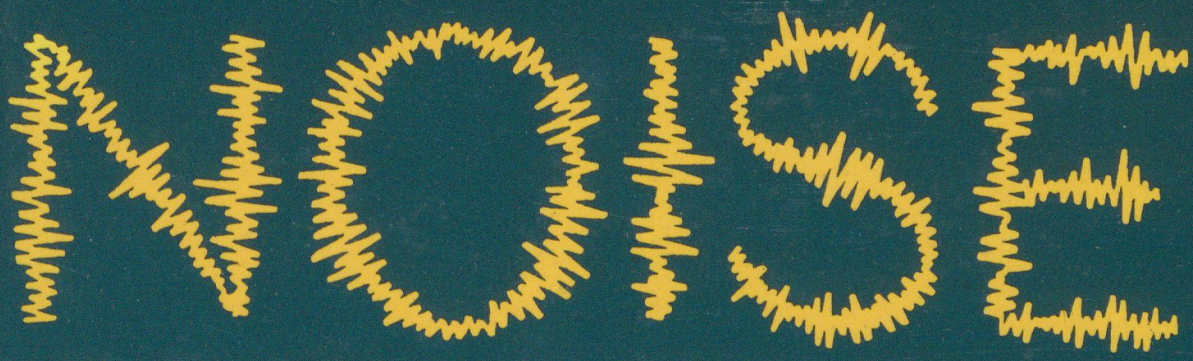

IN PHYSICAL SYSTEMS

INCLUDING 1/f NOISE, BIOLOGICAL SYSTEMS AND MEMBRANES

Edited by A. AMBRÓZY

NOISE IN PHYSICAL SYSTEMS

INCLUDING 1/f NOISE, BIOLOGICAL SYSTEMS AND MEMBRANES

10088

NOISE IN PHYSICAL SYSTEMS

INCLUDING 1/f NOISE, BIOLOGICAL SYSTEMS AND MEMBRANES

10th INTERNATIONAL CONFERENCE
AUGUST 21–25, 1989, BUDAPEST, HUNGARY

EDITED BY
A. AMBRÓZY

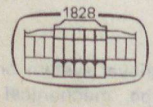

AKADÉMIAI KIADÓ, BUDAPEST 1990

MTA
KIK
0 00003 83285 1

674949

MAGYAR
TUDOMÁNYOS AKADÉMIA
KÖNYVTÁRA

M. TÜD. AKADÉMIA KÖNYVTÁRA
Könyvtár. 4040./19. 90. sz.

ISBN 963 05 5778 9

© A. AMBRÓZY, BUDAPEST 1990

All rights reserved. No part of this publication may be reproduced, stored in a retrieval system or transmitted in any form or by any means: electronic, electrostatic, magnetic tape, mechanical, photocopying, recording or otherwise, without permission in writing from the publishers.

PRINTED IN HUNGARY

SESSIONS

1. General theories of fluctuations and noise
2. Noise in various physical systems (solids, liquids, surfaces, magnetics)
3. Noise in materials (crystalline, amorphous)
4. Quantum noise (squids, masers, lasers, quantum optics)
5. Noise in electron devices (diodes, BJTS, FETS)
6. Noise in biological systems and membrane noise
7. Theories of 1/f noise
8. 1/f noise in physical systems (e.g.materials)
9. 1/f noise in electron devices
10. Measurement techniques
11. Chaos and other fluctuation phenomena

International Advisory committee:

A.Ambrózy,Hungary
V.Bareikis,USSR
L.de Felice,USA
P.H.Handel,USA
C.Heiden,FRG
F.N.Hooge, The Netherlands
B.K.Jones,U.K.
P.Mazzetti,Italy
T.Musha,Japan
M.Savelli,France
A.van der Ziel,USA
C.M.Van Vliet,Canada
D.Wolf,FRG
R.J.Zijlstra,The Netherlands

Local Scientific Committee:

Prof.A.Ambrózy
Prof.T.Berczeli
Dr.T.Geszti
Dr.L.B.Kiss
Prof.P.Szépfalussy

Steering Committee:

Prof.S.Csibi,Chairman,Hungarian Academy of Sciences
Prof.R.Tuschák, Techn.Univ. Budapest
Prof.L.Kállai, Treasurer, High School of Finance and Accountancy
Prof.A.Ambrózy
Dr.P.Bánlaki, Secretary

INVITED SPEAKERS

Moss, F (St.Louis)	The use of analog simulation in studies on noise driven nonlinear dynamical systems
Brophy, J.J. (Salt Lake City)	Noise in materials - some recent results
van der Ziel, A. (Minneapolis)	Experiments on 1/f noise agreements and discrepancies with Handel's predictions
Bareikis, V. (Vilnius)	Fluctuation spectroscopy of hot electrons in semiconductors
Defelice, L.J. (Atlanta)	Excitability and channel kinetics in free-running membrane
Kiss, L. B. (Szeged)	Some recent theories of 1/f noise
Hooge, F.N. (Eindhoven)	Is there a simple empirical relation for 1/f noise?
Kleinpenning, T. (Eindhoven)	1/f noise in electronic devices
Storm, L. (Münster)	Errors associated with the measurement of power spectra by the correlation technique

PREFACE

Towards the end of the 60's the research of fluctuation phenomena became more extensive beginning mainly with investigation of the active devices to continue with physical systems in a wider sense. A series of conferences started in 1968 whose title at present is:

International Conference on Noise in Physical Systems

Places and times of the previous conferences are the following:

Nottingham, United Kingdom	1968
Toulouse, France	1971
Gainesville, USA	1973
Noordwijkerhout, Holland	1975
Bad Nauheim, FRG	1978
Washington, USA	1981

In the late seventies interest in 1/f noise increased suddenly and a parallel series of conferences developed under the title "Conference on 1/f Noise". These are:

Tokyo, Japan	1977
Orlando, USA	1980

The two series merged in 1983:

Montpellier, France	1983

Rome, Italy	1985
Montreal, Canada	1987
Budapest, Hungary	1989

The present one - the tenth - has been sponsored by the Hungarian Academy of Sciences, the State Office for Technical Development and the Technical University of Budapest and held in the campus of the university, August 21-25, 1989.

Nine invited and 118 contributed papers were read in eleven Sessions. An interesting feature of the conference is that all the countries important in noise research were represented.

Only papers presented personally are included in this volume, according to the reaffirmed decision of the International Advisory Board. The papers have been placed in logical order within each session by the Local Scientific Committee of the Conference hoping in this way to facilitate access to the information provided.

Having had ten (twelve) successful gatherings, participants look forward to the continuation. The next two conferences will be held in Kyoto, Japan, 1991 and in the U.S.A., 1994.

A. Ambrózy

TABLE OF CONTENTS

Sessions and Committees v

Invited Speakers vi

Preface vii

SESSION 1

GENERAL THEORIES OF FLUCTUATIONS AND NOISE

PELLEGRINI, B. 3

Electrokinematics theorem and noise

NOUGIER, J.P., VAISSIÈRE, J.C. 7

Langevin noise source of the state occupancy function

MUNAKATA, T., MIMAKI, T., WOLF, D. 11

Estimation of the autocorrelation function of Gaussian random processes from the probability densities of crossing intervals with two levels

TETZLAFF, R., WOLF, D. 15

Recent results for the level-crossing problem of Gaussian random signals

NEIDENOFF, A. 19

"General equivalent noise" of electric networks

SESSION 2

NOISE IN VARIOUS PHYSICAL SYSTEMS
(SOLIDS, LIQUIDS, SURFACES, MAGNETICS)

ZHOU, T., JAMES, M., SINHA, K., DEBNATH, G., MOSS, F. 29

The use of analog simulation in studies on noise driven nonlinear dynamical systems

GOMBOS, G., SZAKÁCS, T. 39

Noise and self-organization in a simple cellular automaton

BARKAUSKAS, R., GANTSEVICH, S.V., KATILIUS, R. 45

Fluctuations and collision-controlled light scattering in nonequilibrium electron-hole plasma

DEDULEVIČ, S., KANCLERIS, Ž., MATULIS, A. 49

Price relation violation in slightly heating electric field

BAREIKIS, V., LIBERIS, J., MATULIONIS, A., MILIUŠYTE, R., SAKALAS, P. 53

Long-range fluctuations of hot electrons in GaAs and InP at 80K

BEBEN, J. 57

Time cross-correlation functions of density fluctuations for potassium adlayer on the (112) W plane

KOCHELAP, V.A., MITIN, V.V., ZAKHLENIUK, N.A., BULASHENKO, O.M. 61

Limitation of spectral density of current fluctuations in semiconductors in strong electric fields

FENG, S. 67

Universal conductance fluctuations and the 1/f noise magnitudes in disordered metals

FORGÁCS, G., BÉAL-MONOD, M.T. 71

Mechanism in conductance fluctuations of mesoscopic disordered systems disobeying universal laws

SESSION 3

NOISE IN MATERIALS (CRYSTALLINE, AMORPHOUS)

BROPHY, J.J. 77

Noise in materials — some recent results

BROPHY, J.J. 87

Diffusion noise in sodium beta alumina

DARGYS, A., MILIUŠYTE, R. 91

Tunnel noise in p-type semiconductors

REGGIANI, L., VARANI, L. 95

The Monte Carlo method for the microscopic interpretation of electronic noise in semiconductors

BORDONE, P., REGGIANI, L., VARANI, L., MITIN, V. 99

Generation-recombination noise in p-Si at 77 K

MITIN, V.V., Van VLIET, C.M. 103

Light hole contribution to noise and diffusion at low temperatures in p-germanium

GOTTWALD, P., AMBRÓZY, A., SZENTPÁLI, B. 109

Hot electron noise in thin GaAs films

MONTORSI, A., BERTOTTI, G. 113

Theory of Barkhausen noise in ferromagnetic materials

MYKOLAITIS, H., PALENSKIS, V., LAUCIUS, J. 117

Modulation noise in magnetic and other nonlinear systems

MYKOLAITIS, H. 121

Investigation of modulation noise in amorphous magnetic alloy

KUROPYATNIK, I.N., ROMANENKO, A.I., CHEREVKO, A.G. 125

Low-frequency noise of high-T_c superconductors

KOGAN, Sh.M., NAGAEV, K.E. 129

The kinetics of fluctuations and the spectral density of noise in resistive states of superconductors

KONOPKA, J., JUNG, G. 135

Characterization of high temperature superconductors by microwave noise emission

SESSION 4

QUANTUM NOISE (SQUIDS, MASERS, LASERS, QUANTUM OPTICS)

van der ZIEL, A. 143

Experiments on 1/f noise agreements and disagreements with Handel's predictions

HANDEL, P.H. 155

General derivation of the quantum 1/f noise effect in physical cross sections and the 1/N factor

ORSAL, B., RANIRIHARINOSY, K., ALABEDRA, R., JOINDOT, I. 159

Correlation between electrical and optical noises in double heterostructure lasers at wavelength $\lambda = 0.83$ micrometer

HANDEL, P.H. 167

Quantum 1/f cross-correlations and spectra

KIL, A.J., ZIJLSTRA, R.J.J., ANDRE, J.D. 171

Localization fluctuations in quantum Hall devices

MÜCK, M., HEIDEN, C. 175

Investigation of noise in relaxation oscillators made of microbridges

HANDEL, P. H. 179

The nonlinearity causing classical and quantum 1/f noise: Sliding scale invariance and quantum chaos definition

SESSION 5

NOISE IN ELECTRON DEVICES (DIODES, BJTS, FETS)

BAREIKIS, V., KATILIUS, R. 189

Fluctuation spectroscopy of hot electrons in semiconductors

KUGLER, S., HEIME, K., SCHLAPP, W., WEIMANN, G. 201

Determination of trap parameters in highly doped semiconductors from low frequency noise spectra

HOFMAN, F., ZIJLSTRA, R. J. J., HENNING, J. C. M. 205

Noise spectroscopy of deep centers in $Al_xGa_{1-x}As$

KRATĚNA, L., ŽDÁNSKÝ, K., ŠIKULA, J., VAŠINA, P., GRMELA, L. 209

Noise and deep level transient spectroscopy of deep level (DX) centres in GaAs-GaAlAs heterostructures

JONES, B. K., TAYLOR, G. P. 213

Spectroscopy of surface states using generation recombination noise

VAŠINA, P., ŠIKULA, J., GRMELA, L., HÜTTEL, I., HLÁVKA, J. 217

Noise diagnostics of GaAlAs heterostructure luminescent diodes

VALENZA, M., RIGAUD, D., KOUADIO, A., LECOY, G., HERAULT, D. 221

Characterization of various types of implanted layers through noise measurements in buried channel MOSFET's

ŠIKULOVA, M., ŠIKULA, J., VAŠINA, P., NEVĚČNÝ, V. 227

Burst noise in p-n junction devices

MATUKAS, J., PALENSKIS, V., PINCEVIČIUS, A., SMETONA, S. 231

The influence of low-energy ion radiation in GaAs surface on the current-voltage, capacitance-voltage and noise characteristics of Schottky-barrier diodes

NERI, B., DILIGENTI, A., ALOE, P., MOZZI, C. 237

$1/f^{\gamma}$ noise in thin gold films and its dependence on process parameters

KONCZAKOWSKA, A., GLADYSZ, H. 241

Noise as a lifetime estimator for bipolar transistors

HASSE, L., KONCZAKOWSKA, A., SPIRALSKI, L. 247

Noise measurements of power semiconductor devices for reliability evaluation

ORSAL, B., MAATOUGUI, A.H., ALABEDRA, R., SAVELLI, M., LEVÊQUE, G., FLACHET, J.C. 251

Noise and impact ionization rates for electrons and holes in $Hg_{0.56}Cd_{0.44}Te$ avalanche photodiode for optical fiber transmission systems at 2.5 μm

LUKYANCHIKOVA, N.B., DEKHTYARUK, N.T. 259

Noise and mechanism of impact ionization in GaAs

BELAN, J., MATISCAK, F., MIKOLAJ, V., STRAPKO, F., LATTA, V. 263

Dependence of voltage fluctuations on the ratio of the avalanche and tunneling current in reference diodes

NERI, B., MARINI, A., SALETTI, R., OLIVO, P. 267

Current noise spectra and fluctuations before breakdown in thin silicon oxides

GHIBAUDO, G. 271

Unified formulation of trapping noise and fluctuation in MOS devices

DIERICKX, B., SIMOEN, E., VERMEIREN, J., COS, S., CLAEYS, C. 275

Anomalous v_{DS} dependent noise in Si MOSFET's at LHe temperature

PERANSIN, J.M., VIGNAUD, P., RIGAUD, D., DUMAS, J.M. 281

Low-frequency noise associated to the gate current of GaAs MESFETs and MODFETs

CARBONE, A., DEMICHELIS, F., MAZZETTI, P. 285

Experimental study of the current noise in CdS photoconducting devices as a function of the wavelength and intensity of the exciting radiation

JINDAL, R.P. 289

Improving photo detector noise performance using noninstantaneous multiplication (amplification)

ŠIKULA, J., VAŠINA, P., SYNEK, S., HÜTTEL, I. 293

Noise of GaAlAs super-LED radiation

ŠIKULA, J., KOKTAVÝ, B., VAŠINA, P., SCHAUER, P., STRÁSKÝ, L. 297

Impulse noise in capacitors

SESSION 6
NOISE IN BIOLOGICAL SYSTEMS AND MEMBRANE NOISE

DeFELICE, L. J. 303
Excitability and channel kinetics in the free-running membrane

GREEN, M. E. 313
Noise spectra of a kinetic model of channel gating based on an electrorheological model of the physical process

SESSION 7
THEORIES OF 1/F NOISE

KISS, L. B. 319
Some recent theories of 1/f noise

ANTON, K., WOLF, D. 331
Simulation of 1/f noise

GINGL, Z., KISS, L. B., VAJTAI, R. 335
$1/f^k$ noise generated by scaled Brownian motion

PALENSKIS, V., ŠOBLICKAS, Z., STADALNIKAS, A. 339
Excess low-frequency noise in semiconductors

KOLEK, A., KUSY, A. 343
A real space renormalization group approach to 1/f noise in random resistor networks

MEADE, M. L 347
Time- and frequency-domain models for fractional noises

WEBER, B., WOLF, D., HANDEL, P. H. 351
Analytical and numerical study of fluctuations in active nonlinear system

Van VLIET, C. M. 357
An alternative theory for quantum 1/f noise based on quantum electrodynamics

WOLF, D., HANDEL, P. H., SEKINE, M. 365
Characteristic functional of physical thermal noise which includes equilibrium 1/f noise

ZAKLIKIEWICZ, A. M. 369
Simple interpretation of 1/f noise phenomenon

SESSION 8

1/f NOISE IN PHYSICAL SYSTEMS (E.G.MATERIALS)

HOOGE, F.N. 375

Is there a simple empirical relation for 1/f noise?

MUSHA, T., BORBÉLY, G., SHOJI, M. 385

Fluctuations of Brillouin scattered light intensity with quartz specimen

BAKSHEE, I.S., POTEMKIN, V.V., SALKOV, E.A., KHIZHNYAK, B.I. 389

1/f noise in Al: The existence of surface noise

TACANO, M., KANAYAMA, T., SUGIYAMA, Y., HASHIGUCHI, S. 393

1/f noise in quarter-micron filaments of GaAs and InP made by focussed ion-beam implantation

BAKSHEE, I.S., GRIN', V.F., KARACHEVTZEVA, L.A., KODALASHVILI, M.Z., SALKOV, E.A., KHIZHNYAK, B.I. 397

1/f noise in n-$Cd_xHg_{1-x}Te$

GOUYET, J.F., SAPOVAL, B., BOUGHALEB, Y., ROSSO, M. 401

Dynamics of disordered fronts: Diffusion and invasion noise

GALPERIN, Yu.M., GUREVICH, V.L., KARPOV, V.G., KOZUB, V.I. 407

Disorder-induced flicker noise

MAY, E.J.P., AL-CHARCHAFCHI, S.H. 411

1/f noise in variable carbon granule resistors

MAY, E.J.P. 417

1/f noise in carbon and asbestos wetted by saline solutions

NEUSTROEV, L.N., OSIPOV, V.V., PANASHCHENKO, O.N. 421

Nyquist 1/f noise in semiconductor-tunneling dielectric-semiconductor structures

SHI, Z.M., DUTOIT, M., ILEGEMS, M. 427

Noise in the tunneling current through thin SiO_2 film at 77 and 295 K

HANDEL, P.H. 433

1/f noise and quantum 1/f approach in ferroelectrics and ferromagnetics

GUNNARSSON, K., SVEDLINDH, P., NORDBLAD, P., LUNDGREN, L., ARUGA, H., ITO, A. 437

Measurements of the equilibrium magnetic noise of a short-range Ising spin glass

SESSION 9

1/F NOISE IN ELECTRON DEVICES

KLEINPENNING, T. G. M. 443

1/f noise in electronic devices

AMBRÓZY, A., GOTTWALD, P., SZENTPÁLI, B. 455

Low frequency noise in thin GaAs layers

LUKYANCHIKOVA, N. B., PETRICHUK, M. V., GARBAR, N. P., SASČIUK, A. P. 461

Connection between the 1/f noise and the noise of generation-recombination type in semiconductors

KARAPATNITSKI, I. A., SYRGABEKOV, I. N., OSIPCHUK, L. K., STAFEEV, V. I. 465

1/f noise in long Si diodes

DIMOPOULOS, G., CHOVET, A. 471

Evidence of 1/f bulk noise sources in SOS devices

FRONEN, R. J. 475

Relation between noncoherent emission and 1/f noise in the light output of laser diodes

ŠIKULA, J., KOKTAVÝ, B., VAŠINA, P., ČERMÁKOVÁ, A. 479

1/f noise, degradation and reliability of GaAsP LED's

DECOUTERE, S., DEFERM, L., CLAEYS, C., DECLERCK, G. 483

Influence of the density of interface traps on the base 1/f noise in vertical npn and lateral pnp transistors

GÜTTLER, H. H., WERNER, J. H., STOLL, H. 487

Excess noise measurements at silicide/silicon Schottky diodes

VANDAMME, L. K. J. 491

1/f noise in CMOS transistors

GHIBAUDO, G., HAFEZ, I. M., BALESTRA, F. 495

Flicker noise in MOS transistors from liquid helium to room temperature

CHANG, J., VISWANATHAN, C. R. 499

Low frequency noise in CMOST's at cryogenic temperatures

CHANG, J., VISWANATHAN, C. R. 503

Flicker noise behavior of MOSFET's after oxide degradation under high gate voltage

HASHIGUCHI, S., IRIE, H. 507

1/f noise in HEMTs

DOUTRELOIGNE, J., De BAETS, J., De RYCKE, I., De SMET, H., Van CALSTER, A., VANFLETEREN, J. 511

A correlation between 1/f noise and short-term drift in poly-CdSe: In thin film transistors

CHEN, T.M., FANG, P., COTTLE, J.G. 515

Electromigration and $1/f^{\alpha}$ noise in Al-based thin films

SUN, M.I., COTTLE, J.G., CHEN, T.M. 519

Determination of Al-based metal film lifetimes using excess noise measurements

ŠOŠTAREC, I. 523

The effects of nuclear irradiation on the low frequency noise of some low noise monolithic operational amplifiers

JONES, B.K., RUSSELL, P.C., XU, Y.Z. 531

Excess noise as an indicator of digital integrated circuit reliability

BÁNLAKI, P. 537

Investigation on the noise of power supply current of CMOS ICs

BALTES, H.P., NATHAN, A., CASTAGNETTI, R. 543

Low frequency noise correlations in superlattice dual-drain magnetic sensors

SESSION 10

MEASUREMENT TECHNIQUES

STORM, L. 551

Errors associated with the measurement of power spectra by the correlation technique

MASOERO, A., MORTEN, B., PRUDENZIATI, M., STEPANESCU, A. 561

An improved technique of measuring the contact noise in thick film resistors

COMALLONGA, J., SAVELLI, M., MARTIN, R., RABARIOELINA, J., MONBLANC, P. 565

1/f noise measurement in 0.1 ohm resistors

TREFÁN, GY., KISS, L.B., GINGL, Z., TÖRÖK, M., HEVESI, I., AMBRÓZY, A. 569

Diffusion noise-generators realized by analog circuits

AMBRÓZY, A., BÁNLAKI, P., GINGL, Z., KISS, L.B., VAJTAI, R., TREFÁN, GY., HEVESI, I. 573

$1/f^k$ noise generators based on computer-random-walk

Van STERKENBURG, S. 577

Noise limited resolution of a Michelson interferometer

NAUMBURGER, V. 581

Noise reduction principles in spectro-ellipsometry

ALABEDRA, R., RIGAUD, D., ORSAL, B., PERANSIN, J.M., VALENZA, M. 585

Real time experimental measurements of noise source correlation in amplifiers and transducers

DMOWSKI, K., JAKUBOWSKI, A. 589

Theoretical signal-to-noise ratio of correlators with exponentially weighted average and weighting function with blanking time

DAMGOV, V.N. 593

Noise properties of negative R, C and L one-ports based on four-frequency parametric systems

HASSE, L.Z., SPIRALSKI, L. 599

Multifunctional noise measurement system for electronic component quality evaluation

SESSION 11

CHAOS AND OTHER FLUCTUATION PHENOMENA

KURTHS, J., BENZ, A.O., BIRKEMEYER, U., ISLIKER, H. 605

Chaotic pulsations in the solar corona

GAFIJCHUK, V.V., KERNER, B.S., OSIPOV, V.V., VASYUNYK, Z.I. 609

A new type of space-time chaos

DAMGOV, V.N., HRISTOV, T.S. 615

Chaos in short-distance Doppler radars with self-detecting oscillators

BULSARA, A.R., SCHIEVE, W.C., JACOBS, E.W. 621

Effect of weak noise on chaotic dynamic systems

ANISHCHENKO, V.S., KRAVTSOV, Yu.A., PIKOVSKII, A.S. 625

Noisy chaos

VOSHCHINSKII, Yu.A., MAGARSHAK, A.S., SHTEINGRADT, D.M. 629

Chaotization of vibrations of a nonautonomous oscillator affected by a noise signal: Experimental study

ZHOU, T., MOSS, F. 635

Stochastic resonance: How increasing the noise can result in more order

RAMIREZ-PISCINA, L., SANCHO, J.M., LINDENBERG, K., de la RUBIA, F.J. 639

Escape over a potential barrier driven by colored noise

VAVRIV, D.M., RYABOV, V.B. 645

Fractal dimensions: Problems of calculations

CHERNESHOV, I.Yu., VAVRIV, D.M. 651

Experimental investigations of dynamical chaos in weakly nonlinear oscillators

BELOGORTSEV, A.B., VAVRIV, D.M. 657

The interaction of resonances and chaos in quasilinear systems

BEHN, U., MÜLLER, R. 663

Electrohydrodynamic instabilities in nematics driven by dichotomous stochastic voltages

MAGARSHAK, A.S., SINKEVICH, A.Yu., SHTEINGRADT, D.M. 667

Amplitude stochastization of oscillations of a nonlinear oscillator with high-frequency pumping modulated by a telegraph random signal

List of Participants 675

Author Index 683

Subject Index 687

SESSION 1

GENERAL THEORIES OF FLUCTUATIONS AND NOISE

10th Int.Conf. on Noise in Physical Systems
1989 Budapest, Hungary

ELECTROKINEMATICS THEOREM AND NOISE

B. PELLEGRINI

Istituto di Elettronica e Telecomunicazioni,
Universita di Pisa
56126 Pisa, Italy

ELECTROKINEMATICS THEOREM

For an electric system of volume Ω and surface A, a new electrokinematics theorem leads to the general equation (1,2)

$$\int_A \left(\varepsilon \frac{\partial \psi}{\partial t} \mathbf{F} - U \mathbf{J} \right) \cdot d\mathbf{A} = \sum_{i=1}^{N} q_i \mathbf{v}_i(\mathbf{r}_i) \cdot \mathbf{F}(\mathbf{r}_i) + \int_\Omega \frac{\partial \psi}{\partial t} \nabla \cdot (\varepsilon \mathbf{F}) \, d\mathbf{r} \quad , \tag{1}$$

where $\mathbf{F}(\mathbf{r},t)$ is an arbitrary irrotational field defined by $\mathbf{F} = -\nabla\phi(\mathbf{r},t)$ in Ω and $\phi = U(\mathbf{r},t)$ on A, with U being a given function of $\mathbf{r}$ and t, $\mathbf{J}$ is the total current density, $\psi(\mathbf{r},t)$ and $\varepsilon(\mathbf{r})$ are the electric potential and the electric permittivity, respectively, and q_i, $\mathbf{r}_i$ and $\mathbf{v}_i$ are the charge, position and velocity of the ith charge carrier of the N(t) carriers contained in Ω at time t.

By specifying $\mathbf{F}$, the integral equation (1) makes it possible to generalize the Ramo-Schockley theorem (3,4) and its extensions (5) from the vacuum devices to any other device, to obtain the energy balance and its components, the Kirchoff law and so on (1,2).

In particular, a meaningful result is obtained from (1) for bipoles with two plan and parallel electrodes, of areas A_1 and A_2 at a distance L, and with a constant permittivity ε. Indeed, from (1), by choosing a $\mathbf{F}(\mathbf{r},t) = F(t)\mathbf{u}$, we find that current i entering Ω across A_2 is given by

$$i = -\frac{1}{L} \sum_{i=1}^{N} q_i v_{ix} + C \frac{dV}{dt} + \frac{1}{L} \int_{A_3} \left(x \mathbf{J}_d + \varepsilon \frac{\partial \psi}{\partial t} \mathbf{u} \right) \cdot d\mathbf{A} \quad , \tag{2}$$

where axis x, unit vector $\mathbf{u}$ and component v_{ix} of $\mathbf{v}_i$ are in a perpendicular direction to the electrodes, $C = \varepsilon A_2/L$ is the capacitance, V is the potential between the electrodes, $\mathbf{J}_d$ is the displacement current and A_3 is the lateral surface of the device.

For a right cylinder the term of (2) depending on $\mathbf{u}$ becomes null, as well as that depending on V if this is constant, i.e. if the terminals are shortcircuited for the AC components. The other term taking into account displacement current $x\mathbf{J}_d/L$ across A_3, can also be neglected, at least for a small surface A_3 and/or for low frequencies. Therefore, by putting $v_{ix} = v_i$ for sake of simplicity, (2) becomes

$$i(t) = -\frac{1}{L} \sum_{i=1}^{N} q_i v_i \tag{3}$$

Equation (3) allows us to perform a direct statistical computation of the spectrum S of the current and, therefore, of any of its noises according to the Wiener-Kintchine theorem

$$S = 2 \int_{-\infty}^{\infty} \Gamma(\theta) \cos(\omega\theta)\, d\theta \quad , \tag{4}$$

where the autocorrelation function $\Gamma(\theta)$ of the current, from (3), becomes

$$\Gamma = \frac{1}{L^2} \lim_{T\to\infty} \frac{1}{T'} \int_{-T'/2}^{T'/2} \left[\sum_{i=1}^{N_T} \sum_{h=1}^{N'_T} q_i v_i(t)\, q_h v_h(t+\theta) \right] dt \quad , \tag{5}$$

in which N_T (N'_T) is the number of all the carriers which, at least during of fraction of the time interval -T'/2, T'/2 (-T'/2+θ, T'/2+θ), are present in the device, and ω is the angular frequency.

Let t'_j and t''_j (j = i, h) be the instants of start and of finish, respectively, of the current pulse $q_j v_j(t)/L$ due to the jth carrier, so that $\sigma_j = t''_j - t'_j$ and $t_j = (t'_j + t''_j)/2$ are the length and intermediate time of such a pulse, respectively. Therefore, we have the average value $\overline{v}_j = \varphi_j L/\sigma_j$ and the fluctuation $\Delta v_j = v_j - \overline{v}_j$ of $v_j(t)$ during the time interval t'_j, t''_j, where φ_j = 1(-1) when the jth charge, by starting from electrode 1 (2), reaches electrode 2 (1), whereas φ_j = 0 if it reaches the start terminal.

For i≠h, Δv_i and Δv_h are uncorrelated so that v_i and v_h give contributions $\Gamma_{ih} = q^2\varphi'_i\varphi'_h F_{ih}/\sigma_i\sigma_h$ to Γ through their average values alone; q is the electron charge, $\varphi'_j = \varphi_j q_j/q$, with its values 1, 0, − 1, indicates when the pulse contribution to the current is positive, null and negative, respectively, and the θ function $F_{ih}(\theta)$ has the shape shown in the side figure for $\sigma_i > \sigma_h$,

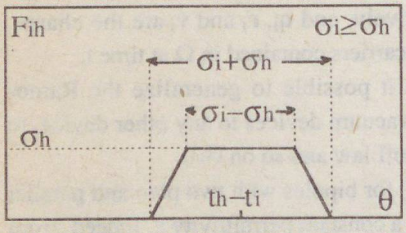

whereas for $\sigma_i < \sigma_h$ these latter quantities are interchanged; in both cases $\int F_{ih}\, d\theta = \sigma_i\, \sigma_h$.

Therefore, if we use N_T^+, N_T^0 and N_T^- to indicate the number of the N_T pulses with φ'_j = 1, 0, -1, respectively, the sum, for i≠h, of the Γ_{ih}'s gives a total contribution Γ_{dc} to Γ which, according to (5), becomes

$$\Gamma_{dc} = q^2 \lim_{T'\to\infty} \frac{1}{T'} \left(N_T^+ \frac{N_T^+}{T'} - N_T^- \frac{N_T^+}{T'} + N_T^- \frac{N_T^-}{T'} - N_T^+ \frac{N_T^-}{T'} \right) = \left(\overline{i}^{+} - \overline{i}^{-} \right)^2 = \overline{i}^{\,2} \quad , \tag{6}$$

where $\overline{i}^{+}$ ($\overline{i}^{-}$) is the average current due to the positive (negative) pulses and $\overline{i} = \overline{i}^{+} - \overline{i}^{-}$ is the average total current. That is, according to (4) and (6), Γ_{dc} leads to the spectrum $S_{dc} = 2\pi\, \overline{i}^{\,2}\, \delta(\omega)$ due to the direct current.

Rather, for i = h, the $(N_T^+ + N_T^-)$ terms $q^2\, v_i(t)v_i(t+\theta)/L^2$ relevant to the carriers crossing the device give a contribution Γ_{ac} to Γ which, from (4) and (5), for $\sigma_m\omega \ll 1$, leads to the spectrum

$$S_{sh} = 2q^2 \lim_{T'\to\infty} \frac{1}{T'} \left(N_T^+ + N_T^- \right) = 2q \left(\overline{i}^{+} + \overline{i}^{-} \right) \quad , \tag{7}$$

with σ_m being the greatest of the σ_i's, whereas N_T^0 pulses make no contribution to S_{sh}.

Equation (7) generalizes the Schottky theorem to any bipole. The problem in applying it is computing $\overline{i}^+$, $\overline{i}^-$ and σ_m. For certain bipoles, such as diodes of various types, this problem is easy to solve, whereas for others, such as resistors, it is more complex. For the latter, however, $\overline{i}^+$, $\overline{i}^-$ and σ_m can be easily computed if their length L is much smaller than the mean free path l_s of the carriers and the applied field is null. Indeed in this case we have [6] $\overline{i}^+ = \overline{i}^- = qnAv_{th}/(2\pi)^{1/2}$ and $\sigma_m \approx L/v_{th}$, where n is the carrier density, A is the cross-section of the device, $v_{th} = (kT/m)^{1/2}$ is the thermal velocity, k is the Boltzmann constant, T is the absolute temperature and m is the carrier effective mass.

By going back to (5), according to the uncorrelation of Δv_i and Δv_h for $i \neq h$, it may be written in the form $\Gamma = \Gamma_{dc} + \Gamma_{ac}$ where Γ_{dc} is given by (6) and Γ_{ac} becomes

$$\Gamma_{ac} = \frac{q^2}{L^2} \lim_{T \to \infty} \frac{N_T}{T'} \int_0^{T'} \Gamma_v(\theta, t')\, dt' \quad , \tag{8}$$

in which $t' = t - t'_i$ and Γ_v is the autocorrelation function of the velocity given by

$$\Gamma_v = \frac{1}{N_T} \sum_{i=1}^{N_T} v_i(t')\, v_i(t'+\theta) = \iint vv' \Phi(v, v', t')\, dv\, dv' \quad , \tag{9}$$

where Φ is the joint probability density function of $v = v(t')$ and $v' = v(t'+\theta)$ on condition that the carrier is still in the device at t'.

While, for $\sigma_m \omega \ll 1$, (4), (8) and (9) again give (7), apart from the shape of $\Gamma_{ac}(\theta)$, in the other cases the part of S deriving from Γ_{ac} depends on such a shape and in particular on that due to carrier scatterings, and to it the N_T^0 pulses also contribute.

For instance, for a resistor with $L \gg l_s$ and a null field, the effects of the scatterings on Γ_{ac} prevail so that we have $\int \Gamma_v dt' \cong \sigma_a (kT/m) \exp(-|\theta|/\tau_s)$ and $N_T = \overline{N}\, T'/\sigma_a$, where τ_s is the scattering time and σ_a is the average value of σ_i. Therefore, in this case, from (4) and (8) we obtain the spectrum S_{th}, relevant to Γ_{ac}, of the thermal noise given by Nyquist's theorem [6]

$$S_{th} = 4kT\, \mathrm{Re}\left[G(j\omega)\right] = \frac{4q^2 n\, l_s\, v_{th}\, A}{L(1+\tau_s^2 \omega^2)} \quad , \tag{10}$$

where $q\tau_s/m = \mu$ is the carrier mobility, $G(j\omega) = q\mu nA/L(1 + j\tau_s\omega)$ is the device conductance and, finally, $l_s = \tau_s v_{th}$.

In particular, from the preceding results relevant to S_{sh} and from (10) for $\tau_s \omega \ll 1$, we find that $S_{th} = S_{sh}$ for $L = (2\pi)^{1/2} l_s$ [6], that is, as might be expected, the shot noise prevails for $L \ll l_s$ and the thermal noise for $L \gg l_s$.

Equations (4), (8) and (9) may be used to compute S in a general form.

In their turn, according to the preceding statistical approach, equations (4) and (5) could be applied to compute the generation-recombination (g-r) and flicker noises, too, by taking into account the N(t) fluctuation induced by charge fluctuation ΔQ in the device defects.

We do not have sufficient space to do this here.

However, we can use the electrokinematics theorem again to compute in a straightforward way the coupling coefficient between the charge fluctuation ΔQ of a defect and the induced fluctuation ΔI of the output current; this coefficient makes it possible to compute such noises using the corpuscular-collective approach [7-9]. To this end we can write (3) in the integral form

$$i = -\frac{1}{L}\int_{\Omega}\left[(J_n+J_p)+(\eta_n+\eta_p)\right] dr \quad , \tag{11}$$

where J_n (J_p) is the density of the drift - diffusion current of the electrons (holes) along the x axis and η_n (η_p) is its fluctuation due to the scatterings.

Through the potential fluctuation ΔV, fluctuation ΔQ generates fluctuations Δn and Δp of the electron and hole concentration, respectively, which, according to (11) and the usual equations of J_n and J_p, lead to the relevant fluctuation ΔI of i in the form [7]

$$\Delta I = -\frac{1}{L}\int_{\Omega}\left(J_n\frac{\Delta n}{n}+J_p\frac{\Delta p}{p}\right) dr \quad . \tag{12}$$

By computing ΔV by means of the Poisson equation, from (12) we obtain

$$\Delta I = -\frac{\left[J_n(x)-J_p(x)\right]}{qL\left[n(x)+p(x)\right]}\Delta Q \quad , \qquad \Delta I = -\,q\,\frac{\left[J_n(x)-J_p(x)\right]}{2kTL\varepsilon}(x-x_1)\,(x_2-x)\,\Delta Q \quad , \tag{13}$$

if the defect, of abscissa x, is in a quasi neutral region or in a depletion layer, respectively, for instance of a p-n junction; x_1 and x_2 are the edges of the depletion layer.

Equation (13) overcomes, by virtue of the electrokinematics theorem, any previous limit or problem arising from the impedance field method [7] and the incompleteness in determining the coupling coefficients by means of the continuity equations alone [8].

Using (13) and the Lorenztian spectrum of ΔQ we can then compute the output spectrum of the g-r and flicker noises of bipolar devices by means of the usual methods [9].

On the other hand, unitary models of the thermal and g-r noises [10] and of the g-r and flicker noises [6,11], as well as their Monte Carlo simulations, have been obtained for unipolar devices again on the basis of the electrokinematics theorem in its form (3).

In conclusion, the electrokinematics theorem allows us to deal with noise phenomena in a general and straightforward way and to obtain new results.

---

1. B. Pellegrini, Phys. Rev. **B34**, 5921 (1986).
2. B. Pellegrini, Alta Frequenza **56** (Italian issue), 157, (1987).
3. S. Ramo, Proc. IRE **27**, 584 (1939).
4. W. Schockley, J. Appl. Phys. **9**, 636 (1938).
5. G. Cavalleri, E.Gatti, G. Fabbri, and V. Svelto, Nucl. Instrum. Methods **92**, 137 (1977).
6. B Pellegrini, Alta Frequenza - Rivista di Elettronica **1** (Italian issue), 3 (1989).
7. B. Pellegrini, Phys. Rev. **B24**, 7071 (1981).
8. B. Pellegrini, Phys. Rev. **B38**, 8269 (1988); ibid., 8279 (1988)
9. B. Pellegrini, Phys. Rev. **B35**, 571 (1987).
10. M. Macucci, B. Pellegrini, L. Reggiani, P. Terreni, J. Appl.Phys. **63**, 5369 (1988).
11. B. Pellegrini, in "Physics of Semiconductor Devices", Ed. S.C. Jain and Radakrishna, (World Scientific, Singapore 1987), p. 220.

10th Int.Conf. on Noise in Physical Systems
1989 Budapest, Hungary

LANGEVIN NOISE SOURCE OF THE STATE OCCUPANCY FUNCTION

J.P. NOUGIER, J.C. VASSIERE

Centre d'Electronique de Montpellier,* Université
des Sciences et Techniques du Languedoc
34060 Montpellier Cedex, France

THE STATE OCCUPANCY FUNCTION

Let us consider a homogeneous semiconductor bar, in an uniform electric field E_s. This system can be described using a Monte Carlo simulation, in which one follows the motion of each electron, using random numbers, as a succession of free flights and scattering events. We assume that this scheme is a correct description of the system. Now let us consider a domain D of volume Ω inside the semiconductor bar. Through the Monte Carlo simulation, we know, at a given time t, which electrons are in the domain D, and in which state they are, within a coarse grained description of the phase space. It is then possible to assign to each state (cell in {k} space) the indicator 1 if it is occupied, and 0 if it is empty: the random function f(k,r,t), which takes the corresponding values 0 or 1, is the state occupancy function (SOF). It describes completely, at time t, the state of the system composed of the electrons in the volume Ω. It follows from its definition that (see eq. (1) of ref. [1]):

$$\sum_{\mathbf{k}} f(\mathbf{k},\mathbf{r},t) = N(\mathbf{r},t) \quad , \tag{1}$$

where N(r,t) is the total number of electrons located in the domain D at time t. The ensemble average value of the SOF is the distribution function (DF), which obeys the Boltzmann equation (BE). Its steady state value will be labelled $f_s(\mathbf{k})$.

The fluctuations of transport parameters, about their steady state value, can be related [2] to the spectral density $S_f(\mathbf{k},\mathbf{k}')$ of the fluctuations of the SOF about $f_s(\mathbf{k})$, which is itself related to the Langevin noise source term $S_\xi(\mathbf{k},\mathbf{k}')$. The fluctuations of the SOF of systems governed by the BE have been studied since more than 30 years by a number of researchers [2][3][4]. The basic result, which had been till now accepted by everybody, is that the Langevin noise source term

* Laboratoire associé qu CNRS, UA 391.

$S_\xi(k,k')$, responsible for the fluctuation of $f(k,r,t)$, can be written as [3][4][5]:

$$S_\xi(k_1,k_2) = \delta_{k_1k_2}\left[\sum_k f_s(k)P(k,k_1) + \sum_k f_s(k_1)P(k_1,k)\right] - \left[f_s(k_1)\,P(k_1,k_2) + f_s(k_2)\,P(k_2,k_1)\right] \quad . \qquad (2)$$

In recent works [6][7], we took $S_\xi(k_1,k_2)$ as being diagonal, i.e.:

$$S_\xi(k_1,k_2) = S_\xi(k_1)\,\delta_{k_1k_2} \quad , \qquad (3)$$

which is in contradiction with eq.(2). The demonstration of eq.(2) lies on the fact that the system is Markovian [3][4]. Eq.(2) obviously satisfies the relation:

$$\sum_k \sum_{k'} S_\xi(k,k') = 0 \quad . \qquad (4)$$

In the present paper, we show that a system described by the BE is not Markovian, and we demonstrate that eq. (2) cannot hold. As a consequence, all subsequent derivations which have been based on that theory are wrong.

THE SYSTEM IS NOT MARKOVIAN

The system of electrons located at time t in the domain D inside the semiconductor bar cannot be Markovian because it is an open system. As explained above, the state of each electron in the domain D can be supposed to be known at time t, through a Monte Carlo simulation. Assuming that this system is Markovian is equivalent to state that the probability to find a given electron in a given state at time t'>t, can be deduced from the knowledge of the system at time t. This is wrong, since at time t'>t, some of the electrons of the system have moved away, due both to drift and diffusion: waiting long enough, all the electrons which were in D at time t will have escaped, so that even at thermal equilibrium, one has $f(k,r,t'\to\infty)\approx 0$: this is obviously wrong, since other electrons, coming from outside D, have replaced those which have escaped. Therefore, the knowledge of the function $f(k,r,t)$ at time t does not give an indication of what could be its value later on: one needs also to know f outside D at time t.

EQUATION (2) DOES NOT HOLD

An essential feature of the actual motion of the electrons, correctly taken into account by the Monte Carlo simulation, is the fact that, due to the random scattering events, the number of electrons in the domain D is not constant, but fluctuates. This fluctuation is not taken into account by usual theories of Markovian processes, which assume that the sum of all the probabilities, i.e. the total number of systems, is constant and do not depend on time (see either eqs (2.10), (3.1), (3.16), (5.1) and (5.3), of ref. [3]) . This is a hypothesis, which is in contradiction with the physics of the system we are dealing with. Therefore the SOF $f(k,r,t)$ cannot be described by the usual theory of Markovian processes.

The SOF $f(\mathbf{k},\mathbf{r},t)$ defined above, is a random function of time, fluctuating between 1 and 0 at random instants. The total number of particles $N(\mathbf{r},t)$ inside D, given by eq.(1), is a random number with an average value N_s. Due to this fluctuation, eq. (2) cannot hold, as is shown below.

It follows from the definition of $f(\mathbf{k},\mathbf{r},t)$ that eq. (1) is satisfied. The SOF is stationary, and its first moment, that is its average value $\langle f(\mathbf{k},\mathbf{r},t)\rangle = f_s(\mathbf{k},\mathbf{r})$, is the steady state distribution function. As a consequence, $f_s(\mathbf{k},\mathbf{r})$ should obey the stationary BE. If f is displaced from steady state, it comes back to it, according to the time dependent BE. For a non-degenerate semiconductor:

$$\frac{\partial\langle f(\mathbf{k},\mathbf{r},t)\rangle}{\partial t} = -\frac{e}{\hbar}\mathbf{E}_s\cdot\nabla_{\mathbf{k}}\langle f(\mathbf{k},\mathbf{r},t)\rangle + \sum_{\mathbf{k}'}\langle f(\mathbf{k}',\mathbf{r},t)\rangle P(\mathbf{k}',\mathbf{k}) - \sum_{\mathbf{k}'}\langle f(\mathbf{k},\mathbf{r},t)\rangle P(\mathbf{k},\mathbf{k}') \quad , \tag{5}$$

which will be written as:

$$\frac{\partial\langle f(\mathbf{k},\mathbf{r},t)\rangle}{\partial t} = \Psi\,\langle f(\mathbf{k}',\mathbf{r},t)\rangle \quad . \tag{6}$$

Let $\tilde{f}(\mathbf{k},\mathbf{r},t)$ be the random fluctuation of $f(\mathbf{k},\mathbf{r},t)$ about its steady state value $f_s(\mathbf{k})$, such that $f(\mathbf{k},\mathbf{r},t) = f_s(\mathbf{k})+\tilde{f}(\mathbf{k},\mathbf{r},t)$, and $\tilde{f}(\mathbf{k},\mathbf{r},\omega)$ the Fourier transform of $\tilde{f}(\mathbf{k},\mathbf{r},t)$: from eq.(6), $\tilde{f}(\mathbf{k},\mathbf{r},\omega)$ is related to the noise force $\xi(\mathbf{k})$ through:

$$(j\omega - \Psi)\,\tilde{f}(\mathbf{k},\mathbf{r},\omega) = \xi(\mathbf{k}) \quad . \tag{7}$$

The Langevin noise source term is

$$S_\xi(\mathbf{k},\mathbf{k}')\,\Delta\nu = \langle\xi(\mathbf{k})\xi^*(\mathbf{k}')\rangle \quad , \tag{8}$$

and:

$$\left\langle \left| \sum_{\mathbf{k}}\xi(\mathbf{k}) \right|^2 \right\rangle = \sum_{\mathbf{k}}\sum_{\mathbf{k}'}\left\langle \xi(\mathbf{k})\,\xi^*(\mathbf{k}')\right\rangle = \Delta\nu \sum_{\mathbf{k}}\sum_{\mathbf{k}'} S_\xi(\mathbf{k},\mathbf{k}') \quad . \tag{9}$$

Eq.(9) shows that eq.(2) is equivalent to:

$$\sum_{\mathbf{k}}\xi(\mathbf{k}) = 0 \quad . \tag{10}$$

Now let us sum eq. (7) over k: since the Boltzmann operator Ψ is such that, for every function of k, thus including $\tilde{f}(\mathbf{k},\mathbf{r},\omega)$

$$\sum_{\mathbf{k}}\Psi\,\tilde{f}(\mathbf{k},\mathbf{r},\omega) = 0 \quad . \tag{11}$$

It follows from eqs (7) and (11) that

$$j\omega\sum_{\mathbf{k}}\tilde{f}(\mathbf{k},\mathbf{r},\omega) = \sum_{\mathbf{k}}\xi(\mathbf{k}) \quad . \tag{12}$$

If, according to eq. (10), we suppose that $\sum_{\mathbf{k}}\xi(\mathbf{k}) = 0$, eq. (12) shows that

$$\sum_{\mathbf{k}}\tilde{f}(\mathbf{k},\mathbf{r},\omega) = 0 \quad . \tag{13}$$

Equations (13) and (3) give then

$$\tilde{N}(r,\omega) = \sum_k \tilde{f}(k,r,\omega) = 0 \quad . \tag{14}$$

The spectral density $S_N(r,\omega)$ of the fluctuations of $N(r,t)$ is then given by:

$$S_N(r,\omega) = \langle \tilde{N}(r,\omega)\tilde{N}^*(r,\omega) \rangle = 0 \quad , \tag{15}$$

and the variance of $N(r,t)$ is, with $\omega=2\pi\nu$:

$$\langle \Delta\tilde{N}^2(r,t) \rangle = \int_0^\infty S_N(r,\omega)\, d\nu = 0 \quad , \tag{16}$$

which is in contradiction with the evidence that $N(r,t)$ fluctuates: thus assuming the classical result given by eq.(2) leads to a physical nonsense given by eq. (16).

CONCLUSION

We have shown in this paper that the classical theory of the fluctuations of the SOF, about steady state, of systems obeying the BE, is wrong. This is due to the fact that such distributions describe open systems, which are not Markovian, contrary to the underlying assumption of the classical theory.

Indeed, as far as space density fluctuations are involved, built in electric fields appear, and one should take into account the space dependent BE associated with the Poisson equation, even in a homogeneous sample in a uniform steady state electric field. We are now tackling this refinement. Instead of eq. (2), we recently proposed the expression (3) for the Langevin source term [1], which does not seem to be in contradiction with the basic description of motion of electrons as given for example by a Monte Carlo simulation. This allowed us to compute the transverse diffusion coefficient at T=300 K in p-type Silicon [6][7].

Work partially supported by the "Groupement Circuits Intégrés Silicium".

REFERENCES

[1] J.P. Nougier, J.C. Vaissière, Phys. Rev. B37, 8882 (1988)

[2] S.V. Gantsevich, V.L. Gurevich, R. Katilius, Riv. Nuovo Cimento 2, 1 (1979)

[3] M. Lax, Revs. Mod. Phys. 32, 25 (1960)

[4] M. Lax, Revs. Mod. Phys. 38, 541 (1966)

[5] S.V. Gantsevich, V.L. Gurevich, R. Katilius, Phys. Rev., to be published.

[6] J.P. Nougier, A. Moatadid, J.C. Vaissière, J. Phys. (Paris) C4, t. 49, 165 (1988).

[7] J.P. Nougier, J.C. Vaissière, Proc. 6th Int. Conf. on Hot Carriers in Semicond., Phœnix, Arizona (USA) (1989), to be published in Solid State Electron.

10th Int.Conf. on Noise in Physical Systems
1989 Budapest, Hungary

ESTIMATION OF THE AUTOCORRELATION FUNCTION OF GAUSSIAN RANDOM PROCESSES FROM THE PROBABILITY DENSITIES OF CROSSING INTERVALS WITH TWO LEVELS

T. MUNAKATA, T. MIMAKI,* D. WOLF**

Tamagawa University, 6-1-1 Tamagawagakuen, Machida-shi, Tokyo, Japan
*University of Electro-Communications, Chofugaoka, Chofu-shi, Tokyo, Japan
**Institut für Angewandte Physik der J.W. Goethe Universität, Frankfurt a.M., FRG

ABSTRACT

Estimation of autocorrelation function from the probability densities of level crossing time interval lengths was studied for Gaussian random processes. The method is based on the fact that the renewal functions for the crossing intervals (called Rice function) are given by a few parameters, which are further represented only by the autocorrelation function of the original random process. We derived the procedure to estimate the autocorrelation function using the ratios of the four Rice functions, which are defined corresponding to the directions of the crossings with the different starting and destination levels. Estimation can be improved by expanding the autocorrelation function in terms of Hermite functions. The method was successfully demonstrated for some Gaussian processes having 7th order Butterworth spectrum with different bandwidths.

THEORY AND RESULTS

The one of the Rice's Q-functions for two crossing levels I_1 and I_2 is defined in the following way:

$Q^{+-}(\tau, I_1, I_2)d\tau$ denotes the conditional probability that the random process crosses downward with level I_2 (indicated by '-' of second superscript) between $t_1+\tau$ and $t_1+\tau+d\tau$, given an upward crossing with level I_1 (indicated by '+' of first superscript) at t_1.

In analogous way $Q^{++}(\tau, I_1, I_2)$, $Q^{-+}(\tau, I_1, I_2)$ and $Q^{--}(\tau, I_1, I_2)$ are defined corresponding to the direction of crossings, respectively (refer to Fig. 1). These Rice functions are written analytically as follows;

$$Q^{+-}(\tau, I_1, I_2) = F(\tau, I_1, I_2) J_1(r, h, k), \qquad (1\text{-a})$$

$$Q^{++}(\tau, I_1, I_2) = F(\tau, I_1, I_2) J_1(-r, h, -k), \qquad (1\text{-b})$$

$$Q^{-+}(\tau, I_1, I_2) = F(\tau, I_1, I_2) J_1(r, -h, -k), \qquad (1\text{-c})$$

and $$Q^{--}(\tau, I_1, I_2) = F(\tau, I_1, I_2) J_1(-r, -h, k), \qquad (1\text{-d})$$

where

$$F(\tau, I_1, I_2) = M_{22}\beta^{-1/2}(1-m^2)^{-3/2}\exp\{I^2/2 - (I_1^2+I_2^2-2mI_1I_2)/(2-2m^2)\}, \quad (2)$$

$$J_1(r, h, k) \equiv \frac{1}{2\pi s}\int_h^\infty dx \int_k^\infty dy (x-h)(y-k)e^{-z}, \qquad (3)$$

$$z = -\frac{x^2+y^2-2rxy}{2(1-r^2)}, \quad s = (1-r^2)^{1/2}, \quad r = \frac{M_{23}}{M_{22}} = \frac{m''(1-m^2)-m\,m'^2}{\beta(1-m^2)-m'^2}, \quad (4)$$

$$h = m'(I_2-mI_1)[M_{22}(1-m^2)]^{-1/2}, \quad (5) \qquad k = m'(I_1-mI_2)[M_{22}(1-m^2)]^{-1/2}. \quad (6)$$

The quantity $m=m(\tau)$ denotes the autocorrelation function of the original random process and $m'=dm(\tau)/d\tau$, $m''=d^2m(\tau)/d\tau^2$. The integration $J_1(r, h, k)$ can be rewritten as

$$J_1(r, h, k) = \frac{he^{-k^2/2}}{2(2\pi)^{1/2}}[1-P(\frac{h-rk}{s})] + \frac{ke^{-h^2/2}}{2(2\pi)^{1/2}}[1-P(\frac{k-rh}{s})]$$

$$+ \frac{s}{2\pi}\exp[-\frac{k^2-2rhk+h^2}{2(1-r^2)}] + (hk + r)K(r, h, k). \qquad (7)$$

where

$$P(x) \equiv \frac{2}{(2\pi)^{1/2}}\int_0^x \exp(-t^2/2)dt, \quad \text{and} \quad K(r, h, k) \equiv \frac{1}{2\pi s}\int_h^\infty dx \int_k^\infty dy\, e^{-z}. \quad (8)$$

If we carefully observe two expressions (5) and (6), the ratio h/k can be used for the determination of autocorrelation function $m(\tau)$. The ratio is simply expressed as

$$h/k = [I_2-mI_1]/[I_1-mI_2], \qquad (9)$$

which contains only $m(\tau)$ and known quantities I_1 and I_2. Then the expression (9) is rewritten as

$$m = [hI_1-kI_2]/[hI_2-kI_1]. \qquad (10)$$

Next, we must determine the quantities h and k from some combinations of Rice functions, which can be obtained numerically or experimentally. Using Eqs (1) and (7), the simple expressions are derived for the ratios of Rice functions as follows;

Definition of Rice's Q-functions

Fig. 1

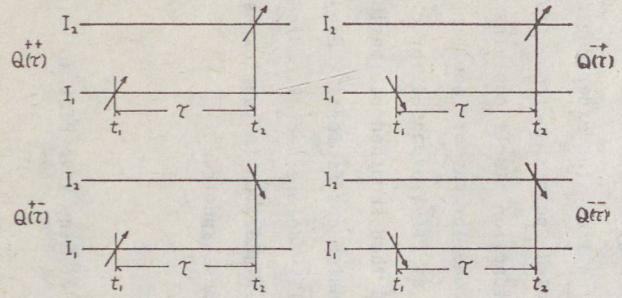

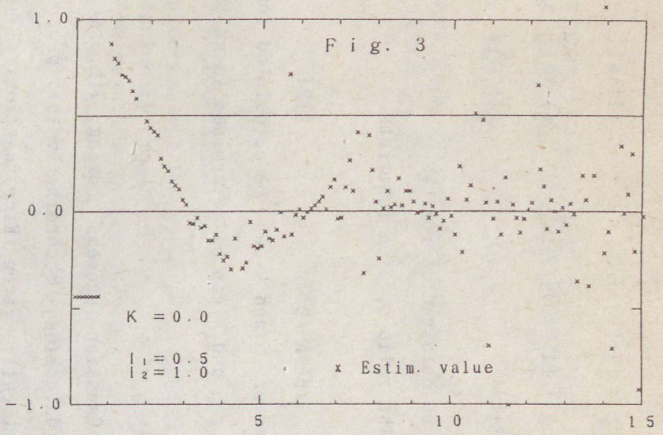

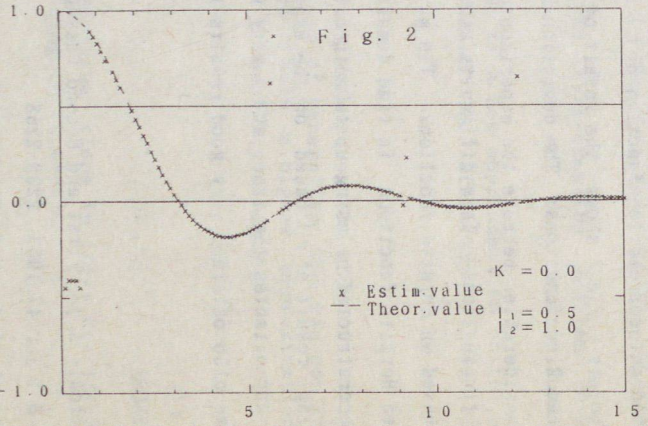

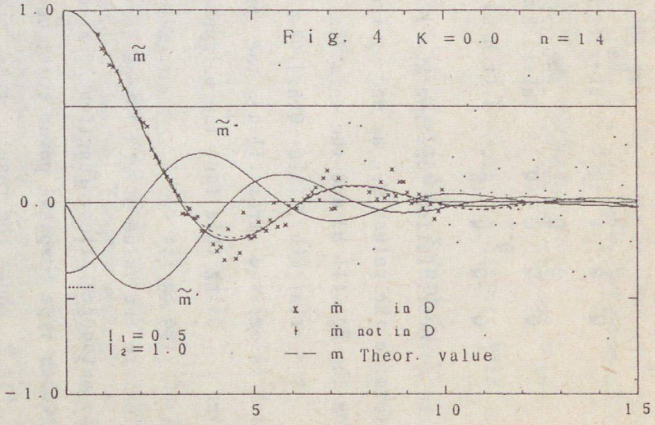

$$a_1 \equiv \frac{Q^{+-}-Q^{++}}{Q^{+-}-Q^{++}-Q^{--}+Q^{-+}} = \frac{-ke^{-h^2/2}}{(hk+r)(2\pi)^{1/2}} + [1-P(h)]/2 \ , \qquad (11\text{-a})$$

$$a_2 \equiv \frac{Q^{+-}-Q^{--}}{Q^{+-}-Q^{++}-Q^{--}+Q^{-+}} = \frac{-he^{-k^2/2}}{(hk+r)(2\pi)^{1/2}} + [1-P(k)]/2 \ , \qquad (11\text{-b})$$

$$a_3 \equiv \frac{Q^{+-}}{Q^{+-}-Q^{++}-Q^{--}+Q^{-+}} = J_1(r,h,k)/(hk+r) \ . \qquad (11\text{-c})$$

Then the autocorrelation function $m(\tau)$ can be obtained as follows.

1) Determine the values a_1, a_2 and a_3 from the ratio of Rice-functions.

2) From the Eq. (11-b) and the relation

$$k = -r[a_1-Q(h)]/\{h[a_1-Q(h)]+(2\pi)^{-1/2}\exp(-h^2/2)\}, \qquad (12)$$

which is derived from (11-a), the parameter h and k can be calculated for given r. Using this fact the parameters r, h and k can be determined so as to satisfy the Eq. (11-c).

3) Calculate the value of $m(\tau)$ from Eq. (10).

Now the autocorrelation function for the Gaussian process having 7th order Butterworth type lowpass power spectrum is determined according to this procedure. Fig. 2 shows the result from theoretically given Rice functions. The obtained autocorrelation function $m(\tau)$ fits very well to the true value, except some points. Fig. 3 shows the result of estimation from the experimentally determined Rice functions. The deviation of estimated points $\hat{m}$ from true value is considerable, because the experimental Rice function itself contains statistical fluctuations. This difficulty can be overcome by way of smoothing procedure based on Hermite functions. The $\hat{m}(\tau)$ was at first expanded by orthonormalized Hermite functions in time domain D, and then smoothed estimation $\tilde{m}(\tau)$ was reconstructed by using up to n-th order expansion coefficients. Fig. 4 shows the final result $\tilde{m}(\tau)$ based on the experimentally determined Rice functions, which approximates the true $m(\tau)$ very well. In addition to the lowpass spectrum we also obtained very good results for bandpass spectrum.

REFERENCES

[1] Rainal, A. J., First and Second Passage Times of Sine Wave Plus Noise; B. S. T. J., 47, 1968, 2239-2258

[2] Rainal, A. J., Axis-Crossing Intervals of Rayleigh Processes; B. S. T. J., July-Aug., 1965, 1219-1224

10th Int.Conf. on Noise in Physical Systems
1989 Budapest, Hungary

RECENT RESULTS FOR THE LEVEL-CROSSING PROBLEM OF GAUSSIAN RANDOM SIGNALS

R. TETZLAFF, D. WOLF

Institut für Angewandte Physik der Universität Frankfurt
D-6000 Frankfurt a.M., FRG

1. INTRODUCTION

Up to now the conditional probability density $P_{o+}(\tau;R)$ $[P_{o-}(\tau;R)]$, that a stationary random process crosses a certain level R for the first time $t=\tau$ with negative [positive]slope given an upcrossing [downcrossing] at t=0, has not been found analytically. Rice [4] calculated in his famous work the functions $Q_{\pm}(\tau;R)$ which approximate $P_{o\pm}(\tau;R)$ at least in the region of small interval length τ. McFadden [2] proposed the so-called "Quasi-Independence Solutions" which approximate $P_{o\pm}(\tau;R)$ in a larger range of τ. Another approach was recently presented by Munakata and Wolf [3], who introduced the so-called multi-states model.
Considering all of the solutions of the level-crossing problem known so far, one has to state that in various cases the true density functions $P_{o\pm}(\tau;R)$ cannot be represented well.
In this paper we present the derivation of a new approximation on the basis of the "Weak Quasi Independence Assumption" for arbitrary values of the level R and interval length τ.

2. THEORY

Let $\xi(t)$ be a continuous Gaussian process with zero mean and unit variance, then $P_{o-}(\tau;R) = P_{o+}(\tau;-R)$. Without loss of generality one can confine to the analysis of $P_{o-}(\tau;R)$. In order to obtain a higher approximation for $P_{o-}(\tau;R)$, we introduce the conditional probability density

$$W_{++/-}(\tau_1,\tau_2;R) = \frac{W_{-++}(\tau_1,\tau_2;R)}{W_{-}(R)} \qquad (1)$$

that $\xi(t)$ crosses the level R with positive slope in $(t+\tau_1, t+\tau_1+d\tau_1)$ and $(t+\tau_1+\tau_2, t+\tau_1+\tau_2+d\tau_2)$ given a downcrossing in (t,t+dt).

$$W_{-++}(\tau_1,\tau_2;R) = E\cdot\int_{-\infty}^{0} x\cdot J(h,k,r)\cdot\exp\{-\frac{Bx^2+Cx}{2}\}dx \qquad (2)$$

can be derived as a function of J(h,k,r) which can be quickly and precisely

calculated [5]. The quantities h, k, r, B, C and E - presented in the Appendix - are functions of the M_{ij}'s, being the cofactors of the ij-th elements in the determinant

$$|\underline{\underline{M}}| = \begin{vmatrix} ß & -\psi''(\tau_1) & -\psi''(\tau) & 0 & -\psi'(\tau_1) & -\psi'(\tau) \\ -\psi''(\tau_1) & ß & -\psi''(\tau_2) & \psi'(\tau_1) & 0 & -\psi'(\tau_2) \\ -\psi''(\tau) & -\psi''(\tau_2) & ß & \psi'(\tau) & \psi'(\tau_2) & 0 \\ 0 & \psi'(\tau_1) & \psi'(\tau) & 1 & \psi(\tau_1) & \psi(\tau) \\ -\psi'(\tau_1) & 0 & \psi'(\tau_2) & \psi(\tau_1) & 1 & \psi(\tau_2) \\ -\psi'(\tau) & -\psi'(\tau_2) & 0 & \psi(\tau) & \psi(\tau_2) & 1 \end{vmatrix}$$

of a six-dimensional Gaussian density. $\psi(\tau)$ is the autocorrelation function of $\xi(t)$. The primes denote differentiations and $ß=-\psi''(0)$, $\psi(0)=1$. Thus the function - introduced by M.S. Longuet-Higgins [1] -

$$X_-(\tau;R) = \int_0^\tau W_{++/-}(\tau_1,\tau-\tau_1;R)d\tau_1 = \sum_{n=0}^{\infty} n\cdot P_{2n-}(\tau;R) \quad , \tag{3}$$

is obtained which enables us to determine the higher approximation

$$QX_-(\tau;R) \equiv Q_-(\tau;R)-X_-(\tau;R) = P_{o-}(\tau;R) - \sum_{n=1}^{\infty} n\cdot P_{(2n+2)-}(\tau;R). \tag{4}$$

Furthermore, assuming [6] that a level-crossing time-interval is statistically independent of the adjacent (2n+2) level-crossing time-intervals ($n\geq 1$), the infinite sum in Eq.(4) can be represented by the convolution of $P_{o-}(\tau;R)$ with

$$Y(\tau;R) = \int_0^\tau \frac{W_{+++}(\tau_1,\tau-\tau_1;R)}{W_+(R)}\, d\tau_1 \tag{5}$$

where

$$W_{+++}(\tau_1,\tau_2;R) = -E\cdot\int_0^\infty x\cdot J(h,k,r)\cdot\exp\{-\frac{Bx^2+Cx}{2}\}dx. \tag{6}$$

Finally the unknown distribution density $P_{o-}(\tau;R)$ can be determined by solving numerically the Volterra integral equation of the second kind

$$P_{o-}(\tau;R) = QX_-(\tau;R) + P_{o-}(\tau;R) * Y(\tau;R) \quad . \tag{7}$$

3. RESULTS

Our solution was evaluated numerically for several processes $\xi(t)$ with fourth-order Butterworth bandpass power spectra. In Fig.1a-d typical solutions of Eq.(7), designated $P^{**}_{o-}(\tau;R)$, $Q_-(\tau;R)$, and $QX_-(\tau;R)$ are compared to measured densities $P_{o-}(\tau;R)$ for R=0.5 and different ratios $\kappa=f_1/f_2$ of the cut-off frequencies of high and lowpass, resp. As it can be seen, the approximation $QX_-(\tau;R)$ is an improvement, but becomes negative for increasing τ. On the other hand, comparing all of the results one finds $P^{**}_{o-}(\tau;R)$ to be

a nearly perfect representation of the true density. This statement holds within the entire range of τ as well as with all values of R and κ.

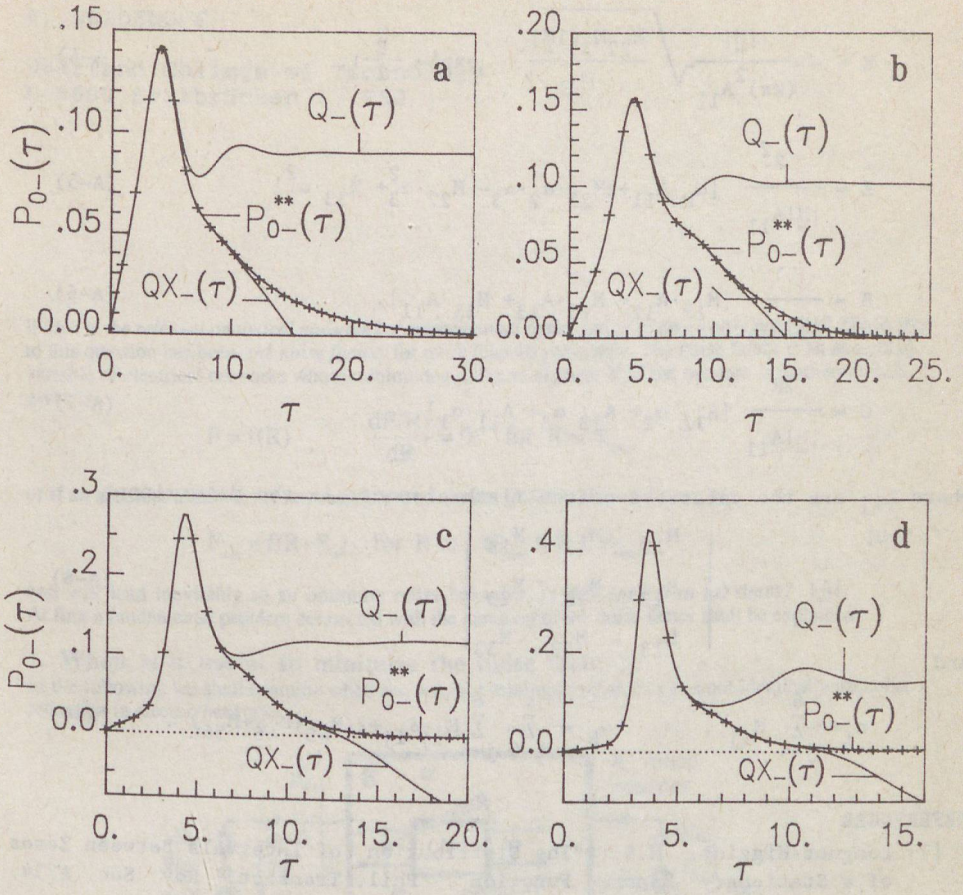

Fig.1a-d. Calculated approximations (——) and measured values of $P_{0-}(\tau;R)$ (+++) for R=0.5 and κ= 0.0 (a), 0.2 (b), 0.5 (c), 0.8 (d)

APPENDIX

Concerning (2) and (6) the following functions were introduced

$$h(x) = -\frac{1}{\sqrt{A_{11}M_{33}|\underline{M}|}} \cdot [A_{21}\cdot x + (M_{23}\cdot\alpha_3 - M_{33}\cdot\alpha_2)\cdot R], \qquad (A\text{-}1)$$

$$k(x) = -\frac{1}{\sqrt{A_{11}M_{22}|\underline{M}|}} \cdot [A_{31}\cdot x + (M_{23}\cdot\alpha_2 - M_{22}\cdot\alpha_3)\cdot R], \qquad (A\text{-}2)$$

$$r = -\frac{M_{23}}{\sqrt{M_{22}\,M_{33}}}\,, \tag{A-3}$$

$$E = -\frac{|\underline{\underline{M}}|}{(2\pi)^2 A_{11}}\sqrt{\frac{M_{22}M_{33}|\underline{\underline{M}}|}{A_{11}}}\cdot\exp\{-\frac{\hat{E}}{2}\}, \tag{A-4}$$

$$\hat{E} = \frac{R^2}{|\underline{\underline{M}}|A_{11}}\,[\alpha_R\cdot A_{11}+2M_{23}\cdot\alpha_2\cdot\alpha_3-M_{22}\cdot\alpha_3^2+M_{33}\cdot\alpha_2^2] \tag{A-5}$$

$$B = \frac{1}{|\underline{\underline{M}}|A_{11}}\,[M_{12}\cdot A_{12}+M_{13}\cdot A_{13}+M_{11}\cdot A_{11}], \tag{A-6}$$

$$C = \frac{2R}{|\underline{\underline{M}}|A_{11}}\,[A_{12}\cdot\alpha_2+A_{13}\cdot\alpha_3+A_{11}\cdot\alpha_1], \tag{A-7}$$

where A_{ij} are the cofactors of the ij-th elements in the determinant

$$|\underline{\underline{A}}| = \begin{vmatrix} M_{11} & M_{12} & M_{13} \\ M_{12} & M_{22} & M_{23} \\ M_{13} & M_{23} & M_{33} \end{vmatrix} \tag{A-8}$$

and

$$\alpha_i = \sum_{j=4}^{6} M_{ij}\,, \qquad \alpha_R = \sum_{i=4}^{6}\sum_{j=4}^{6} M_{ij}\delta_{ij}+2(M_{45}+M_{46}+M_{56})\,. \tag{A-9}$$

REFERENCES

[1] Longuet-Higgins, M.S.: "The Distribution of Intervals Between Zeros of a Stationary Random Function", Phil. Transact. Roy. Soc. A254, 1962, pp.557-599

[2] McFadden, J.A.: "The Axis-Crossing Intervals of Random Functions", Trans. Inst. Radio Engrs. IT2, 1956, pp.146-150, IT4, 1958, pp.14-24

[3] Munakata, T. and Wolf, D. : "On the Distribution of the Level-Crossing Time-Intervals of Random Processes", Proc. 7th Int. Conf. on Noise in Physical Systems, Montpellier 1983, pp:49-52.

[4] Rice, S.O.: "Distribution of the Fades in Radio Transmission", Bell Syst.Tech. J. 37, 1958, 581-635

[5] Tetzlaff, R.: "Simulation und Analyse des Pegelkreuzungsverhaltens bandbegrenzter Rayleighprozesse", Diplomarbeit, Institut für Angewandte Physik der Universität Frankfurt am Main, 1985

[6] Wolf, D. and Brehm, H.: "Die Verteilungsdichte der Zeitintervalle zwischen Nulldurchgängen bei Gaußschen stochastischen Signalen", AEÜ 27, 1973, pp.477-489

"GENERAL EQUIVALENT NOISE" OF ELECTRIC NETWORKS

A. NEIDENOFF

Saarland College of Technology
D-6600 Saarbrücken 1, FRG

Which is the relevant analytical variable for mathematical optimization of an electric network? The answer to this question has been *the noise factor* for more than 40 years now. The noise factor is an analytical variable of electrical networks whose minimum e.g. for an element R of the network is mathematically given by

$$F = f(R) \qquad \frac{dF(R)}{dR} = 0 \quad \text{for } R = R_{opt} \tag{1a}$$

or if an absolute minimum is impossible the minimum inside a given range

$$F_{min} = f(R=R_x) \quad \text{for } R \text{ in } (R_{min} \le R \le R_{max}) \tag{1b}$$

and will lead inevitably to an optimum noise behavior. ***Is this correct at all times?***
At first a fundamental problem connected with the handling of the noise factor shall be explained.

1. When is it useful to minimize the noise factor?

In the following we shall examine when and why the minimum noise factor is not identical with noise reduction in electric networks.

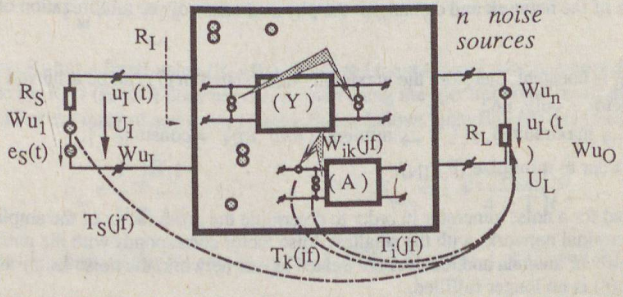

Fig.1 *The general noisy network with partially correlated noise sources*

The network in fig. 1 has two decisive points, the signal generator with the input noise source and the signal load (signal sink), where more two-terminal and four-terminal noisy networks are active. (The load is also noisy and it has its own noise generator. This is the last /n-th/ noise source of the network.)

The effective value U_L at the signal load R_L is given by

$$U_L = \sqrt{\frac{1}{\tau}\int_0^\tau u_L^2(t)\,dt} \qquad U_L = \sqrt{\frac{1}{\tau}\int_0^\tau |e_s(t)\,T_s(jf)|^2\,dt} \tag{2}$$

The signal power P_{SO} in R_L for any time function - included pure noise* - is given by

$$P_{so} = \frac{U_L^2}{R_L} \qquad P_{so} = \frac{1}{\tau R_L}\int_0^{\tau} |e_s(t)\, T_s(jf)|^2 \, dt \tag{3}$$

The output noise voltage spectral density, Wu_O in $[V^2s]$ at R_L

$$Wu_o(f) = \sum_{i=1}^{n}\left(\sum_{k=1}^{n} T_i(jf)\, T_k^*(jf)\, W_{ik}(jf)\right) \tag{4}$$

determines the noise power P_{NO} at the signal load R_L

$$P_{NO} = \frac{U_{NL}^2}{R_L} = \frac{1}{R_L}\int_0^{\infty} Wu_o(f)\, df = \frac{1}{R_L}\int_0^{\infty} \sum_{i=1}^{n}\left(\sum_{k=1}^{n} T_i(jf)\, T_k^*(jf)\, W_{ik}(jf)\right) df \tag{5}$$

The signal to noise ratio SNR between the two ($SNR_O = P_{SO}/P_{NO}$) is the value which has to be maximized, if noise reduction is meant to be useful at all! Minimizing the noise factor F does not always have this effect.

The noise factor is defined as follows:

$$F = \frac{SNR_I}{SNR_O} \qquad F = \frac{P_{SI}/P_{NI}}{P_{SO}/P_{NO}} \qquad F = \frac{P_{SI}\,P_{NO}}{P_{NI}\,P_{SO}} \tag{6}$$

Even the first glance reveals that the two variables 'noise factor' F and 'signal to noise ratio' SNR_O at the signal load can never be mathematically identical, although the latter one is inevitably the relevant variable in noise optimization:

$$SNR_o = \frac{P_{SO}}{P_{NO}} \qquad SNR_o = \frac{P_{SI}}{P_{NI}}\,\frac{1}{F} \tag{7}$$

Therefore they should not be considered as especially close related, and more important, one can only expect that the minimum of F will lead to a maximum of SNR_O, if during the analytical reduction of the noise factor the parameter P_{NI} in Eq.(7) is not neglected. The remaining parameter P_{SI} is generally not correlated with the noise of the network and cannot put the physical sense of the minimization of F in doubt.

In a few applications P_{NI} is constant, therefore the maximum value stated in (7) can be achieved by minimizing the noise factor F only, i.e.:

$$\{\, SNR_O \rightarrow \text{maximum} \,\},\ \text{if}\ \{\, F \rightarrow \text{minimum } \textit{and}\ P_{IN} = \text{constant}^{**} \,\},$$
$$\text{in order to minimize } (F.P_{IN}). \tag{8}$$

If an antenna is exchanged for a noise generator in order to determine the noise factor of the amplifier, then the amplifier (the four-terminal network) with the smallest noise factor corresponds with the maximum value stated in (7). If however antenna and receiver are treated as one network, the noise factor must no longer be applied, as Eq.(8) is no longer fulfilled.

The minimum noise factor of a cascaded network, if arranged to its optimum /Friis' theorem/, will also only lead to the maximum value stated in (7) because P_{NI} remains constant and (8) is fulfilled.

It has to be concluded that ***not the minimum of the noise factor by itself but the minimum of the product $F\ P_{NI}$ will lead to a valid noise optimization of electrical networks***, when the question: "When is it adequate to minimize the noise factor?" has to be answered generally valid.

---

* - e.g. radioastronomy

** - or possibly even a minimum

Moreover in all standard works published in the last 3 to 4 decades (e.g.: [1] ,[2], [3], [4], [5], [6]...) noise matching is stated as the mathematical optimization of electric networks. In reality this is, however, just one example which can be used to show that the noise factor by itself cannot be the correct physical variable or analytical expression for the optimization of noisy networks.

2. Why is the noise matching meaningless?

Wu_1 be defined as the noise spectrum of the signal source. If R_I is the input impedance of the general four-terminal network (fig.1) and Wu_I is the input noise spectrum to the four-terminal network in fig.1, and when the noise matching with the integral noise factor is applied, it is premised that the input noise power is given by:

$$P_{NI} = \frac{\overline{U_I^2}}{R_I} = \frac{Wu_1 \Delta f}{R_I} = Wu_1 \left(\frac{R_I}{R_S + R_I} \right)^2 \frac{\Delta f}{R_I} = Wu_1 \frac{R_I \Delta f}{(R_S + R_I)^2} \qquad (9)$$

The noise matching contradicts the method discussed in chapter 1, where it is tried to find the minimum of F by varying R_S respectively P_{NI} . Apart from this common mistake there are also contradictions to basic principles in noise matching included.

Even more basic mistakes are made when doing integral or spectral noise matching, namely:

Error 1.) During noise matching it is assumed, that the noise spectral density Wu_1 in the signal source is generally described by the thermal noise of R_S, ($Wu_1 = 4kTR_S$) ?! But the one has not got anything to do with the other, even if a passive solderable resistor is concerned. It is especially not the case for an active two-terminal network, the e.m.f of which is caused by the transformation of mechanical energy, by the energy of an electromagnetic field (antenna)* or by an electric network (and all its noise) connected in series.

Due to error 1 Eq. (9) is converted to:

$$P_{NI} = \frac{4kTR_S R_I \Delta f}{(R_S + R_I)^2} \qquad (10)$$

Error 2.) In order to make further progress towards integral noise matching a simple expression for the input noise power P_{NI} is usually assumed. The step in (11) is being justified by declaring that the usual power matched connection is being applied, i.e. for $R_S=R_I$ follows:

$$P_{NI} = k\,T\,\Delta f \qquad (11)$$

This means that R_S has a **fixed** value ($R_S=R_I$). It has to be questioned why one now starts to look for an optimum value for R_S?! (Error 2 does not occur when using the spectral noise factor as here this step is not necessary.) For the integral and spectral noise factor follows from Eq.(10) due to error 2:

$$F_{int} = \frac{P_{eq}(R_S)}{k\,T\,\Delta f} \qquad F_{spec} = 1 + \frac{Wu_{NW}(R_S)}{4\,k\,T\,R_S} \qquad (12)$$

Error 3.) Instead of looking for the minimum of { $F(R_S)\,P_{NI}(R_S)$ } as (7) and (8) would suggest, i.e.:

$$\frac{\partial (F\,P_{NI})}{\partial R_S} = 0 \qquad (13)$$

the minimum of F only is determined in noise matching procedures:

---

* - Not even thermal radiation received by an antenna does allow this assumption, as the space in which the antenna is located is never a pure abstract black body. After all, ***is it useful to receive with the antenna in a pure abstract black body?*** The thermal radiation is a neglectable portion of the radiation finally received by the antenna.

$$\frac{\partial F}{\partial R_s} = 0 \qquad (14)$$

This is analytically possible, but because of more mistakes the signal-to-noise ratio in the load R_L cannot be maximized, which then results in no useful noise reduction being achieved.

Another way of showing why the noise matching is meaningless can be followed with the following thought experiment:
Given are the following two identical electrical networks in fig. 2 .

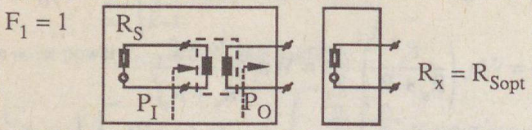

Fig. 2 *Cascaded network and its equivalent two-terminal network*

The transformer be ideal, without noise and consequently has the noise factor $F_1 = 1$. Depending on whether it has been adapted as far as its power is concerned, its power transfer function will be less or equal to 1 ($P_O/P_I \leq 1$), without having any effect on the value of the noise factor F_1 . As it is possible to obtain any value for R_x for the complete two-terminal network, it is also possible to select the value R_{Sopt}. This should reduce the noise factor of the complete network to a minimum if one accepts noise matching.

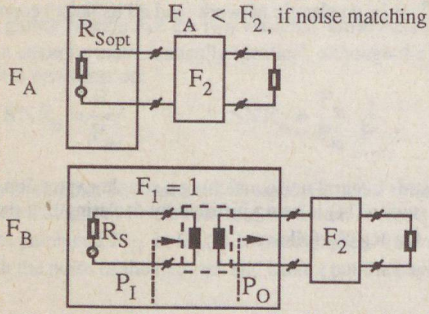

Fig. 3 *Cascaded network for the Friis theorem*

Friis theorem tells however, that in the above case the expression for the noise factor of the cascade is given by:

$$F_B = F_1 + \frac{F_2 - 1}{\left(\frac{P_o}{P_I}\right)} \quad \text{, and} \quad F_B \geq F_2 \quad \text{for} \quad \frac{P_o}{P_I} \leq 1 \quad . \qquad (15)$$

As

$$\frac{P_o}{P_I} \leq 1 \qquad (16)$$

the transformer can only increase the noise factor and not decrease (as $P_O/P_I \leq 1$ and $F_1 = 1$). As the two results are contradictory for two identical electrical networks, $F_A < F_2$ and $F_B \geq F_2$, only one can be correct.
Every network can be described by the network structure shown in fig. 1 or fig. 3. ***This is why the statements made here can be inductively related back from figure 1 to every type of network. This is also why the statements made here are generally valid.***

3. Theory

As the noise reduction of electric networks cannot make use of the noise factor, a new analytical function is required, which leads in all cases to a maximum signal to noise ratio at the network output SNR_O when it is mathematically treated and minimized. With P_{SO} from Eq.(3) and P_{NO} from Eq.(5) follows

$$SNR_o = \frac{\frac{1}{\tau R_L}\int_0^{\tau} |e_s(t)\, T_s(jf)|^2 \, dt}{\frac{1}{R_L}\int_0^{\infty} \sum_{i=1}^{n}\left(\sum_{k=1}^{n} T_i(jf)\, T_k^*(jf)\, W_{ik}(jf)\right) df} \tag{17}$$

The basic assumption shall be that the considered network be linear, stationary and in steady-state conditions*. (The signal transfer function $T_S(jf)$ is invariant with respect to time.)

$$SNR_o = \frac{\frac{1}{\tau}\int_0^{\tau} |e_s(t)|^2 \, dt}{\frac{1}{|T_s(jf)|^2}\int_0^{\infty} \sum_{i=1}^{n}\left(\sum_{k=1}^{n} T_i(jf)\, T_k^*(jf)\, W_{ik}(jf)\right) df} \tag{18}$$

In communications practice noise problems are treated spectral, i.e. the network is investigated at certain defined frequencies or in a very limited frequency range ($\Delta f \approx df$), which is due to signal selection and filtering of signals. Taking into account this additional limitation one obtains for $SNR_O(\Delta f)$.

$$SNR_o(\Delta f) = \frac{\frac{1}{\tau}\int_0^{\tau} |e_s(t)|^2 \, dt}{\frac{\Delta f}{T_s(jf)\, T_s^*(jf)} \sum_{i=1}^{n}\left(\sum_{k=1}^{n} T_i(jf)\, T_k^*(jf)\, W_{ik}(jf)\right)} \tag{19}$$

The signal $e_S(t)$ at the networks input and Δf are uncorrelated to the network, even if a noise signal is being fed to the networks input, so that as final goal function of noise optimization an expression $W_{eq}(f)$ of the following type remains:

$$SNR_o(\Delta f) = \frac{\frac{1}{\tau}\int_0^{\tau} |e_s(t)|^2 \, dt}{W_{eq}(f)\, \Delta f} \qquad SNR_o(\Delta f) = \frac{\text{constant}}{W_{eq}(f)} \tag{20}$$

where $$W_{eq}(f) = \frac{1}{T_s(jf)\, T_s^*(jf)} \sum_{i=1}^{n}\left(\sum_{k=1}^{n} T_i(jf)\, T_k^*(jf)\, W_{ik}(jf)\right)$$

---

* - This limitation is not very tight, as the noise signals in the network are so weak that even a nonlinear network could then be considered as linear. Further on one would not intend to investigate switching processes (non-steady state conditions) and noise problems at the same time.

The term W_{eq} in Eq. (20) shall be called 'general equivalent noise' (g.e.n.), as - in effect - it is an equivalent transfer of noise sources to the signal source. Equivalent, as the effect of the individual noise sources onto the signal output remain unchanged:

$$W_{eq}(f) = \sum_{i=1}^{n} \left(\sum_{k=1}^{n} K_i(jf)\, K_k^{*}(jf)\, W_{ik}(jf) \right) \qquad K_i(jf) = \frac{T_i(jf)}{T_s(jf)} \qquad K_k(jf) = \frac{T_k(jf)}{T_s(jf)} \tag{21}$$

The g.e.n. W_{eq} is the contribution of the individual noise generators and their cross-correlations to the total **output** noise in a noiseless network with an equivalent noise source in the signal input:

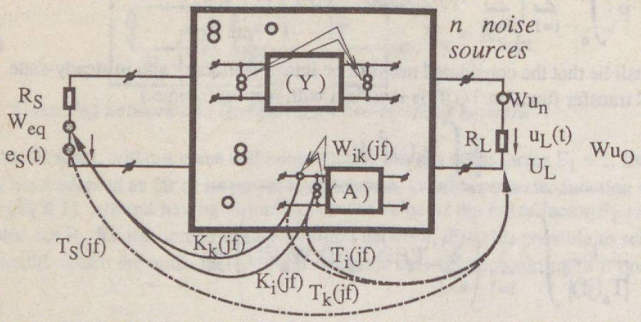

Fig. 4 *Linear transposition of the noise source to the g.e.n. of the network*

The g.e.n. has the following characteristics:

a) It is a real expression and a (voltage or current) spectral density, which corresponds to the type of the utilized signal source, as it is generated under the direct influence of the signal transfer function:

The signal source is a voltage source:

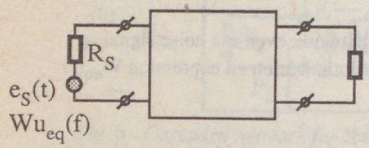

g.e.n. is a voltage spectral density

The signal source is a current source:

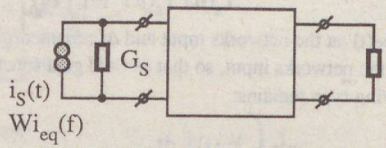

g.e.n. is a current spectral density

Fig. 5 *Possible variants of the 'general equivalent noise'*

b) $K_{ik}(jf)$ in Eq.(21) shall be called weighting factor of $W_{ik}(jf)$. $K_{ik}(jf)$ for i = 1(1)n and k = 1(1)n are the weighting factors of the individual spectral densities with which they contribute to the networks' g.e.n. They are functions of the parameters of the network of higher order and consequently define alone the effect of the corresponding noise source on the SNR_O at the networks output.

c) The analytic modifications of the noise free network during the noise reduction affect the weighting factors K(jf). The weighting factors modify g.e.n. (see Eq.(21)) in such a way that the new value of g.e.n. generates the same amount of noise at the signal output as would do the individual noise sources directly (see Eq.(4)). ***It appears amazing that the intensity of the noise source is not relevant at all as the weighting factors can shift it to any value at the signal output!***

Consequently the analytic noise optimization of a network is far more efficient than e.g. cooling of the network.

Noise reduction occurs under specific conditions for the signal parameters and the passive components:

$$W_{eq} = f(\omega_0, K, Q, R_1..R_m, C_1..C_n, L_1..L_p) \rightarrow \min \qquad (22)$$

for: signal frequency: $f_s := \text{parameter}$

signal parameters: $K_{min} \le K \le K_{max}$, $Q_{min} \le Q \le Q_{max}$

passive components: $R_{min} \le R_i \le R_{max}$, $C_{min} \le C_j \le C_{max}$, $L_{min} \le L_k \le L_{max}$

The advantage of the g.e.n. is that the decisive criterion for a network's optimum noise behavior, the signal-to-noise ratio, can be directly controlled and optimized. The transfer function $T_S(jf)$ doesn't have to be considered any more, the network is noiseless, the signal-to-noise ratio can no longer be changed by the network, and the complete noise optimization of any network can be achieved. ***Not only the network with the minimum noise level can be chosen even the most noisy network can be computed, to see by how much the noise level can change:***

$$W_{eq} = f(\omega_0, K, Q, R_1..R_m, C_1..C_n, L_1..L_p) \rightarrow \max \qquad (23)$$

(parameters as in Eq. (22))

The circuit in fig. 6, an active RC-low-pass filter of the 2nd order that can be integrated, is an example of complete noise optimization in a network.

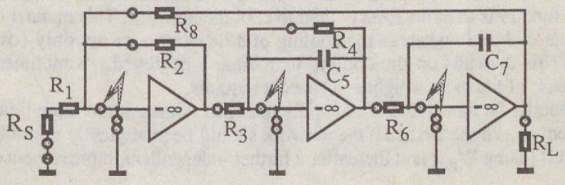

Fig. 6 *Active RC-low-pass filter of the 2nd order*

For a given network with the same circuit diagram and constant signal transfer function the predictable maximum and minimum noise levels lie very far apart which can always be verified experimentally.

Tab.1 shows the method to test the new way of noise reduction: two variants that have been selected from many others and that have been physically realized in pairs and experimentally tested.

Tab.1 *Experimental circuits for the low-pass in Fig. 6*

f_o = 121,9 kHz Q = 3,005 K = 1

R_{min} = 100Ω R_{max} = 1MΩ C_{min} = 56pF C_{max} = 0,47µF

20% tolerance for all R and C

	Output noise voltage u_{ON} for Δf = 108 kHz									
	R_1	R_2	R_3	R_4	C_5	R_6	C_7	R_8	R_{eq}	u_{ON}
optimal	100Ω	1MΩ	100Ω	10,3kΩ	382pF	1MΩ	0,45µF	100Ω	144kΩ	43,9 µV
most noisy	1MΩ	100Ω	464Ω	70,0kΩ	56pF	100Ω	65,6pF	1MΩ	5,87TΩ	287 mV

The computed differences in the output noise level (for minimum and maximum of W_{eq}) reached in the diverse networks up to 110 dB while the signal transfer function was maintained constant. More than 15 networks, that were experimentally tested, proved that the method of noise reduction and the measured results agreed ideally. In the case of theoretical 76.31 dB , s. Tab.2, (minimum to maximum g.e.n. and also minimum to maximum noise voltage at the output) the experiments gave 70 dB ***at room temperature without any technical parts having been changed.***

Some principal questions, which arose empirically in connection with noise levels in networks, can be plausibly answered with the help of the above mentioned 'general equivalent noise' W_{eq}:

- *'Does a network's resistor R, that is generating thermal noise, have to be large or small in order to achieve maximum noise reduction?'* This is answered by the function $W_{eq}(R)$.

- *'Why is the noise in a network with many noise generators sometimes less than the noise in a network with fewer noise generators? And why is this not always the case?'* A complicated network with several elements has got more free parameters which can be modified without affecting the signal transfer function. Hence the noise of a larger network can be reduced more efficiently applying the weighting factors $K_{ik}(jf)$. That is also why an analytically optimized larger network will generate less noise than a smaller network, even if the smaller network has also been optimized analytically.
- *'What effect on the noise does it have, if the network is fed back to itself? Does this increase the noise or does it reduce it? How should the feedback be introduced?'* A feedback generates additional coefficients in the weighting factors. Therefore the optimization of a network with feedback is more efficient with respect to its noise than an optimization of a network without feedback. A feedback has to consider those noise sources whose weighting factors are less affected.
- *'Is it theoretically possible for a network to amplify an electric signal without making any noise? If so, how could this be explained?'* The answer is yes, if it is a network, whose set of linear equations generates a well-populated matrix. Its weighting factors allow taking into account all noise sources utilizing all parameters, so that they can be asymptotically reduced to zero.

Reducing noise levels in networks by using the 'general equivalent noise' is very advantageous in an economic sense, as it supplies only one defined electrical value for each component and the components' cost does not depend on its electrical values. Therefore the network costs the same whether it has been designed to have optimum noise levels or not. This means that an increase in noise optimization will not result in an increase in production costs at all!

With respect to a network's thermal noise it is more effective to reduce the thermal noise analytically - by reducing the weighting functions to almost zero - than to cool the network. This manner of proceeding creates no additional material costs whereas the cooling of a network does not only cost more, ***it is also only partly efficient.*** (This depends on the cooling temperature achieved.) Sometimes cooling can't even be carried out because of the extra weight and space it requires.

Nevertheless it will generally be most effective to apply both procedures at the same time to obtain optimum noise reduction, i.e.: in the first step the network should be analytically optimized with respect to nonthermal noise levels (using W_{eq}) and thereafter a further independent improvement can be made by cooling the network.

4. Conclusions

When using a network it is not so important to find out how many noise generators there are in each active element. It is also not so important to find out how strong they are or how they have come to be. The weighting factors define alone the effect of the corresponding noise source on the SNR_O at the networks output. ***The intensity of the noise source is not relevant at all as the weighting factors can shift it to any value at the signal output!***

A noise generator in a network becomes interesting only when it constitutes a considerable part to the outgoing noise (at the network's output). In a complete mathematical optimization it is decisive for the values of all parameters to respect the final value of the 'general equivalent noise' $W_{eq}(R_k)$.

ACKNOWLEDGEMENTS

This work was financially supported by the ZHPK and the Rector of Saarland College of Technology and Telefunken AG.

References

[1]	Bittel, H., L.Storm Rauschen, Eine Einführung ...	Springer	1971
[2]	Connor, F.R. Noise, Second Edition	Edward Arnold	1982
[3]	Landstorfer, F., H.Graf Rauschprobleme der Nachrichtentechnik	Oldenbourg	1981
[4]	Meinke, H., F.W.Gundlach Taschenbuch der Hochfrequenztechnik	Springer	1986
[5]	Motchenbacher, C.D., F.C.Fitchen Low-Noise Electronic Design	John Wiley & Sons	1973
[6]	Ott, H.W. Noise Reduction Techniques in Electronic Systems	John Wiley & Sons	1976

SESSION 2

NOISE IN VARIOUS PHYSICAL SYSTEMS
(SOLIDS, LIQUIDS, SURFACES, MAGNETICS)

10th Int.Conf. on Noise in Physical Systems
1989 Budapest, Hungary

THE USE OF ANALOG SIMULATION IN STUDIES ON NOISE DRIVEN NONLINEAR DYNAMICAL SYSTEMS

T. ZHOU,* M. JAMES,** K. SINHA,+ G. DEBNATH,+ F. MOSS

Department of Physics, University of Missouri at St. Louis
St. Louis, MO 63121, USA

I. Introduction

The simulation of complex, in particular stochastic, problems in nonlinear dynamics by means of electronic circuit modeling is by now a well-established technique for rapidly obtaining the behavioral properties of model systems over wide ranges of parameter values with reasonable accuracy. The techniques, which have recently been reviewed in detail[1,2], will be briefly outlined here. An example electronic circuit model of the simplest, archetypal bistable system is shown in Fig. 1. This circuit mimics a Brownian particle moving in the one-dimensional potential,

$$U(x) = -\frac{1}{2}x^2 + \frac{1}{4}x^4, \tag{1}$$

for which the Langevin equation, which describes the motion in the limit of large damping, is

$$\dot{x} = x - x^3 + V_{n(t,\tau)} \, . \tag{2}$$

where V_n is a random noise, which is usually Gaussian and may be either "white" or "colored". In the former case, one assumes that the noise correlation time τ, is << any

---

*permanent address, Institute for Semiconductors, Chinese Academy of Sciences, Beijing, PRC

**present address, Department of Physics, University of Wisconsin at Parkside, Kenosha, WI 53141, USA

+present address, Department of Electrical Engineering, Michigan State University, East Lansing, MI 48824, USA

other time scale in the problem; while in the latter, τ can be $\cong$ or >> than such time scales. The noise intensity D, and τ are defined by the auto correlation functions,

$$\langle V_n(t)V_n(s)\rangle = 2D\delta(t - s) \tag{3}$$

of the white noise, and

$$\langle V_n(t)V_n(s)\rangle = \frac{D}{\tau}\exp[-|t - s|/\tau] \tag{4}$$

for the colored. In the simulation, this noise is derived from a wide bandwidth noise generator[3] driving a linear, single pole filter whose cutoff frequency is $\omega_n = 1/\tau_n$.

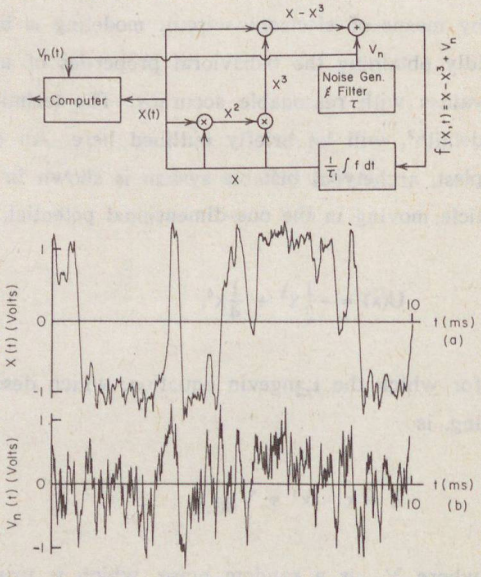

Fig. 1. A schematic outline of the analog simulator of a bistable system driven by colored noise. The x symbols refer to analog multipliers[4]. The ± symbols refer to standard summation circuits using operational amplifiers. The ∫ is an integrator, i.e. an operational amplifier with a feedback capacitor and an input resistor with time constant $\tau_i = R_iC_f$. (a) below is an example output x(t), and (b) shows the noise V_n, which in this case is colored with $\tau = 2.0$

The integrator time constant τ_i establishes the characteristic time scale of the system against which all other times are measured. The dimensionless noise correlation time of Eq. (4) is thus defined by $\tau = \tau_n/\tau_i$. Quasi-white noise is thus represented when $\tau \langle < 1$, and colored noise when $\tau \cong$ or $\rangle > 1$. The noise intensity is given by Eq. (4) in the limit t $\rightarrow$ s in terms of the mean square noise voltage, which is a measured quantity,

$$\langle V_n^2\rangle = \frac{D}{\tau}. \tag{5}$$

The circuit is a closed loop system, with the integrand of the stochastic differential equation Eq. (2), $x - x^3 + V_n(t,\tau)$, generated by appropriate combinations of voltages applied to the input of the integrator. The output of the integrator is the solution x(t). In essence, Eq. (2) is solved by collecting charge on a capacitor (the feedback capacitor of the integrator). This technique is not limited to inertia less systems. Damped oscillators can easily be fabricated using two integrators with the same time constant[5]. Systems with periodic[6] and even random[7] or other special purpose[8] potentials have also been modeled with the aid of an hybrid technique which allows one to write an arbitrary forcing function into a programmable, read only memory (PROM) which functions as a look-up table when combined with an ADC and a DAC[6].

The output voltages of such circuit models are then fed to analog-to-digital converters (ADCs) (not shown) and the digitized results analyzed by the computer[9] using the Asyst software[10]. Ensemble averages of the following measured quantities are produced: 1-d stationary and time evolving probability densities of position and residence time, 2-d stationary probability densities and power spectra and correlation functions.

In the following, we outline three experiments and briefly review some experimental results obtained from recent simulations.

II. Colored Noise Effects

The circuit shown in Fig. 1 and the model represented by Eqs (1), (2) and (4) were used in early studies on colored noise effects in nonlinear systems[11], approximate theories of which have only recently become accurate for large τ and about which controversy remains[12]. We show here two noise color induced features of the 2-d stationary probability density $P(x,V_n)$. These features are interesting, because they cannot be accounted for with any approximate 1-d theory - the colored noise problem is inherently multi-dimensional[13] - and hence they played a role in the stimulation of current theoretical advances. The first effect is a skewing of the contours of $P(x,V_n)$[14]. Fig. 2 (a) shows an example $P(x,V_n)$ measured on the system shown in Fig. 1 for $\tau = 4$, which is strongly colored noise. The skewing effects show up in the cross-sections taken at rather high altitude , as in Fig. 2 (b) and near the separatrix, as in Fig. 2. (c).

By contrast, cross-sections measured for $\tau << 1$ are nearly symmetric "dog bone" shaped items as shown, for example in Fig. 3 (a), which was measured on a different but nevertheless bistable potential[8]. The sequence in Fig. 3 shows the effect of increasing τ while holding other conditions constant. Fig. 3 (c) depicts the second color induced feature: the appearance of a "hole" or depression in $P(x,V_n)$ for $\tau > \tau_c$, where τ_c is a critical value. This is a topological phase transition marked by the bifurcation of the one saddle point connecting the two peaks, shown in the center of (b), to the two saddles, indicated by arrows in (c).

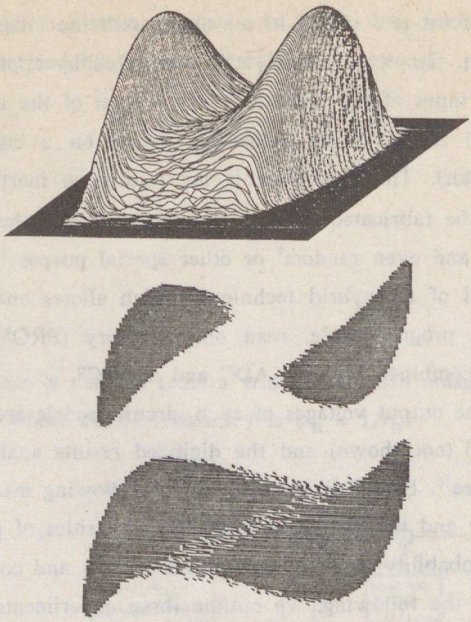

Fig. 2 (a) A two dimensional probability density $P(x,V_n)$. The probability density is the vertical coordinate, x is the horizontal and V_n is the isometric. (b) A cross-section cut through the object shown in (a) above the separatrix, and (c) a cut near the separatrix. Skewing at large τ tends to squeeze the probability toward the lower left-to-upper right diagonal.

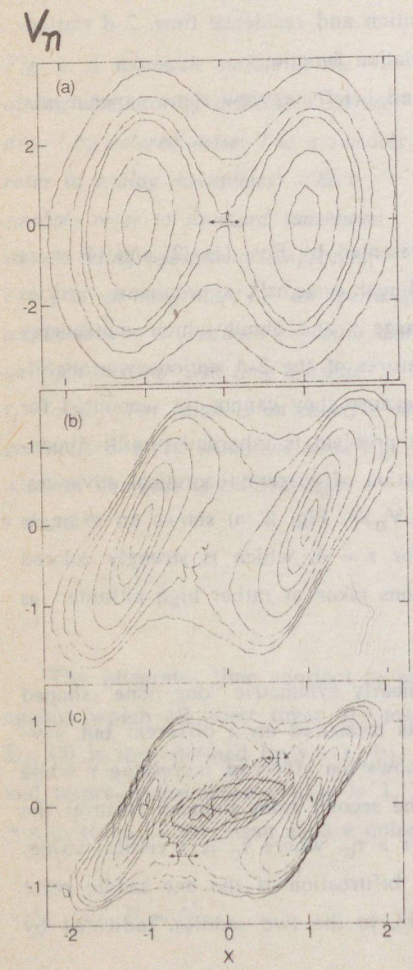

Fig. 3. Contours of constant probability cut through $P(x,V_n)$ measured on a "soft" bistable potential described in Ref. 8. (a) for τ = 0.1 or quasi-white noise; (b) for $\tau = 1.5 \cong \tau_c$; and (c) for τ = 5.0. Note the bifurcation of the single saddle (b) into two, off axis saddles shown by the arrows in (c).

This topological transformation, originally discovered with analog simulators[7,8], has since been confirmed with matrix continued fraction numeric techniques[15,16]. The appearance of two off axis saddles is significant since it graphically demonstrates that one dimensional approximations, for example for the mean first passage time between peaks, *must* break down for large τ, in particular for $\tau \geq \tau_c$.

One early approximate theory, albeit limited to small values of τ, predicted the skewing effect[17], though the holes have so far been demonstrated only numerically.

III. Phase Locking and Chaos in a Two Dimensional Laser Model

A laser, viewed a macroscopic dynamical system is an inherently three dimensional system comprising the field intensity I, population inversion F and the atomic polarizability. The polarizability is often adiabatically eliminated so that a representation in terms of dimensionless quantities is[18]

$$\dot{I} = 2K_0 I(AF - k) \tag{6}$$

$$\dot{F} = \gamma[1 - F(1 + I)], \tag{7}$$

where K_0 is a constant, A is the cavity gain, γ is a polarizability ratio and k is a cavity loss rate. The system shown has a virtual Hopf bifurcation which leads to a damped natural frequency $\omega \cong [2K_0\gamma(A - 1)]^{1/2} + O(\gamma^{3/2})$. In this example, we externally modulate the cavity loss k with amplitude m at frequency Ω,

$$k = 1 + m\cos(\Omega t). \tag{8}$$

Fig. 4 shows the analog simulator of this system[19].

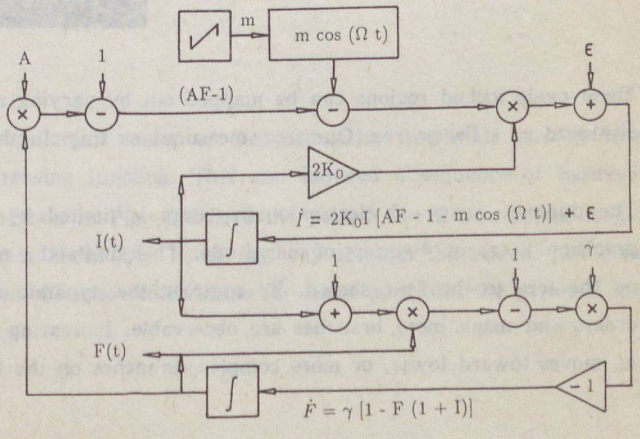

Fig. 4. Simulator of an externally driven 2-d laser model. An offset adjustment ϵ is shown but not mentioned in the text.

Since the system is now three dimensional, it is potentially chaotic, and because there are two independent frequencies we should observe mode locking. We expect mode locking whenever the ratio $\lambda = \omega/\Omega$ is a rational fraction, and the accessible fractions to be given by the well-known Farey arithmetic[20]. Mode locking was observed by plotting the return map of the simulator response I(t) on an oscilloscope. The return map is obtained by plotting a dot on the scope screen at a time clocked by one signal (the modulation) at the location of a maximum (vertical) versus the location of the last previous maximum (horizontal) of the other signal (the simulator output). The dot pattern is stationary for a mode lock, rotates rapidly when the two waves are unlocked, spreads into patterns of irregularly placed dots of various shapes for chaos, and fills more-or-less uniformly a circular or oblong shape for random noise. The number of dots in the return map is the denominator of λ. An example lock for $\lambda = 2/3$ is shown in Fig. 5.

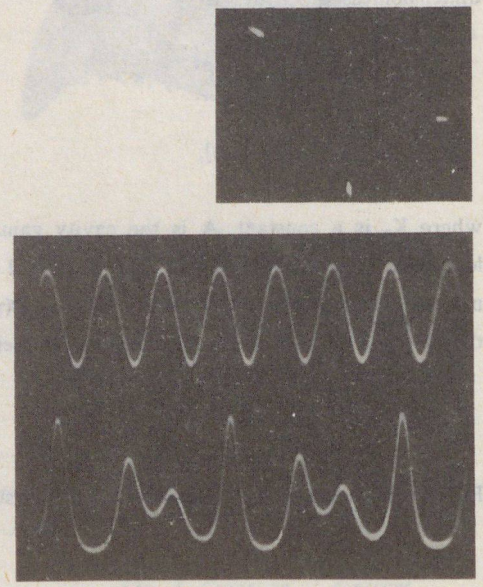

Fig. 5. Photographs of the oscilloscope screen. Upper photo is the return map of I(t). The lower photo shows the modulation k above and the actual time trace of I(t) below. For this lock $\lambda = 2/3$. When unlocked, the dots on the return map rotate rapidly and the waveforms shown below are no phase locked.

These mode locked regions can be mapped out by varying m and λ. The results are often displayed as a Farey tree. Our tree, measured on this simulator is shown in Fig. 6.

The dynamic range of electronic simulators is limited by their own internal noise and precision to about 4 orders of magnitude. This limits the number of observable branches on the tree to the four shown. By contrast, the dynamic range of real lasers is some 9 orders and many more branches are observable. Increasing the strength of the modulation m, moves toward lower, or more complex, branches on the tree.

Fig. 6. A Farey tree observed in the simulator shown in Fig. 4 on the interval [1/2,1/1]. Mode locks for Farey fractions > 7/11 were washed out by the internal circuit noise.

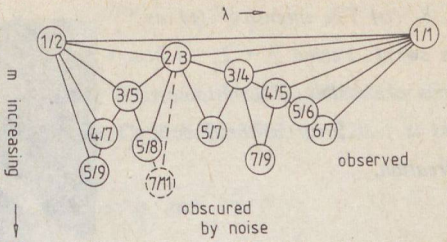

The regions around the two strongest locks at $\lambda = 1$ and $1/2$ have been explored in detail as shown in Fig. 7, where a quantity $X_m \propto \sqrt{A}$ is plotted versus λ. Increasing the laser gain A, moves the system toward chaos. For each value of A (or X_m), the frequency of the modulation is varied and the regions of locked and unlocked modes are depicted. The regions between and below the curves are locked, and are called "Arnold tongues". The tongues terminate in chaos for large A, as shown by the large error bars near the top. The tongue at $\lambda = \frac{1}{2}$ is unique to this system in that it encloses no area.

Fig. 7. The gain-frequency phase plane showing the first two Arnold tongues. The symbols are experimental data measured on the simulator. The curves are the theory of Ref. 18. The onset of chaos is marked by the large error bars near the tops of the tongues.

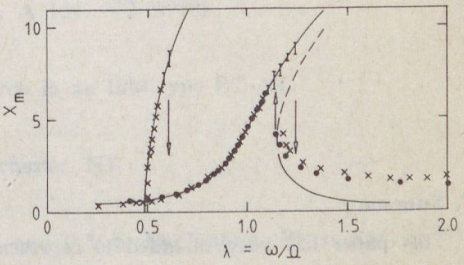

Chaos can also be induced by larger values of the modulation amplitude m. We have swept m with a linearly increasing function. This also induced a sequence of harmonic bifurcations. An example is shown in Fig. 8, where the period 1 → 2 bifurcation is just noisy, and the onset of chaos is about 2/3 of the way through the sweep, just prior to the period 2 → 3 bifurcation. Chaotic return maps for fixed m within the period 2 and 3 regions are shown below.

Fig. 8. (a) The intensity I(t) as m is swept. Period 1 → 2 → 3 bifurcations are visible. The onset of chaos is just prior to the 2 → 3 bifurcation.

(a)

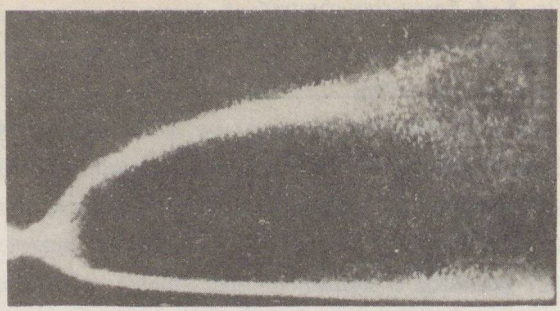

(b) Chaotic, period 2 return map.



(c) Chaotic, period 3 return map.



IV. Summary

This paper has been intended to represent the results of some recent selected analog simulations and to convey something of a tutorial aspect. Both discussions have been necessarily brief, but hopefully they will convey a flavor of this type of research activity and provide the groundwork for anyone who might wish to build a simulator as an addendum to their own research topics. Greater detail can be found in the references.

V. Acknowledgements

We are grateful to a large number of people for stimulating discussions. Of the many, a few are of special note: P. Hanggi, P. Mandel, L. Kiss, L. Schimansky-Geier, L. Fronzoni, F. Marchesoni and P. Jung. Parts of this work were supported by the British Science and Engineering Research Council, The U. S. Office of Naval Research and N.A.T.O.

References

1. L. Fronzoni in **Noise in Nonlinear Dynamical Systems, Vol. 3**, edited by F. Moss and P.V.E. McClintock (Cambridge University Press, Cambridge 1989) p. 222.

2. P.V.E. McClintock and F. Moss in *op. cit.*, Ref. 1. p. 243.

3. Quan-Tech Laboratories, Model 420

4. Analog Devices, AD534 or Burr-Brown, MPY534.

5. F. Moss, P. Hanggi, R. Mannella and P.V.E. McClintock, Phys. Rev. A **33**, 4459 (1986).

6. K. Vogel, H. Risken, W. Schleich, M. James, F. Moss and P.V.E. McClintock, Phys. Rev. A **35**, 463 (1987)

7. G. Debnath, F. Moss, F. Marchesoni, Th. Leiber and H. Risken, J. Stat. Phys. 54, 1381 (1989).

8. F. Marchesoni and F. Moss, Phys. Lett. A **131**, 322 (1988)

9. Data Translation Model 2820 ADC boards in an IBM type PC-AT.

10. Asyst Software Technologies, Inc., Rochester, NY.

11. P. Hanggi, T. Mroczkowski, F. Moss and P.V.E. McClintock, Phys. Rev. A **32**, 695 (1985).

12. see, for example, the following Comments and citations therein:

(a) G. Tsironis, K. Lindenberg, E. Peacock-Lopez and B. West, Phys. Rev. Lett. **63**, 214 (1989)

(b) P. Jung and P. Hanggi, Phys. Rev. Lett. **63**, 215 (1989)

(c) P. Jung, F. Marchesoni and P. Hanggi, Phys. Rev. Lett. **63**, 216 (1989)

(d) G. Tsironis, P. Grigolini, K. Lindenberg, R. Mannella and V. Palleschi, Phys. Rev. Lett. **63** 217 (1989).

13. see for example, H. Risken, **The Fokker Planck Equation** (Springer-Verlag, Berlin 1989)

14. F. Moss and P.V. E. McClintock, Z. Phys. B **61**, 381 (1985).

15. P. Hanggi, P. Jung and F. Marchesoni, J. Stat. Phys. **54**, 1367 (1989).

16. F. Moss, F. Marchesoni, Th. Leiber and H. Risken, J. Stat. Phys., to be published.

17. W. Ebeling and L. Schimansky-Geier in **Noise in Nonlinear Dynamical Systems, Vol.1**, edited by F. Moss and P.V.E. McClintock (Cambridge University Press, Cambridge) p. 279.

18. T. Erneux, S. Baer, and P. Mandel, Phys. Rev. A **35**, 1165 (1987).

19. M. James and F. Moss, J. Opt. Soc. Am. B **5**, 1121 (1988).

20. see for example, P. Bak, T. Bohr and M. Jensen, Phys. Scr. **T9**, 50 (1985).

10th Int.Conf. on Noise in Physical Systems
1989 Budapest, Hungary

NOISE AND SELF-ORGANIZATION IN A SIMPLE CELLULAR AUTOMATON

G. GOMBOS, T. SZAKÁCS

Research Institute for Technical Physics,
Hungarian Academy of Sciences
P.O.Box 76, H-1325 Budapest, Újpest 1

We have examined the effect of external noise on self-organizing processes in simple cellular automaton systems (CA). We have taken the CA constructed previously for the study of two-dimensional nucleation crystal growth, then we have made alterations in order to apply it as antiferromagnetic Ising-model. We show a way how to take further steps towards the problem of anisotropy and 'long range' local interactions. We give a qualitative analysis of the connection between the simulated self-organizing and the actual real properties of the system.

INTRODUCTION

Self-organizing processes that take place in nonlinear, non-equilibrium systems give us numerous examples that a certain magnitude of additive, external noise can advance ordering (e.g. fluctuations in external temperature in nucleation crystal growth, the temperature of the spin-system in antiferromagnetic phase transitions, etc.). In the past decade there were various applications of CA in modelling self-ordering (1). We consider CA that represent existing physical self-ordering phenomena (2D nucleation crystal ripening, antiferromagnetic phase transition). Our aim is to decide whether, in the presence of external noise, the ordering is advanced or not. To accomplish this goal we have used Vichniac's CA in a modified form which is fit to describe anisotropic behaviour and the effect of - local, but not short range - interactions (like secondary chemical bonds). To describe the degree of ordering we have in-

troduced a parameter that can be regarded as an order parameter.

THE METHOD

Our CA consists of uniform elements (cells). It is a spatio-temporally discrete network in which the cells change their states simultaneously. The dynamics is given by a spatially and temporarily local rule, the transition function which determines the state of a given cell at time t+1 as a function of the states of the neighbouring cells at time t. We have introduced two states: we have taken a Mooreian neighbourhood (a cell with its 8 immediate neighbours) and a periodic boundary condition. The transition function is given by the following implicit form:

$$S_{kl}(t) := \sum_{ij}^{i+j-1} (-1) \; a_{ij} \; x_{k+i,l+j}(t) \qquad (i,j=-1,0,1) \qquad (1)$$

$$x_{kl}(t+1) := \begin{cases} 0 & A-1 < S_{kl}(t) \\ 0 \text{ or } 1 \text{ at random} & -A \leq S_{kl}(t) \leq A-1 \\ 1 & S_{kl}(t) < -A \end{cases} \qquad (2)$$

where k, l are the cartesian co-ordinates of the cell, $x_{kl}(t)$ is the state of the cell at time t, a_{ij} is a non-negative integer, A is the magnitude of the noise. By this definition the ensueing evolutions tend to iterate to a chessboard-like configuration which we will take as the ordered state of the CA.

Let us define a quantity, B, the following way:

$$B := \sum (x_{ik}(t) \; \overline{\text{XOR}} \; x_{i+1,k}(t) + x_{ki}(t) \; \overline{\text{XOR}} \; x_{k,i+1}(t)) \qquad (3)$$

where 0 = false, 1 = true and $\overline{\text{XOR}}$ is identical to exclusive OR negated; i=1,2,..,N, N is the size of the CA (N+1pl). This construction gives B = 0 in the ordered state. It is a good assumption to say that, in the case of crystal ripening, B is a

monotonous function of the free energy or the free enthalpy, while in the case of the antiferromagnetic Ising-model it is connected to magnetization.

We have calculated the time evolution of B and its momenta for thousands of arbitrary initial patterns. The distribution of B shows a non-gaussian behaviour, therefore, as a corollary of the Wiener-Khinchin theorem shown by Haken, the response of the system given to external noise can be described by the 2nd and 4th momenta (m_2 and m_4).

RESULTS

First in (1) we put $a_{ij} = 1$. This CA was first used by Vichniac for a qualitative modelling of nucleation without noise (A = 0) (2).

Figures 1-4 show the evolutions of the (central) momenta of B. It can be seen that small noise magnitudes advance ordering (A = 1, 2), but A = 3 stops it completely.

In the case of nucleation crystal growth the Gibbs-potential plays the role of the order parameter (3). Beside a better ordered state, for crystal ripening external noise is quickening the pace of events as well, an effect which is not reproduced by our simulations. The behaviour of m_2 helps us to divide the process into two parts: after a short transient stage it decreases, the process becomes less sensitive to the actual macroscopic state, while in the second part the opposite is true. This corresponds quite well to the two stages of crystal ripening or, in the antiferromagnetic model, the starting of quenching of the antiparallelly oriented domains (4). This fact and the graphs of m_2 and m_4 prove that B can be regarded as an order parameter.

We have carried out similar investigations using other transition rules - anisotropic growth (different a_{ij}-s) is strongly suggested by practice. The initial saturation was modified by giving different probabilities to the values 0 and 1 when generating the pattern. This is important, for the above physical systems are basically controlled by the initial saturation. Then, to improve our method we have changed the neigh-

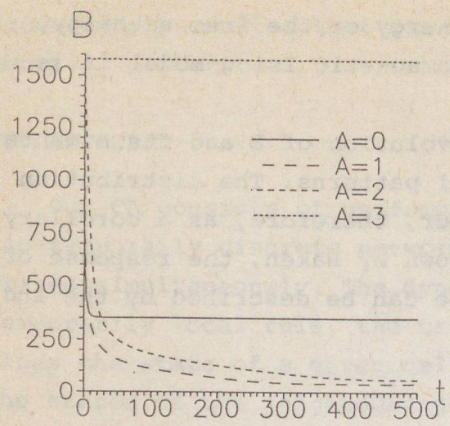

Fig. 1

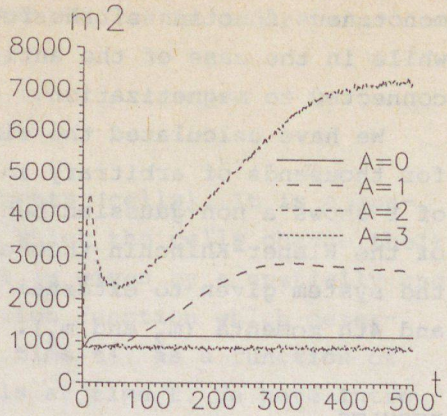

Fig. 2

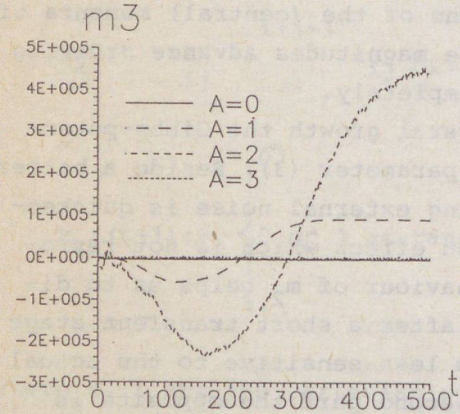

Fig. 3

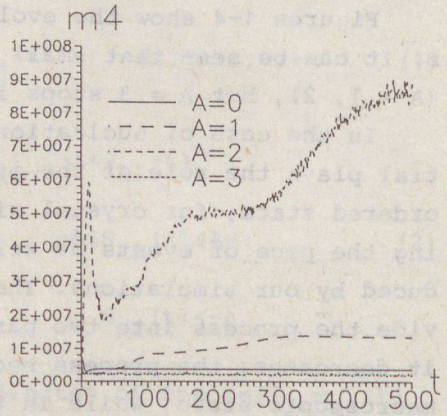

Fig. 4

bourhood after a couple of steps; in (1) we put i,j = -2,..,2 in a_{ij}. A reason for this change was that in nucleation secondary chemical bonds, interactions with longer range can also play a significant role after a given time.

Only extreme saturation produced qualitative results really different from the previous ones. The ordering is largely dependent on the point of time when the neighbourhood is expanded, or, in other words, on the macroscopic configuration preceding the presence of longer range interactions. The degree of

ordering of the final state is always increased, but temporary disordering may occur in some cases. We will give further details concerning other transition functions in the near future.

REFERENCES

1. Wolfram, S., Rev. Mod. Phys. 55, 601 (1983).
2. Vichniac, G.Y., Physica 10D, 96 (1984).
3. Gibbs, J.W., Trans. Conn. Acad. Sci. 3, 108, 343 (1875-78).
4. Ulbricht, H., et al.: Thermodynamics of Finite Systems..., Teubner Texte zur Physik, Band 17, BSB. Teubner, Leipzig 1988.

10th Int.Conf. on Noise in Physical Systems
1989 Budapest, Hungary

FLUCTUATIONS AND COLLISION-CONTROLLED LIGHT SCATTERING IN NON-EQUILIBRIUM ELECTRON-HOLE PLASMA

R. BARKAUSKAS, S.V. GANTSEVICH, R. KATILIUS

Semiconductor Physics Institute, Lithuanian Academy of Sciences
Vilnius 232600, Lithuanian SSR

A typical excess noise measurement is that of a noise power emitted by a sample as a whole into the circuit or the waveguide. The method provides information about fluctuations integrated over the sample volume, namely, those of the total current through the sample. On the other hand, fluctuations in small volumes inside the sample also deserve investigation since these fluctuations carry information about spatially-inhomogeneous kinetic processes in the spatially-homogeneous semiconductor. Such fluctuations can be studied via light-scattering experiments. Indeed, light scattering probes the spectrum of charge density fluctuations in solid state plasma (see, e.g. Abstreiter et al. 1984). Light is scattered from charge density fluctuation the wavevector of which, $\vec{q}$, equals the difference of the scattered and incident light wavevectors, and in this way the space-time Fourier analysis of these fluctuations is performed. The method is based on the expression for differential cross-section of light scattering which in the simple case of parabolic energy band structure and isotropic free carrier masses can be written as

$$\frac{d\sigma}{d\vartheta\, d\omega} = \frac{V_0^2}{2\pi}\left(\frac{e^2}{mc^2}\right)^2 \langle \delta n^2 \rangle_{\vec{q}\omega}\,, \qquad (1)$$

where $\langle \delta n^2 \rangle_{\vec{q}\omega}$ is the spectral density of carrier density fluctuations, V_0 is the scattering volume.

The aim of our paper is to investigate hot carrier density-density correlation functions in collisional multicomponent semiconductor plasma in which several different species may be present (many-valley structure, electrons and holes). The results can be used for quantitative interpretation of light scattering experiments in semiconductors.

By using the earlier derived classical diagrammatic technique especially suited for kinetic and fluctuation problems (Barkauskas et al. 1984), the equations for two-time two-point correlation functions describing fluctuations in non-equilibrium electron-hole plasma are obtained. The possible many-valley structure of conduction and/or valence band as well as intervalley transitions are taken into account. The solutions of the equations needed to calculate the scattered light spectrum in collision-controlled limit are constructed using the inverse evolution operator technique. The evolution operator takes into account the self-consistent Coulomb fields. On the other hand, electron-electron, hole-hole and electron-hole collisions are neglected compared to the lattice scattering. Thus the electron and hole concentrations n_e and n_h are supposed not to be high.

The electron-hole, electron-electron and hole-hole correlation functions in the long-wave low-frequency quasineutral limit (the "hydrodinamic approximation", see Barkauskas et al. 1984) are expressed in terms of transport characteristics of the non-equilibrium electron-hole plasma:

$$\langle \delta n_e^2 \rangle_{\vec{q}\omega} = \langle \delta n_e \delta n_h \rangle_{\vec{q}\omega} = \frac{2q^2 \tau_M}{V_0 \Delta_{\vec{q}\omega}} \left(\frac{n_e D_e}{\tau_{hM}^2} + \frac{n_h D_h}{\tau_{eM}^2} \right), \quad \omega \tau_M \ll 1 \qquad (2)$$

(cf. van Vliet 1970); here $D_{e,h}$ are the diffusion coefficients of electrons and holes, τ_{eM} and τ_{hM} are the electron and hole Maxwellian relaxation times while $\tau_M = (\tau_{eM}^{-1} + \tau_{hM}^{-1})^{-1}$. The frequency dependence of the correlation function is determined by the denominator

$$\Delta_{\vec{q}\omega} = (\omega - \vec{q}\vec{v}_a)^2 + q^4 (D_a + D_{\vec{v}})^2 \qquad (3)$$

describing the drift and spreading of the fluctuation; $\vec{v}_a$ is the ambipolar drift velocity in the electric field $\vec{E}$, and $D_a + D_{\vec{v}}$ is the total coefficient of ambipolar diffusion consisting of two terms: $D_a = (D_e\tau_{eM} + D_h\tau_{hM})/(\tau_{eM} + \tau_{hM})$ is the ordinary ambipolar diffusion coefficient and $D_{\vec{v}} = (\vec{q}\vec{v}_h - \vec{q}\vec{v}_e)^2\tau_M^3 / \tau_{eM}\tau_{hM}q^2$ is the convective term appearing due to finite time of Maxwellian relaxation. It describes the spreading of the fluctuation in $\vec{q}$ direction caused by combined action of Coulomb forces and different driving of electrons and holes by the external electric field (Gelmont and Shur 1971). The constant $D_{\vec{v}}$ emerges in the denominator of Eq. (2) only, i.e. it influences the evolution but not the source of the ambipolar fluctuations standing in the nominator of Eq. (2).

Let us note that in the frequency region $q^2 D_a \ll \omega \lesssim \tau_M^{-1}$ the low plateau in the spectral lineshape is predicted. It vanishes only at $\omega \gg \tau_M^{-1}$, and its contribution to the integral intensity can be comparable with that of the central line (Barkauskas et al. 1989). This can be seen from the expression for the integral intensity of light scattering:

$$\frac{d\sigma}{d\vartheta} = \frac{V_0 e^4}{c^4}\left\{\frac{n_e D_e}{D_a + D_{\vec{v}}}\cdot\frac{\tau_M}{\tau_{hM}}\cdot\left[\frac{\tau_M}{\tau_{hM}}\left(\frac{1}{m_e}+\frac{1}{m_h}\right)^2 + q^2 D_h\tau_{hM}\frac{1}{m_e^2} + \right.\right.$$

$$\left.\left. + q^2 D_{\vec{v}}(\tau_{eM}+\tau_{hM})(1+q^2 D_h\tau_{hM})/m_e^2\right] + e \leftrightarrow h\right\}. \qquad (4)$$

The many-valley structure of the energy band makes the fluctuation and light scattering spectra rather complicated (Barkauskas et al. 1989). In special cases of high symmetry the contribution of unscreened "mass fluctuations" due to intervalley transitions and intravalley diffusion of carriers (Gantsevich et al. 1971) and that of ambipolar quasineutral density fluctuations described above can be separated. The last contribution can be written as

$$\left(\frac{d\sigma}{d\Omega d\omega}\right)_a = \frac{V_0 e^4}{8\pi c^4}\left[\vec{e}_s\cdot\left(\frac{1}{s_e}\sum_{je}\overleftrightarrow{m^{-1}_{je}} + \frac{1}{s_h}\sum_{jh}\overleftrightarrow{m^{-1}_{jh}}\right)\cdot\vec{e}_i\right]^2 \left(\delta n_e + \delta n_h\right)^2_{\vec{q}\omega}, \quad (5)$$

where $\vec{e}_i$ and $\vec{e}_s$ are the unit polarization vectors of the incident and scattered fields, $\overleftrightarrow{m^{-1}_{j\,e,h}}$ is the inverse mass tensor in the $j_{e,h}$-valley, $s_{e,h}$ is the number of the equivalent valleys in the conduction and valence bands. Expressions (2) should be inserted into Eq. (5).

The quasi-neutrality of these two types of fluctuations ensures their relatively high level and should facilitate observation of light scattering from many-valley electron-hole plasma in semiconductors. The "mass fluctuation" contribution strongly depends on light polarization and vanishes in special geometry. This should help to separate the contributions of mass fluctuations and ambipolar fluctuations in experiments.

REFERENCES

Abstreiter G., Cardona M., and Pinczuk A. 1984 "Light scattering by free carrier excitations in semiconductors". In Light Scattering in Solids IV, Eds. M. Cardona and G. Guntherodt. Springer-Verlag, Berlin, p. 5-150.

Barkauskas R., Gantsevich S.V., Kagan V.D. and Katilius R. 1984 "Electron fluctuations under phonon nonequilibrium conditions". Sov. Phys. JETP 60, p. 187-193.

Barkauskas R., Gantsevich S.V., and Katilius R. 1989 "Electromagnetic wave scattering from nonequilibrium collisional multicomponent plasma in semiconductors". Fiz. Tverd. Tela (Leningrad) 31, in press.

Gantsevich S.V., Gurevich V.L., Kagan V.D., and Katilius R. 1971 "Collision-controlled light scattering from hot solid state plasma". In Proceed. of the 2d Intern. Conf. on Light Scattering in Solids, Paris, Ed. M. Balkanski. Flammarion, p. 94-97.

Gelmont B.L. and Shur M.S. 1971 "The instability of quasi-neutral waves in a semiconductor with two kinds of carriers" Phys. Lett. 35A, p. 353-354.

Van Vliet K.M. 1970 "Noise sources in transport equations associated with ambipolar diffusion and Shockley-Read recombination". Solid State Electronics 13, p. 649-657.

10th Int.Conf. on Noise in Physical Systems
1989 Budapest, Hungary

PRICE RELATION VIOLATION IN SLIGHTLY HEATING ELECTRIC FIELD

S. DEDULEVIČ, Ž. KANCLERIS, A. MATULIS

Semiconductor Physics Institute,
Lithuanian Academy of Sciences
Vilnius 232600, Lithuanian SSR

The violation of various Callen-Welton relations between the system dissipation and fluctuation characteristics is a well-known feature of the nonequilibrium electron gas. Among these relations the Price relation between the spectral density of current fluctuations $(\delta j_i \delta j_k)_\omega$ and the diffusion tensor D_{ik} is of considerable interest because for this relation to be violated the essential two-particle collisions are necessary. The quantitative characteristic of the Price relation violation is the correlation tensor Δ_{ik} which may be defined in the following way:

$$(\delta j_i \delta j_k)_{\omega \to o} = (e^2 n/V)(D_{ik}+D_{ik}-\Delta_{ik}) \qquad (1)$$

where V is the system volume, n is the electron concentration. When the electron system is in the thermodynamic equilibrium or when two-particle collisions are absent, the correlation tensor Δ_{ik} vanishes and the Price relation holds. According to the above said, the tensor Δ_{ik} is a convenient quantitative characteristic of the electron system "nonideality".

As far as we know, neither in gas-discharge nor in semiconductor plasma has the tensor Δ_{ik} been measured experimentally yet. Theoretically Δ_{ik} has been estimated by Gantsevich et al.(1979) and Barkauskas and Katilius(1979) using electron temperature approximation. An attempt has also been made to calculate Δ_{ik} for hot electrons using the Monte Carlo technique (Lugli and Reggiani.1986). These calculations revealed that in the case of a strong electric field Δ_{ik} could be observed only in the high electron concentration region (n

$\sim 10^{18} cm^{-3}$). To carry out an experiment, however, with the samples of such electron concentration in a strong electric field is very difficult.

In view of the coulomb ee-scattering being most efficient in the low energy region we performed the diffusion tensor D_{ik} and the correlation tensor Δ_{ik} calculations in the case of warm electrons expecting the correlation tensor to be significant under lower electron concentration.

The calculations were performed in the case of the medium electron concentration, when ee-scattering and the energy relaxation via electron-phonon scattering is of the same efficiency, i e. the following conditions were supposed to be satisfied:

$$\tau_p << \tau_{ee} \simeq \tau_\varepsilon \tag{2}$$

where τ_p and τ_ε are the characteristic times of electron momentum and energy relaxation.

According to Gantsevich et al.(1979) the diffusion tensor can be defined as

$$D_{ik} = \int d^3p (p_i/m) \Psi_k(p) \tag{3}$$

where the function $\Psi_k(p)$ satisfies the following kinetic equation

$$eE(\partial/\partial p)\Psi_k(p) - S\Psi_k = (p_k/m - V_k)(\partial/\partial n) nF(p). \tag{4}$$

Here $S\Psi_k$ is the linearized collision term,

$$V_k = (\partial/\partial n) \int d^3p (p_k/m) F(p) \tag{5}$$

and $F(p)$ is the nonequilibrium stationary electron distribution function.

When the conditions (2) are satisfied the expression for tensor Δ_{ik} is the following:

$$\Delta_{ik} = -\int d^3p \{(p_i/m)\Phi_k + (p_k/m)\Phi_i\} \tag{6}$$

where the function Φ_k satisfies the same equation as Ψ_k with the operator $(\partial/\partial n)n$ on the right side of Eq.(4) replaced by $n(\partial/\partial n)$.

According to the main idea of the warm electrons longitudinal and transverse components of the diffusion tensor

and the correlation tensor were expanded into E-series and presented as

$$D_{\perp} = D_o\{1+\gamma_{\perp}(E/E^*)^2\}, \tag{7}$$

$$D_{\parallel} = D_o\{1+\gamma_{\parallel}(E/E^*)^2\}, \tag{8}$$

$$\Delta_{ik} = \delta_{ik} D_o \gamma_B (E/E^*)^2. \tag{9}$$

Here D_o is the diffusion coefficient of equilibrium electron gas and $E^*=(3mkT/2\tau_p\tau_\varepsilon)^{1/2}$.

We restricted our calculations to the case of covalent semiconductors. The asymmetric parts of the collision terms were replaced by the momentum time relaxation approximation and the linearized Landau collision term, properly describing the low energy singularity of the coulomb ee-scattering, was included into the equations for symmetric parts of the functions Ψ_k and Φ_k. These equations were solved making use of the two-particle Monte Carlo technique.

Without going into particulars we present the final results for a semiconductor with a parabolic isotropic heavy-hole band of p-type Ge which has rather strong optical scattering what proved to be essential for the Price relation to be violated. (For details of the calculation refer to Kancleris and Matulis(1987) and Dedulevič et al.(1989)). In Fig.1 the coefficients $\gamma_{\perp}$,$\gamma_{\parallel}$ and γ_B are plotted as functions of the hole concentration. To show the ee-scattering influence the curves for $\gamma_{\perp}$ and $\gamma_{\parallel}$ with(1,3,5) and without(2,4) the two-particle scattering are given. Comparing the curves one can conclude that the ee-scattering plays an essential role in the medium concentration region ($n \sim 10^{14}$-10^{15} cm^{-3})in the case of warm electrons. As seen from Fig.1 in this region the coefficient γ_B is of the same order as diffusion tensor E^2-corrections and is of significance.

We also performed calculations for a model system with only quasi-elastic scattering taken into account and in this case the value of the coefficient γ_B was found to be less then 10% compared with those of $\gamma_{\perp}$ and $\gamma_{\parallel}$. This fact indicates the role of optical scattering to be of equal importance in

violating of the Price relation. This scattering enhances the ee-interaction via so-called compound scattering mechanism.

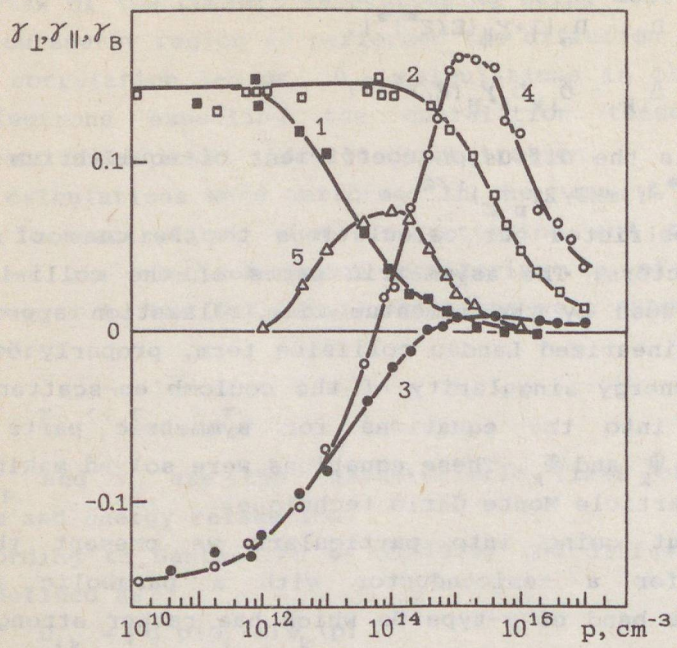

Fig.1. Warm electron coefficients: 1,2-$\gamma_\perp$; 3,4-$\gamma_\parallel$; 5-γ_B; 1,3,5-with ee-scattering; 2,4-without ee-scattering.

References

Barkauskas R. and R. Katilius (1979). Sov.Phys. JEPT, 50(3), 576-582.

Dedulevič S., Kancleris Ž. and A. Matulis (1989). Zn. Eksp. Teor. Fiz. 95(5), 1701-1710. (In Russian)

Gantsevich S. V., Gurevich V. L. and R. Katilius (1979). Riv. Nuovo Cim., 2(5), 1-87.

Lugli P. and L. Reggiani (1986). Proc. of 8th Intern. Conf. Noise in Phys. Systems 1985, NHPC, Amsterdam, 235-238.

Kancleris Ž. and A. Matulis (1987). J. Phys. C. 20, 1273-1284.

LONG-RANGE FLUCTUATIONS OF HOT ELECTRONS IN GaAs AND InP AT 80 K

V. BAREIKIS, J. LIBERIS, A. MATULIONIS, R. MILIUŠYTĖ, P. SAKALAS

Semiconductor Physics Institute, Lithuanian Academy of Sciences
Vilnius, 232600, Lithuanian SSR

INTRODUCTION

At strong electric fields (E) the dominant noise source in GaAs and in InP is the intervalley one and it can be suppressed by the reduction of sample length (Bareikis et al.1985). It has been supposed that at electric fields which are not high enough for the intervalley transfer the electron runaway related noise may manifest itself (Bareikis et al.1987). This noise is caused by the specific scattering mechanism in these materials, where polar-optical small angle scattering dominates and electrons can gain high drift component of mean energy. We demonstrate that rare events of large angle scattering create the long range fluctuations which can be suppressed in short samples.

EXPERIMENTAL

The longitudinal noise temperature Tn(E) is measured in microwave range. The electrons are heated by 1μs pulses of dc voltage U (repetition rate 125Hz). The details of the technique are described elsewhere (Bareikis et al.1985). From the data on Tn(E) and small signal conductivity, the spectral density of current fluctuations SJ(E) is determined. MOCVD grown low doping ($10^{15}cm^{-3}$) epitaxial layers of GaAs and InP are used to produce n^+-n-n^+ structures. The interelectrodal distances l were in 1 ÷ 10 micron range.

RESULTS AND DISCUSSION

Fig. 1 illustrates the main effect in InP: 1) the slow growth of Tn at intermediate fields (up to 3 kV/cm) is in contrast to

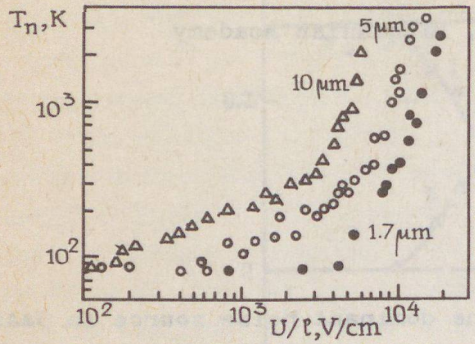

Fig. 1. Noise temperature vs average electric field (U/l) for different lengths of samples.

the rapid increase of Tn at high fields, 2) the magnitude of Tn is proportional to the sample length. The normalised spectral density of current fluctuations as a function of the average (U/l) electric field for different lengths of samples is plotted in Fig. 2. A decrease of Sj(E) is observed at fields below 1kV/cm.

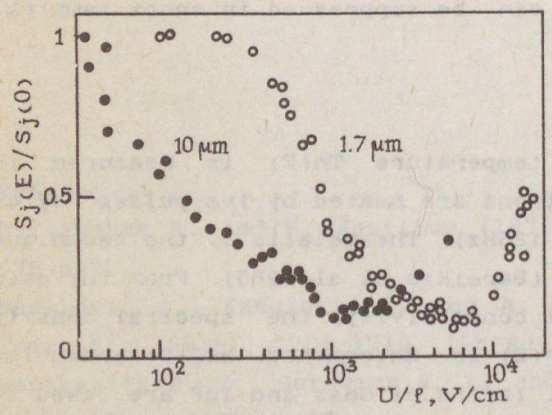

Fig. 2. Current fluctuation spectral density vs average electric field for different lengths of samples.

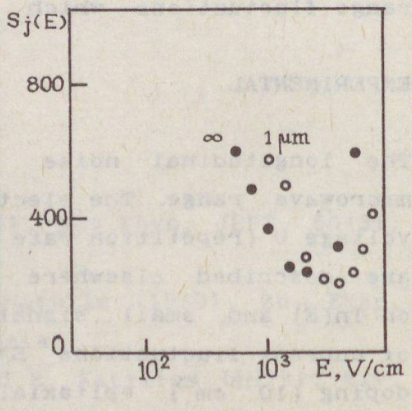

Fig. 3. Simulated spectral density of current fluctuations vs electric field for different lengths of samples.

This can be interpreted in terms of convective noise. At higher fields Sj(E) increases. As the sample length is decreased the minimum of Sj(E) is shifted to the higher fields. The similar results are obtained for GaAs, too. The intervalley separation energy being lower in GaAs, the decrease in Sj(E) takes place in a more narrow field range.

To interpret the results on velocity fluctuations the Monte Carlo simulation for 1 micron and long InP samples within one valley model (Brennan and Hess. 1984) is performed. The electric field is supposed to be uniform. Electron scattering on acoustic and optical phonons as well as on ionized impurities is taken into account. Results of simulation show (Fig. 3.) that the dependence Sj(E) is similar to that obtained experimentally. Since one valley model is used, the increase of Sj(E) at higher E is not associated with the intervalley scattering. It is caused by the enhanced velocity fluctuations due to the electrons which try and fail to run away because of large angle scattering at high energies. Such failed runaway events, need comparatively long time and much space. They give rise to long-range fluctuations. In short samples the electrons leave

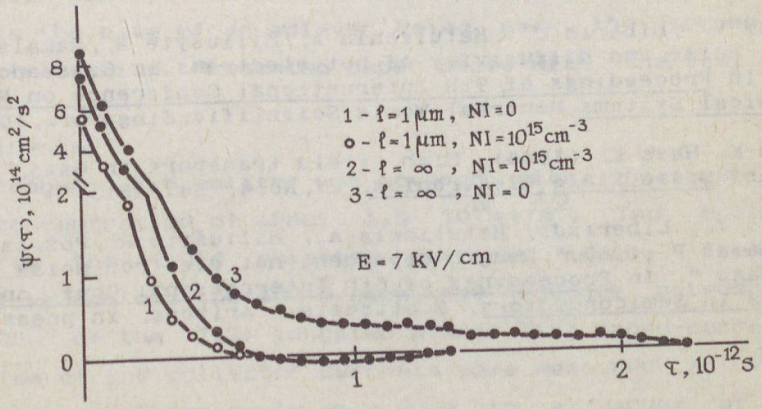

Fig. 4. Correlation function vs time of long and short samples for different doping levels.

the sample before they gain enough energy and therefore higher E is needed for this noise source to manifest. Thus, the size effects arise from inefficient chaotization of the electron motion. The simulated autocorrelation function (Fig. 4) confirms this reasoning. Fig. 4. illustrates that ionized impurity scattering influences the long-range fluctuations: for short samples the influence is negligible, for long ones the impurity scattering hinders the runaway effect and reduces the long-range fluctuations. Other aspects of the large angle scattering of high energy electrons by impurity levels have been discussed (Bareikis et al. 1989).

CONCLUSIONS

The long range fluctuations of hot electron velocity arising from large angle scattering at high energies has been observed in GaAs and InP at 80 K. These fluctuations are suppressed as the sample length is reduced and/or ionized impurity scattering is introduced.

REFERENCES

Bareikis V., Kibickas K., Liberis J., Miliušytė R., Sakalas P. (1985). Noise in short n^+-n-n^+ GaAs diodes. In Proceedings of the 8th International Conference on Noise in Physical Systems, Rome, North-Holland, 203-205

Bareikis V. , Liberis J. , Matulionis A., Miliušytė R., Sakalas P. (1987). Noise and diffusivity of hot electrons in GaAs and InP at 80K. In Proceedings of 9th International Conference on Noise in Physical Systems. Montreal, World Scientific, Singapore, 109-111

Brennan K. Hess K. (1984). High field transport in GaAs, InP and InAs. Solid State Electronics, 27, No. 4, 347-351.

Bareikis V., LiberisJ., Matulionis A., Miliušytė R., Požela J., and Sakalas P. 1989 " Length dependent hot electron noise in doped GaAs ". In Proceedings of 6th International Conf. on Hot Carriers in Semiconductors, Scottsdale, Arizona, in press.

TIME CROSS-CORRELATION FUNCTIONS OF DENSITY FLUCTUATIONS FOR POTASSIUM ADLAYER ON THE (112) W PLANE

J. BEBEN

Institute of Experimental Physics
Wroclaw University, Poland

Introduction

Surface diffusion phenomena are an interesting problem from the point of view of noise generation. Surface movement of adatoms causes local fluctuations of the concentration and can be described using the theory of density fluctuations developed by Smoluchowski [1]. The Field Emission Microscopy (FEM) technique can be used to investigate surface phenomena by analysis of field emission current fluctuations [2]. In the case when the fluctuations of the field emission current are caused by concentration fluctuations of adsorbed atoms and the Fick's law is to be valid, the theories of Timm and Van der Ziel [3] or Gomer [4] can serve to determine the diffusion coefficient [5]. Papers by Mazenko et al. [6] discuss the case of an adlayer being near the second-order phase transition. Presented paper deals with the last case.

Experimental

A tungsten FEM emitter was covered with potassium atoms with concentration of about 1.5 10^{18}at/m^2. Two collectors measured the field emission currents coming from two slit-like regions (50*300 Å each, the distance between them was 300Å) of the (112) tungsten plane. Time cross-correlation function of the collector currents were measured at various temperatures. Experiments were done in a vacuum of about 10^{-8}Pa. The obtained correlation functions are shown in Fig.1

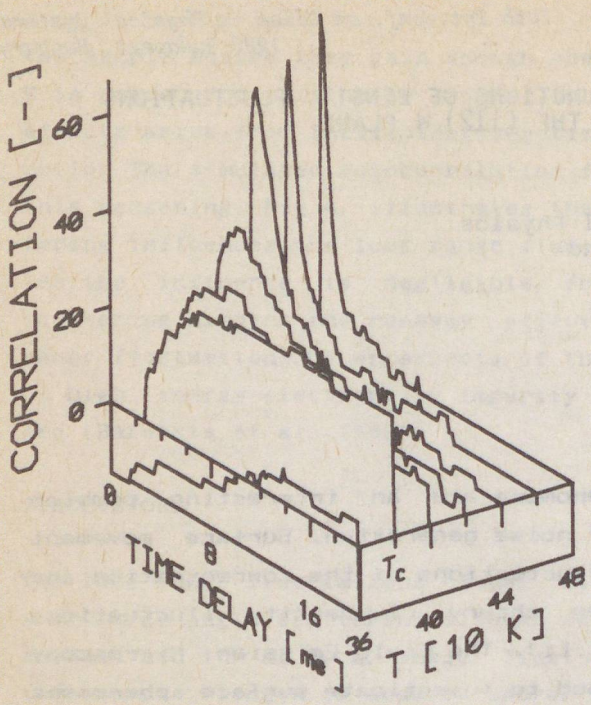

Fig.1 The evolution of the experimental correlation functions with temperature. The curve for 380K with the slowest decay corresponds to the critical temperature, T_c. The curve for 360K has negative values and cannot be fitted by a Gaussian.

Discussion

Beyond the critical region where the Fick's law is valid, the cross-correlation functions of density fluctuations should have a long-time limit given by

$$CC(\tau) \simeq (\tau)^{-d/z} \qquad (1)$$

where τ is the time delay, $CC(\tau)$ is the cross-correlation function and d is dimensionality of the system. According to Mazenko et al. [6] similar long time limit is expected in the critical region and for critical temperature, T_c, we should have

$$CC(\tau) \simeq (\tau)^{-\eta/z} \qquad (2)$$

where η is the usual critical index and z is the dynamical critical index.

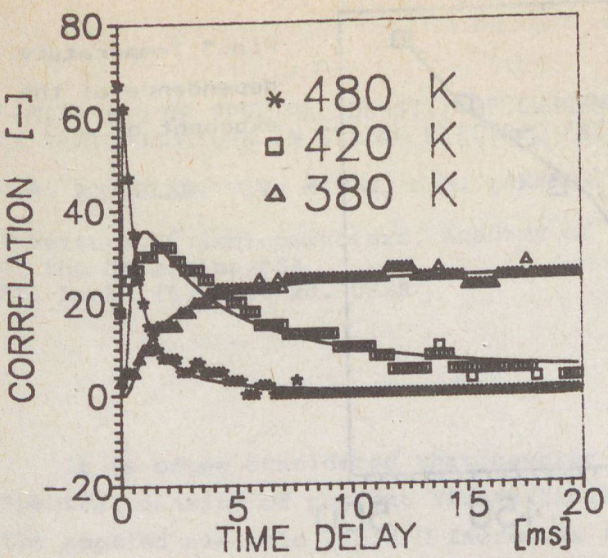

Fig.2 Three chosen experimental cross-correlation functions (stars, squares and triangles). The solid lines are the fitted curves.

To compare the experimental results with the theoretical prediction, the formula

$$CC(\Delta,\tau) = S\ (4\pi D\tau)^{-d/2} \exp\left[-\Delta^2/4D\tau\right] \qquad (\ )$$

which is valid beyond the critical region, was used. Taking the distance between the probe regions Δ=300Å, the S, d and the diffusion coefficient D were found to obtain the best fit with experimental points. Fig.2 shows the results for three chosen temperatures. The temperature dependence of the exponent d/2 is presented in Fig.3.

The above fitting procedure enables to obtain the exponent d/2, the value of which is an indicator of an adsorbate state. According to [6] it should change when the system approaches to the critical temperature, starting from a value 1 to η/z=1/15 for the Ising model. The obtained results, as shown in Fig.3 indicate that for the examined adsorption system the second-order phase transition occurs and the critical temperature is about 380K. For lower temperatures (see Fig.1, curve for 360K) the correlation function has negative values in a large delay time interval and cannot be fitted by a Gaussian curve. A question arises what mechanism

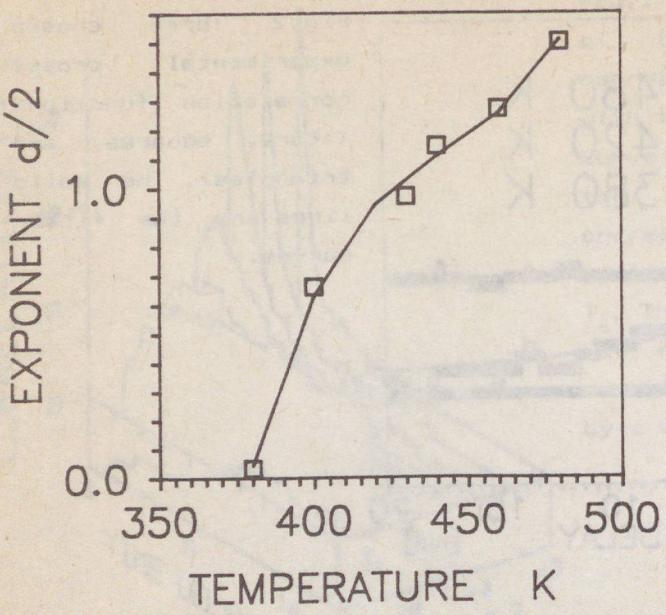

Fig.3 Temperature dependence of the exponent d/2.

is responsible for this. Creation of potassium islands is not possible because of strong repulsive Coulomb interaction of adsorbed atoms. The existence of commensurate and incommensurate regions seems to be more probable below the critical temperature where the above interpretation would be inadequate.

Work supported by the Polish Ministry of Education within the Central Project of Basic Research CPBP 01.08.A.

References

[1]. S.Chandrasekhar, Rev. Mod.Mhys. 15(1943)1.

[2]. Ch. Kleint, H.-J.Gasse, Naturforsch. 15a(1960)87.

[3]. G.W.Timm and Van der Ziel, Physica 32(1966)1333.
K.M.Van Vliet and E.R.Chenette, Physica 31(1965)985.

[4]. R.Gomer, Surface Sci. 38(1973)373.

[5]. J.Bęben, Ch.Kleint, R.Męclewski, Z.Phys.B Cond.Matter 69(1987)319; Surface.Sci. 213(1989)438.

[6]. G.Mazenko, J.R.Banawar and R.Gomer, Surface Sci. 107(1981)459; see also: G.F.Mazenko, Surface Mobilities on Solid Materials, ed. by Vu Thien Binh, Plenum Press, New York and London 1981, pp. 27-62.

10th Int.Conf. on Noise in Physical Systems
1989 Budapest, Hungary

LIMITATION OF SPECTRAL DENSITY OF CURRENT FLUCTUATIONS IN SEMICONDUCTORS IN STRONG ELECTRIC FIELDS

V.A. KOCHELAP, V.V. MITIN, N.A. ZAKHLENIUK, O.M. BULASHENKO

Institute of Semiconductors, Academy of Sciences
of the Ukrainian SSR
Pr. Nauki 45, Kiev-28, USSR

It is often considered that carrier mean energy $\bar{\varepsilon}$ and spectral density of current fluctuations $S(\omega, E)$ increase when the applied electric field E increases (1, 2). However, this is true only for quasielastic scattering of carriers. For several semiconductor materials (p-Ge, InSb, etc.) there is a strong interaction between the carriers and optical phonons. In this case carrier energy relaxation is essentially inelastic and new important features of transport and noise characteristics arise at low lattice temperature T. For such situation four characteristic electric fields, E_c, E_o, E^-, E^+, may be introduced. These fields have the following meaning: E_c corresponds to the beginning of the carrier heating; at $E > E_o$ the contribution of the optical phonon emission to the carrier energy balance becomes essential; E^- shows when streaming motion occurs; up to E^+ the carrier's penetration into the active energy region $\varepsilon > \hbar\omega_o$ is negligibly small (ε is the carrier energy, $\hbar\omega_o$ is the optical phonon energy). Transport and noise of the hot carriers for the interval of the fields $E > E^-, E^+$ were considered earlier (3, 4). The transport phenomena for E from the interval $E < E^-, E^+$ were studied, too (5).

In our report for the first time we investigated the current noise for the case $K_oT < \hbar\omega_o$, in pure and doped semiconductors when the main mechanism of energy loss of hot carriers is the optical phonon emission, and momentum scattering is controlled by any other mechanism. The investigation was carried out on the basis of the analysis of the correlation function equation and of the direct Monte Carlo simulation.

Analytical results were obtained for the model in which the optical phonon emission is taken into account for the ensemble of hot carriers. For the case $E < E^{-}$ the distribution function is almost isotropic in the passive energy region ($\varepsilon < \hbar\omega_o$) and it is near zero in the active region. For such a model the field and frequency dependences of the spectral density of current fluctuations are calculated in detail.

Principal qualitative peculiarities of the current noise are the following. For both pure and doped semiconductors the growth of noise intensity is limited in strong electric fields ($E > E_o$).

In pure semiconductors the spectral density $S(\omega, E)$ is field independent and isotropic (the longitudinal component $S_{\parallel}$ is equal to the transfer component $S_{\perp}$, i.e. the convective contribution to the fluctuations disappears). In the low-frequency limit we obtain that the mean energy, mobility and spectral density are saturated:

$$\bar{\varepsilon}_{sat} = \frac{9}{25}\hbar\omega_o, \quad \mu_{sat} = \frac{9}{8}\sqrt{\frac{\pi k_o T}{\hbar\omega_o}}\,\mu(0), \quad S_{sat} = \frac{9}{32}\sqrt{\frac{\pi\hbar\omega_o}{k_o T}}\,S(\omega, 0),$$

where $\mu(0)$ and $S(\omega, 0)$ are the low-field values of mobility and spectral density. In this limit the noise temperature T^n equals $T^n = \hbar\omega_o/4k_o$. At high frequencies there is $1/\omega^2$ dependence of $S(\omega, E)$ and noise temperature T^n equals $T^n = 2\hbar\omega_o/9k_o$.

In heavily doped semiconductors, when carrier momentum scattering is controlled by ionized impurities, $\bar{\varepsilon}$, μ and S are nonmonotonous functions of the electric field, and they decrease as $1/E$ with increasing E for $E > E_o$. In the low-frequency limit we have essential anisotropy of S: $S_{\parallel}/S_{\perp} = 8\,(2\pi^2 - 3)/3\pi^2$. At high frequencies there is nontrivial frequency dependence of the spectral density: $S(\omega, E) \sim \frac{1}{\omega^2}\ln\omega$ and the noise temperature depends on ω and decreases when E increases.

The qualitative peculiarities of the current noise in the low-frequency limit are illustrate in Figs 1-4, where the results are shown for the model with p-Ge parameters at two tem-

peratures: T = 15 K, E_c = 74 V/m (dashed lines) and T = 30 K, E_c = 200 V/m (continuous lines). Figures 1 and 3 correspond to the pure material, Figs 2 and 4 to the doped material with impurity concentration $N_A = 10^{21}$ m^{-3}. Limitations of the electric fields that were mentioned above are taken into account.

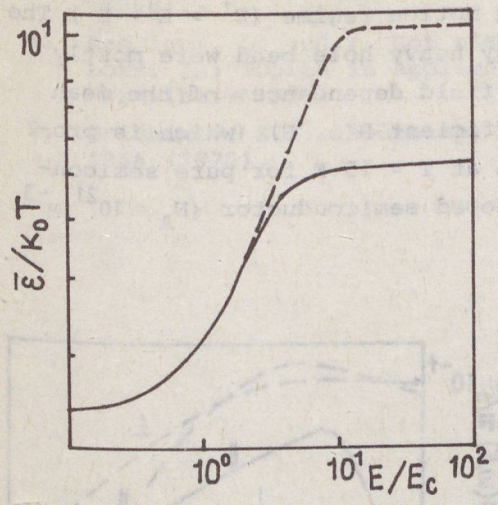

Fig. 1

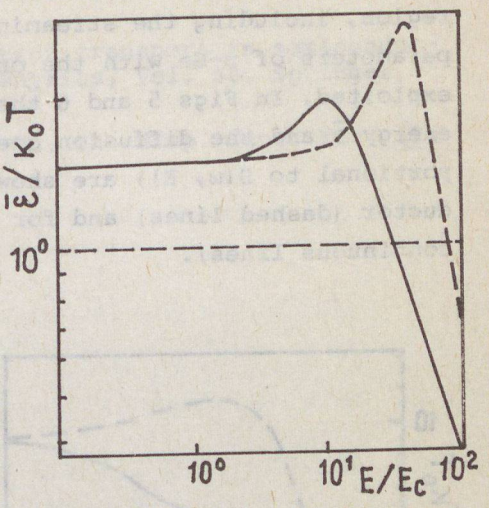

Fig. 2

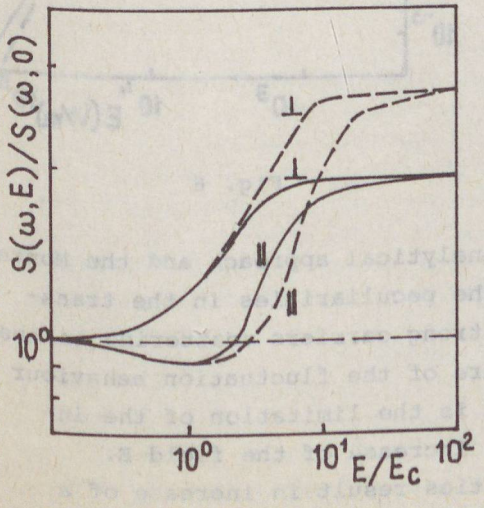

Fig. 3

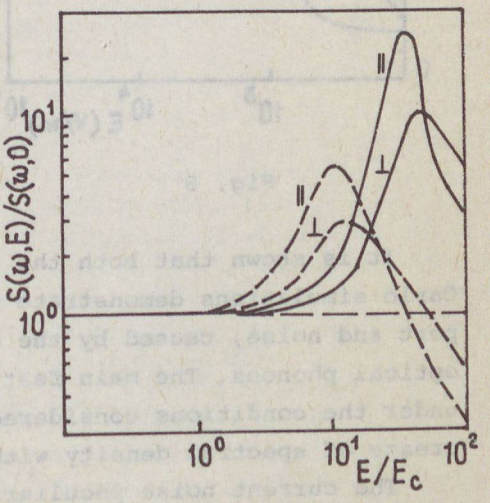

Fig. 4

As a prolongation of the investigation for the model described above, in this report we present also the results of the Monte Carlo simulations. This method permits to consider the case of small anisotropy and the case of arbitrary anisotropy of the distribution function. Thus we can study the transport and fluctuation phenomena in the wide electric field region, including the streaming motion regime ($E^+ > E > E^-$). The parameters of p-Ge with the only heavy hole band were mostly exploited. In Figs 5 and 6 the field dependences of the mean energy $\bar{\varepsilon}$ and the diffusion coefficient $D(\omega, E)$ (which is proportional to $S(\omega, E)$) are shown at T = 15 K for pure semiconductor (dashed lines) and for doped semiconductor ($N_A = 10^{21}$ m^{-3}, continuous lines).

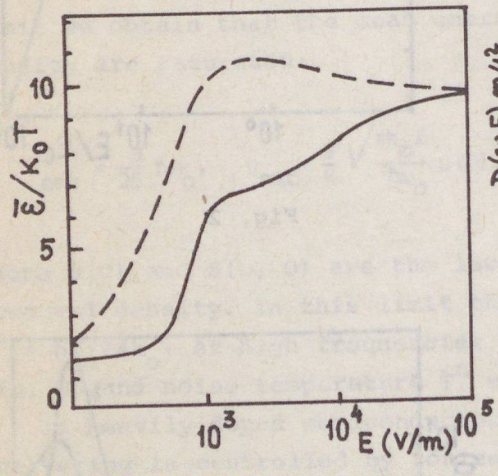

Fig. 5

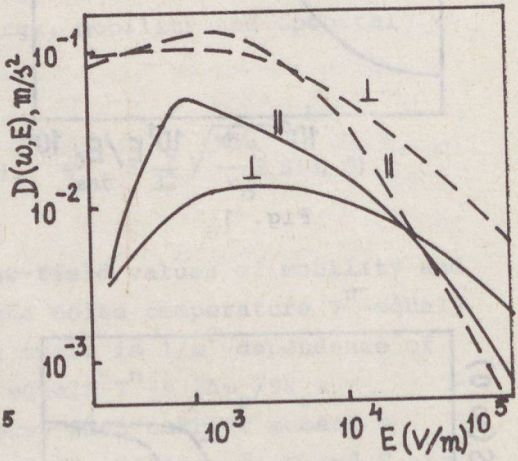

Fig. 6

It is shown that both the analytical approach and the Monte Carlo simulations demonstrate the peculiarities in the transport and noise, caused by the strong carriers scattering on the optical phonons. The main feature of the fluctuation behaviour under the conditions considered is the limitation of the increase of spectral density with increase of the field E.

The current noise peculiarities result in increase of a signal-noise relation, which is important for use in different semiconductor devices.

REFERENCES

1. Price, P.J., In: Fluctuation Phenomena in Solids. Ed. R.E. Burges. Academic Press, New York 1965, p. 355.
2. Gantsevich, S.V., Gurevich, V.L., Katilius, R., Rivista del Nuovo Cimento 2, 1 (1979).
3. Levinson, I.B., Matulis, A., Zh. Eksp. Teor. Fiz. 54, 1466 (1968).
4. Reggiani, L. (ed.), Hot electron transport in semiconductors. In: Topics in Applied Physics, Vol. 58. Springer, Heidelberg 1985.
5. Gribnikov, Z.S., Kochelap, V.A., Zh. Eksp. Teor. Fiz. 58, 1046 (1970).

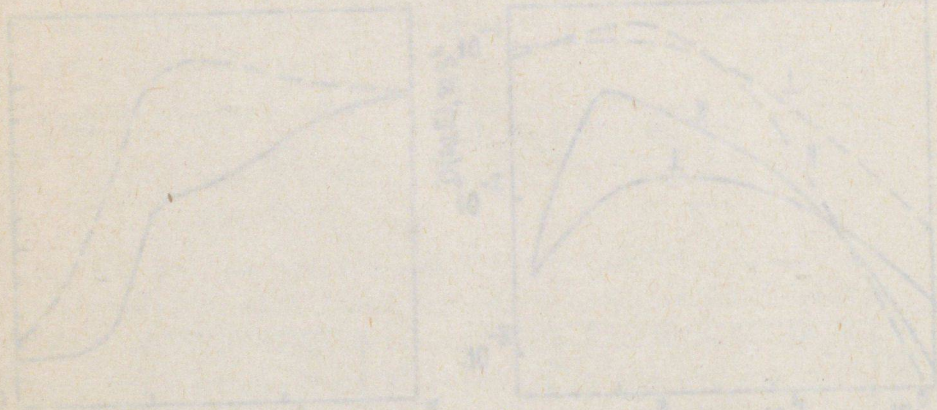

10th Int.Conf. on Noise in Physical Systems
1989 Budapest, Hungary

UNIVERSAL CONDUCTANCE FLUCTUATIONS AND THE 1/f NOISE MAGNITUDES IN DISORDERED METALS

S. FENG

Department of Physics, Solid State Science Center,
University of California
Los Angeles, CA 90024, USA

This paper contains mainly work that I did in collaboration with Lee and Stone, which was published sometime ago.[1] I will also give an account of some recent experimental studies related to our subject matter.

$1/f$ noise is a phenomenon which encompasses many fields of science and our daily life. In this paper we shall confine our attention to a particular example of $1/f$ noise: the conductance $1/f$ noise in disordered metals. We shall see that at low temperatures, quantum interference effects play an important role in determining the magnitudes of $1/f$ noise magnitudes in such systems.

We first specify the theoretical model that we consider, with all the necessary parameters. Our system consists of a piece of metal, of dimensions L_x, L_y, and L_z, with the direction z being the current-carrying direction. Our sample is supposed to be disordered, i.e. it contains some impurity atoms which scatter the transporting electron. The amount and the strength of the impurity scattering can be summarized as usual by the elastic scattering rate $1/\tau$ (computed at the Fermi energy). The associated elastic scattering mean free path is then given by $l = v_F\tau$. We will work exclusively in the so-called weak localization limit $k_F l > 1$. We should emphasize here that the elastic scattering events only change the momentum of the transporting electron but not energy, so that the phase shift between the scattered electron wavefunction and the incident one is a *fixed* quantity, thus the electron wavefunction is still a *coherent* wavefunction, albeit being of a more complicated (in general multiply scattered) form. It is also to be noted that τ or l is independent of temperature, as only elastic processes are involved. The phase breaking scattering processes in a disordered metal can be summarized by an inelastic scattering rate for the transporting electron, $1/\tau_{in}$. Such processes include the scattering by phonons and other electrons. In general, as $T \to 0$, $1/\tau_{in} \to 0$. This is because the amount of thermally excited excitations in the system which inelastically scatter electrons decreases with temperature. It is important to emphasize that inelastic scatterings are phase breaking scattering processes such that interference effects get cut off beyond the time scale τ_{in}. Thus we can distinguish the following two qualitatively different regimes for a theoretical description of the conductance noise magnitudes in disordered metals.

(1) $\tau \gg \tau_{in}$. From the above definitions, this regime is achieved at relatively high temperatures with a relatively low degree of disorder. In this regime, the transporting electron suffers many phase breaking inelastic scattering events inbetween the phase coherent elastic scattering events, so that it is not so important to worry about the phase information

of the electron wavefunction too much, and we can just simply treat the transporting electron as a semi-classical object. This is exactly the assumption for using the conventional Boltzmann transport theory which we learned from textbooks. The average conductance of a metallic sample in this regime is given by the Drude formula, and the theoretical model for calculating the $1/f$ noise amplitudes has also been available for some time.[2]

The basic idea for estimating the noise amplitudes in this semi-classical regime, which is also referred to sometimes as the "local interference model", is the following. The noise generating mechanism is that a fraction of the impurities can move around randomly during experimental measurement time. These motions could be due to thermal activations or quantum tunnelings of impurities to hop among local energy minima, or diffusions of impurities along grain boundaries. Whenever such an impurity motion takes place, a modification of the scattering cross-section that this impurity atom poses to the transporting electrons results. This gives rise to fluctuations of the conductance of the system, which is of course the noise one measures. If the activation energies for different moving impurities follow a wide (compared to k_BT) distribution, this results in a $1/t$ distribution for the time constants of the moving impurities, and the noise spectrum can be determined to follow a $1/f$ form. This is of course is the standard McWhorter picture for explaining the $1/f$ noise spectrum. Even if one does not want to stick to this particular model for the $1/f$ spectrum, or even if the measured noise spectrum is not of a $1/f$ form, it is still a meaningful question to consider the variance of the conductance noise δG^2, which is simply the integrated noise magnitude $\int d\omega S_G(\omega)$. (We subtract off the thermal white noise from the noise spectrum before this integration, so as to include only noise generated by impurity motions.) Within the local interference model, we can write the conductance noise variance, following Kogan and Nagaev,[2] as

$$\frac{\delta G^2}{G^2} = \frac{p\beta^2}{N_i}(\frac{\tau_{in}}{\tau})^2,$$

where N_i is the total number of impurities in the sample, p is the fraction of moving impurities, and β is a number of order 0.1 which measures the average relative change in scattering cross-section of moving impurities. For the $1/f$ spectrum, one can obtain δG^2 from the noise magnitude at 1 Hz approximately through $\delta G^2 \approx 20 S_G(1Hz)$, because of the insensitivity of δG^2 to the frequency cutoffs in the $1/f$ spectrum. We re-emphasize that because this semi-classical theory for estimating the noise magnitudes disregards the possible phase coherence for the electron wavefunction, it is only applicable in the "clean" limit $\tau_{in} \ll \tau$.

We now come to consider the opposite limit, namely when the above inequality reverses, which is sometimes called the quantum diffusive regime.

(2) $\tau \ll \tau_{in}$: this is a regime favored for a relatively large concentration of impurities and at low temperatures. In this regime, a transporting electron suffers many phase perserving elastic scatterings with impurity atoms inbetween phase breaking inelastic collisions. Thus in order to describe the electron transport processes properly, it is crucial to include the phase information of the coherent electron multiple scattering wavefunction (by impurities), up to a length scale of the so-called inelastic diffusion length (or phase coherence length) $L_{in} = \sqrt{D\tau_{in}}$. Here the diffusion constant $D = v_F^2\tau/3$ describes the random walk nature of electron's scattering events with impurities. Many interesting

properties arise in this quantum diffusive regime of electron transport. One of the celebrated examples is electron localization or weak localization. In our problem here, we can now ask the question of what is the conductance fluctuations induced by moving a few impurities in a sample. For purposes of illustration, we shall give the results only for the quasi-2D case $t \ll L_y = L_z \equiv L$, where the thickness of the film is taken to be $l \ll t \ll L_{in}$. First we consider the really low temperature case so that $L_{in} > L$. This is the so-called mesoscopic regime. Suppose we move just one impurity a distance δr, the resultant average conductance change can be estimated to be

$$\delta G_1^2 \equiv < (G - G')^2 > = 0.96 \frac{e^2}{h} \frac{l}{t} \frac{C(k_F \delta r)}{(k_F l)^2},$$

where $C(x) = 1 - Sin^2(x)/x^2$. Note that this result does not decay with the size of the system L provided $L \leq L_{in}$! This result is qualitatively different from the corresponding one from the semi-classical picture. First of all, this reflects a dramatically large amount of conductance fluctuations which are induced by just one moving impurity. This is seen by comparing this result with the situation that if we move *all* the impurities randomly, we obtain the so-called "universal conductance fluctuations" value of $\delta G^2 \approx (\frac{e^2}{h})^2$. Thus moving one impurity in a quasi-2D film in the mesoscopic regime gives rise to conductance fluctuations which is a finite fraction of that induced by moving all the impurities. This surely is a fantastic manifestation of the novel transport phenomena due to quantum phase coherence. If more than one impurity moves around, we have the following two different situations. For the case of a small number of moving impurities, we have the unsaturated regime $p \ll (l/L)^2$, with the corresponding conductance fluctuations $\delta G^2 \approx p N_i \delta G_1^2$, i.e. the conductance fluctuations from moving different impurities simply add. If we move too many impurities such that $p \gg (l/L)^2$, then the conductance fluctuations saturate at the universal value e^2/h.

The above results can be extended to treat a macroscopic sample such that $L \gg L_{in}$. Physically, as there is no phase coherence beyond the length scale L_{in}, one can divide the sample up into regions of size L_{in}, the fluctuations of each phase coherence "box" can be obtained from the above results, and the fluctuations of the entire system should be added incoherently from each boxes, i.e.

$$\delta G^2 = \delta G^2 (L = L_{in}) (\frac{L_{in}}{L})^2.$$

In the unsaturated limit $p \ll (l/L_{in})^2$, the conductance noise measured in variance due to a fraction p moving impurities can be calculated to be

$$\frac{\delta G^2}{G^2} = 18\pi p \frac{L_{in}^4}{k_F^4 l^4 L^3 t},$$

where we have absorbed the C function into the definition of p. In the saturated limit $p \gg (l/L_{in})^2$, we have

$$\frac{\delta G^2}{G^2} = 18\pi \frac{L_{in}^2}{k_F^4 l^2 L^2 t^2}.$$

A very novel feature of these expressions is the fact that as one lowers temperature, because L_{in} gets longer and longer, the noise magnitudes will keep going up, until saturating at the full quantum level $\approx e^2/h$ when $L_{in} \geq L$. This is a very different picture compared to our intuition and the semi-classical theory.

Another very unique feature of the conductance fluctuations due to moving impurities in the quantum diffusive regime is that when a magnetic field is applied transverse to the film, the noise magnitude reduces exactly to one half its value in the absence of the field, with a crossover field $B_c \approx \phi_0/L_{in}^2$. This is due to the following fact: in the absence of magnetic field, both electron interference paths which are symmetric and anti-symmetric under time reversal contribute equally to the conductance fluctuations. When the sample is subject to a field $B > B_c$, those interference paths which are anti-symmetric upon time reversal stop contributing to the fluctuations.

We now briefly discuss some recent experiments on noise in disordered metals in light of the above theoretical picture. First there was the measurement of the Purdue group[3] on the telegraph noise in disordered Bi films and wires at low temperatures $< 1K$. At such low temperatures one can actually observe conductance "jumps" due to individual impurity motions, as the time constant for such motions is very long and is due to quantum tunneling across potential barriers, and the frequency of such impurity motion is very low so that typically at a given moment only one impurity hop occurs. The typical magnitudes observed in these experiments are in an order of magnitude agreement with the theoretical predictions presented above. The temperature dependence of the noise magnitudes from the experiment and the theory, when the value of L_{in} from independent measurements was used, is also in rather good agreement. The negative temperature dependence of the noise magnitudes in disordered C films near the metal-insulator transition at low temperatures was later measured by the Illinois group.[4] In a recent experimental study of Bi films at a slightly higher temperature regime $T < 70K$ done at Bell Labs, both the negative temperature dependence and the $1/2$ reduction of the noise magnitudes in a magnetic field were clearly demonstrated. The actual number for the noise magnitudes can be fitted well by the above theory, using reasonable (but unkown) estimates for the fraction of moving impurities p.

In summary, we presented an outline for the recent theoretical development of the noise magnitudes in disordered metals based on the "universal conductance fluctuations" mechanism, which is valid in the low temperature regime. This new theoretical framework for estimating noise magnitudes compares well with recent experimental studies.

REFERENCES

1. S. Feng, P. A. Lee, and A. D. Stone, Phys. Rev. Lett. **56**, 1960, 2772(E) (1986); see also *Quantum Effects in Small Disordered Systems*, edited by B. L. Altshuler, P. A. Lee, and R. A. Webb, (Elsevier, 1989).
2. Sh. M. Kogan and K. E. Nagaev, Sov. Phys. Solid State **24**, 1921 (1982).
3. D. E. Beutler *et al.*, Phys. Rev. Lett. **58**, 1240, 2608(E) (1987).
4. G. A. Garfunkel *et al.*, Phys. Rev. Lett. **60**, 2773 (1988).
5. N. Birge and B. Golding, Phys. Rev. Lett. **62**, 195 (1989).

MECHANISM IN CONDUCTANCE FLUCTUATIONS OF MESOSCOPIC DISORDERED SYSTEMS DISOBEYING UNIVERSAL LAWS

G. FORGÁCS, M.T. BÉAL-MONOD*

Department of Physics, Clarkson University, Potsdam, N.Y. 13676, USA; and Central Research Institute for Physics 1525 Budapest, P.O.Box 49, Hungary
*Laboratoire de Physique des Solides, Université Paris-Sud, 91400 Orsay, France

It has been established both theoretically (1) and experimentally (2) that there exist conductance fluctuations of the order e^2/h (e is the electric charge, h is Planck's constant) in mesoscopic disordered electronic systems. More precisely

$$(\text{var } G)^2 = \langle G^2 \rangle - \langle G \rangle^2 \sim (e^2/h)^2. \qquad (1)$$

Here G is the macroscopic conductance and $\langle\ \rangle$ denotes the sample to sample average which, as demonstrated by Lee et al. (3), can be replaced by the average over the disorder. The content of Eq. (1) is the following: the conductance fluctuations are independent of sample size, degree of disorder and the dimensionality, i.e. they are universal. Equation (1) is valid only at low temperatures, where the elastic mean free path is smaller than the inelastic mean free path. The fact that Eq. (1) is independent of the degree of disorder, i.e. the concentration of impurities in the metal, is true in the so-called weak localization limit, namely when $k_F l \gg 1$, where k_F is the Fermi momentum, l is the elastic mean free path.

As a separate development it has been shown recently (4) that when interaction between the impurities in the theory of Anderson localization (5) is taken into account, new qualitative features occur. In particular, such interaction may account for the experimental fact of localization induced by annealing (6).

It is then natural to ask how the interaction between impurities affects the universal conductance fluctuations (UCF) in disordered mesoscopic systems. Moreover, since it has been claimed that these fluctuations may be at the origin of the 1/f noise (at least in disordered metallic systems), we ask how the above interaction affects 1/f noise. It has to be emphasized that the interaction between impurities, in our opinion, must be taken into account to describe correctly the metal-insulator transition via localization. In many systems such a transition occurs at 50% impurity concentration (6) and it is hard to believe that at such concentrations effects of interaction are unimportant. These interactions, provided they are of short range, do not change the universal properties of the Anderson transition (they do not change the values of critical exponents) but may change the nonuniversal aspects, like the value of the critical concentration (at which the transition takes place).

We have reexamined the theoretical calculation leading to UCF in the presence of impurity interaction. Our model of the disordered metal is a lattice gas with two kinds of atoms one of them being the host the other the impurity. In this way quenched disorder is built into the system by allowing each site to exist in two possible states (host and impurity) with appropriate probabilities. Assuming nearest neighbour interactions between the atoms a correlated probability distribution for the complete state of the system can be derived. The electrons are scattered by both kinds of atoms and the conductivity of the system is calculated in the usual way (4, 7), using the Kubo formula. The final expression is obtained by averaging the result for a given impurity configuration with the correlated probability distribution derived on the basis of interactions. As a result we obtain

$$\text{var } G \sim e^2/h \ (1+\gamma), \tag{2}$$

where γ is a relatively complicated expression in terms of the concentration and interaction parameters of the impurities. The full expression for γ is given explicitly in Ref. (8). The im-

portant consequence of the impurity interaction is then that some universal aspects of UFC are lost. Since the value of γ is sensitive to the sign of the interactions (namely whether they are attractive or repulsive), it should be possible to observe experimentally our effect Eq. (2) by choosing repulsive and attractive impurities to measure "UCF".

In Ref. (9) it has been shown that by moving a single impurity in two dimensions, one can induce conductance fluctuations of the same order as in Eq. (1). It was then argued that such a sensitivity of conductance fluctuations to the impurity motion may provide an explanation for 1/f noise. Our calculation with interaction between impurities may be applied also to this question. Indeed, our results show that the expressions derived in Ref. (9) do change in the presence of interactions. The appearing correcting factors, similar to $(1+\gamma)$ in Eq. (2), again strongly depend on the nature of the interactions. Therefore, beside the fact that the universal nature of the fluctuations is lost, the fluctuations caused by the motion of a single impurity are either strongly enhanced or weakened. As a consequence, if the results of Ref. (9) are indeed relevant to the theory of 1/f noise, our findings relate the amplitude of the noise to the interaction between the impurities. Careful experimental studies of this amplitude, with varying impurity content are, therefore, suggested.

REFERENCES

1. Altshuler, B.L., JETP. Lett. 41, 648 (1985).
   Altshuler, B.L., Khmelnitskii, D.E. JETP. Lett. 42, 359 (1985).
   Stone, A.D., Phys. Rev. Lett. 54, 2692 (1985).
   Lee, P.A., Stone, A.D., Phys. Rev. Lett. 55, 1622 (1985).
   Imry, Y., Europhys. Lett. 1, 249 (1986).
2. Umbach, C.P., et. al., Phys. Rev. B30, 4048 (1984).
   Webb, R.A., et. al., Phys. Rev. Lett. 54, 2696 (1985).
   Washburn, S., et. al., Phys. Rev. B32, 4789 (1985).
   Licini, J.C., et. al., Phys. Rev. Lett, 55, 2987 (1985).
   Scocol, W.J., et. al., Phys. Rev. Lett. 56, 2865 (1986) and 58, 1039 (1987).

Kaplan, S.B., Hazstein, A., Phys. Rev. Lett. 56, 2403 (1986).

3. Lee, P.A., Stone, A.D., Fukuyana, H., Phys. Rev. B35, 1039 (1987).

4. Beal-Monod, M.T., Forgacs, G., Phys. Rev. B37, 6646 (1988).

5. Lee, P.A., Ramakrishnan, T.V., Rev. Mod. Phys. 57, 287 (1985).

6. Lesueur, J. Dumoulin, L., Nedellec, P., Phys. Rev. Lett. 55, 2355 (1985).

Lesueur, J., Ph. D. Thesis, Orsay, 1985 (unpublished).

7. Abrikosov, A.A., Gorkov, L.P., Dzyaloshinskii, I.E., Methods of Quantum Field Theory in Statistical Physics. Prentice-Hall, Englewood Cliffs 1963.

8. Beal-Monod, M.T., Forgacs, G., J. Phys. (Paris) (in press).

9. Altshuler, B.L., Spviak, B.Z., JETP. Lett, 42, 447 (1985).

Feng, S., Lee, P.A., Stone, A.D., Phys. Rev. Lett 56, 1960 and ibid. erratum 56, 2772 (1986).

SESSION 3

NOISE IN MATERIALS
(CRYSTALLINE, AMORPHOUS)

10th Int.Conf. on Noise in Physical Systems
1989 Budapest, Hungary

NOISE IN MATERIALS – SOME RECENT RESULTS

J.J. BROPHY

Department of Physics, University of Utah
Salt Lake City, Utah 84112, USA

INTRODUCTION

A rich variety of electrical fluctuation phenomena in solid materials have been measured and analyzed since the invention of electronic amplification. It is possible, for example, to observe 1/f noise, conductivity fluctuations arising from generation-recombination noise and Nyquist noise in the same semiconductor specimen. Similarly, the Nyquist theorem yields quantitative measurements of magnetic losses in ferromagnetic materials in terms of magnetic flux density fluctuations and Barkhausen noise spectra show relaxation time constants associated with irregularities in the motion of domain walls. Critical fluctuations in second-order phase transitions in solids, analogous to critical opalescence in gas-liquid mixtures, are reported in ferroelectrics and in the new high temperature superconductors.

These experiments, and many others, provide background for several recent studies of noise in materials. Of particular interest are fluctuation conductivity in high temperature superconductors, noise spectroscopy in solids, noise in amorphous materials, and noise effects in solid ionic conductors.

HIGH TEMPERATURE SUPERCONDUCTORS

Since the superconducting phase transition is of second order, it has associated with it critical point thermodynamic fluctuations (1,2,3). Because of critical fluctuations, Cooper pairs have a finite existence probability above T_C. This leads to so-called excess, or fluctuation, conductivity, which can be calculated from the current-current correlation function and the fluctuation-dissipation theorem. In terms of the reduced temperature, $\varepsilon=(T-T_C)/T_C$, the fluctuation conductivity in the case of bulk (three-dimensional) fluctuations can be written as (3,4),

$$\Delta\sigma_{3D} = \frac{e^2}{32h} \frac{1}{\xi(0)} \varepsilon^{-1/2} \quad (1)$$

where $\xi(0)$ is the zero temperature coherence length. For two-dimensional fluctuations,

$$\Delta\sigma_{2D} = \frac{e^2}{16h} \frac{1}{d} \varepsilon^{-1} \quad (2)$$

where $d << \xi$ is the characteristic length of the two-dimensional system.

Some experimental measurements suggest that $Y_1Ba_2Cu_3O_{7-x}$ is three-dimensional (4) in character, in spite of the well known layer-like structure, while others (5,6) indicate two-dimensional behavior. It seems likely that the discrepancy can be attributed to differences in experimental conditions, for detailed measurements (7) on (Y, Ho, and Sm) $Ba_2Cu_3O_{7-x}$ show both dimensionalities in different temperature ranges, as illustrated in Fig. 1. Other results (8,9) on T1-Ba-Ca-Cu-0 and Bi-Sr-Ca-Cu-0 materials indicate strictly two dimensional fluctuation behavior.

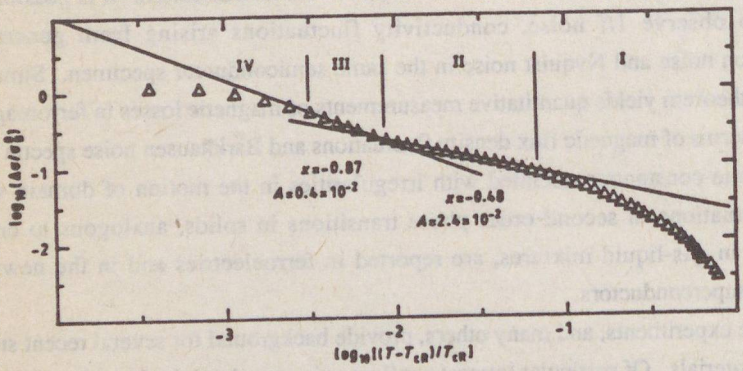

Figure 1. Normalized excess conductivity of $Y_1Ba_2Cu_3O_{7-x}$ as a function of the reduced temperature. Three-dimensional fluctuations are observed in region II and two-dimensional fluctuations in region III. From reference (7).

Experimental results yield in-plane coherence lengths of 10 A° to 15 A° and transverse coherence lengths as small as 2 A°. These are many orders of magnitude smaller than those in ordinary superconductors. Small values of ξ in Eqs. (1) and (2) yield significant values of excess conductivity and explain why the effect is observed in bulk high temperature superconductors, but not in normal superconductors except under very special conditions, such as in amorphous materials.

Thermodynamic fluctuations also influence the specific heat anomaly at the superconducting transition, causing departures from the specific heat jump predicted by

BCS theory. Comparison of experimental results with expressions analogous to Eqs. (1) and (2), as illustrated in Fig. 2, confirm the three-dimensional nature of the fluctuations in $YBa_2Cu_3O_{7-x}$ single crystal.

Current noise in (Y or Er)$Ba_2Cu_3O_{7-x}$ ceramics is 1/f noise above the transition temperature (11, 12) and is much larger than in metals, requiring a Hooge constant of about 10^3. The noise is greater in the transition region than in the normal state and exhibits a peak at the same temperature as the peak in $(dR/dT)^2$, but a thermal fluctuation model underestimates the noise by many orders of magnitude. No current noise is measurable in the superconducting state. The granular nature of the ceramic is important in that samples with smaller grains and more grain-grain contacts show greater noise.

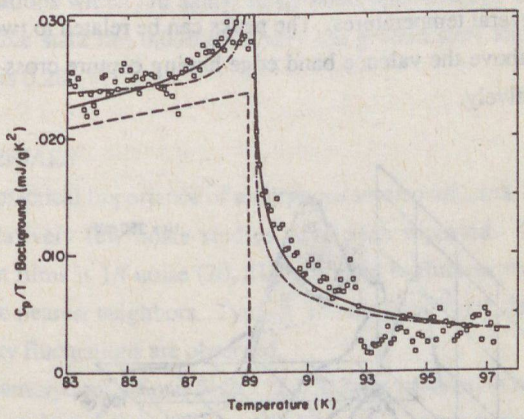

Figure 2. Comparison of experimental specific heat data with BCS theory supplemented by critical fluctuation contributions for 3D (solid curve) and 2D (dash-dot curve) behavior. From reference (10).

Other noises in high temperature superconductors include detection of highly energetic spin fluctuations by light scattering (13). The spin excitations are correlated with carrier concentration as adjusted by altering the oxygen content. Magnetic flux noise is detected in $Y_1Ba_2Cu_3O_{7-x}$ thin film rings using a dc SQUID (14). The noise spectrum is 1/f noise and the magnitude depends upon the microstructure of the film.

NOISE SPECTROSCOPY IN SOLIDS

Carrier trapping transitions lead to characteristic features in current noise power spectra which can be used to identify discrete trap levels in semiconductors. For example,

if a noise power spectrum is a combination of 1/f noise and a single Lorentzian,

$$S(f) = \frac{A}{f} + \frac{B\tau}{1+(2\pi f\tau)^2} \tag{3}$$

where A and B are constants and τ is a characteristic time. Properties of the second term can be extracted from the total spectrum by plotting fS(f) vs. f since, from Eq. (3),

$$fS(f) = A + \frac{B\tau f}{1+(2\pi f\tau)^2} \tag{4}$$

and the 1/f noise contribution appears as only an additive constant. This approach is referred to as noise spectroscopy.

The technique has been applied to boron-doped silicon polycrystalline thin films (15) under experimental conditions such that noise processes within the grains dominate over grain boundary effects. Typical noise spectra plotted in accordance with Eq. (4) are shown in Fig. 3 for several temperatures. The peaks can be related to two deep trap levels at 0.05 and 0.20 eV above the valence band edge having capture cross sections of 10^{-19} and 10^{-17} cm^2, respectively.

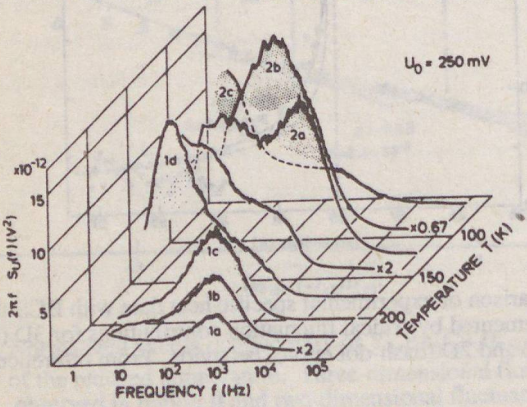

Figure 3. Noise spectroscopy analysis of p-type silicon films. From reference (15).

In coarse-grained films, and for applied voltages such that the average potential drop across a grain-grain boundary exceeds the potential barrier at the boundary, carrier transitions at grain boundary states dominate the noise (16). It proves possible to account for the measured 1/f noise in terms of spatial potential fluctuations at the interfaces caused by a random distribution of grain boundary defects. Noise spectrographic analysis shows a broad peak indicating a distribution of characteristic time constants. The extent of the 1/f

slope of the noise power spectra extends from one decade in frequency for a silicon bicrystal to three decades for a coarse-grained polycrystal.

Deep trap levels at 0.37 and 0.47 eV with capture cross sections of 4×10^{-16} and 7×10^{-15} cm^2 respectively are found from the low frequency noise spectra of n-type InGaAs at different temperatures (17). Similar trap depths are found in A1GaAs/GaAs heterostructures (18) with, however, much greater capture cross sections, 5×10^{-14} and 2×10^{-13} cm^2. By assuming that the traps are located within the surface depletion region, concentrations are determined to be about $10^{17} cm^{-3}$ for both traps.

Below a 145°K phase transition, electrical conductivity in Mo_2S_3 can be described by a double-well potential model in which carriers can exist in either a weakly-conducting ground state or a more highly-conducting metastable state. Transitions between states lead to conductivity fluctuations which are analyzed by noise spectroscopy (19). The results show that the metastable state lies 0.026 eV above the ground state and that the energy barrier between states is 0.28 eV.

AMORPHOUS MATERIALS

In spite of the practical importance of amorphous semiconductors, most particularly silicon thin films, relatively few noise studies have been reported. Current noise in amorphous silicon thin films is 1/f noise (20, 21) attributed to fluctuations in the phonon-assisted hopping rate to nearest neighbors. Typical values, 5×10^{-2}, for the Hooge constant associated with mobility fluctuations are observed.

Hydrogenated amorphous silicon films (21, 22) have Lorentzian noise spectra with a characteristic turnover frequency of about 100 Hz. This arises from a characteristic trapping time associated with a narrow band of states near the Fermi level. The analysis yields the density of states at the Fermi level, which is $1.5 \times 10^{16} cm^{-3} eV^{-1}$ for intrinsic samples and $3.5 \times 10^{19} cm^{-3} eV^{-1}$ for a n-type sample. The latter figure is in good agreement with the density of active donors expected from the doping level. The Lorentzian character of the spectrum was first noted in hydrogenated amorphous silicon resistors (22).

Tunnel junctions of amorphous silicon and hydrogenated amorphous silicon thin films can be made small enough in area ($100 \mu^2$) so that transitions to individual electron traps can be observed (24) at low temperatures. The result is a telegraph noise signal from which the trapping kinetics can be obtained. The measurements are consistent with a model in which the energy of the trap state shifts with electron occupancy, possibly the result of two different ionic spatial configurations. The number of trapping noise sources is essentially the same for hydrogenated and nonhydrogenated films. Recently, telegraph noise signals have been observed in large area junctions as well (25). This is explained by assuming that the junction current is confined to microchannels ($<1 \mu m^2$) and that individual traps control current in the channels.

Large conductance fluctuations are reported at the annealing temperature of doping modulated hydrogenated amorphous silicon multilayers (26).

SUPERIONIC CONDUCTORS

The superionic conductor Naβ″alumina is a solid electrolyte with room temperature conductivity typical of semiconductors and with essentially zero electronic conductivity. Conduction results from the high mobility of the sodium ions and it turns out that the sodium ions can easily be replaced in the structure by other mono- or di-valent ions (27).

Current noise in these superionic conductors is observed using liquid electrodes containing the same mobile ion species as in the solid electrolyte. Initial low frequency contact noise attributed to ionic shot noise at the electrode/electrolyte interface during the buildup of an electric double layer (28) decays away so that low-noise contacts are achieved after ageing for several hours. Nyquist noise pertaining to the conductivity of the bulk electrolyte is observed at frequencies above about 10 Hz.

Conductivity fluctuations in sodium (29), silver (30) and lead (31) β″alumina ceramics and single crystals result from diffusion noise of the mobile ions, since measured noise power spectra vary as $f^{-3/2}$ and the noise magnitude increases as the square of the current. The standard expression for the noise voltage spectral density, S(V, f, T), arising from diffusion can be written (32)

$$\frac{S(V,f,T)}{V^2} = \frac{4}{N}\left[\frac{D}{2L^2}\right]^{1/2} \omega^{-3/2} \qquad (5)$$

where N is the number of diffusing entities, D is the diffusion constant, L is the sample length, T is the temperature, V is the applied voltage and ω is the angular frequency. This expression is valid above a characteristic frequency given by $2D/L^2$ and Poisson statistics are assumed.

The noise level predicted by Eq. (5) is many orders of magnitude smaller than observed experimentally for all mobile ion species if N is taken to be the known concentration of mobile ions, about 10^{21} cm^{-3}. This discrepancy is attributed to ordering and correlation effects between the mobile ions, since the derivation of the standard expression assumes independent diffusing entities. Diffuse scattering x-ray structure analysis (33) confirms ordering that is a function of temperature. Correlation lengths range from 10 to 200°A and increase in the order Ag, Na, Pb.

It is convenient to compare experimental diffusion noise results for the different mobile ion species by computing an effective ion density using Eq. (5). The results, Fig. 4, indicate that the effective ion densities are slightly thermally activated ($\approx$ 0.1 eV) and that the different mobile ion species differ by many orders of magnitude.

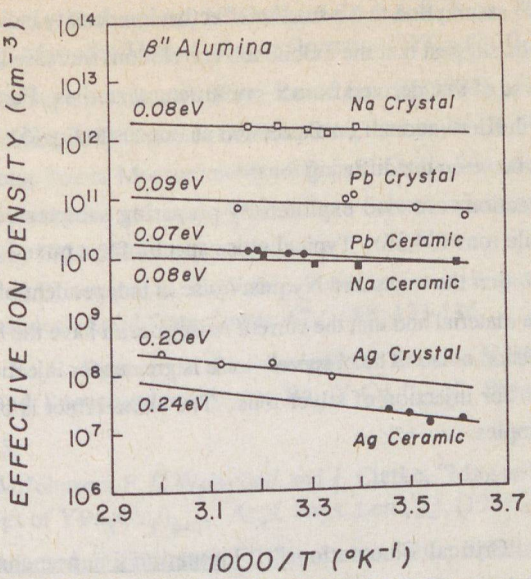

Figure 4. Calculated effective ion density for sodium, silver and lead β" alumina ceramics and single crystals.

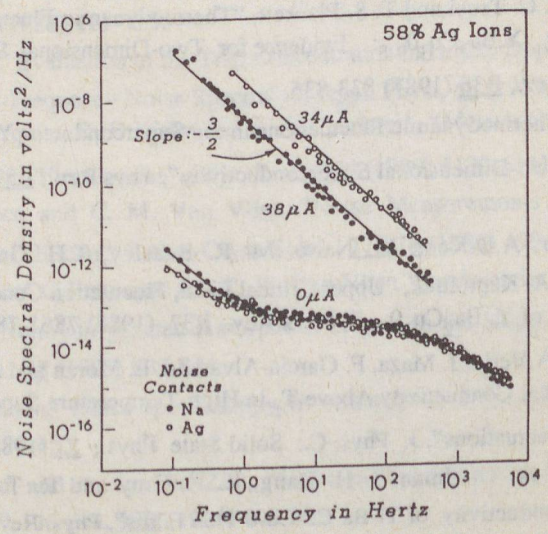

Figure 5. Nyquist and current noise spectra for a mixed Ag/Na β"alumina ceramic. From reference (35).

Under the rather crude assumption that a smaller effective ion density indicates increased ordering, these results suggest that the mobile ion correlations increase in the order Pb, Na, Ag, just the reverse of that derived from x-ray structural studies. Further quantitative interpretation awaits the derivation of an expression analogous to Eq. (5) that includes the effect of correlations between the diffusing ions.

Ion-ion interactions are also explored by preparing samples containing two (or more) different mobile ions (34,35). Typical noise spectra for a mixed Ag/Na β″alumina ceramic, Fig. 5, show that the measured Nyquist noise is independent of the ionic species in the liquid electrode material and that the current noise spectra have the $f^{-3/2}$ slope characteristic of diffusion noise. The observed noise is greater for injection of sodium ions into the mixture than for injection of silver ions. The same effect is observed in mixed Ca/Na β″alumina samples.

REFERENCES

1. A. Münster, "Critical Fluctuations", Fluctuation Phenomena in Solids, R.E. Burgess (ed), Academic Press Inc., New York (1965) 180-264.
2. N. G. Van Kampen, Stochastic Processes in Physics and Chemistry, North-Holland Publishing Co., Amsterdam (1981) 323-326.
3. W. J. Skocpol and M.Tinkham, "Fluctuations Near Superconducting Phase Transitions", Rep. Prog. Phys., 38 (1975) 1049-1097.
4. P. P. Freitas, C. C. Tsuei and T. S. Plaskett, "Thermodynamic Fluctuations in the Superconductor $Y,Ba_2Cu_3O_{9-\delta}$: Evidence for Two-Dimensional Superconductivity", Phys. Rev., B36 (1987) 833-835.
5. M. Ausloos, "Thermodynamic Fluctuations in the Superconductor $Y,Ba_2Cu_3O_{9-y}$: Evidence for Two-Dimensional Superconductivity", Phys.Rev., B37 (1988) 611-614.
6. B. Oh, K.Char, A.D.Kent, M. Naito, M. R. Beasley, T.H. Geballe, R. H. Hammond and A. Kaptulmik, "Upper Critical Field, Fluctuation Conductivity, and Dimensionality of Y, $Ba_2Cu_3O_{7-x}$", Phys. Rev., B37, (1988) 7861-7864.
7. Felix Vidal, J. A.Veria, J. Maza, F. Garcia-Alvarado, E. Moran and M. A. Alario, "Excess Electrical Conductivity Above T_c in High-Temperature Superconductors, and Thermal Fluctuations", J. Phys. C.: Solid State Phys., 21 (1988) L99-L606.
8. F. H. Kim, A. M. Goldman, J. H. Kang, K. E. Gray and R. T. Kampwirth, "Fluctuation Conductivity of Tl-Ba-Ca-Cu-0 Thin Films", Phys. Rev. 39, (1989) 12,275-12,278.
9. G.Balestrino, A. Nigro, R. Vaglio, and M. Marinelli, "Thermodynamic Fluctuations in the 110-K Bi-Sr-Ca-Cu-0 Superconductor: Evidence for Two-Dimensional Behavior," Phys. Rev., B39 (1989) 12,264-12,266.

10. S. E. Inderhees, M. B. Salamon, N. Goldenfield, J. P. Rice, B. G. Pazol and D. M. Ginsberg, "Specific Heat of Single Crystals of $YBa_2Cu_3O_{7-x}$: Fluctuation Effects in a Bulk Superconductor", Phys. Rev. Lett., 60 (1988) 1178-1180.

11. J. A.Testa, Yi Song, X.D.Chen, J. Golben, Sung-Ik Lee, B. R. Patton and J. R. Gaines, "1/f Noise Power Measurements of Copper Oxide Superconductors in the Normal and Superconductors in the Normal and Superconducting States", Phys. Rev., B38 (1988) 2922-2925.

12. B. W. Ricketts, R.Driver and H. K. Welsh, "Low Frequency Excess Noise in Bulk $YBa_2Cu_3O_7$ Samples", Solid State Comm. 67 (1988) 133-136.

13. K. B. Lyons, P. A. Fleury, L. F. Schneemyer and J. V. Waszcak, "Spin Fluctuations and Superconductivity in Ba_2 Y Cu_3O_{6+x}", Phys. Rev. Lett.,60 (1988) 732-735.

14. M. J. Ferrari, M.Johnson, F. C.Wellstood and J. Clarke, "Magnetic Flux Noise in Thin-Film Rings of $YBa_3Cu_3O_{6+x}$," Appl. Phys. Lett., 53, (1988) 695-697.

15. A. J. Madenach and J. H.Werner, "Deep-Level-Noise Spectroscopy of Ion-Implanted Polysilicon Thin Films," Phy. Rev.,B38, (1988) 1958-1962.

16. A. J. Madenach and J. H. Werner, "Noise Spectroscopy of Silicon Grain Boundaries", Phys. Rev.,B38 (1988) 13150-13162.

17. S.Kugler, K.Steiner, U.Seiler and K. Heime, "Low-Frequency Noise Measurements on n-InGaAs/InP Junction Field-effect Transistor Structures," Appl. Phys. Lett., 52, (1988) 111-113.

18. S. Kugler, "Evaluation of the Trap Concentration in Highly Doped Semiconductors from Low-Frequency Noise Spectra", J. Appl. Phys., 66 (1989) 219-222.

19. R. L.Fagerquist, R. D.Kirby and E. A. Pearlstein, "Metastable States in Mo_2S_3: Conductivity Fluctuations", Phys. Rev., B39 (1989) 5139-5151.

20. A.D'Amico and C. M. Van Vliet, "Noise Measurements in Thin Films of Amorphous Silicon", J. Non-Cryst. Solids, 77&78 (1985) 499-502.

21. A. D'Amico, G.Fortunato and C. M. Van Vliet,"Conductivity and Noise in Thin Films of Nonhydrogenated Amorphous Silicon in the Hopping Regime", Solid State Elec., 28 (1985) 837-844.

22. J.C. Anderson, "Noise Spectroscopy in Amorphous Silicon Films", Phil. Mag., B (1983) 31-45.

23. S. K. Kim and A. van der Ziel, "Noise in Hydrogenated Amorphous Silicon Resistors", Physica, 98B (1980) 303-305.

24. C.T. Rogers, R. A. Buhrman, H.Kroger and L.N.Smith, "Characterization of Individual Electron Traps in Amorphous Si by Telegraph Noise Spectroscopy", Appl. Phys. Lett.,49 (1986) 1107-1109.

25. R. Arce and L. Ley, "Observation of Random Telegraph Noise in Large Area a-Si: H/a-$Si_{1-x}N_x$:H Double Barrier Structures", Mat. Res. Soc. Symp. Proc., 119 (1989).

26. H. Fitzsche, S. H. Yang and J. Takada, "Metastable Non-Equilibrium Conductance States in Doping-Modulated a-Si:H Multilayers", Mat. Res.Soc. Symp. Proc., 118 (1988) 257-284.

27. G. C. Farrington and B. Dunn, "Divalent Beta″-Aluminas: High Conductivity Solid Electrolytes for Divalent Cations", Solid State Ionics, 7 (1982) 267-281.

28. C. K. Kuo and J. J.Brophy, "The Kinetics of Contact Noise of Naβ″Alumina", J. Appl. Phys., 65 (1989) 3484-3486.

29. J. J. Brophy and S. W.Smith, "Current Noise in Sodium β″Alumina Ceramic", J. Appl. Phys., 58, (1985) 351-354.

30. J. J. Brophy, "Current Noise in Silver β″Alumina Ceramics and Single Crystals", J. Appl. Phys., 61, (1987) 581-584.

31. J. J. Brophy, "Noise in Lead β″Alumina", Noise in Physical Systems, C. M. Van Vliet (ed), World Scientific Publishing Co., Singapore, (1987) 307-310.

32. K. M. Van Vliet and J. R.Fassett, "Fluctuations Due to Electronic Transitions and Transport in Solids", Fluctuation Phenomena in Solids, R. E. Burgess (ed), Academic Press, Inc., New York (1965) 268-351.

33. G. Collin, J. P. Boilot, Ph. Colomban and R. Comes, "Host Lattices and Superionic Properties in β- and β″−Alumina. I. Structures and Local Correlations", Phys. Rev., B34, (1986) 5838-5860.

34. C. K. Kuo and J. J. Brophy, "Conductivity Fluctuations in Mixed Sodium/Cadmium β″-Alumina", submitted to Solid State Ionics.

35. J. J. Brophy, "Current and Thermal Noise in Mixed Na/Ag β″-Alumina", to be published.

10th Int. Conf. on Noise in Physical Systems
1989 Budapest, Hungary

DIFFUSION NOISE IN SODIUM BETA ALUMINA

J.J. BROPHY

Department of Physics, University of Utah
Salt Lake City, Utah 84112, USA

INTRODUCTION

Conductivity fluctuations associated with diffusion noise of the mobile sodium ions have been observed in ceramic (1) and single crystal (2) Naβ″alumina. The measured noise levels are similar in both materials and are much larger than predicted by the standard theory of diffusion noise (3), which is attributed to correlation effects between the mobile ions. These correlation effects are expected to be stronger in Naβalumina compared to the β″ structure, but preliminary results on ceramic specimens of Naβalumina indicate that the noise levels are about the same (4). This work reports experimental measurements of diffusion noise in single crystal Naβ″alumina.

EXPERIMENTAL TECHNIQUE

The four corners of single crystal platelets of melt-grown Naβalumina (5) 0.5 x 0.5 x 0.05 cm^3 are sealed into plastic test tubes containing a 0.5 M solution of NaI in propylene carbonate to provide longitudinal current contacts and transverse noise contacts. Noise spectra at the transverse contacts are measured with a PAR 113 amplifier and a digital FFT analyzer.

The NaI solution yields low-noise contacts after aging for several hours (6) and Nyquist noise of the sample bulk resistance can be observed at frequencies above about 100 Hz, Fig. 1. Room temperature conductivity determined from Nyquist noise measurements is $1.5 \times 10^{-3}(\text{ohm-cm})^{-1}$, somewhat smaller than literature values (7), whereas the thermal activation energy, 0.17 eV, is in satisfactory agreement. The current noise spectra vary as $f^{-3/2}$, characteristic of diffusion noise (3) and increase as the square of the current.

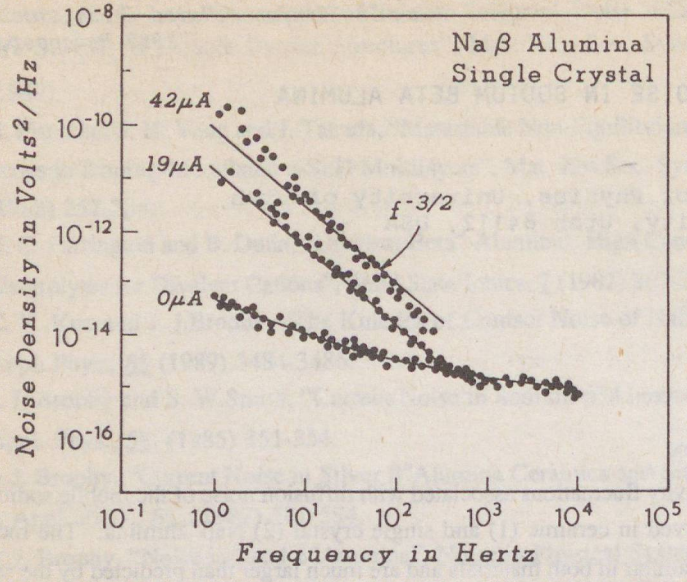

Figure 1. Nyquist and current noise spectra of a Naβalumina single crystal.

DISCUSSION

The observed current noise levels are thermally activated with an activation energy of 0.4eV, somewhat smaller than Naβ″alumina (2), and are much larger than that predicted by the standard expression for diffusion noise (3),

$$\frac{S(V,f,T)}{V^2} = \frac{2}{N}\left[\frac{2D}{L^2}\right]^{1/2} \omega^{-3/2} \qquad (1)$$

where S(V,f,T) is the spectral noise density, V is the applied dc voltage, N is the number of diffusing ions, D is the diffusion constant, L is the sample length, ω is the angular frequency, and Poisson statistics are assumed. Equation (1) applies above a critical angular frequency given by $L^2/2D$ and is derived on the basis of independent diffusing entities. The discrepancy between Eq.(1) and experimental data is attributed to correlations between the diffusing ions which lead to a smaller effective value of N than the known number of sodium ions given by the chemical composition of Naβalumina. This is similar to Naβ″alumina results.

The standard expression, Eq. (1), may be used to calculate an effective value of N in order to compare measurements from Naβalumina with those from Naβ″alumina. As shown in Figure 2, the calculated effective ion density is significantly smaller in the case of the β form compared to the β″ structure and both are very much smaller than the chemical

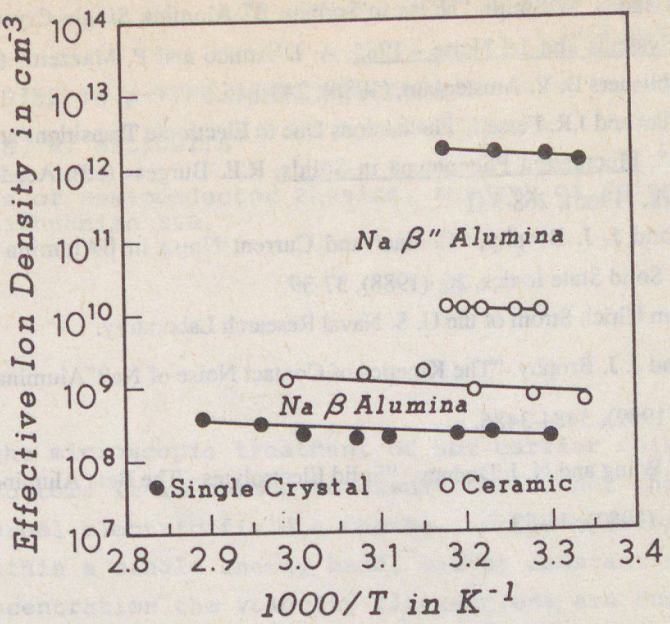

Figure 2. Calculated effective ion density for ceramic and single crystal Naβalumina and Naβ″alumina.

density, about 10^{21}ions/cm^3. The agreement between ceramic and single crystal samples is satisfactory in Naβalumina but less so for Naβ″alumina.

The lower value of the effective ion density for Naβalumina is consistent with increased ion-ion correlation effects characteristic of the β crystalline structure compared to the β″ form. A more quantitative interpretation awaits the development of an analytical treatment of diffusion noise that includes correlation effects.

ACKNOWLEDGMENT

The author is deeply grateful to Dr. Chu Kun Kuo who made many of the experimental measurements, to Dr. Ulrich Strom who supplied the Naβalumina single crystals, and to the Office of Naval Research for support of the research in part.

REFERENCES

[1] J. J. Brophy and S. W. Smith, "Current Noise in Sodium β″ Alumina Ceramics", J. Appl. Phys., 58, (1985), 351-354.

[2] J. J. Brophy and S. W.Smith, "Noise in Sodium β″ Alumina Single Crystals", Noise in Physical Systems and 1/f Noise - 1985, A. D'Amico and P. Mazzetti (eds), Elsevier Science Publishers B. V. Amsterdam, (1986), 243-246.

[3] K. M. VanVliet and J.R. Fassett,"Fluctuations Due to Electronic Transitions and Transport in Solids", Fluctuation Phenomena in Solids, R.E. Burgess (ed), Academic Press Inc., New York, (1965), 268-351.

[4] C. K. Kuo and J. J. Brophy, "Contact and Current Noise in βAlumina and Nasicon Ceramics", Solid State Ionics, 26, (1988), 37-39.

[5] Obtained from Ulrich Strom of the U. S. Naval Research Laboratory.

[6] C. K. Kuo and J. J. Brophy, "The Kinetics of Contact Noise of Naβ″Alumina", J. Applied Phys., 63, (1989), 3484-3486.

[7] J. Bates, J. C.Wang and N. J. Dudney, "Solid Electrolytes - The Beta Aluminas", Physics Today, July, (1982), 46-53.

10th Int.Conf. on Noise in Physical Systems
1989 Budapest, Hungary

TUNNEL NOISE IN p-TYPE SEMICONDUCTORS

A. DARGYS, R. MILIUŠYTĖ

Institute of Semiconductor Physics, Academy of Sciences
of the Lithuanian SSR,
Vilnius

In the microscopic treatment of hot carrier noise in bulk semiconductors it is common to assume that under the action of the external electric field a charge carrier between collisions moves within a single energy band, and at constant charge carrier concentration the velocity fluctuations are due to intraband and interband carrier collisions with lattice imperfections. If energy bands are close enough, as for example near the degeneracy point of the valence band of the covalent semiconductors, a new noise source, which will be called tunnel noise, will appear. As shown in (1, 2), the external electric field mixes up the wavefunctions of light (l) and heavy (h) mass bands and, as a result, hole intervalence tunnelling transitions become important if hole trajectory passes near the degeneracy point. Due to the intervalence tunnelling the hole velocity between collisions will assume more complicated character. Below, with the help of the Monte Carlo method, the contribution of the intervalence tunnelling has been evaluated in p-type germanium.

In Fig. 1 the solid curves demonstrate the time dependence of the hole velocity component parallel to the electric field (E = 11 kV/cm) in the limit of zero spin-orbit interaction (3). At the moment t = 0 the hole is in the heavy mass band and has the following wavevector components perpendicular and parallel to $\vec{E}$: $(k_{\perp 0}, k_{\parallel 0}) = (a,-a); (a, 0); (a, a)$ for curves 1, 2 and 3, respectively; $a = 1.89 \cdot 10^6$ cm^{-1}. The l- and h-bands are considered to be parabolic and spherical with the effective masses

$m_h = 0.34\ m_0$, $m_l = 0.05\ m_0$. For comparison, the velocity in the absence of tunnelling, $v_\parallel = eEt/m_h$, is plotted by dashed curve too. The case of infinite spin-orbit interaction was considered in (4). Since the general character of the dependence of the velocity on the electric field and time is similar in both cases, in the Monte Carlo calculations the formulas for the simpler one, i.e. when spin-orbit interaction is neglected, have been used.

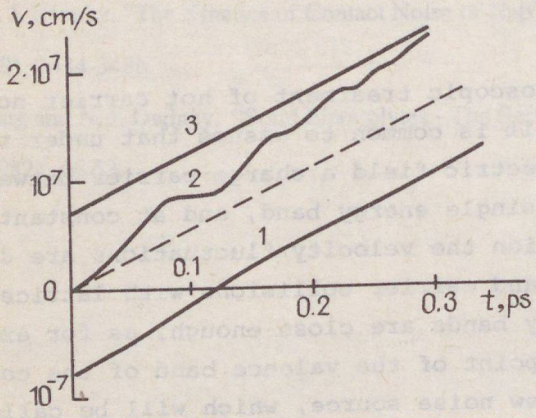

Fig. 1. Hole velocity in the presence (solid lines) and absence (dashed line) of the intervalence tunnelling

At not too high electric fields the curves in Fig. 1 can be approximated by the following formula (3):

$$v_\parallel = (k_{\parallel 0} - Et)\left[\frac{1}{m_h} + \left(\frac{1}{m_l} - \frac{1}{m_h}\right) P_{12}(t)\right], \tag{1}$$

$$P_{12}(t) = \Theta^2 \left\{\frac{1}{(Z^2+1)^4} + \frac{1}{(Z_0^2+1)^4} - \frac{2\cos\left[\frac{1}{\Theta}\left(\frac{Z^3-Z_0^3}{3} + Z - Z_0\right)\right]}{(Z^2+1)^2 (Z_0^2+1)^2}\right\}, \tag{2}$$

where $\Theta = 2eE/[\hbar^2 (m_l^{-1} - m_h^{-1}) k_{\perp 0}^3]$ is tunnelling constant, $Z = (k_{\parallel 0} - Et)/k_{\perp 0}$, $Z_0 = k_{\parallel 0}/k_{\perp 0}$, $k_{\parallel 0}$ and $k_{\perp 0}$ are parallel and perpendicular to the electric field E wavevector components at the the moment t = 0. From Eqs (1) and (2) and Fig. 1 one can see

that the inclusion of the intervalence band tunnelling yields two new effects: (i) the damped fast velocity oscillations with the variable frequency due to hole tunnelling to and from the light mass band (the last term in Eq. (2)); (ii) the increment in the hole acceleration after the hole has passed the region near the point $\vec{k} = 0$, where tunnelling is most pronounced.

We have calculated the spectral densities of velocity fluctuations, S and S_t, when intervalence tunnelling is absent and present, respectively, by the Monte Carlo method (5) at the lattice temperature 77 K and for parameter values typical of spherical bands of Ge. Only (instantaneous) scattering on acoustic and optical vibrations were included. The population of 1-band has been neglected, however, in calculating the hole velocity autocorrelation function the tunnelling to 1-band between collisions was taken into account with the help of Eqs (1) and (2). Since 1-band population makes up about 6% of the total population, the error due to this approximation is expected to be small.

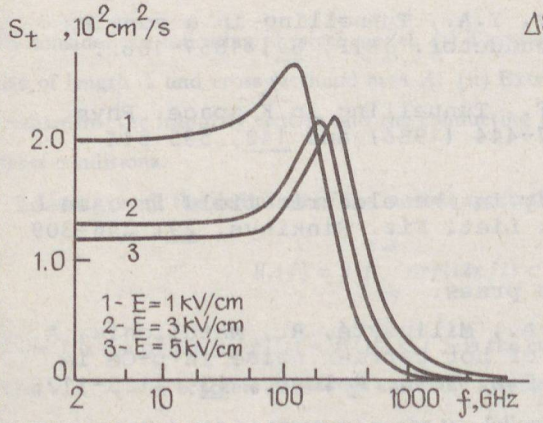

Fig. 2. Spectral density of velocity fluctuations at three values of the electric field E

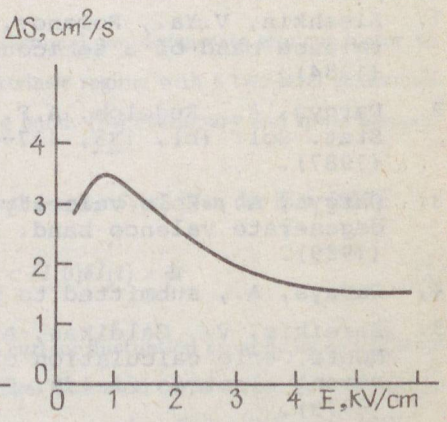

Fig. 3. Increment in spectral density at low frequencies due to intervalence tunnelling as a function of electric field

Figure 2 shows the parallel to the electric field spectral density of velocity fluctuations, S_t, for three values of the electric field. The contribution of tunnel noise, $\Delta S = S_t - S$, at frequencies smaller than 10 GHz is shown in Fig. 3. The form of ΔS is conditioned by two competing processes: (i) the increase of the tunnelling probability with E and (ii) the decrease of the number of holes in the region of the degeneracy point, where tunnelling is most effective, due to hot carrier effects. It has been found that in the considered frequency range the main contribution to ΔS comes from the first two terms in Eq. (2), i.e. from the increment in the acceleration. In p-Ge the contribution of the tunnel noise to the total noise, as seen from Fig. 2 and Fig. 3, is small and does not exceed a few percents. However, in the materials, for example p-ZnSe and ZnTe, for which the distance between l- and h-bands is smaller in a larger portion of the Brillouin zone, the tunnel noise contribution to S is expected to be larger by an order of magnitude.

REFERENCES

1. Aleshkin, V.Ya., Romanov, Y.A., Tunnelling in a complex valence band of a semiconductor. JETP, 87, 1857-1862. (1984).
2. Dargys, A., Rudolph, A.F., Tunnelling in $\vec{K}$-space. Phys. Stat. Sol. (b), 135, 437-444 (1986) and 140, 535-544 (1987).
3. Dargys, A., Hole velocity in the electric field in case of degenerate valence band. Liet. Fiz. Rinkinys, 29, 298-309 (1989).
4. Dargys, A., submitted to press.
5. Bareikis, V., Galdikas, A., Miliušytė, R., Matulionis, A., Monte Carlo calculation of hot carrier noise in p-Ge in strong electric fields. Fiz. Tekn. Polupr., 13, 1123-1126 (1979).

10th Int.Conf. on Noise in Physical Systems
1989 Budapest, Hungary

THE MONTE CARLO METHOD FOR THE MICROSCOPIC INTERPRETATION OF ELECTRONIC NOISE IN SEMICONDUCTORS

L. REGGIANI, L. VARANI

Dipartimento di Fisica e Centro Interuniversitario
di Struttura della Materia, Università di Modena
41100 Modena, Italy

1. INTRODUCTION

The Monte Carlo (MC) method, by providing a microscopic simulation of charge transport in a given physical system, offers a unique theoretical approach to investigate different sources of noise and corresponding spectral densities. In particular, by giving an exact solution of the appropriate master equation for any strength of the applied electric field, this method applies to ohmic as well as to non-ohmic (hot-electron) conditions. In this paper we present the theory underlying the application of the MC method and provide new calculations for the case of p-Si.

2. THEORY AND RESULTS

We consider the following physical model. (i) Two-terminal non-degenerate semiconductor device of length L and cross-sectional area A. (ii) Extrinsic regime with a two-level conduction mechanism, the impurity centers and the conducting band. (iii) Stationary and space homogeneous conditions.

Let us recall the definition of the current spectral density $S_I(f)$ [Van der Ziel, 1970]:

$$S_I(f) = 2\int_{-\infty}^{\infty} exp(i2\pi ft) < \delta I(0)\delta I(t) > dt \tag{1}$$

where f is the frequency, $\delta I(t) = I(t) - < I >$ is the current fluctuation around the steady state value $< I >$, and brackets denote an ensemble average. The total current $I(t)$, as measured in the outside circuit, can be expressed in the two following equivalent forms [Pellegrini, 1986]:

$$I(t) = \frac{e}{L} N_I v_d^r(t) = \frac{e}{L} N(t) v_d(t) \tag{2}$$

where e is the modulus of the electron charge, N_I is the total number of traps, $v_d^r(t) = \frac{1}{N_I}\sum_{i=1}^{N_I} v_i(t)$ is the reduced carrier drift velocity (which accounts for the time spent by the carriers on the impurities, the so-called trapping time), $N(t)$ is the number of carriers in the

conducting band (free carriers), and $v_d(t) = \frac{1}{N(t)} \sum_{i=1}^{N(t)} v_i(t)$ is the free carriers drift velocity (which neglects the trapping time).

The last expression on the right-hand side of Eq. (2) lends itself to an exact decomposition of $S_I(f)$ in terms of different noise sources. Indeed, from Eq. (2) $S_I(f)$ can be given the two following equivalent expressions [Reggiani et al, 1988]:

$$S_I(f) = \frac{2e^2}{L^2} N_I \int_{-\infty}^{\infty} exp(i2\pi ft) < \delta v_d^r(0) \delta v_d^r(t) > dt \qquad (3a)$$

$$S_I(f) = S_{Ivd}(f) + S_{Igr}(f) + S_{Icr}(f) \qquad (3b)$$

where

$$S_{Iv_d}(f) = \frac{2e^2}{L^2} < N >^2 \int_{-\infty}^{\infty} exp(i2\pi ft) < \delta v_d(0) \delta v_d(t) > dt \qquad (4)$$

$$S_{Igr}(f) = \frac{2e^2}{L^2} < v_d >^2 \int_{-\infty}^{\infty} exp(i2\pi ft) < \delta N(0) \delta N(t) > dt \qquad (5)$$

$$S_{Icr}(f) = \frac{2e^2}{L^2} < N >< v_d > \int_{-\infty}^{\infty} exp(i2\pi ft)[< \delta N(0) \delta v_d(t) > + < \delta v_d(0) \delta N(t) >]dt \qquad (6)$$

As seen from Eq. (3b), the total spectral density S_I is decomposed into the sum of three terms which are related respectively to fluctuations in free carrier drift velocity (S_{Iv_d}), number (S_{Igr}), and correlation between number and drift velocity (S_{Icr}). For the isotropic case here considered S_I and S_{Iv_d} have a longitudinal and a transverse component with respect to the electric field. From their definition in terms of correlation functions (see Eqs. 5,6) it appears that S_{Igr} and S_{Icr} have only the longitudinal component and are proportional to $< v_d >^2$ and $< v_d >$, respectively. Therefore, they describe excess noise and, as expected, vanish at equilibrium and/or when the noise is measured in a direction perpendicular to the applied field. Clearly, S_{Igr} and S_{Icr} are identically zero when in steady-state the traps are fully ionized, since it implies $\delta N(t) = 0$. We notice that, when two particle interaction is neglected, it is:

$$< \delta v_d(0) \delta v_d(t) >=< \delta v(0) \delta v(t) > / < N > \; ; \; < \delta N(0) \delta N(t) >=< \delta u(0) \delta u(t) >< N > \qquad (7)$$

where $v(t)$ is the instantaneous velocity of the single carrier and $u(t)$ is the random telegraph signal: $u(t) = 1$ when the particle is free and $u(t) = 0$ when the particle is trapped.

The MC method, by providing an exact solution of the appropriate master equation describing the problem at end, represents the most up-dated method to evaluate the different correlation functions entering the noise spectral density of Eqs. (3-6). Previous efforts have succeeded in interpreting noise data in Si in the absence of trapping phenomena [Reggiani et al, 1981], with and without carrier-carrier scattering [Lugli and Reggiani, 1985] and, recently, in the presence of trapping phenomena [Reggiani et al, 1987b]. Here we extend this last result by evaluating the frequency dependent spectrum for the case of p-type Si at 77 K when carrier-carrier interaction is neglected. The details of the numerical calculation and of the microscopic model are reported by Reggiani et al.(1987a).

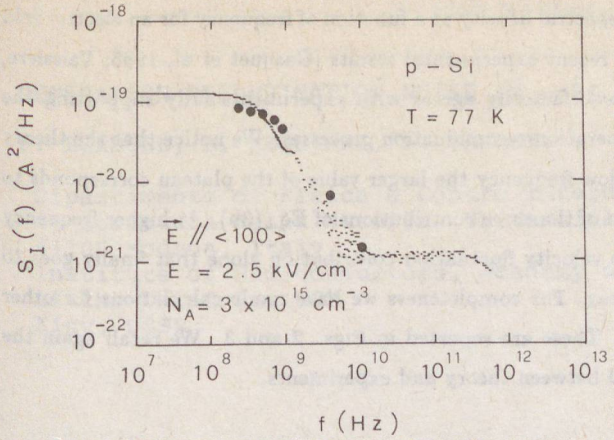

Fig. 1 - Direct Monte Carlo output of the current spectral density in the direction of the electric field as a function of frequency for the case of holes in Si at 77 K with an acceptor concentration $N_A = 3 \times 10^{15}\ cm^{-3}$, $L = 1.5\ cm$ and $A = 3.0 \times 10^{-3}\ cm^{-2}$. Full circles represent experimental results [Gasquet et al, 1985; Vaissiere, 1986].

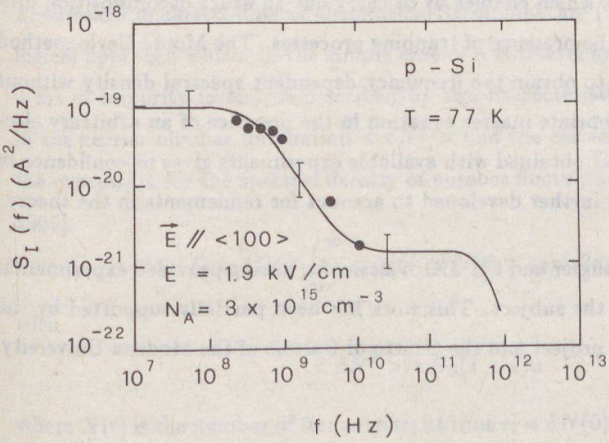

Fig. 2 - Current spectral density in the direction of the electric field $E = 1.9\ kV/cm$ as a function of the frequency for the case of holes in Si at 77 K with an acceptor concentration $N_A = 3 \times 10^{15}\ cm^{-3}$, $L = 1.5\ cm$ and $A = 3.0 \times 10^{-3}\ cm^{-2}$. The curve reports Monte Carlo calculations with bar indicating uncertainties. Full circles represent experimental results [Gasquet et al, 1985; Vaissiere, 1986]

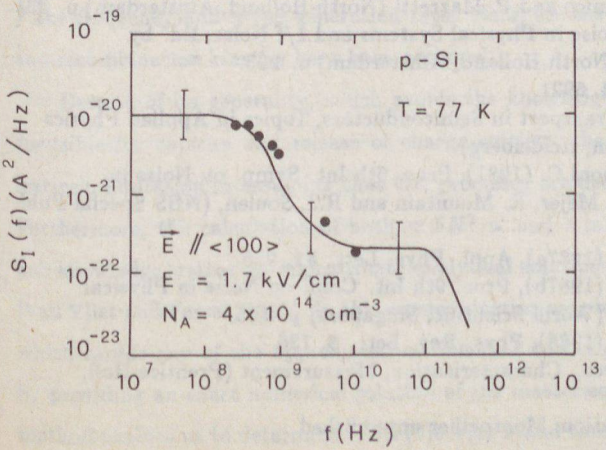

Fig. 3 - Current spectral density in the direction of the electric field $E = 1.7\ kV/cm$ as a function of the frequency for the case of holes in Si at 77 K with an acceptor concentration $N_A = 4 \times 10^{14} cm^{-3}$, $L = 1.5\ cm$ and $A = 3.0 \times 10^{-3}\ cm^{-2}$. The curve reports Monte Carlo calculations with bar indicating uncertainties. Closed circles represent experimental results [Gasquet et al, 1985; Vaissiere, 1986]

Figure 1 shows the theoretical spectral density as a function of frequency for an electric field $E = 2.5\ kV/cm$ as compared with recent experimental results [Gasquet et al, 1985, Vaissiere, 1986]. As it can be seen theory satisfactorily agrees with experiments fully supporting the microscopic model used to treat generation-recombination processes. We notice that the theory gives evidence of two plateaus. At low frequency the larger value of the plateau corresponds to the total noise coming from the sum of the three contributions of Eq. (3b). At higher frequency the second plateau comes from the velocity fluctuation contribution alone that finally goes to zero with the usual Lorentzian decay. For completeness we have made calculations for other fields and acceptor concentrations. These are reported in Figs. 2 and 3. We recall again the rather satisfactory agreement found between theory and experiments.

3. CONCLUSIONS

We have presented a general theory which enables us to carry out an exact decomposition procedure of different noise sources in the presence of trapping processes. The Monte Carlo method is shown to be a fruitful procedure to obtain the frequency dependent spectral density without approximations in solving the appropriate master equation in the presence of an arbitrary electric field. The satisfactory agreement obtained with available experiments gives us confidence in predicting that this method will be further developed to account for refinements in the theory.

Authors wish to thank Prof. J.P. Nougier and Dr. J.C. Vaissier for having provided experimental data and for helpful discussions on the subject. This work has been partially supported by the CEE ESPRIT II BRA 3017 NOISE project and the Centro di Calcolo of the Modena University.

REFERENCES

Gasquet D., Azais B., Vaissiere J.C. and Nougier J.P. (1985), Noise in Physical Systems and 1/f Noise, Ed. by A. D'Amico and P. Mazzetti (North-Holland, Amsterdam) p. 231.

Lugli P. and Reggiani L. (1986), Noise in Physical Systems and 1/f Noise, Ed. by A. D'Amico and P. Mazzetti (North-Holland, Amsterdam) p. 235.

Pellegrini B. (1986), Phys. Rev. **34**, 5921.

Reggiani L. (1985), Hot Electron Transport in Semiconductors, Topics in Applied Physics Vol. 58 (Springer-Verlag, Berlin, Heidelberg).

Reggiani L., Brunetti R. and Jacoboni C. (1981), Proc. 6th Int. Symp. on Noise in Physical Systems, Eds. P.H.E. Mejer, R. Mountain and R.J. Soulen, (NBS Special Publ. 614 Washington) p. 414.

Reggiani L., Lugli P. and Mitin V. (1987a), Appl. Phys. Lett. **51**, 925.

Reggiani L., Lugli P. and Mitin V. (1987b), Proc. 9th Int. Conf. on Noise in Physical Systems, Ed. C.M. Van Vliet, (World Scientific, Singapore) p. 105.

Reggiani L., Lugli P. and Mitin V. (1988), Phys. Rev. Lett. **8**, 736.

Van der Ziel A. (1970), Noise, Source, Characterization, Measurement (Prentice-Hall, New Jersey).

Vaissiere J.C. (1986), PhD Dissertation, Montpellier unpublished.

10th Int.Conf. on Noise in Physical Systems
1989 Budapest, Hungary

GENERATION-RECOMBINATION NOISE IN p-Si AT 77 K

P. BORDONE, L. REGGIANI, L. VARANI, V. MITIN*

Dipartimento di Fisica e Centro Interuniversitario
di Struttura della Materia, Università di Modena
41100 Modena, Italy
*Institute of Semiconductors, Academy of Sciences
of the Ukrainian SSR
Kiev, USSR

1. INTRODUCTION

Theoretical understanding of Generation-Recombination (GR) noise is based on a phenomenological approach which, in the simple case of a two-level system (e.g. the conducting band and a set of impurity levels), is described by two characteristic parameters: namely, the variance in the carrier number fluctuation $< \delta N^2 >$ and the carrier lifetime τ. These parameters enter the expression for the spectral density of number fluctuation, $S_{\delta N}(f)$, as [Van Vliet and Fasset, 1965]:

$$S_{\delta N}(f) \equiv 4Re\{ \int_0^\infty < \delta N(0)\delta N(t) > exp(i2\pi ft)\, dt \} = \frac{4 < \delta N^2 > \tau}{1 + (2\pi f\tau)^2} \qquad (1)$$

with

$$< \delta N^2 >= N_0(1-u)u \quad ; \quad \tau = \frac{u}{\gamma} \qquad (2)$$

where $N(t)$ is the number of free carriers at time t, $< \delta N(0)\delta N(t) >$ the autocorrelation function of number fluctuations, N_0 the total number of impurities, u the average fraction which is ionized, f the frequency and γ the generation rate. Here, for the sake of simplicity, linear generation and recombination kinetics have been assumed.

Despite of its generality, which avoids the knowledge of the microscopic mechanisms responsible for capture and release of charge carriers, the phenomenological approach has an intrinsic limitation in assuming that GR processes are decoupled from scattering mechanisms. Furthermore, the calculation of both $< \delta N^2 >$ and τ in terms of the kinetic, to the best of our knowledge, relies on approximate analytical solutions of the appropriate master equation [Van Vliet and Fasset, 1965]. In this communication we present a Monte Carlo (MC) simulation which avoids any of the approximations inherent to the phenomenological approach. Indeed, by providing an exact numerical solution of the master equation in momentum space, the MC method enables us to determine $< \delta N(0)\delta N(t) >$ and thus $S_{\delta N}(f)$. Accordingly, we can obtain

$< \delta N^2 >$, verify the eventual exponential decay of $< \delta N(0)\delta N(t) >$ and, in this case, calculate τ within quite general conditions. As an example we consider p-type Si at 77 K.

2. THEORY AND RESULTS

By definition, for the present system the correlation function of number fluctuations is:

$$< \delta N(0)\delta N(t) >= \sum_{i,j=1}^{N_0} < [u_i(0) - u][u_j(t) - u] >$$

$$= N_0 < \delta u_i(0)\delta u_i(t) > + \sum_{i \neq j=1}^{N_0} < \delta u_i(0)\delta u_j(t) > \qquad (3)$$

where $u_i(t)$ is the instantaneous state of a single carrier which can assume the two values 0 and 1 according to the cases when it is trapped or free, and $\delta u_i(t) = u_i(t) - u$.

The second term in the r.h.s. of Eq. (3) describes the cross correlations due to particle-particle interaction. In the present approach it will be neglected since this interaction will not be considered. The quantity $< \delta u_i(0)\delta u_i(t) >$ is evaluated in the standard way, as for the case of the velocity-fluctuations correlation function [Jacoboni and Reggiani 1983], by means of a MC simulation, within a stationary condition. More specifically, we consider a uniform semiconductor sample of cross-sectional area A and length L. In addition to the scattering mechanisms with phonons and ionized impurities, we introduce the GR processes within the cascade model assisted by acoustic phonons (the most relevant mechanism for the case at hand) taking $\gamma = 2.9 \times 10^9\ s^{-1}$ [Reggiani et al, 1989]. Then, the instantaneous value of $u_i(t)$ is recorded for a sampling time T_0 sufficiently long to detect the vanishing value of the correlation function (typically $T_0 \simeq 0.1 \mu s$). The average fraction of ionized carriers is finally determined from the ratio between the total time spent in the valence band and the total time of the simulation.

The results of the MC simulation are compared with those of the phenomenological approach in Figs. 1 and 2. We remark that the values of u have been determined under quite different conditions: e.g. by changing alternatively the acceptor concentration, the electric field strength, the lattice temperature and so on. As a general trend, we have found that the MC results well agree with the phenomenological approach for the case of $< \Delta N^2 >$. On the contrary, significant deviations occur for τ which exhibits values larger than predicted by the phenomenological approach. We ascribe these effects to the strong coupling between GR processes and scattering mechanisms which occur in the lowest energy region of the carrier energy-distribution function. Indeed, GR processes mostly occur below the 1 *meV* energy region, where the probability of capture exceeds that of scattering mechanisms thus coupling GR and scattering processes. This interpretation is supported by the fact that, at increasing field strengths, MC results get closer

MAGYAR TUDOMÁNYOS AKADÉMIA KÖNYVTÁRA

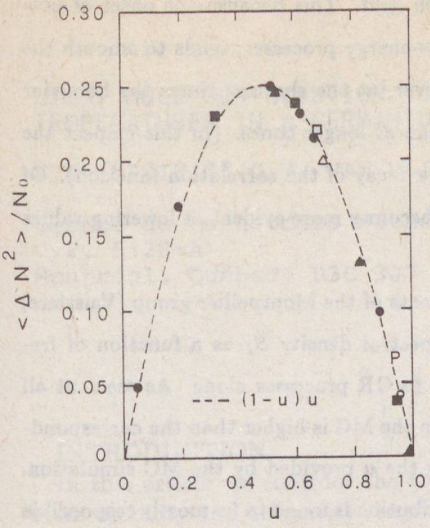

Fig. 1 - Values of $< \delta N^2 > /N_0$ as a function of the fraction of free carriers u in p-Si at 77 K. Symbols refer to MC simulations, dashed curve refers to the phenomenological approach.

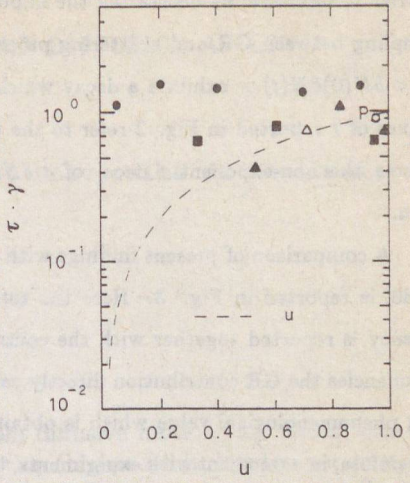

Fig. 2 - Values of $\tau\gamma$ as a function of the fraction of free carriers u in p-Si at 77 K. Symbols refer to MC simulations, continuous curve refers to the phenomenological approach.

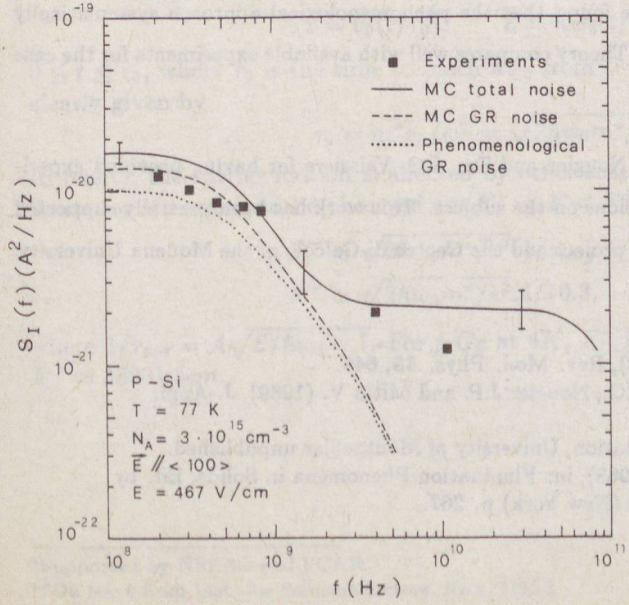

Fig. 3 - Spectral density of current fluctuation as a function of frequency for the case of p-Si at 77 K for an acceptor concentration $N_A = 3 \times 10^{15} cm^{-3}$ and an electric field $E = 467\ V/cm$. Continuous (dashed) curve reports the MC calculations for the total (GR) contributions, dotted curve refers to the results obtained for the GR contribution using the phenomenological approach. Points refer to experiments of the Montpellier group [Vaissiere, 1986].

to those of the phenomenological approach at the given field. This because the onset of hot-carrier phenomena, by decreasing the importance of low-energy processes, tends to smooth the coupling between GR and scattering processes. Moreover, at the shortest times the behavior of $< \delta N(0)\delta N(t) >$ exhibits a decay which is faster than at longer times. (In this respect the values of τ reported in Fig. 2 refer to the the long time decay of the correlation function). Of course, this non-exponential decay of $< \delta N(0)\delta N(t) >$ becomes more evident at lowering values of u.

A comparison of present findings with the experiments of the Montpellier group [Vaissiere, 1986] is reported in Fig. 3. Here the total current spectral density S_I as a function of frequency is reported together with the contribution due to GR processes alone. As seen, at all frequencies the GR contribution directly calculated from the MC is higher than the corresponding phenomenological value which is obtained by using the u provided by the MC simulation. Therefore, in agreement with experiments, the GR contribution is found to be mostly responsible for the large plateau value which is exhibited at the lowest frequencies.

3. CONCLUSIONS

We have reported the first microscopic theory of Generation Recombination noise for the case of the acoustic-phonon cascade model. The use of a Monte Carlo simulation has enabled us to solve exactly the master equation of the problem. Results agree with the phenomenological approach available from literature in the limit when the fraction of free carriers is larger than 0.8, while for lower values we have found that the phenomenological approach systematically underestimates the carrier lifetime. Theory compares well with available experiments for the case of p-Si at 77 K.

Authors wish to thank Prof. J.P. Nougier and Dr. J.C. Vaissiere for having provided experimental data and for helpful discussions on the subject. This work has been partially supported by the CEE ESPRIT II BRA 3017 project and the Centro di Calcolo of the Modena University.

REFERENCES

Jacoboni C. and Reggiani L. (1983), Rev. Mod. Phys. **55**, 645.
Reggiani L., Varani L., Vaissiere J.C., Nougier J.P. and Mitin V. (1989), J. Appl. Phys. to be published.
Vaissiere J.C. (1986), Ph D Dissertation, University of Montpellier unpublished.
Van Vliet K.M. and Fasset J.R. (1965), in: Fluctuation Phenomena in Solids, Ed. by R.E. Burgess, Academic Press (New York) p. 267.

LIGHT HOLE CONTRIBUTION TO NOISE AND DIFFUSION AT LOW TEMPERATURES IN p-GERMANIUM*

V.V. MITIN,** C.M. VAN VLIET

Centre de Recherches Mathématiques, Université de Montréal,
C.P. 6128-A
Montréal, Québec, H3C 3J7

INTRODUCTION

In this article we consider the transition from diffusive motion (low fields, constant mobility and diffusivity) to streaming motion (higher fields, low temperature, $kT \ll \hbar w_0$). Streaming motion is realized when impurity scattering and acoustical phonon scattering are almost absent, and when the number of thermally available phonons is low, so that the main scattering event is optical phonon (or polar optical phonon) emission (Reggiani, 1985). The motion is then near "ballistic". A carrier is accelerated in the electric field F until it reaches the energy $\mathcal{E} \approx \hbar w_0$, where $\mathcal{E}$ is its kinetic energy $\frac{1}{2}m^* v_k^2$, and w_0 is the optical phonon frequency. The critical velocity is denoted as v_0, i.e. $v_0 = \sqrt{2\hbar w_0/m^*}$. When v_k equals v_0, or is slightly larger (Komigawa, 1982; Andronov and Pozela, 1983; Peters et al., 1985) an optical phonon is emitted and the carrier energy reverts to zero. For the ideal streaming process we have the simple equations,

$$v = v_0(t/\tau_0), \qquad \mathcal{E} = \hbar w_0 (t/\tau_0)^2, \tag{1}$$

$0 \le t \le \tau_0$, where τ_0 is the time to reach $\hbar w_0$ from $\mathcal{E} = 0$. This streaming period is clearly given by

$$\tau_0 = m^* v_0 / eF = \sqrt{2\hbar w_0 m^*}/eF. \tag{2}$$

In reality, the carrier motion is affected by other scattering mechanisms. Thus the limits for streaming to be observed are $F^- < F < F^+$, where

$$F^- \simeq \sqrt{2\hbar w_0 m^*/e^2}(1/\tau_{imp} + 1/\tau_{ac}), \tag{3a}$$

$$F^+ \simeq \sqrt{2\hbar w_0 m^*/e^2}\,\mathcal{A}/10.3, \tag{3b}$$

where $1/\tau_{opt} = \mathcal{A}\sqrt{\mathcal{E}/\hbar w_0 - 1}$. For *p-Ge* at $4K$, F^- is approximately $10V/cm$ and $F^+ \approx 3000V/cm$.

*Supported by NSERC and FCAR
**On leave from Inst. for Semiconductors, Kiev, USSR

APPROACH

A many particle (our sample involved a few thousand holes) Monte Carlo (MC) approach was employed to compute the drift velocity ($v_d = \langle v \rangle$), the mean energy ($\langle \mathcal{E} \rangle$), the normalized velocity-velocity correlation function $C^*(\tau)$, and the diffusivities $D_{||}$ and $D_\perp$ (longitudinal and transverse, respectively). The definitions are:

$$C^*(\tau) = \langle \delta v(t)\, \delta v(t+\tau) \rangle / \langle v \rangle^2, \tag{4}$$

$$D(w \to 0) = \int_0^\infty d\tau\, C^*(\tau) \langle v \rangle^2. \tag{5}$$

For previous results involving the MC method, see Bareikis et al. (1981), Jacoboni and Reggiani (1983), Brunetti and Jacoboni (1984), and Kochelap et al. (1989). For a discussion on the frequency dependence of D, see Van Vliet and van der Ziel (1979). The optical phonon energy for p-Ge is $\hbar w_0/k = 430K$. The main new results of this paper are that light hole motion, as well as interband scattering (light hole band – heavy hole band) is taken into account. For the effective masses we took $m_1 = 0.0423$ and $m_2 = 0.346$. We will see that the presence of light holes drastically modifies the behaviour, as previously given by Bareikis et al.

RESULTS INVOLVING THE HEAVY HOLE BAND ONLY

MC results for v_d and $\langle \mathcal{E} \rangle$ are shown in Figs. 1 and 2, respectively for three impurity levels: $N_A = 0$ (curves 1), $N_A = 10^{20} m^{-3}$ (curves 2), and $N_A = 10^{22} m^{-3}$ (curves 3)

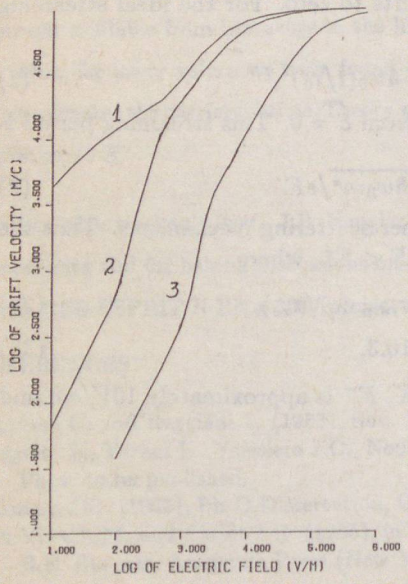

Fig. 1 Field dependence of drift velocity.

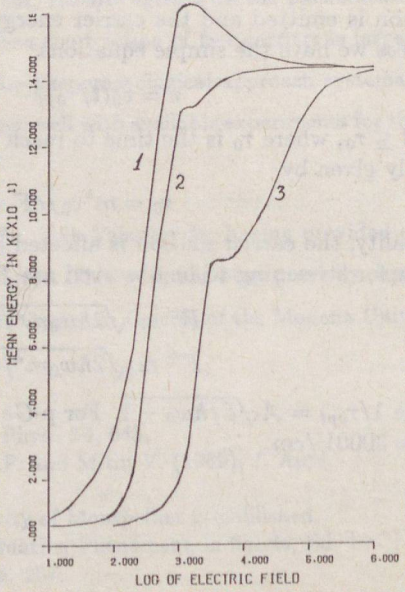

Fig. 2 Field dependence of mean energy $\langle \mathcal{E} \rangle$ in Kelvins.

The drift velocity shows no anomalies, which were not discussed before. The saturation value is $v_0/2$ as follows from Eq (1), using time averaging (period $(0, \tau_0)$) instead of ensemble averaging.

For the dependence of $\langle \mathcal{E} \rangle$ on the field there is a sharp rise with a maximum at about $3 \times 10^3 V/m$ at which field the optical phonon emission rate approaches the acoustical scattering rate. Then $\langle \mathcal{E} \rangle$ decreases to the saturation value $\hbar w_0/3k = 143.3K$, as it should according to Eq (1). When impurity scattering is added, the maximum does not develop, but a kink in the monotonic increase occurs near the field where optical phonon emission sets in and the process proceeds towards pure streaming.

The transition from diffusive behaviour to streaming is most clearly visible in the diffusivity, see Fig. 3.

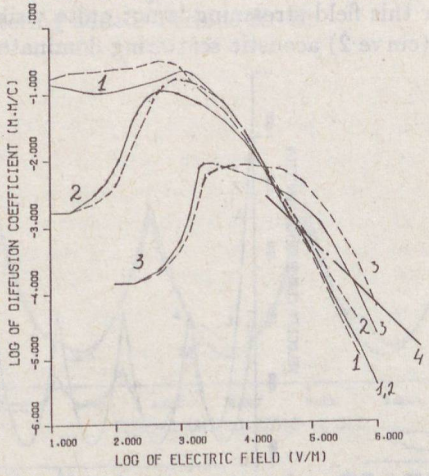

Fig. 3 Field dependence of $D_\perp$ (broken lines) and $D_{||}$ (full lines) for three impurity concentrations, N_A.

When streaming sets in, $D_\perp \to 0$ since there is no velocity component perpendicular to the electric field, while $D_{||} \to 0$ because of the periodicity of $C^*(\tau)$ under pure streaming, see below. Curve 4 is due to interband scattering, discussed in the next section.

Some analytical results for pure streaming are easily derived. The velocity $v(t)$ follows a "saw-tooth" profile. Thus, for all $t \geq 0$, we have

$$v(t) = v_0 \cdot (t/\tau_0) - v_0 \sum_{n=1}^{\infty} \theta(t - n\tau_0), \tag{6}$$

where $\theta(t)$ is the Heaviside (unit step) function. From this, one finds with some

algebra,

$$C^*(\tau) = [\langle v(t)\, v(t+\tau)\rangle / \langle v\rangle^2 - 1]$$

$$= \frac{1}{12} \cdot \left[1 - 6\frac{\tau}{\tau_0}\left(1 - \frac{\tau}{\tau_0}\right) - 12\sum_{n=1}^{\infty}\left(\frac{\tau}{\tau_0} - n\right)\theta(\tau - n\tau_0)\right]. \quad (7)$$

This is a periodically repeated parabola; notice, $C^*(\tau + \tau_0) = C^*(\tau)$. For $\tau = 0$ or τ_0 its value is 0.333; for $\tau = \tau_0/2$ its minimum yields -0.166. When the ensemble average for D, Eq (5), is replaced by an average over an interval $((n-1)\tau_0, n\tau_0)$, its value is found to be zero.

The MC results for $C^*(\tau)$ are shown in Fig. 4 ($F = 500V/m$), Fig. 5 ($F = 5000V/m$), and Fig. 6 ($F = 5 \times 10^4 V/m$). In all cases, curves (1) refer to optical phonon emission only, while in curves (2) acoustical phonon scattering is taken into account.

In Fig. 4, $\tau_0 = 7.64 \times 10^{-10} sec$ as is found from Eq (2), with m^* taken to be the heavy hole mass m_2. For this field streaming is not quite visible (curve 1 is a "weak" parabola); in reality (curve 2) acoustic scattering dominates.

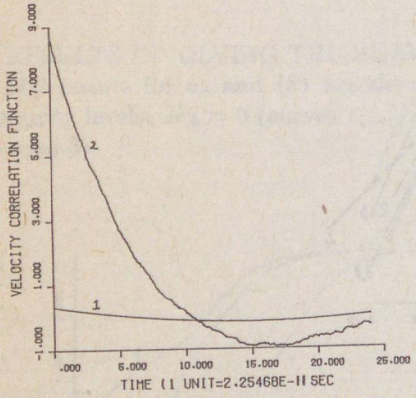

Fig. 4 Velocity correlation function for $F = 500V/m$.

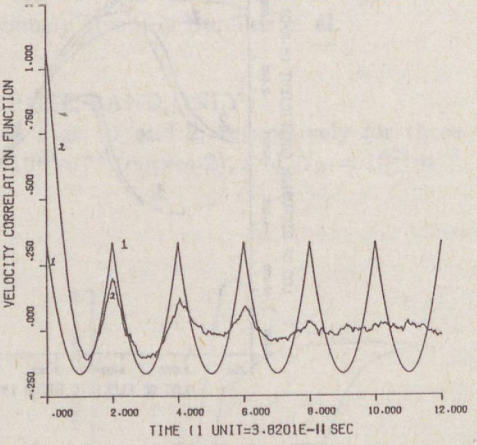

Fig. 5 Velocity correlation function for $F = 5000V/m$.

Fig. 5 (curve 1) shows the parabolas for pure streaming, τ_0 being now $7.64 \times 10^{-11} sec$. However, acoustic phonon scattering causes rapid damping (curves 2). This is even more clear in Fig. 6 where $C^*(\tau)$ for periods 20–25 is shown.

EFFECT OF MOTION OF LIGHT HOLES AND INTERBAND SCATTERING

For the light holes the transit time to reach the energy $\hbar w_0$ is shorter since the mass is smaller. Thus, as in Eq (2)

$$\tau_{02} = \sqrt{2\hbar w_0 m_2}/eF, \quad \tau_{01} = \sqrt{2\hbar w_0 m_1}/eF = \sqrt{\gamma}\,\tau_{02}. \quad (8)$$

For the interband scattering time under streaming conditions we have (Costalo and Reggiani, 1973; Bir and Picus, 1961)

$$\frac{1}{\tau} = \frac{1}{\tau_1} + \frac{1}{\tau_2} = \frac{1}{\tau_{02}} \frac{(1+\gamma^2)}{\sqrt{\gamma}(1+\gamma^{3/2})}; \quad (9)$$

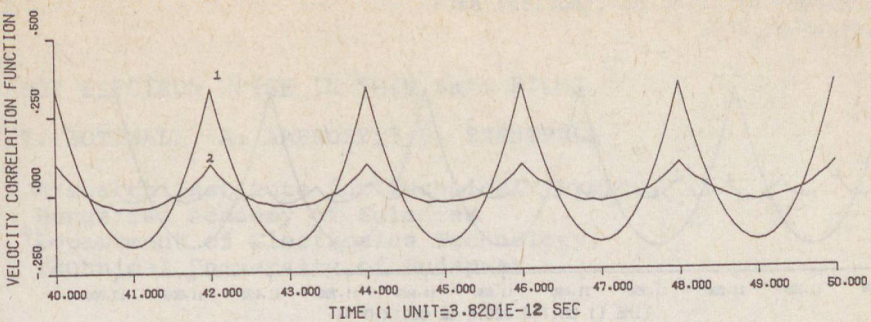

Fig. 6 Velocity correlation function for $F = 50000V/m$. Heavy-hole motion only. Curve 1: pure streaming; curve 2: acoustical phonon scattering added. Periods 20–25.

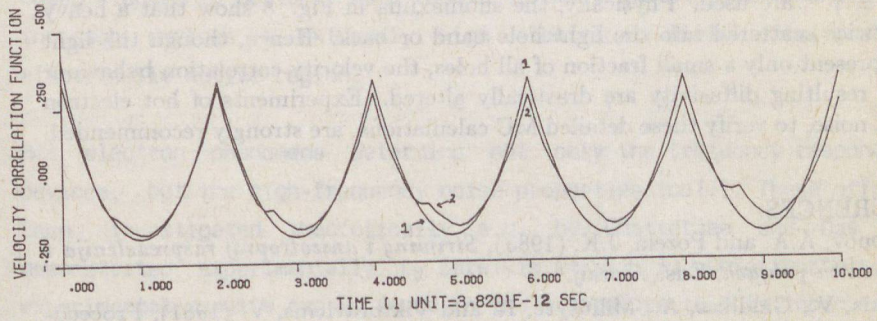

Fig. 7 Velocity correlation function for $F = 50000V/m$. Curve 1: heavy-hole motion only. Curve 2: effect of light hole motion and interband scattering. Periods 0–5.

we must consider here that after optical phonon emission, a heavy hole can be scattered into the light hole band (time constant τ_2) or vice versa (time constant τ_1). The diffusivity due to interband scattering has the form (Brunetti et al., 1981),

$$D_{||} = \nu_1 \nu_2 (\langle v_1 \rangle) - \langle v_2 \rangle)^2 \tau, \tag{10}$$

where ν_1 and ν_2 are the fractions of holes in the two bands. One easily finds, $D_{||} = 64.5/F \ \ m^2/sec$, F in V/m. This is the dominant diffusivity, see curve 4 of Fig. 3.

Detailed MC calculations of $C^*(\tau)$ for $F = 5 \times 10^4 V/m$ are presented in Figs. 7 and 8. Curves 1 give the results for heavy-hole streaming only (they reveal the same parabolas as in Fig. 6). Curves 2 show the effect of the addition of light holes. In particular, Fig. 8 shows that a "quasi-periodicity" of $\approx \tau_{02}/3$ develops.

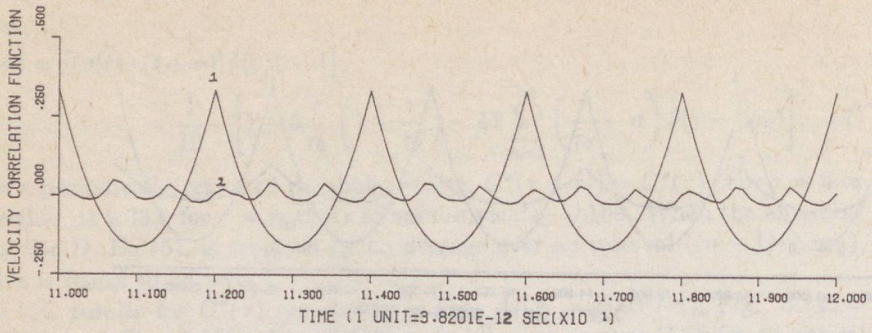

Fig. 8 Velocity correlation function for $F = 50000V/m$. Curve 1: heavy-hole motion only. Curve 2: effect of light hole motion and interband scattering. Periods 55–60.

From Eq (9) one finds indeed that $\tau \approx \tau_{02}/3$ when the previously given values of $m_2/m_1 \equiv \gamma^{-1}$ are used. Physically, the submaxima in Fig. 8 show that a heavy hole is twice scattered into the light hole band or back. Hence, though the light holes represent only a small fraction of all holes, the velocity correlation behaviour and the resulting diffusivity are drastically altered. Experiments of hot electron Johnson noise, to verify these detailed MC calculations, are strongly recommended.

REFERENCES

Andronov, A.A. and Pozela, J.K. (1983), *Striming i anizotropnij raspredelenija v skreshchenich polijach*, Eds., Gorkij.

Bareikis, V., Galdikas, A., Miliusyté, R. and Viktoravicius, V. (1981), Proceedings Sixth International Conference on *Noise in Physical Systems*, P.H.E. Meijer, R.D. Mountain and R.J. Soulen, Eds., National Bureau of Standards, 406.

Bir, G.L. and Pikus, G.E. (1961), Sov. Phys. Solid State **2**, 2039; **2**, 2287.

Brunetti, R., Jacoboni, C. and Reggiani, L. (1981), Journal de Physique **42**, (Colloque C7, supplément au No. 10), C7–117.

Costalo, M. and Reggiani, L. (1973), Phys. Stat. Sol. (b) **58**, 461.

Jacoboni, C. and Reggiani, L. (1983), Rev. Mod. Physics **55**, 645.

Kochelap, V.A., Mitin, V. and Zakhleniuk, N.A. (1989), Zh. Exp. Theoret. Fiziki **95**, 775.

Komigama, S. (1982), Adv. Phys. **31**, 255.

Peters, F.M., Van Puymbroeck, W. and Devreese, J.T. (1985), Phys. Rev. **B31**, 5322.

Reggiani, L (1985), *Hot electron transport in semiconductors*, Ed., Springer Verlag, Berlin-Heidelberg.

Van Vliet, K.M. and van der Ziel, A. (1979), Physica **99A**, 337.

HOT ELECTRON NOISE IN THIN GaAs FILMS

P. GOTTWALD, A. AMBRÓZY,* B. SZENTPÁLI

Research Institute for Technical Physics,
Hungarian Academy of Sciences
*Department of Electronics Technology,
Technical University of Budapest

INTRODUCTION

Because of their excellent high-frequency properties multivalley semiconductors with nonequivalent valleys are widely used in realising of high speed electronic devices. As a result of small geometrical dimensions - used in such devices - extremely high electrical field exist inside their electrically active region.

Hot electron phenomena determine not only the frequency response of the devices, but the high-frequency noise properties too[1]. These effects have been investigated theoretically e.g. by Chatterjee and Das [2] and demonstrated experimentally by Bareikis et al. [3]. Unfortunately only few experimental results can be found in the literature to this topic.

We present now results and discussion of an experimental work carried out for studying the field and frequency dependence of the noise current spectral density generated by this GaAs epitaxial layers under the influence of strong electric field.

METHOD

For the investigations small dimensional planar resistors were fabricated by standard GaAs microelectronic technology on a MESFET-like epitaxial layer structure. To avoid the Gunn instability in the active layer lower doping has been chosen than usual in MESFET's. Fig.1 shows the layout of the resistor chip and summarizes the main geometrical and technological parameters with the common notations.

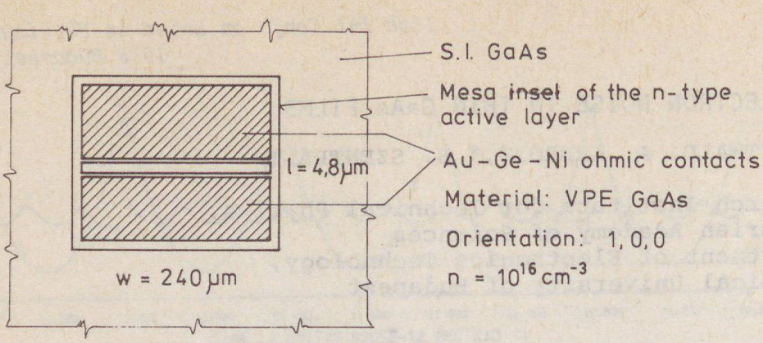

Fig. 1 The layout and the main parameters of the resistor chip.

At properly low measurement frequencies (in our case 1, 2 and 3 GHz) the samples performed the small signal stability criteria given by Copeland [4], because the doping X length product was about 5 X 10^{12} cm^{-2} and the frequency X length product was in the range of 10^{6} $cm.s^{-1}$ even at the highest measurement frequency.

The layer thickness was chemically etched down in the region between the ohmic contacts, until reaching a nominal low field resistance value of 50 ohms. The resistor chips were mounted on a ceramic plate as terminations of microstrip lines with a characteristic impedance also of 50 ohms. For lowering the parasitic inductances multiwire bonding was applied. The noise current generated by the DC biased planar GaAs resistors were measured by a calibrated low noise microwave receiver [5].

Correction according to the system noise was made also in the calculation of the final result.

RESULTS and DISCUSSION

The full line curves in Fig. 2 show the obtained fieldstrength dependence of the equivalent noise ratio (ENR) in form of the relative noise temperature (RNT) at the frequencies of 1, 2 and 3 GHz. On the other hand the dotted curve corresponds to the measurement of Bareikis et al. at 10 GHz. [3].

It should be noted that the DC bias causes a considerable increase of the small signal resistance of the sample, which results in an impedance mismatch in the measurement circuit. Approximate calculation have shown, that

the correction needed of the above measurement results does not alter the character of the fieldstrength and frequency dependence of the RNT values. It has to be mentioned, that the temperature rise of the sample caused by the biasing DC power was not more than about 100 K. Namely, calculations of the thermal resistance between the active layer and the ambient gave a value of not more than 200 $K.W^{-1}$.

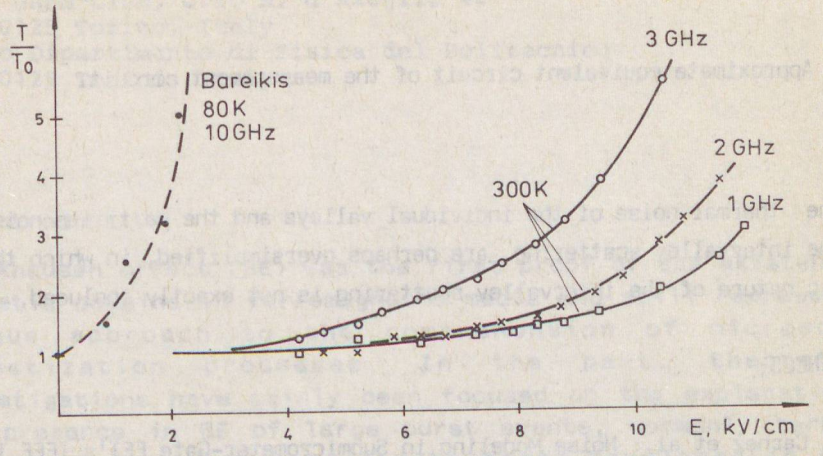

Fig.2 Measured fieldstrength dependence of the relative noise temperature at different measurement frequencies.

As the measurements show there is a considerable frequency dependence of the generated noise current density. The result obtained by Bareikis et al. at 10 GHz seems to correspond to this frequency dependence. The increase of the RNT values against the frequency cannot be explained by the parasitics of the measurement circuit having basically low-pass filter characteristic.

Fig.3 shows the small signal equivalent circuit of the measurement circuit indicating also the calculated values of the parasitic reactances.It is obvious from this Figure, that the circuit parasitics may be neglected at the relative low measurement frequencies.

Finally we note, that although the theory given in [2] predicts a strong frequency dependence in the real part of the microwave small signal mobility, this theory also does not explain immediately the observed frequency dependence of the hot electron noise. So we believe, that the theories characterizing the hot electron noise in multivalley semiconductors as the sum

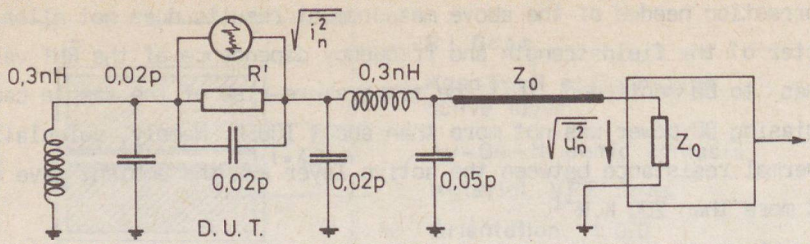

Fig.3 Approximate equivalent circuit of the measurement circuit.

of the thermal noise of the individual valleys and the partition noise due to the intervalley scattering, are perhaps oversimplified, in which the energetic nature of the intervalley scattering is not exactly included.

REFERENCES:

[1] B. Carnez et al.: Noise Modeling in Submicrometer-Gate FET's IEEE Trans. Electron Devices, pp. 784-789. 1981.

[2] A.Chatterjee and P. Das: Current noise in multivalley semiconductors. Noise in Physical Systems and 1/f noise.
Conf. Proc. pp. 161-164. Elsevier, 1983.

[3] V.Bareikis et al.: Size dependent diffusion and microwave noise in GaAs and InP. Proc. of the 19th Int. Conf. on the Phys. of Semiconductors. pp. 1427-1430. 1988. Warsaw

[4] J.A.Copeland: Characterisation of Bulk Negative-Resistance Diode Behaviour. IEEE Trans. Electron Devices, ED-14, 1967 pp. 461-463.

[5] The measurements were made at the University of Aachen (Dep. of. Sol. State El.) by the receiver of a noise measuring system manufactured by AILTECH.

10th Int.Conf. on Noise in Physical Systems
1989 Budapest, Hungary

THEORY OF BARKHAUSEN NOISE IN FERROMAGNETIC MATERIALS

A. MONTORSI,* G. BERTOTTI

Istituto Elettrotecnico Nazionale Galileo Ferraris
and GNSM-CISM, c.so M. d'Azeglio 42
I-10125 Torino, Italy
*Also Dipartimento di Fisica del Politecnico
I-10129 Torino, Italy

1. Introduction

Barkhausen effect (BE) was the first proof of the existence of magnetic domains in ferromagnetic media and still represents a unique approach to the comprehension of microscopic magnetization processes. In the past, theoretical investigations have mainly been focused on the explanation of the presence in BE of large burst events, commonly termed B pulses or B avalanches. The theories developed in [1,2] interpreted these burst events as due to the clustering of many elementary domain wall (DW) jumps, leading to useful descriptions of B noise statistical properties. Nonetheless, a gap remained as for the physical interpretation of the mechanism connecting the avalanches to DW dynamics.

As proposed in [3,4], this gap can be filled up by studying the motion of a 180° DW in a randomly perturbed medium, in the frame of the theory of stationary Markov processes. It is well known [5] that a linear relationship holds in metallic systems between DW velocity and magnetic field H. In terms of the magnetic flux rate of change $\dot{\Phi}$ (proportional to DW velocity), one can write

$$\sigma G \dot{\Phi} = H - H_c , \qquad (1)$$

where σ is the electrical conductivity and G=0.1356. The local coercive field H_c randomly fluctuates as a consequence of the perturbations that the DW encounters in its motion, and induces fluctuations of $\dot{\Phi}$ responsible for BE. Information on the stochastic behavior of H_c was obtained in [6,7], leading to the conclusion [3] that H_c is a random function of DW position, i.e. Φ, obeying the Langevin equation:

$$dH_c/d\Phi + (H_c - \langle H_c \rangle)/\xi = dW/d\Phi . \qquad (2)$$

Here ξ is the correlation length implied by the finite interaction range of lattice perturbations with the DW and $W(\Phi)$ is a Wiener-Levy process characterized by $\langle|dW|^2\rangle = 2Ad\Phi$, with A an unknown constant.

Equations (1) and (2) contain all the basic information about DW motion (and henceforth eventually about BE) once some suitable hypothesis on the nature of the internal field H is made. We expect that $H=H_a-H_m$, where H_a is the applied field and H_m is the magnetostatic counterfield. If we assume that DW motion is taking place in a portion of the hysteresis loop characterized by a constant differential permeability μ, the average magnetization of the system will change at a constant rate $\dot{I}$ if we apply an external field H_a such that $\dot{H}_a=\dot{I}/\mu$. In these conditions $\dot{\Phi}$ is a stationary process, with $\langle\dot{\Phi}\rangle=S\dot{I}$ (S is the sample cross-section). Inspection of Eq.(1) shows then that the simplest consistent assumption for the magnetostatic contribution is $\dot{H}_m=\dot{\Phi}/Su$. After introducing the time constants $\tau=\sigma GS\mu$ and $\tau_c=\xi/S\dot{I}$ and the dimensionless parameters $c=\sigma G\dot{I}/A\mu$, $z=c\dot{\Phi}/S\dot{I}$, $h_c=-\sigma G/A\ H_c/\tau$, $w=-\sigma G/A\ W/\tau$, the time derivative of (1) together with eq. (2) (rewritten with respect to time) read

$$dz/dt + (z-c)/\tau = dh_c/dt \qquad (3)$$

$$dh_c/dt + z/c\ (h_c-\langle h_c\rangle)/\tau_c = dw/dt\ , \quad \langle|dw|^2\rangle = 2z\ dt/\tau. \qquad (4)$$

The process z is markovian, and its statistical properties are fully determined by the solution of the Fokker-Planck equation associated with Eqs. (3) and (4). Due to the non-linear term in (4) this solution is not yet known in the most general case. The limit $\tau_c\to\infty$, which physically corresponds either to a low $\dot{I}$ regime or to long-range DW interactions, was considered in [4]. In the next section, we present further approximate analytical solutions in different limits, which cover the conditions of main physical interest in BE experiments.

2. Results and discussion

We start with the Fokker-Planck equation associated with Eqs (3) and (4). In terms of z and of $y=z-c-(h_c-\langle h_c\rangle)$, it reads

$$\frac{\partial}{\partial t}P - \frac{\partial}{\partial z}\left[(z-c)\left(1+\frac{\tau}{\tau_c}\frac{z}{c}\right)P\right] + \frac{\tau}{\tau_c}\,y\frac{\partial}{\partial z}\left(\frac{z}{c}P\right) - (z-c)\frac{\partial}{\partial y}P = c\frac{\partial^2}{\partial z^2}\left(\frac{z}{c}P\right) \qquad (5)$$

The first limit we shall consider is that of high $\dot{I}$, where $\dot{\Phi}$ shows only small fluctuations around its average $S\dot{I}$. Hence in

Eq.(4) we can assume $z \ll c$ and $\langle |dw|^2 \rangle = 2c\, dt/\tau$, which implies that all the terms z/c of Eq.(5) can be approximated by 1. Equation (5) then becomes a bivariate linear Fokker-Planck equation, the solution of which is known in the literature (see for example [8]). In particular one obtains that in this limit the stationary probability distribution $P_0(z,y)$ is the product of two gaussians in z and y,

$$P_0(z,y) = 1/(2\pi a)\ (\tau/\tau_c)^{1/2}\ \exp\{-[(z-c)^2 + \tau/\tau_c\ y^2]/2a\} \quad (6)$$

with $a = c/(1+\tau/\tau_c)$, and the autocorrelation function $R(\Delta t)$ reads

$$R(\Delta t) = a\ \{[\exp(-\Delta t/\tau) - \tau/\tau_c\ \exp(-\Delta t/\tau_c)]/(1 - \tau/\tau_c)\}. \quad (7)$$

Taking the Fourier transform of $R(\Delta t)$ and recalling that $z = c\dot{\Phi}/S\dot{I}$, we obtain the power spectrum $F(\omega)$ of the BE flux rate $\dot{\Phi}$ as

$$F(\omega) = 4\ SI\ A/(\sigma G)^2\ \omega^2/[(\omega^2+\tau^{-2})(\omega^2+\tau_c^{-2})]\ . \quad (8)$$

Remarkably enough, Eq.(8) exhibits all the basic features of the spectra observed in BE experiments:
- in the high ω region $F(\omega)/S\dot{I} \propto k\ \omega^{-2}$, with k independent of $\dot{I}$ and μ;
- $F(\omega)$ exhibits a maximum which increases with increasing μ or decreasing $\dot{I}$, according to power laws which are in substantial agreement with experimental results [4];
- the frequency of the maximum increases with increasing $\dot{I}$ or with decreasing μ.

Concerning the amplitude probability distribution P_0, we can work out a more realistic approximation, in which the terms z/c in the left-hand side of Eq.(5) are approximated by 1, while the one in the right-hand side is kept exact. This corresponds to estimating the decay of h_c correlations on the basis of the average, instead of instantaneous, DW velocity. Being interested in the stationary case, we can drop out the time derivative term. Besides, as we just need the z dependence, we can integrate over y (and over the initial conditions). The $\partial P_0/\partial y$ term then disappears because of the boundary conditions. On the other hand, we can evaluate the y integral of the yP_0 term by using for P_0 the high $\dot{I}$ expression given by Eq.(6). The result is zero, and, after the reparametrization $\check{c} = c(1+\tau/\tau_c)$, $\check{z} = z\check{c}/c$, we end up with the following equation for $P_0(\check{z})$:

$$\frac{\partial}{\partial \check{z}}\ [(\check{z}-\check{c})P_0] + \frac{\partial^2}{\partial \check{z}^2}(\check{z}P_0) = 0\ . \quad (9)$$

The solution is

$$P_0(\tilde{z}) = \tilde{z}^{\tilde{c}-1} \exp(-\tilde{z})/\Gamma(\tilde{c}) \qquad (10)$$

The value $\tilde{c}=1$ identifies a crossover between a regime in which P_0 diverges for $\tilde{z}\to 0^+$ and one in which it goes to zero. This result has a clear physical meaning. When $\tilde{c} < 1$, we are in presence of a burst-like behavior, where a DW spends most of the time with velocity almost zero, while for $\tilde{c} > 1$ we have a continuous DW motion, where the $\tilde{z}\to 0$ condition has a negligible probability to occur.

It is quite remarkable that the expression (10) for P_0 reproduces exactly the one found in [4] for the limit $\tau_c \to \infty$, apart from a rescaling $\tilde{z}\to z$ and $\tilde{c}\to c$. Thus Eq. (10) seems to be a distinctive feature of BE. This is well confirmed by comparison with experimental data given in [9] and in a forthcoming paper, where it is also shown that the power-law divergence of P_0 when $\tilde{c} < 1$ implies scaling properties in the distribution of B pulses, which can be described in terms of a fractal structure of fractal dimension $D=1-\tilde{c}$ [10].

The analysis of BE experiments according to (8) and (10) is of great interest in that it gives definite information on the parameters of the theory, A and ξ. In our opinion, important progress in the comprehension of ferromagnetic hysteresis will be achieved by investigating the dependence of these parameters on $\dot{I}$ and μ, as well as on the microstructural properties of a given material.

References

[1] H. Bittel, IEEE Trans Magn. MAG-5, 359 (1969).
[2] G. Montalenti, Z. Angew Phys. 28, 29 (1970).
[3] G. Bertotti in "Magnetic Excitations and Fluctuations II", U. Balucani,S.W. Lovesey, M.G. Rossetti and V. Tognetti eds. (Springer, Berlin 1987), p. 135.
[4] B. Alessandro, C. Beatrice, G. Bertotti and A. Montorsi, J. Appl. Phys. 64, 535 (1988).
[5] H.J. Williams, W. Shockley and C. Kittel, Phys. Rev. 80, 1090 (1950).
[6] J.A. Baldwin, G.M. Pickles, J. Appl. Phys. 43, 4746 (1972).
[7] R. Vergne, J.C. Cotillard and J.L. Porteseil, Revue Phys. Appl. 16, 449 (1981).
[8] N.G. van Kampen, "Stochastic processes in physics and chemistry" (North-Holland, Amsterdam 1981), p. 228.
[9] B. Alessandro, C. Beatrice, G. Bertotti and A. Montorsi, SOFT-Conference (Madrid, 1989), to appear on Anales de Fisica.
[10] B. Alessandro, C. Beatrice, G. Bertotti and A. Montorsi, "Domain wall dynamics and BE in metallic ferromagnetic materials. Theory and Experiments.", preprint submitted to Phys. Rev.

10th Int.Conf. on Noise in Physical Systems
1989 Budapest, Hungary

MODULATION NOISE IN MAGNETIC AND OTHER NONLINEAR SYSTEMS

H. MYKOLAITIS, V. PALENSKIS, J. LAUČIUS

Department of Radiophysics, Vilnius University
Lithuanian SSR

A modulation (or excess) low-frequency noise in an output signal of the system originates from temporal fluctuations of its transfer characteristic. In this connection there is an essential difference between linear and nonlinear systems: the fluctuations in various regions of the nonlinear transfer characteristic may be independent. Futhermore, the output signal of such system contains higher harmonics of the input signal.

The purpose of the present paper is to ascertain the relationship between distribution of both the fluctuation intensity and the length of independently fluctuating parts of the transfer characteristic and a phase distribution of the modulation noise occuring near to the harmonics for a magnetic system. However, the conclusions of the paper are applicable to any nonlinear systems [1].

We discuss a modulation noise in a magnetic system, containing a coil with nonlinear ferromagnetic core, placed in an exciting external magnetic field

$$H(t) = H_m \sin(2\pi t/T) - H_0, \tag{1}$$

where H_0 is the weak ($H_0 \ll H_m$) steady field. Then the first harmonic of the corresponding magnetic flux density

$$B_1(t) = B_{01} \sin(2\pi t/T - \varphi). \tag{2}$$

The magnetic hysteresis loop (HL) of the core is described by two sets of numerals – coordinates of the HL points plotted in a H–B diagram. According to this we can rewrite Eq. (1) for the i-th point:

$$H_i = H_m \sin[2\pi(i-1)/T] - H_0; \quad i = 1, 2, .., k, ..., N. \tag{3}$$

Here N is the total number of the HL points. In our discussion we consider a uniform time (or angular) distribution of the HL points, however, our method is correct for another distribution law, too. Fluctuations of the loop's k-th element have been taken by a slight modulation of the magnetic flux density value of the k-th HL point:

$$B_{kj} = B_k + F\sin(2\pi j/J); \quad j = 0, 1, 2, ..., J. \tag{4}$$

Here F is the amplitude of the modulation: $F \ll B_{max}$, where B_{max} is the maximum value of B_i; J is the period of the modulation expressed in T units. A coil-induced-voltage E* is proportional to a time derivative of a magnetic flux in the core. When a cross-section area of the core is set to be 1, E* is obtained from Eq. (3)–(4) as follows:

$$E^*_{ij} = -\frac{2\pi}{N} \frac{B_{i+1,j} - B_{ij}}{\arcsin[(H_{i+1} + H_0)/H_m] - \arcsin[(H_i + H_0)/H_m]}. \tag{5}$$

Spectral amplitudes of n-th harmonic of the induced signal (HIS) E* is found by means of a Fourier analysis in analogy to a principle of synchronous detection:

$$a_{jn\xi} = -(1/\pi)\sum_{i=1}^{N} E^*_{ij}[\cos n[\arcsin[(H_i + H_0)/H_m] + \xi]][\arcsin[(H_{i+1} + H_0)/H_m] - \arcsin[(H_i + H_0)/H_m]] \quad (6)$$

$$b_{jn\xi} = -(1/\pi)\sum_{i=1}^{N} E^*_{ij}[\sin n[\arcsin[(H_i + H_0)/H_m] + \xi]][\arcsin[(H_{i+1} + H_0)/H_m] - \arcsin[(H_i + H_0)/H_m]]$$

where ξ is the phase of the detector control signal. Here and in the following all phases are defined with respect to the exciting field phase. In terms of vector diagram these amplitudes may be interpreted as projections of the n-th HIS vector into two perpendicular axes, one of which (corresponding to $b_{jn\xi}$) is at the angle of ξ to the exciting field vector. According to this the phase and the absolute value of the n-th HIS vector are determined from the following relations:

$$|\vec{E}_{jn}| = b_{jn\xi}, \quad \varphi_{jn} = \xi \quad \text{, if } a_{jn\xi} = 0 \text{ and } \partial(a_{jn\xi})/\partial\xi < 0. \quad (7)$$

Using Eq. (4)–(6) we may obtain the spectral amplitudes for the first harmonic of the modulation signal to occur in the n-th HIS:

$$c_{n\xi} = (2/J)\sum_{j=0}^{J-1} a_{jn\xi}\sin(2\pi j/J), \quad (8)$$

$$d_{n\xi} = (2/J)\sum_{j=0}^{J-1} b_{jn\xi}\sin(2\pi j/J).$$

Signal of this harmonic may be described on the vector diagram by vector $\vec{E}_{tn}$, the absolute value and the phase of which may be expressed in analogy to Eq. (7):

$$|\vec{E}_{tn}| = d_{n\xi}, \quad \psi^*_n = \xi \quad \text{, if } c_{n\xi} = 0 \text{ and } \partial(c_{n\xi})/\partial\xi < 0. \quad (9)$$

Digital computations were performed for several types of a real HL featuring different rates of both rectangularity and saturation. All these types of HL have produced essentially the same results. In the following all numerical data correspond to the HL illustrated in Fig. 1, where values of H and B are given in arbitrary units. The HL was described by 60 points (N = 60) under uniform time (or angular) distribution. The k-th element of the HL in Fig. 1 is shown to be modulated. The modulation frequency is set to be 20 times lower than the exciting field's one, i. e. J = 20. The modulation amplitude F = 0,01 against $B_{max} \approx 2$.

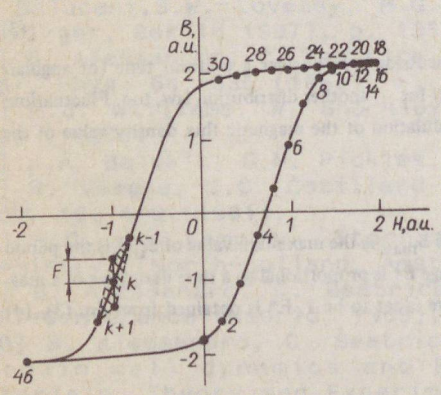

Fig. 1. Hysteresis loop under analysis.

The results of the computation lead to the establishing of the modulation noise vector model. According to this model the phase distribution of the modulation noise intensity is described in terms of vector diagram. The fluctuations of HL cause complex modulation of the output signal, which may be represented on the vector diagram of n-th HIS by the noise vector $\vec{E}_{tn}$. The sum of both $\vec{E}_{tn}$ and the vector of unmodulated HIS $\vec{E}_{on}$ yields the resultant vector of the modulated n-th HIS:

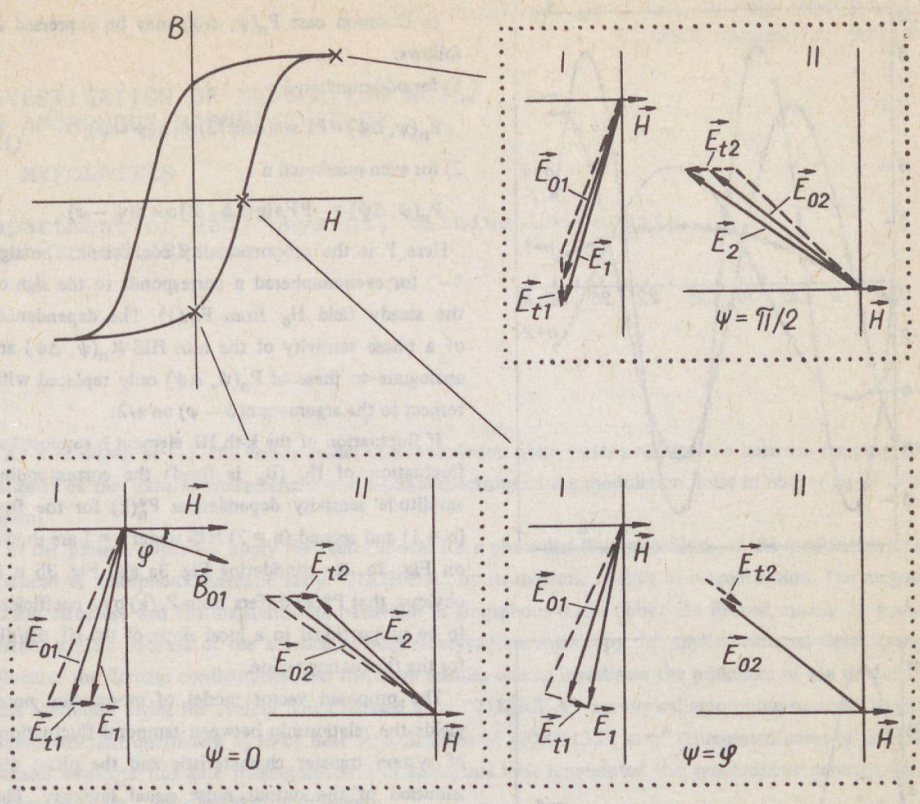

Fig. 2. Vector diagrams of the first (I) and second (II) HIS for angular position of fluctuating element $\psi = 0$; φ; $\pi/2$.

$\vec{E}_n = \vec{E}_{tn} + \vec{E}_{on}$.

The phase of $\vec{E}_{tn}$ equals to $-n\psi_k$, where ψ_k is the angular position of the k-th element:

$$\psi_k = \arcsin\,[(H_k + H_0)/H_m]. \tag{10}$$

The absolute value of $\vec{E}_{tn}$ is proportional to the amplitude of modulation F and also depends on the angular length of the fluctuating element $\Delta\psi$:

$$\Delta\psi = 2\pi r/N, \tag{11}$$

where r is the number of fluctuating points.

Vector diagrams of both the first (I) and the second (II) HIS for several angular positions of the fluctuating element are shown in Fig. 2. From the diagrams it is apparent that fluctuations in the region of the coercive field H_c with angular position $\psi(H_c) \equiv \varphi$ provide a phase modulation for the first HIS and an amplitude modulation for the second one. Naturally, in case of independent fluctuations in some parts of the HL the resultant noise vector of n-th HIS equals to the sum of the noise vectors induced by every part of the HL.

We define the projection of the noise vector $\vec{E}_{tn}$ into the direction of the vector $\vec{E}_{on}$ as an amplitude sensivity of the n-th HIS to HL fluctuations P_n (k, r). The dependence $P_n(k)$ for the first four harmonics under r = 1 is shown in Fig. 3a.

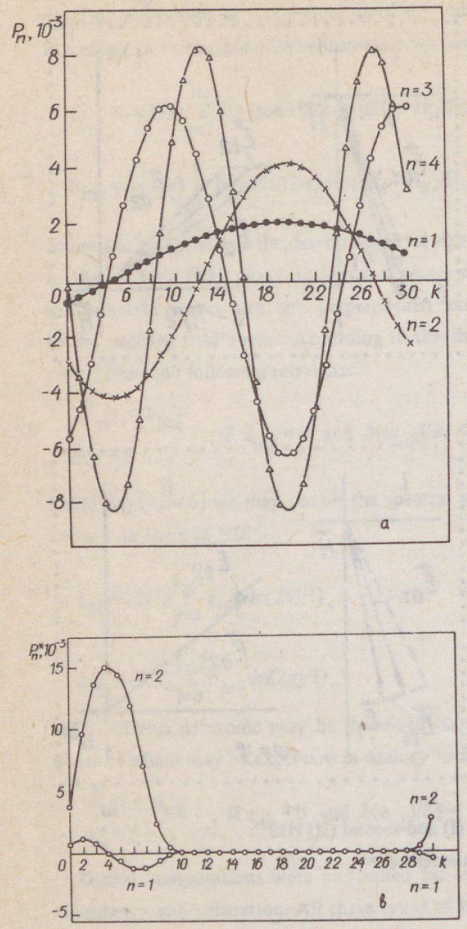

Fig. 3. Amplitude sensivity of n-th HIS vs serial number of fluctuating point when HL fluctuations are represented by fluctuations of: a) magnetic flux density; b) magnetic field.

In common case $P_n(\psi, \Delta\psi)$ may be expressed as follows:

1) for odd-numbered n

$$P_n(\psi, \Delta\psi) = PF \sin(n\Delta\psi/2) \sin n(\psi - \varphi); \qquad (12)$$

2) for even-numbered n

$$P_n(\psi, \Delta\psi) = -PF \sin(n\Delta\psi/2) \cos n(\psi - \varphi).$$

Here P is the proportionality coefficient. The sign "–" for even-numbered n corresponds to the sign of the steady field H_0 from Eq.(1). The dependences of a phase sensivity of the n-th HIS $R_n(\psi, \Delta\psi)$ are analogous to these of $P_n(\psi, \Delta\psi)$ only replaced with respect to the argument $n(\psi - \varphi)$ on $\pi/2$.

If fluctuation of the k-th HL element is supposed as fluctuation of H_k (B_k is fixed) the corresponding amplitude sensivity dependences $P_n^*(k)$ for the first (n = 1) and second (n = 2) HIS under r = 1 are shown on Fig. 3b. By considering Fig. 3a and Fig. 3b it is obvious, that $P_n^*(k)$ differs from $P_n(k)$ by a coefficient to be proportional to a local slope of the HL dB/dH for the fluctuating region.

The proposed vector model of modulation noise yields the relationship between temporal fluctuations of system transfer characteristic and the phase distribution of the output noise signal intensity. The model is applicable and essential not only to magnetic systems, but to any nonlinear systems, too, such as ferroelectrics, semiconductor devices, etc. It is evident, that the model includes also a modulation noise in linear systems. For these systems vectors $\vec{E}_{tn}$ and $\vec{E}_{on}$ are collinear, so fluctuations of the transfer characteristic cause only an amplitude modulation of the output signal.

REFERENCE

1. Mykolaitis H., Palenskis V., Laučius J. "Analysis of the modulation noise caused by the remagnetization of a ferromagnet." Liet. fiz. rink. 28 (2), 211–218, 1988 (in Russ.).

10th Int.Conf. on Noise in Physical Systems
1989 Budapest, Hungary

INVESTIGATION OF MODULATION NOISE IN AMORPHOUS MAGNETIC ALLOY

H. MYKOLAITIS

Department of Radiophysics, Vilnius University
Lithuanian SSR

As it is shown in [1], the vector model of a modulation noise yields a relationship between temporal fluctuations of the transfer characteristic and a phase spectrum of the modulation noise in output signal of the system.

In the present paper we apply the vector model for a phase-distribution analysis of the modulation noise, produced in amorphous magnetic alloy "71KHCP-A" by its dynamic cycling of magnetization. The magnetic domain structure and the magnetization behaviour in amorphous metal ribbon are formed mostly by random internal stresses because of the absence of magnetocrystalline anisotropy. An applied external elastic tension influences the domain configuration and therefore enables one to investigate the principles of the modulation noise formation under the cycling. The Co-based alloy "71KHCP-A" is a typical amorphous one with negative magnetostriction coefficient λ_s to be near zero. Samples of 120X2X0,25 mm^3 represented cores of the experimental two-core flux-gate magnetometer. An analogous lock represented the synchronous detector which has been used for a noise signal demodulation.

The detector allows to measure the noise during the small time interval the angular position of which with respect to magnetization cycle depends on the phase ξ of the detector control signal. The variation of ξ from 0° to 360° leads to the clockwise displacement of the interval analysed along the hysteresis curve starting from the point H(t) = 0. The amplitude of excitation field H_m = 45 A/m was large enough to reach a sufficient saturation at frequency f = 5 kHz.

Hysteresis loop of the sample under tension σ is shown in Fig. 1. Hysteresis loop's fluctuations have been investigated directly in a form of the induced noise voltage. Phase-distribution diagram of the noise intensity is shown in Fig. 2. The measured values of the noise spectral density are divided by the number of output coil windings w squared. The diagram shows a particular variation of the noise intensity along the hysteresis curve. The curves along both branches of the hysteresis loop exibit the same intensity distribution. Maxima of the intensity occur at the steep parts of the loop around H_c. These regions correspond to the phase of $130^o \div 180^o$ (or $310^o \div 360^o$). Noise intensity in these regions exceeds by about 25÷30 dB the one occurring in the saturation regions. The tension σ leads to an appreciable decrease of the noise intensity.

The established fluctuations of the hysteresis loop may be considered as a sum of statistically independent elementary fluctuations having proper characteristics. According to the vector model each of these fluctuations is represented on the vector diagram of the n-th harmonic of the induced signal (HIS) by its own noise vector. The resultant noise vector produces complete complex modulation of the HIS, corresponding to the phase-distribution diagram of modulation noise. Fig. 3a and 3b show rough vector diagrams of the first and second HIS respectively. The noise phase-distribution diagrams of these HIS are plotted too. The noise voltage is presented at frequency Δf = 25 Hz under σ = 0. We see that the fluctuations of hysteresis curve cause really a com-

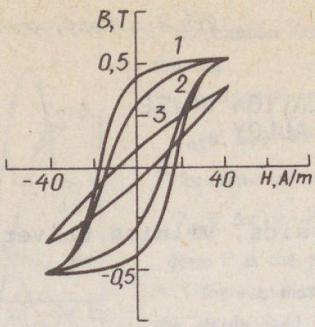

Fig. 1. Hysteresis loop under tension σ, MPa = 0 (1); 72,5 (2); 145 (3).

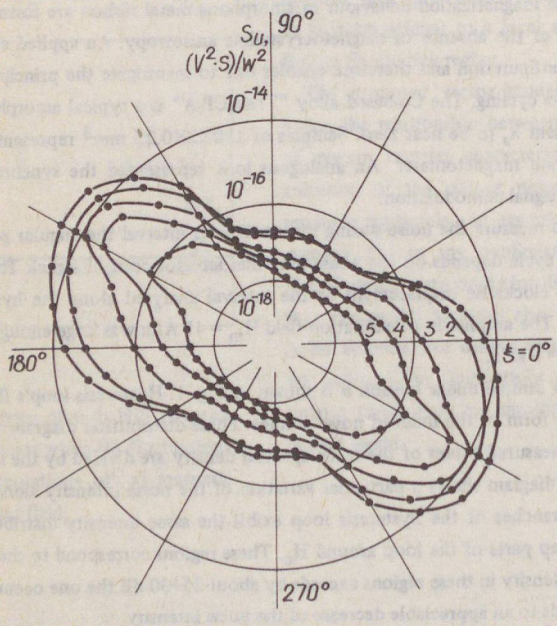

Fig. 2. Phase-distribution diagram of induced noise voltage.
Tension σ, MPa = 0 (1); 36,3 (2); 72,5 (3); 108,8 (4); 145 (5).

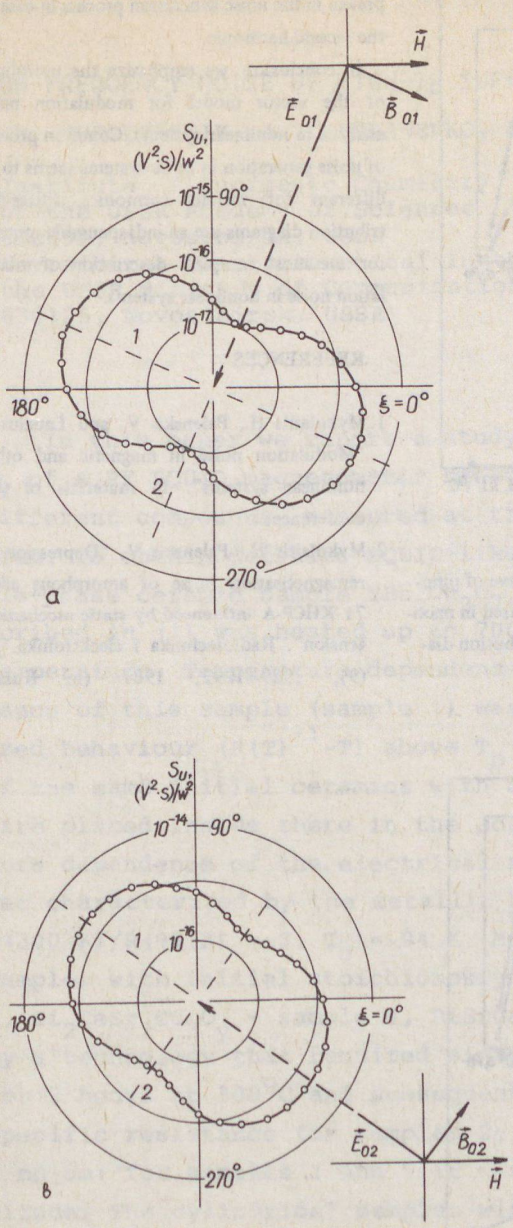

Fig. 3. Vector diagram and modulation noise phase-distribution diagram for the first (a) and second (b) HIS. Tension $\sigma = 0$.

plex modulation of the output harmonics. A phase modulation prevails for the first HIS and amplitude modulation – for the second one. This fact is in complete agreement with conclusions of the vector model, accounting the real distribution of fluctuation intensity along the hysteresis curve (Fig. 2). The noise phase-distribution diagram in Fig. 3a allows to distinguish at least two different fluctuation processes in the cycling period. One of them is related to the process of domain structure rearrengement corresponding to the steep parts of hysteresis loop. The other one performs the noise behaviour in the saturation regions. A presence of several independent noise mechanisms produces different performances of the modulation noise to be measured at various points of the phase-distribution diagram.

Namely, the noise intensity dependence on the static uniform tension σ of the samples is presented in Fig. 4a and 5a for the regions of phase-distribution diagrams corresponding to both the maximum (1) and minimum (2) modulation noise intensities of the first and second HIS, respectively. It has been established that the noise decreases under the tension σ, if $\lambda_s \sigma < 0$. The effect can be explained by enhancement of reversibility in the magnetization process with increasing the stress. Pinning centres (regions of internal stress extreme gradient, nonmagnetic inclusions, etc.) impede a reversible motion of the domain walls resulting in Barkhausen jumps. These jumps are the main source of modulation noise. The pinning centres are to be eliminated out of the magnetization process, because reversible rotation of the directions of domain magnetization substitutes the irreversible domain wall motion. As far as the dependence $S_u(\sigma)$ is concerned, the pinning centre may be characterised by an effective stress σ_{eff} [2]. Derivative $\partial S_U/\partial \sigma$ gives a distribution of the centres as the function of σ_{eff} (Fig. 4b and 5b). It is evident, that pinning centres of large σ_{eff}

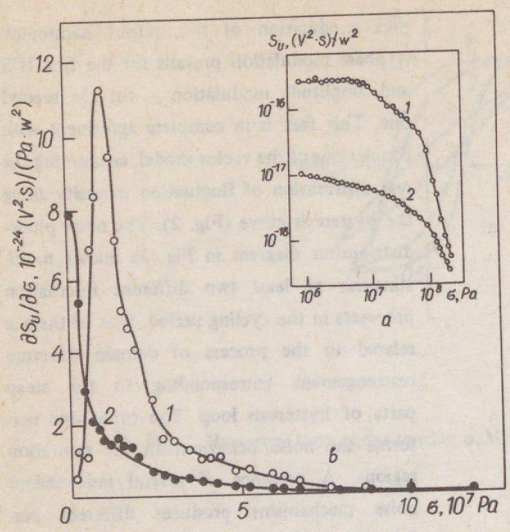

Fig. 4. Spectral density S_u (a) and distribution curve of pinning centres (b) vs tension σ for the first HIS measured in maximum (1) and minimum (2) regions of phase-distribution diagram.

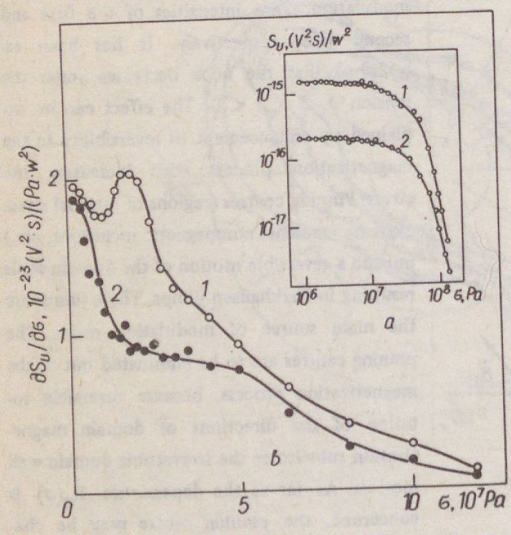

Fig. 5. Same as Fig. 4 for the second HIS.

prevail in the noise generation process in case of the second harmonic.

In conclusion we emphasize the usefulness of the vector model for modulation noise analysis in nonlinear systems. Common process of noise generation in these systems seems to be different for various harmonics. Phase-distribution diagrams are an indispensable requisit for the most complete description of modulation noise in nonlinear systems.

REFERENCES

1. Mykolaitis H., Palenskis V. and Laucius J. "Modulation noise in magnetic and other nonlinear systems". In materials of this conference.
2. Mykolaitis H., Palenskis V. "Depression of remagnetisation noise of amorphous alloy 71 KHCP-A influenced by static mechanical tension". Radiotechnika i elecktronika. 33 (9), 1989–1992, 1987 (in Russ.).

LOW-FREQUENCY NOISE OF HIGH-T_c SUPERCONDUCTORS

I.N. KUROPYATNIK, A.I. ROMANENKO, A.G. CHEREVKO*

Institute of Inorganic Chemistry, Siberian Branch
of the USSR Academy of Sciences
630090, Novosibirsk, USSR
*Novosibirsk Electrotechnical Institute of Communications,
the USSR Ministry of Communications
630125, Novosibirsk, USSR

In this paper we report a study of the noise spectral power S_f of a RF SQUID magnetometer based on bulk superconductors of different compounds, measured at the temperature of liquid helium. To obtain definite SQUID-like properties, an initial single-phase ceramic sample $YBa_2Cu_3O_{7-x}$ obtained by the method described in (1) was heated up to 700°C and then quenched to room temperature. Temperature dependence of the electrical resistance of this sample (sample 1) was characterized by the localized behaviour $(R(T)^{-1} \sim T)$ above T_c = 70 K. Sample 2 was a piece of the same initial ceramics with a 0.2 mm diameter platinum wire placed inside there in the course of preparation. Temperature dependence of the electrical resistance for this sample was characterized by the metallic behaviour $(R(T) \sim T)$ with $R(300\ K)/R(95\ K) = 3$, T_c = 94 K. Multiphase bismuth ceramic samples with initial stoichiometry $BiSr_{0.83}CuCa_{0.5}O_x$ - sample 3, $Bi_2CaSr_2Cu_3O_y$ - sample 4, $BiSrCaCu_2O_z$ - sample 5 were made by a technology that required sintering of the initial oxides for 2 hours at 800°C and subsequent cooling for 8 hours. The specific resistance for samples 2, 3 and 4 was found to be 5 mΩ·cm; for samples 1 and 5 it was higher by an order of magnitude. The cylindrical samples with a diameter of 1.5-3 mm and 8 mm in length, used in our measurements, were placed in the inductance coil of the tank circuit of a standard RF SQUID magnetometer tuned at 30 MHz and modulated at 9 kHz. To study the magnetic properties of SQUIDs, the signal characteristics were measured, i.e. a dependence of voltage V_D at the output on magnetic field ΔH (Fig. 1).

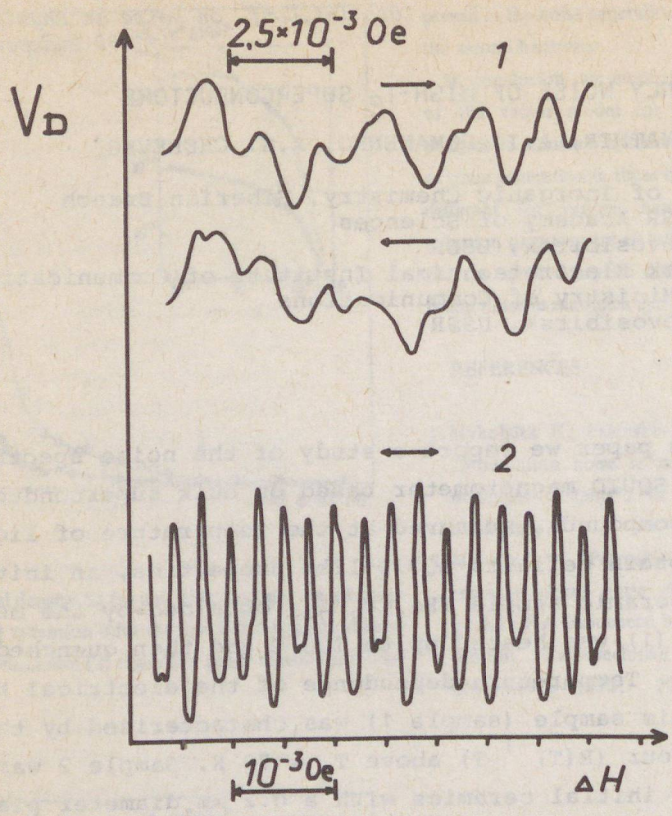

Fig. 1. Dependence of voltage V_D at the output of SQUID electronics on magnetic field ΔH at a temperature of 4.2 K: curve 1 (averaged on the basis of 10 cycles of field sweep) - for sample 1; curve 2 - for sample 2. Curves $\rightarrow$ and $\leftarrow$ are placed apart for better representation.

Curve 1 is characterized by complex periodicity and hysteresis. With magnetic field sweep frequency about 10^{-3} Hz temporal effects appearing in the sample led to a significant ambiguity in the form of signal response. For sample 2 field dependence of V_D was characterized by one period and lack of both hysteresis and temporal effects. Field period was found to be 2.5×10^{-8} T (2.5×10^{-4} Oe), which corresponds to the quantization loop area of 8×10^{-8} m^2, whereas the cross-section of the platinum wire was 3×10^{-8} m^2. The maximum period for quenched sample 1 was found to be 2×10^{-7} T and hence the typical loop area $s \sim 10^{-8}$ m^2.

S_f of a SQUID magnetometer based on the samples under study was recorded by the SK4-72 spectrum analyzer over the frequency range of $0.05\text{-}2\times10^4$ Hz at a temperature of 4.2 K. A niobium screen was used for screening, without attenuating the magnetic field of the Earth. A band-width of the SQUID magnetometer operated in a feed-back mode was 2 kHz for sample 1 and 10 kHz for sample 2. Magnetometer disbalance in the magnetic flux was adjusted close to zero using the additional magnetic field. In each case, SQUID sensitivity was calibrated on magnetic field.

S_f of sample 1 is a set of curves, where curve 2 (Fig. 2) is a typical representative. Below 10 Hz, S_f tends to the dependence $1/f^2$. Studies of S_f behaviour for bismuth ceramic sample 3 gave similar results. For samples 4 and 5, the signal-to-noise ratio was insufficient for stable SQUID operation in the feed-back mode. Curve 1 (Fig. 2) shows the most stable SQUID

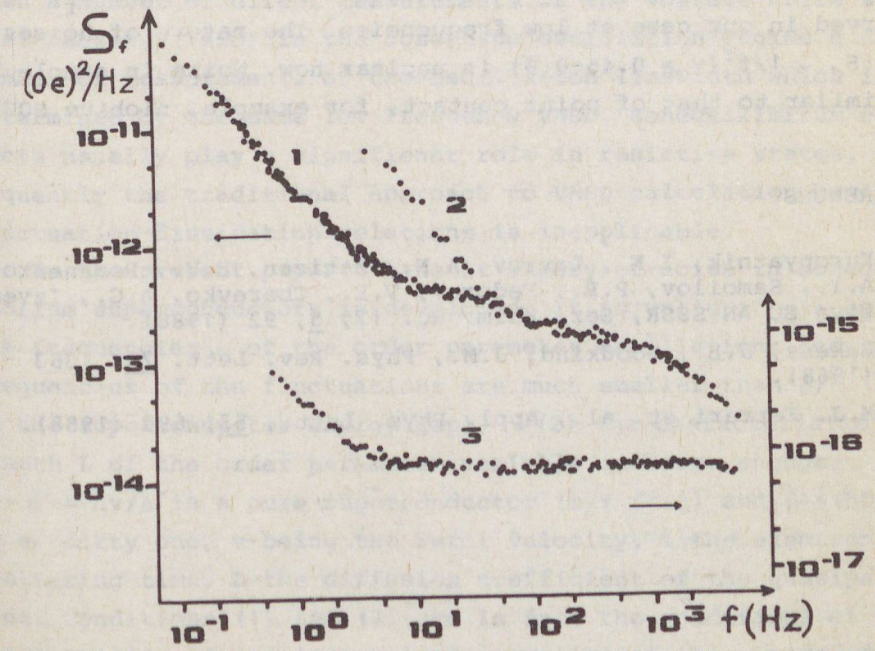

Fig. 2. Noise spectral power S_f versus frequency f: curves 1 and 2 - S_f of SQUID magnetometer based on sample 1; curve 3 - S_f for sample 2.

operation with sample 1. For this state below 10 Hz, $S_f \sim 1/f^{\gamma}$, $\gamma = 1.1\text{-}1.2$. S_f of sample 2 (curve 3 in Fig. 2) below 10 Hz is approximated by the same dependence, for higher frequencies there is the white noise. Within the range of 10-500 Hz, the noise was observed with $S_f \sim 1/f^{\gamma}$ ($\gamma = 0.45\text{-}0.6$). Such S_f dependence is seen in all curves of types 1 and 2 of sample 1, and also of sample 3. The decreasing S_f at frequencies above 1 kHz for sample 1 arose from the amplitude-frequency characteristics of the magnetometer. While measuring S_f for sample 2, noise with a component $1/f^2$ was not observed. $1/f^2$ noise observed in quenched samples of yttrium (sample 1) and also bismuth (sample 3) ceramics is accompanied by random in-time magnetic flux jumps. Such behaviour can arise from transitions between metastable current states of Josephson net (this seems to be similar to phase-sleep phenomena in weakly connected superconductors (2)) or from creep of the magnetic flux trapped in a sample (3). If these processes are characterized by exponential distribution of characteristic times, one expects to find $S_f \sim 1/f$, observed in our case at low frequencies. The nature of noises with $S_f \sim 1/f^{\gamma}$ ($\gamma = 0.45\text{-}0.6$) is unclear now. Noise in sample 2 is similar to that of point contact, for example, niobium SQUID.

REFERENCES

1. Kuropyatnik, I.N., Lavrov, A.N., Matizen, E.V., Romanenko, A.I., Samoilov, P.P., Fedorov, V.E., Cherevko, A.G., Izvestiya SO AN SSSR, Ser. Khim. No. 17, 5, 92 (1988).
2. Lukens, J.E., Goodkind, J.M., Phys. Rev. Lett. 20, 1363 (1968).
3. M.J. Ferrari et. al., Appl. Phys. Lett., 53, 695 (1988).

10th Int.Conf. on Noise in Physical Systems
1989 Budapest, Hungary

THE KINETICS OF FLUCTUATIONS AND THE SPECTRAL DENSITY OF NOISE IN RESISTIVE STATES OF SUPERCONDUCTORS

Sh.M. KOGAN, K.E. NAGAEV

Institute of Radioengineering and Electronics,
USSR Academy of Sciences
Moscow, 103907, USSR

Nonequilibrium resistive states are often realized in superconductors. Examples are the S-c-S contacts (S is a bulk superconductor, c is a constriction or a microbridge) in the regime of Josephson oscillations, vortex motion in type II superconductors, irradiation of superconductors by microwaves, quasiparticle injection. In the case of S-c-S contacts there has been a number of direct measurements of the voltage noise spectral density (VNSD) in the Josephson oscillation regime and a number of measurements of the oscillation linewidth which is determined by the same low-frequency VNSD. Nonequilibrium effects usually play a significant role in resistive states. Consequently the traditional approach to VNSD calculation based on fluctuation-dissipation relations is inapplicable.

In the present paper a kinetic theory of noise in nonequilibrium superconductors is developed. It is valid if (1) both the frequencies ω of the order parameter oscillations and the frequencies of the fluctuations are much smaller than $\Delta/\hbar$ (2Δ is the superconductor energy gap), (2) the characteristic length L of the order parameter variable is large enough: $L \gg \xi = \hbar v/\Delta$ in a pure superconductor ($\hbar/\tau \ll \Delta$) and $L \gg (\hbar D/\Delta)^{1/2}$ in a dirty one, v being the Fermi velocity, τ the electron scattering time, D the diffusion coefficient of the quasiparticles. Conditions (1) and (2) are in fact the conditions of the applicability of quasiparticle description of the superconductor kinetics.

The basis of the present theory is the equation of Boltzmann-Langevin type for the fluctuations of quasiparticle dis-

tribution function $\delta f(\varepsilon\vec{n}\vec{r}\,t)$ which is a function of energy variable ε, unit vector $\vec{n}$ in the quasimomentum direction, space coordinate $\vec{r}$ and time t. We used the kinetic equation for the distribution function $f(\varepsilon\vec{n}\vec{r}\,t)$ derived by Shelankov (1980) who, in turn, proceeded from the equations for Green's functions of the superconductor (Larkin et al. 1977). If conditions (1) and (2) are fulfilled the kinetic equation for the fluctuations has the form

$$\delta[\, a_z\frac{\partial f}{\partial t} + a^2 v\vec{n}\frac{\partial f}{\partial \vec{r}} + (a_z v\vec{n}\dot{\vec{p}}_s + i a_y\dot{\Delta} + a^2\dot{\Phi})\frac{\partial f}{\partial \varepsilon} + I(\varepsilon\vec{n}\vec{r}\,t)] = \delta J(\varepsilon\vec{n}\vec{r}\,t). \quad (1)$$

Here $\delta(...)$ means that the expression in brackets has to be linearized, $\vec{p}_s = \hbar(\partial\chi/\partial\vec{r})/2 - e\vec{A}/c$ and $\Phi = \hbar\chi/2 + e\phi$ are the gauge invariant momentum and potential, χ is the order parameter phase, $\vec{A}$ and ϕ are the electromagnetic field potentials, $a_i = (R_i - A_i)/2$, R_i and A_i are the components of the expansions of the retarded $\hat{R}$ and advanced $\hat{A}$ matrix Green functions of the superconductor in Pauli matrices ($R = R_i\tau_i$), the point over $\vec{p}_s$, Δ and Φ denotes time derivative. The collision integral I is equal to the difference of quasiparticle fluxes outgoing of and ingoing into the state $\varepsilon\vec{n}$:

$$I(\varepsilon\vec{n}\vec{r}\,t) = \int d\varepsilon' \int d\vec{n}'\,[\, J_1(\varepsilon\vec{n}, \varepsilon'\vec{n}') - J_1(\varepsilon'\vec{n}', \varepsilon\vec{n}) + J_2^+(\varepsilon\vec{n}, \varepsilon'\vec{n}') - J_2^-(\varepsilon\vec{n}, \varepsilon'\vec{n}')\,] . \quad (2)$$

The quasiparticle fluxes in this expression can be presented in the form:

$$J_1(\varepsilon\vec{n}, \varepsilon'\vec{n}') = W_1(\varepsilon\vec{n}, \varepsilon'\vec{n}')f(\varepsilon\vec{n})[\,1 - f(\varepsilon'\vec{n}')\,],$$
$$J_2^+(\varepsilon\vec{n}, \varepsilon'\vec{n}') = W_2^+(\varepsilon\vec{n}, \varepsilon'\vec{n}')f(\varepsilon\vec{n})f(\varepsilon'\vec{n}'),$$
$$J_2^-(\varepsilon\vec{n}, \varepsilon'\vec{n}') = W_2^-(\varepsilon\vec{n}, \varepsilon'\vec{n}')[\,1 - f(\varepsilon\vec{n})]\,[\,1 - f(\varepsilon'\vec{n}')\,] . \quad (3)$$

Depending on the signs of the energies ε and ε' these fluxes correspond to scattering transitions within one branch of the quasiparticle spectrum, to transitions between different branches, and to creation or annihilation of quasiparticle

pairs. The coefficients W_1, W_2^+ and W_2^- have the sense of transition probabilities.

The correlation function of the random extraneous fluxes δJ (Langevin sources) in the r.h.s. of Eq. (1) can be found taking into account that different transition processes of the quasiparticles and consequently the corresponding scattering fluxes between different states and in different points $\vec{r}_1$ and $\vec{r}_2$ and time instants t_1 and t_2 are uncorrelated. Each of these scattering processes is a Poisson-like random process and therefore the correlation function of the fluxes δJ is

$$\langle \delta J(\varepsilon_1 \vec{n}_1 \vec{r}_1 t_1) \delta J(\varepsilon_2 \vec{n}_2 \vec{r}_2 t_2) \rangle = -\frac{1}{N_F} \delta(t_1 - t_2) \delta(\vec{r}_1 - \vec{r}_2) [\, \delta(\vec{n}_1 - \vec{n}_2) *$$

$$* \delta(\varepsilon_1 - \varepsilon_2) \int d\varepsilon' \int d\vec{n}' [\, J_1(\varepsilon_1 \vec{n}_1, \varepsilon' \vec{n}') + J_1(\varepsilon' \vec{n}', \varepsilon_1 \vec{n}_1) + J_2^+(\varepsilon_1 \vec{n}_1, \varepsilon' \vec{n}') +$$

$$+ J_2^-(\varepsilon_1 \vec{n}_1, \varepsilon' \vec{n}')] - J_1(\varepsilon_1 \vec{n}_1, \varepsilon_2 \vec{n}_2) - J_1(\varepsilon_2 \vec{n}_2, \varepsilon_1 \vec{n}_1) + J_2^+(\varepsilon_1 \vec{n}_1, \varepsilon_2 \vec{n}_2) +$$

$$+ J_2^-(\varepsilon_1 \vec{n}_1, \varepsilon_2 \vec{n}_2)] \,. \qquad (4)$$

Here N_F is the density of states at the Fermi energy.

Equation (1) should be supplemented by the linearized self-consistency equation for the energy gap Δ (λ is the interaction constant):

$$\delta\Delta = -i\lambda \int d\varepsilon \int d\vec{n} \; \delta[\, a_y f] \qquad (5)$$

and by the linearized electroneutrality condition and the expression for the current density fluctuation:

$$\delta\Phi(\vec{r}\, t) = \int d\varepsilon \int d\vec{n} \; \delta[\, a^2 (f - 1/2)] \,, \quad \delta j(\vec{r}\, t) = eN_F v \int d\varepsilon \int d\vec{n} \; \vec{n} \delta[\, a_z f] \,. \qquad (6)$$

Equations (1)-(6) form a complete system for the fluctuation kinetics in superconductors.

The method developed has been used to calculate the VNSD across a long ($L >> (\hbar D/\Delta)^{1/2}$) S-c-S junction in the regime of strong self-stimulation of superconductivity, i.e. in the range of current that corresponds to the plateau on the current-voltage characteristic (CVC) of the contact. The effect of self-stimulation is caused by a strong deviation of the quasi-

particle distribution function $F(\varepsilon) = f(-\varepsilon)-f(\varepsilon)$ from equilibrium (Aslamazov et al. 1976). The current suppresses the order parameter Δ in the microbridge against its value Δ_o in the banks. The quasiparticles with energies $\varepsilon < \Delta_o$ turn out to be trapped in a well and can escape into the banks only after obtaining an energy $\varepsilon > \Delta_o$. For these quasiparticles the time of establishing equilibrium is the energy relaxation time which is large at low temperatures. Owing to the impurity scattering of the quasiparticles in the well, the jittering well walls cause a diffusion flux of quasiparticles towards higher energies, so that their number at the gap decreases and consequently the order parameter and the supercurrent increase (Aslamazov et al. 1976). Averaging Eq. (1) over the contact volume and over a great number of Josephson oscillation periods we derive an equation of energy diffusion for the fluctuations $\delta F(\varepsilon)$ of the isotropic distribution function. At low frequencies it takes the form:

$$\delta\left[\frac{\partial}{\partial\varepsilon}\left(D_\varepsilon\frac{\partial F}{\partial\varepsilon}\right) - I_{ph}\right] = \delta J_{ph} + \frac{\partial}{\partial\varepsilon}\delta j_\varepsilon, \tag{7}$$

I_{ph} and δJ_{ph} are the collision integral and the random extraneous flux corresponding to the phonon scattering, δj_ε is the fluctuation of the diffusion flux along the "energy axis" and the coefficient of this diffusion is

$$D_\varepsilon = \frac{\Delta_o}{\hbar}\, 4e^2\overline{U^2}\,\Delta^2(\varepsilon^2 - \Delta^2)^{-1}, \tag{8}$$

$U(t)$ being the instantaneous voltage across the contact, the bar denotes averaging over time. The principal source of noise in the region of plateau on the CVC are the fluctuations δj_ε of the diffusion flux which are caused ultimately by the randomness of the impurity scattering. The correlation function of $\delta j(\varepsilon t)$ is proportional to D_ε (analogue of the fluctuation-dissipation relation):

$$\langle\delta j_\varepsilon(\varepsilon_1 t_1)\delta j_\varepsilon(\varepsilon_2 t_2)\rangle_\omega = \frac{D_\varepsilon}{\overline{V(\varepsilon)}\overline{N_F}}\,\delta(\varepsilon_1 - \varepsilon_2). \tag{9}$$

Here $V(\varepsilon)$ is the contact volume accessible for quasiparticles with a given energy ε, the subscript ω denotes the Fourier transform.

The fluctuations δj_ε cause fluctuations of the distribution function at energies $\varepsilon \cong \Delta$ and consequently (through Eq. (5)) fluctuations $\delta\Delta$ of the energy gap. If a supercurrent $\vec{j}_s = \pi e N_F D \Delta F(\Delta) \vec{p}_s/\hbar$ is flowing through the junction the fluctuations $\delta\Delta$ cause fluctuations of the supercurrent δj_s. As the total current is fixed, these fluctuations lead to fluctuations δj_n of the normal current which result in voltage fluctuations. The corresponding VNSD at zero frequency is

$$S_U^{(s)}(0) = 4kT \frac{R_d^2}{R_n} \frac{\Delta_o}{kT} \Delta_o^2 \left(4e^2 \bar{U}^2\right)^{-1}. \qquad (10)$$

Here R_d and R_n are the small-signal and normal resistances of the contact. Usually $S_U^{(s)}$ is much greater than S_U^n which is caused by the Nyquist noise source in the normal resistance of the contact and was calculated earlier (Likharev et al. 1972). With respect to this result one can understand why the measured VNSD is as a rule 3÷10 times greater than its value predicted by Likharev and Semenov. One can understand also the observed shift of the VNSD (as a function of $\bar{U}$) with respect to the maximum of $R_d(\bar{U})$ and the decrease of VNSD as the temperature approaches the critical temperature T_c and Δ_o tends to zero.

REFERENCES

1. Aslamazov, L.G., Larkin, A.I., Zh. Eksp. Teor. Fiz. 70, 1340 (1976).
2. Larkin, A.I., Ovchinnikov, Yu.N., Zh. Eksp. Teor. Fiz. 73, 299 (1977).
3. Likharev, K.K., Semenov, V.K., Pis'ma Zh. Eksp. Teor. Fiz. 15, 625 (1972).
4. Shelankov, A.L., Zh. Eksp. Teor. Fiz. 78, 2359 (1980).

10th Int.Conf. on Noise in Physical Systems
1989 Budapest, Hungary

CHARACTERIZATION OF HIGH-TEMPERATURE SUPERCONDUCTORS BY MICROWAVE NOISE EMISSION

J. KONOPKA, G. JUNG

Instytut Fizyki PAN
02-668 Warszawa, Poland

The discovery of superconductivity in ceramic oxides among which the best known are yttrium (YBCO), bismuth (BCSCO) and thallium (TCBCO) compounds evoked much of excitement not only because of the possibly new mechanism of superconductivity which may be involved in these compounds, but also owing to their potential applications. Several technological procedures have been proposed to obtain bulk materials and thin films. It appears, however, that most of the oxide superconductors grow in the form of agglomerates of anisotropic grains separated by nonstoichiometric or structurally damaged interface material. The granularity strongly influences the electric and magnetic properties of the material.

Almost all methods known in solid state physics were applied to characterize the high-Tc materials. In this paper we propose still another approach. It relies on the measurement of the noise emanating from the superconductor. Such a noise arises, in principle, owing to the energy conversion in microregions of the material which are characterized by strong nonlinear response to the d.c. electric energy supplied to the sample. These nonlinearities are also strongly dependent on the external magnetic field. The magnetic field constitutes then yet another experimental variable. Measurements of the noise energy spectrum as a function of the temperature (T), the bias current (I) and the magnetic field (B) may provide reliable information on the degree of granularity, twining and on the density and strength of the flux pinning centres. Most of these information is difficult to obtain by other methods.

The noise spectrum emanating from the superconductor may extend even up to the Terahertz range. It is composed of a background noise attributed to the low-frequency dissipative processes, mainly a viscous flux flow, and the excess emission lines due to radiating Josephson junctions and their interaction with moving flux structures. Every Josephson junction present in the investigated material should convert d.c. to a.c. energy satisfying Josephson frequency-voltage relation ($f/V \cong 483.6$ MHz/μV). The energy involved in such a process in a single junction is of the order of 10^{-12} to 10^{-15} W, and is mostly dissipated inside the material. Only a part of this energy, still decreased by the impedance mismatch, radiates from the surface to the external world. Therefore this method is mostly suitable for the investigation of surface layers and thin film superconductors.

We found that the exploration of the noise emission at microwave frequencies in an experimental arrangement in which the waveguide output provides an excellent isolation from 1/f noise and other low frequency noise sources give good insight into the physical processes occurring in high-temperature superconductors. Our experimental holder realized for X-band is presented in Fig. 1. The superconducting sample (a thin film strip or a rectangular bar, generally 3.5 mm long and 0.1 to 0.5 mm wide) is connected by 4 leads. The printed circuit together with output waveguide flange form the capacitively connected load for the fundamental TE01 mode. Microwave radiation from the film is detected by a wide-band superheterodyne receiver (T_{noise} = 560 K), tuned either to 11.3 or 12.6 GHz. The 3 dB receiver bandwidth is close to 250 MHz. The signal power amplified by an IF amplifier is measured by a wide band bolometric head (1).

Our method has been applied to several YBCO and BCSCO thin film samples deposited by different techniques on various substrates. In Fig. 2 we present a typical spectrum of the YBCO film deposited by pyrolysis on ZrO_2 substrate. Significant excess emission is a manifestation of pronounced granularity and a relatively flat background, not increasing with bias current, is an indication of a large concentration of strong pinning

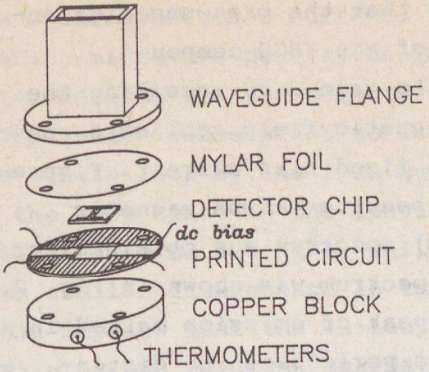

Fig. 1. X-band waveguide holder for measurements of microwave noise emission from high-Tc thin films

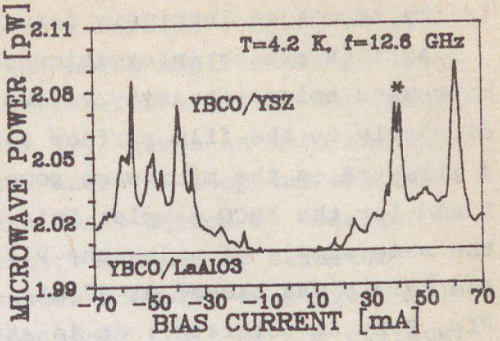

Fig. 2. Wide-band noise emission from YBCO films: granular on ZrO_2 and almost epitaxial on $LaAlO_3$.

centres. In contrast, the flat lower curve obtained for magnetron deposited YBCO on $LaAlO_3$ substrate indicates that the film is almost epitaxial. Similar behaviour was obtained for other samples deposited on $LaAlO_3$ substrates. Figure 3 compares the noise emission and the dynamic resistivity of YBCO and BCSCO magnetron deposited films. Electron microscopic tests revealed that BCSCO films are significantly less granular and more densely packed than the corresponding YBCO films. This feature is perfectly reflected in the X-band noise spectra of both materi-

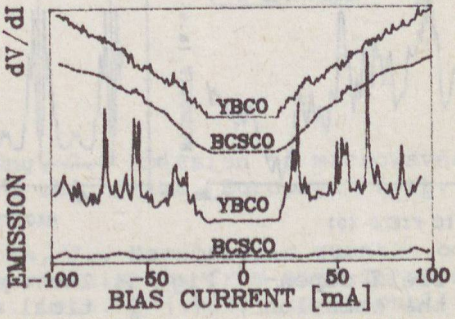

Fig. 3. Comparison of microwave noise emission and dynamic resistivities of magnetron deposited YBCO and BCSCO samples.

als. We would like to add, however, that the pronounced granularity is not an intrinsic feature of the YBCO compound.

An interesting information can be gained by recording the microwave noise intensity versus magnetic field applied perpendicularly to the film surface for a fixed bias current. Figure 4 illustrates the microwave power spectrum versus magnetic field for the YBCO sample. This P(B) spectrum was obtained for the same sample of which the P(I) spectrum was shown in Fig. 2. The sample was biased at 37 mA (at peak of emission marked in Fig. 2 by an asterisk). At least two periods can be distinguished in this recording. The Fourier spectrum of the large period marked by the frame is shown as an insert. Careful analysis of this spectrum suggests that the noise may come from a radiating multi-junction interferometer, actually a 13-loop cluster (2). Indeed the simplified theoretical model of the 13 identical Josephson junctions connected in parallel by superconducting electrode can generate quite a similar spectrum. Figure 5 shows the results of such a calculation (the plot of

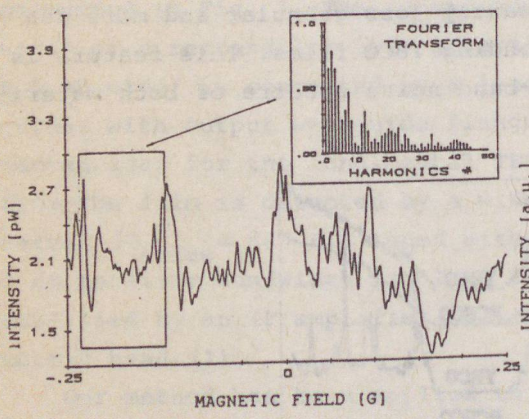

Fig. 4. Magnetic field dependence of the emission line marked by asterisk in Fig. 2. Insert shows the Fourier transform of "large" period.

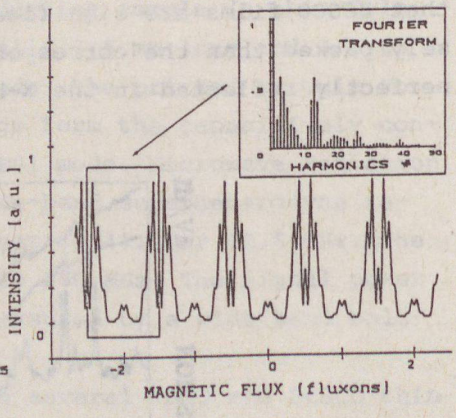

Fig. 5. The square of the critical current vs. magnetic field calculated for 13-loop quantum interferometer. Insert shows Fourier transform of single period.

the squared critical current, which is proportional to the radiating microwave power). An important information can be also obtained from the periodicity of the noise amplitude. The large period which corresponds to the increase of the flux threading the single loop by the flux quantum (Φ_o) gives an information of the loop size (in the considered case the loop surface was estimated to be 200 μm^2), while the small period is associated with similar flux change in the entire multi-loop structure (this implies that the 13-loop cluster occupies some 2900 μm^2). Similarly one may even estimate the upper limit of the critical current of a single weak link contributing to the particular emission peak (at a given bias current) (2).

Independent microstructural tests have been performed in order to verify the applicability of the proposed method. The agreement between microscopic and microwave noise tests was very good. The microwave noise tests can be always easily performed along with standard superconducting transition measurements providing an instant microstructural information without the need of a sophisticated electron microscopic equipment.

ACKNOWLEDGEMENTS

The authors thank S.J. Lewandowski for his help and advice in preparing the manuscript. Technical assistance in thin film fabrication given by P. Gierłowski and W. Kula is gratefully acknowledged. This work was supported by Polish Government grant CPBP 01.9.

REFERENCES

1. Konopka, J., Jung, G., Emission of microwaves from d.c.-biased Y-Ba-Cu-O thin films. Europhys. Lett. 8 549-553 (1989).
2. Jung, G., Konopka, J., Macroscopic quantum coherence effects in microwave emission from high-Tc superconducting films. Europhys. Lett. 9 (1989) (to be published).

SESSION 4

QUANTUM NOISE
(SQUIDS, MASERS, LASERS, QUANTUM OPTICS)

10th Int.Conf. on Noise in Physical Systems
1989 Budapest, Hungary

EXPERIMENTS ON 1/f NOISE AGREEMENTS AND DISAGREEMENTS WITH HANDEL'S PREDICTIONS

A. van der ZIEL

EE Department, University of Minnesota
Minneapolis, MN 55455, USA

Abstract. In most electronic devices Handel's theory of 1/f noise is verified experimentally. The theories of acceleration 1/f noise and 1/f noise in n-type Silicon require more work. Generation-recombination 1/f noise does not fit Handel's theory. The collector 1/f noise in BJTs needs a new model.

1. INTRODUCTION

In 1969 Hooge introduced the following 1/f noise relation[1]

$$\frac{S_I(f)}{I^2} = \frac{\alpha_H}{fN} \qquad \text{(Hooge equation)} \qquad (1)$$

Here α_H is the Hooge parameter, $N = I\tau/e$ is the number of carriers in the system; τ is the carrier transit time in collision-free devices and corresponds to the drift time in collision-dominated devices.

α_H can always be defined but may not always have meaning. For long resistors ($L > 1000$ μ meter)[1,2] $\alpha_H = 2\text{-}5\times10^{-3}$; it is apparently an invariant of the system. α_H decreases with decreasing length[3] and can be orders of magnitude smaller for short devices (FETs, pn diodes and BJTs).

In non-uniform devices N must be replaced by the number $\Delta N(x) = N(x)\Delta x$ of carriers in the section Δx. Equation (1) then becomes a distributed noise source.

Handel's quantum 1/f noise theory[4] gives a derivation of Eq. (1) that expresses α_H in terms of fundamental parameters of the system:

$$\alpha_H = \frac{4\alpha}{3\pi}\frac{\Delta v^2}{c^2} \qquad (2)$$

where c is the velocity of light, Δv the change in velocity along the electron path, and $\alpha = 2\pi q^2/hc$ (emu) is the fine structure constant for conglomerates of charge q. For single electrons and holes $\alpha = \alpha_o = 2\pi e^2/hc = 1/(137)$. The 1/f current noise is associated with the low frequency Bremsstrahlung emitted by accelerated or decelerated electrons.

If a(t) is the electron acceleration,

$$\Delta v = \int_0^\tau a(t)dt \quad \text{and} \quad F(0) = \int_0^\tau a(t)dt \tag{3}$$

is the l.f. Fourier transform of a(t). Equation (2) may thus be written[5]

$$\alpha_H = \frac{4\alpha_o}{3\pi}\left(\frac{q}{e}\right)^2 \frac{[F(0)]^2}{c^2} \tag{3a}$$

For secondary emission processes $q/e = I_a/I_{pr} = \delta$ and I_{pr} is the primary current; for vacuum photodiodes q/e = n, the average number of electrons emitted per incoming photon, and for most other processes q/e = 1.

2. 1/f NOISE IN COLLISION-FREE DEVICES

2a. Secondary emission 1/f noise[6,7]

$$(\alpha_H)_{theo} = \frac{4\alpha_o}{3\pi}\delta^2\left(\frac{\Delta v}{c}\right)^2; \quad S_I(f) = (\alpha_H)_{exp}\frac{eI_a}{f\tau_{da}} \tag{4}$$

$$\tau_{da} = \frac{2d_{da}}{\Delta v}; \quad \Delta v = \left[\frac{2e}{m}(V_a - V_d)\right]^{1/2} \tag{4a}$$

Hence $S_I(f)$ varies as $(\Delta v)^3$, corresponding to $(V_a - V_d)^{3/2}$.

Equating $(\alpha_H)_{theo} = (\alpha_H)_{exp}$ yields d_{da}, the electron path length. For tube # 1 $d_{da} = 4.8 \pm 0.3$ mm (average over 7 independent measurements); for tube #2 $d_{da} = 7.0 \pm 0.6$ mm (average over 7 independent measurements). This is excellent agreement.

2b. Vacuum photodiode 1/f noise[8]

In these devices one has quantum 1/f noise due to acceleration of electrons and photoemission noise due to fluctuations in the cathode work function. The quantum part yields

$$\alpha_H = \frac{4\alpha_o}{3\pi} n^2 \left(\frac{\Delta v}{c^2}\right)^2 \quad ; \quad S_I(f) = \alpha_H \frac{eI_a}{f\tau_{ca}} \tag{5}$$

$$S_I(\infty) = 2eI_a n \quad ; \quad \tau_{ca} = \frac{2d_{ca}}{\Delta v} \quad ; \quad \Delta v = \left[\frac{2e}{m} V_a\right]^{1/2} \; ; \qquad (5a)$$

experimentally n = 1.52. The work function fluctuation spectrum is

$$\text{const.} \frac{eI_a{}^2 V_a{}^0}{f^{3/2}} \quad \text{and is due to diffusion of ions.} \qquad (6)$$

$$\text{Put } S_I(f) - S_I(\infty) = A + BV_a{}^{3/2} \qquad (7)$$

where A varies as $1/f^{3/2}$ and B as 1/f. Experimentally,

$A(100) = 6\times10^{-24}$ A²/Hz ; $A(10) = 3.3\times10^{-22}$ A²/Hz ;

$B(100) = 8.0\times10^{-27}$ A² V$^{3/2}$/Hz $B(10) = 7.3\times10^{-26}$ A² V$^{3/2}$/Hz

$f^{3/2}$ A = (8±2)10^{-21} A² Hz$^{1/2}$; fB = (7.6±0.4)$\times10^{-25}$ A² V$^{3/2}$

fB yields d_{ca} (0.60±0.03) cm. This is very good agreement.

2c. Partition 1/f noise in pentodes (6AU6) (cathode noise suppression)

Since the device has two current-carrying electrodes 2 (screen grid) and a (anode)[9,10], we introduce v_a, v_2, I_a, I_2 and N_a, N_2:

$$S_p(f) = \frac{4\alpha_o v_a v_2}{3\pi c^2} \frac{I_a I_2}{f(N_a N_2)^{1/2}} \qquad (8)$$

$$v_a = \left(\frac{2e}{m} V_a\right)^{1/2} \quad ; \quad v_2 = \left(\frac{2e}{m} V_2\right)^{1/2} \qquad (8a)$$

$$N_2 = I_c(\tau_{m1}+\tau_{12})/e \quad ; \quad N_a = N_2 + I_a\tau_{2a}/e \qquad (8c)$$

$$\tau_{m1} = \frac{3d_{m1}}{(2e/m)^{1/2} V_m{}^{1/2}} \quad ; \quad \tau_{12} = \frac{2d_{12}}{(2e/m)^{1/2}(V_{m1}{}^{1/2}+V_2{}^{1/2})} \quad ;$$

$$\tau_{2a} = \frac{2d_{2a}}{(2e/m)^{1/2}(V_2{}^{1/2}+V_a{}^{1/2})} \qquad (8d)$$

6AU6 has d_{m1} = 0.12 mm; d_{12} = 1.0 mm, d_{2a} = 3.0 mm

case(a) V_{m1} = 2.0V; V_a = 454V; V_2 = 134V

case(b) V_{m1} = 2.0V; $V_a = V_2$ = 134V

$$\frac{S_p(10)_a}{S_p(10)_b} = 1.75 \text{ (theory)}, 1.74\text{(exp)}; \quad \frac{(v_a)_a}{(v_a)_b} = 1.84$$

3. 1/f NOISE IN SEMICONDUCTOR RESISTORS AND FETs

In resistors and FETs one can apply Eq. (2) provided that Δv is now the change in velocity between collisions and that averages are taken over k-space. The theory of section 1c can be applied and the parameter F(0) can be introduced. If a(t) is the acceleration

$$a(t) = \frac{h}{m^*}\frac{dk}{dt} \quad , \quad F(0) = \frac{h}{m^*}\Delta k \tag{9}$$

Equation (9) relates the 1/f noise to scattering processes, and as a consequence the 1/f noise can be described as mobility 1/f noise. The Handel noise sources can be translated into scattering noise sources. In addition there can be surface 1/f noise via carrier tunneling.

3a. Scattering processes[11,12]

1. Normal collision processes (phonon interaction)
   In Si at 300K $\alpha_{Hn} = 3.5\times10^{-9}$; $\alpha_{Hp} \simeq 1.0\times10^{-8}$ (estimated)
2. Umklapp to next Brillouin zone

$$h\Delta k = \frac{h}{a} \quad ; \quad \alpha_H = \alpha_{Hu} = \frac{4\alpha_o}{3\pi}\left(\frac{h}{m^* ac}\right)^2 \tag{10}$$

Occurs in silicon PMOS devices under strong inversion or in $Hg_{1-x}Cd_xTe$ for small x (degeneration); a is the lattice spacing.

3. Umklapp + Intervalley scattering in n-type Si

N-type Si has 6 equivalent valleys; each valley has one opposite valley that gives Umklapp noise by scattering and four adjacent valleys that give intervalley noise by scattering.

If one has multiple collision processes one uses the mobility fluctuation model. One writes[12]

$$\frac{1}{\mu} = \Sigma\frac{1}{\mu_i} \quad ; \quad \frac{\delta\mu}{\mu^2} = \Sigma\frac{\delta\mu_i}{\mu_i{}^2} \quad , \text{ or} \tag{11}$$

$$\alpha_H = \Sigma\,\alpha_{Hi}\left(\frac{\mu}{\mu_i}\right)^2 \quad ; \quad \alpha_{Hi} = \frac{[S_I(f)]_i}{I^2} f_N = \frac{4\alpha_o}{3\pi}\frac{[F_i(0)]^2}{c^2} \tag{11a}$$

$$\text{Generally } \frac{\mu}{\mu_i} \simeq \exp\left(-\frac{\Theta}{4T}\right) \tag{11b}$$

where $\Theta = \Theta_D$ (Debye temperature) for Umklapp processes.

For Umklapp plus normal processes (1+2)

$$\alpha_H = \frac{4\alpha_o}{3\pi}\left(\frac{h}{m^*ac}\right)^2 \exp\left(-\frac{\Theta_D}{2T}\right) + \alpha_{Hn}\left[1 - \exp\left(\frac{-\Theta_D}{4T}\right)\right]^2 \qquad (12)$$

At 300°K and p-channel Si JFETs (process 1); $(\alpha_H)_{theo}=10^{-8}$; $(\alpha_H)_{exp} \simeq 10^{-8}$. At T = 300°K and n-channel Si JFETs (processes 1 and 3): $(\alpha_H)_{exp} = 2.5\times10^{-8}$. Temperature dependence both theoretically and experimentally $\exp(\Theta_D(2T)\alpha_H(\infty)\cdot(\alpha_H)_{theo}$ is due to process (1, 3a, 3b; normal + Umklapp + intervalley. Low-noise P-channel MOSFETs $(\alpha_{Hp})_{exp} = 4\times10^{-7}$ and $(\alpha_{Hp})_{theo} = 4.2\times10^{-7}$ at 300°K, by proper choice of m* [weighted average, Eq. (12)].

α_H for n-channel Si needs further study.

3b. Coherent state 1/f noise[14]; Acceleration 1/f noise[15]

In long semiconductor resistors $\alpha_H = (2\text{-}5)\times10^{-3}$ (Hooge), and in short devices (α_H) corresponds to collision 1/f noise and is much smaller; according to Eq. (2) $4\alpha_o/3\pi = 3.09\times10^{-3}$ and $\Delta v^2/c^2 \ll 1$. Therefore a quantum theory had to be developed that could explain the high values of α_H.

To that end Handel developed the coherent state quantum 1/f noise theory. It yields $\alpha_H = 2\alpha_o/\pi = 4.6\times10^{-3}$, in agreement with experiment.

Because in medium length semiconductor resistors α_H seems to decrease with decreasing device length one would expect a new noise source that accounts for this effect. Such a model is the acceleration 1/f noise model. Due to the applied d.c. field E the acceleration produces Bremsstrahlung between collisions, whereas collision processes produce collision noise pulses. The latter are independent and hence are added quadratically. The Bremsstrahlung pulses generated between pulses are generated coherently and hence add linearly; they give therefore a large effect for large device lengths d.

Since a force eE is applied to the electron, the acceleration $a(t) = eE/m^*_n$ and the drift velocity $u_d = \Delta x/\Delta t = \mu_n E$. Therefore the Fourier transform F(0) of a(t) is

$$F(0) = \int_o^d \frac{eE}{m^*_n}\frac{\Delta t}{\Delta x}\,dx = \int_o^d \frac{eE}{m^*_n \mu_n E}\,dx = \frac{d}{\tau_n} \qquad (13)$$

where $\tau_n = m^*_n\mu_n/e$ is the average time between collisions for electrons; it is of the order of 10^{-12} sec. The corresponding Hooge parameter is

$$(\alpha_H)_{acc} = \frac{4\alpha_o}{3\pi} \frac{[F(0)]^2}{c^2} = \frac{4\alpha_o}{3\pi} \left(\frac{d}{c\tau}\right)^2 \qquad (14)$$

If $(\alpha_H)_{coll}$ is the Hooge parameter due to collisions, then

$$(\alpha_H)_{tot} = (\alpha_H)_{coll} + (\alpha_H)_{acc} \qquad (14a)$$

Experiment. Applied to a resistor or MOSFET:

$$S_I(f) = \frac{\alpha_H e \mu I_d V_d}{f d^2} \quad , \quad \text{or} \quad \frac{S_I(f)}{\mu I_d V_d} = \frac{\alpha_H}{d^2} \frac{e}{f} \qquad (15)$$

is independent of d, if and only if α_H varies as d^2.

Peng[16] obtained the following results for silicon MOSFETs at 10 Hz, with units of different lengths built on the same substrate.

α	14 μm	19 μm	24 μm	194 μm	Average
$\frac{S_I(f)}{\mu I_d V_d} \times 10^{20}$	4.1	3.5	5.5	5.5	4.6±0.8

$$\frac{\alpha_H}{d^2} = 2.9 = \frac{3.09\times10^{-3}}{(c\tau)^2} \quad ; \quad \tau = 1.1\times10^{-12} \text{ sec}$$

Similar results were obtained for large numbers of Si P-type MOSFETs and N-type MOSFETs. All had units of different length built on the same substrate. α_H always varied as d^2, except for very low d, and all had $\tau \approx 10^{-12}$ sec, which is of the order of the time constant associated with the scattering process. The devices of very short length had α_H independent of d, because in that case scattering 1/f noise predominates over acceleration 1/f noise.

The longest units had d = 194 μm; this was not long enough to produce $\alpha_H = 4.6\times10^{-3}$, as expected for coherent state 1/f noise. Peng's curves did not saturate for the largest d and the above model does not give saturation because full coherence is assumed. A finite coherence length would give the desired effect. As long as saturation effects have not been observed, the possible transition from acceleration noise to coherent state 1/f noise remains an open question.

Long silicon JETs do not show the effect. In p-type Si-resistors with high doping and d up to 900 μ meter the acceleration 1/f noise was masked by contact 1/f noise. Further studies are on the way.

4. DIFFUSION 1/f NOISE[17]

According to the Einstein relation $eD = kT\mu$, the diffusion constant D

and the mobility μ in semiconductors are directly related, so that a fluctuation in μ would correspond to a fluctuation in D. Consequently one would expect for a section Δx at x

$$\frac{S_I(x,f)}{I^2(x)} = \frac{S_D(x,f)}{D^2(x)} = \frac{\alpha_H}{fN(x)\Delta x} \quad . \tag{16}$$

4a. Diode 1/f noise

Applying this to a short n^+-p diode having a length w_p of the p-region and averaging over x and x' yields

$$S_I(f) = \frac{2eI_n}{4f\tau_{dn}} \alpha_H \ln \frac{N(0)}{N(w_p)} \tag{17}$$

where $\tau_{dn} = w_p^2/2D_n$ as the diffusion time of electrons through the p-region, whereas "short" means $w_p \ll L_n$, $L_n = (D_n\tau_n)^{1/2}$ and τ_n is the electron life time in the p-region.

N(0) and $N(w_p)$ are the electron concentration at the junction and at the p-contact, respectively. A calculation shows

$$\frac{N(0)}{N(w_p)} = \frac{D_n/w_p + s_{cn}}{D_n/w_p + s_{cn}\exp(-eV/kT)} \tag{17a}$$

where s_{cn} is the electron surface recombination velocity at the p-contact (6×10^6 cm/sec in n-type Si). For short p^+-n diodes s_{cn} must be replaced by s_{cp} [(4×10^6 cm/sec) in p-type Si].

Diffusion 1/f noise in Si diodes is often masked by generation recombination type 1/f noise. For n^+-p-n and p^+-n-p silicon devices this is less often the case.

For long n^+-p diodes it must be taken into account that the noise generated at x is detected at the junction (x=0) and is thus attenuated by a factor $\exp(-x/L_n)$, as indicated in ref. [18].

Carrying out the calculation one obtains for the external circuit

$$S_I(f) = \alpha_{Hn} \frac{eI}{f\tau_n} f(a) \tag{18}$$

where $$f(a) = \left[\frac{1}{3} - \frac{1}{2a} + \frac{1}{a^2} - \frac{1}{a^3}\ln(1+a)\right] \tag{18a}$$

$a = [N(0)-N_n]/N_n = [\exp(eV/kT)-1]$ and N_n is the equilibrium electron concentration in the p-region.

Wu et al.[19] showed that the voltage dependence of $S_I(f)$ for long $Hg_{1-x}Cd_xTe$ n^+-p diodes was given by (18) and that α_{Hn} had the value $(3\text{-}5)\times10^{-3}$ as expected for coherent state 1/f noise. Fang et al.[20] measured α_{Hp} for long p^+-n Si diodes at back bias and elevated temperatures and found $\alpha_{Hp} = 4\times10^{-3}$, again as expected for coherent state 1/f noise. This is good agreement.

To determine τ_n for long diodes, one measures the diode admittance Y. For n^+-p diodes operating in the diffusion mode

$$Y = g_o(1+j\omega\tau_n)^{1/2} \tag{19}$$

where g_o is the l.f. differential conductance Wu[19] found $\tau_n = 2\times10^{-7}$ sec. For short diodes $\tau_n = w_n^2/2D_n$ is much smaller. Unless α_{Hn} is much smaller, this results in a much larger $S_I(f)$.

Wu found a case where τ_n was 2×10^{-7} sec and $\alpha_{Hn} \simeq 5\times10^{-5}$. This could be Umklapp 1/f noise. If Umklapp 1/f noise can occur, normal collision 1/f noise would not be detectable.

4b. Transistor 1/f noise

By analogy with n^+-p and p^+-n short diodes one would expect for n^+-p-n transistors at forward bias [Eqs. (17)-(17a)]

$$S_{I_B}(f) = \alpha_{Hp}\frac{2eI_b}{4f\tau_{dE}}\ln\left[\frac{(D_p/W_E)+s_{cp}}{D_p/W_E}\right] \tag{20}$$

$$S_{I_C}(f) = \alpha_{Hn}\frac{2eI_c}{4f\tau_{dB}}\ln\left[\frac{(D_n/W_B)+v_n}{D_n/W_B}\right] \tag{20a}$$

It is here assumed that I_B is caused by hole injection into the emitter, diffusion of holes through the emitter, followed by collection by the emitter contact, whereas I_E is caused by electron injection into the base, diffusion through the base and collection by the collector. $\tau_{dE} = W_E^2/2D_p$ and $\tau_{dB} = W_B^2/2D_n$ are diffusion times. s_{cp} is the contact recombination velocity at the emitter contact and v_n the limiting velocity of electrons at high fields. It was found that $S_{I_B}(f) \ll S_{I_C}(f)$ for $I_C/I_B \simeq \beta_F$, as expected[22].

It was first assumed that α_{Hp} and α_{Hn} corresponded to normal collision 1/f noise and occasionally a specimen of a given device type showed agreement with experiment[21]. It was later understood that the situation was more complex.

Fang et al.[22] measured many transistors with widely different f_T =

$(2\pi\tau_{dB})^{-1}$. At low currents I_C and for the same device type, α_{Hn} differed little from unit to unit. At low I_C and for device types with widely different f_T, α_{Hn}/τ_{dB} differed little from type to type.

For devices with different factors $(1+v_nW_B/D_n)$ the expression $1/4(\alpha_{Hn}/\tau_{dB})\ln(1+v_nW_B/D_n) = f_c$ differed little from type to type. If one writes

$$S_{I_C}(f) = 2eI_cf_c/f;\ f_c = \frac{fS_I(f)}{2eI_c} \tag{21}$$

then f_c is an invariant of the system and has the value 15-20 Hz for most units and types. This may give important clues to the collector 1/f noise model, and indicates how Handel's theory must be modified.

At larger currents f_c increases with increasing current I_C; the increase differs from unit to unit and from type to type. This is probably caused by non-uniform current flow through the emitter-base space charge region (emitter crowding) and does not indicate that Hooge's equation is invalid.

5. GENERATION-RECOMBINATION (g-r) TYPE 1/f NOISE

When Peng et al[20] analyzed the 1/f noise of long p^+-i-n Silicon power diodes operating at 410°K and biased in the back direction, they found that $S_I(f)/(I)$ was independent of current. They therefore conjectured

$$S_I(f) = \alpha_H e|I|/f\tau \tag{22}$$

To prove this one observes that $|\Delta I(x)| = eN_T(x)\Delta x/\tau$ is the current generated in the section Δx and that Hooge's equation for the section Δx is

$$\Delta S_I(x)\Delta x = \frac{\alpha_H[\Delta I(x)]^2}{f^\gamma N_T(x)\Delta x} = \frac{(eN_T(x)\Delta x/\tau)^2\alpha_H}{f^\gamma N_T(x)\Delta x} = \frac{e\alpha_H}{f^\gamma\tau}|\Delta I(x)| \tag{23}$$

Integration yields Eq. (22). The spectra of their units all had $\gamma = 1$.

Van der Ziel et al[23] also solved the a.c. Fletcher equation and obtained $Z_{tot} = 1/Y_j + Z_m$. Here Y_j is the admittance of the n^+-i diode and Z_m the modulation impedance due to modulation of the carrier density in the i-region by the a.c. current. If the i-region extends from $-d < x < d$, the solution is

$$p(x) = p(I)\frac{\cosh x/L}{\cosh d/L};\quad Y_j = g_o\frac{L}{L'}\frac{\tanh(d/L')}{\tanh d/L} \tag{24}$$

where $P(x) = (P(I)$ at $x = \pm d$; $g_o = dI/dV$ and $L' = L(1+j\omega\tau)^{-1/2}$ the a.c. diffusion length. For long diodes ($d/L \gg 1$) $\tanh d/L \approx 1$, or

$$Y_j = g_o L/L' = g_o(1+j\omega\tau)^{1/2} \qquad (24a)$$

and the current flow at the boundaries is by diffusion. For $d/L \ll 1$, $p(x) = P(I)$ for all x, $\tanh d/L' = d/L'$ and

$$Y_j = g_o(L/L')^2 = g_o(1+j\omega\tau) \qquad (24b)$$

diffusion is negligible and the current flow is by generation-recombination and drift.[23]

In addition one can evaluate Z_m as a function of frequency. It is found that Z_m has an inductive component. This leads to a complicated resonance for $d/L \gg 1$[20] and to a simple resonance for $d/L \ll 1$.[23]

Measurements on relatively short p-i-n $Hg_{1-x}Cd_xTe$ p-diodes at T = 80K and x = 0.20 yielded $\tau = 10^{-7}$ sec and $2\times10^{-5} < \alpha_H < 2\times10^{-6}$. The spectrum was $1/f^{\gamma}$ with $\gamma \neq 1$, indicating that the noise is not quantum 1/f noise, but g-r type 1/f noise.[23]

Equation (2) can be used to calculate the quantum limit set by direct band to band transitions. If a hole-electron pair is generated, the average energy of the free electron is 3kT/2 and hence $\Delta v_n^2 = 3kT/m^*_n$. For holes we have in the same way $\Delta v_p^2 = 3kT/m^*_p \ll \Delta v_n^2$. Hence in good approximation

$$\alpha_H = \frac{4\alpha_o}{3\pi}\frac{3kT}{m_n^* c^2} \qquad (25)$$

For T = 80°K we have $m^* = 0.0073\ m_o$, and $\alpha_H = 1.7\times10^{-8}$. It is doubtful whether this limit can be reached.

Acknowledgement. This review is based on papers written by the University of Minnesota quantum 1/f noise project, supported by NSF grants and ARO contract DAA-29-85-K02356.

References

1. F. N. Hooge, Phys. Lett, A-29, 139 (1969); Physica, 83B, 9 (1976).
2. H. Hanafi and A. van der Ziel, Physica, 94B, 351 (1978).
3. G. Bosman, R. J. J. Zijlstra and A. D. van Rheenen, Phys. Lett., 78A, 385; 80A, 571 (1980).
4. P. H. Handel, Phys. Rev. Lett. 34, 1492 (1975); Phys. Rev., 22, 745 (1988).
5. A. van der Ziel, A. D. van Rheenen and A. N. Birbas, Phys. Rev. B, July 15 (1989).
6. P. Fang and A. van der Ziel, Physica, 147B, 311 (1987).
7. A. van der Ziel, P. Fang and A. D. van Rheenen, J. Appl. Phys. 65, 1766 (1989).

8. P. Fang, L. He, Q. Peng, H. Kang and A. van der Ziel, J. Appl. Phys. 65, 1766 (1989).
9. A. van der Ziel, C. J. Hsieh, P. H. Handel, C. M. van Vliet and G. Bosman, Physica, 124B, 299, (1984); Physica, 145B, 195 (1987).
10. A. van der Ziel and P. H. Handel, 125B, 286 (1984).
11. A. van der Ziel, P. H. Handel, X. C. Zhu and K. Duh, IEEE Trans. El. Dev., ED-32, 667 (1985).
12. G. Kousik, C. M. Van Vliet, G. Bosman and P. Handel, Adv. Phys. 34, 663 (1985).
13. A. Pawlikiewicz, A. van der Ziel, G. Kousik and C. M. Van Vliet, Sol. State Electron, 31, 2331 (1981).
14. P. H. Handel, in Noise in Physical Systems and 1/f Noises, Eds. A. d'Amico and P. Mazetti, New York, NY, Elsevier (1986), p. 465.
15. A. van der Ziel, J. Appl. Phys., 63, 903 (1988); Q. Peng, A. N. Birbas, A. van der Ziel, A. D. van Rheenen and K. Amberiadis, J. Appl. Phys., 63, 907 (1988).
16. Q. Peng, private communication.
17. T. G. M. Kleinpenning, Physica, 98B, 289 (1980).
18. A. van der Ziel, Proc. IEEE, 76, 2331 (1981) (review paper).
19. X. L. Wu, J. B. Anderson and A. van der Ziel, IEEE Trans. El. Dev., ED-34, 602 (1987).
20. P. Fang, L. He, A. D. van Rheenen, A. van der Ziel and Q. Peng, Sol. State Electron, 32 (1989).
21. A. H. Pawlikiewicz, A. van der Ziel, G. Kousik and C. M. Van Vliet, Sol. State Electron; 31, 831 (1988).
22. R. Z. Fang, A. C. Young, A. D. van Rheenen and A. van der Ziel, to be published.
23. A. van der Ziel, P. Fang, L. He, X. L. Wu and A. D. van Rheenen, J. Vac. Science Technology; A-7, 550 (1989): A detailed theory is in preparation.

10th Int.Conf. on Noise in Physical Systems
1989 Budapest, Hungary

GENERAL DERIVATION OF THE QUANTUM 1/f NOISE EFFECT IN PHYSICAL CROSS SECTIONS AND THE 1/N FACTOR

P.H. HANDEL

Physics Department, University of Missouri
St. Louis, MO 63121, USA

In the fourteen years since the discovery of the Quantum 1/f Effect, the derivation of quantum 1/f noise was presented in the elementary terms of Schrödinger's statistical catalogue model, using second quantization only for photons [1], or not at all [2]-[6]. This approach is natural in view of the close connection between this new effect and diffraction [3] which is usually treated without second quantization, in the statistical catalogue model based on the single-particle solution of the Schrödinger equation, normalized to the number of particles N. Just as the superposition of elementary phase-shifted waves allows for the simplest and most intuitive description of diffraction through a slit, the simplified description of quantum 1/f noise in terms of interference beats between the non-bremsstrahlung part and the slightly frequency-shifted partial scattered waves with bremsstrahlung energy losses, will always provide the simplest and most elementary quantitative derivation of the quantum 1/f effect, easily accessible even at the undergraduate level, in agreement with the experiment [7].

The present paper presents the second-quantized derivation of the Quantum 1/f Effect in a more general form which determines the scattered current from the simultaneous observation of a sample of N outgoing particles. The minimal outgoing sample for defining particle-particle correlations in the scattered wave consists of two particles, and therefore at the Montreal Conference the effect was calculated for the case of two outgoing particles. Since the general derivation also yields a 1/N factor for bosons and a 1/(N-1) for fermions, and since the simplifying restriction to N=2 was promptly used by some people to misinterpret and discredit the theory, a presentation of the general case of N bosons or N fermions will be of interest to all.

We start with the expression of the Heisenberg representation state $|S\rangle$ of N identical bosons of mass M emerging at an angle θ from some scattering process with various undetermined bremsstrahlung energy losses reflected in their one-particle waves $\varphi_i(\xi_i)$

$$|S\rangle = (N!)^{-1/2} \Pi_i \int d^3\xi_i \varphi_i(\xi_i) \psi^+(\xi_i) |0\rangle = \Pi_i \int d^3\xi_i \varphi_i(\xi_i) |S^o\rangle, \qquad (1)$$

where $\psi^+(\xi_i)$ is the field operator creating a boson with position vector ξ_i and $|0\rangle$ is the vacuum state, while $|S^o\rangle$ is the state with N bosons of position vectors ξ_i with i = 1.....N. All products and sums in this paper run from 1 to N, unless otherwise stated.

To calculate the particle density autocorrelation function in the outgoing scattered wave, we need the expectation value of the operator

$$O(\mathbf{x}_1,\mathbf{x}_2) = \psi^+(\mathbf{x}_1)\psi^+(\mathbf{x}_2)\psi(\mathbf{x}_2)\psi(\mathbf{x}_1), \tag{2}$$

known as the operator of the pair correlation. This corresponds to a density autocorrelation function. The presence of two-particle coordinates in the operator O does not mean that we are considering two-particle interactions, it only means that the expectation value which we are calculating depends on the relative position of the particles. Using the well known commutation relations of the boson field operators,

$$\psi(\mathbf{x})\psi^+(\mathbf{y}) - \psi^+(\mathbf{y})\psi(\mathbf{x}) = \delta(\mathbf{x} - \mathbf{y}), \tag{3}$$

$$\psi(\mathbf{x})\psi(\mathbf{y}) - \psi(\mathbf{y})\psi(\mathbf{x}) = 0, \tag{4}$$

$$\psi^+(\mathbf{x})\psi^+(\mathbf{y}) - \psi^+(\mathbf{y})\psi^+(\mathbf{x}) = 0, \tag{5}$$

we first calculate the matrix element

$$N!\langle S^o|O|S^o\rangle = \Sigma'_{\mu\nu}\Sigma'_{mn}\delta(\eta_\nu-\mathbf{x}_1)\delta(\eta_\mu-\mathbf{x}_2)\delta(\xi_n-\mathbf{x}_1)\delta(\xi_m-\mathbf{x}_2)\Sigma_{(i,j)}\Pi'_{ij}\delta(\eta_j-\xi_i). \tag{6}$$

Here the prime excludes $\mu=\nu$ and $m=n$ in the summations and excludes $i=m$, $i=n$, $j=\mu$ and $j=\nu$ in the product. The summation $\Sigma_{(i,j)}$ runs over all permutations of the remaining N-2 values of i and j. On the basis of this result we now calculate the complete matrix element

$$\begin{aligned}\langle S|O|S\rangle &= [1/N(N-1)]\ \Sigma'_{\mu\nu}\Sigma'_{mn}\int d^3\eta_\mu\int d^3\eta_\nu\int d^3\xi_m\int d^3\xi_n \\ &\varphi_\mu^*(\eta_\mu)\varphi_\nu^*(\eta_\nu)\varphi_m(\xi_m)\varphi_n(\xi_n)\delta(\eta_\nu-\mathbf{x}_1)\delta(\eta_\mu-\mathbf{x}_2)\delta(\xi_n-\mathbf{x}_1)\delta(\xi_m-\mathbf{x}_2). \\ &= [1/N(N-1)]\ \Sigma'_{\mu\nu}\Sigma'_{mn}\ \varphi_\mu^*(\mathbf{x}_2)\varphi_\nu^*(\mathbf{x}_1)\varphi_m(\mathbf{x}_1)\varphi_n(\mathbf{x}_2)\end{aligned} \tag{7}$$

The one-particle states are spherical waves emerging from the scattering center located at x=0:

$$\varphi(\mathbf{x}) = (C/x)e^{iKx}\,[1 + \Sigma_{\mathbf{k}l}b(\mathbf{k},l)e^{-iqx}\,a^+_{\mathbf{k},l}]. \tag{8}$$

Here C is an amplitude factor, K the boson wave vector magnitude, $b(\mathbf{k},l)$ the bremsstrahlung amplitude for photons of wave vector $\mathbf{k}$ and polarization l, while $a^+_{\mathbf{k},l}$ is the corresponding photon creation operator, allowing the photon state to be created from the vacuum if Eq. (8) is inserted into Eq. (1). The momentum magnitude loss $q=Mck/\hbar K\equiv 2\pi Mf/\hbar K$ is necessary for energy conservation in the Bremsstrahlung process. Substituting Eq, (8) into Eq. (7), we obtain

$$\langle S|O|S\rangle = |C/x|^4\{N(N-1) + 2(N-1)\Sigma_{\mathbf{k},l}|b(\mathbf{k},l)|^2[1+\cos q(x_1-x_2)]\}, \tag{9}$$

where we neglected a small term of higher order in $b(\mathbf{k},l)$. To perform the angular part of

the summation in Eq. (9), we calculate the current expectation value of the state in Eq. (8), and compare it to the well known cross section without and with bremsstrahlung

$$j = (\hbar K/Mx^2)[1 + \Sigma_{kl}|b(k,l)|^2] = j_o[1 + \alpha A \int df/f], \qquad (10)$$

where the quantum fluctuations have disappeared, where $\alpha = e^2/\hbar c$ is the fine structure constant, $\alpha A = (2\alpha/3\pi)(\Delta v/c)^2$ is the fractional bremsstrahlung rate coefficient, also known in QED as the infrared exponent, and where the 1/f dependence of the bremsstrahlung part displays the well-known infrared catastrophe, i.e., the emission of a logarithmically divergent number of photons in the low frequency limit. Here Δv is the velocity change $h(K-K_o)/M$ of the scattered boson, and $f = ck/2\pi$ the photon frequency. Eq. (9) thus gives

$$\langle S|O|S\rangle = |C/x|^4\{N(N-1) + 2(N-1)\alpha A \int [1+\cos q(x_1-x_2)]df/f\}, \qquad (11)$$

which is the pair correlation function, or density autocorrelation function along the scattered beam with $df/f = dq/q$. The spatial distribution fluctuations along the scattered beam will also be observed as fluctuations in time at the detector, at any frequency f. According to the Wiener-Khintchine theorem, we obtain the spectral density of fractional scattered particle density ρ, (or current j, or cross section σ) fluctuations in frequency f or wave number q by dividing the coefficient of the cosine by the constant term N(N-1):

$$\rho^{-2}S_\rho(f) = j^{-2}S_j(f) = \sigma^{-2}S_\sigma(f) = 2\alpha A/fN, \qquad (12)$$

where N is the number of particles or current carriers used to define the current j whose fluctuations we are studying. Note that our result is not affected by any phase factors which may multiply the individual wave functions of the N particles, because to each phase factor present in $|S\rangle$, there will be a conjugate in $\langle S|$. Quantum 1/f noise is thus a fundamental 1/N effect. The exact value of the exponent of f in Eq. (12) can be determined by including the contributions from all real and virtual multiphoton processes of any order (infrared radiative corrections), and turns out to be $\alpha A - 1$, rather than -1, which is important only philosophically, since $\alpha A \ll 1$. The spectral integral is thus convergent at f=0.

For fermions we repeat the calculation replacing in the derivation of Eq. (6) the commutators of field operators by anticommutators, which finally yields in the same way

$$\rho^{-2}S_\rho(f) = j^{-2}S_j(f) = \sigma^{-2}S_\sigma(f) = 2\alpha A/f(N-1), \qquad (13)$$

which causes no difficulties, since $N \geq 2$ for particle correlations to be defined, and which is practically the same as Eq. (12), since usually $N \gg 1$. Eqs. (12) and (13) suggest a new notion of physical cross sections and process rates which contain 1/f noise, and express a fundamental law of physics, important in most high-tech applications.

We conclude that the conventional quantum 1/f effect can be explained in terms of interference beats between the part of the outgoing DeBroglie waves scattered without bremsstrahlung energy losses above the detection limit (given in turn by the reciprocal duration T of the 1/f noise measurement) on one hand, and the various parts scattered with

bremsstrahlung energy losses; but there is more to it than that: exchange between identical particles is also important. This, of course, is just one way to describe the reaction of the emitted bremsstrahlung back on the scattered current. This reaction thus reveals itself as the cause of the quantum 1/f effect, and implies that the effect cannot be obtained with the independent boson model. The effect, just like the classical turbulence-generated 1/f noise [8],[9] is a result of the scale-invariant nonlinearity of the equations of motion describing the coupled system of matter and field. Ultimately, therefore, this nonlinearity is the source of the 1/f spectrum in both the classical and quantum form of the theory. We can say that the quantum 1/f effect is an infrared divergence phenomenon, this divergence being the result of the same nonlinearity. The new effect is, in fact, the first time-dependent infrared radiative correction. Finally, it is also deterministic in the sense of a well determined wave function, once the initial phases γ of all field oscillators are given. In quantum mechanical correspondence with its classical turbulence analog, the new effect is therefore a quantum manifestation of classical chaos which we can take as the definition of a certain type of quantum chaos.

Acknowledgment: The author thankfully acknowledges the magnanimous support of Annie and Edward Karcich of Salinas, CA, over the last 25 years, as well as the vitally important sponsorship of AFOSR, ARO and NVEOL.

REFERENCES

1. P.H. Handel: "1/f Noise - an 'Infrared' Phenomenon", Phys. Rev. Letters 34, p.1492 - 1494 (1975).

2. P.H. Handel: "Quantum Approach to 1/f Noise", Phys. Rev. 22A, p. 745 (1980).

3. T.S. Sherif and P.H. Handel: "Unified Treatment of Diffraction and 1/f Noise", Phys. Rev. A26, p.596-602, (1982).

4. P.H. Handel and D. Wolf: "Characteristic Functional of Quantum 1/f Noise", Phys. Rev. A26, 3727-30 (1982).

5. G.S. Kousik, C.M. van Vliet, G. Bosman and P.H. Handel: "Quantum 1/f Noise associated with Ionized Impurity Scattering and Electron-phonon Scattering in Condensed Matter", Advances in Physics 34, p. 663-702, (1986).

6. P.H. Handel: "Starting Points of the Quantum 1/f Noise Approach", Submitted to Physical Review B.

7. A. Van der Ziel, "Unified Presentation of 1/f Noise in Electronic Devices; Fundamental 1/f Noise Sources", Proc. IEEE 76, 233-258 (1988); review paper.

8. P.H. Handel: "Turbulence Theory for the Current Carriers in Solids and a Theory of 1/f Noise", Phys. Rev. A3, 2066 (1971).

9. P.H. Handel: Instabilitäten, Turbulenz und Funkelrauschen in Halbleitern III; Turbulenz im Halbleiterplasma und Funkelrauschen. Z. Naturforschg.**21a**, 579 (1966).

10th Int.Conf. on Noise in Physical Systems
1989 Budapest, Hungary

CORRELATION BETWEEN ELECTRICAL AND OPTICAL NOISES IN DOUBLE HETEROSTRUCTURE LASERS AT WAVELENGTH λ = 0.83 MICROMETER

B. ORSAL, K. RANIRIHARINOSY, R. ALABEDRA, I. JOINDOT*

C.E.M. (UA 391), U.S.T.L.
34060 Montpellier Cedex, France
*C.N.E.T., Lannion
route de Trégastel, 22301 Lannion, France

ABSTRACT

In this work the influence of the D.H. laser electrical parameters on the electrical and optical fluctuations is discussed. The correlation between electrical and optical noises at 100KHz is obtained.

INTRODUCTION

In the first part, the noise equivalent circuit of D.H. laser diode is described. In the second part, the white noise in the optical power outputs P and electrical fluctuations $S_v(f)$ are shown. At last, in the third part, the coherence function between electrical and optical noises versus drive current is presented.

1. LASER CHARACTERISTICS AND NOISE EQUIVALENT CIRCUIT

Laser is index guided Sharp LMT 10 used for optical fibres at a wavelength of 0.8 µm. In this double heterostructure semi-conductor laser, an effective lateral step Δn_L over the active region is induced through evanescent field coupling (1).

The noise equivalent circuit of a semiconductor monomode laser diode (Fig. 1) is derived from the rate equations including Langevin noise sources taking into account Harder's theory (2, 3):

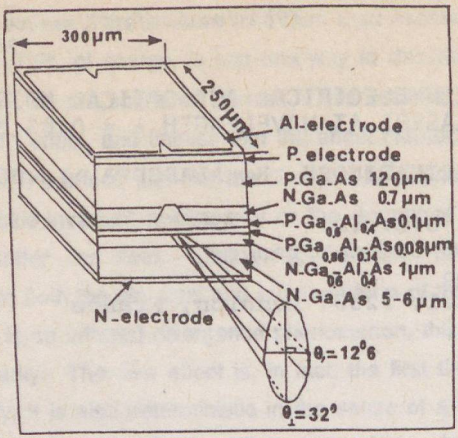

Fig. 1

$$\frac{dn}{dt} = \frac{i}{q} + \frac{n}{\tau_s} - (E_{cv} - E_{vc})s + f_N(t) \tag{1}$$

$$\frac{ds}{dt} = (E_{cv} - E_{vc})\, s + \gamma \frac{n}{\tau_s} - \frac{s}{\tau_{ph}} + f_s(t) \tag{2}$$

n and s are the total number of electrons in net gain medium rate g_o and photons in the single lasing mode. The pump rate is i/q, τ_s the spontaneous lifetime, τ_{ph} the photon lifetime. E_{cv}s is the downward stimulated rate, E_{vc}s the upward stimulated rate due to stimulated absorption. The net gain rate is by definition the net emission stimulated $g = E_{cv} - E_{vc}$ and $\gamma \frac{n}{\tau_s}$ is the spontaneous emission coupled into the lasing mode. $f_N(t)$ and $f_S(t)$ are Langevin source terms for electrons and photons. The spectral density $S_i(f)$, $S_v(f)$ and the cross spectral density $S_{iv}(f)$ do not depend on frequency f and are given by computing $F_N(f)$, $F_S(f)$, the Fourier transforms of $f_N(t)$ and $f_S(t)$. We obtain after Mc Cumber (4):

$$S_i = \frac{\bar{i}_n^{\,2}}{\Delta F} = 2\, C\, \frac{m\, V_T}{n_o} \langle |F_N(f)|^2 \rangle \tag{3}$$

$$S_v = \frac{\bar{v}_n^{\,2}}{\Delta F} = 2\, L^2\, (q\, g_o)^2 \langle |F_s(f)|^2 \rangle \tag{4}$$

$$S_{iv} = \frac{\overline{i_n V_n}}{\Delta F} = + 2 LC \frac{m V_T}{n_o} q g_o \langle |F_n(f) \quad F_s(f)| \rangle \qquad (5)$$

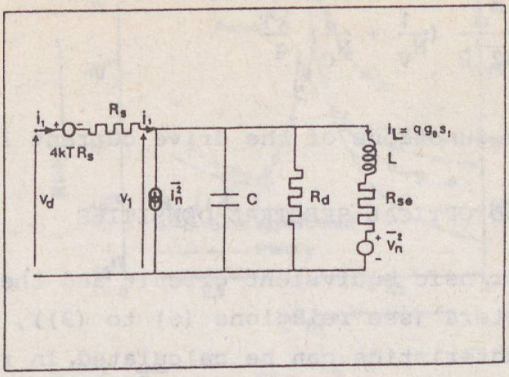

Fig. 2

The current noise source i_n in parallel represents mainly the fluctuations in electron population. The voltage noise source v_n is due to the shot noise of the gain mechanism fluctuations of the photon population (4). In Fig. 2, C is the usual diffusion capacitance resulting from the storage effect of the injected carriers. R is a modified differential diode resistance which approaches the conventional $\frac{mV_T}{i_o}$ expression in the absence of photons. L is a differential inductance due to photons. R_{se} is a resistance related to spontaneous emission current given by emission coupled into the lasing mode. All parameters can be written:

$$C = \frac{q}{mV_T} n_o \qquad (6)$$

$$R_d = \frac{mV_T}{q\, n_o \left(AS_o + \frac{1}{\tau_{nsp}}\right)} \qquad (7)$$

$$L = \frac{mV_T}{q\, n_o\, G_o \left(AS_o + \frac{\gamma}{\tau_{nsp}}\right)} \qquad (8)$$

$$R_{se} = \frac{mV_T \gamma}{q \tau_{ph} S_o G_o (AS_o + \frac{\gamma}{\tau_{nsp}})} \quad (9)$$

$$mV_T = 2 + \frac{n_o}{2\sqrt{2}\,\Omega} (\frac{1}{N_V} + \frac{1}{N_C}) \frac{kT}{q} \quad (10)$$

R, L, C, R_{se} are functions of the drive current I_L.

2. ELECTRICAL AND OPTICAL SPECTRAL DENSITIES

From the intrinsic equivalent circuit and the knowledge of extrinsic parameters (see relations (6) to (9)), the noise modulation characteristics can be calculated. In relations (11) to (14) Z (ω) is the diode impedance, $\frac{\overline{v_d^2}}{\Delta F}$ the voltage noise spectral density, $S_s(f) = \frac{\overline{S_n^2}}{\Delta f}$ the number photon noise spectral density, S_n the instantaneous photon number due to noise current i_{n_L}.

$$Z(\omega) = \frac{V_1(\omega)}{I_1(\omega)} = \frac{1}{LC} \left(\frac{R_{s_e} + j L\omega}{[\frac{1}{LC}(1 + \frac{R_{se}}{R_d}) - \omega^2] + j\omega(\frac{R_{se}}{L} + \frac{1}{R_d C})} \right) \quad (11)$$

$$Z(\omega) = \frac{(R_{s_e} + j L\omega)}{LC\ D} \quad (12)$$

$$S_{V_D}(f) = \frac{\overline{V_d^2}(\omega)}{\Delta f} = 4k\,TR_s + \frac{[R_{se}^2 + (\omega L)^2]\frac{\overline{i_n^2}}{\Delta f} + \frac{\overline{V_n^2}}{\Delta f} + 2\frac{\overline{i_n V_n}}{\Delta f} R_{se}}{(LC)^2 D(\omega)\ D^*(\omega)} \quad (13)$$

Electrical and optical noise curves versus I_L/I_S are shown in Fig. 3. The relative intensity noise (RIN) spectrum is given by:

$$RIN = \frac{S_{\Delta S}(f)}{S_o^2} = \frac{\overline{i_n^2} - 2(\overline{i_n v_n})/R_d + \overline{v_n^2}\,[1/R_d^2 + (C\omega)^2]}{(L\,C\,q\,G_o S_o)^2\ |D|^2} \frac{1}{\Delta f} \quad (14)$$

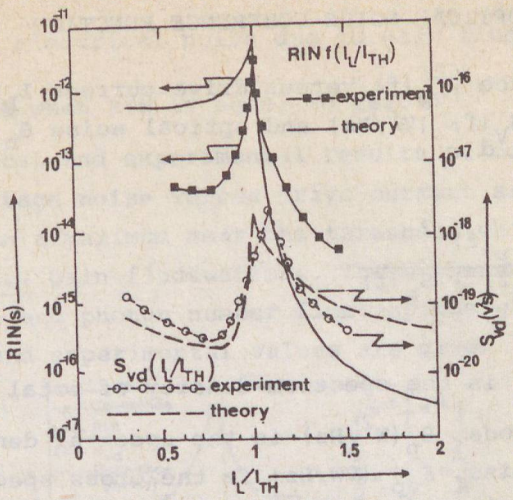

Fig. 3

$$RIN = \frac{S_{\Delta S}(f)}{S_o^2} = \frac{\overline{\Delta P^2}}{\bar{P}^2} = \frac{\overline{\Delta I_{ph}^2}}{\bar{I}_{ph}^2} \qquad (15)$$

where S_o is the average photon number, $\bar{P}$ the average optical power and $\bar{I}_{ph}$ the detected average photocurrent. So, the optical photocurrent noise spectrum is given by:

$$S_{\Delta S}(f) = \frac{\overline{i_n^2} - 2(\overline{i_n\, v_n})/R_d + \overline{v_n^2}\,[1/R_d^2 + (C\omega)^2]}{(L\ C\ q\ G_o)^2\ |D|^2}\ \frac{1}{\Delta f} \qquad (16)$$

At medium frequency (f = 100 KHz), relations (13) and (16) become (4):

$$S_{V_d} = 4k\ T\ R_s + \frac{R_{se}^2\ \frac{\overline{i_n^2}}{\Delta f} + \frac{\overline{v_n^2}}{\Delta f} + 2\ R_{se}\ \frac{\overline{i_n\ v_n}}{\Delta f}}{(1 + \frac{R_{se}}{R_d})^2} \qquad (17)$$

$$S_{I_{ph}} = I_{ph}^2\left(\frac{\overline{i_n^2} - 2(\overline{i_n\, v_n})/R_d + \overline{v_n^2}\,[1/R_d^2 + (C\omega)^2]}{(L\ C\ q\ G_o)^2\ |D|^2}\ \frac{1}{\Delta f}\right) \qquad (18)$$

3. ELECTRICAL-OPTICAL NOISE COHERENCE FUNCTION

The coherence $\gamma^2_{vp}(f)$ versus drive current I_L between the voltage noise $S_{V_d}(f)$ (V^2/Hz) and optical noise $S_p(f)$ in (W^2/Hz) is given by:

$$\gamma^2(f) = \frac{|S_{vp}(f)|^2}{S_{V_d}(f) \cdot S_p(f)} \tag{19}$$

where $S_{V_d}(V^2/Hz)$ is the spectrum density of total voltage noise of the laser diode, $S_p(W^2/Hz)$ is the spectral density of light output power noise, S_{vp} (VW/Hz) is the cross spectral density between power noise and electrical noise.

The experimental setup is described in another paper (5). Equation (19) can be also written as:

$$\gamma^2 I_{phV_d} = \frac{|S_{I_{ph} V_d}(f)|^2}{S_{I_{ph}}(f) \cdot S_{V_d}(f)} \tag{20}$$

where $S_{I_{phV_d}}(f)$ is the cross spectrum between photocurrent noise and electrical noise. Theoretical results of coherence function (2) are given by the following relation:

$$\gamma^2 I_{phV} = \frac{1}{1 + \dfrac{(\overline{i_a^2} + \overline{i_g^2})(\overline{u_n^2} + \overline{v_a^2})}{|a|^2 (\overline{v_1^2})^2} + \dfrac{|a|^2(\overline{u_n^2} + \overline{v_a^2}) + (\overline{i_g^2} + \overline{i_a^2})}{|a|^2 \overline{v_1^2}}} \tag{21}$$

where $\overline{i_a^2}$: current amplifier noise 9×10^{-24} A^2 s (5)

$\overline{v_a^2}$: voltage amplifier noise 6.4×10^{-19} V^2 s

$\overline{v_n^2}$: voltage noise due to serial resistance = 4 k T R_s ΔF

$\overline{i_g^2}$: pure shot noise of the photocurrent

$\overline{v_1^2}$: laser electrical noise due to gain fluctuations

$|a|^2\ \overline{v_1^2} = 0$ when RIN is equal to zero.

The theoretical and experimental results of coherence function, RIN and voltage noise versus drive current are shown in Fig. 4. We obtain a maximum near the threshold which can be explained by optical gain fluctuations. These phenomena are related to voltage and photon number fluctuations given by $S_{\Delta S}(f)$ (14). Computed and experimental values are given in Table 1.

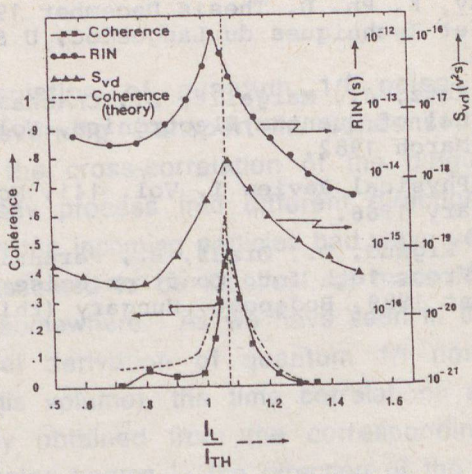

Fig. 4

Table 1

I_L	0.8 I_{TH}	1.05 I_{TH}	1.25 I_{TH}
$g(s^{-1})$		g_m	
$\frac{\overline{v_1^2}}{\Delta f}(V^2S)$	4×10^{-19}	2×10^{-18}	1.5×10^{-19}
$\lvert a\rvert^2(A^2/V^2)$	5×10^{-6}	1.4×10^{-2}	3.5×10^{-2}
$\gamma^2_{I_{phV}}(f)$ (computed)	0.07	0.6	0.06
$\gamma^2_{I_{phV}}(f)$ (experimental)	0.06	0.5	0.05

CONCLUSION

The coherence increases as the gain and decreases when the optical mode gain saturates.

REFERENCES

1. Agrawal, G.P., Lateral analysis of quasi-index guided injection lasers: transition from gain to index guiding. Journal of Lightwave Technology, Vol. LT2, No. 4, pp. 537-543, August 1984.
2. Raniriharinosy, K. Ph. D. Thesis December 1988, Université des Sciences et Techniques du Languedoc, U.S.T.L., Montpellier, France.
3. Harder, Ch., Katz, J., Margalit, S., Chacham, J.S., Yariv, A., IEEE Journal of Quantum Electronics, Vol. QE18, No. 3, pp. 333-337, March 1982.
4. Mc Cumber, Physical Review I, Vol. 141, No. 1, pp. 306-322, January 1966.
5. Alabedra, R., Rigaud, D., Orsal, B., Peransin, J.M., Valenza, M., Proc. 10th Int. Conf. on Noise in Physical Systems, August 1989, Budapest, Hungary (this volume).

10th Int.Conf. on Noise in Physical Systems
1989 Budapest, Hungary

QUANTUM 1/f CROSS-CORRELATIONS AND SPECTRA

P.H. HANDEL

Physics Department, University of Missouri
St. Louis, MO 63121, USA

The calculation of quantum 1/f noise in various kinetical coefficients governing transport in condensed matter, requires a knowledge of the cross-correlation of the outgoing current densities scattered by any process into different directions with wave vectors **K'** and **K"** when the incoming particles had wave vectors $\mathbf{K}_1$ and $\mathbf{K}_2$. The particles are assumed to be identical, of mass M, with wave functions which overlap somewhere. As we have seen in the preceding paper [1] on the general derivation of quantum 1/f noise in physical cross sections (in this volume), the time correlations and frequency spectra can be readily obtained from the corresponding spatial correlations along the outgoing beams in the direction of the detector which is now replaced by two detectors in the directions of **K'** and **K"** respectively. Working again in the Heisenberg representation, we limit ourselves to the simplest case of two particles described by the outgoing spherical waves

$$\varphi(x) = (C/x)\exp(iK_1x)[1 + \Sigma_{k,l}b(k,l)\exp(-iq_1x)a^+_{k,l}]|0> \qquad (1)$$

$$\chi(x) = (C/x)\exp(iK_2x)[1 + \Sigma_{k,l}\beta(k,l)\exp(-iq_2x)a^+_{k,l}]|0> \qquad (2)$$

where now b corresponds to the momentum change $\mathbf{K'}-\mathbf{K}_1$, while β has an independent phase and corresponds to the momentum change $\mathbf{K"}-\mathbf{K}_2$ of the second particle. As in the preceding paper [1] mentioned above, for bosons we obtain the current density autocorrelation function

$$A(K_1,K_2,K',K";x_1x_2) = \langle S|O|S\rangle = (K'K"/2M)\langle 0|\chi(x_1)\varphi(x_2)|^2$$

$$+\chi^*(x_1)\varphi^*(x_2)\chi(x_2)\varphi(x_1) +\chi^*(x_2)\varphi^*(x_1)\chi(x_1)\varphi(x_2) +|\chi(x_2)\varphi(x_1)|^2|0\rangle$$

$$= (K'K"/M)\{[1 + \Sigma_{k,l}|b(k,l)|^2][1 + \Sigma_{k,l}|\beta(k,l)|^2]$$

$$+(1/2)\exp[iK'(x_2-x_1)-iK"(x_2-x_1)][1 + \Sigma_{k,l}|\beta(k,l)|^2\exp -iq(x_2-x_1)]$$

$$[1 + \Sigma_{k,l}|b(k,l)|^2\exp iq(x_2-x_1)] + [x_1 \leftrightarrow x_2]\}$$

$$= (K'K"/M)\{[1 +\Sigma_{k,l}|b(k,l)|^2][1 +\Sigma_{k,l}|\beta(k,l)|^2] + \cos(K'-K")(x_2-x_1)$$

$$+ \Sigma_{k,l}|\beta(k,l)|^2\cos[(K'-K"-q)(x_2-x_1) +\Sigma_{k,l}|b(k,l)|^2\cos[(K'-K"+q)(x_2-x_1)$$

$$+ \Sigma_{k,l}\Sigma_{k',l'}|\beta(k,l)|^2|b(k',l')|^2\cos[(K'-K"+q'-q)(x_2-x_1)]\}. \qquad (3)$$

Except for K'=K" all terms which are not constant are rapidly oscillating and do not yield low frequency noise contributions; as usual, only practically unobservable high $1/\Delta f$ noise terms are present in this case in the quantum fluctuations. For K'=K", however, we get low frequency noise down to arbitrarily low frequencies, because the momentum magnitude changes $q=kMc/\hbar K$ and $q'=k'Mc/\hbar K$ caused by the soft photon emission are arbitrarily small. We obtain the spatial quantum 1/f current density cross-correlation

$$A(K_1,K_2,K',K";x_1x_2) = (h^2K'K"/M)\{[1+\Sigma_{k,l}|b(k,l)|^2][1+\Sigma_{k,l}|\beta(k,l)|^2]$$

$$+ \{1 + \Sigma_{k,l}[|b(k,l)|^2 + |\beta(k,l)|^2]\cos q(x_2-x_1)\}\delta_{K',K"}$$

$$+ \Sigma_{k,l}\Sigma_{k',l'}|\beta(k,l)|^2|b(k',l')|^2\cos[(q'-q)(x_2-x_1)]\delta_{K',K"}\}. \qquad (4)$$

Note that the restriction indicated by the Kronecker symbols $\delta_{K',K"}$ refers only to the magnitude of the outgoing wave vectors, or to the kinetic energies of the outgoing particles, and that their outgoing and incoming directions can be different. Therefore, only particles of the same energy have quantum 1/f noise cross-correlations, and particle groups of different energy will yield independent quantum 1/f noise

contributions, a result which was anticipated empirically by Kleinpenning [2] in semiconductors. Performing the angular integrations contained in the softaron lattice sums of Eq. (4), as indicated in the preceding paper mentioned at the start, and using the relation dk/k = df/f, with f=ck/2π, we obtain

$$A(\mathbf{K}_1,\mathbf{K}_2,\mathbf{K}',\mathbf{K}'';x_1x_2) = (\hbar^2K'K''/M)\{[1 + \alpha A_1\int df/f][1 + \alpha A_2\int df/f]$$

$$+ [1 + \alpha\int(A_1 + A_2)\cos\, q(x_2-x_1)\ (df/f)]\delta_{K',K''}$$

$$+ \alpha^2A_1A_2\int(df/f)\int(df'/f')\cos[(q'-q)(x_2-x_1)]\delta_{K',K''}\}. \qquad (5)$$

Here $A_1 = 2\hbar^2(K'-K_1)^2/3\pi M^2c^2$ and $A_2 = 2\hbar^2(K''-K_2)^2/3\pi M^2c^2$. We may call this approximation the independent bremsstrahlung model. Neglecting the last term which is a noise of noise contribution, applying the Wiener-Khintchine theorem, and using again the relation dk/k = df/f, to connect wave number spectra to frequency spectra, we obtain the cross-spectral densities of the rate fluctuations $\Delta w(\mathbf{K}_1,\mathbf{K}')$ from $\mathbf{K}_1$ to $\mathbf{K}'$, and $\Delta w(\mathbf{K}_2,\mathbf{K}'')$ from $\mathbf{K}_2$ to $\mathbf{K}''$

$$S_{\Delta w}(\mathbf{K}_1,\mathbf{K}_2,\mathbf{K}',\mathbf{K}'') = (\alpha/2f)(A_1+A_2)\langle w(\mathbf{K}_1,\mathbf{K}')\rangle\langle w(\mathbf{K}_2,\mathbf{K}'')\rangle\delta_{K',K''}(2/N) \qquad (6)$$

for bosons.

For fermions we replace everywhere in the derivation of Eq. (3) the boson field commutators by fermion field anticommutators and obtain in the same way

$$A(\mathbf{K}_1,\mathbf{K}_2,\mathbf{K}',\mathbf{K}'';\mathbf{x}_1,\mathbf{x}_2) = (1/2)[|\chi(\mathbf{x}_1)|^2|\phi(\mathbf{x}_2)|^2 + (1\Leftrightarrow 2)]$$
$$-(1/4)[\chi^*(\mathbf{x}_1)\phi^*(\mathbf{x}_2)\chi(\mathbf{x}_2)\phi(\mathbf{x}_1) + (1\Leftrightarrow 2)]$$
$$= [1 + \Sigma_{\mathbf{k},l}|\beta(\mathbf{k},l)|^2][1 + \Sigma_{\mathbf{k},l}|b(\mathbf{k},l)|^2] - (1/2)\cos[(K_1-K_2)(x_1-x_2)]$$
$$-(1/2)\Sigma_{\mathbf{k},l}[|\beta(\mathbf{k},l)|^2 + |b(\mathbf{k},l)|^2]\cos[(K_1-K_2)(x_2-x_1) + q(x_1-x_2)]$$
$$-(1/2)\Sigma_{\mathbf{k}\mathbf{k}'ll'}|\beta(\mathbf{k},l)|^2|b(\mathbf{k}',l')|^2\cos(K_1-K_2+q'-q)(x_1-x_2). \qquad (7)$$

Applying again the smoothing operation as in Eq. (3), we obtain now

$$AK_1,K_2,K',K'';x_1,x_2) = [1+\Sigma_{\mathbf{k},l}|\beta(\mathbf{k},l)|^2][1+\Sigma_{\mathbf{k},l}|b(\mathbf{k},l)|^2]$$
$$-1/2\ \{1 + \Sigma_{\mathbf{k},l}[|\beta(\mathbf{k},l))|^2 + |b(\mathbf{k},l)|^2]\cos[q(x_1-x_2)]\delta_{K1,K2}$$
$$-(1/2)\Sigma_{\mathbf{k}\mathbf{k}'ll'}|\beta(\mathbf{k},l)|^2|b(\mathbf{k}',l')|^2\cos(q-q')(x_1-x_2)\delta_{K1,K2}. \qquad (8)$$

For elastic scattering we have $K' = K_1$ and K'' and K_2, provided the scattering center is fixed or very massive (e.g. a crystal). In conclusion, for fermions we obtain in the same way as for Eq.(6)

$$S_{\Delta w}(\mathbf{K}_1,\mathbf{K}_2,\mathbf{K}',\mathbf{K}'') = (\alpha/f)(A_1+A_2)\langle w(\mathbf{K}_1,\mathbf{K}')\rangle\langle w(\mathbf{K}_2,\mathbf{K}'')\rangle\delta_{K',K''}(1/N-1), \quad (9)$$

where the last factors have been added in Eqs. (6) and (9) in an attempt to generalize the results, derived here for N=2, to the case of N particles in the final state, on the basis of the result of the preceding papers [1],[4].

Our result in Eq. (9) differs somewhat from a heuristic generalization of the basic quantum 1/f noise formula used in a previous paper [3].

Acknowledgment: The author thankfully acknowledges the magnanimous support of Annie and Edward Karcich of Salinas, CA, over the last 25 years, as well as the vitally important sponsorship of AFOSR, ARO and NVEOL.

REFERENCES

1. P.H.Handel: "General Derivation of the Quantum 1/f Noise Effect in Physical Cross Sections and the 1/N Factor" in this volume.

2. T.G. Kleinpenning, Physica B94 , 141 (1978).

3. G.S. Kousik, C.M. Van Vliet, G. Bosman, and P.H. Handel, Advances in Physics 34, 663-702 (1986).

4. P.H. Handel: "Starting Points of the Quantum 1/f Noise Approach." Submitted to Phys. Rev.

10th Int.Conf. on Noise in Physical Systems
1989 Budapest, Hungary

LOCALIZATION FLUCTUATIONS IN QUANTUM HALL DEVICES

A.J. KIL, R.J.J. ZIJLSTRA, J.P. ANDRÉ*

Fysisch Laboratorium
P.O. Box 80 000, 3508 TA Utrecht, The Netherlands
*Laboratoire d'Electronique et de Physique Appliquée
94450 Limeil-Brevannes, France

We present measurements of electrical noise in GaAs/AlGaAs heterostructures operating under integral quantum Hall effect (QHE) conditions [1,2]. At liquid helium temperatures and in strong magnetic fields perpendicular to the GaAs/$Al_xGa_{1-x}As$ interface the Hall conductance is quantized in units of e^2/h with an accuracy better than 0.1 ppm. Under these circumstances the energy of the high-mobility electrons in the two-dimensional electron gas (2DEG) at the interface is entirely quantized: the density of states consists of a series of Landau levels. The quantization of the Hall conductance appears in magnetic field ranges where the Fermi level lies between two Landau levels.

As noise measurements provide detailed information on the nature of charge transport we hoped to gain a better understanding of the nature of electrical conduction in the QHE regime. Furthermore, since noise sets an ultimate limit to accuracy of the quantum Hall resistance, noise measurements are also of metrological interest.

In our experiments we used MOCVD-grown GaAs/$Al_xGa_{1-x}As$ material with x=0.34. At 1.6 K the mobility of the electrons in the 2DEG was 12.3 m^2/Vs and the 2D electron density was $4.3 \times 10^{15} m^{-2}$ after cooldown in the dark. The direct current through the rectangular samples was of the order of 20 μA and was kept constant. The spectral noise intensity of the Hall voltage and that of the longitudinal or Shubnikov-de Haas (SdH) voltage was measured under QHE conditions in the frequency range 0.5 Hz to 100 kHz. Furthermore the cross spectral noise intensity of the Hall voltage and the SdH voltage was measured. The noise spectra generally consist of two distinct components, one of which is current and frequency independent, whereas the other component depends on both current and frequency. The frequency independent or white noise component could be identified as thermal noise [3].

The frequency dependent part of the noise consists of two Lorentzians with corner frequencies of the order of 1 Hz and 100 Hz respectively. The noise has a quadratic current dependence in the entire frequency range considered. Therefore the noise can be interpreted as generation-recombination (g-r) noise due to trapping-detrapping transitions.

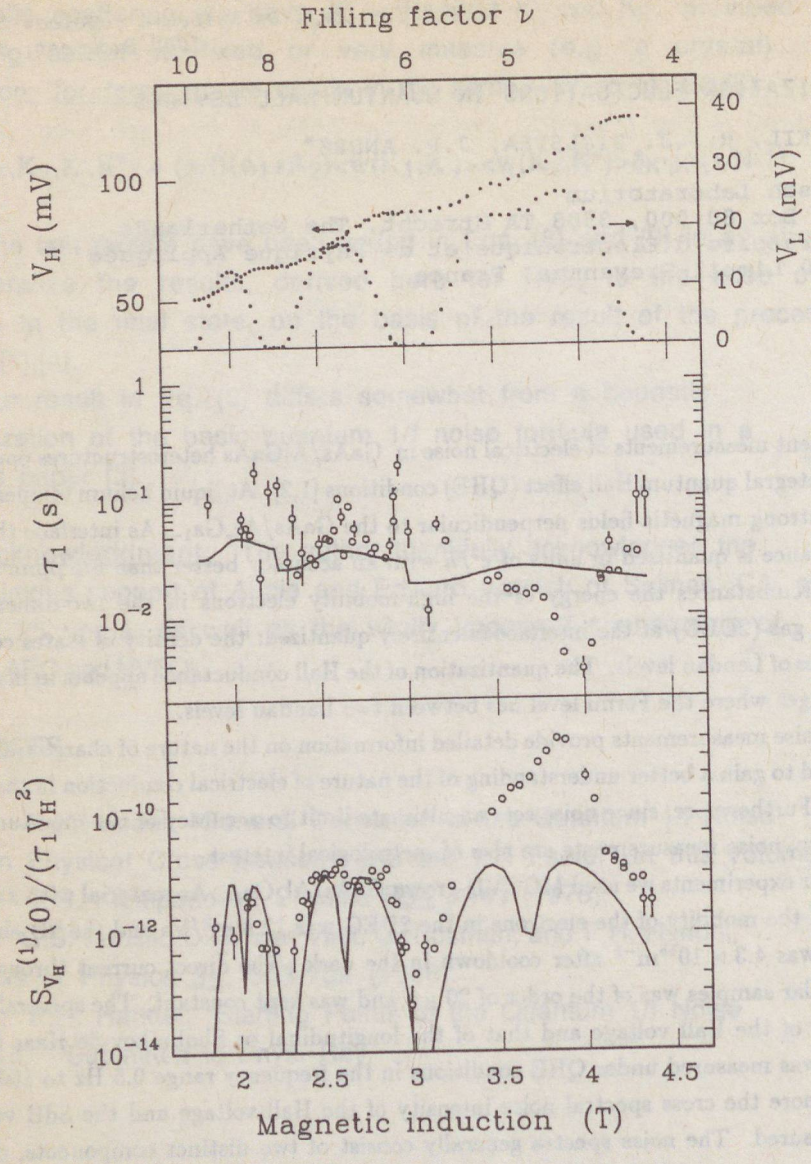

Figure 1: Relative noise intensity $S_{V_H}^{(1)}(0)/(\tau_1 V_H^2)$ and relaxation time τ_1 of the low-frequency Lorentzian in the Hall voltage noise vs. magnetic induction. The channel current was 20 μA and the temperature was 1.6 K. The solid lines are the results of model calculations. As an indication of the magnetic field ranges associated with the quantum Hall regime, the d.c. Hall voltage V_H and SdH voltage V_L are shown as well.

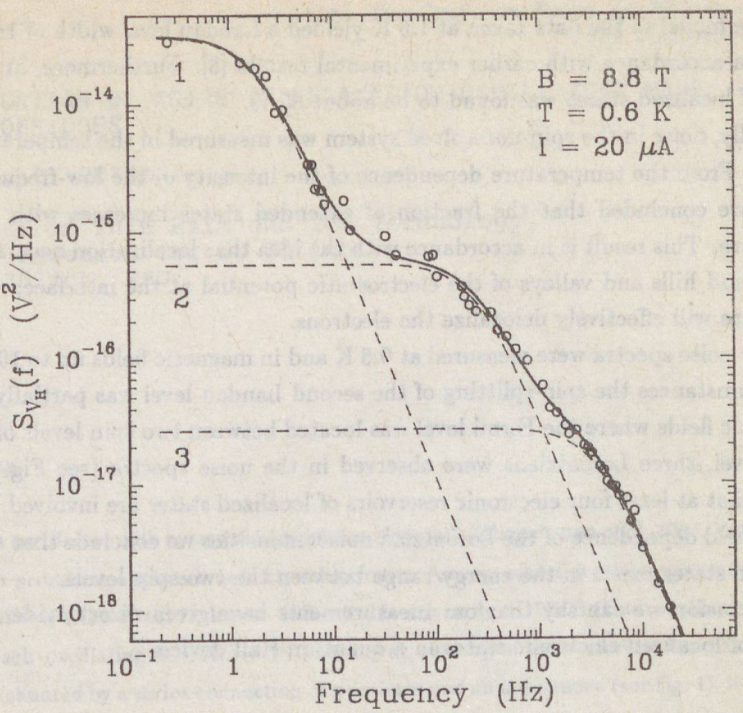

Figure 2: Spectral intensity $S_{V_H}(f)$ of the excess noise in the Hall voltage, measured at 0.6 K and at $B = 8.8$ T. The current I through the 2DEG was $I = 20$ μA. The solid line is a fit. The three Lorentzians are indicated separately by dashed lines.

In order to elucidate the origin of the *g-r* noise, spectra were measured as a function of magnetic field [4] and temperature. The low-frequency plateaus of the two Lorentzians showed maxima and minima as a function of magnetic field. The relaxation times of the Lorentzians showed a less pronounced behavior due to experimental error. In Fig. 1 the results for the low-frequency Lorentzian are shown.

The experimental results were fitted to a model based on *g-r* noise theory [7]. Fluctuations in the number of free electrons due to trapping in localized states in both tails of one Gaussian-shaped Landau level were calculated. This type of localization is generally thought to be essential for the explanation of the QHE itself [5,6]. The free or extended states in the center of the Landau level determine the electrical transport properties of the 2DEG. Transitions within one Landau level give rise to two Lorentzians in the noise spectra, since three electronic reservoirs are involved. By varying the magnetic field the Fermi level is swept through the Landau levels. When the Fermi level approaches a mobility edge, the calculated *g-r* noise intensity is found to show a similar behavior as in the experiment. A fair agreement between calculations and experiment could be established in the regime where the spin-splitting of the Landau levels was not resolved (see Fig. 1).

A fit of the model to the data taken at 1.6 K yielded a Landau level width of 1±0.2 meV, which is in accordance with earlier experimental results [8]. Furthermore, at 1.6 K the fraction of localized states was found to be about 85 %.

Secondly, noise in the spin-unresolved system was measured in the temperature range 4 to 15 K. From the temperature dependence of the intensity of the low-frequency noise intensity we concluded that the fraction of extended states increases with increasing temperature. This result is in accordance with the idea that localization occurs on closed orbits around hills and valleys of the electrostatic potential at the interface; raising the temperature will effectively delocalize the electrons.

Finally noise spectra were measured at 0.6 K and in magnetic fields up to 10 T. Under these circumstances the spin-splitting of the second Landau level was partially resolved. At magnetic fields where the Fermi level was located between two spin levels of the same Landau level, three Lorentzians were observed in the noise spectra (see Fig. 2). This indicates that at least four electronic reservoirs of localized states are involved. From the magnetic field dependence of the Lorentzian noise intensities we conclude that a reservoir of localized states exists in the energy range between the two spin levels.

In conclusion we can say that our measurements have given direct evidence for the existence of localized electronic states in a quantum Hall device.

References

[1] K. von Klitzing, G. Dorda and M. Pepper, *Phys. Rev. Lett.* **45**, 494 (1980).

[2] For reviews see: K. von Klitzing, Rev. Mod. Phys. **58**, 519 (1986); *The Quantum Hall Effect*, edited by R.E. Prange and S.M. Girvin (Springer-Verlag, New York, 1987); H. Aoki, *Rep. Prog. Phys.* **50**, 655 (1987).

[3] A.J. Kil, J.C.D. Verhagen, R.J.J. Zijlstra, M.F.H. Schuurmans and J.P. André, to be published.

[4] A preliminary account has been given in: A.J. Kil, R.J.J. Zijlstra, P.M. Koenraad, J.A. Pals and J.P. André, *Solid State Comm.* **60**, 831 (1986); R.J.J. Zijlstra and A.J. Kil, *Proceedings of the 9th International Conference on Noise in Physical Systems and the 5th International Conference on 1/f noise*, Montreal (1987), edited by C.M. van Vliet, World Scientific, Singapore, p. 139, and A.J. Kil, R.J.J. Zijlstra, B.M. van der Doef, J.A. Pals and J.P. André, *Physica Scripta* **38**, 212 (1988).

[5] H. Aoki and T. Ando, *Solid State Comm.* **38**, 1079 (1981).

[6] D.C. Tsui and S.J. Allen, *Phys. Rev. B* **24**, 4082 (1981).

[7] K.M. van Vliet and J.R. Fassett in *Fluctuation Phenomena in Solids*, edited by R.E. Burgess, Academic Press, New York (1965), p. 268.

[8] J.P. Eisenstein, H.L. Störmer, V. Narayanamurti, A.Y. Cho, A.C. Gossard and C.W. Tu, Phys Rev. Lett. **55**, 875 (1985).

10th Int.Conf. on Noise in Physical Systems
1989 Budapest, Hungary

INVESTIGATION OF NOISE IN RELAXATION OSCILLATORS MADE OF MICROBRIDGES

M. MÜCK, C. HEIDEN

Institute of Thin Film and Ion Technology,
Nuclear Research Center Jülich
D-5170 Jülich, FRG

Introduction

Relaxation oscillators with hysteretic Josephson elements (Zimmerman et al. 1967, Vernon et al. 1968) offer promising applications in cryoelectronics. Among others are thermometers, local oscillators for rf-SQUIDs (Mück et al. 1988 a), RO-driven dc-SQUIDs (Gudoshnikov et al. 1989) and self-oscillating SQUIDs (SOS, Mück et al. 1988 b). If the hysteretic Josephson element is shunted by a series connection of a resistor and an inductance (see fig. 1), it may switch periodically between the superconducting and the resistive state. If a constant bias current I_B satisfies the condition

$$I_{cmax} < I_B < I_{cmin} \cdot \{(R_R + R_S)/R_S\} \qquad (1)$$

a series of short pulses can be measured across the Josephson element with a frequency

$$f \approx (R_S/L_S) \cdot \{\ln((I_B - I_{cmin})/(I_B - I_{cmax}))\}^{-1} \qquad (2)$$

where I_{cmin} and I_{cmax} are the minimum and maximum critical current, respectively (cf. fig. 1), R_S and L_S are the resistance and inductance of the shunt, and R_R is the resistance of the Josephson element in the resistive state.

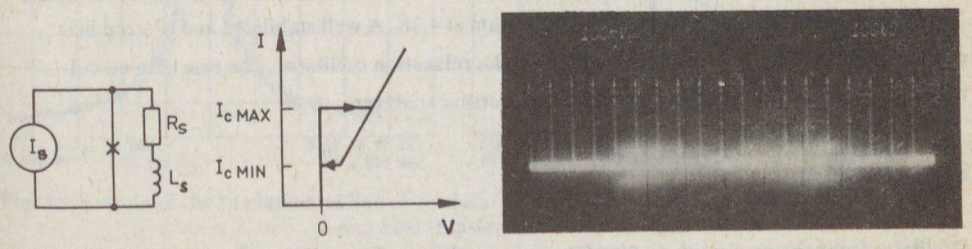

Fig. 1 Schematic I-V-characteristics of a hysteretic Josephson element (centre) and circuit diagram (left) and generated voltage pulses (right) of a relaxation oscillator, using a microbridge as Josephson element (see also fig. 2).

Essential to obtain highest sensitivity of relaxation oscillator based devices is to minimize any noise generated by the device itself. Unfortunately, it is found that under some circumstances, relaxation oscillators made of microbridges have an intrinsic noise much higher than pure thermal noise. To optimize the operation of the above mentioned devices, it is necessary to investigate all possible sources generating this excess noise. On the basis of such an investigation, the preparation and operation parameters may be changed until the excess noise is reduced to a minimum value.

Experimental Details

In all our experiments, microbridges (see fig. 2) are used as Josephson elements. They are prepared from Nb, NbN, and Nb_3Ge thin films, typically between 30 nm and 150 nm thick, using e-beam lithography and reactive ion etching, as reported elsewhere (Rogalla 1985). The microbridges exhibit critical currents I_{cmax} of approx. 5mA for Nb and 15mA for NbN and Nb_3Ge. Because of the large critical current densities in the microbridges, a hysteresis is observed in the I-V-characteristics, which is due to self-heating. The series connection of resistor and inductance is realized by either a short piece of wire or an evaporated Cu-strip. Typical oscillator frequencies are about 15MHz with a 3mm long wire or 300Mhz with a 200μm long and 100μm wide Cu-strip.

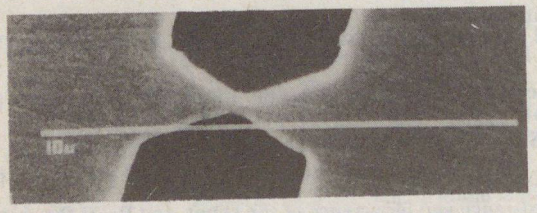

Fig. 2 SEM picture of a Nb_3Ge microbridge

All measurements were performed in liquid helium at 4.2K. A well stabilized and filtered bias current I_B of up to 100mA could be imposed in the relaxation oscillator. The resulting ac-voltage was investigated on an oscilloscope or a spectrum analyzer.

Results and discussion

Oscillator frequencies of up to $f = 800$MHz and ac-voltages of up to 300 mV could be generated by these relaxation oscillators. Investigating the frequency spectrum of a relaxation oscillator with a spectrum analyzer, a relative linewidth of $10^{-4} < \delta f(\text{-3dB})/f < 10^{-1}$ is found (see fig.3). This linewidth was found to depend on several parameters, like temperature, frequency, bias current, the material used for the microbridge and the inductance and resistance of the shunt.

There are several reasons for fluctuations in I_B, I_{cmax} and I_{cmin}. The noise of the room-temperature current source was measured to be so small that its effect on the oscillator noise can be neglected. Superimposed on I_B is the thermal current noise of the shunt resistor R_S and the normal resistance of the bridge R_N. Since R_S usually is much smaller than R_N, for oscillator frequencies up to about R_S/L_S this noise is dominated by R_S, leading in first approximation to a relative linewidth of $\delta f \approx (f_0/I_B)\sqrt{4kT/L_S}$. The influence of the current noise depends on oscillator frequency. At higher frequencies, the role of R_N becomes dominant since the noise due to R_S is band limited by L_S.

Considering a pure thermal noise, the amplitude distribution of the above mentioned bias current fluctuations is Gaussian, which leads to a certain shape of the emission lines. Since the oscillator is frequency modulated by the noise current, the resulting line shape differs from a Gauss-curve, because of contributions of the sidebands.

To determine the frequency spectrum of the noise which frequency modulates the oscillator, its output signal was fed to a frequency to voltage converter and then analyzed by an af spectrum analyzer. Over the investigated frequency range from 0.1 Hz to 10 kHz, the oscillator noise usually was found to be white. Only in case of Nb microbridges, sometimes a $1/f$-noise was found below 2Hz.

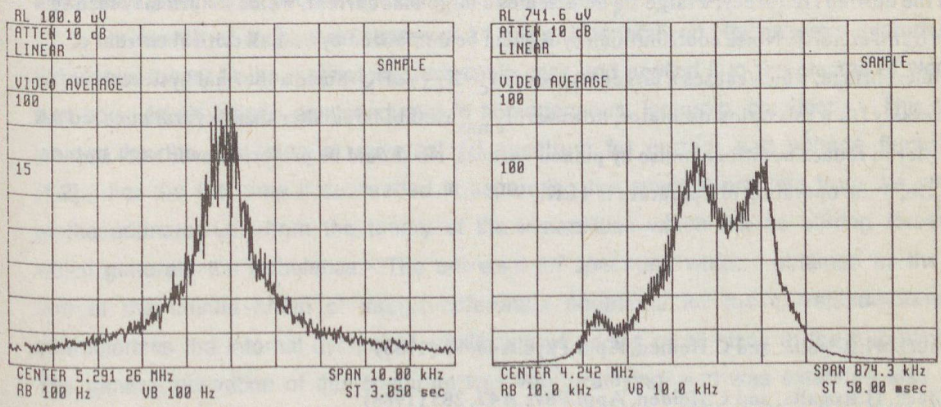

Fig. 3 Spectrum of the fundamental line of a relaxation oscillator exhibiting thermal noise (left) and heat transfer noise (right)

Increasing the bias current leads to a sudden increase in linewidth at a certain bias current (usually about 40mA). The emission lines then exhibit several maxima (cf. fig.3). The linewidth and the number of maxima are increasing with increasing bias current. This phenomenon is only found, if the microbridge is immersed in liquid helium above the λ-point. This leads to the

assumption, that this additional noise is produced by fluctuations in the heat transfer from the bridge to the helium bath. A poorer heat removal by a helium gas bubble leads to an increase in temperature of the microbridge and an increase in frequency. Since this frequency change is comparatively small ($<10^{-1}$), this indicates, that most of the heat produced by dissipation in the bridge is carried away by the substrate.

The above mentioned mechanisms of thermal- and heat removal noise are sufficient to explain the observed linewidths on relaxation oscillators with Nb microbridges. Relaxation oscillators with NbN or Nb_3Ge microbridges even without heat transfer noise show a much larger linewidth ($\approx 10^{-2}$), compared to thermal noise, which must be generated by a further noise source, which influences I_{cmax} and I_{cmin}. Since NbN and Nb_3Ge films exhibit stronger pinning of vortices than Nb films, and I_{cmax} depends on pinned vortices in the bridge region, it is assumed that the noise is caused by a changing number and location of pinned vortices in the microbridge. Further investigations are needed here however.

Consequences

For practical applications of relaxation oscillators, e.g. in self-oscillating SQUIDs, one has to minimize all the above mentioned noise sources. If only thermal noise produced by R_S and R_N is considered, the inductance L_S should be made as large as possible. On the other hand, to obtain the desired frequency, a large L_S determines a large bias current, which in turn may lead to heat transfer noise. Noise contributions by R_N can be minimized by a small critical current of the microbridge, which causes a larger R_N, since $I_c \approx 2 \triangle / eR_N$. Since a thermal hysteresis is neccessary for a relaxation oscillator, however, I_{cmax} cannot be smaller than several hundred μA. In order to reduce additional noise by pinned vortices, Nb should be preferred over NbN and Nb_3Ge, if the operating temperature is 4.2K.

References

M.Mück, H.Rogalla, and C.Heiden, Appl.Phys.**A46**, 97 (1988)

M.Mück, H.Rogalla, and C.Heiden, Appl.Phys.**A47**, 285 (1988)

H.Rogalla, B.David, and M.Mück "SQUID'85, Superconducting Quantum Interference Devices and Their Applications", edited by H.D.Hahlbohm and H.Lübbig, W. de Gruyter, Berlin 1985, page 671

S.A.Gudoshnikov et al., IEEE Trans.MAG-**25**, 1178 (1989)

F.L.Vernon and R.J.Pedersen, J.Appl.Phys.**39**, 2661 (1968)

J.E.Zimmerman and A.H.Silver, Phys.Rev.Lett.**19**, 14 (1967)

10th Int.Conf. on Noise in Physical Systems
1989 Budapest, Hungary

THE NONLINEARITY CAUSING CLASSICAL AND QUANTUM 1/f NOISE: SLIDING SCALE INVARIANCE AND QUANTUM CHAOS DEFINITION

P.H. HANDEL

Physics Department, University of Missouri
St. Louis, MO 63121, USA

The motion of many nonlinear systems is known to become unstable at certain critical values of of the relevant parameters, which correspond to bifurcation points. Turbulence is obtained then as the limit of a sequence of instabilities (Hopf bifurcations). The sequence of bifurcations leads to turbulence, which is a form of chaos. It is in fact one of the aims of the study of deterministic chaos in fluids, to understand the mechanisms of fully developed turbulence which implies irregular behavior in time and space.

On the other hand, whenever an electric current is carried by a small number of particles, low-frequency fluctuations with a spectral density inversely proportional to f are noticed. This 1/f noise was an unsolved fundamental problem of electrophysics and electronics ever since people learned to amplify electrical signals.

In search of a universal theory of 1/f noise, I generalized Heisenberg's hydrodynamic turbulence theory to the magnetohydrodynamic case and applied it to the plasma of electrons and holes in an infinite semiconductor in homogeneous, isotropic conditions. This theory yielded for the first time a universal 1/f spectrum for current and voltage fluctuations [1,2]. For the first time it succeeded in separating the spectral problem from the problem of the sources, i.e., from the theory of the instabilities which act as stirring forces and which generate the turbulence. The universal 1/f spectrum, which I obtained as the solution of the infinite chain of integro-differential equations for the correlation functions, characterizes the internal dynamical equilibrium of eddies of all sizes in the turbulent field. The general derivation of this spectrum was very gratifying, and was extended also to the case of metals [2], but was useless for practical 1/f noise applications, being limited to an infinite-sample homogeneous, isotropic, turbulence concept with unknown stirring forces. Without a theory of the instabilities generating the turbulence, the theory was incomplete.

Although I found some new instabilities, none of them was a zero-threshold instability as required by the physical 1/f noise. From 1963 to 1974 I tried to quantize this turbulence theory to eliminate the need for classical instabilities. This led to the quantum

1/f theory [3-9] which is the quantum equivalent of the old turbulence theory, a quantum manifestation of classical chaos which we use to define the notion of quantum chaos.

The quantum 1/f theory describes a fundamental law of nature, a new aspect of Quantum Mechanics (QM), expressed by the simple universal equation $S_{\delta\sigma/\sigma} = 2\alpha A/fN$. This means that the generally accepted notion of constant cross sections σ and process rates in QM is insufficient in practice, and all we can observe, according to the postulates of QM, are the scattered currents per unit incoming flux, i.e., what I call the physical cross sections σ and process rates (PCS&PR). The latter differ from their average (which is the usual notion of cross section) by a quantum fluctuation which is a function of time. I found that this fluctuation contains in addition to the well-known, trivial, Poissonian shot noise (with a white spectrum) expressing the discrete nature of matter, a fundamental part $\delta\sigma$, arising universally, according to the principles of QM, from the infrared-divergent coupling of the scattered particles to photons, and to other massless quanta. The above universal equation shows that the spectral density $S_{\delta\sigma/\sigma}(f)$ of fractional cross section fluctuations is twice the known fractional bremsstrahlung rate $\alpha A/f$ associated with the scattering cross section σ, divided by the number of carriers N used for testing the cross section. The bremsstrahlung coefficient αA is derived below semiclassically, and is also known as the infrared exponent in Quantum Electrodynamics (QED), with $\alpha = e^2/\hbar c = 1/137$, and $A = (2/3\pi)(\Delta v/c)^2$ in the non-relativistic case. Here Δv is the velocity change of the particles in the scattering process, and c the speed of light.

The Quantum 1/f Effect [3-9] is a fundamental fluctuation of physical cross sections and process rates, known also as quantum 1/f noise, and caused by the infrared-divergent coupling of current carriers to low frequency photons and to other infraquanta. The physical origin of quantum 1/f noise is easy to understand. Consider for example the scattering of current carriers, e.g., electrons on a center of force of arbitrary nature. The scattered electrons reaching a detector at a given angle away from the direction of the incident beam are described by DeBroglie waves of a frequency corresponding to their energy. However, some of the electrons have lost energy in the scattering process, due to the emission of Bremsstrahlung. Therefore, part of the outgoing DeBroglie waves is shifted to slightly lower frequencies. When we calculate the probability density in the scattered beam, we obtain also cross terms, linear both in the part scattered with and without bremsstrahlung. These cross terms oscillate with the same frequency as the frequency of the emitted bremsstrahlung photons. The emission of photons at all frequencies results therefore in probability density oscillations at all frequencies. The corresponding current density fluctuations are obtained by multiplying the probability density oscillations by the velocity of the scattered current carriers. Finally, these current fluctuations present in the scattered beam will be noticed at the detector as low frequency current fluctuations, and will be interpreted as fundamental cross section fluctuations in the scattering cross section of the

scatterer. Although the wave function φ of each carrier is split into a Bremsstrahlung part and a non-Bremsstrahlung part, no quantum 1/f noise can be observed from a single carrier. A single carrier will only provide a pulse in the detector. Many carriers are needed to produce the Quantum 1/f Effect, just as in the case of electron diffraction patterns, where each individual particle is diffracted, but unless we repeat the experiment many times, or use many particles, no diffraction pattern can be seen. A single particle only yields a point of impact on the photographic plate in diffraction, or a pulse in the detector in the 1/f noise case. While incoming carriers may have been Poisson distributed, the scattered beam will exhibit super-Poissonian statistics, or bunching, due to this new effect which we may call Quantum 1/f Effect. The Quantum 1/f Effect is thus a many-body or collective effect, best described through the two-particle wave function and the pair-correlation function.

Let us estimate the magnitude of the Quantum 1/f Effect by starting with the classical (Larmor) formula $2q^2\mathbf{a}^2/3c^3$ for the power radiated by a particle of charge q and acceleration $\mathbf{a}$. The acceleration can be approximated by a delta function $\mathbf{a}(t) = \Delta\mathbf{v}\delta(t)$ whose Fourier transform $\Delta\mathbf{v}$ is constant and is the change in the velocity vector of the particle during the almost instantaneous scattering process. The one-sided spectral density of the emitted Bremsstrahlung power $4q^2(\Delta\mathbf{v})^2J/3c^3$, obtained by substituting $\mathbf{a}$ in the Larmor formula by its Fourier transform and multiplying by J, is therefore also constant, provided the average number J of particles scattered per second is constant. The number $4q^2(\Delta\mathbf{v})^2J/3hfc^3$ of emitted photons per unit frequency interval is obtained by dividing with the energy hf of one photon. The probability amplitude of photon emission $[4q^2(\Delta\mathbf{v})^2J/\ 3hfc^3]^{1/2}e^{i\gamma}$ is given by the square root of this photon number spectrum, including also a phase factor $e^{i\gamma}$. Let ψ be the Schrödinger wave function of the scattered outgoing charged particles, which can be constructed from single-particle wave functions. The beat term in the probability density $|\psi|^2$ is linear both in this Bremsstrahlung amplitude and in the non-Bremsstrahlung amplitude. Its spectral density will therefore be given by the product of the squared probability amplitude of photon emission (proportional to 1/f) with the squared non-Bremsstrahlung amplitude which is independent of f. The resulting spectral density of fractional probability density fluctuations is obtained by dividing with $|\psi|^4$ and is therefore

$$|\psi|^{-4}S_{|\psi|^2}(f) = 8q^2(\Delta\mathbf{v})^2/3hfNc^3 = 2\alpha A/fN = j^{-2}S_j(f), \qquad (1)$$

where $\alpha = e^2/\hbar c = 1/137$ is the fine structure constant and $\alpha A = 4q^2(\Delta\mathbf{v})^2/3hc^3$ is known as the infrared exponent in quantum field theory, and is known as the quantum 1/f noise coefficient, or Hooge constant, in electrophysics.

The spectral density of current density fluctuations is obtained by multiplying the probability density fluctuation spectrum with the squared velocity of the outgoing particles. When we calculate the spectral density of fractional fluctuations in the scattered current j, the outgoing velocity simplifies, and therefore Eq. (1) also gives the spectrum of current

fluctuations $S_j(f)$, as indicated above. The scattered current per unit incoming flux is the physical cross section, and therefore the low-frequency scattered current fluctuations will be interpreted as fluctuations in the physical scattering cross section. The quantum expectation value of the physical cross section is constant and represents the usual definition of the cross section. The occurrence of the fourth power of a wave function in Eq. (1) is due to the expression of the two-particle wave function as a product of two one-particle wave functions. The quantum 1/f noise contribution of each carrier is independent, and therefore the quantum 1/f noise from N carriers is N times larger; however, the current j will also be N times larger, and therefore in Eq. (1) a factor N was included in the denominator for the case in which the cross section fluctuation is observed on N carriers simultaneously. The 1/N factor is derived in my "General Derivation ....." paper in this volume.

The fundamental fluctuations of cross sections and process rates are reflected in various kinetic coefficients in condensed matter, such as the mobility μ and the diffusion constant D, the surface and bulk recombination speeds, and recombination times τ and the rate of tunneling in semiconductors. Therefore, the spectral density of fractional fluctuations in all these coefficients is given also by Eq. (1).

We conclude that the conventional Quantum 1/f Effect can be explained in terms of interference beats between the part of the outgoing DeBroglie waves scattered without bremsstrahlung energy losses above the detection limit (given in turn by the reciprocal duration T of the 1/f noise measurement) on one hand, and the various parts scattered with bremsstrahlung energy losses on the other hand. This, of course, is just one way to describe the reaction of the emitted bremsstrahlung back on the scattered current. This reaction thus reveals itself as the cause of the Quantum 1/f Effect. The effect, just like our classical turbulence-generated 1/f noise described below, is a result of the nonlinearity of the equations of motion describing the coupled system of matter and field. Ultimately, therefore, this nonlinearity is the source of the 1/f spectrum in both the classical and quantum form of the theory. We can say that the Quantum 1/f Effect is an infrared divergence phenomenon, this divergence being the result of the same nonlinearity. The new effect is, in fact, the first time-dependent infrared radiative correction. Finally, it is also deterministic in the QM sense of a well determined wave function, once the initial phases γ of all field oscillators are given. In QM correspondence with its classical turbulence analog, the new effect is therefore a quantum manifestation of classical chaos which we can take as the definition of a certain type of quantum chaos. It differs from its classical turbulence analogue only through the probabilistic interpretation of the wave function.

In the case of homogeneous, isotropic turbulence [1,2] caused in the electron-hole plasma of an infinite sample of a symmetric intrinsic semiconductor by dynamical instabilities of any kind, we start from the equations

$$\nu \mathbf{v}^+ = (e/2c)\mathbf{v}^- \times \mathbf{B} - (1/n)\nabla P, \tag{2}$$

$$\nu \mathbf{v}^- = 2e[\mathbf{E} + \mathbf{v}^+ \times \mathbf{B}/c] - (2/n)\nabla(P_p - P_n), \tag{3}$$

$$\nabla \cdot \mathbf{v}^+ = 0 \qquad (n = \text{const}), \tag{4}$$

$$\nabla \times \mathbf{E} = -(1/c)\partial \mathbf{B}/\partial t, \tag{5}$$

$$\nabla \times \mathbf{B} = 2\pi e n \mathbf{v}^-/c, \tag{6}$$

$$\nabla \cdot \mathbf{B} = 0. \tag{7}$$

Here n is the total carrier concentration including an equal number of electrons and holes, ν/e their reciprocal mobility assumed to be the same for electrons and holes, P_n and P_p the partial pressures of electrons and holes, P the total carrier pressure, $2\mathbf{v}^+$, $\mathbf{v}^-$ the sum and the difference of the carrier drift velocities. Inertial terms proportional to the effective masses of the carriers, as well as electrostatic terms and compressibility terms have been neglected here in a consistent way [1,2], because we are interested in the low-frequency domain only. Although we do not work this out here, this system of equations can be shown to admit an energy theorem. Performing a Fourier expansion and substituting $\mathbf{E}$ from Eq. (3) into Eq. (5), we obtain with Eq. (6)

$$\partial \mathbf{B}(\mathbf{k})/\partial t + \mu k^2 \mathbf{B}(\mathbf{k}) = i\mathbf{k} \times \sum_{\mathbf{k}'} \mathbf{v}^+(\mathbf{k}') \times \mathbf{B}(\mathbf{k}-\mathbf{k}'), \tag{8}$$

where $\mu = c^2\nu/4\pi n e^2$. Eqs. (2) and (6) yield

$$\mathbf{v}^+(\mathbf{k}) = (i/4\pi\nu n) \sum_{\mathbf{k}''} \{\mathbf{B}(\mathbf{k}'')[\mathbf{k}'' \cdot \mathbf{B}(\mathbf{k}-\mathbf{k}'')] - \mathbf{k}''[\mathbf{B}(\mathbf{k}'') \cdot \mathbf{B}(\mathbf{k}-\mathbf{k}'')]$$
$$-(\mathbf{k}/k^2)(1-\delta_{\mathbf{k},0})[\mathbf{k}'' \cdot \mathbf{B}(\mathbf{k}-\mathbf{k}'')\ \mathbf{k} \cdot \mathbf{B}(\mathbf{k}'') - \mathbf{B}(\mathbf{k}'') \cdot \mathbf{B}(\mathbf{k}-\mathbf{k}'')\ (\mathbf{k} \cdot \mathbf{k}'')]\}. \tag{9}$$

Substituting this into Eq. (8), we obtain the fundamental dynamical field-equation of turbulence in the electron-hole plasma of a symmetric intrinsic semiconductor

$$\partial b_\beta(\mathbf{k},t)/\partial t + \mu k^2 b_\beta(\mathbf{k},t) = \sum_{\mathbf{k}'\mathbf{k}''} b_j(\mathbf{k}-\mathbf{k}',t)\ b_l(\mathbf{k}'',t)\ b_m(\mathbf{k}'-\mathbf{k}'',t)$$
$$\cdot(k_j\delta_{\beta s} - k_s\delta_{\beta j})[k_s\delta_{lm} - k_m''\delta_{ls} + (k_s'/k'^2)(1-\delta_{\mathbf{k}',0})(k_m''k_l' - \mathbf{k}' \cdot \mathbf{k}''\delta_{lm})], \tag{10}$$

in terms of $\mathbf{b} \equiv \mathbf{B}/\sqrt{2\pi\nu n}$.

Multiplying Eq. (10) with $b_\alpha^*(\mathbf{k},t-\tau)$ and taking the average over a statistical ensemble which represents our notion of stationary turbulence, we obtain in quasi-stationary conditions

$$\partial w_{\alpha\beta}(\mathbf{k},\tau)/\partial\tau + \mu k^2 w_{\alpha\beta}(\mathbf{k},\tau)$$
$$= \sum_{\mathbf{k}'\mathbf{k}''} \langle b_\alpha^*(\mathbf{k},t-\tau) b_j(\mathbf{k}-\mathbf{k}',t) b_l(\mathbf{k}'',t) b_m(\mathbf{k}'-\mathbf{k}'',t)\rangle R_{jml\beta}, \tag{11}$$

with $w_{\alpha\beta}(\mathbf{k},\tau) \equiv (L/2\pi)^3 \langle b_\alpha^*(\mathbf{k},t-\tau) b_\beta(\mathbf{k},t)\rangle$, where L is the edge of the cubic normalization box, and

$$R_{jml\beta} \equiv (k_j\delta_{\beta s} - k_s\delta_{\beta j})[k_s\delta_{lm} - k_m''\delta_{ls} + (k_s'/k'^2)(1-\delta_{\mathbf{k}',0})(k_m''k_l' - \mathbf{k}' \cdot \mathbf{k}''\delta_{lm})]. \tag{12}$$

Multiplying Eq. (10) with more magnetic field components and averaging, we obtain equations connecting the fourth-order correlation tensor to the sixth-order tensor, and so on [1,2]. To end this infinite chain of equations for the correlation functions, we make a quasinormality assumption which expresses the fourth-order moment appearing in Eq. (11) according to the scheme

$$\langle ABCD\rangle = \langle AB\rangle\langle CD\rangle + \langle AC\rangle\langle BD\rangle + \langle AD\rangle\langle BC\rangle, \tag{13}$$

valid if the four field components would approximate a joint normal distribution. This yields the closed equation

$$\partial w_{\alpha\beta}(\mathbf{k},\tau)/\partial\tau + \mu k^2 w_{\alpha\beta}(\mathbf{k},\tau) = (2\pi/L)^3 w_{\alpha j}(\mathbf{k},\tau)\sum_{\mathbf{k}'} w_{|m}(\mathbf{k}',0) R_{jm|\beta}(\mathbf{k},\mathbf{k}'). \quad (14)$$

Isotropic turbulence requires $w_{\alpha\beta} = A_1(k)\delta_{\alpha\beta} + A_2(k)k_\alpha k_\beta$, with coefficients A_1 and A_2 related through Eq. (7), yielding $w_{\alpha\beta}(\mathbf{k},\tau) = (1/2)[\delta_{\alpha\beta} - k_\alpha k_\beta/k^2]u(k,\tau)$, where $u(k,\tau) = \sum_\alpha w_{\alpha\alpha}(\mathbf{k},\tau)$. Therefore, the scalar correlation function $u(k,\tau)$ satisfies the dynamical equation of homogeneous, isotropic, stationary turbulence

$$\frac{\partial v(k,x)}{\partial |x|} + v(k,x) = -\frac{1}{2} v(k,x) \int \frac{d^3k'}{k'^3} \frac{k^2 + \mathbf{k}\cdot\mathbf{k}'}{(\mathbf{k}+\mathbf{k}')^2}\left[1 - \left(\frac{\mathbf{k}\cdot\mathbf{k}'}{kk'}\right)^2\right] v(k',0), \quad (15)$$

where $v(k,x) \equiv k^{-3}u(k,\tau)$, and $x = \mu\tau k^2$ is a dimensionless variable replacing τ. We convince ourselves that the integral is independent of k, provided $v(k,x)$ does not depend on its first argument, by setting $\mathbf{k}'/k \equiv \kappa$. This yields a solution. However, with $v = e^{-m|x|}$ we get a logarithmic divergence at $\kappa = 0$. We look for an exact solution of the form

$$v(k,x) = hk^\varepsilon e^{-|x|m(k)}, \text{ or } u(k,x) = (h/k^{3-\varepsilon})\, e^{-|x|m(k)}, \quad (16)$$

where $m(k)$ is very close to a constant, almost independent of k, and h is a constant proportional to the intensity of the turbulence, or the turbulence level. Substituting this into Eq. (15) and performing the integration, we obtain a finite result only for $0 < \varepsilon < 2$:

$$m(k) = 1 + h\, r(\varepsilon) k^\varepsilon, \text{ with } r(\varepsilon) = [2\pi^2 \cot an(\varepsilon\pi/2)]/[(1-\varepsilon^2)(3-\varepsilon^2)]. \quad (17)$$

We notice that $m(k)$ is indeed practically constant when $0 < \varepsilon << 1$ is very small, arbitrarily small. The value $\varepsilon = 0$ leads to a logarithmic divergence, but we can set $\varepsilon = 0$ for practical purposes.

The spectral density corresponding to Eq. (16) with $\varepsilon = 0$ is

$$w_{\alpha\beta}(\omega) = (1/\pi)\int_0^\infty \cos\omega\tau\, d\tau \int w_{\alpha\beta}(k,\tau)\, d^3k$$

$$= \tfrac{4}{3}\delta_{\alpha\beta}\int_0^\infty k^2 dk \int_0^\infty d\tau\, u(k,\tau)\cos\omega\tau = \tfrac{4}{3} h\delta_{\alpha\beta}\int_0^\infty \frac{mk\,dk}{\omega^2 + m^2k^2} = \frac{\pi}{3}\frac{h}{\omega}\delta_{\alpha\beta}. \quad (18)$$

This is a 1/f spectrum. At the low frequency end we do not get a divergent spectral integral, because the more exact form of the spectrum with a finite small $\varepsilon << 1$ is

$$\int_0^\infty \frac{mk^{1+\varepsilon}dk}{\omega^2 + m^2k^4} = \frac{1}{\omega^{1-\varepsilon/2} m^{\varepsilon/2}} \int_0^\infty \frac{x^{1+\varepsilon}dx}{1+x^4}, \quad (19)$$

which is proportional to $f^{\varepsilon/2-1}$. It is interesting to note that for $\varepsilon << 1$ cotan $\varepsilon\pi/2 \approx 2/\varepsilon\pi$ in Eq. (17), and that the value of ε calculated from Eq. (17) is therefore proportional to h, or to the intensity of the turbulence. This feature of the classical theory is expressed with fascinating clarity in the quantum form of the theory, where ε is replaced by the infrared exponent $2\alpha A$ which also appears as a intensity factor multiplying the quantum 1/f noise.

The essential element which led to the 1/f spectrum in the classical turbulence theory is the *nonlinearity* of the equations of motion, caused by the reaction of the electric currents back on themselves via the generated electromagnetic field. The same feedback reaction, via the electromagnetic field, also caused the nonlinearity in the quantum 1/f theory, and in QED in general, leading in the same way to an identical 1/f spectrum, this time with a physically more meaningful $\varepsilon=2\alpha A$. This *nonlinearity* induces the coupling between various scales of turbulence and leads to the dynamical equilibrium between eddies of all sizes, expressed by the 1/f spectrum. In the $\varepsilon=0$, or $\alpha A=0$, limit, this dynamical equilibrium assumes both for the quantum case and for homogeneous, isotropic turbulence in the unbounded semiconductor sample the simplest form, characterized by scale-homogeneity, or scale invariance. Indeed, for $\varepsilon=0$, replacing in Eqs. (15) and (16) k and k' by λk and $\lambda k'$, while also replacing τ by τ/λ^2, (or ω by $\lambda^2\omega$), Eq. (15) is not affected, and λ drops out. We conclude that *in the weak turbulence limit ($\varepsilon=0$) we obtain perfect self-similarity of the turbulence process at all scales in space and time, classically and quantum-mechanically*. The implied scale invariance is caused by the absence of any characteristic length or time scale, or by the presence of a sliding scale. Indeed, the frequency scale μk^2 is a function of the size of the eddies, given by the wave number k which can have any value. The actual frequency and wave-number spectra are closely related fractals, but in the weak-turbulence limit they approach an exact 1/f and $1/k^3$ spectrum respectively. We are thus understanding the nonlinear dynamics which shapes this fractal.

Our classical turbulence theory can be extended to the case of metals [2] or degenerate extrinsic semiconductors in the Drude model. The system of integro-differential equations is quite different, and leads to a third-order nonlinearity in the resulting closed equation of motion, or nonlinear field-equation, which replaces Eq. (9). The corresponding infinite chain of equations for the correlation tensors now goes in steps of one. The third-order correlation can be eliminated between the first and second equations in the chain. The resulting dynamical equation [2] for homogeneous, isotropic, stationary turbulence, which replaces Eq. (15), with the same notations, using $\mathbf{e}_3$ as the unit vector of the third axis, is

$$-\frac{\partial^2 v(k,x)}{\partial x^2} + v(k,x)$$

$$= -\frac{1}{2}\int\frac{d^3\kappa}{\kappa^3}\,\frac{1+\kappa\cdot\mathbf{e}_3}{|\mathbf{e}_3+\kappa|^3}\left[1-\frac{(\kappa\cdot\mathbf{e}_3)^2}{\kappa^2}\right]v(\kappa k,\kappa^2 x)\,v(k|\mathbf{e}_3+\kappa|,x|\mathbf{e}_3+\kappa|^2). \qquad (20)$$

This also admits, in the $\varepsilon=0$ limit of weak turbulence, a solution v(k,x) which does not depend on the first argument, and $u(k,x) = k^{-3}e^{-xm(x)}$, this time with an x-dependent m. With the change of variables $t=\omega\tau$ and $k'=k/\sqrt{\omega}$ in the second (middle) form of Eq. (18), x remains invariant, and a factor $1/\omega$ will appear in front of the integrals which themselves will just yield a constant factor independent of ω or k. We thus obtain again a universal 1/f spectrum. As is shown in detail elsewhere [2], this 1/f spectrum is ex-

pressed in the corresponding current and voltage fluctuations which can be observed in the semiconductor or metallic medium. We conclude that the 1/f spectrum is a general property of electrically conducting systems in interaction with the electromagnetic field, a property which is caused by the scale-invariant nonlinearity of the equation of motion of the system of carriers and field in mutual interaction (sliding scale invariance), and which finds its clearest expression in the Quantum 1/f Effect.

The author thankfully acknowledges the support of Annie and Edward Karcich of Salinas, CA, as well as the vitally important sponsorship of AFOSR, ARO and NVEOL.

REFERENCES

1. P.H. Handel: Instabilitäten, Turbulenz und Funkelrauschen in Halbleitern III; Turbulenz im Halbleiterplasma und Funkelrauschen. Z. Naturforschg.**21a**, 579 (1966).

2. P.H. Handel: "Turbulence Theory for the Current Carriers in Solids and a Theory of 1/f Noise", Phys. Rev. A3, 2066 (1971).

3. P.H. Handel: "1/f Noise - an 'Infrared' Phenomenon", Phys. Rev. Letters 34, p.1492 - 1494 (1975).

4. P.H. Handel: "Quantum Approach to 1/f Noise", Phys. Rev. 22A, p. 745 (1980).

5. T.S. Sherif and P.H. Handel: "Unified Treatment of Diffraction and 1/f Noise", Phys. Rev. A26, p.596-602, (1982).

6. P.H. Handel and D. Wolf: "Characteristic Functional of Quantum 1/f Noise", Phys. Rev. A26, 3727-30 (1982).

7. G.S. Kousik, C.M. van Vliet, G. Bosman and P.H. Handel: "Quantum 1/f Noise associated with Ionized Impurity Scattering and Electron-phonon Scattering in Condensed Matter", Advances in Physics 34, p. 663-702, (1986).

8. P.H. Handel: "Starting Points of the Quantum 1/f Noise Approach", Submitted to Physical Review.

9. A. Van der Ziel, "Unified Presentation of 1/f Noise in Electronic Devices; Fundamental 1/f Noise Sources", Proc. IEEE 76, 233-258 (1988); review paper.

SESSION 5

NOISE IN ELECTRON DEVICES
(DIODES, BJTS, FETS)

10th Int.Conf. on Noise in Physical Systems
1989 Budapest, Hungary

FLUCTUATION SPECTROSCOPY OF HOT ELECTRONS IN SEMICONDUCTORS

V. BAREIKIS, R. KATILIUS

Semiconductor Physics Institute,
Lithuanian Academy of Sciences
Vilnius 232600, Lithuania

INTRODUCTION

Cut-off frequencies in semiconductor high-speed devices are determined by drift velocity of electrons. Favourable conditions for extension of frequency range are created in high-mobility materials and high electric fields. As a result, the electrons are heated, and this leads to excess noise. In microvawe region the excess noise consists of two main parts: hot electron thermal and intervalley noise. Here we shall deal with hot electron noise in two widely-used materials: GaAs and InP. The hot electron noise in these materials and heterojunctions was widely investigated during the last years (Bareikis et al.1980, 1987, Gasquet et al.1983, 1985, Whiteside et al. 1987, Van Rheenen et al.1987). To maximize the drift velocity and minimize the noise, the transistors with short gate length were invented, where favourable conditions for an enhancement of drift velocity due to overshoot effect were created. Since transient behaviour is different for drift velocity, noise and diffusion, the special investigation of microwave noise and electron diffusivity in short samples is of present interest.

Usual noise spectroscopy involves the determination of steps in noise spectrum at $\omega\tau \sim 1$, where τ is the time of characteristic process responsible for the corresponding noise source. The similar information can be obtained changing

the electron transit through the sample time τ_{tr}, since slow processes are cut off. Thus, changing the sample length L as well as the electric field strength $\vec{E}$, one effectively investigates the different noise sources. So, alongside with ω - spectroscopy, L - E - spectroscopy seems shaping nowadays as a modern tool of hot electron investigation. In the limiting case of very short samples the ballistic regime is reached. This case was discussed in detail (Nougier 1983; Schmidt et al. 1983), and we shall restrict ourselves to discussion of intermediate cases.

THEORY

The general principles of hot electron noise theory are well-known and well-founded. The theory is based on the Boltzmann-Langevin equations or the kinetic equations for correlation functions (see, e.g. Gantsevich et al. 1979). In principle, these equations describe the noise processes in samples of any length, as long as collision duration and scatterer dimensions can be neglected. The only problem is that of correct boundary conditions. It is rather difficult, however, to find analytic solutions in practically important cases. For this reason, numerical methods for hot electron noise are widely used (Boittiaux et al. 1983; Junevičius and Reklaitis, 1986).
The Boltzmann-Langevin and correlation-function methods are equivalent provided the correct sources $y_{\vec{p}}$ are used in the Boltzmann - Langevin equation. (Gantsevich et al. 1979). In particular, the correlation properties of these sources are the same, independently of the sort of fluctuations considered: spatially nonhomogeneous or homogeneous, i.e. fluctuations developing in time and space or only in time. We pay attention to this problem because recently there were attempts (Nougier and Vaissiere, 1989) to revise the correlation properties of source term in Boltzmann-Langevin equation obtained by Lax (1960) and by many others. Space-dependent state-occupancy fluctuations around a spatially-homogeneous steady state, $\delta F_{\vec{p}}(\vec{r},t)$ obey the Boltzmann-Langevin equation

$$\left(\frac{\partial}{\partial t}+\vec{v}\frac{\partial}{\partial \vec{r}}+\Psi_{\vec{p}}\right)\delta F_{\vec{p}}(\vec{r},t)=y_{\vec{p}}(\vec{r},t)\,, \qquad (1)$$

where $\Psi_{\vec{p}}$ is the (linearized) Boltzmann operator. As far as physical mechanisms accompanied by carrier number variation (such as generation-recombination processes) are not taken into account, the space-dependent fluctuations should obey the continuity equation ($\delta N=\sum_{\vec{p}}\delta F_{\vec{p}}$, $\delta\vec{j}=\sum_{\vec{p}}\vec{v}\,\delta F_{\vec{p}}$):

$$\frac{\partial}{\partial t}\delta N(\vec{r},t)+\mathrm{div}\,\delta\vec{j}(\vec{r},t)=0\,. \qquad (2)$$

Since the Boltzmann operator conserves the carrier number: $\sum_{\vec{p}}\Psi_{\vec{p}}=0$, the Langevin source should have the property

$$\sum_{\vec{p}} y_{\vec{p}}(\vec{r},t)=0\,. \qquad (3)$$

Otherwise the summation of Eq.(1) over $\vec{p}$ would not lead to the continuity equation (2), i.e. Eq.(1) would be incompatible with carrier conservation.

Spatially-homogeneous fluctuations are those extending over a volume Ω large enough the carrier number fluctuations to be suppressed due to Coulomb forces ($\Omega > L_D^3$, L_D is the Debye length). Such fluctuations obey the spatially-homogeneous Boltzmann-Langevin equation

$$\left(\frac{\partial}{\partial t}+\Psi_{\vec{p}}\right)\delta F_{\vec{p}}(t)=y_{\vec{p}}(t)\,. \qquad (4)$$

Here should be $\sum_{\vec{p}}\delta F_{\vec{p}}(t)=\delta N(t)=0$, and this is compatible with $\sum_{\vec{p}} y_{\vec{p}}(t)=0$ as was emphasized by Gantsevich et.al(1989). We should like to stress that in this as well as other aspects, the contemporary kinetic theory of fluctuations is noncontradictory and well-grounded. We should like to recommend to use it wider to investigate fluctuations in intermediate-length samples.

ENERGY FLUCTUATIONS (CONVECTIVE NOISE)

While reducing the sample length, noise sources are one after

another eliminated. One of such sources is energy-fluctuation-induced noise (convective noise). It follows from the kinetic theory that in the case of nearly elastic scattering for sufficiently long samples the ratio of the longitudinal to transverse noise temperatures, $T_{n\parallel}/T_{n\perp}$, is expressible through the ratio of small-signal to cord conductivities, $\sigma_\parallel = \partial J/\partial E$ and $\tilde{\sigma} = J/E$, in a following way (Shulman 1970, Katilius and Miliušytė 1980)

$$\frac{T_{n\parallel}}{T_{n\perp}} = \frac{1}{4}\left(\sqrt{\frac{\sigma_\parallel}{\tilde{\sigma}}} + \sqrt{\frac{\tilde{\sigma}}{\sigma_\parallel}}\right)^2 \geq 1 . \qquad (5)$$

In short sample, when the transit time becomes less than the energy relaxation time, $\tau_{tz} < \tau_\varepsilon$ (at the same time, $\tau_{tz} > \tau_p$ where τ_p-the momentum relaxation time), the energy processes do not manifest itself. As a result, J-E characteristic of a sample becomes less nonlinear. The ratio (5) then approaches unity. Since $T_{n\parallel}$ of the short sample approaches $T_{n\perp}$ of the long sample, it follows that the longitudinal noise temperature is reduced in short samples when the energy relaxation process is cut off.

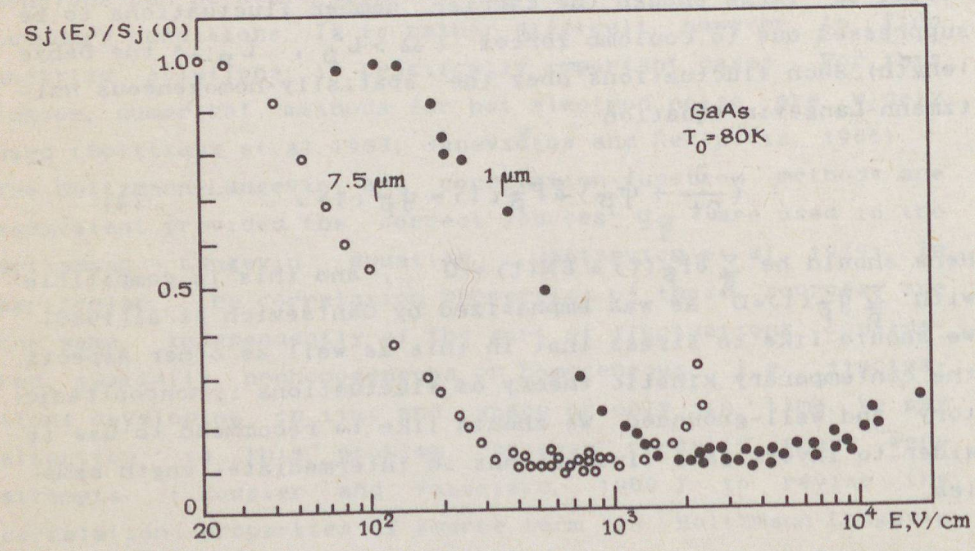

Fig. 1. Relative spectral density of current fluctuations vs electric field for various length n^+-n-n^+ structures, $n=3\cdot10^{15}cm^{-3}$ (Bareikis et al. 1988a).

At the same time, the spectral density of current fluctuations, S_j, being partly suppressed by the convective noise in the long sample, is increased in the short sample. This is illustrated in Fig. 1 which demonstrates the remarkable enhancement of S_j in short sample in moderate fields ($E \lesssim 0.5$ kV/cm) in GaAs at 80K at 10 GHz. One should be aware, of course, that due to peculiarities of scattering mechanisms in GaAs, the convective noise concept is of restricted applicability to this material. Similar results were obtained in InP (Bareikis et al. 1988, 1989a). We see that the noise vs length characteristic is quite informative and in some sense can be used instead of spectral characteristic of noise.

INTERVALLEY NOISE

Intervalley noise offers another possibility to demonstrate spectroscopic potentialities of noise vs length characteristic measurements. Fig. 2 shows $S_j(E) / S_j(0)$ deduced from $T_{n\parallel}$ and $\sigma_{\parallel}$ measurements performed in GaAs at 10 GHz in samples of various lengths at 293 K. The decrease of $S_j(E)$ well below the equilibrium value typical for the micron-length samples is in contrast to the increase of $S_j(E)$ in long ones. This effect is due to the intervalley noise suppression in short samples.

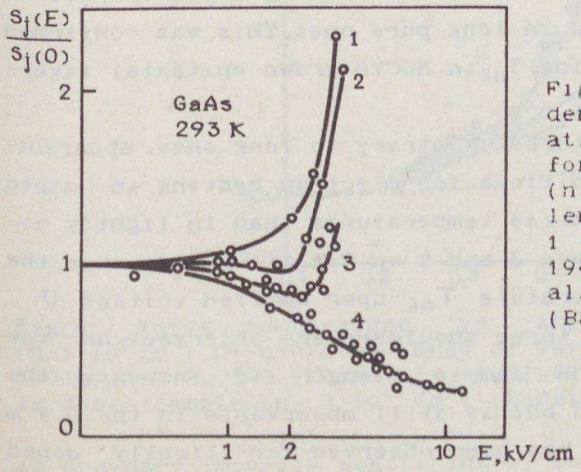

Fig. 2. Relative spectral density of current fluctuations vs electric field for the n^+-n-n^+ structures ($n=3\cdot10^{15}$ cm^{-3} of various length (in microns) : 1 -1000 (Bareikis et al. 1980); 2-11.0 (Gasquet et al. 1985); 3-7.5 and 4-1.0 (Bareikis et al. 1986).

An electron should travel a rather long distance in a given electric field to accumulate the intervalley separation energy. Therefore, in the case of short samples a region of electric fields exists where GaAs behaves as one-valley semiconductor in which a decrease of $S_j(E)$ is due to convective noise influence on the hot-electron noise, as was explained above. At 300 K lattice temperature, in contrast to 80 K (Fig. 1), this influence is observed up to 1μm - length sample indicating that τ_ε remains smaller than τ_{tz}. Let us note that cut-off of intervalley scattering in short samples not only reduces the noise but simultaneously leads to an enhancement of drift velocity.

NOISE IN SHORT DOPED SAMPLES

The noise spectrum in short samples is quite sensitive to the doping level of the sample. We shall demonstrate that doping may enrich the noise spectrum, enlarging diagnostic possibilities of the noise-vs-length spectroscopy. Different noise sources can reveal themselves in the noise vs electric field dependence of the short sample.

Doping introduces extra scattering of electrons, and heating of electrons by an electric field is hindered. For this reason, the thermal noise of hot electrons in long doped samples is expected to be lower than in long pure ones. This was confirmed experimentally by measuring $T_{n\parallel}$ in MOCVD grown epitaxial layers of GaAs (see Fig. 3).

In submicron doped structures, contrary to long ones, apparently less favourable conditions for electron heating in doped material lead to higher noise temperatures than in lightly doped samples (Compare curves 3 and 4 on Fig. 4). Beside this, the dependence of noise temperature $T_{n\parallel}$ upon applied voltage U reveals some structure: three shoulders are observed on the curves 1-3 on Fig. 4. As the sample length is increased the structure tends to smooth but is still observable in the 0.9 m sample. No such structure has been observed for slightly doped samples of the same length (see curve 4 on Fig. 4). The structure is more expressed in the plot $S_j(U)$ (Fig. 5).

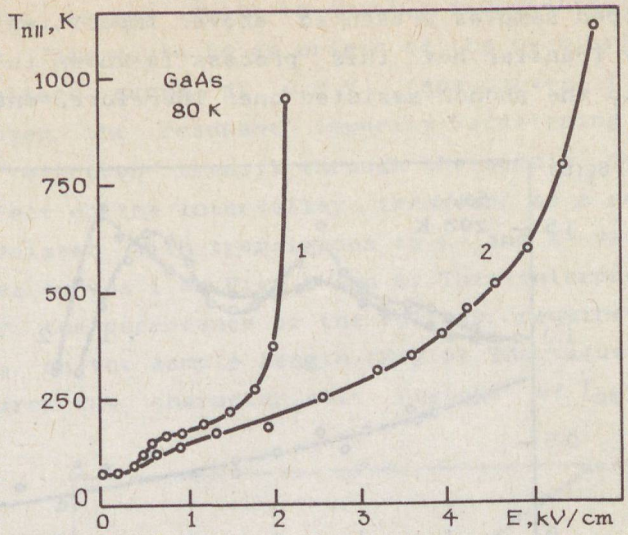

Fig. 3. Noise temperature vs electric field for long samples with various doping level: 1-n = $3 \cdot 10^{15}$ cm^{-3}; 2-n = $3 \cdot 10^{17}$ cm^{-3} (Bareikis et al. 1989b).

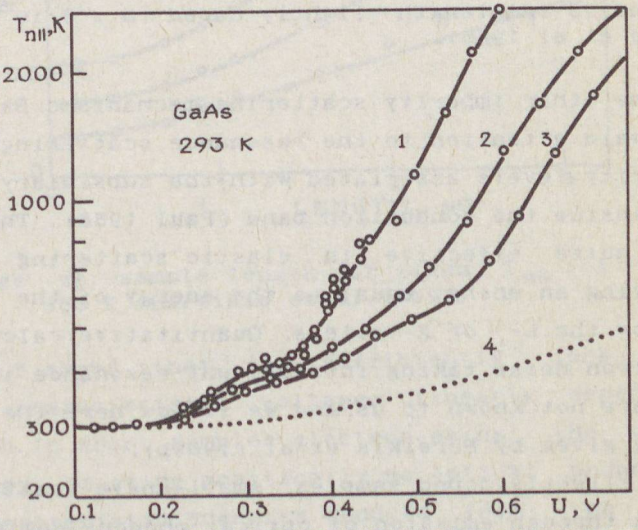

Fig. 4. Noise temperature vs applied voltage for doped (n=$3 \cdot 10^{17}$cm^{-3}) n^+-n-n^+ structures of various lengths(in microns): 1-0.2; 2-0.7; 3-0.9(Bareikis et al. 1989b); 4-1μm-length lightly doped sample (n= $3 \cdot 10^{15}$ cm^{-3}) (Bareikis et al. 1986)

An ordinary impurity scattering by Coulomb interaction which becomes inefficient in high E does not explain the results

in short doped samples presented above. Impurities assist an intervalley transfer but this process is known to be weak as compared to the phonon-assisted one. Therefore, one must con-

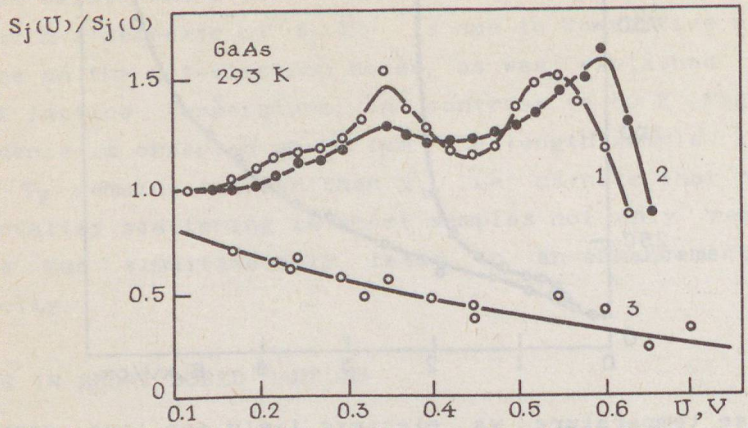

Fig. 5. Relative spectral density of current fluctuations vs applied voltage for doped ($n = 3 \cdot 10^{17} cm^{-3}$) n^+-n-n^+ structures of various length (in microns): 1-0.2; 2-0.7 (Bareikis et al. 1989a) and 3-1μm-length lightly doped ($n = 3 \cdot 10^{15} cm^{-3}$) sample (Bareikis et al. 1986).

sider some other impurity scattering mechanisms. Bareikis et al. (1989b) paid attention to the resonance scattering on the shallow impurity levels associated with the subsidiary valleys and located inside the conduction band (Paul 1968). This mechanism could be quite effective in elastic scattering of hot electrons having an energy equal to the energy of the levels situated below the L- or X-valleys. Quantitative calculations of hot electron noise taking into account resonance impurity scattering are not known to us, and we follow here the qualitative reasoning given by Bareikis et al. (1989b).

In short slightly-doped samples, small-angle scattering of hot electrons through emission of optical phonons dominates. Electrons can gain high drift component of mean energy and leave the sample before being transferred to upper valleys. As a result, the noise characteristics of short slightly -doped samples are smooth and monotonic (see curve 4 on Fig. 4 and curve 3 on Fig. 5). The resonance impurity scattering, being an elastic large-angle scattering, changes the ratio of the hot

electron mean energy drift to chaotic components increasing the last one. This could be an origin of the pecularity on the noise vs voltage curve at 0.2 V (see curves 1 on Figs. 4 and 5). Moreover, the resonant impurity scattering enhancing the time of electron transit through the sample can have an indirect effect on the intervalley transfer. As a result, two maxima associated with transitions to L- and X- valleys are observed (see curves 1 on Figs. 4 and 5). This interpretation is confirmed by the dependence of the voltage, required to reach the same $T_{n\parallel}$, on the sample length (Fig. 6). The values of $T_{n\parallel}$ are chosen from the characteristic regions of $T_{n\parallel}$ vs U plot

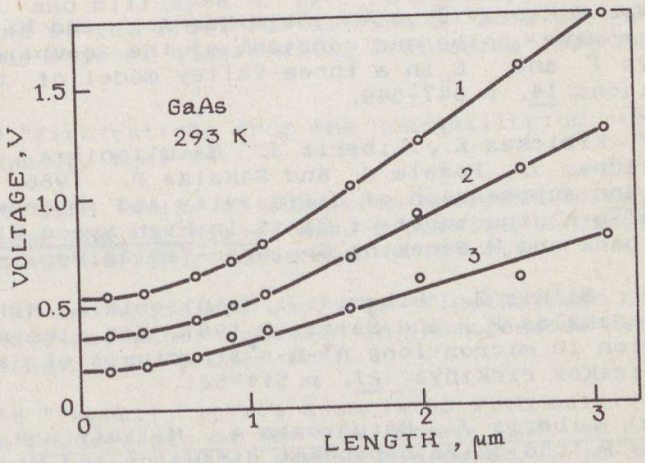

Fig. 6. Voltage vs sample length for fixed $T_{n\parallel}$: 1 - 1500 K, 2 - 500 K, 3 - 350 K (Bareikis et al. 1989b)

(Fig. 4). Fig. 6 shows that for sufficiently long samples ($\sim 1\mu m$) the characteristic voltages linearly depend on the sample length. In short samples electron gains the characteristic energy emitting practically no optical phonons. The limiting characteristic energies deduced from the extrapolation of the curves on Fig. 6 are 0.2, 0.38 and 0.55 eV. The last two values can be associated with the Γ-L and Γ-X energy separation while the first one should be attributed to the impurity resonance level position.

CONCLUSIONS

The theoretical and experimental evidence exists of the possibility to suppress effectively the hot-electron noise level by selection of the sample length, doping, and electric field strength. The length-dependence of the noise spectrum enables one to separate various noise sources (intervalley, energy fluctuation as well as resonance scattering induced noises). In this sense, one may speak about the hot electron fluctuation "length spectroscopy".

REFERENCES

Bareikis V., Viktoravičius V., Galdikas A., and Miliušytė R. 1980 "Microwave noise and constant of the coupling between the valleys Γ and L in a three-valley model of GaAs". Sov. Phys. Semicond. 14, p. 847-849.

Bareikis V. Kibickas K., Liberis J. Matulionis A., Miliušytė R., Paršeliūnas J., Požela J. and Sakalas P. 1986 "Velocity overshoot and suppression of diffusivity and microwave noise in short n^+-n-n^+ structures of GaAs". In High Speed Electronics, Eds. B. Kallback and H. Beneking. Springer-Verlag, Berlin, p. 28-31.

Bareikis V., Bilkis Z., Liberis J., Matulionis A., Miliušytė R., Požela J., Sakalas P., and Šaltis R. 1987 "Hot electron noise and diffusion in micron-long n^+-n-n^+ structures of GaAs an InP". Lietuvos fizikos rinkinys 27, p. 511-521.

Bareikis V., Liberis J., Matulionis A., Miliušytė R., Požela J., and Sakalas P. 1988 "Size dependent diffusion and microwave noise in GaAs and InP". In Proceedings of the 19th Intern. Conf. on the Physics of Semiconductors, Warsaw, Institute of Physics PAN, p. 1427-1430.

Bareikis V., Liberis J., Matulionis A., Miliušytė R., and Sakalas P. 1989a "Long-range fluctuations of hot electrons in GaAs and InP at 80 K". These Proceedings.

Bareikis V., Liberis J., Matulionis A., Miliušytė R., Požela J. and Sakalas P. 1989b "Length dependent hot electron noise in doped GaAs". In Proceedings of 6th Intern. Conf. on Hot Carriers in Semiconductors, Scottsdale, Arizona, in press.

Boittiaux B., Constant E., and Ghis A. 1983 "Simulation of diffusion noise in a device". In Noise in Physical Systems and 1/f Noise, Eds. M. Savelli, G. Lecoy, and J. P. Nougier. North-Holland, Amsterdam, p. 19-22.

Gantsevich S. V., Gurevich V. L., and Katilius R. 1979 "Theory of fluctuations in nonequilibrium electron gas". Rivista del Nuovo Cimento, 2(5), p. 1-87.

Gantsevich S.V., Gurevich V.L., and Katilius R. 1989"Comment on Fluctuations of the hot-carrier state-occupancy function in homogeneous semiconductors". Phys. Rev. B, in press.

Gasquet D., Fadel M., and Nougier J.P. 1983"Noise of hot electrons in indium phosphide". In Noise Physical Systems and 1/f Noise, Eds. M. Savelli, G. Lecoy, and J.P. Nougier. North-Holland, Amsterdam, p. 169-171.

Gasquet D., de Murcia M., Nougier J.P., and Gontrand C. 1985 "Transport parameters of hot electrons in GaAs at 300 K". Physica 134B, p. 264-268.

Junevičius D. and Reklaitis A. 1988"Monte Carlo particle investigation of noise in short n^+-n-n^+ GaAs diodes". Electronics Lett. 24, p. 1307-1308.

Katilius R. and Miliušytė R. 1980 "Anisotropy of current fluctuations and of the electron diffusion in a strong electric field in the case of quasielastic scattering". Sov. Phys JETP 52, p. 320-324.

Lax M. 1960 "Fluctuations from the nonequilibrium steady state". Rev. Mod. Phys. 32, p. 25-64.

Nougier J.P. 1983 "Noise of submicron devices". In Noise in Physical Systems and 1/f Noise, Eds. M. Savelli, G. Lecoy, and J.P. Nougier. North-Holland, Amsterdam, p. 153-159.

Nougier J.P. and Vaissiere J.C. 1988 "Fluctuations of the hot-carrier state-occupancy function in homogeneous semiconductors". Phys. Rev. B37, p. 8882-8887.

Paul W. 1968 "Impurity levels associated with multi-conduction bands". In Proceedings of the 9th Intern. Conf. on the Physics of Semiconductors, Moscow. Nauka, Leningrad, p. 16-26.

Schmidt R.R., Bosman G., van Vliet C.M., van der Ziel A., Eastman L.F., and Hollis M. 1983 "Noise in near-ballistic n^+-n-n^+ and n^+-p-n^+ gallium arsenide submicron diodes". In Noise in Physical Systems and 1/f Noise, Eds. M. Savelli, G. Lecoy, and J.P. Nougier. North-Holland, Amsterdam, p. 173-176.

Shulman A.Ya. 1970 "Correlation functions of nonequilibrium fluctuations in semiconductors in electron temperature approximation". Sov. Phys. Solid State 12, p. 922-925.

Van Rheenen A.D., Bosman G., and Morkoc H. 1987 "Hot electron noise in a square quantum-well device". In Ninth Intern. Conf. on Noise in Physical Systems, Montreal, Ed. C.M. Van Vliet. World Scientific, Singapore, p. 151-157.

Whiteside C.F., Bosman G., and Morkoc H. 1987 "Study of hot electron properties in GaAs/AlGaAs heterojunction interfaces" In Ninth Intern. Conf. on Noise in Physical Systems, Montreal, Ed. C.M. Van Vliet. World Scientific, Singapore, p. 92-96.

10th Int.Conf. on Noise in Physical Systems
1989 Budapest, Hungary

DETERMINATION OF TRAP PARAMETERS IN HIGHLY DOPED SEMICONDUCTORS FROM LOW-FREQUENCY NOISE SPECTRA

S. KUGLER, K. HEIME,[+] W. SCHLAPP,[*] G. WEIMANN[*++]

Sonderforschungsbereich 254, Universität Duisburg
D-4100 Duisburg 1, FRG
*Forschungsinstitut der Deutschen Bundespost
D-6100 Darmstadt, FRG

N-GaAs/AlAs-superlattice heterostructure field-effect transistors were investigated by low frequency noise measurements. The spectra show dominant generation-recombination contributions and at low frequencies an additional 1/f-component. From the analysis of the g-r-noise two traps could be determined with activation energies of 0.59 and 0.36eV. A model which allows the calculation of the trap concentration is proposed and successfully applied to the measurements.

I. Introduction

The generation-recombination (g-r) noise arising from an exchange of a charge carrier with a deep donor (DX-centre) is well known to be the dominant noise source in n-AlGaAs/GaAs heterostructure field-effect transistors (HFET) [1,2]. This deep centre is responsible for capturing electrons from the two-dimensional electron gas (TEG) occurring in a triangular shaped potential well at the AlGaAs/GaAs-interface. The performance of these devices suffers in the presence of this trap, persistent photoconductivity and a collaps of the I-V-characteristic occur in the dark at low temperatures. In order to reduce the influence of this trap an improved HFET structure was used. Instead of a homogeneously doped AlGaAs layer a superlattice consisting of doped GaAs and undoped AlAs was grown. In this superlattice HFET (SLHFET) no degradation of the device performance was observed at low temperatures.

II. Sample Preparation and Experimental Procedure

Superlattice GaAs/AlAs-HFETs grown by MBE were investigated. The sample consists of a 1μm thick undoped GaAs buffer layer grown on a (100) oriented GaAs substrate. Three sequential undoped GaAs/AlAs layers of thickness 2 and 1.6nm, resp., form the spacer followed by a superlattice of 17 (Si-) doped GaAs/undoped AlAs layers of the same thickness. On top an undoped GaAs cap layer was grown (Fig. 1). Calculations using the Kronig-Penney model indicate an effective band gap which corresponds to a homogeneous $Al_xGa_{1-x}As$-layer of 31% Aluminum. The doping and the

---

[+]now with : RWTH Aachen, D-5100 Aachen, FRG
[++]now with : Technische Universität München, D-8046 Garching, FRG

sheet carrier concentrations in the TEG were $1.2 \times 10^{18} cm^{-3}$ and $4.5 \times 10^{11} cm^{-2}$, resp. The mobility was $6,400 cm^2/Vsec$ at room temperature and exceeded 130,000 at 77K. The devices were HFETs with gate lengths of 1 and 2μm and drain-source spacings of 5μm. Also ungated devices were investigated with drain-source spacings of 5, 15, 30, and 60μm. The measurements were performed under constant current conditions in the frequency and temperature range from 1Hz to 25kHz and from 50 to 370K, resp.

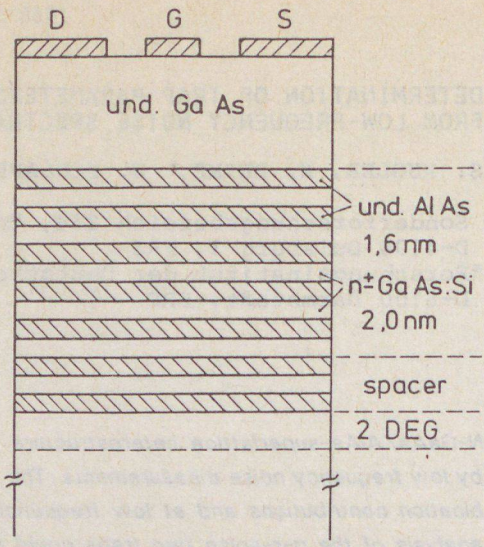

Fig. 1: Schematic cross-section of the investigated device

III. Results and Discussion

The devices were investigated in the ohmic regime. The spectra of the ungated FET are similar to the ones with a gate electrode. At high temperatures they show a superposition of a 1/f- and a g-r-noise contribution. At lower temperatures the 1/f-noise is masked by the increasing g-r-noise amplitude. Additionally a second Lorentzian occurs.

The gate doesn't influence the shape of the spectra, only the noise amplitude increases at the same drain current by pinching-off the channel. This is understood by an increasing drain-source voltage due to a higher channel resistance.

From the analysis of the 1/f-component a Hooge-parameter α_H of $1\text{-}2 \times 10^{-5}$ could be evaluated at room temperature. This value is close to the umklapplimit after Handel's theory [3]. This umklapp-1/f-noise should be a fundamental noise source in semiconductors like n-GaAs, which have satellite valleys at the zone boundary [4].

The activation energies ΔE_T and capture cross-sections σ_T of the electron traps are determined in an Arrhenius-plot of $\log(\tau T^2)$ versus 1/T. This plot yields two

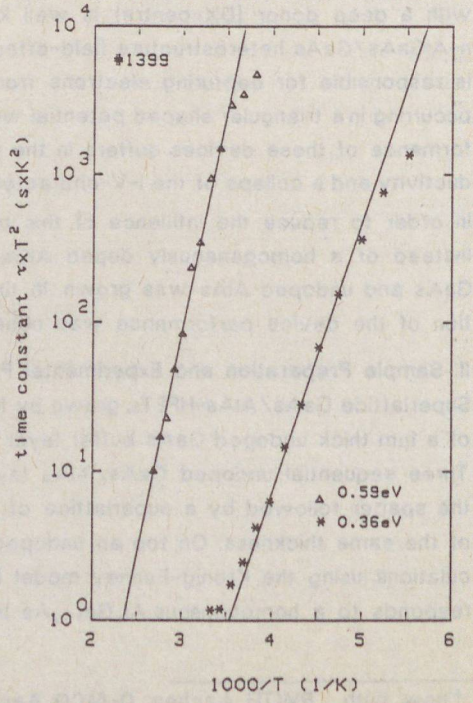

Fig. 2 :Arrhenius-plot of the SLHFET

deep levels with activation energies of 0.59 and 0.36eV. The corresponding capture cross-sections are $5 \cdot 10^{-14}$ and $1.4 \cdot 10^{-14} cm^2$, resp (Fig. 2).

In the following a model which allows the calculation of the trap concentrations is proposed. Existing models of weakly doped semiconductors [5] could not be adapted to this case because these models assume a shift of the Fermi-level through the trap-level by varying the temperature. In highly doped semiconductors, however, the Fermi-level is pinned near the conduction band edge at appropriate temperatures and is therefore always far away from the trap level. A way out of this dilemma is the assumption that the g-r-noise is "located" within the surface space charge region [6]. In order to simplify the calculations a homogeneous $Al_xGa_{1-x}As$ layer with an effective Al-content of 31% is assumed instead of the superlattice.

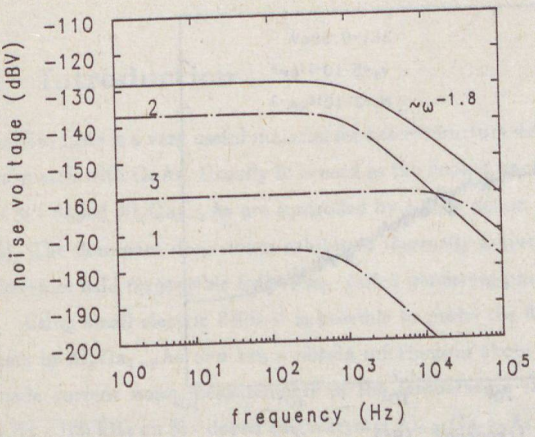

Fig. 3 : Superposition of the spectra obtained within the surface space charge region spectrum 1 is near the surface, 2 at the Fermi-level and 3 deeper in the space charge region.

At the GaAs surface the Fermi-level is pinned near midgap. This potential height propagates through the cap layer to the GaAs/AlGaAs-interface where the conduction band is additionally enhanced with respect to the Fermi-energy by a band discontinuity of about 0.3eV. The shape of the conduction band is assumed to be parabolic with a barrier height of Φ_s=0.8eV.

Due to the fact that within the depletion region the distance between the Fermi-level and the trap-level is not constant, the time constant τ and the fluctuation probability $f_T(1-f_T)$ also become spatially dependent, f_T is the occupation probability.

Each point within the depletion region contributes to the noise having its own Lorentzian-type spectrum. The full g-r-noise spectrum is obtained by a superposition of all surface elements within the space charge region (SCR) (Fig. 3).

$$S_N = N_T L W \int_{SCR} \frac{f_T(y)\,(1-f_T(y))\,\tau(y)}{1+\omega^2\tau(y)^2}\,dy \qquad (1)$$

L and W are the length and width of the device and N_T is the trap concentration. From Fig. 3 it is seen that the resulting spectrum is not a pure Lorentzian with a low-pass filter characteristic but modified with an $\omega^{-1.8}$-decrease at high frequencies. The time constant of the full spectrum is very close to that obtained when the Fermi-level lies on the trap-level :

$$\tau = \left[N_C v_{th} \sigma_T \exp\left\{ \frac{\Delta E_T}{k_B T} \right\} (B+1) \right]^{-1} \qquad (2)$$

where v_{th} is the thermal velocity, N_c the density of states in the conduction band, k_B is Boltzmann's constant and B the degeneracy of the trap. The time constant follows an Arrhenius law, eq. (2) illustrates that the use of the Arrhenius-plot as described above is valid.

The trap concentration is obtained as the best fit of the measured spectrum with the calculated one after eq (1) (Fig. 4). From this calculation the trap concentration follows as $2 \cdot 10^{16} cm^{-3}$ for the 0.59eV trap and to $8 \cdot 10^{16} cm^{-3}$ for the trap at 0.36eV. The latter one is due to the DX-centre, which in homogeneous AlGaAs layers occurs with two different levels at 0.4eV and concentrations in the order of $10^{17} cm^{-3}$ and which is reduced in concentration in the SLHFET. Therefore the influence of this trap on device performance is reduced.

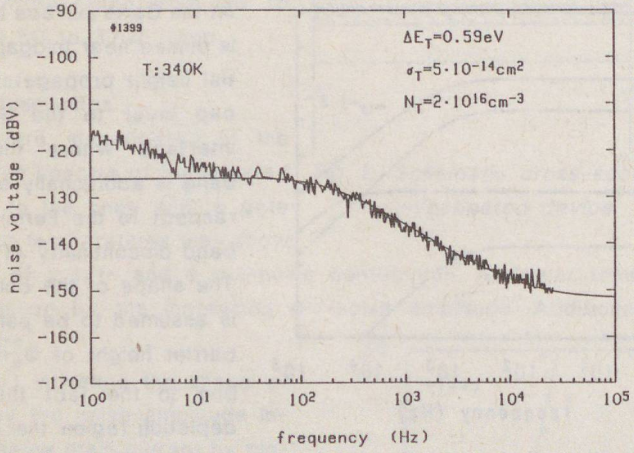

Fig. 4 : Measured noise spectrum at 340K in comparison to the calculated one

IV. Conclusion

G-r-noise was observed in n-GaAs/AlAs superlattice HFETs. The origin of this noise were two electron traps with activation energies of 0.59 and 0.36eV. A model which allows the calculation of the trap parameters is discussed. The trap concentrations were obtained as $2 \cdot 10^{16}$ and $8 \cdot 10^{16} cm^{-3}$, resp.

Acknowledgement

We are indebted to G. Howahl and U. Doerk for device preparation. The work was supported by Deutsche Forschungsgemeinschaft (Sonderforschungsbereich 254).

References

[1] L. Loreck, H. Dämbkes, K. Ploog, K. Heime, IEEE Electr. Dev. Lett. 5, 9 (1984)
[2] J.R. Kirtley, T.N. Theis, P.M. Mooney, S.L. Wright, J. Appl. Phys. 63, 1541 (1988)
[3] P.H. Handel, Phys. Rev. A 22, 795 (1980)
[4] A. van der Ziel, Proc. IEEE 76, 233 (1988)
[5] A.D. van Rheenen, G. Bosman, R.J.J. Zijlstra, Solid State Electr. 30, 259 (1988)
[6] S. Kugler, J. Appl. Phys. 66, 219 (1989)

10th Int.Conf. on Noise in Physical Systems
1989 Budapest, Hungary

NOISE SPECTROSCOPY OF DEEP CENTERS IN $Al_xGa_{1-x}As$

F. HOFMAN, R.J.J. ZIJLSTRA, J.C.M. HENNING*

Fysisch Laboratorium
P.O.Box 80000, 3508 TA Utrecht, The Netherlands
*Philips Research Laboratories
P.O.Box 80000, 5600 JA Eindhoven, The Netherlands

1 Introduction

$Al_xGa_{1-x}As$ is a very useful material for heterostructure devices because of its small ($\leq$0.14 %) [1] lattice mismatch with GaAs. Usually Si is used as the dopant to create n - type layers. The electrical properties of Si - doped $Al_xGa_{1-x}As$ are controlled by a deep donor, the so - called DX - center when $x > 0.22$ [2] [3]. The dominant deep donor exhibits a thermally activated capture cross-section for electrons and is therefore held responsible for the so - called persistent photoconductivity effect [4].

Using small electric fields it is possible to probe the fluctuations in the number of free charge carriers in $Al_xGa_{1-x}As$ and hence obtain information about the traps causing these fluctuations [5]. We made current noise measurements in the temperature range 77 - 300 K and in the frequency range 1 Hz - 100 kHz on Si - doped single crystal $Al_{0.31}Ga_{0.69}As$. The thermal depth of the donors responsible for the conduction followed from Hall effect measurements.

2 Experimental setup

We made noise measurements on Si - doped MO-VPE grown $Al_{0.31}Ga_{0.69}As$ with $N_H(300K) = 1.3 \times 10^{23}m^{-3}$ using electric fields low enough to ensure that the behaviour of the sample was ohmic. The thickness of the sample was 4 μm, and it was provided with Sn contacts. The substrate was semi - insulating GaAs. It was mounted in a N_2 flow or a N_2 bath cryostat. The measuring technique was conventional [5]. The Hall and specific resistivity measurements were made using the *van de Pauw* technique [6].

3 Experimental results and discussion

3.1 Hall effect measurements

Using the van de Pauw technique both the specific resistivity and the Hall mobility were measured. In figure 1 the Hall electron concentration is shown as a function of inverse temperature. The electron concentration is determined by a deep donor at temperatures above 170 K. At temperatures below 170 K the slope of the N_H versus 1000/T curve becomes less steep because the electrons can't surmount

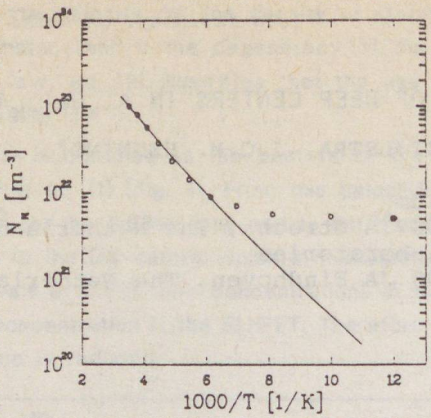

Figure 1: Hall electron concentration as a function of inverse temperature in $Al_{0.31}Ga_{0.69}As$. The drawn line is a fit to data,using the values of table 1. For details see text

the capture barrier to the donor level and the donor is *not* in thermal equilibrium with the Γ - valley. It is known that the dominant donor is compensated [3]. The Hall electron concentration was analyzed using :

$$N_H = \frac{(N_\Gamma.\mu_\Gamma + N_L.\mu_L + N_X.\mu_X)^2}{N_\Gamma.\mu_\Gamma^2 + N_L.\mu_L^2 + N_X.\mu_X^2} \quad (1)$$

in which N_Γ, N_L and N_X are the electron concentrations in the three lowest conduction band valleys, and μ_Γ,μ_L and μ_X are the electron mobilities in these valleys. We used the energy positions for the valleys as given by Henning *et al* [7] correcting for the temperature dependence of the different gaps [8]. At a temperature of 300 K the minimum of the L - valley is located 75 meV above the Γ - valley and the X - valley has an energy of 170 meV above the Γ - valley. We assumed $\frac{\mu_\Gamma}{\mu_L} = 8.5$ [9] and $\frac{\mu_\Gamma}{\mu_X} = 25$ (we used the quotient of the L and X conductivity effective masses [1] independent of the temperature). With these values it appears that the Fermi - level is pinned at some 50 meV below the Γ valley. The drawn line is a computerfit using the charge - neutrality condition with the values given in table 1.

Table 1: parameters used in the numerical simulations, B_d is the degeneracy, E_d is the thermal depth of the donor.

compensation	$6.510^{23}m^{-3}$	
	trap 1	trap 2
N_d	$2.510^{24}m^{-3}$	$4.10^{24}m^{-3}$
E_d	- 54 meV	-125 meV
B_d	2	2
σ_d	$10^{-19}m^2$	$1.210^{-19}m^2$
E_{σ_d}	300 meV	230 meV

3.2 Noise measurements

The noise measurements were done under ohmic conditions. In the temperature range studied apart from thermal noise two Lorentzians and 1/f noise could be distinguished. The generation - recombination (g - r) noise relaxation times and low frequency plateau values were obtained numerically and are shown in figure 2 and figure 3. The measured spectra consist at most temperatures of *two* Lorentzians indicating that we deal with a *three* - level system. We assumed that we essentially deal with only the lowest Γ - valley and with *two* trapping levels. Transitions between different trapping levels are very rare, so we didn't take them into account.

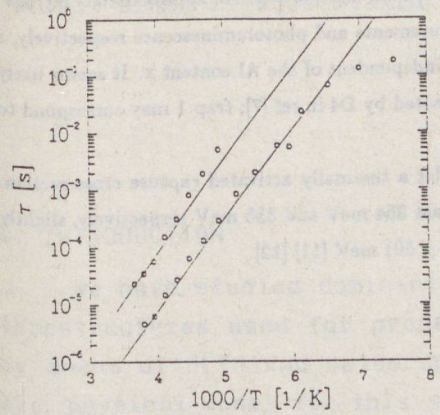

Figure 2 : g - r noise relaxation times as a function of inverse temperature. The drawn lines are fits to data using the values given in table 1. For details see text.

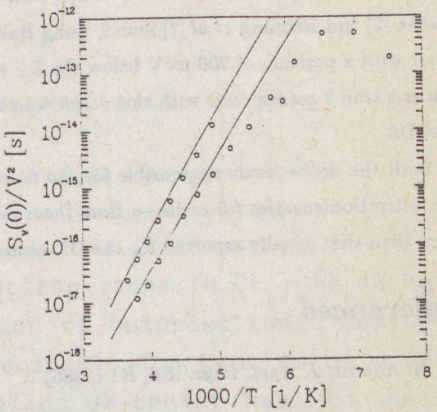

Figure 3 : g - r noise low frequency plateau values as a function of inverse temperature. The drawn lines are fits to data, using the values as given in table 1. For details see text.

The g - r noise theory of three-level systems is well known [10]. The behaviour of the fluctuations is governed by the so - called relaxation matrix M with elements depending on the derivatives of the transition currents from level i to j, p_{ij}, with respect to the populations of the levels n_K. The eigenvalues of M are the inverse relaxation times $\frac{1}{\tau_1}$ and $\frac{1}{\tau_2}$. The plateau values corresponding to the two relaxation times are given by :

$$\frac{S_N}{N^2}(1) = 4.\frac{\tau_1^3.\tau_2}{\tau_2 - \tau_1}.\left[p^0_{12}.\left(\frac{1}{\tau_1} - M_{22} - M_{12}\right) + p^0_{13}.\left(\frac{1}{\tau_1} - M_{22}\right)\right].\frac{1}{N^2} \qquad (2)$$

The expression for $\frac{S_N}{N^2}$ (2) is exactly the same with τ_1 and τ_2 everywhere interchanged. Superscript 0 denotes thermal equillibrium values and N is the number of electrons in the Γ - valley. The transition currents can be expressed as :

$$p_{1i} = \sigma.v_{th}.\frac{N.P_i}{Volume} \qquad (3)$$

where N is the number of conduction band electrons, P_i is the number of empty traps, σ is the capture cross-section of the trap and the volume is the volume of the sample. Using these expressions we could

make computerfits with the parameters given in table 1, resulting in the drawn lines in fig 1, fig 2 and fig 3. It proved to be absolutely necessary to assume that the capture cross-sections of the two traps were thermally activated, as formally described by : $\sigma(T) = \sigma_d.exp(-E_{\sigma_d}/(kT))$.

4 Conclusions

The conduction at high temperatures is caused by a donor with a thermal depth of 54 meV, slightly less than that found by Chand *et al* [3] 84 meV, but they neglected the temperature dependence of the effective density of states of the conduction bands and the difference in the Hall electron concentration and the total number of free electrons. Using their data we find a thermal depth of approximately 60 meV. Saxena [2] and Henning *et al* [7] found, using Hall measurements and photoluminescence respectively, a donor with a position of 200 meV below the L - valley, independent of the Al content x. It seems likely that our trap 2 corresponds with this donor which is denoted by D4 in ref [7]; trap 1 may correspond to level D3.

Both the donor levels responsible for the noise exhibit a thermally activated capture cross-section. The activation energies for emission from these centers are 354 meV and 355 meV respectively, slightly lower than that usually reported for the DX-center (430 ± 50) meV [11] [12].

References

[1] S. Adachi, *J. Appl. Phys.* **58**, R1 (1985)

[2] A. K. Saxena, *Phys. Stat. sol.* (b) **105**, 777 (1981)

[3] N. Chand, T. Henderson, J. Klem, W. T. Masselink, R. Fischer, *Phys. Rev.* **B 30**, 4481 (1984)

[4] D. V. Lang, R. A. Logan, M. Jaros, *Phys.Rev.***B 19**, 1015 (1979)

[5] F. Hofman, R. J. J. Zijlstra, J. C. M. Henning, *Sol. St. El.* **31**, 279 (1988)

[6] L. J. van der Pauw, *Philips Res. Rpts* **13**, 1 (1958)

[7] J. C. M. Henning, J. P. M. Ansems, P. J. Roksnoer, *Semicond. Sci. Technol.* **3**, 361 (1988)

[8] D. E. Aspnes, *Phys. Rev.* **B 14**, 5331 (1976)

[9] A. Sagar, *Phys. Rev.* **117**, 93 (1960)

[10] K. M. van Vliet, J. M. Fasset in *Fluctuation phenomena in solids*, edited by R. E. Burgess, Academic Press New York and London, Chapter VII (1965)

[11] Mooney, P. M. ,Caswell, N. S., Wrigth, S. L. ,*J. Appl. Phys.* **62**, 4786 (1987)

[12] Calleja, E. ,Gomez, A. , Muñoz, E. , *Appl. Phys. Lett.* **52**, 383 (1988)

10th Int.Conf. on Noise in Physical Systems
1989 Budapest, Hungary

NOISE AND DEEP LEVEL TRANSIENT SPECTROSCOPY OF DEEP LEVEL (DX) CENTRES IN GaAs-GaAlAs HETEROSTRUCTURES

L. KRATĚNA, K. ŽDÁNSKÝ, J. ŠIKULA,* P. VAŠINA,* L. GRMELA*

Institute of Radio Engineering and Electronics,
Czechoslovak Academy of Sciences
182 51 Praha 8, Czechoslovakia
*Department of Physics, Technical University
662 37 Brno, Czechoslovakia

1. INTRODUCTION

We have studied dominant electron traps in $Ga_{1-x}Al_xAs$ heterostructures used for preparation of optoelectronic devices by means of DLTS and noise spectroscopy. The problem of a valid physical model for this so-called DX-center has not been solved definitely [1-4]. As the DLTS measurements are carried out under non-equilibrium conditions we attempted to compare in this report these results to those obtained by noise spectroscopy.

The samples used for the DLTS and noise measurements were $Ga_{0.65}Al_{0.35}As$ double heterostructures prepared by liquid phase epitaxy and are described in detail in a parallel report [6].

The DLTS measurements were carried out on a standard deep level spectrometer. The peak belonging to the DX center was measured with different rate windows and the T^2 corrected Arrhenius plot of the emission rate vs. temperature T was drawn. The values of the activation energy $E = (0.32 \pm 0.01)eV$ and electron capture cross-section $c_n = (3 \pm 0.3) \times 10^{-13}$ cm^2 were obtained.

2. EXPERIMENT AND RESULTS

From the current fluctuation spectral density $S_i(\omega)$ we may determine the relaxation time τ and the dispersion σ^2 in homogeneous samples according to the formula [5]

$$\sigma^2 = \frac{(bn_o + p_o)^2 V}{2\pi I^2 b^2} \int_0^\infty S_i(\omega) \, d\omega \qquad (1)$$

where n_o, p_o are equilibrium electron and hole concentrations, I is the current, V is the volume and b is the electron-hole mobility ratio.

The electron capture cross section c_n and the relaxation time τ are related by the equation

$$\tau^{-1} = c_n N_c \exp[(E_t - E_c)/kT] \quad , \qquad (2)$$

where N_c is the effective density of states in the conduction band and E_t is the energy of the trap in the band gap. The concentration dispersion follows the equation [5]

$$\sigma^2 = \frac{1}{2} N_t / \{1 + \cosh [(E_t - E_{F_n})/kT]\} \qquad (3)$$

where N_t is the trap concentration and E_{F_n} is the quasi-Fermi level of electrons. To determine the three quantities, i.e. the trap concentration N_t, its energy level E_t and the capture cross-section c_n we have to carry out the measurements of the spectral density $S_i(\omega)$.

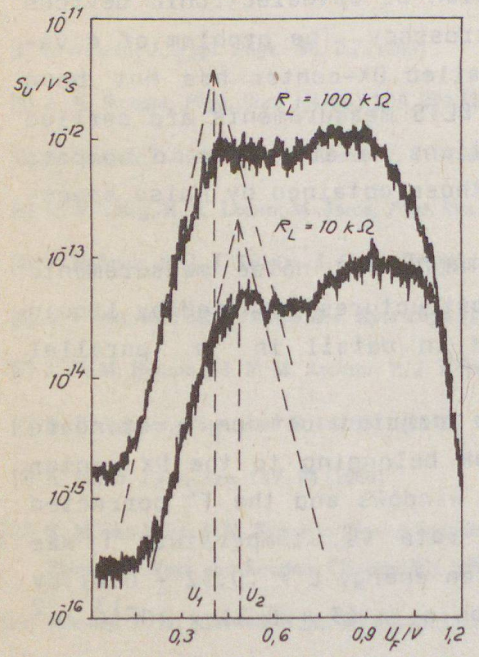

Fig.1 Voltage spectral density S_U vs. forward voltage U_F plot. The indicated maxima at U_1, U_2 correspond to the appropriate energy level

The concentration dispersion will have extreme value in the case when the trap energy level will be equal to quasi-Fermi level for electrons E_{F_n}.

If we suppose that

$$\Delta E_F = E_{F_n} - E_{F_o} = eU_F - \Delta(eU_B) \tag{4}$$

where U_F is forward voltage, ΔU_B is the voltage drop on the effective series resistance of the junction then the maximum value of the concentration dispersion will take place for the voltage U_{Fmax} measured across the p-n heterojunction

$$U_{F_{max}} = \frac{E_t - E_{F_o}}{e} + \Delta U_B \ . \tag{5}$$

Here E_F is the equilibrium Fermi level.

In Fig.1 we show the voltage spectral density S_U versus forward DC voltage applied to the diode U_F. It is seen that decreasing the diode current shifts the maximum to lower voltages. Let the value of the voltage extrapolated to zero junction current be U_x. Then it holds that

$$R_i I = U_k - U_x \tag{6}$$

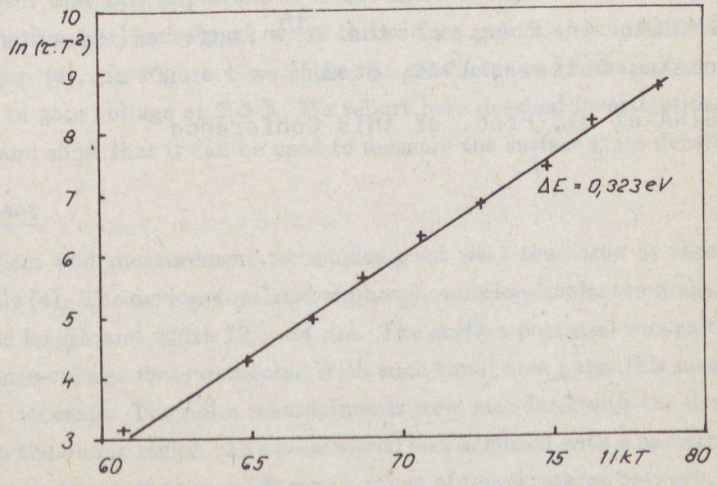

Fig.2 Arrhenius diagram for the DX center

where U_k (k=1, 2) are the corresponding values of U_{Fmax} in Fig.1 and R_i is an effective series resistance of the junction. Thus we can obtain the energy level of the dominant trap in $Ga_{1-x}Al_xAs$ heterojunction and to compare its value with that we have calculated from the DLTS spectra. As from the diagram in Fig.1 it is $\Delta E = (0,35 \pm 0,05)$ eV we conclude that the agreement of the activation energy values obtained by DLTS spectroscopy and by noise measurements is good.

In Fig.2 we show the Arrhenius plot for the DX center in the same sample of the double heterostructure.

REFERENCES

[1] J.R. KIRTLEY et al., in Noise in Physical Systems and 1/f Noise, edited by C.M. Van Vliet, Montreal (1987)

[2] T.N. THEIS, in Defects in Semiconductors, edited by H.J. von Bardeleben (Trans Tech Publications Ltd., Switzerland, 1986), p.393

[3] K. ŽĎÁNSKÝ and Le Thanh Binh, phys.stat.sol.(a), 105, K51 (1988)

[4] K. ŽĎÁNSKÝ and Le Thanh Binh, phys.stat.sol.(a) to be published

[5] J. ŠIKULA, in Proc. of the 6th Conf. of Czechoslovak Physicists, Ostrava, 1979, p.43

[6] P. VAŠINA et al., Proc. of this Conference

10th Int.Conf. on Noise in Physical Systems
1989 Budapest, Hungary

SPECTROSCOPY OF SURFACE STATES USING GENERATION-RECOMBINATION NOISE

B.K. JONES, G.P. TAYLOR

Department of Physics, University of Lancaster
Lancaster, LA1 4YB, United Kingdom

Abstract

The generation-recombination resistance fluctuations observed in the resistance of buried-channel MOSFETs is shown to be due to transitions between surface-states and the channel. This noise can be used as a new form of surface-state spectroscopy.

Introduction

Many reports have been made that the 1/f noise of the resistance fluctuations in the channel of a depletion or buried-channel MOSFET decreases significantly as the surface depletes (1)(2)(3)(4). This is because the dominant carrier trapping states at low frequencies change from being the high density surface states to the low density bulk states within the channel Debye region. However, high resolution studies have shown that this improvement in the noise is degraded by a large generation-recombination (g-r) noise peak when the surface potential is in the middle of the energy gap (4). In Figure 1 we show the conductance fluctuation at 10 Hz as a function of gate voltage at 295 K. We report here detailed investigations of this g-r process and show that it can be used to measure the surface state density.

Experiment

The devices and measurement techniques used were the same as those described previously (4). The devices consisted of phosphorous ion-implanted n-channel devices with gate length and width 12 × 64 μm. The surface potential was calculated from capacitance-voltage measurements. With such small area gates this measurement is not very accurate. The noise measurements were standard with the device channel biased in the ohmic region. The noise signal was acquired with a spectrum analyser. All the measurements were made over a range of temperatures between 130 and 360 K.

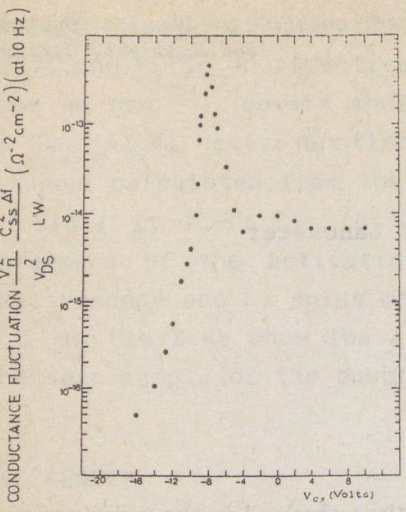

Figure 1

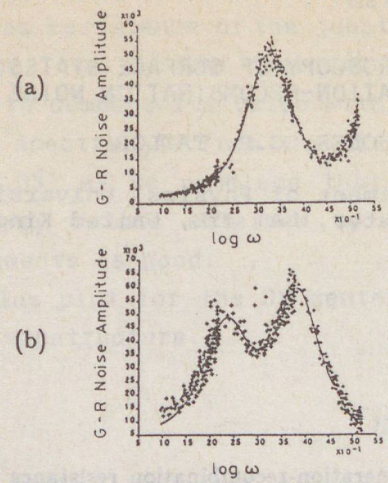

Figure 2

To obtain accurate measurement of the g-r noise in the presence of the large 1/f noise the excess noise spectrum was taken between 1 Hz and 25 kHz and a plot of $S_v \times f$ was made. The g-r signal is then a peak at the characteristic frequency, f_0, and the 1/f signal is a constant background. The data were then fitted to the background and the theoretical expressions for one or two g-r peaks as shown in Figure 2(a)(b).

Results

The data fitted well to the theoretical curves. Under some conditions of temperature and gate voltage two g-r processes were seen simultaneously. The characteristic frequencies, f_0, of the g-r processes were plotted in various ways but it was found that the only satisfactory analysis was to assume that the process involved was thermally activated over an energy related to the surface potential. With this assumption the results fell on three curves, as shown in Figure 3, which indicates that three processes are operating simultaneously. The surface potential is measured relative to the valence band. In the lower half of the band gap the process becomes faster near the valence band but some of the data show that the process also speeds up towards the conduction band above the flat band energy.

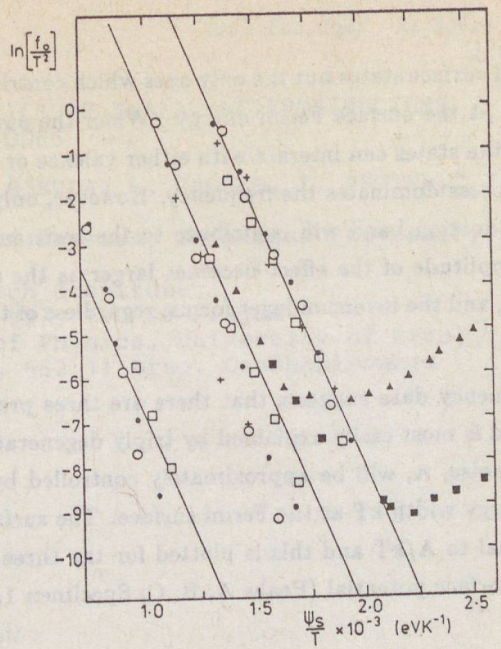

Figure 3

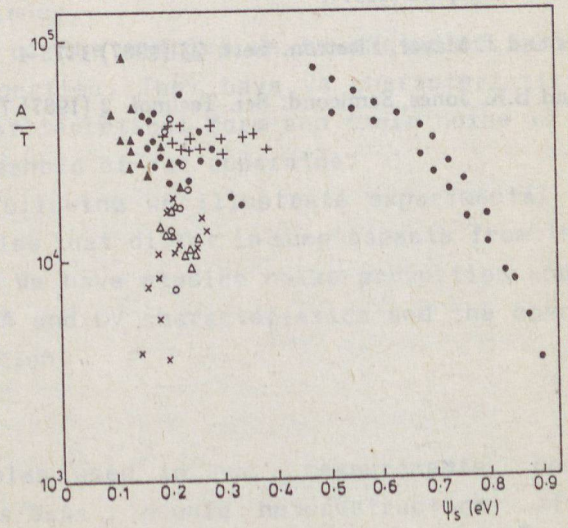

Figure 4

Discussion

There is a continuum of surface states but the only ones which contribute significantly to the noise are those at the surface Fermi energy. When the surface potential is within the energy gap the states can interact with either valence or conduction band carriers. The faster process dominates the frequency. However, only the trapping of electrons from the conduction band will contribute to the resistance fluctuation of the n-channel. The amplitude of the effect becomes larger as the surface potential nears the valence band, and the inversion layer forms, regardless of the time constant variation.

The characteristic frequency data suggests that there are three processes all acting to the valence band and is most easily explained by triply degenerate surface states. The amplitude of the noise, A, will be approximately controlled by the number of surface states in an energy width kT at the Fermi surface. The surface state density N_{SS} is thus proportional to A/kT and this is plotted for the three levels in Figure 4 as a function of the surface potential (Peaks A, B, C; Specimen 1, ▲, ●, + and Specimen 2 △, ○, x.

References

1) K. Amberiadis and A. van der Ziel, Solid-State Electron 26 (1981) 1009-17.

2) R.H.M. Clevers, Ninth Int. Conf. on Noise in Physical Systems, Montreal 1987, World Scientific, Singapore (1988).

3) C. Carruthers and J. Mavor, Electron. Lett. 23 (1987) 1173-4.

4) S.A. Hayat and B.K. Jones, Semicond. Sci. Technol. 2 (1987) 732-5.

10th Int.Conf. on Noise in Physical Systems
1989 Budapest, Hungary

NOISE DIAGNOSTICS OF GaAlAs HETEROSTRUCTURE LUMINESCENT DIODES

P. VAŠINA, J. ŠIKULA, L. GRMELA, I. HÜTTEL,* J. HLÁVKA**

Department of Physics, Technical University,
662 37 Brno
*Radio Research Institute,
Novodvorská 997, 100 00 Prague
**Department of Physics, University of Brno,
Kotlárská 2, 662 11 Brno, Czechoslovakia

1. INTRODUCTION

Noise characteristics can be used as an efficient tool for non-destructive diagnostics of GaAlAs light-emitting diodes which operate in the near-infrared region. Their "strip geometry" heterostructure gives high luminescent power and quantum efficiency.

Majority of the samples we have studied exhibit all the mentioned properties. They have VA characteristics which are very near their teoretical form and their noise is in proximity of the threshold of our apparatus.

In the following we illustrate experimental results obtained on samples that differ in some aspects from the mentioned ensemble. We have studied noise properties and their correlation to VA and CV characteristics and the spectrum of the emitted radiation.

2. EXPERIMENT

The samples used in our measurements consisted of $Al_{0.35}Ga_{0.65}As/GaAs$ double heterostructure (Fig.1). They were grown by liquid phase epitaxy at about 800°C. Subsequently

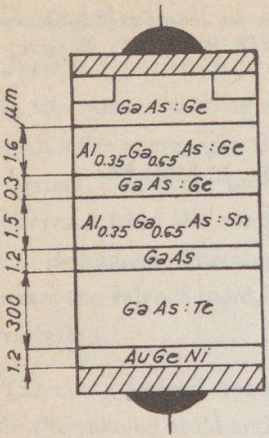

Fig.1 A cross-section of the GaAlAs LED

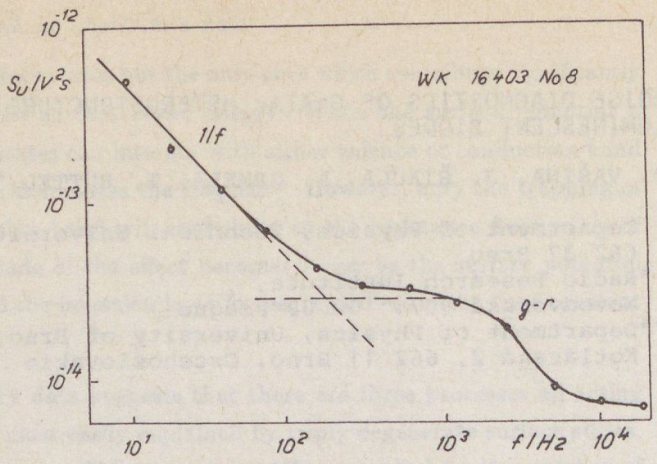

Fig.2 The voltage spectral density S_u vs frequency plot for No 8 sample at T=297 K, I = 1 μA

the n-type S_n doped $Al_{0.35}Ga_{0.65}As$ layer, the p-type Ge doped GaAs layer, the p-type Ge doped $Al_{0.35}Ga_{0.65}As$ layer, and the p^+-type Ge doped GaAs contact layer were grown on the n^+-type (100) - oriented GaAs substrate. Metal contacts on both sides of the heterostructure plate were produced by vacuum evaporation and a short - time annealing.

3. RESULTS AND DISCUSSION

The voltage fluctuation spectral density S_u vs. frequency f plot for No 8 sample of the LED and a current of 1 μA is shown in Fig. 2. Two components are apparent, one of the 1/f type and the other following the $(1 + \tau^2 \omega^2)^{-2}$ law. The magnitude of the total spectral density at 1 kHz is by 4 orders higher than that of the shot noise. The spectrum of the emitted radiation from the mentioned LED is in Fig.3. Two peaks in the curve are apparent. The nominal wavelength main peak of the LED is at 860 nm. Relative magnitude of the peaks depends on the forward current.

The photon energy corresponding to the other peak is by 0,15 eV lower. This peak is observed only in samples that exhibit excess noise and whose V/A characteristics differ from the theoretical shape.

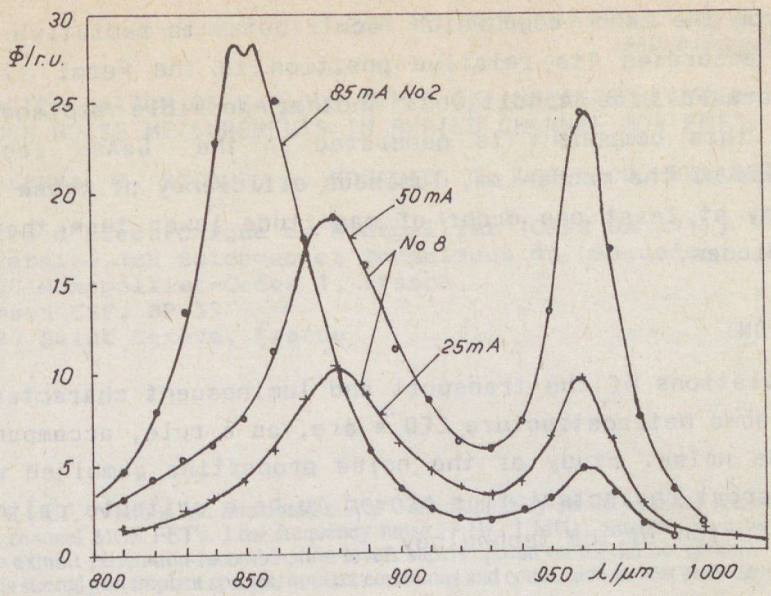

Fig.3 The emitted spectra of various samples for three values of the forward current

The light output fluctuations of our samples are similar to those referred to in our paper on super - LED´s [1]. In the range below 100 Hz their spectral density Si follows the $1/f^a$ dependence where $a \approx 2$, and $I^{5/2}$ law, where I is the LED current. This conforms to the results of [2].

Optical output vs. LED current fluctuation cross-correlation measurements were carried out. They showed that LED´s having an excess noise gave rise to a correlation coefficient $B(\tau)$ different from zero. The B vs. delay τ plot was found to be exponential with the time constant of about 1 ÷ 5 ms slightly dependent on the current I_F. The B(0) vs. I_F plot has a maximum at a current of 5 ÷ 10 mA, the maximum value being equal to about 15%.

It has been published [3] that donor-related deep level (DX) traps in the GaAlAs heterostructure act as a source of noise. Dominant mechanism of this noise is the g-r process related to these levels. We deal with this in [4].

To explain the above-mentioned behaviour we assume that there is an energy level in the band gap which is 0,15 eV

apart from the band edge which contributes to radiative transitions according its relative position to the Fermi level under forward bias conditions. Another possible explanation is that this component is generated in the GaAs region. Regardless of the mechanism, luminous efficiency of these samples is by at least one order of magnitude lower than that of normal diodes.

CONCLUSION

Deviations of the transport and luminescent characteristics of some heterostructure LED´s are, as a rule, accompanied by excess noise. Study of the noise properties combined with the transport characteristics proved to be a suitable criterion for evaluation of the technology.

REFERENCES

[1] J. ŠIKULA et al., phys.stat.solidi, 111 a, 367, (1989)

[2] R.J. FRONEN, L.K.J. VANDAMME et al.: IEEE Journ. of Quant. Electronics, 24, 724, (1988)

[3] J.R. KIRTLEY et al.: in Proc. of the 9th Int. Conf. on Noise in Phys.Systems, 70, (1987)

[4] J. ŠIKULA et al., Proc. of this Conference

10th Int.Conf. on Noise in Physical Systems
1989 Budapest, Hungary

CHARACTERIZATION OF VARIOUS TYPES OF IMPLANTED LAYERS THROUGH NOISE MEASUREMENTS IN BURIED CHANNEL MOS FET's

M. VALENZA, D. RIGAUD, A. KOUADIO, G. LECOY, D. HERAULT*

Centre d'Electronique de Montpellier (CNRS UA 391),
Université des Sciences et Techniques du Languedoc
34060 Montpellier-Cedex 1, France
*Thomson CSF, BP 55
38120 Saint Egrève, France

ABSTRACT. Various ion-implanted layers were studied by means of noise measurements in buried channel MOS FET's. Low frequency noise (1 Hz- 1 MHz) has been investigated; noise spectra exhibit generation-recombination levels superimposed on the 1/f component. G.R. noise depends strongly on implant species, implant conditions and conduction modes in the layer.

I) INTRODUCTION

Ion-implantation has become a standard technics in the integrated circuit processing.The implant is followed by temperature processing steps in order to activate the dopant atoms and to avoid the implantation induced lattice damage. The first order characteristics (I-V, Threshold voltage, mobility, ...) are not affected by the previous processes. However, it has been reported in literature [1,2] that the noise properties of ion-implanted MOS transistors and nonimplanted ones are different. The aim of this paper is to show that G.R. noise component observed only in the case of ion-implanted MOS Transistors can be associated to the implantation process.

II) DEVICE STRUCTURE AND EXPERIMENTAL SETUP

In order to analyse the properties of CCD's output amplifiers, the characteristics [(I_{DS}-V_{DS}) and noise] of the MOS Transistors used for these integrated amplifiers have been studied.

Three types of buried channel MOS FET's on Si (p-type:$3.10^{15}cm^{-3}$) have been investigated:

i)- Single implantation of Phosphorus (140 kev ; 1.1×10^{12} cm^{-2}). These MOS T are called "a".

ii)- Single implantation of Phosphorus (180 kev ; 2.1×10^{12} cm^{-2}). These MOS T are called "b".

iii)- Double implantation: Phosphorus (180 kev ; 2.1×10^{12} cm^{-2})
followed by Boron (100kev ; 5.5×10^{11} cm^{-2}). These MOS T are called "c".

Phosphorus implantations were annealed at 1050°C for 210 min. and Boron implantations at the same temperature for 140 min.

Each type of MOS T has been designed with the following geometry rates: $\frac{W}{L}=\frac{200}{15}$ and $\frac{200}{60}$.

Upon the same wafer enhancement MOS T (called "d")were available with a ratio $\frac{W}{L}=\frac{200}{60}$.

For each device a substrate electrode B is available and the equivalent SiO_2 thickness is 105 nm.

All the contacts were independently biased. The noise was measured between Source and Drain. The Source, Gate and Bulk electrodes were a-c short-circuited. After amplification the noise spectral densities were performed by using F.F.T. analyzers from 1 Hz to 1 MHz. The noise spectral intensity of the Drain current versus freqency is obtained when the Channel resistor and the bias Drain resistor are taken into account.

III) EXPERIMENTAL RESULTS

a) The first measurements were made at $V_G = V_S = V_B = 0$. The I_{DS} - V_{DS} characteristics (at room temperature) are plotted in Fig 1 for the four types of MOS T . These curves exhibit three domains of conduction : The ohmic and saturation regions followed by a third region where a multiplication effect occurs. This last mechanism is confirmed by a hole current appearing in the substrate electrode B.

b) In order to calculate the carrier mobility μ and the number N of conduction carriers, I_{DS} versus V_{GS} characteristics for various V_{GS} values were plotted in the ohmic region where the condition is: $V_{DS} < (V_{GS} - V_T) / 10$ (V_T is the threshold voltage).

The channel resistor R_C is given by: $R_C = \frac{dV_{DS}}{dI_{DS}} = \frac{L^2}{\mu C V^*_{GS}}$ where $\mu = \frac{\mu_0}{1+\theta V^*_{GS}}$;

$V^*_{GS} = V_{GS} - V_T$; $C = C_{ox}.W.L$; θ is the reduction factor of mobility.

N is given by : $N = \frac{L^2}{q\mu R_C}$.

The other parameters have their conventional meaning.

The calculated values are reported in Table1.

For enhancement MOS T "d", a mobility value of 700 cm^2/Vs is obtained.

Taking into account the results of the various mobilities it seems that a surface conduction is predominant for the MOS T "a","c" and "d" whereas a bulk conduction occurs for the MOS T"b".

TABLE 1

MOS T	a	b	c
V_T (V)	-4	-6	-6
μ_0 (cm^2/Vs)	750	1200	610
θ	$23\ 10^{-3}$	$58\ 10^{-3}$	$6.3\ 10^{-3}$
N at V_{GS}=0	$2\ 10^7$	$3\ 10^7$	$3\ 10^7$

c) The channel current noise spectra for MOS T "c" are reported in Fig 2 for various Drain bias conditions. At low Drain voltages the noise intensity exhibits 1/f noise followed by a white noise in the high frequency range.This white noise has to be associated with the thermal noise of the channel. Moreover generation-recombination noise is superimposed on 1/f noise in the saturation region of the I_{DS}-V_{DS} characteristics. This result is in agreement with literature [3,4].

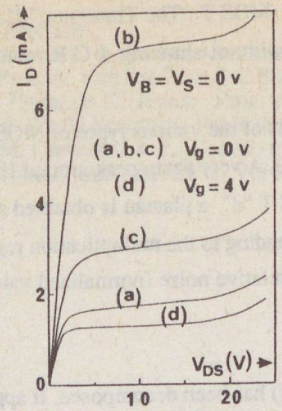

fig:1

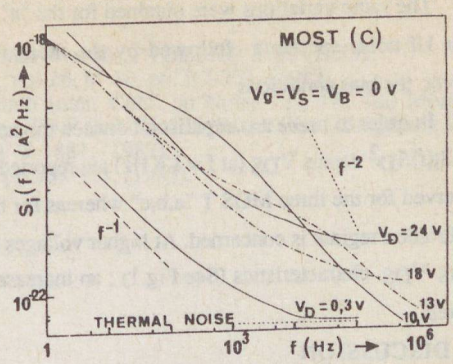

fig : 2

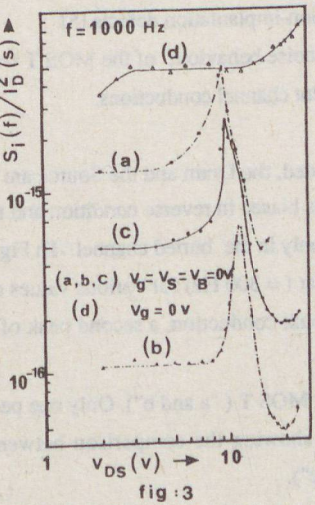

fig : 3

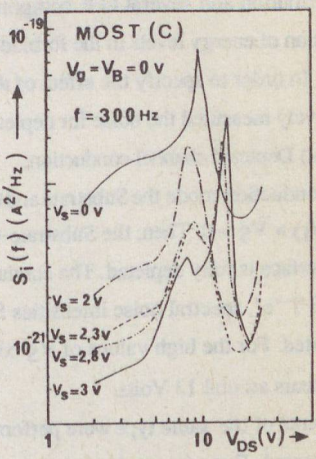

fig : 4

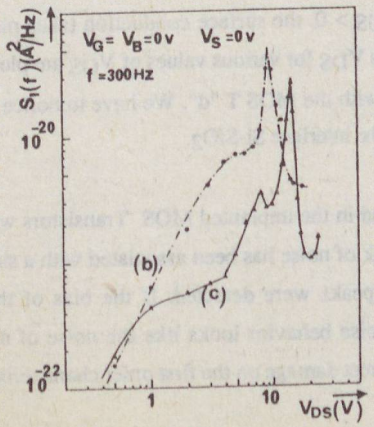

fig:5

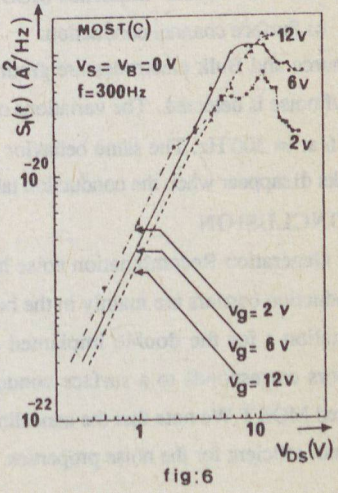

fig:6

The same variations were obtained for the "a" and "b" MOS T . The Transistor "d" exhibits only a 1/f noise spectrum followed by the thermal noise without showing a G.R. component whatever the bias conditions.

In order to make a comparison between the noise levels of the various types of MOS T, the ratios $S_i(f)/I_D^2$ versus V_{DS} (at f = 1 KHz) are reported in Fig 3. A very sharp peak around 10 Volts is observed for the three MOS T "a,b,c" whereas for the MOS T "d" a plateau is obtained as far as the saturation regime is concerned. At higher voltages corresponding to the multiplication regime of the I_{DS}-V_{DS} characteristics (See Fig.1) , an increase of the relative noise (normalized values) is observed.

IV) DISCUSSION

Starting from results given in Fig.2, the spectrum $S_i(f)$ has been decomposed. It appears a 1/f contribution and several G.R components.These G.R spectra can be associated with a discrete distribution of energy levels in the forbidden gap created by ion-implantation defects.[5]

In order to specify the effect of these levels on the noise behaviour of the MOS T we have successively measured the noise for depleted and enhancement channel conductions.

a) Depleted channel conduction:

In this conduction mode the Substrate and the Gate are grounded, the Drain and the Source are biased so that $V_D > V_S > 0$. Then, the Substrate-Channel junction is biased in reverse condition and the Si-SiO_2 interface is fully depleted. The conduction takes place only in the buried channel. In Fig.4, for the MOS T "c", spectral noise intensities $S_i(f)$ versus V_{DS} (at f = 300 Hz) for various values of V_S are reported. For the high values of V_S corresponding to a bulk conduction, a second peak of noise level appears around 13 Volts.

Experiments of the same type were performed with the other MOS T ("a and b"). Only one peak has been detected. Experimental results are plotted in Fig.5 showing the comparison between the "Single" and the "Double" implanted MOS T (type "b" and "c").

b) Surface channel conduction:

The Source and Bulk electrodes are grounded. For $V_{GS} > 0$, the surface conduction takes place. Only 1/f noise is detected. The variations of $S_i(f)$ versus V_{DS} for various values of V_{GS} are plotted in Fig.6 at f= 300 Hz. The same behavior is observed with the MOS T "d". We have to notice that the peaks disappear when the conduction takes place at the interface Si-SiO_2.

V) CONCLUSION

Generation-Recombination noise has been found in the implanted MOS Transistors when the conduction carriers are mainly in the bulk. One peak of noise has been associated with a single implantation ; for the double implanted device two peaks were detected. If the bias of these transistors corresponds to a surface conduction, the noise behavior looks like the noise of non-implanted MOS T.We note that the annealing effects correct damage on the first-order characteristics but are not efficient for the noise properties.

REFERENCES

[1] K. Nakamura, O. Kudoh, M.Komoshida: J.A.P.Vol 46, n°7,pp.3189-3193 (1975)
[2] H.S.Park, A. Van der Ziel: Sol. Stat. Elec., Vol 26, n° 10, pp.747-751, (1983).
[3] S.A. Hayat, B.K. Jones: Proc. of the Ninth Inter. Conf. on Noise . pp.477-480 Montreal (1987).Ed. World Scientific Publishing Co.Pte.LTD.P.O.BOX 128, Farrer Road. Singapore 912.
[4] R.H.M. Clevers: J.A.P., Vol 62, n°5, pp.1877-1881, (1987).
[5] J.R. Troxell: Sol. Stat. Elec., Vol 26, n° 6, pp.539-548, (1983).

10th Int.Conf. on Noise in Physical Systems
1989 Budapest, Hungary

BURST NOISE IN PN JUNCTION DEVICES

M. ŠIKULOVÁ, J. ŠIKULA, P. VAŠINA, V. NEVĚČNÝ

Technical University
Technická 2, 616 96 Brno, Czechoslovakia

1. INTRODUCTION

We investigated the burst noise in semiconductor p-n junction diodes, Schottky diodes, LED´s (including heterostructures), bipolar transistors and integrated circuits. From our experiments it follows that the origin of the burst noise is of the same nature in all these devices and its source is located in the depletion layer of the p-n junction.

2. Theory

Our approach is based upon the physical model of Hsu and others [1]. According to this model, the burst noise is generated by means of a defect in the crystal structure of the semiconductor. The conductivity of the defect has two discrete values (α , β) and causes modulation of the sample current. In this way a secondary process, Y(t), is produced, which has two states. The primary process, X(t), is represented by occupation of the defect trap by an electron or a hole. We assume that the X(t) process is a three-state, homogeneous and markovian process.

The Y(t) secondary process of the current modulation is a two-state one, because: i) no current passes through the trap when it is occupied by an electron, ii) emission of an electron into the valence or conductance band or capture of a hole by the trap makes the current pass through the defect. We can see that two states of the X(t) process are projected onto one state of the Y(t) process. Diagrams showing the states of the primary and secondary processes and the corres-

ponding transition probability intensities are in Figs 1a and b, respectively.

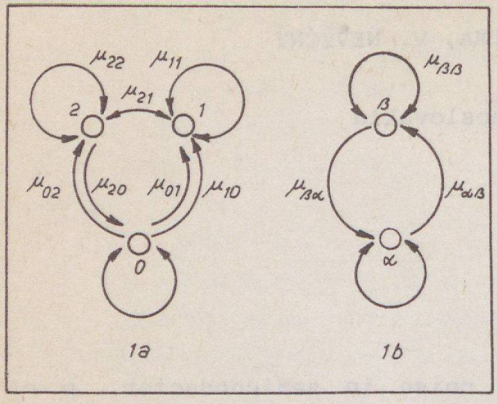

Fig.1 Diagram of the transition intensities of the primary and secondary processes

For a three-state primary process X(t) from the Kolmogorov´s equations the absolute probability distribution and transition probability p are derived.

We suppose that the 0-state of the X(t) process is transformed into the α -state of the secondary process Y(t), while the two states 1 and 2 of the X(t) process are transformed into the β -state of Y(t).

Then

$$p_{\alpha\alpha}(t) = \Pi_\alpha + b_1 \tau_1 \exp(t/\tau_1) + b_2 \tau_2 \exp(t/\tau_2) \qquad (1)$$

where Π_α is an absolute probability distribution of Y(t) process in the α state, b_1, b_2 are functions of the transition probabilities and τ_1, τ_2 are relaxation times.

The spectral density of the Y(t) process is

$$S_y(\omega) = \frac{I_B^2 \Pi_\alpha}{\pi} \left(\frac{-b_1 \tau_1^2}{1+\omega^2 \tau_1^2} + \frac{-b_2 \tau_2^2}{1+\omega^2 \tau_2^2} \right) \qquad (2)$$

where I_B is the amplitude of the burst noise.

In a special case of an N-type semiconductor in low injection conditions we have the dispersion of the secondary process Y(t):

$$D\{Y(t)\} = \frac{I_B^2/2}{1 + \mathrm{ch}\,[(E_t - E_{Fn})/kT]} \qquad (3)$$

where E_{Fn} and E_t are quasi-Fermi and trap energies, respectively. In the low frequency region the spectral density is determined by the dispersion only. The dispersion of the current fluctuations has a maximum value when the quasi-Fermi

level E_{Fn} coincides with that of the traps E_t. Similarly, we find the spectral density of the current fluctuations:

$$S_{iB} = \frac{D\{Y(t)\}}{\pi} \cdot \frac{\tau}{1 + \omega^2\tau^2} \cdot \qquad (4)$$

In a general case for the three-state X(t) primary process the spectral density consists of two components with relaxation times given by the capture of electrons and the capture of holes.

3. EXPERIMENTAL

All samples we have measured exhibited the burst noise and simultaneously the excess current in the low-voltage region. The excess current component varies as $I \sim \exp(\beta_1 U)$ with $\beta_1 \ll \beta_2$ and is independent of temperature. The exponent β_2 of the ordinary current varies with the temperature and corresponds to the g-r process in the p-n junction ($\beta_2 = e/2kT$).

The temperature measurement of the saturation current corresponding to the excess current curve makes it possible to evaluate the activation energy E_a. Our measurements give for GaAs LED No 11 E_a = 0.4 eV, which corresponds to [3] for the contact potential of some metals, as for example Au with p-type galium arsenide.

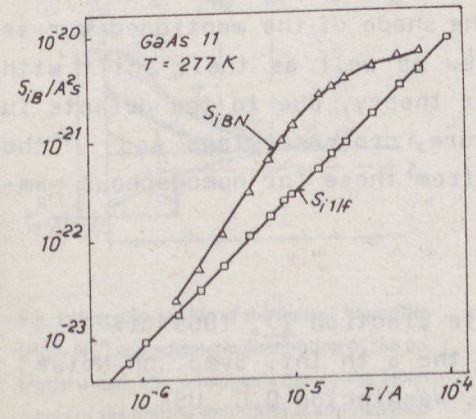

Fig.2 The spectral density of current fluctuations in the two states of the secondary process

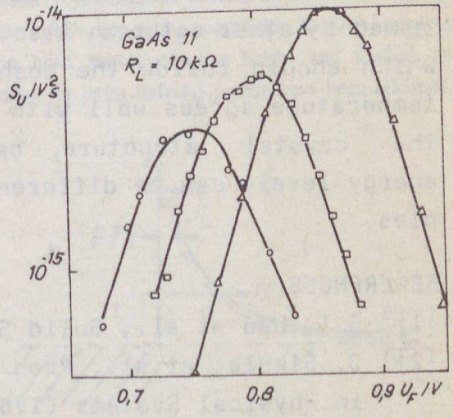

Fig.3 Voltage spectral density of the burst noise component as a function of the forward voltage U_F for three different temperatures

The current dependence of the current spectral density for the two mentioned states for f = 1 kHz are in Fig.2. The lower curve corresponds to the 1/f noise (0-state), the upper to the 1-state. Subtracting the values of the curves gives the spectral density of the burst noise.

Fig.3 illustrates a plot of the voltage spectral density vs. the forward voltage U_F at three different temperatures. One may see that the maxima of the curves shift towards lower voltages when increasing the temperature. It is to be noted that when the diode is fed from a constant current supply all the maxima appear at the same voltage.

Our model makes it possible to explain the observed spectral density as a function of frequency, which depends on the relaxation times of both electrons and holes and to determine the energy of the trap which controls the burst noise. The results that we have obtained on a number of diodes of various materials give, however, only a qualitative agreement. As example we show our results of measurements of GaAs LED´s, which feature the following properties: $n_o = 2.10^{17}$ cm^{-3}, the p-region has been produced by diffusion with the surface concentration p = 10^{20} cm^{-3}. Taking that τ is in the order of 10^{-4} s, for the maxima of the curves in Fig.3 we find the I_{BN} to be of the order of 10^{-8} A which is a good agreement with our results of other measurements and with values published by other authors. Also, the shape of the mentioned curves which should follow the cosh law as well as their shift with temperature agrees well with our theory. Due to the defects in the crystal structure, capture cross-sections and the energy levels can be different from those for homogeneous samples.

REFERENCES

[1] S.T. Hsu et al., Solid State Electron 13, 1005 (1970)

[2] J. Šikula, et al., Proc. of the 6 th Int. Symp. on Noise in Physical Systems (1981), Washington D.C. USA

[3] C.A. Mead, Sol.State Electr. 9, 1023 (1966(

[4] J.C. Martin, G. Blasquez.: Solid State Electron. 14, 89, (1971)

10th Int.Conf. on Noise in Physical Systems
1989 Budapest, Hungary

THE INFLUENCE OF LOW-ENERGY ION RADIATION IN GaAs SURFACE ON THE CURRENT-VOLTAGE, CAPACITANCE-VOLTAGE AND NOISE CHARACTERISTICS OF SCHOTTKY-BARRIER DIODES

J. MATUKAS, V. PALENSKIS, A. PINCEVIČIUS, S. SMETONA

Department of Radiophysics, Vilnius University,
Lithuanian SSR

There is currently a great deal of interest in the use of ion beam techniques for semiconductor devices processing. Schottky-barrier diodes (SBD) are in widespread use in the mixing and direct detection due to their excellent high-frequency properties.

The effects of radiation on the current-voltage (I–V), capacitance-voltage (C–V) and noise characteristics of Al-nGaAs Schottky-barrier diodes have been studied. SBD have been fabricated on the nGaAs plates, radiated by low-energy ($E < 2$ keV) Ar^+, N^+ and O^+ ions. I–V, C–V and noise of SBD have been measured in a wide temperature range from 77 to 380 K both for forward and backward bias. A preliminary study of I–V and noise characteristics of Schottky diodes on nGaAs surfaces to an Ar^+ ion bombardment in the 0,8–6 keV range has been done earlier [1]. It is shown that bombardment of nGaAs surface by Ar^+ ions allows to produce Schottky diodes with very low forward bias voltage, and that such diodes have practically the same level of noise as those fabricated without the bombardment.

The distribution of the potential in Al-nGaAs interface upon both Schottky-barrier height and ionized impurities (or point defects) profile have been calculated

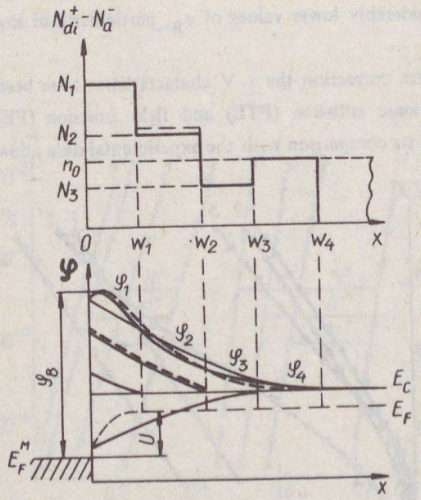

Fig. 1. Step-like profile of the ionized impurities ($N_d^+ - N_a^-$) and schematic distribution of the potential φ and it's components due to the increments of the ionized impurities at any step junction in the interface layer. The dotted curves present the shift of the potentials due to the change of the impurity N_2. U is the forward diode voltage.

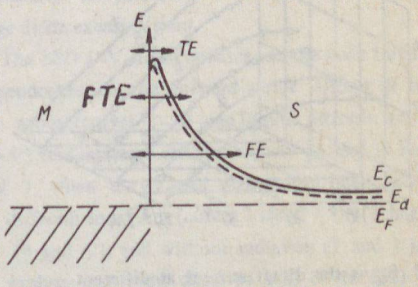

Fig. 2. The current flowing through the Schottky-barrier contact mechanisms: thermionic emission (TE), field-thermionic emission (FTE) and field emission (FE).

also. We solve the Poisson equation with a sharply defined edge of the depletion layer at x = w (Fig. 1). Assuming that ionized impurity ($N_d^+ - N_a^-$) profile is step-like shape with any number of steps and accounting that potentials $\varphi_i(w_i)$ and its derivatives $\varphi_i'(w_i)$ from both left and right sides at any step junction are equal the analytical expressions for the potential distribution $\varphi(x)$ and C–V characteristic (or for the depletion depth w) of SBD have been obtained. For four-step profile (Fig. 1) we can write:

$$w = \left[\frac{2\epsilon(\varphi_B - E_F - qU)}{q^2 n_0} + \frac{N_2 - N_1}{n_0} w_1^2 + \frac{N_3 - N_2}{n_0} w_2^2 + \frac{n_0 - N_3}{n_0} w_3^2\right]^{1/2}; \quad (1)$$

$$\varphi_4(x) = (qn_0/2\epsilon)(w - x)^2 = A(w - x)^2, w_3 \leqslant x \leqslant w; \quad (2a)$$

$$\varphi_3(x) = \varphi_4(x) + A[(N_3 - n_0)/n_0](w_3 - x)^2, w_2 \leqslant x \leqslant w_3; \quad (2b)$$

$$\varphi_2(x) = \varphi_3(x) + A[(N_2 - N_3)/n_0](w_2 - x)^2, w_1 \leqslant x \leqslant w_2; \quad (2c)$$

$$\varphi_1(x) = \varphi_2(x) + A[(N_1 - N_2)/n_0](w_1 - x)^2, 0 \leqslant x \leqslant w_1, \quad (2d)$$

where all the variables are presented in Fig. 1; $A = qn_0/2\epsilon$; ϵ is the dielectric constant. As it is seen from the Eqs (2a)–(2d) the potential $\varphi(x)$ may be decomposed into components (Fig. 1), i. e. any ionized impurity increment gives an additional square term $a_i(w_i - x)^2$. The fluctuation, for example, of the ionized impurity concentration N_2 deals to change in the potentials $\varphi_2(x)$ and $\varphi(x)$, which are shown in Fig. 1 by dotted curves. These results allow us to compose in such a way the profile of ionized impurities to obtain SBD with desirable parameters. It is worth to point that the usual technique for evaluating the Schottky-barrier height from the extrapolation of the $1/C^2$ curve to zero gives only an effective value φ_B^* which differs from the real value φ_B (see the Eq. (1)). In addition, the value φ_B^* extracted from I–V characteristics, taking into account only thermionic emission of charge carriers, provides sometimes considerably lower values of φ_B, particularly at low temperatures.

On the basis of those results and owing to the image-force correction the I–V characteristics have been calculated including thermionic emission (TE), field-thermionic emission (FTE) and field emission (FE) (Fig. 2). The calculation of I–V and C–V characteristics and its comparison with the experimental data allow us to conclude that the field-thermionic emission is the main mechanism of the charge carriers transport through the Schottky barrier, especially at low temperatures.

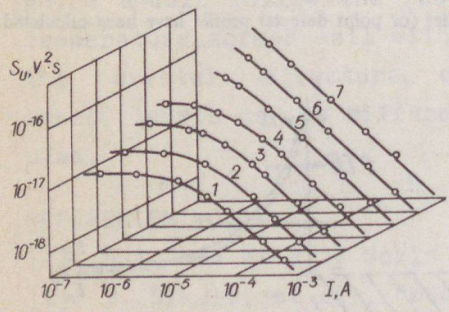

Fig. 3. S_U vs the direct current at different temperatures in the white noise region. T, K: 1 – 356; 2 – 350; 3 – 337; 4 – 335; 5 – 319; 6 – 291; 7 – 251.

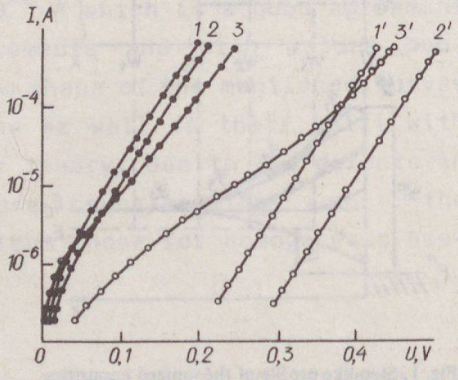

Fig. 4. I–V characteristics at different SBD annealing temperatures T_{ann} on both clean (opened dots) and radiated surfaces nGaAs by N^+ (closed dots). T_{ann}, K: 573 (2; 2'); 673 (1; 1'); 773 (3; 3'). Diameter of the Schottky contact D = 0,5 mm. $\Phi = 10^{15}$ cm^{-2}.

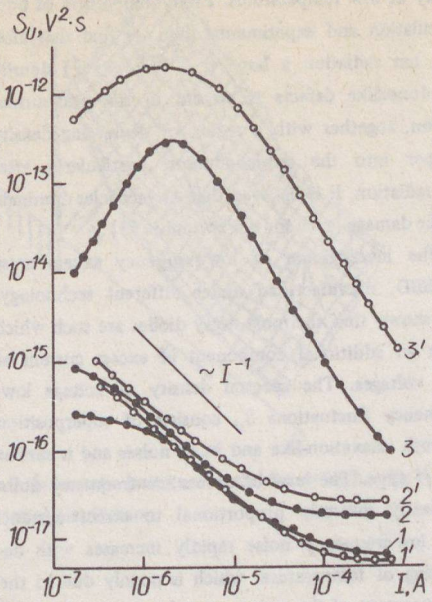

Fig. 5. S_u vs the direct current for the same SBD as in Fig. 4.

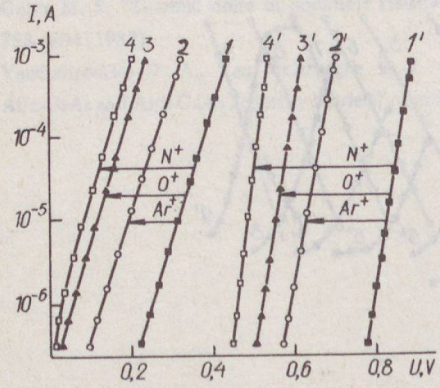

Fig. 6. I–V characteristics at room (curves 1–4) and liquid nitrogen (curves 1'–4') temperatures, when the nGaAs surface has been radiated by ions: Ar^+ (2; 2'), O^+ (3; 3'), N^+ (4; 4') and without the radiation (1; 1'). T_{ann} = 673 K. D = = 0,5 mm (except the SBD by Ar^+ radiation for which D = 0,25 mm). $\Phi = 10^{15}$ cm^{-2}.

It has been shown that the noise of SBD in the range of the white spectrum is consistent upon the idea of the thermal noise in nonlinear resistive elements independently of technology and nonideality of I–V characteristics, and is well described by Gupta's formula [2]:

$$S_u = \frac{\langle \Delta U^2 \rangle}{\Delta f} = 4kT\left(\frac{dU}{dI} + \frac{1}{2} I \frac{d^2U}{dI^2}\right)_{I=I_{dc}} \qquad (3)$$

where S_u is the spectral density of the voltage fluctuations ΔU; I is the current; I_{dc} is the direct (constant) current; U is the bias voltage. In Fig. 3 the solid curves present the calculation data by Gupta's formula (3), points – the direct measurement results in the white noise range. A good agreement is obtained for all regions of I–V characteristics. The Schottky formula $S_i = 2qI$ is valid only for ideality factor m = 1 of I–V characteristics $I = I_0 (\exp(qU)/(mkT) - 1)$.

Thermal annealing of the SBD after metal Al contact deposition is performed under helium gas at different temperatures during 15 min. Fig. 4 gives the variations of typical I–V characteristics as a parameter of the annealing temperature (573 K, 673 K and 773 K) for Schottky diodes fabricated on both the clean (opened dots, curves 1'–3') and the radiated surface nGaAs by 1 keV energy nitrogen ions with dose $\Phi = 10^{15}$ cm^{-2} (closed dots, curves 1–3). As it is seen from those results the annealing temperature, exceeding 673 K, leads to a large excess current at low bias-voltages. For the same SBD as in Fig. 4 the low-frequency noise intensity dependences on forward diode current at the noise measuring frequency 1 kHz are presented in Fig. 5. The large noise intensity at annealing temperature 773 K is attributed to the large diode excess current.

The SBD I–V characteristics and the noise intensity dependences on the forward diode current at both the room (curves 1–4) and liquid nitrogen (curves 1'–4') temperatures are respectively plotted in Fig. 6 and 7, when the nGaAs surface has been radiated by different ions: Ar^+ (curves 2 and 2'), O^+ (3 and 3'), N^+ (4 and 4'), and without radiation (1 and 1'). As an analysis shows the observed shift of the SBD I–V characteristics to the lower bias-voltages (Fig. 6) is related not only to the reduction of barrier height, but to the increase of barrier transparency too, espe-

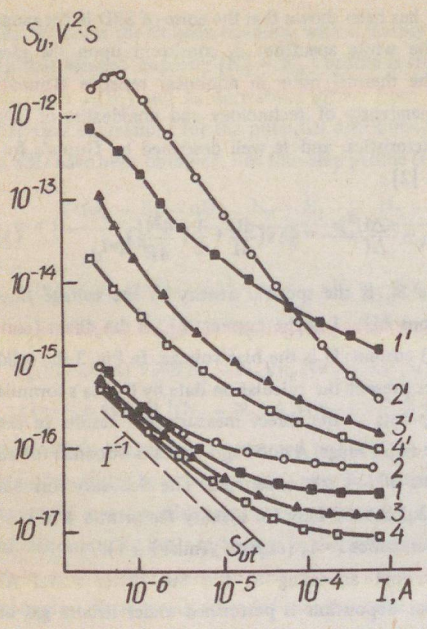

Fig. 7. S_u vs the direct current for the same SBD as in Fig. 6 (f = 1 kHz; S_{ut} is the white noise level).

cially at low temperatures. From comparison of both calculation and experimental data we find that after the ion radiation a large ($\sim 10^{18}$ cm^{-3}) density of donorlike defects is present in the near-surface region, together with a region of decreasing density deeper into the semiconductor, particularly after O^+ radiation. It is believed that As vacancies dominate in the damage layer and act as donors [3].

The investigation of low-frequency excess noise of SBD, manufactured under different technology, has shown that the most noisy diodes are such which have an additional component of excess current at low voltages. The spectral density of voltage low-frequency fluctuations S_u consists of superposition of both relaxation-like and burst noises and is similar to 1/f type. The level of excess low-frequency noise is nearly inversely proportional to direct current. The low-frequency noise rapidly increases with decreasing of temperature, which is mainly due to the enhancement of the excess current component. Fig. 8

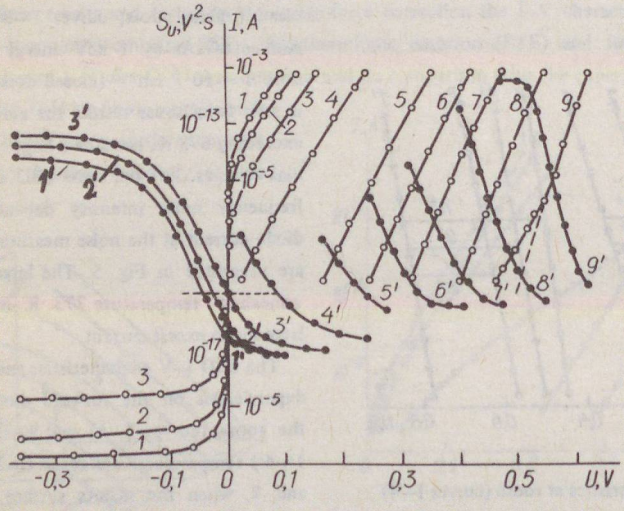

Fig. 8. Current I (opened dots) and the noise intensity S_u (closed dots) dependence on the bias-voltage U at different temperatures; T, K; 374 (1; 1'); 360 (2; 2'), 336 (3; 3'), 284 (4; 4'); 224 (5; 5'), 190 (6; 6'); 158 (7; 7'); 124 (8; 8'); 77 (9; 9'). T_{ann} = 673 K; f = 1 kHz; D = 0,5 mm; O^+ radiation: $\Phi = 10^{15}$ cm^{-2}.

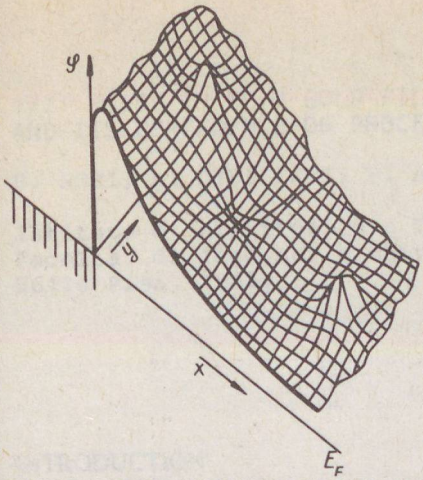

Fig. 9. Schematic pattern of a real Schottky-barrier potential distribution.

shows typical dependences of current (opened dots) and spectral density of noise S_u (at 1 kHz, closed dots) at different temperatures on the bias-voltage in both the forward and backward directions. The low-frequency noise results are explained on the basis of nonhomogeneous metal-semiconductor contact potential energy model, which includes various pits and humps in the space-charge region, as it is shown in Fig. 9. The thermally activated capture and emission of electrons by the traps in the space-charge region introduce random fluctuations of the potential energy barrier both width and height, which lead to the current fluctuations.

Thus, the surface bombardment with low-energy ions allows to produce zero-bias SBD, which are very important for the mixing and direct detection of weak microwave signals.

REFERENCES

1. Matukas J., Palenskis V., Pincevičius A., Petrauskas G., Smetona S., Žukauskas S. "Investigation of current-voltage characteristics and noise of Schottky diodes on bombardment conditions of the surface of gallium arsenide by argon ions". Liet. fiz. rink. 26(5), 618–626 (1986) (in Russ.).
2. Gupta M. S. "Thermal noise in nonlinear resistive devices and its circuit representation". Proc. IEEE. 70, 788–804 (1982).
3. Vanderbroucke D. A., Van Meivhaeghe R. L., Laflere W. H., Cardon F. "Sputter-induced damage in Al/n-GaAs and Al/p-GaAs Schottky barriers". Semicond. Sci-Techn. 2(5), 293–298 (1987).

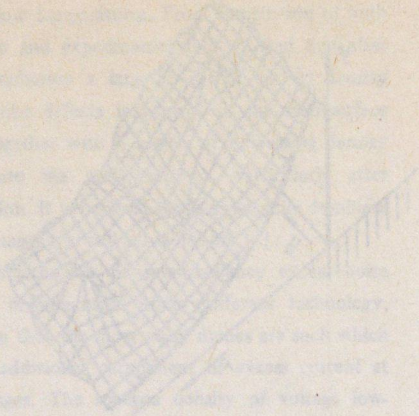

10th Int.Conf. on Noise in Physical Systems
1989 Budapest, Hungary

$1/f^{\gamma}$ NOISE IN THIN GOLD FILMS AND ITS DEPENDENCE ON PROCESS PARAMETERS

B. NERI, A. DILIGENTI, P. ALOE, C. MOZZI

Istituto di Elettronica e Telecomunicazioni,
Facoltà di Ingegneria, Università di Pisa
56126 Pisa, Italy

INTRODUCTION

Low-frequency noise is usually absent in thin continuous metal films [1],except at very low frequencies when the dc current density j and the absolute temperature T exceed critical values which depend on the material and on its microstructure.In this case the noise displays an $1/f^{\gamma}$ behavior ($\gamma \geq 2$) which has been attributed to dislocation kinetics [2] and,more recently ,to electromigration (EM) occurring along grain-boundaries (GB) [3].

To detect EM noise it is necessary to perform measurements below 1 Hz (typically from 10 mHz to 1 Hz) and to this end the use of an Ultra Low Noise Amplifier [3] is essential.

For Al and Al/Si resistors the origin of $1/f^2$ noise has been reasonably attributed to EM along GBs : the activation energies obtained using a proportionality relationship [3] between the vacancy flux J and the power spectral density of resistance fluctuations S_R are consistent with data in literature.Moreover the relationship can be simply deduced from a model based on the dependence of the mean life time of GB vacancies on the stress conditions (temperature T and current density j).Further proof is the correlation existing between the resistance of the stripes to EM and their E_a value deduced by means of the noise technique [4].

In this paper the results obtained with thin Au films are described and discussed.The aims of the work were: i) to prove that,even in this case,$1/f^2$ noise is caused by EM and ii) to evaluate the activation energy E_a.

Technological problems related to fabrication of the samples and the heavy dependence of noise spectra on process parameters did not allow a completely satisfactory achievement of the objective.

EXPERIMENTS.

The measurement system is made up of three basic parts: a Wheatstone bridge, one of the arms of which consists of the resistor under test, cascaded with a preamplifier with a very low noise figure (ULNA) whose output is linked to a spectrum analyzer.

The test patterns employed have a four-contact configuration which is suitable for the measurement of the resistance temperature coefficient (TCR).

The constant current I_o which flows in the sample is supplied by dry lead batteries.The films were deposited by means of RF sputtering or by thermal evaporation on SiO_2/Si substrates.Before noise measurements each sample was observed at the SEM and then packaged on To-3 containers.

The resistors investigated belong to three different groups:

a) AuTi : samples whose adhesion to SiO_2 was enhanced by interposing a very thin Ti layer between Au and Si O_2.Au was sputtered on a heated substrate (~ 300°C).

b) AuCr/A : samples with Chromium dots only in the pad area for bonding improvement. A means that the film was purposely thermally annealed to allow grain growth (t_{anneal} = 1 hr,T = 673 K in air [5]).

c) AuCr/B : samples obtained as above;the annealing was only that required by the packaging of the resistor (t_{anneal} = 1 hr,T = 443 K in air).

The effect of different annealing conditions is shown by Fig.1 and Fig.2 which represent SEM pictures of the film surface.AuCr/A samples show an evident grain structure.

TCR also reflects the different grain structure of AuCr/A and AuCr/B: average values are $3.60x10^{-3}$ and $3.35x10^{-3}$ K^{-1} respectively and this difference ($\Delta_{TCR}\% \approx 7\%$),according to the Mayadas model [6],means either a greater average value of grain dimension or a smaller defectivity at GBs for the samples with greater TCR.

The first remarkable result is that for *all* the group b) samples the noise is *not detectable*,even under the most severe stress conditions (j = 1.75 $x10^6$ A/cm^2,T = 353 K) obtainable with the experimental set-up.On the contrary,group c) samples from the same evaporation run give rise,when properly stressed,to $1/f^2$ spectra.Using the proportionality relationship between S_R and the vacancy flux an Arrhenius plot was constructed to evaluate the activation energy.A typical result is shown in Fig.2.If this plot is compared with those obtained previously for Al or Al/Si,shown in Fig. 3,a greater dispersion of the experimental results can be noted.The difference between the film structures can be seen by comparing Fig.2 with Fig.3: in the case of Al/Si well defined grains can be observed.

Besides Au is characterized by very poor adhesion to dielectric substrates,so that it was difficult to obtain reliable low-temperature annealed samples (annealing at higher T seems to improve adhesion).

Arrhenius plots referring to AuTi samples show a better correlation between the points but the activation energy is greater than the previous one (average E_a value ≈ 1 eV) and the points concern spectra with shapes different from $1/f^2$,that is γ is often ≠2.

It is well known that Ti interdiffuses along Au GBs at temperatures as high as 300 °C [7],so that the noise spectra are probably caused by Ti rather than Au diffusion and thus the activation energy concerns Ti diffusion into Au.



Fig.1. SEM picture of AuCr/A sample.TCR = 3.60×10^{-3} K^{-1}.

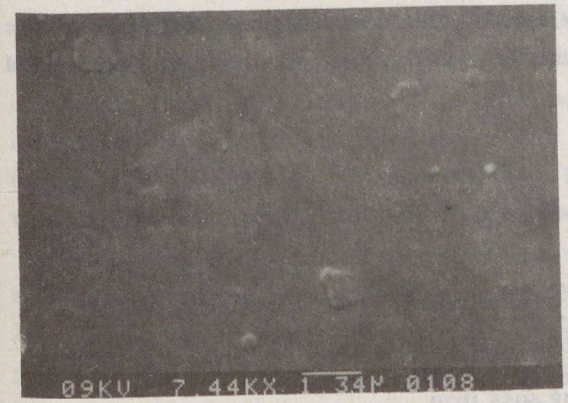

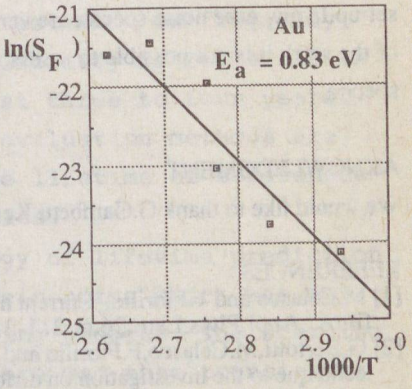

Fig.2. SEM picture of AuCr/B sample.Less evident grain structure.TCR = 3.35×10^{-3} K^{-1}.On the right : typical Arrhenius plot.

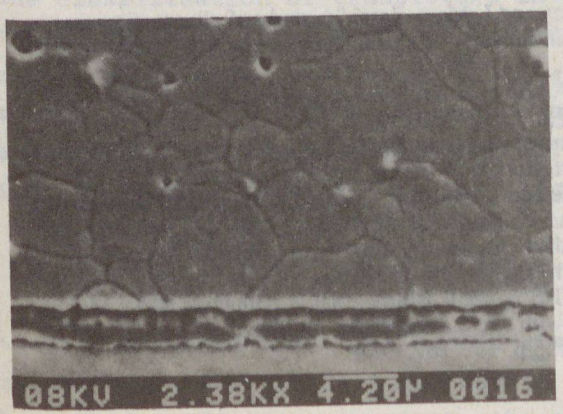

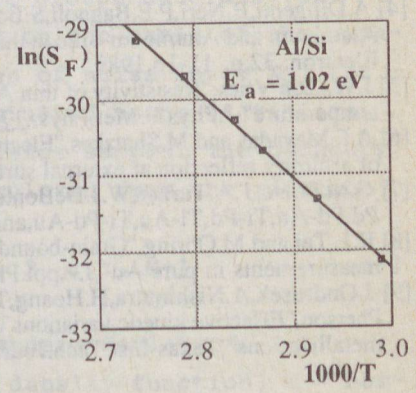

Fig.3. SEM of Al/Si sample.On the right : typical Arrhenius plot.

However,E_a values found for non-annealed samples ($\approx$ 0.80 eV) are in agreement with the data in literature [8],even though a greater activation energy was expected because the noise technique usually operates at lower stress conditions than those traditionally employed to evaluate E_a.In fact E_a seems to depend on measurement conditions [9].

CONCLUSIONS

Noise measurements performed on thin Au films seem to give further evidence that low-frequency $1/f^2$ spectra originate from vacancy movements (EM) along GBs.The activation energy deduced for non-annealed samples is tendentially in agreement with the relationship $E_{ai} = AT_{mi}$,which,for pure metals,foresees an activation energy proportional to the melting point of the material. As regards the E_a value,lower than expected,it must be noted that this result was obtained for samples characterized by very small grain dimension (smaller TCR),and it was impossible to find E_a for films with the structure of Fig.1 (greater TCR) with our experimental set-up.In any case noise spectra are very sensitive to the process parameters,so that at this stage of the work it is not possible to assess whether other sources of noise are superimposed on EM spectra.

AKNOWLEDGMENT

We would like to thank G.Gambetti Kenologia snc for film thickness measurements.

REFERENCES

[1] M.Celasco and F.Fiorillo,"Current noise measurements in continuous metal thin films",Appl.Phys.Lett.,26,p. 211-212,1975.
[2] G.Bertotti,M.Celasco,F.Fiorillo and P.Mazzetti,"Application of the current noise technique to the investigation on dislocations in metals during plastic deformation",J.Appl.Phys.,50,p. 6948-6955,1979.
[3] B.Neri,A.Diligenti and P.E.Bagnoli,"Electromigration and low-frequency resistance fluctuations in Aluminum thin-film interconnections" IEEE Trans.on El.Dev.,ED-34,p. 2317-2322,1987.
[4] A.Diligenti,B.Neri,P.E.Bagnoli,S.Bea and L.Mantellassi,"A study of electromigration in Aluminum and Aluminum-Silicon thin film resistors using noise technique",Solid-State Electron.,32,p. 11-16,1989.
[5] J.W.C.de Vries,"Resistivity of thin Au films as a function of grain diameter and temperature",J.Phys.F:Met.Phys.,17,p. 1945-1953,1987.
[6] A.F.Mayadas and M.Shatzkes,"Electrical-resistivity model for polycrystalline films: the case of arbitrary reflection at external surfaces",Phys.Rev.B,1,p. 1382-1389,1970.
[7] G.M.Poate,T.A.Turner,W.J.DeBonte and J.Yahalom,"Thin-film interdiffusion.I.Au-Pd,Pd-Au,Ti-Pd,Ti-Au,Ti-Pd-Au,and Ti-Au-Pd",J.Appl.Phys.,46,p. 4275-4283,1975.
[8] K.L.Tai and M.Ohring,"Grain-boundary electromigration in thin films.II.Tracer measurements in pure Au",J.Appl.Phys.,48,p. 36-45,1977.
[9] J.Ondrusek,A.Nishimura,H.Hoang,T.Sugiura,R.Blumenthal,H.Kitagawa and J.Mc Pherson,"Effective kinetic variations with stress duration for multilayered metallizations",Texas Inst.Tech.Jour.,5,p. 157-167,1988.

10th Int.Conf. on Noise in Physical Systems
1989 Budapest, Hungary

NOISE AS A LIFETIME ESTIMATOR FOR BIPOLAR TRANSISTORS

A. KONCZAKOWSKA, H. GŁADYSZ*

Institute of Electronic Technology,
Technical University of Gdansk
80-952 Gdansk, Poland
*Scientific Manufacturing Semiconductor Center
ul. Komarowa 5, 02-675 Warszawa, Poland

PROBLEM STATEMENT

The current interest in the links between low-frequency noise of semiconductors and their reliability is reflected in a number of works published in the past three to four years. Principal problems are discussed and evaluation methods are surveyed which aimed at predicting the lifetime of semiconductors based on their 1/f noise properties.

This paper presents the methodology of lifetime prediction of bipolar transistors by means of their noise which was measured at the output of the manufacturing process. The starting point in the research work reported here was that transistors with long lifetime expectation generate a small level, and those with short lifetime generate a high level of 1/f noise. The classification of transistors into groups according to their 1/f noise level X was performed on the basis of the method proposed below. The boundary values of noise level X_{bi} for each group of classification were evaluated using statistical parameters of a representative transistor sample. The boundary values of noise level X_{bi} can be calculated from the relation:

$$X_{bi} = \bar{X} + s\, z_i \qquad i = 1, 2, \ldots, M-1 \qquad (1)$$

where $\bar{X}$ = sample mean, s = sample standard deviation, z_i = areas under standardized normal density function, M = number of classification groups in the sample.

For example, for M = 4 the probability associated with each group must be P = 1/M = 0.25, and the required values of z_i are:

$z_1 = -0.67$, $z_2 = 0$, $z_3 = +0.67$. In this case all transistors from the sample are classified into the following groups:

$X_j \leq X_{b1}$: group 1, very good devices with probably very long lifetime,

$X_{b1} < X_j < X_{b2}$ group 2, good devices with probably long lifetime,

$X_{b2} \leq X_j < X_{b3}$ group 3, devices with probably short lifetime,

$X_j \geq X_{b3}$ group 4, potentially bad devices with probably very short lifetime,

where X_j = value of transistor noise level, j = 1, 2, ..., N,

N = number of transistors in the sample.

This classification can be verified by reliability tests.

EXPERIMENTS AND RESULTS

Measurement of noise parameters (noise factor F[dB] at different frequencies from 10 Hz to 1000 MHz and equivalent noise voltage U_n[nV] measured in the frequency range 10-50 Hz), and static parameters (transistor leakage current I_{CBO} and current gain h_{21E}) has been performed in 8 samples (50 devices each) of BF 414 transistors which were taken immediately after manufacturing, before (at time t = 0 h), during and after the following tests:

A - aging test, constant power dissipation equal to 300 mW, sample I - 1500 hours, sample II - 5000 hours of aging,

B - impact test, acceleration equal to 150 g, 3000 to 100,000 impacts - sample III,

C - temperature cycling, 1 cycle=storage for 20 minutes at extreme temperatures ($-55^{o}C$; $+125^{o}C$), 5 to 100 cycles - sample IV,

D - cooker test, storage in superheated steam at $+125^{o}C$ for 6 hours, procedure repeated 10 times - sample V,

E - step-stress test, duration of test during every step for samples VI, VII, VIII equal to 6, 12, 48 hours, respectively and power dissipation $P = P_o + i\Delta P$, where P_o = 450 mW, ΔP = 50 mW.

The investigations performed in sample I were treated as preliminary research. The mean values of the noise factor F[dB] for this sample at all measured frequencies versus aging time are presented in Fig. 1. The noise factor significantly decreased after 250 hours of aging for all devices.

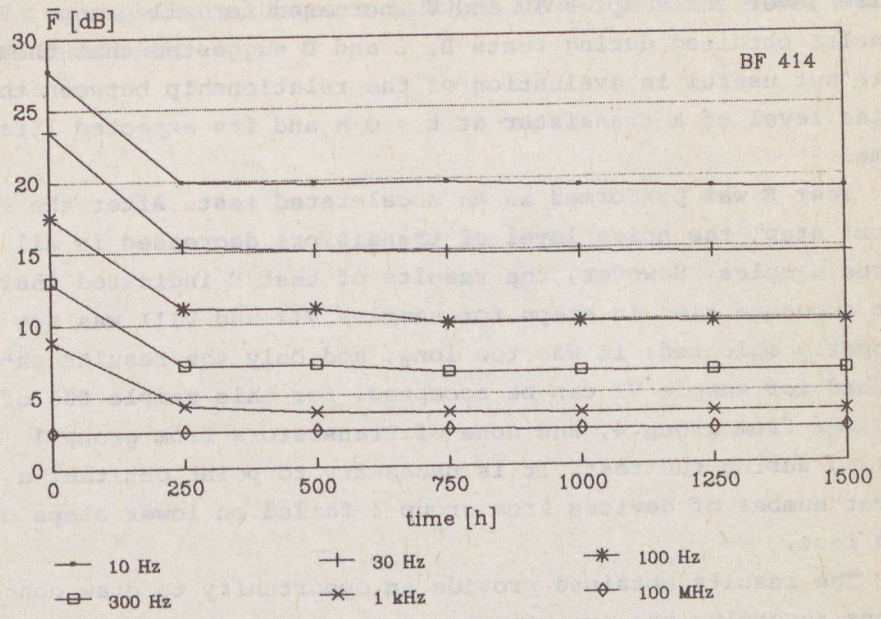

Fig. 1. The mean values of noise factor F[dB] versus time

The results obtained during sample I aging allow to select the frequency f = 10 Hz for noise factor measurement, as the most adequate for predicting a lifetime of transistors. For samples II-VIII only F[dB] at f = 10 Hz and U_n[nV] were measured. For sample II the boundary values of noise factor were found to be: F_{b1} = 21 dB, F_{b2} = 23.5 dB, F_{b3} = 25.5 dB, and all transistors were classified into four groups. Two transistors from group 4 failed after 250 hours. Transistors from group 1 had a small level of noise during the test. However, the aging time 5000 hours is too short in comparison with the lifetime of contemporary manufactured transistors, therefore this test is still continued, and another test (test E) has also been applied.

To detect the influence of impact, of temperature cycling and of storage in superheated steam on the level of transistor noise, tests B, C, and D were performed. Transistors from these samples were classified into four groups as described above. During test B the values of noise and static parameters of transistors from sample III did not change. The mean values of noise level for samples IV and V increased for all groups. The results obtained during tests B, C and D suggested that these were not useful in evaluation of the relationship between the noise level of a transistor at t = 0 h and its expected lifetime.

Test E was performed as an accelerated test. After the first step, the noise level of transistors decreased in all three samples. However, the results of test E indicated that the exposure time in steps for samples VII and VIII was not properly selected; it was too long, and only the results obtained for sample VI can be accepted. For this sample 80% of devices from group 4, and none of transistors from group 1 failed during the test. It is necessary to point out that a great number of devices from group 4 failed on lower steps of the test.

The results obtained provide an opportunity to draw conclusions regarding the experiments.

CONCLUSIONS

For predicting the lifetime of transistors BF 414, the noise factor F[dB] measured at f = 10 Hz or equivalent noise voltage U_n[nV] measured in the frequency range 10-50 Hz can be applied.

The results of measurements which were obtained during the reliability tests allow the following conclusions:

- a correlation exists between the noise level of transistors and the value of current gain,
- before failure the noise level of transistors rapidly increases,
- the properties of transistors improve after the first hours of aging, noise decreases, current gain increases,

- transistor parameters do not change during the impact testing,
- transistors with a high noise level from group 4 failed during the step-stress; transistors from samples VII and VIII failed very quickly; the duration of test was too long.

It is concluded that the results of the experiments, although satisfactory, require further investigations which are still continued.

10th Int.Conf. on Noise in Physical Systems
1989 Budapest, Hungary

NOISE MEASUREMENTS OF POWER SEMICONDUCTOR DEVICES FOR RELIABILITY EVALUATION

L. HASSE, A. KONCZAKOWSKA, L. SPIRALSKI

Institute of Electronic Technology,
Technical University of Gdansk
80-952 Gdansk, Poland

INTRODUCTION

The quality (reliability) of semiconductor devices depends on the procedures of manufacturing and on the quality (purity) of materials applied in the production process. Accelerated tests are used in typical reliability investigations. Their costs for power devices are relatively high.

The basic failures of power semiconductors are related to defects of microstructure due to surface overheating. The defects are reflected in an increase of 1/f noise level or in the occurrence of burst noise. Therefore they may be detected on the basis of level and type of noise generated by the devices. Better possibilities of defect detection arise for the reverse bias, both before the breakdown and in the breakdown region. It reveals instabilities "built in" an element during production (residues of adhesive drops, incorrect insertion of tungsten disc, translocation of lead terminals) which cause a higher level of noise or occurrence of burst noice. These investigations are nondestructive and allow to evaluate the reliability of each device individually.

PROCEDURE OF INVESTIGATIONS

The investigations were carried out on TOO-40-12 thyristors and DOO-1006 power diodes (LAMINA) as follows:

1. Preliminary measurement of statical characteristics:
   - conduction: U_{TM}[V]/I_{TM} = 500 A 25°C,
   - blocking: I_{DRM}[mA]/U_{DRM} = 1200 V 25°C, 125°C,

- reverse I_{RRM}[mA]/U_{RRM} = 1200 V 25°C, 125°C,

where $U_{TM}(I_{TM})$ - repeatable peak forward voltage (current),
$I_{DRM}(U_{DRM})$ - repeatable peak blocking current (voltage),
$I_{RRM}(U_{RRM})$ - repeatable peak reverse current (voltage).

2. Noise measurements for reverse bias:
   - level of power spectral density (PSD) G_n at 30 Hz, 75 Hz, 124 Hz, 1 kHz,
   - detection of burst noise,
   - noise power in frequency band 1.5 Hz...150 Hz.
3. Classification into following groups:
   - devices potentially defective: on the basis of high noise or of a significant burst noise or of a sharp slope of PSD at low frequencies,
   - good devices.
4. Typical reliability tests:
   - temperature cycles 3 * (-40°C; +125°C),
   - vibrations 2 * (||&⊥), 6 h, harmonic, 5 g, 50-100 Hz,
   - mechanical shocks 15 g, (||&⊥), 250±10 shocks,
   - investigation of voltage stability: I_R, I_D, time 0 h, 16 h, 24 h, 32 h, 125°C, U_{RRM} = U_{DRM} = 1200 V.
5. Measurement of statical characteristics as in item 1.
6. Final measurement of noise as in item 2.
7. Classification into following groups:
   - defective devices: catastrophically or partially,
   - good devices,
   - devices rejected on the basis of noise and reliability tests.

ANALYSIS OF EXPERIMENTAL RESULTS

The noise measurements were performed on 26 thyristors and 10 diodes in the reverse bias at voltages 100 V, 200 V and 300 V versus frequency (30 Hz-1 kHz). The results obtained for thyristors and for diodes were similar, and the analysis of thyristor investigation is only quoted.

The block diagram of noise measurement system for preliminary selection of semiconductor devices is presented in Fig. 1. The detailed noise measurements were carried out in a system

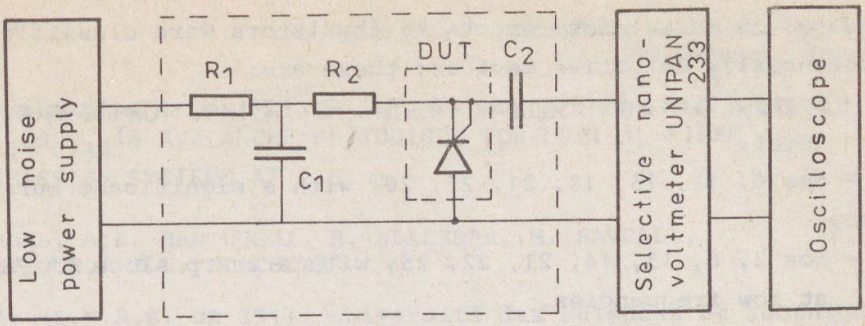

Fig. 1. Block diagram of measurement system

consisting of: low noise power supply, testing set-up, multichannel recorder 7005 B&K, digital event recorder 7502 B&K, graphic level recorder 2307 B&K and narrow-band frequency analyser 2010 B&K. The representative examples of noise measurements are presented in Fig. 2.

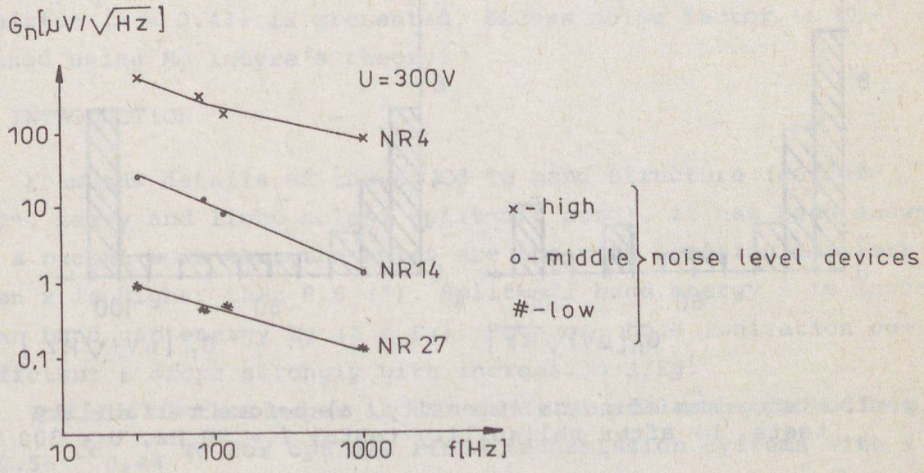

Fig. 2. Typical results of PSD for selected thyristors

It was found that the highest level of noise and greatest differences in the noise intensity for the investigated devices existed at frequency 30 Hz and reverse bias voltage 300 V. For this reason the description of experimental results was limited to the results of measurements at frequency 30 Hz and bias 300 V.

Based on noise measurements 16 thyristors were classified as potentially defective devices; these are:

- Nos 1, 2, 4, 8, 10, 15, 16, 18, 21, 28, with a high noise level,
- Nos 6, 13, 15, 18, 21, 25, 26, with a significant burst noise,
- Nos 2, 6, 13, 14, 21, 22, 25, with a sharp slope of PSD at low frequencies.

After the reliability tests, 15 thyristors (1, 2, 4, 6, 8, 13, 16, 18, 19, 20, 21, 22, 24, 28, 34) were found as defective devices (11 previously classified as potentially bad - underlined numbers). The noise level of thyristors measured after the reliability tests has been increased for all devices (see Fig. 3).

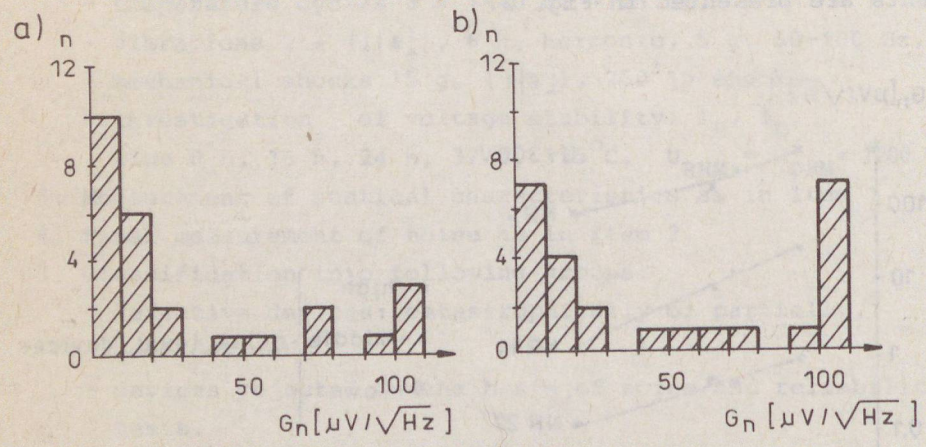

Fig. 3. Histograms of noise intensity, a) before reliability tests, b) after reliability tests; f = 30 Hz, U = 300 V

CONCLUSIONS

Based on the investigations it can be concluded that a general relationship exist between noise level or type of 1/f noise and lifetime of power semiconductor devices. These investigations can be treated only as preliminary research, and the particular selection of the criterion for these devices can be formulated after more numerous experiments.

10th Int.Conf. on Noise in Physical Systems
1989 Budapest, Hungary

NOISE AND IMPACT IONIZATION RATES FOR ELECTRONS AND HOLES IN $Hg_{0.56}Cd_{0.44}Te$ AVALANCHE PHOTODIODE FOR OPTICAL FIBRE TRANSMISSION SYSTEMS AT 2.5 μm

B. ORSAL, A.H. MAATOUGUI, R. ALABEDRA, M. SAVELLI,
G. LEVÊQUE,* J.C. FLACHET**

C.E.M. (C.N.R.S. UA 391), Université des Sciences et Techniques du Languedoc, 34060 Montpellier Cedex, France; *Laboratoire Spectroscopie U.V. des Solides (C.N.R.S. UA 790), Université des Sciences et Techniques du Languedoc, 34060 Montpellier Cedex, France; **S.A.T. 41 rue Cantagrel, 75013 Paris, France

Experimental results on the $Hg_{0.56}Cd_{0.44}Te$ avalanche photodiode are shown. In the first part of the paper both multiplication coefficients M_n and M_p are determined. The coefficients α and β are calculated so that the ratio $k = \beta/\alpha$ is deduced. For the first time the multiplication noise at this composition ($x = 0.44$) is presented. Excess noise factor is obtained using Mc Intyre's theory.

1. INTRODUCTION

From the details of the Hg Cd Te band structure (conduction, heavy and light holes, split-off band), it has been shown in a recent work that the holes are the most ionizing carriers when x is higher than 0.6 (1). Split-off band energy Δ is lower than band gap energy Eg ($\Delta < Eg$). However, hole ionization coefficient β drops strongly with increasing Δ/Eg.

The aim of this paper is the study of avalanche photodiode $Hg_{0.56}Cd_{0.44}Te$ for optical fibre transmission systems with x equal to 0.44. This alloy composition leads to devices that are well-suited for 2.5 μm detection. Bandgap Eg is exactly equal to 0.48 eV, the ratio Δ/Eg is equal to 1.6 at this composition ($x \cong 0.44$).

2. DEVICE STRUCTURE

All the APD's were processed by Société Anonyme des Télécommunications in a planar technology on $Hg_{0.56}Cd_{0.44}Te$

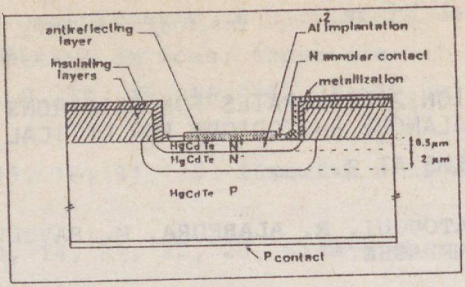

Fig. 1

wafers with the same crystallographic orientation (Fig. 1) (2). It is worth mentioning that we have a n^+ n^- p junction where the n region has a lower dope than the substrate ($N_A = 10^{16}$ cm^{-3}). The main characteristics are as follows:

Diameter of sensitive area	30 µm
Dark current at -10 V	1 µA < I_{obs} < 5 µA
Bandgap energy (x = 0.44)	0.48 eV
Response at 2 µm<λ<2.56 µm	0.3 A/W < σ_o < 0.5 A/W
Wavelength range	1.5 µm - 2.55 µm
Capacitance at -10V	0.5 pF
Bandwidth at M = 5	500 MHz
Diameter of active region	110 µm

3. ELECTRIC ANALYSIS

3.1. C-V curves

C-V characteristics show a $V^{-1/2}$ dependence between 4 and 14 V. These measurements show neither $V^{-1/3}$ variation nor $V^{-1/2}$ variation below 4 V. The concentration profile is shown in Fig. 2.

The n^+ type layer is formed by aluminium-ion implantation (60 KeV 10^{14} cm^{-2}). The n^- type layer is due to propagation of defects following the implantation (3). The extension of this layer is about 2 µm. At the n-p junction, the transition between n and p sides is gradual with a gradient of about $2x10^{19}$ cm^{-4}. The effective doping is $N_B \cong 4.8 \times 10^{15} cm^{-3}$. The p

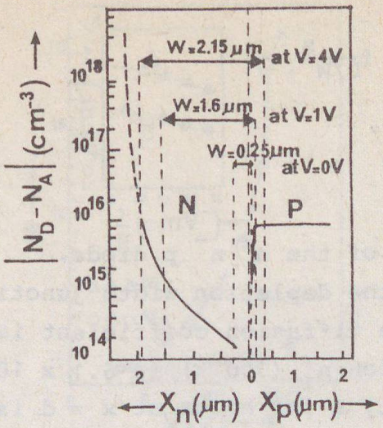

Fig. 2

type dope density obtained by linear part of $1/C^2$ curves is about 10^{16} cm^{-3} when voltage is higher than 4 V (4).

3.2. I-V characteristics

From the I-V characteristics in Fig. 3, the diode ideality factor n = 1 points to a diffusion current dominated diode:

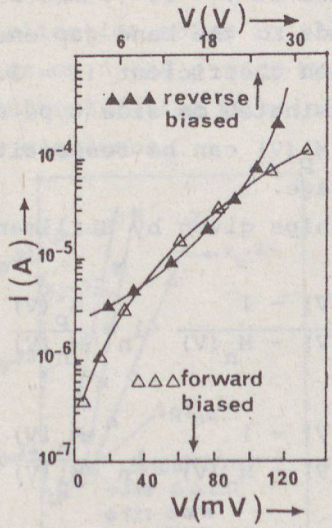

Fig. 3

$$I_o = \frac{q A_{ni}^2 D}{N_d W} \left(\frac{s}{D/W + s}\right) \quad (1)$$

$$I = I_o \left\{\exp\left(\frac{qV}{kT}\right) - 1\right\} \quad (2)$$

W is the base length of the $n^+ n^- p$ diode.

$W = d - W(V)$ is the depletion width junction area equal to 1.32×10^{-4} cm^2. Hole diffusion coefficient is about 2 cm^2/s. Intrinsic concentration n_i (300 K) is 6.1×10^{13} cm^{-3}. Surface recombination velocity s for holes at x = d is 10^4 cm/s. The I_o increase is in qualitative agreement with an increasing depletion width W under reverse bias conditions and a reduced short diode width W = d - W(V) as can be seen from Eq. (1). Above 6 V, the dark current increase is due to impact ionization and breakdown voltage appears at 30 V. It is due to avalanche phenomenon.

3.3. Spectral response and multiplication coefficients

Figure 4 shows the multiplication coefficients M_n, M_p. The maximum of M is obtained at V = 29 V. The wavelength cut-off $\lambda_c \sim 2.56$ µm corresponds to the band gap energy (0.48 eV) with x = 0.44. The absorption coefficient (λ = 2.50 µm) is 2×10^4 cm^{-1} (4). Devices were illuminated on side type n or on side type p separately. $M_n(V)$ and $M_p(V)$ can be respectively deduced at λ = 2.5 µm versus voltage.

By using relationships given by Stillman for P.I.N.A.P.D.'s:

$$\beta(E) = \frac{1}{W(V)} \frac{M_p(V) - 1}{M_p(V) - M_n(V)} \ln \frac{M_p(V)}{M_n(V)} \quad (3)$$

$$\alpha(E) = \frac{1}{W(V)} \frac{M_n(V) - 1}{M_p(V) - M_n(V)} \ln \frac{M_n(V)}{M_p(V)} \quad (4)$$

We obtain electron ionization coefficient $\alpha(E)$ and the same for holes $\beta(E)$ (Fig. 4).

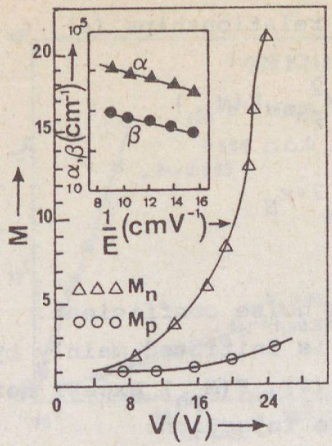

Fig. 4

For electric field E ≅ 2 x 10^5 Vcm^{-1}, the ratio $K(E) = \frac{\alpha(E)}{\beta(E)}$ is about (16 ± 1). This result is given for the first time at this composition.

4. NOISE MEASUREMENTS

The measurement principle has been shown in a previous work (4). We present multiplication noise in illumination conditions in both injection cases on n and p side types (Fig. 5). So, in the first case, the multiplication is mainly initiated by holes, in the second case by electrons.

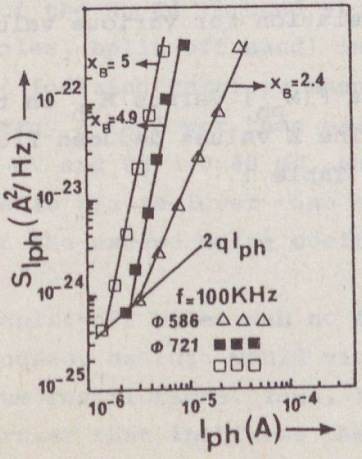

Fig. 5

Noise is given by relationships (4):

$$S_{i_{ph}} = 2\,q\,I_{ph_{inj}}\,M_{ph}^{2}\,F(M_{ph}) \tag{5}$$

$$= 2\,q\,I_{ph_{inj}}\,M^{2+x_N} \tag{6}$$

where x_N is the excess noise coefficient.
As the multiplication is initiated mainly by the holes generated in the n^+ region (4), $F(M_{ph})$ excess noise factor can be written under pure hole injection:

$$F(M_p) = M_p\left[1 + \left(\frac{1-k}{k}\right)\left(\frac{M_p-1}{M_p}\right)\right] \tag{7}$$

Experimentally $F(M_{ph})$ is given by the ratio:

$$F_{exp}(M_{ph}) = \frac{S_{i_{ph}}(f)}{2\,q\,I_{ph_{inj}}\,M^{2}} = M_{ph}^{x_N} \tag{8}$$

$$M_{exp} = \frac{I_{ph}(V)}{I_{ph_{inj}}} \tag{9}$$

The excess noise factor $F(M_{ph})$ will be deduced and analysed by using Mc Intyre's relation for various values of the ratio $K(E) = \beta(E)/\alpha(E)$.

Figure 6 represents $F(M_{ph})$ versus M_{ph} in the injection case mentioned previously. The K values deduced from previous results are presented in Table 1.

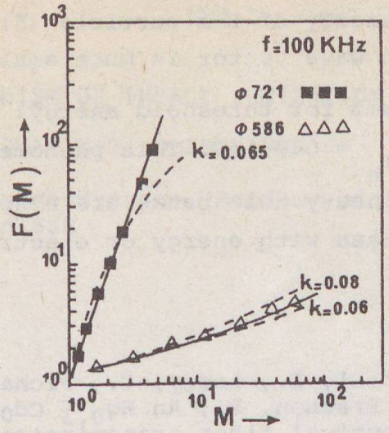

Fig. 6

Table 1

Injection	Excess noise coefficient x_n	Excess noise factor (M = 5)	$K = \beta/\alpha$
Holes	3.0 ± 0.1	2.4	0.06
Electrons	0.4 ± 0.1	50	0.06

5. DISCUSSION

Experimental results have shown that electrons are the most ionizing carriers with a ratio $K^{-1} = \alpha/\beta = 16 \pm 1$.

From details of the Hg Cd Te band structure (conduction, heavy and light holes, split-off band) in a previous work, the holes are the most ionizing carriers when $x > 0.6$ with the split-off band energy Δ is lower than band gap energy (5). In our case $\Delta = 0.84$ eV and $Eg = 0.48$ eV, the ratio Δ/Eg is higher than 1, and the ratio β/α is lower than one, leading to a strong increase in the excess noise coefficient under pure hole injection (6).

In our case, split-off holes can no longer be considered in the ionization process, as this would violate conservation of energy and momentum restrictions. Thus, if one allows a heavy hole to be the carrier that initiates the multiplication process, one can treat this case by calculation in order to deter-

mine the threshold energy of the particle (5). Thus one finds $K^2_{i_e} << K^2_{i_h}$. Electron wave vector is much smaller than hole wave vector. It is the same for threshold energy:

$E_{i_e} \cong 0.54$ eV, $E_{i_h} = 0.94$ eV. This phenomenon is due to the fact that light and heavy hole bands are nonparabolic. The effective masses increase with energy or electric field (7).

REFERENCES

1. Alabedra, R., Orsal, B., Lecoy, G., Pichard, G., Pichard, J., Meslage, J. Fragnon, P., An $Hg_{0.3}$ $Cd_{0.7}$ Te avalanche photodiode for optical fiber transmission systems at λ = 1.3 µm. I.E.E.E. T.E.D. Vol. E.D. 32, pp. 1302-1306, July 1985.
2. Royer, M., Brossat, T., Fragnon, P., Meslage, J., Pichard, G., Nguyen Duy, T., Ann. Telecom. 98 (1983) 62.
3. Bubulac, L.O., Tennant, W.E., Riedel, R.A., Magee, T.J., J. Vac. Sci. Techn. (21), pp. 251-254, May-June 1982.
4. Matougui, A., Ph. D. Thesis, C.E.M.-U.S.T.L., Montpellier, June 1989.
5. Lecoy, G., Orsal, B., Alabedra, R., I.E.E.E. J. Q.E, Vol. Q.E 23, No. 7, July 1987.
6. Orsal, B., Alabedra, R., Lecoy, G., Flachet, Y., 9th International Conference on Noise in Physical Systems, Montreal, May 25-29, 1987.
7. Levêque, G., $Hg_{0.4}$ $Cd_{0.6}$ Te bands structure GRECO, II-VI, Toulouse, October 1988.

10th Int.Conf. on Noise in Physical Systems
1989 Budapest, Hungary

NOISE AND MECHANISM OF IMPACT IONIZATION IN GaAs

N.B. LUKYANCHIKOVA, N.T. DEKHTYARUK

Institute of Semiconductors, Academy of Sciences
of the Ukrainian SSR
Kiev-28, USSR

Noise investigations offer considerable scope for studying the physical processes in semiconductor materials and devices. Some results of such investigations of impact ionization in GaAs are presented in this work.

P^+-n diodes as well as p^+Ge-nGaAs heterodiodes and Pt-nGaAs Schottky diodes have been studied. Donor concentration in GaAs was equal to 10^{16} cm^{-3}, acceptor concentrations both in p^+GaAs and p^+Ge were equal to 10^{18} cm^{-3}.

Spectral densities of the short current noise S_i were measured at f = 20 Hz to 200 kHz. The spectral density of the open circuit voltage noise S_u was measured at f = 70 kHz. Measurements were carried out at $i = 10^{-7}$-10^{-2} A.

Excess white noise with properties typical for the avalanche noise was observed in $S_i(f)$ spectra at $f \gtrsim 1$ kHz measured not only in the region of the avalanche breakdown but also in the wide interval of pre-breakdown electrical fields $E = (1{,}7\text{-}4)\cdot 10^5$ $V\cdot cm^{-1}$.

The comparatively slow rise of S_i and rather slow decrease of S_u with increasing i in the pre-breakdown field region show that under these conditions the ratio k of the impact ionization coefficients for electrons and holes differs considerably from unity and $kM < 1$ where $M = \exp\alpha l_a$ is the multiplication factor for the carriers multiplied more effectively, α is the higher impact ionization coefficient, l_a is the thickness of the avalanche region, the primary current being formed by the charge carriers multiplied more effectively /1/.

In this case it is possible to determine the value of k by two independent methods: (i) from dependence $S_i(i,M,k)/2/$, (ii) from dependence $S_u(i,M,k,W,\partial\alpha/\partial E)$ where W is the width of the diode space charge region /3/ and the value of $\partial\alpha/\partial E$ being estimated from the measured dependence $\ln M(E) = \alpha(E)\, l_a(E) \sim \alpha(E)W(E)$.

As a result, it was found that the value of k decreased by a factor of more than 100 in the electric field range studied in which M is increased from $M_1 \approx 10$ to $M_2 \approx 10^3$. This fact indicates that the multiplication process studied is not connected with the band-to-band impact ionization for which the equality $k \approx 1$ is known to take place for GaAs /4/.

This conclusion was supported also by the fact that the values of α observed were several times higher than the band-to-band ionization coefficients for electrons and holes in GaAs over the studied range of the pre-breakdown fields /4/.

Because α is increased by a factor of $(l_{a1}/l_{a2})(\ln M_2/\ln M_1) \leq 3$ then the observed decrease of k by a factor of 100 is due mainly to the essential decrease of the smaller impact ionization coefficient with increasing E. This experimental result as well as the other effects observed cannot be explained in the frames of the band-to-band impact ionization model at all.

We have developed the model of impact ionization of the deep centres by hot electrons and holes which opens up the possibility for explanation of all experimental results observed. Let us denote the probability of ionization of a i-type carrier by a j-type hot carrier by C_{ij}. According to the model proposed, at $C_{ij}/C_{jj} > C_{ii}/C_{ji} > 1$ and $C_{ii}/C_{ij} > 1$, the higher and smaller impact ionization coefficients are equal, respectively,

$$\alpha_i = (N_t/v_i)C_{ij} \sim \exp(-E_{ijo}/E),$$

$$\alpha_j = (N_t/v_j)(C_{ij}C_{ji}/C_{ii}) \sim \exp\{[E_{iio} - (E_{ijo}+E_{jio})]/E\}$$

and we have

$$k = \alpha_j/\alpha_i = (C_{ji}v_i)/(C_{ii}v_j) \sim \exp[(E_{iio}-E_{jio})/E]$$

where N_t is the density of the ionized centres, v_i and v_j are the drift velocities of a i- and j-type carrier in the avalanche region, respectively. It is taken into account here

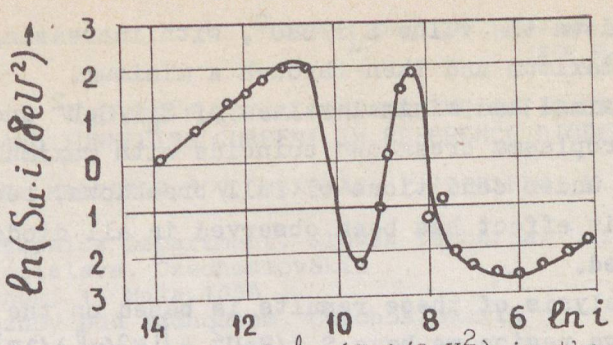

Fig.1. Current dependences of $\ln (S_u i/8eU^2)$ in the avalanche breakdown region.

that $C_{ij} \sim \exp(-E_{ijo}/E)$ and E_{ijo} is a function of the energy position of the level and of the carrier free path length.

It is seen that: (i) the value of α_i may be rather high and so may exceed the band-to-band ionization coefficients if N_t is sufficiently high; (ii) the value of k may be significantly lower than unity and, at $E_{iio} > E_{jio}$, may decrease with increasing electric field; (iii) the value of α_j is decreased with increasing electric field at $E_{iio} > (E_{ijo}+E_{jio})$.

In addition, the facts that k is independent of N_t, α_i is a function of N_t and, hence, M is a function of N_t, make it possible to explain the different values $S_i/2ei = M(kM+2)$ and $S_u i/8eU^2 = M(kM+2)/\left[(\ln M)^2(kM+1)m^2\right]$ observed at given E and, hence, at constant k in different diodes. Here $m = (E/\alpha_i)(\partial\alpha_i/\partial E)$ and U is the voltage drop across the diode.

All these allows to connect phenomena described above with the impact ionization of the deep levels in GaAs.

The noise measurements show that, as far as E approaches the avalanche breakdown value, the value of k approaches unity (due to the increase of the band-to-band impact ionization contribution) and then k has a tendency for a new decrease.

It is known that at the breakdown region only the value of S_u is to be measured. As a result of these measurements, an effect has been observed that may also be connected with some unusual features of impact ionization. This effect consists of the following (Fig.1).

1. Under conditions both of microplasma breakdown and

full breakdown the value $S_u i/8eU^2$, with increasing i, passes through a maximum and then through a minimum.

2. Maximal and minimal values of $S_u i/8eU^2$ under conditions of microplasma breakdown coincide with maximal and minimal values under conditions of full breakdown, respectively.

3. This effect has been observed in all diode structures investigated.

An analysis of these results is based on the fact that in breakdown region we have $S_u i/8eU^2 = \{[E\partial(\alpha l_a)/\partial E]^2 k\}^{-1}$, $\alpha l_a = \ln k/(k-1)$, and l_a being practically independent of E. It shows that this effect may be connected with a sharp peak in the dependence $\alpha(E)$ at $E \approx 5{,}5$ V·cm^{-1}. Note that Pearsall /6/ had already observed such a maximum by the method different from the noise one. Our results may be considered as an important reason for the existence of such effect.

Thus, our noise investigations have enabled us to find and to study two new physical effects connected with some peculiar features of impact ionization in GaAs.

References

1. N.B.Lukyanchikova, N.T.Dekhtyaruk, Noise investigation of the impact ionization in GaAs. Phys. stat. solidi (a) 91, No.1, pp.279-286, 1985.
2. R.J.McIntyre, Multiplication noise in uniform avalanche diodes. IEEE Trans. Electron Devices ED-13, No.1, pp.164-168, 1966.
3. J.A.Ringo, P.O.Lauritzen, Low-frequency white noise in reference diodes. Solid-State Electron. 15, No.6, pp.625-634, 1972.
4. G.E.Bulman, V.M.Robbins, G.E.Stillman, Noise and characteristics of the impact ionization processes in GaAs. IEEE Trans. Electron Devices ED-32, No.11, pp.2454-2465, 1985.
5. N.B.Lukyanchikova, Impact ionization of deep levels in GaAs IMPATT diodes. Fizika i technika poluprovodnikov 23, No.2, pp.332-337, 1989.
6. T.R.Pearsall, The band structure dependence of impact ionization by hot carriers in semiconductors: GaAs. Solid-State Electron. 21, No.1, pp.297-302, 1978.

DEPENDENCE OF VOLTAGE FLUCTUATIONS ON THE RATIO OF THE AVALANCHE AND TUNNELING CURRENT IN REFERENCE DIODES

J. BELAN, F. MATISCAK,* V. MIKOLAJ, F. STRAPKO, V. LATTA

Microelectronics Department, Slovak Technical University
812 19 Bratislava, Czechoslovakia
*Tesla Roznov, 1, Maja 1000
756 61 Roznov pod Radhostem, Czechoslovakia

Measurements of a noise in subsurface reference Zener diodes at various values of the multiplication factor are reported. The low 1/f voltage noise at low multiplication factor of the reference Zener diodes was observed.

Reference Zener diode applications have led to increased interest in low-noise voltage fluctuations and reliability in low-voltage breakdown junctions. These diodes are interesting for high-speed, high-resolution D/A and A/D converters. Previous monolithic converters with references, which have used emitter-base Zener diodes, have proven unstable with time, temperature, and power cycling [1]. The device design of subsurface Zener diodes [1] avoids surface instabilities entirely.

Noise measurements were performed with the aid of the low-frequency measurement shielding chamber, where the analyzed sample, the low noise preamplifier and the battery source were located. The amplified noise signal is then processed by an FFT analyzer unit, which contains a digital signal processor, amplifiers, high-pass filters and a 12-bit A/D converter, which are controlled by an 8-bit microprocessor. For frequency analysis a Fast Fourier Transform with 1024 points was used. The FFT analyzer unit was connected to a PC AT by the RS232C interface. Two frequency spectra, taken at different sampling rates, were stitched together for each broad-band spectrum. The averaging of the spectral lines in a higher frequency range was made with the aid of the evaluation of 128 or more time domains with 1024 points. In the lower frequency range the evaluation

consists of 16 time domains, in which fewer spectral lines were averaged at lower frequencies and more at higher frequencies.

We have made measurements of the voltage noise of the subsurface Zener diodes breaking down between 5 and 7 volts at various values of the reverse current. The subsurface Zener diodes investigated in this study were manufactured for a reference circuit of A/D and D/A 12-bit convertor. Fig. 1 illustrates the device design of subsurface reference Zener diode [1]. The resistance from either anode to the active Zener site is composed of both lateral r_{bb} as well as small section or pinch resistance. One anode is fed with a bias current, and the other anode is used as a sense connection for the error correction circuitry.

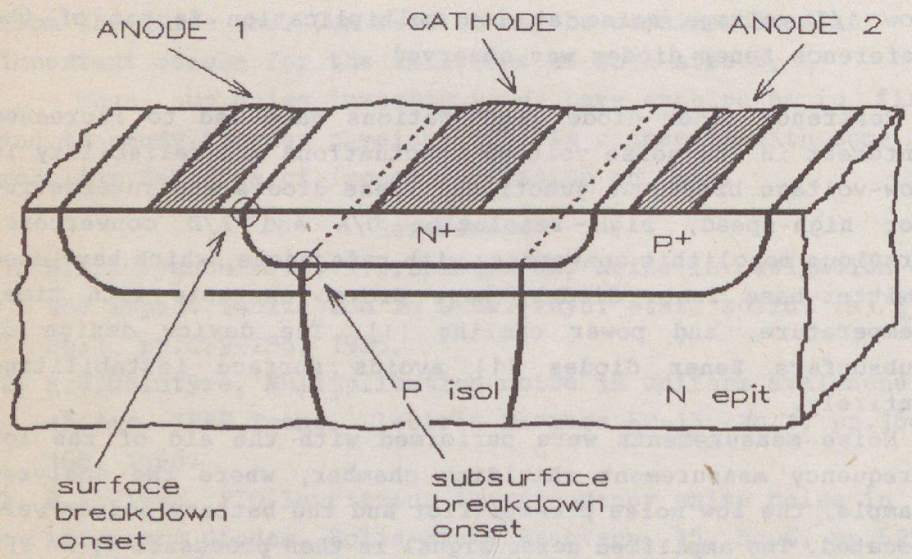

Fig. 1. The device configuration of the measured subsurface Zener diodes.

The noise properties of the reference Zener diodes are dependent on the ratio of the avalanche current I_a and tunneling current I_t [3]. The multiplication factor is defined as $M=I_r/I_t$, where I_r is the p-n junction reverse current . The dependence of the noise spectral voltage density $S_u(f)$ on 1/M is plotted in Fig. 2. The change of the slope of the spectral voltage density of the white noise and the occurrence of 1/f noise show that two different breakdown phenomena are present.

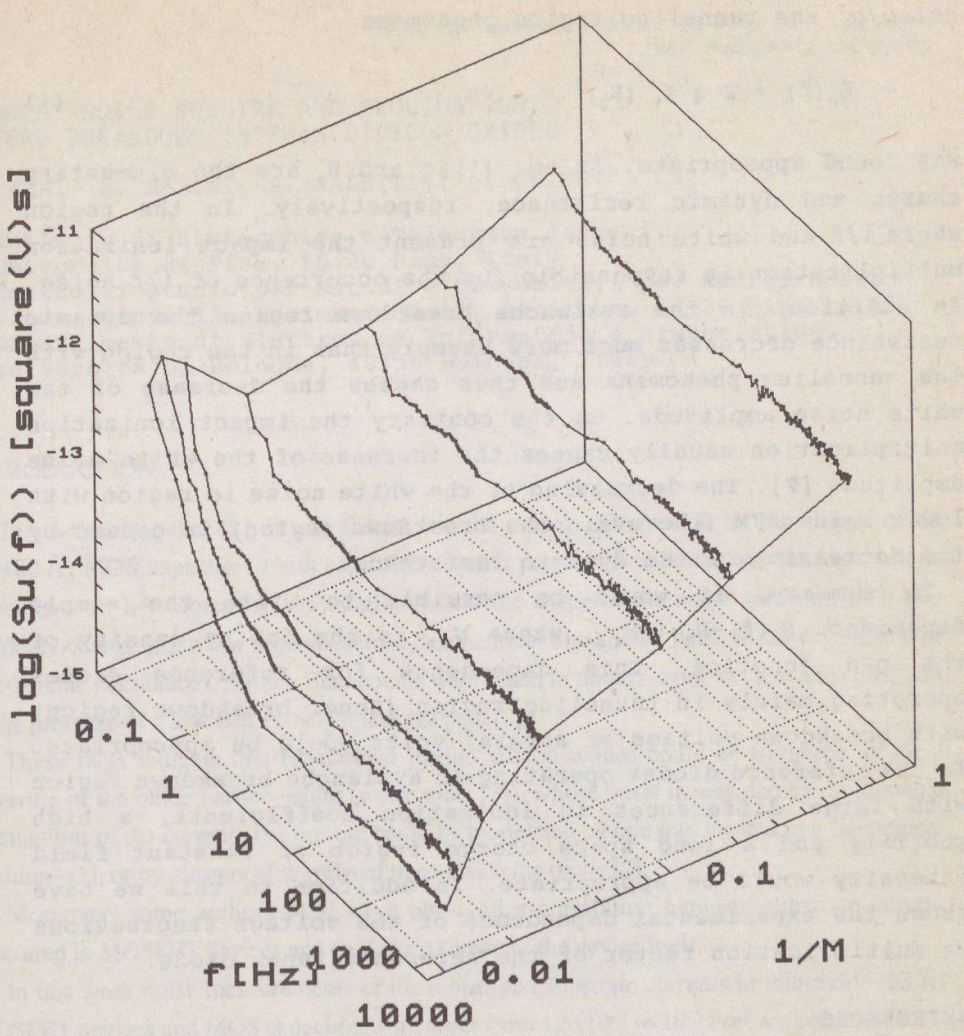

Fig. 2. The noise spectral voltage density $S_u(f)$ of the subsurface Zener diode versus frequency and versus 1/M, where M is the multiplication factor.

At a higher value of 1/M (only the white noise is present) mainly the tunneling phenomenon takes place whereas at a lower value of 1/M (1/f and white noise are present) mainly the avalanche breakdown takes place. For the region where M is approximately equal to 1, only the simple equation for the shot

noise of the tunneling region phenomena

$$S_u(f) = 2\,q\,I_t\,(R_D)^2 \qquad (1)$$

was found appropriate. In eq. (1) q and R_D are the elementary charge and dynamic resistance, respectively. In the region where 1/f and white noise are present the impact ionization multiplication is responsible for the occurrence of 1/f noise. In addition, in the avalanche breakdown region the dynamic resistance decreases much more steeply than in the region with the tunneling phenomena and thus causes the decrease of the white noise amplitude. On the contrary the impact ionization multiplication usually causes the increase of the white noise amplitude [2]. The decreasing of the white noise in region with lower value 1/M (the avalanche breakdown region) is caused by the decreasing of the dynamic resistance.

In summary, it would be possible to write the simple dependence $S_u(f) \approx R_D \approx 1/N_{A,D}$, where $N_{A,D}$ is the doping density of the p-n junction. This dependence for reference diodes operating mainly in tunneling region (Zener breakdown region) with breakdown voltage of several volts would be appropriate. In the reference diodes operating in avalanche breakdown region with large differences in ionization coefficients, a high mobility and a long space charge region of constant field intensity would be appropriate. In addition to this we have shown the experimental dependence of the voltage fluctuations on multiplication factor of the reference Zener diode.

REFERENCES

1. M.P. TIMKO and P.R. HOLLOWAY, "Circuit techniques for achieving high speed-high resolution A/D conversion", IEEE J. Solid-State Circuits SC-15, pp. 1040, (1980).

2. W. LUKASZEK, A. VAN DER ZIEL and E. R. CHENETTE, "Investigation of the transition from tunneling to impact ionization multiplication in silicon p-n junctions", Solid State Electr. 19, pp. 57, (1976).

3. J. BELAN and V. MIKOLAJ, "Voltage noise of breakdown region of subsurface Zener diodes", Phys. Stat. Sol. (a) 112, pp. K119, (1989).

10th Int.Conf. on Noise in Physical Systems
1989 Budapest, Hungary

CURRENT NOISE SPECTRA AND FLUCTUATIONS BEFORE BREAKDOWN IN THIN SILICON OXIDES

B. NERI, A. MARINI, R. SALETTI,* P. OLIVO**

Istituto di Elettronica e Telecomunicazioni,
Università di Pisa, 56126 Pisa, Italy
*Centro di Studio per Metodi e Dispositivi per Radiotrasmissioni, Consiglio Nazionale delle Ricerche, 56126 Pisa, Italy
**Dipartimento di Elettronica Informatica e Sistemistica,
Università di Bologna, 40136 Bologna, Italy

INTRODUCTION

In a previous paper [1], it was shown that the tunneling current I_t in thin silicon-oxide (60÷80 Å) MOS capacitors (with area of 10^{-4} cm^2) presents a 1/f noise whose magnitude is dependent on I_t^2. Moreover, the amplitude and the shape of the noise spectrum of I_t (S_t) suddenly change just a few seconds before the electrical breakdown when I_t shows bi-stable or multi-stable fluctuations. Similar fluctuations were found in thinner-oxide devices and correlated to the presence of a low-barrier-height leakage path [2].

These facts indicate that breakdown in thin silicon oxides could be triggered by local lowering of the oxide barrier-height (weak spots [3]), whose onset is revealed by multi-stable fluctuations of the current. The current could be modulated by one trap located in a "strategical position" [1], or by clusters of correlated traps inside the oxide [2].

Moreover, some authors [4,5] have observed a correlation between substrate current measured in MOSFET devices and oxide breakdown of the device itself.

In this work noise measurements of the tunnel and substrate currents in thin-oxide (63 Å) MOSFET devices and MOS capacitors with areas from 1.6×10^{-7} to 10^{-5} cm^2 are presented.

EXPERIMENTS

The measurement setup and the sample structure for the two kinds of devices examined are shown in Fig.1. ULNA1 and ULNA2 are two equal and independent Ultra-Low-Noise Amplifiers designed by us for these experiments. Their input resistance is much higher than R_1 and R_2 respectively, and their equivalent input noise is negligible in the frequency range above 100 mHz, as compared to the Johnson noise of R_1 and R_2.

Preliminary measurements were performed on the MOSFETs at a fixed stress voltage V_a=8.4 V. They show that the noise spectrum of I_p (S_p), measured in the range 0.4÷40 Hz, emerges from the system background noise only in the final part of the device operating time (some tens of seconds before breakdown). On the other hand, the spectrum S_t is measurable

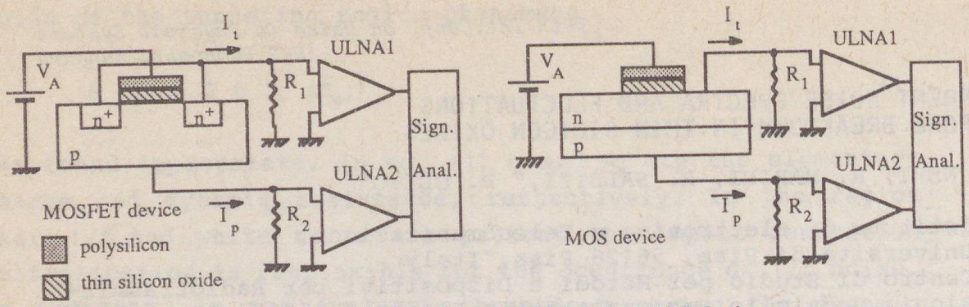

Fig.1: Experimental setup for measurements in MOSFET and MOS devices.

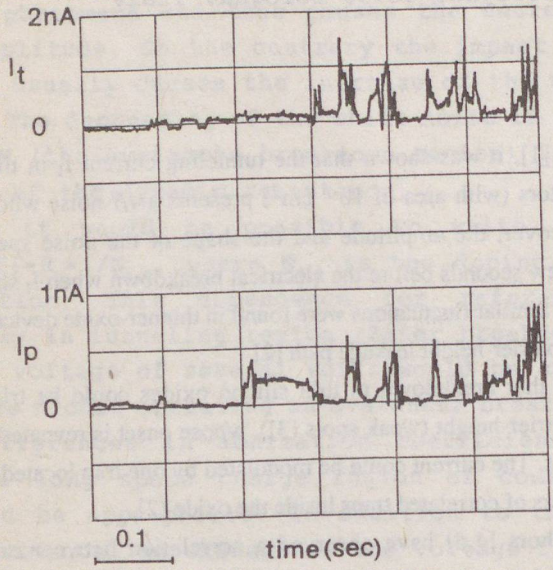

Fig.2: Correlated fluctuations of tunnel and substrate currents before breakdown in a MOSFET.

during the entire life of the device and shows the same frequency dependence already observed in MOS capacitors (i.e. flicker noise with a frequency exponent close to 1) [1].

Moreover, the contemporaneous time-observation of I_t and I_p showed for the first time that both I_t and I_p present random multi-stable fluctuations in the final stage of the device operating time. These fluctuations are sometimes fully correlated and their amplitude is of the same order of magnitude. Correlated pulses are easily recognizable in the plots of I_t and I_p versus time reported in Fig.2. Accurate tests were performed in order to exclude the possibility of systematic interactions between the two measuring channels.

In order to investigate the dependence of the current noise spectra on sample geometry we plan to perform a more complete set of measurements on MOSFET devices with different area and oxide thickness when a suitable number of samples is available.

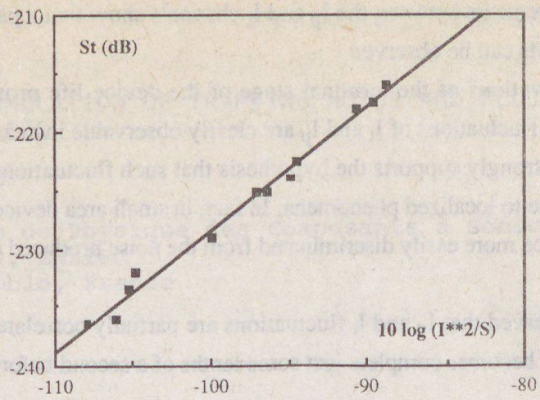

Fig.3 Current noise spectra at 100 mHz versus I^2/S for MOS devices.

As far as MOS capacitors are concerned, the dependence of S_t on the current I_t was investigated for four different values of V_a and three groups of devices, each characterized by a different area. Usually, the noise measurement was started only when I_t was reduced by a factor of at least 2.5 with respect to its peak value. In this way the current can be considered almost constant during the measurement. In fact, I_t shows the typical decreasing exponential-like dependence on stress time for a given value of the gate stress voltage [6]. The noise spectrum was flicker-like with a frequency exponent of about 1 in these devices too.

The expected dependence of S_t on the current density j and area S, considering uniformly distributed and independent fluctuators, is expressed at a given frequency by the relationship

$$S_t(j,S) = A\, j^2\, S = A\, I^2 / S \qquad (1)$$

where A is a constant depending on the physical characteristics of the oxide and I is the value of I_t at which noise measurement was performed.

Fig.3 shows the value of S_t measured at 100 mHz versus I^2/S for the three groups of devices tested. The fit with Eq.(1) is represented by the straight line. The good fit means that neither boundary nor current crowding effects were observable, at least in flicker noise generation, even in the smallest area devices.

Finally, the measurement of the mean value and the low frequency noise spectrum of the substrate current I_p and its correlation with S_t during the first part of the device life was attempted. The main results are:

a) the mean value of I_p is about 3 orders of magnitude smaller than that of I_t and is at present not measurable in the smallest area devices, at least with this measurement configuration, because of leakage current of the device package (even tens of pA);
b) only a few devices show excess low frequency noise in I_p in the first part of their operating life; in these cases the measured noise shows a 1/f spectrum;

c) cross spectrum measurements between the I_p and I_t channels show that a partial correlation between the two currents can be observed.

Moreover, time-observations of the terminal stage of the device life prove that the time interval in which bi-stable fluctuations of I_t and I_p are clearly observable increases when device area decreases. This fact strongly supports the hypothesis that such fluctuations, which always precede breakdown, are due to localized phenomena. In fact, in small area devices the effect of a single local fluctuator can be more easily discriminated from the noise produced in the remaining area of the device.

In addition, it was observed that I_p and I_t fluctuations are partially correlated even in MOS capacitors. The correlation becomes complete just some tenths of a second before breakdown.

CONCLUSIONS

Noise measurements on tunneling and substrate currents in MOS and MOSFET devices have shown that the current noise spectra S_t and S_p, respectively, are flicker-like with a frequency exponent very close to 1 during the first part of the life of the samples. S_t is proportional to the product I^2/S in the explored range of S and I, that is between 1.6×10^{-7} and 10^{-5} cm^2, 1.6×10^{-9} and 1.15×10^{-7} A respectively, in MOS devices.

Moreover, it has been shown for the first time that a correlation between the random telegraphic pulses affecting the currents I_t and I_p exists just before breakdown in both MOS and MOSFET devices. This experimental observation cannot be explained by the existing models for thin-oxide electrical breakdown. It is therefore necessary to develop a new model or improve the existing ones to take into account this interesting and new phenomenon.

Finally, noise observations can also be useful to detect the onset of electrical breakdown, because the device failure is always preceded by current pulses. It is in fact possible to stop the experiment just before breakdown when early pulses are detected. Sample characteristics at breakdown onset could thus be investigated with standard techniques.

REFERENCES

[1] B.Neri, P.Olivo, B.Riccò, "Low frequency noise in silicon-gate metal-oxide-silicon capacitors before oxide breakdown", Appl.Phys.Lett. 51, p.2167, December 1987.

[2] K.R.Farmer, R.Saletti, R.A.Buhrman, "Current fluctuations and silicon oxide wear-out in metal-oxide-semiconductor tunnel diodes", Appl.Phys.Lett. 52, p.1749, May 1988.

[3] T.N.Nguyen, P.Olivo, B.Riccò, "A new failure mode of very thin thermal SiO_2 films", Proc. of the IEEE Int. Rel. Phys. Symp. (RPS), p.66, 1987.

[4] Z.A.Weinberg, M.V.Fischetti, Y.Nissan-Cohen, "SiO_2-induced substrate current and its relation to positive charge in field-effect transistors", J.Appl.Phys. 59, p.824, Feb.1986.

[5] I.C.Chen, S.Holland, K.K.Young, C.Chang, C.Hu, "Substrate Hole Current and Oxide Breakdown", Appl.Phys.Lett. 49, p.669, 1986.

[6] P.Olivo, B.Riccò, E.Sangiorgi, "Electron trapping/detrapping within thin SiO_2 films in the high field tunneling regime", J.Appl.Phys. 54, p.5267, Sept.1983.

10th Int.Conf. on Noise in Physical Systems
1989 Budapest, Hungary

UNIFIED FORMULATION OF TRAPPING NOISE AND FLUCTUATION IN MOS DEVICES

G. GHIBAUDO

Laboratoire de Physique des Composants à Semiconducteurs,
UA-CNRS 840, ENSERG
38016 Grenoble, France

1. INTRODUCTION

Fliker noise in MOS transistors is generally attributed to carrier number fluctuations due to the dynamic trapping of electrons (or holes) by oxide interface traps (McWhorter 1957, Reimbold 1984, Uren et al.1985). In particular, it is now established that the observation of random telegraph signals (RTS) on small area devices arise from individual carrier trapping (Uren et al.1985, Restle 1988). All these features put forward the necessity of having a unified approach for the modelling both of the current fluctuation intensity and of the trapping noise level in MOS devices.

Therefore, in this paper, a generalized formulation of the trapping effects which are responsible for the current fluctuations and, in turn, of the trapping noise in a MOS structure is proposed.

2. ANALYSIS AND DISCUSSION

As a matter of fact, when carriers are trapped into the oxide, a subsequent change in the interfacial oxide charge δQ_{ox} is induced. For the point of view of the MOS theory, this oxide charge fluctuation can be simply regarded as a flat–band voltage fluctuation $\delta V_{fb}=-\delta Q_{ox}/(WLC_{ox})$ where C_{ox} is the gate oxide capacitance, W and L are the channel width and length, respectively. This flat–band voltage fluctuation gives then rise to an inversion charge fluctuation and, finally, to a drain current fluctuation δI_d. Since, in the gate charge conservation equation, the gate voltage V_g and the flat–band voltage V_{fb} play a symetric role, it is easy to prove that (Ghibaudo 1989) :

$$\delta I_d = \left(\frac{dI_d}{dV_{fb}}\right)\delta V_{fb} = \left(-\frac{dI_d}{dV_g}\right)\delta V_{fb} = -g_m\,\delta V_{fb} \qquad (1)$$

where g_m is the device transconductance. As a result, making use of the analytical expression of g_m (Ghibaudo 1986) yields for the normalized current fluctuation in the case of an enhanced–mode MOSFET operating at room temperature :

$$\frac{\delta I_d}{I_d} = \frac{g_m}{I_d} \cdot \frac{\delta Q_{ox}}{W\ L\ C_{ox}} = \frac{q}{\alpha\ W\ L\ kT} \cdot \frac{\delta Q_{ox}}{(C_{ox} + C_d + C_{it} + C_i)} \cdot \frac{\mu_{eff}}{\mu_o} \qquad (2)$$

where C_d is the depletion capacitance, C_{it} is the interface state capacitance, C_i is the inversion charge capacitance, kT/q is the thermal voltage, μ_{eff} is the effective mobility, μ_o is the low field mobility and α is a numerical constant (α = 1–2 from weak to strong inversion (Ghibaudo 1986).

Eqs. (1) and (2) clearly point out that, for a given charge fluctuation, the gate voltage dependence of $\delta I_d/I_d$ results from that of the transconductance–current ratio g_m/I_d. As illustrated in Fig. 1, this explains why the current fluctuation are maximum in weak inversion. In contrast, they decrease monotonically in strong inversion as g_m/I_d because of the inversion charge screening.

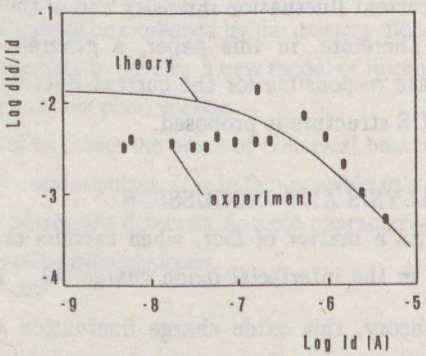

Fig. 1 : Experimental (after Uren et al 1985) and theoretical (Eq. (2)) variations of the current fluctuation intensity $\delta I_d/I_d$ with drain current I_d for small area devices (parameters : L.W=0.4μm^2, Oxide thickness t_{ox}=40nm, V_t=0.6V).

It should also be noted that Eq. (1) is quite general and can be applied, without loss of generality, to depletion mode MOS transistors and also to devices operating at room, low and very low temperatures.

In the same context, starting from Eq. (1), it is easy to derive the corresponding drain current spectral density as :

$$S_{Id} = g_m^2\ S_{Vfb} \qquad (3)$$

where S_{Vfb} is the flat–band voltage spectral density. Eq. (3) clearly shows that, what

is generally called the equivalent input gate voltage spectral density is, in fact, nothing but the flat–band voltage spectral density associated with the oxide charge fluctuation in the MOS structure.

Eq. (3) can then be advantageously used to recover, in a generic way, the Reimbold formula. In the case, for example, of an enhanced–mode MOSFET operating at room temperature, one obtains (Ghibaudo 1987a, 1987b) :

$$\frac{S_{Id}}{I_d^2} = \left(\frac{g_m}{I_d}\right)^2 \frac{S_{Qox}}{W\ L\ C_{ox}^2} = \frac{q^2}{\alpha^2 W\ L\ kT^2} \frac{S_{Qox}}{(C_{ox} + C_d + C_{it} + C_i)^2} \frac{\mu_{eff}^2}{\mu_o^2} \qquad (4)$$

in which S_{Qox} is the oxide charge spectral density per unit of area.

Therefore, as for the current fluctuations (see Eq. (2)), the gate voltage dependence of S_{Id}/I_d^2 emerges essentially from the gate voltage dependence of g_m/I_d as exemplified in Fig. 2 and Fig. 3 for room and liquid helium temperatures.

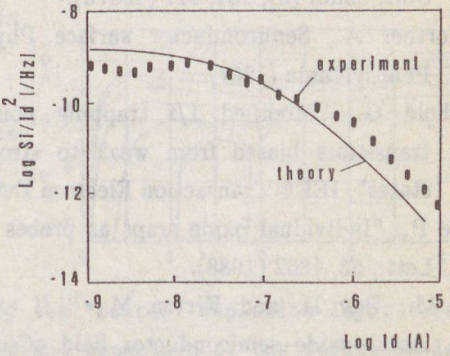

Fig. 2 : Experimental (after Uren et al 1985) and theoretical (Eq. (4)) variations of S_{Id}/I_d^2 with drain current I_d (parameters : W=L=100μm, t_{ox}=40nm, V_t=0.6V).

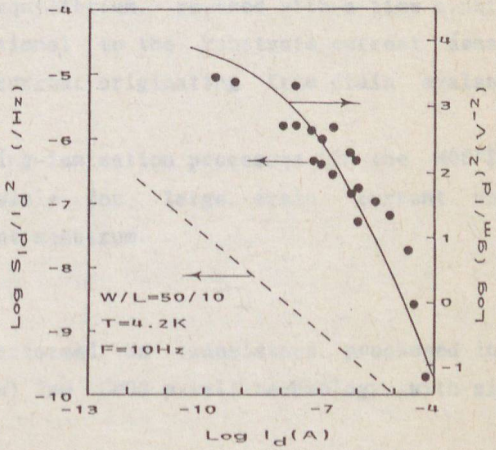

Fig. 3 : Experimental variations of S_{Id}/I_d^2 and $(g_m/I_d)^2$ with drain current as obtained at liquid helium temperature (parameters : W=100μm, L=50μm, t_{ox}=120nm).

3. CONCLUSION

A unified formulation, which provides both the current fluctuation intensity and the current noise level arising from charge trapping in MOS devices, has been achieved. This has been made possible using a proper analysis of the charge trapping phenomenon in terms of flat–band voltage fluctuations. In particular, the prevailing role played by the gate voltage (or drain current) dependence of the transconductance–current ratio g_m/I_d has been clearly emphasized.

REFERENCES

Ghibaudo G., "An analytical model of conductance and transconductance for enhanced mode MOSFETs", Phys. Stat. Solidi (a), 95, 323 (1986).

Ghibaudo G., "A simple derivation of Reimbold's drain current spectrum formula for flicker noise in MOSFETs", Sol. Stat. Electron, 30, 1037 (1987a).

Ghibaudo G., "Calculation of surface charge noise at the Si–SiO_2 interface", Phys. Stat. Solidi (a), 104, 917 (1987b).

McWorther A., Semiconductor surface Physics, Pennsylvania Press University, Pennsylvania (1957).

Reimbold G., "Modified 1/f trapping noise theory and experiments in MOS transistors biased from weak to strong inversion – Influence of interface states", IEEE Transaction Electron Devices, ED–31, 1190 (1984).

Restle P., "Individual oxide traps as probes into submicron devoces", Appl. Phys. Lett., 53, 1862 (1988).

Uren M., Day D. and Kirton M., "1/f and random telegraph noise in silicon metal–oxide–semiconductor field effect transistors", Appl. Phys. Lett., 47, 1195 (1985).

ANOMALOUS V_{DS} DEPENDENT NOISE IN Si MOSFET'S AT LHe TEMPERATURE

B. DIERICKX, E. SIMOEN, J. VERMEIREN, S. COS, C. CLAEYS

IMEC
B-3030 Leuven, Belgium

1. INTRODUCTION

n- or p-MOSFET's operated at liquid Helium (LHe) temperature show anomalies, which are related to free carrier freeze-out. Their current-voltage characteristics feature the so-called 'kink' and 'hysteresis' at typical drain voltages of 1 to 5 V (fig. 1).

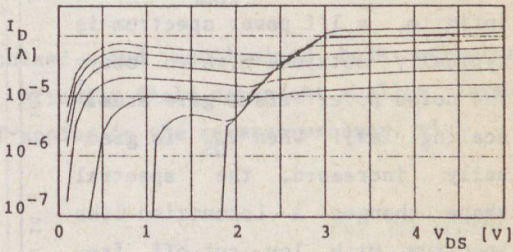

Fig. 1 I_D vs. V_{DS} characteristics of a 20x20µm large nMOSFET, T = 4.2 K, on a semilogarithmic scale. V_{GS}=0.8 to 1.8 V,step 0.2

These anomalies are explained by the "forced depletion layer formation" (FDLF), which is the slow build-up and breakdown of the depletion layer by shallow impurity impact ionization and trapping processes in the substrate [1]. This results in a dynamic equilibrium, reached with a time constant τ_{FDLF} which is inversely proportional to the substrate current density (this is the secondary hole current originating from drain avalanche multiplication).

As will be shown, these trapping-ionization processes in the MOSFET's depletion layer, are responsible for large drain current noise contributions, with a V_{DS} dependent spectrum.

2. EXPERIMENTAL

The noise measurements were performed on transistors processed in a modified (for cryogenic operation) 3µm CMOS p-well technology, with sizes ranging from 3x3 to 100x100 μm^2.

At LHe temperature, the base level equivalent gate noise increases by a factor 3 to 10 compared to room temperature, to levels around 10 μV/√Hz; but additionally a strong V_{DS} dependent excess noise is found, similar to earlier reports [2]. It is observed that the presence of the anomalous kink and hysteresis coincides with onset of this noise. This is most pronounced in nMOSFET's, which also suffer most from the anomalies.
Figure 2 shows a set of drain current noise spectra obtained from the MOSFET referred to in fig. 1.

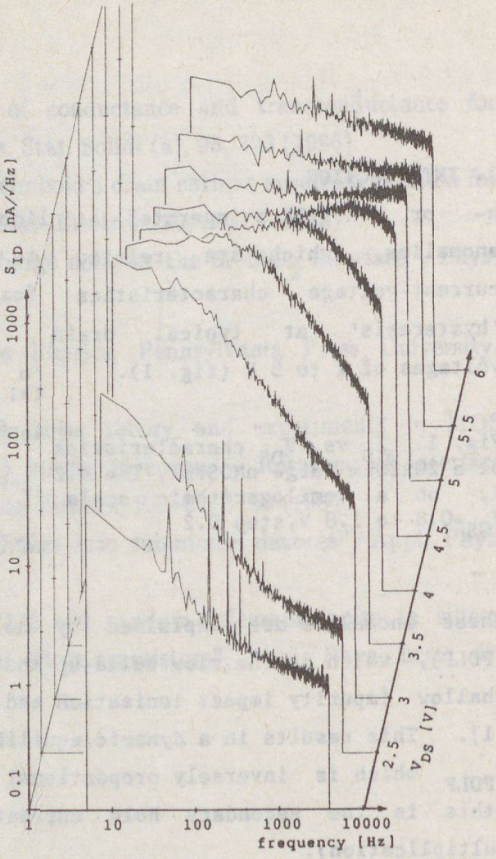

Fig. 2 Set of drain current noise (S_{ID}) spectra for 9 consecutive drain voltages ranging from 2 to 6 V. The frequency ranges from 5 to 4000 Hz.

At low drain biases (<2V), i.e. where the substrate current is virtually zero, and τ_{FDLF} is quasi infinite, a 1/f power spectrum is typically obtained (which obeys the noise power versus gate area^{-1} scaling law). When V_{DS} is gradually increased, the spectral shape changes. A Lorentzian-like spectrum with low cut-off frequency f_c appears, and its low-pass edge shifts towards higher frequencies as V_{DS} increases. Beyond 5 V obviously one just sees the white noise part of the Lorentzian spectrum.

It is worth mentioning that these spectra are not pure Lorentzians, but show a slight resonance with a quality factor of about 1. In a similar experiment on older sets of transistors more pronounced resonances were found in the spectra at frequencies in the sub-kHz region. They are probably of the same nature as the spontaneous oscillations seen in a frozen-out bulk semiconductor [3], but the origin of the different behavior is not understood yet.

3. DISCUSSION

The origin of the drain voltage dependent anomalous noise cannot be attributed to the drain avalanche multiplication current, as this would cause a high bandwidth white shot noise spectrum; furthermore it is not observed at room temperature, although the avalanche current is in the same order of magnitude there. The shape of the excess noise spectra suggests a generation-recombination (GR) type of noise, as suggested in [2], however, the consequent shift of the f_c frequency of the spectrum and the resonant behaviour ask for additional explanations. As found in the FDLF model [1], the secondary bulk current indeed induces a generation-recombination like mechanism in the bulk of the transistor. The traps involved are just the majority dopant bandgap states. Generation normally does not take place at deep cryogenic temperatures, however, under sufficient field conditions, dopant atoms are ionized by impact of substrate current holes, as:

$$\frac{\partial N_A^-}{\partial t} = p \cdot A_{ii} \cdot N_A^o \qquad (1)$$

where N_A^- and N_A^o are the ionized and non-ionized bulk acceptor concentrations, and $A_{ii}(F)$ is the strongly field-dependent shallow level impact ionization rate constant. Trapping is the reverse process, with

$$\frac{\partial N_A^-}{\partial t} = - p \cdot B_T \cdot N_A^- \qquad (2)$$

where B_T is the field-dependent trapping rate constant.
The hole density p may be estimated from the majority carrier bulk current J_B using the mobility expression. The time constant to reach equilibrium for the processes in eq. (1) and (2), i.e. the FDLF mechanism, then is found to be [1]

$$\tau_{FDLF} = \frac{\mu \cdot q \cdot F}{J_B \cdot (A_{ii}+B_T)} \qquad (3)$$

In this formula only J_B varies significantly. From simulations of the bulk behaviour [1] one knows that the other parameters are relatively constant values.

Derivation of an expression for the drain current spectrum

The time constant of eq. (3) strictly speaking also equals the average GR

time constant of carriers trapped by bulk dopant states. The spectrum of the bulk charge fluctuations may be approximated by

$$S_{QB}(f) = \frac{q^2.V.N_A}{2} \cdot \frac{\tau}{1 + (2\pi f\tau)^2} \qquad [C^2/\sqrt{Hz}] \qquad (4)$$

wherein V is the volume of interest, as $V.N_A$ is the number of interacting charges. The translation of bulk charge fluctuations to effective bulk potential spectrum proceeds via the bulk-to-channel capacitance C_B. This last one is difficult to estimate, because the depletion layer is not as nicely delineated as at room temperature, but also because the fluctuating charge is not localized in a small volume. A first estimate for C_B is the bulk-to-channel depletion layer, and an estimate for V is a few times this depletion layer volume. Finally the drain current noise spectrum -at least the part of it originating from the described mechanism- is found via the bulk effect transconductance g_{mb}:

$$S_{ID}(f) = g_{mb}^2.S_{VB}(f) = \frac{g_{mb}^2.q^2.V.N_A}{2.C_B^2} \cdot \frac{\tau}{1 + (2\pi f\tau)^2} \qquad (5)$$

where the bulk current density is included via the FDLF time constant τ (cfr. eq. (3)).

4. CONCLUSIONS

Figure 3 shows extracted values of the Lorentzian cut-off frequency and base level versus bulk current. The linear dependence between f_c ($=\tau^{-1}$) and substrate current I_B, and the inverse root dependence between the spectrum's horizontal level and I_B, are perfectly in agreement with formulae (3) and (5). Also the high amplification from DC bulk current to drain current noise is explained by the prefactors in (5).

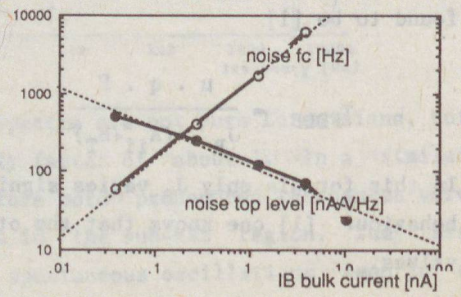

Fig. 3 Lorentzian cut-off frequencies f_c and top levels, extracted from the data of fig. 2.

REFERENCES

[1] B. Dierickx, L. Warmerdam, E. Simoen, J. Vermeiren and C. Claeys, "Model for hysteresis and kink behavior of MOS transistors operating at 4.2 K", IEEE Trans. Electron Dev. vol.35-7, p.1120 (1988).

[2] E.H. Hendriks and R.J.J. Zijlstra, "Diffusion and inter-valley noise in (100) n-channel Si-MOSFETs from T=4.2 to 295K", Solid State El., vol.31-2, p.171 (1988).

[3] S.W. Teitsworth, R.M. Westervelt and E.E. Haller, "Nonlinear oscillations and chaos in electrical breakdown in Ge", Phys. Rev. Letters, vol.51-9, p.825 (1983).

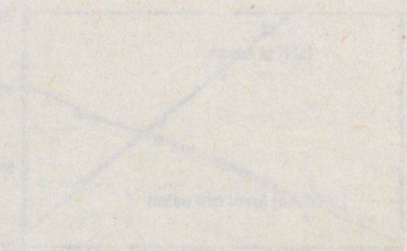

10th Int.Conf. on Noise in Physical Systems
1989 Budapest, Hungary

LOW-FREQUENCY NOISE ASSOCIATED TO THE GATE CURRENT OF GaAs MESFETs AND MODFETs

J.M. PERANSIN, P. VIGNAUD, D. RIGAUD, J.M. DUMAS*

Centre Electronique de Montpellier (CNRS UA 391),
U.S.T.L. 34060 Montpellier Cedex, France
*CNET Lannion, Route de Trégastel,
22301 Lannion, France

Abstract : The results of measurements are presented concerning the gate current noise in GaAs FET's. The devices tested were Schottky structures biased in reverse voltage. A model is proposed that yields an evaluation of a parasitic active conductance in parallel to an ideal diode.

1 Introduction

Schottky barriers are commonly used in numerous FET gate structures. The white noise component presented by the gate current is investigated in the frequency range of 10Hz to 10^5Hz. We have explored the discrepancy between the obtained levels and the ideal shot noise [1]. This experimental study was made on several types of commercial GaAs MESFET's made by NEC and RTC, and MODFET's made by NEC, FUJITSU, and SONY. The results indicate that various noise sources are involved : 1) a shot noise type 2) a thermal noise through a fixed parallel conductance 3) a thermal noise through a leakage conductance depending on the gate voltage.

In the common source configuration the noise behaviour in FET is generally represented by two current noise generators : output i_{dn} and input i_{gn} in the usual conventional representation. In our experimental set-up the generator i_{dn} is shorted and i_{gn} is directly evaluated through a converter current voltage with a negligible input impedance. Thus the device can be seen as a Schottky diode in a reverse bias.

2 Comparison between the gate-channel diode characteristics

The various I_G-V_{GS} charateristics are shown in fig.1 in the voltage range where the noise measurements were performed. For all types of devices the gate electrode is formed in a recess structure with a geometrical settling far to be perfect for a metal-semiconductor contact. Such structures suffer from parasitic edge effects wich explain the scattering in results between samples. This makes it difficult to find a model. At low currents fig.1 shows a linear relationship wich can be associated with a conductance G_o, see also table 1. When I_G increases two trends are observed. A part of MESFETs and the MODFETs (R17, R114, N11, S3, F4, N30) show a current of the form $I_G \propto V_{GS}^4$. These variations suggest a mechanism of carrier injection related to the important fields located at the gate edges [2]. The other part of MESFETs follows a more conventional behaviour of a reverse biased Schottky diode associated with an interfacial disturbed layer. A simple physical model shows for GaAs : $I_R \propto \exp(-0{,}26\ \chi^{1/2}\ \delta)$ where the barrier height field dependence χ and the layer thickness δ are used as adjusting parameters [3].

3 Gate current noise behavior

The white part of the spectral density $S_i(f)$ associated to i_{ng} is plotted in the form of $I_{eq} = S_i(f)/2q$, in fig.2a experimentally obtained from MODFETs. As a result, I_{eq} values follow strictly the I_G increases. The noise source is then a full shot noise mechanism related to the current through the metal-semiconductor junction . From fig.2b it can be seen that for a part of the MESFETs the white noise behaves quite differently. At low currents the noise level is flat independently from I_G. Considering a thermal noise contribution we can express this term as $4kTG_{no}$ where G_{no} is the equivalent noise conductance. The values are reported in table 1. The result $G_o \approx G_{no}$ shows that a dominating parallel conductance masks the junction leakage current effect. At the high currents I_{eq} moves towards I_G but remains lower than the gate current. In this section the spectral density is then found varying as $I_G(1-\alpha)$ with $0<\alpha<1$. It is evident that the major part of the current generates shot noise.

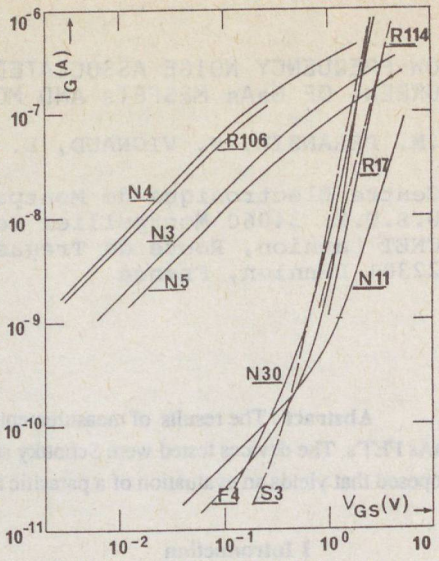

Fig.1 : I_G-V_{GS} DC Characteristics

The last results presented in fig.2c show that white level increases with I_G, but with a ratio $(1-\alpha)$ weakly bias dependent. In this devices $G_o < 10^{-9}$ S is too low to permit the detection of the associated thermal noise.

Table 1

	Code	No.	G_o (S)	G_{no} (S)	I_{eq} (nA)	V_{ref} (mV)
RTC	190	R17	$<10^{-9}$			
	CFX1726	R106	$5.3\ 10^{-7}$	$5.8\ 10^{-7}$	29.0	49
	CFX1726	R114	$4.4\ 10^{-9}$			
	41137	N3	$1.8\ 10^{-7}$	$1.9\ 10^{-7}$	9.5	52
	41137	N4	$7.0\ 10^{-7}$	$7.4\ 10^{-7}$	37.0	51
NEC	41137	N5	$1.2\ 10^{-7}$	$1.1\ 10^{-7}$	5.4	52
	NE720	N11	$2.7\ 10^{-9}$			
	NE202	N30	$<10^{-11}$			
SONY	2SK878	S3	$<10^{-11}$			
FUJI.	FHX01FA	F4	$2.2\ 10^{-11}$			

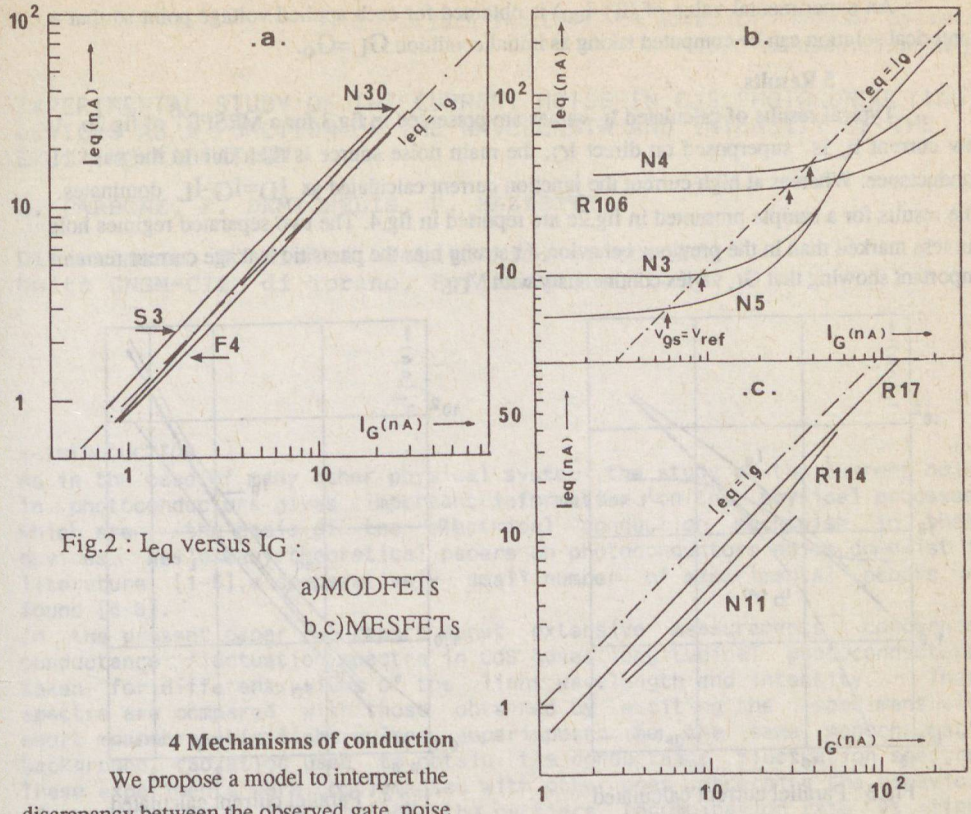

Fig.2 : I_{eq} versus I_G :
a)MODFETs
b,c)MESFETs

4 Mechanisms of conduction

We propose a model to interpret the discrepancy between the observed gate noise current and the shot noise taken as reference. The starting point is an equivalent circuit composed by a reverse diode in parallel with a conductance G_L. Taking various forms this element allows to represent the dispersion of input characteristics.

I_G is then separated in two parts : $I_G=I_D+I_L$ (1) where I_L is the parasitic current and I_D the current crossing the Schottky contact. The total spectral density is : $S_{IG} = S_{ID} + S_{IL}$ (2) . We postulate that I_D generate a full shot noise density : $S_{ID} = 2qI_D$. The parasitic conductance gives a corresponding noise density : $S_{IL} = 4kT\beta G_L$ where β is a coefficient of non-linearity [4], so that the total noise can be expressed on the form : $I_{eq}=I_{Deq}+I_{Leq}$ (3) , with $I_{Deq}=I_D$ as element of comparison and $I_{Leq}= S_{IL}/2q= 2kT\beta G_L/q$.

At low voltage in the case of MESFETs of fig.2b the difference between (1) and (3) gives : $I_{eq}-I_G=(2kT\beta G_L/q)-I_L\geq 0$ (4) where Id is eliminated.The experimental evaluation of bias voltage at the limit $I_{eq}-I_G=0$ can be taken as a reference since at low level $G_L \rightarrow G_o=G_{no}$ and $\beta=1$. We have $I_L=G_L*V_{GS}=G_o*V_{ref}$ and hence from (4) $V_{ref}=2kT/q=50$ mV at room temperature. This was confirmed by results reported in table 1.

At high voltage with $I_{eq}-I_G<0$ we observe that G_L cannot be seen as constant in fig.2c as in fig.2b. Now, we consider a value of leakage conductance function of voltage with $I_{Leq}=(2kT/q)(\partial I_L/\partial V_{GS})$. In that way the relation of currents becomes a differential equation

$$2kT/q.(\partial I_L/\partial V_{GS})-I_L+(I_G-I_{eq})=0 \quad (5)$$

An experimental value of (I_G-I_{eq}) is obtained for each applied voltage point so that a numerical solution can be computed taking as initial condition G_L=G_O.

5 Results

Typical results of calculated I_L values are presented in fig.3 for a MESFET of fig.2b. At low current I_L is superposed on direct I_G, the main noise source is then due to the parallel conductance. Whereas at high current the junction current calculated as I_D=I_G-I_L dominates. The results for a sample presented in fig.2c are reported in fig.4. The two separated regimes hold but less marked than in the previous behavior. At strong bias the parasitic leakage current remains important showing that G_L varies continuously with V_{GS}.

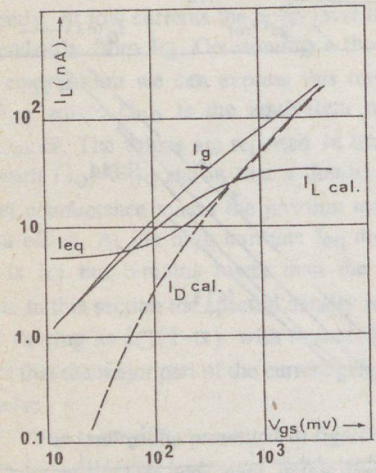

Fig.3 : Parallel current calculated for MESFET N5

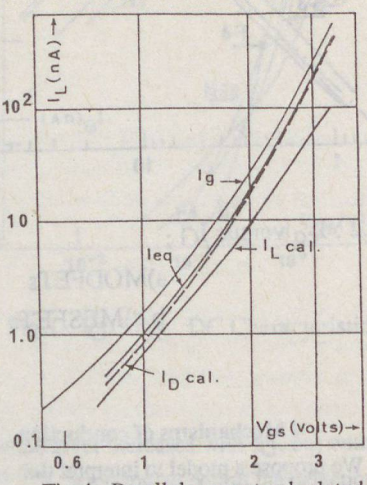

Fig.4 : Parallel current calculated for MESFET R17

In summary the study of the equivalent input noise have shown different noise sources, corresponding to various types of input characteristics. Some samples are governed by a pure shot noise source. Important parasitic conductances, including current partition, are revealed in the others. We distinguish between two possible effects of these leakage currents. A current wich tends to vanish at high polarity and a leakage current increasing with the gate current.The physical nature of the surface is at the origin of the observed effects. We believe that the current path originates in defects at the surface, the surface treatment and the oxydation being implicated during the gate-recess process.

References

1-PERANSIN J-M., VIGNAUD P., RIGAUD D.,DUMAS J-M.,
Bias dependence of low-frequency gate noise in GaAs MESFETs, Electron.Lett., 1989, 25, p.439

2-LAMPERT M.A., MARK P., Current injection in solids
(ACADEMIC PRESS, NY, 1970) Chap. IV

3-SHOU M., WEIYMAN W., GaAs Schottky barrier and its applications in GaAs FET's with high doped channel, Inst. Phys. Conf. Ser; 74, 1984, GaAs and related compounds, p.64

4-VAN DER ZIEL A., Noise : Sources, characterisation, measurement (Prentice-Hall, NJ, 1970)

10th Int.Conf. on Noise in Physical Systems
1989 Budapest, Hungary

EXPERIMENTAL STUDY OF THE CURRENT NOISE IN CdS PHOTOCONDUCTING DEVICES AS A FUNCTION OF THE WAVELENGTH AND INTENSITY OF THE EXCITING RADIATION

A. CARBONE, F. DEMICHELIS, P. MAZZETTI

Dipartimento di Fisica, Politecnico di Torino,
Unità GNSM-CISM di Torino, Politecnico, Italy

1-INTRODUCTION

As in the case of many other physical systems,the study of the current noise in photoconductors gives important information on the physical processes which are the basis of the electrical conduction mechanism in these devices. While many theoretical papers on photoconductors noise do exist in literature [1-5],a comparatively small number of experimental papers are found [6-8].

In the present paper we report about extensive measurements concerning conductance fluctuation spectra in CdS based longitudinal photoconductors, taken for different values of the light wavelength and intensity. These spectra are compared with those obtained by exciting the specimens with short monochromatic light pulses superimposed to the same monochromatic background radiation used to obtain the conductance fluctuation spectra. These experiments were complemented with other ones concerning the behaviour of the noise power density and the carriers recombination rate vs. light intensity.

From the whole set of these measurements some important conclusions can be drawn. In particular they quite clearly show that the conductance fluctuation spectra of CdS type photoconductors are constituted by two different noise components,as already pointed out by Van Vliet et al. [7]. The first one dominates the low frequency part of the spectrum and it is actually a photoinduced noise strictly related to the carrier recombination rate,which depends both on the light wavelength and on the light intensity. An additional noise component,dominating the high frequency part of the spectrum is also present. This second component,which is not a photoinduced noise, has a rather flat power spectrum and can be reasonably attributed to fast spontaneous trapping processes of the majority carriers.

Another important point that has been clarified is the origin of the abrupt change of about 1 decade of the low frequency noise power density observed when the light wavelength λ crosses the value λ_c ,corresponding to the CdS energy gap [9]. As shown in the following,this effect is related to a corresponding abrupt change in the carriers recombination rate,and can be quantitatively accounted for by this effect.

While a full description of all these results is outside the scope of the present paper,in the following the main experimental results leading to the above conclusions will be reported. An extended paper, now in preparation, will give a fuller account of the experiments outlined above.

2-EXPERIMENTAL RESULTS

A detailed description of the experimental set-up has been given in a

previous paper [9]. The photoconductor is connected to a constant voltage supply through a resistor R_i. The voltage fluctuations at the ends of R_i are amplified and sent to a signal analyzer, which gives the power spectrum $\phi_V(f)$. The relative conductance fluctuation power spectrum of the photoconductor, $\phi_G(f)/G_o^2$, is obtained through the relation:

$$\frac{\phi_G(f)}{G_o^2} = \left(\frac{R_o+R_e}{R_o}\right)^2 \cdot \left[1 + \frac{(2\pi f)^2\, C_e^2\, R_o^2\, R_e^2}{(R_o+R_e)^2}\right] \cdot \frac{\phi_V(f)}{V^2} \qquad (1)$$

where G_o and R_o are respectively the average conductance and resistence of the photoconductor, R_e is the equivalent resistence of R_i in parallel with the amplifier input resistence, C_e is the equivalent capacity in parallel with R_e, V is the d.c. voltage drop at the ends of R_e and f is the frequency. The light is sent to the photoconductor through an optical light guide connected to the output window of a monochromator.
Photoresponse measurements are obtained by superimposing brief flashes of light to the main light source, constituted of an halogen lamp connected to a regulated d.c. power supply.
Light intensity fluctuations of the source in excess to the normal shot noise were checked to be very limited, as shown by fig.1, which reports the power spectrum of the photocurrent noise generated in a saturated high quality Gillod Boutry vacuum photodiode put in place of the photoconductor.

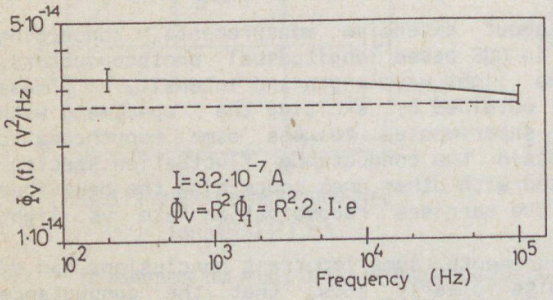

Fig.1 - Shot noise power spectrum of a saturated vacuum photodiode illuminated by the monochromatic light used to excite the CdS photoconductor. I is the photocurrent, V is the voltage drop at the ends of R, in series with the photodiode, $\phi_V(f)$ the power spectrum of V, and e is the electron charge. Dotted line is the theoretical spectrum.

A calibrated photocell was used to measure light intensity in the different physical conditions under which spectra measurements were taken. The main results concerning the effect of the light wavelength on the relative conductance noise spectrum are summarized in the curves of fig.2 and 3. They refer to a specific CdS photocoducting device, but practically identical results were found for all the other tested CdS devices. All the reported results were reproducible over different runs within the indicated bars. Thermal noise was subtracted.
Measurements at different λ values were made by adjusting the light intensity in such a way to keep the conductance constant. There can be noticed a large variation of about 1 decade in the power spectral density at low frequencies when the light wavelength crosses the critical value λ_c corresponding to the energy gap of CdS. This effect is related to a corresponding abrupt change in the conductivity relaxation time after a small monochromatic light pulse of very short duration (about 2 μs) superimposed to the continuous radiation at which the noise spectra were taken.
In fig.2 dotted lines represent the square modulus of the Fourier transform of the conductivity relaxation pulses divided by G_o^2, obtained at two different wavelengths, slightly above and below λ_c. It can be noticed that these spectra are not purely lorentzian ones.

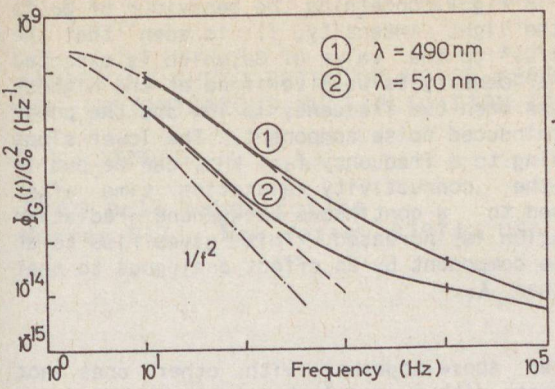

Fig.2 - Relative conductance noise power spectra at two different wavelengths sligtly above and below the energy gap of CdS. Dotted lines represent the energy spectra of the photoresponse pulses of the same specimens excited with very short light pulses whose intensity ratio was equal to the square root of the ratio of the superimposed monochromatic radiation intensities.

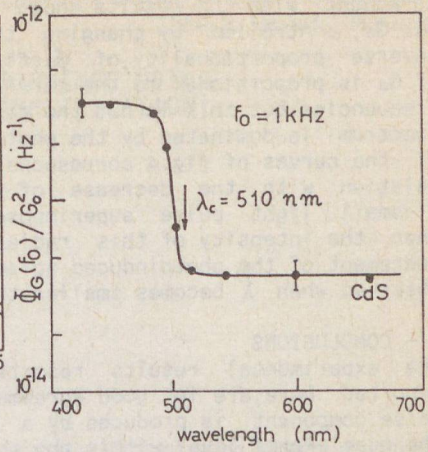

Fig.3 - Behaviour of $\phi_G(f)/G^2$ vs. the wavelength of the exciting radiation at 1 kHz. λ_c is the light wavelength corresponding to the energy gap of CdS. The conductance G_o of the photoconductor is kept constant when λ is varied by adjusting the light intensity.

While the absolute amplitudes of these spectra are arbitrary, their relative position is physically meaningful, because they correspond to light pulses whose amplitude ratio was the same as that expected for the spontaneous fluctuations of the continuous radiation in the two conditions considered, i.e. equal to the square root of the ratio of the intensities needed to keep G_o constant when λ was changed.

Comparison with the noise spectra (full lines) clearly show that the low frequency part of these spectra is actually due to photoinduced noise, while a second noise component should be responsible for the high frequency behavior of the spectra.

The existence of two noise components having different origins is also in good

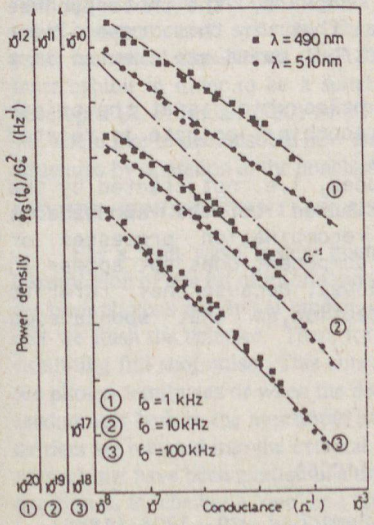

Fig.4 - Behaviour of $\phi_G(f)/G_o^2$ vs. G_o for different values of the freqency f: the deviation from the expected G_o^{-1} slope at low frequency is correlated with an observed decrease of the conductance relaxation time when G_o increases.

agreement with the results shown in fig.4, concerning the behaviour of $\phi_G(f)$ vs. G_o, controlled by changing the light intensity. It is seen that the inverse proportionality of $\phi_G(f)/G_o^2$ to the value of G_o, which is expected if G_o is proportional to the carrier density, is well verified at the highest frequencies, but this is not the case when the frequency is low and the power spectrum is dominated by the photoinduced noise component. The lower slope of the curves of fig.4 corresponding to a frequency f_o=1 kHz, can be put in relation with the decrease of the conductivity relaxation time after a small light pulse superimposed to a continuous background radiation when the intensity of this radiation is increased. This gives rise to an increment of the photoinduced noise component by an effect analogous to that observed when λ becomes smaller than λ_c.

3 - CONCLUSIONS

The experimental results reported above, together with other ones not reported here, are in good agreement with a model where the photoinduced noise component is produced by a corresponding photoinduced fluctuation of the quasi-Fermi level within the photoconductor. This fluctuation produces a noise amplification effect on the photocurrent, and this is in agreement with the fact that the photoinduced noise component is larger than expected by the photon number spontaneous fluctuation, as observed also in [7].

In the model, whose development will be given in a forthcoming paper, it is assumed that the shift of the Fermi level towards the conduction band is due to the formation of a positive space charge due to trapping of the minority carriers or the formation of ionized centers during illumination, and that it is the position of the electrons quasi-Fermi level within the energy gap of the photoconductor that determines the conductance value of the device.

The decay time of the photocurrent after a light pulse is determined by the recombination rate of the excess positive charge created during the flash, and is influenced both by the light wavelength and the light intensity. In particular the increase of this recombination rate when the light wavelength becomes smaller than λ_c, as shown by the photoresponse spectra reported in Fig.2, is due to the fact that in this case light absorption becomes very strong and hole - electron pairs are created in a small layer at the photoconductor surface.

In this case it is the smaller mobility of the holes which is at the origin of the positive space charge, while the larger recombination rate is related to the larger density of carriers of both signs.

The other noise component, which is not photoinduced, i.e. not created by the photon number fluctuation, should be attributed to the spontaneous fluctuation of the space charge related to recombination processes or trapping of the majority carriers. This noise component does not appear in the photoresponse spectra of fig. 2 (dotted lines), because they refer to relaxation pulses averaged by synchronous detection, so that spontaneous fluctuations were smooted out.

REFERENCES

[1] K.M. Van Vliet and J. Blok, Physica 22, 525 (1956)
[2] R.L. Petritz, Phys. Rev. 104, 1508 (1956)
[3] K.M. Van Vliet and J. Blok, Physica 22, 231 (1956)
[4] J.T. Ubbink, Phisica 52, 253 (1971)
[5] I.K. Blokhin and V.A. Kholodnov, Sov. Phys. Semicond. 20, 1208 (1986)
[6] C.I. Shulman, Phys. Rev. 98, 384 (1955)
[7] K.M. Van Vliet, J. Blok, C. Ris and J. Steketee, Physica 22, 723 (1956)
[8] S. Kruizinga and R.J.J. Zijlstra, Phys. Letters 28 A, 399 (1968)
[9] A. Carbone, F. Demichelis, P. Mazzetti, Proc. M.R.S., San Diego (1989)

10th Int.Conf. on Noise in Physical Systems
1989 Budapest, Hungary

IMPROVING PHOTO DETECTOR NOISE PERFORMANCE USING NON-INSTANTANEOUS MULTIPLICATION (AMPLIFICATION)

R.P. JINDAL

AT&T Bell Laboratories
Murray Hill, New Jersey 07974, USA

ABSTRACT

In the classical mode of photodiode operation the device response to an incident photon is effectively instantaneous. In this mode, the inherent gain fluctuations result in a degradation in the noise performance of the photodiode. It is shown how, operation in the non-instantaneous mode, results in the elimination of this noise penalty with a trade off in terms of the effective device gain bandwidth product.

INTRODUCTION

In the classical approach to design low noise photodiodes, exhibiting gain, the photodiode response time τ_p is assumed to be very small compared to the measurement time t_m. The signal multiplication process is therefore treated as instantaneous (Shockley and Pierce, 1938) (temporally deterministic). We have examined the consequences of departing from this classical wisdom and have analytically examined (R. P. Jindal, 1987a,b) a general noise problem where τ_p can be small, comparable to or larger than t_m. Later, the idea of having τ_p larger than t_m (temporally random) has been applied to the problem of level and pulse detection (R. P. Jindal, 1988a) in the case of light wave communication systems. These approximate analytical results have later been verified by exact numerical simulations (R. P. Jindal, 1988b). Further, criteria that a physical phenomenon must exhibit in order to be a suitable candidate for implementing this concept have also been developed (R. P. Jindal, 1989) with finite medium avalanching as an example. In the present work we would like to demonstrate how one can improve the noise performance of conventional detector structures by operation in the nonclassical mode.

REVIEW OF NONINSTANTANEOUS OPERATION

For a light wave system operating at a bit rate B per second, the time available for the transmission of one bit of information is 1/B seconds. This is referred to as t_m. For each bit interval we have photons arriving at random instants of time at the receiver. At the beginning of a bit time slot we flush the detector. Then, for each incident photon the detector initiates a constant current exhibiting full shot noise. This current terminates when the carrier generation process initiated by the photon terminates or when the detector is flushed at the end of the bit interval. We thus permit randomness both in the number of carriers generated per photon and also the times at which these carriers are released into the external circuit. Near the end of the time slot, we count the number of carriers that have been emitted in a time interval τ short compared to the bit time slot t_m and make a decision as to whether a 'one' or a 'zero' was transmitted. At this point, the detector is flushed and is poised for receiving the next bit in the following time slot.

One requirement for operating a device in the non-instantaneous multiplication mode is that its response to an incident photon is the generation of a constant current. This current is allowed to have a fluctuating duration and can exhibit full shot noise. Now, in general, an amplifying device

converts an input voltage or current into an amplified output voltage or current. Thus if one can modulate the device input voltage or current with a photon-generated charge, one should investigate the possibility of operating the device in the noninstantaneous mode. With this basic idea in mind, as an example of a voltage to current converting device, we shall examine the operation of a JFET as a light pulse detector. As an example of a current to current converting device we shall examine the possibility of operating a photoconductive detector (PCD) in the noninstantaneous mode. The consequent improvement in the noise performance will also be quantified.

PHOTOCONDUCTIVE DETECTORS

Consider a photoconductive detector structure shown in Fig. 1. The p^+ diffusion are biased at a potential negative with respect to the n^+ diffusions. The sample temperature is such that the photo active impurities in the substrate are unionized. Electromagnetic radiation ionizes these impurities liberating an electron and leaving behind an ionized impurity (positive fixed charge) for each photon. The liberated electron travels to the n^+ diffusion with transit time t_r constituting a current flow. The photodetector gain $\overline{M}$ is given by τ_p/t_r where τ_p is the electron life time.

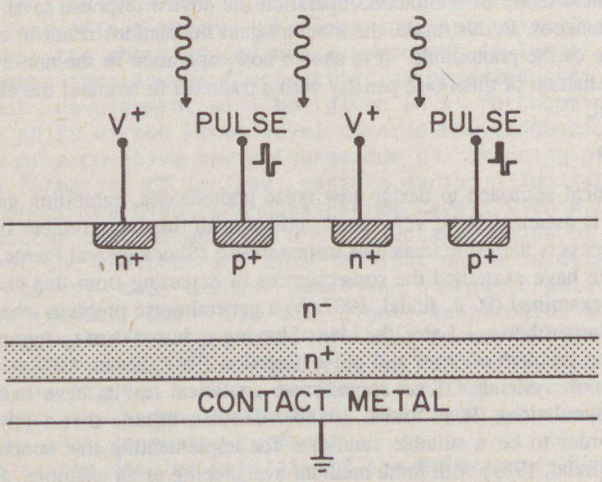

Fig. 1 A conceptual photoconductive detector dealing with the issue of fast reset.

PCDs suffer from a number of noise mechanisms (A. van der Ziel, 1976) of which the g-r part cannot be suppressed by conventional methods. This noise can essentially be viewed as fluctuations in carrier life time τ_p. This gives rise to fluctuating gain M and hence excess noise. When g-r noise is the dominant noise mechanism, for the conventional mode of operation, the signal to noise ratio (S/N) of a PCD can be shown to be

$$(S/N)_{out} = \frac{(S/N)_{in}}{1+var(\tau_p)/\tau_p^{\,2}} \qquad (1)$$

In order to operate a PCD in the noninstantaneous mode one should pick a τ_p large compared to the optical pulse width t_m to be detected. Then each incident photon generates a constant current which continues till quenched at the end of the bit interval. All these individual currents are sampled near the end of the bit interval in a time τ small compared with t_m and the bit is detected. Operated in this mode one should be able to get rid of the g-r noise limitation of the PCD since the effective gain

(R. P. Jindal, 1988a,b) $G = M\tau/\tau_p = \tau/t_r$ is essentially free of any noise associated with fluctuations in τ_p.

PCD RESETTABILITY

The underlying principle of our approach is to increase the electron population to a high level so as to enhance the impurity deionization rate by several orders of magnitude. This can be done by momentarily forward biasing the p^+ diffusion which introduces a large number of holes and electrons into the epi region. For an indirect band gap semiconductor where direct band to band recombinations are improbable, provided the electron hole plasma density is not too high, this will result in a quick neutralization of all the ionized impurities (localized mid-gap states). Then, as we reverse bias the p^+ diffusion the injected holes and excess electrons will be recollected in a single transit time. The detector is now ready for use for the next optical pulse.

FET OPERATION AS A RANDOM DETECTOR

Although, in principle, any transconductance exhibiting device is suitable for the following discussion, we shall discuss the operation of a JFET in the noninstantaneous mode. It has been shown (Shannon and Lohstroh, 1974) how a silicon JFET can be used as an optical detector. Consider the JFET biased as shown in Fig. 2. The essential idea is to apply a voltage reset pulse to the gate of a JFET through a series capacitor. This results in a momentary forward conduction of the gate diode charging this series capacitor. When this resetting pulse terminates, the capacitor charge results in a gate reverse bias with the JFET biased at pinch off. Then for each incident photon the generated charge results in a gate current partially neutralizing the charge responsible for the gate bias. This results in an increase in the channel conductance and hence the channel current. This process of gate current integration continues for the "frame time" till the next resetting pulse is applied. During this time the device can be read repeatedly in a nondestructive manner at the drain.

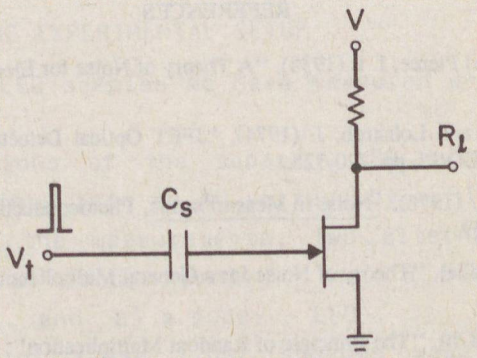

Fig. 2 Biasing circuit for the JFET.

As suggested (Shannon and Lohstroh, 1974) for maximum charge gain, one needs to integrate the drain current over the whole "frame time". Now, the effective charge generated by a photon is directly proportional to the gap between its arrival time t_{ar} and the following reset pulse. Thus the gain per photon fluctuates in sympathy with the photon arrival time t_{ar} resulting in a degradation in the signal to noise ratio. Calculating var(t_{ar}) based on Poisson statistics of the photon arrival process, one can evaluate var(M) and hence arrive at the signal to noise ratio at the output of this

FET amplifier as

$$(S/N)_{out} = \frac{(S/N)_{in}}{1+\bar{n}\, t_m/3} \qquad (2)$$

The above expression assumes gain fluctuations as the dominant noise source and hence quantifies the degradation in the S/N ratio due to them. Going back to the problem of random detection, to eliminate this gain fluctuation noise one should sample the drain current at the end of the optical pulse ("frame time") over a time window τ small compared with optical pulse width t_m. In this manner, although with a reduced gain, this excess noise mechanism can be completely eliminated.

Note that in both the above examples the improvement in the noise performance does not come for free. The noise reduction is accompanied with a reduction in the device gain.

CONCLUSIONS

We have shown that both current to current and voltage to current converting conventional devices can be operated in the noninstantaneous multiplication mode. Specific examples discussed are for a photoconductive device and a JFET both attaining the ideal limit set by shot noise limited input signal to noise ratio albeit with a reduced gain.

ACKNOWLEDGEMENT

I would like to acknowledge the interaction with an anonymous reviewer which motivated me to present the case for the photoconductive devices. Also, I am reminded of a discussion with Serge Luryi regarding the possibility of the existence of such an effect in the operation of a photon drag detector (S. Luryi, 1987) structure. Discussions with John Brews and Serge Luryi regarding the resettability of the PCD were extremely helpful. Support from Bill Lynch and Simon Sze is greatly appreciated.

REFERENCES

1. Shockley, W. and Pierce, J. R.(1938), "A Theory of Noise for Electron Multipliers", IRE *26*, pp. 321-332.
2. Shannon, J. M. and Lohstroh, J. (1974), "JFET Optical Detectors in the Charge Storage Mode", IEEE-TED *21*, pp. 720-728.
3. Van der Ziel, A. (1976), Noise in Measurements, Photoconductive Detectors, Wiley, New York, pp. 146-159.
4. Jindal, R. P. (1987a), "Theory of Noise for a General Multiplication Process", IEEE-EDL *8*, pp. 315-317.
5. Jindal, R. P. (1987b), "The Principle of Random Multiplication", 9th Intl. Conf. on Noise in Physical Systems, Montreal, Canada, pp 241-244.
6. Luryi, S. (1987), "Photon-Drag Effect in Intersubband Absorption by a 2-D Electron Gas", Physical Review Letters *58*, pp. 2263-2266.
7. Jindal, R. P. (1988a), "Attaining the Ideal Detection Limit Using Random Multiplication", JAP *63*, pp. 2824-2827.
8. Jindal, R. P. (1988b),"A Monte Carlo Simulation of a Photodetector operating in the Random Limit", JAP *64*, pp. 6845-6850.
9. Jindal, R. P. (1989), "A Physical Principle to Implement Random (noninstantaneous) Multiplication Photodetector", IEEE-EDL-10(2), pp. 49-51.

10th Int.Conf. on Noise in Physical Systems
1989 Budapest, Hungary

NOISE OF GaAlAs SUPER-LED RADIATION

J. ŠIKULA, P. VAŠINA, S. SYNEK, I. HÜTTEL*

Technical University
CS-662 37 Brno
*Radio Research Institute
Novodvorská 997, CS-100 00 Prague, Czechoslovakia

INTRODUCTION

Recently, Fronen and Vandamme in [1] have dealt extensively with the 1/f spectra of intensity fluctuations in the optical emission of semiconductor lasers.

We present our measurements of optical output fluctuations of GaAlAs super - LED´s in the sub-laser operation mode and compare the results with those of [1].

THE SAMPLES AND THE EXPERIMENTAL SETUP

The super - LED samples we have measured were manufactured according to [2].

The fluctuations of the super - LED output intensity have been transformed into an AC voltage by a PIN photodiode. In the course of the measurements, two alternative sources of light have been used, namely : a) a battery powered incandescent lamp, and b) a super - LED .

The outputs of these light sources were adjusted so as to produce equal DC responses of the PIN diode. In this way we could discriminate between the excess and the shot noise. Furthemore, we have measured the cross - correlation function $B(\tau)$ of the light intensity fluctuations and those of the LED forward current.

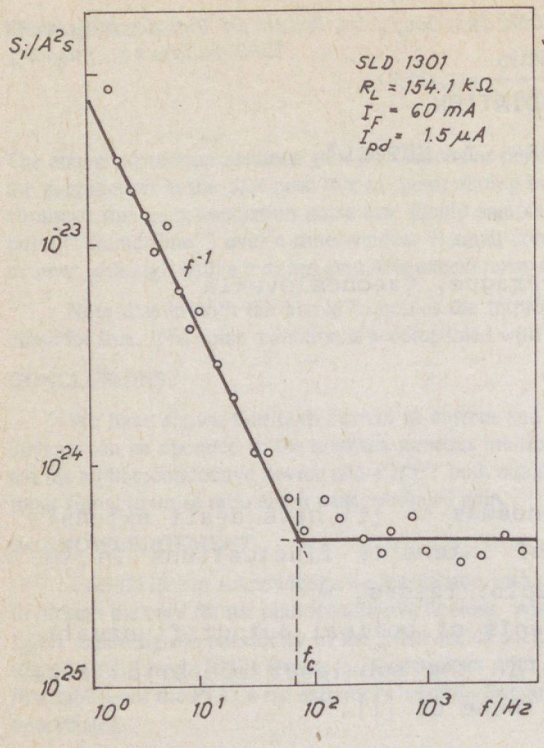

Fig.1 The noise spectral density as a function of frequency

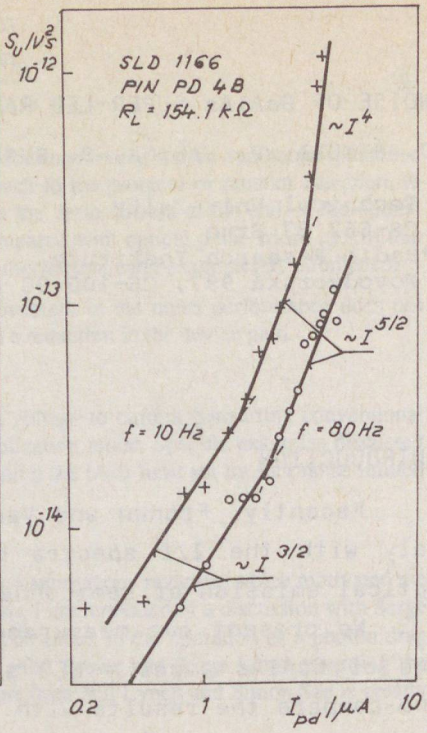

Fig.2 The noise spectral density as a function of the photocurrent

RESULTS AND DISCUSSION

Fig.1 shows the photodetector current fluctuation spectral density S_I vs. frequency f plot at a DC photodetector current I_{pd} of 1,5 uA. The pertinent super - LED forward current was 60 mA, which corresponds to an optical output power of 1,5 milliwatts. The measured spectrum below the cut-off frequency f_c is of the 1/f type. We have shown in [2] that f_c depends on the DC current I_{pd}. At higher values of I_{pd} we have obtained spectra of the $1/f^a$ - type, where the exponent a reaches as much as 4 and the reproducibility of the measured values becomes poor. We suppose that this is due to the super - LED technology, in which the optical feedback is not sufficient to maintain stable laser oscillations.

In view of the theory given in [1], we have carried out a detailed analysis of the $S_u(I_{pd})$ curves at various frequencies. Here $S_u = R_L^2 \cdot S_I$, is the voltage fluctuation spectral density, R_L is the photodetector load resistance. Fig.2 shows two $S_u(I_{pd})$ plots for f = 10 and 80 Hz. At 10 Hz the curve has all three regions mentioned in [1], that is, $S_u \propto I_{pd}^{3/2}$, $I_{pd}^{5/2}$, I_{pd}^{4}; in a good agreement with [1]. At 80 Hz only two regions appear.

It is to be noted that some super - LED´s give $S_u(I_{pd})$ curves which do not obey the mentioned laws.

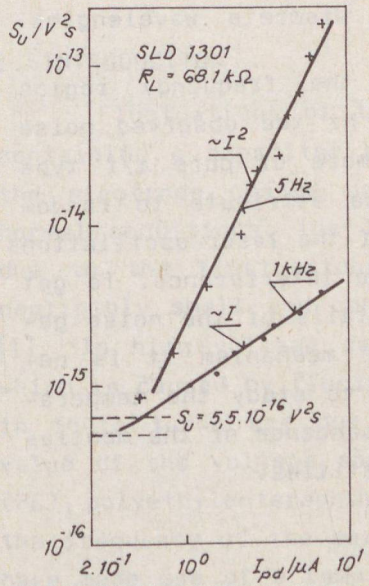

Fig.3 The noise spectral density as a function of the photocurrent for another diode

For example, a super-LED No 1301 at 5 Hz and a load resistance of 68,1 kΩ gives a $S_u(I_{pd})$ plot which can be fairly approximated by a square - law curve (see Fig.3., where for comparison the shot noise spectral density at 1 kHz is drawn).

We explain this result in the following way. Due to the fact that the slope of the $S_u(I_{pd})$ curve changes within the course of one order of the current I_{pd}. To distinguish between the 3/2 and 5/2 laws, one has to carry out high-precision measurements in a great number of points. More precise measurements confirm the power laws proposed by [1] for this diode as is clear from Fig.2. The cross -correlation measurements between the light output fluctuations and the current fluctuations of these diodes show that LED´s having high excess noise give a certain cross-correlation. On the other hand, the LED´s whose noise is near the theoretical value, exhibit the correlation factor near zero.

CONCLUSIONS

Our measurements carried out on super - LED´s show that in the low - frequency region there exists an excess noise of the optical output which is of the 1/f - type. For low and medium level of injection the current spectral density vs. current I plot obeys the 3/2 and 5/2 laws, which is in a good agreement with the theory of Fronen and Vandamme [1].

For the high injection level near the lasing the current spectral density varies as I^4. From spectroscopic measurements (see Fig.4) it is seen that a fraction of the emitted radiation contains coherent components at discrete wavelengths.

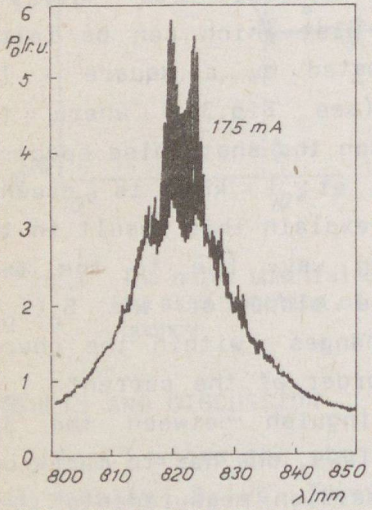

In the frequency region near 1 Hz the observed noise is no more of pure 1/f type which we attribute to random onset of the laser oscillations and mode interference. To get more details of the noise generation mechanism it is necessary to study the temperature dependence of the mentioned quantities.

Fig.4 Light output of the super - LED as a function of the wavelength

REFERENCES

[1] R.J. FRONEN, L.K.J. VANDAMME, IEEE Journ. of Quant. Electronics, 24, 724, (1988)

[2] J. ŠIKULA, P. VAŠINA, I. HÜTTEL, phys.stat. solidi, 111 (a), 367 (1989)

10th Int.Conf. on Noise in Physical Systems
1989 Budapest, Hungary

IMPULSE NOISE IN CAPACITORS

J. ŠIKULA, B. KOKTAVÝ, P. VAŠINA, P. SCHAUER, L. STRÁSKÝ*

Department of Physics, Technical University of Brno
662 37 Brno
*Tesla
612 45 Brno, Czechoslovakia

1. INTRODUCTION

Fluctuations of the electric current in a circuit containing a capacitor may be due to fluctuations of either the electrode charge or the dielectric permittivity. Under normal conditions, the thermal noise of a capacitor which is due to the fluctuations of the dielectric polarization is negligibly small and cannot be measured by present apparatus [1]. In high-voltage capacitors there is a measurable noise which is caused by fluctuations of the electrode charge which, in their turn, are due to the partial discharges. When the value of the voltage applied to capacitors with polyethylene (PE), polyethylenterephthalate (PET), and some others, is steady, the frequency of the partial discharges is low. Therefore, we have made use of a ramp voltage with a small rate of growth.

2. EXPERIMENT

Experimental analysis of the fluctuations generated in capacitors was carried out in a setup in which the DC voltage was fed to a series combination of the studied capacitor and a load resistor R_L. The noise voltage across R_L, which is analyzed by a selective amplifier, is proportional to the current fluctuations. Its time dependence is shown in Fig.1.

The shape of the voltage decay depends on the capacitance and the load resistance R_L.

The impulse noise of Fig.1 is produced in many cases by partial discharges on the metal-insulator interface. The gene-

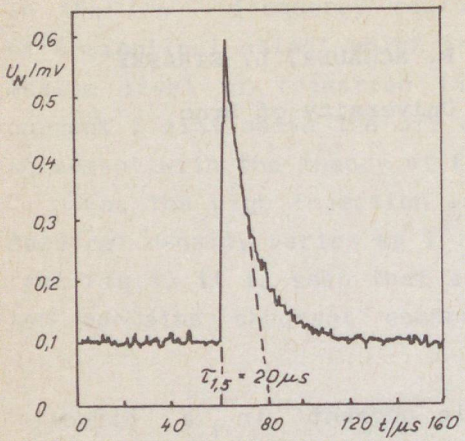

Fig.1 Time dependence of the noise voltage across the load resistance R_L

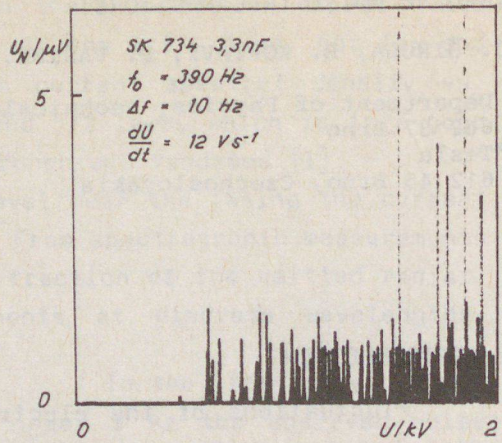

Fig.2 The noise voltage U_N as a function of the applied slowly growing DC voltage

ration of the partial discharges depends on the field strength and its time rate, and on the surface and bulk defect concentration.

Present models of the partial discharges are based upon the assumption that they are generated in the cavities in the insulator bulk and on the metal-insulator interface. These models are deterministic. They calculate the mean discharge frequency from the values of the bulk and surface conductivities and from the ignition and extinction voltages. In fact, both assumptions lead to the impulse time separation and amplitude fluctuations that depend on the ignition and extinction voltages only.

In stationary state the noise measurement is possible only in samples with a high bulk conductivity where reaching the equilibrium state takes from milliseconds to seconds. This is the case of PVC foils. On the other hand, measurement of insulators such as PET (polyethylene terephthalate) would lead to the times between two subsequent impulses of the order of 10^3 to 10^8 seconds.

In these cases it is necessary to carry out the measurements in a quasi-stationary mode, with slowly increasing field strength, as is shown in Fig.2, where on the x-axis a ramp

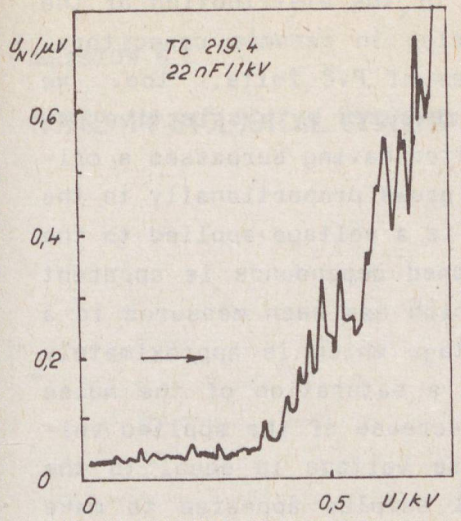

Fig.3 The noise voltage vs. a slowly groving DC voltage diagram for a PVC foil capacitor

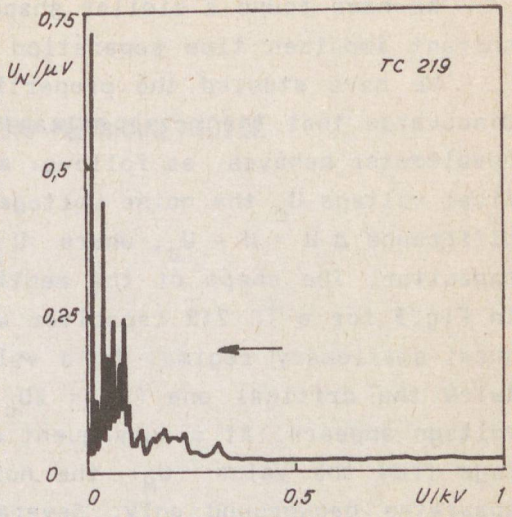

Fig.4 Noise voltage of the capacitor appearing when the DC voltage is slowly decreased

voltage with a rate of 10V/s is indicated and on the y-axis a noise voltage measured by a selective voltmeter is drawn. Our experimental study which was carried out on ensembles of Tesla and Siemens capacitors show that the critical voltage U_c is in many cases lower than the nominal one.

It follows that any growth of the applied voltage to its nominal value can make the capacitor generate current impulses.

Capacitors having relatively high electrical conductivity in the dielectric act as sources of a measurable noise even in the steady state, when the electric field strength in the dielectric is constant. The distribution of the intervals between two subsequent impulses $w(\tau)$ follows an exponential

law:

$$w(\tau) = \lambda \exp(-\lambda\tau) ,$$

where λ is the mean value of the impulse frequency.

We have found a similar shape of the distribution of the current impulses time separation also in ceramic capacitors.

We have studied the properties of PVC foils, too. We discovered that the noise voltage measured by a selective nanovoltmeter behaves as follows: after having surpassed a critical voltage U_C the noise voltage grows proportionally to the difference $\Delta U = U - U_C$, where U is a voltage applied to the capacitor. The shape of the mentioned dependence is apparent in Fig.3 for a TC 219 capacitor which has been measured in a quasi-stationary regime. At a voltage which is approximately twice the critical one ($U_M = 2U_C$) a saturation of the noise voltage appears. At a subsequent decrease of the applied voltage from the value U_M the noise voltage is equal to the apparatus background only. Several samples appeared to make a source of the noise even at a low external electrical field strength, as is seen from Fig.4.

DISCUSSION AND CONCLUSION

Partial discharges make a source of random current impulses and cause charging of the dielectric. The partial dicharge generation is a non-deterministic process. Its stochastic nature is evidenced by the exponential distribution of the impulse time separation as well as an exponential amplitude distribution.

REFERENCE

[1] L.F. Pender, H.J. Wintle: J.Appl.Phys., 50 (1), 361,(1979)

SESSION 6

NOISE IN BIOLOGICAL SYSTEMS AND MEMBRANE NOISE

10th Int.Conf. on Noise in Physical Systems
1989 Budapest, Hungary

EXCITABILITY AND CHANNEL KINETICS IN THE FREE-RUNNING MEMBRANE

L.J. DeFELICE

Department of Anatomy and Cell Biology, Emory University
Atlanta, Georgia 30322, USA

Introduction

The problem addressed here is how action potentials in nerve, heart, and other excitable tissues are related to the time-variant and voltage-dependent kinetics of ion channels in the membranes of these cells. Another way to state this question is: how do channels function in unclamped, free-running membranes? In free-running membranes, the voltage changes during action potentials and when the membrane is at rest. When channels open and close, the local voltage changes. Other channels sense this voltage, change their kinetics, and open or close accordingly. The extent to which channels will sense other channels depends on channel density, lipid bilayer capacitance, and intracellular and extracellular resistivity. In this chapter we will be dealing with the relatively simple problem of a space-clamped membrane in which the potential is the same everywhere.

The usual approach to the above question is to first describe the ionic currents under voltage clamp (Hodgkin & Huxley, 1952). For purposes of discussion we will consider only Na and K currents. The procedure is to apply voltages to (1) a space-clamped axon under conditions that (2) separate currents so only one type of current is being measured. (3) Apply a series of voltage steps that span the normal range of the action potential and record the currents at each step. (4) Build a model that describes the time-variant, voltage-dependent kinetics of the particular current being measured, and (5) repeat the process for each current. Having a model for each current allows us to combine them in their natural ratio and to predict the action potential. We are also able to calculate the time course of each current during the action potential. These are called the action currents.

The macroscopic models can also be used to predict the inherent voltage noise, current noise, and single-channel kinetics if we make certain interpretations. This part of the theory has been described elsewhere (Clay & DeFelice, 1983; DeFelice & Clay, 1983). The predictions are, however, not exclusive, thus if we want to know the properties of individual channels, we have to measure them.

Since it is impossible to measure current under voltage clamp and voltage under current clamp at the same time and place, the above procedure is the only way we have of finding the action currents. We do not have to apply steps, necessarily, but we do have to go through the modeling procedure. Brennecke & Lindemann (1974) got around this limitation by measuring the current and voltage at nearly the same time using a fast switching technique. However, their method has not been used to record action currents but to avoid using two electrodes in traditional voltage-clamp experiments.

Methods

Here we demonstrate another method of finding the action currents that relies on single-channel data obtained during the action potential. The channel currents are from a small patch of membrane. We assume that the membrane outside the patch experiences uniform potential, so one of the critical limitations is (1) knowing the voltage at the patch, a version of the space-clamp problem. We are in a better position, however, to (2) separate currents, because at the single-channel level we exclude, by inspection, patches that contain more than one kind of channel. However, the possibility of small unresolved channels always exists. (3) No voltage protocols are necessary because the voltage is driven by the cell, and (4) no model is needed because the average behavior over many action potentials automatically includes open-channel currents, channel kinetics, and dynamic open-close probabilities, however complicated. (5) Repeating the measurements for each category of channel contributing to the voltage is essential, and we assume all channels of a type to be independent and identical. If not, there should be enough channels in the patch to represent their interdependent, average properties.

To describe the new method, we imagine one Na channel in a cell-attached patch on a spontaneously beating heart cell. The Na channel density in most cells makes the presence of only one Na channel in a typical patch highly unlikely, but extending the argument to more channels is straightforward. The average Na current in the patch, $\langle i_{Na}(t) \rangle$, is a miniature version of the Na action current through the corresponding Na channels outside the patch. The time integral of the Na action current, scaled by channel density and membrane capacity, is the contribution of Na to the action potential (DeFelice, 1983; DeFelice & Levi, 1984).

Not only ionic current but capacitive currents and leak currents also flow through the patch. In the case of Na, this subtraction is crucial because the Na action current and the capacitive transient overlap. Wellis et al. (1989) devised a procedure to remove these background currents in the patch:

$$c[dV(t)/dt] + gV(t) + i_o$$

The first term is the capacitive current; the second is a passive, linear leak, and the third is an offset current. By fitting these terms to a region of the action potential that does not include the Na current, and by extrapolating back into Na domain, Wellis et al. were able to separate the Na

current from the capacitive current. In the following discussion we assume that the capacitive and leak currents have been subtracted.

Theory

We assume that:

$$C(dV/dt) + \Sigma I_i(t) = 0$$

where the first term is the capacitive current through the cell, and the second term is the sum of all the ionic currents. $V(t)$ is the cell action potential. We assume that the equation holds, for example, in small, spontaneously beating heart cells isolated in tissue culture. Since we are considering only Na and K currents, the equation becomes:

$$dV = -(I_{Na}/C)dt - (I_K/C)dt$$

If other currents are present, they simply add to the above expression. The macroscopic currents, I, depend on voltage and change with time. They are composed of the individual ionic currents according to:

$$I(V(t)) = N * i(V(t)) * p(V(t),t))$$

where N is the total number of channels of a certain kind. This formula expresses the prevailing view of channels: on the time scale we are interested in, N is a constant; the open-channel current, i, depends on voltage (and varies with time only if the voltage does); and the open-channel probability, p, has an explicit dependence on time as well as voltage. Examples would be:

$$i(V) = \gamma(V-E)$$

and

$$p(V, t) = e^{-\beta t}/(e^{-\beta t} + e^{-\alpha t})$$

where γ is the single channel conductance (which may or may not depend on voltage), V is the transmembrane voltage, E is the channel reversal potential (which we normally assume to be constant), and α and β are rate constants that depend on V. The membrane is unclamped, thus i, α, and β are parametric functions of time (see Clay & DeFelice, 1983, for more detailed models).

For our purposes we consider only the average value of $i * p$ over many beats, thus:

$$avg\ [i(V(t)) * p(V(t),t)] \equiv \langle i \rangle$$

thus

$$I = N\langle i \rangle$$

where $\langle i \rangle$ is the measured average current through a particular kind of channel. Using this notation for average current, and integrating the above expression for dV, gives an equation for the action potential in terms of the currents:

$$V(t) = -(N_{Na}/C)\int_0^t \langle i_{Na}(u) \rangle du - (N_K/C)\int_0^t \langle i_K(u) \rangle du$$

where u is a dummy variable of integration, and we set the constant of integration, V(0), to

zero. Rewriting the expression as:

$$V(t) = V_{Na}(t) + V_K(t)$$

defines the contribution of each ion pathway to the potential: V_K is the part due to K, V_{Na} is the part due to Na, and so on for other currents. Thus:

$$V_{Na}(t) = -(N_{Na}/C)\int_0^t \langle i_{Na}(u)\rangle du$$

$$V_K(t) = -(N_K/C)\int_0^t \langle i_K(u)\rangle du$$

The integrands are measurable quantities, and the formulas determine the relative proportion of Na and K to the action potential through the constants scaling factors N/C.

Examples

So far we have considered the action potential as if it were a voltage protocol. If ion conductances were strictly voltage-dependent, the currents from spontaneously beating cells and action potential-driven cells would be identical. In simple cases we expect exact correspondence, but if factors besides voltage regulate channels, there may be only a qualitative relationship between voltage clamp currents and action currents.

As a first example, consider a highly simplified squid axon membrane that contains one K channel and one Na channel. This situation is illustrated in Fig. 1.

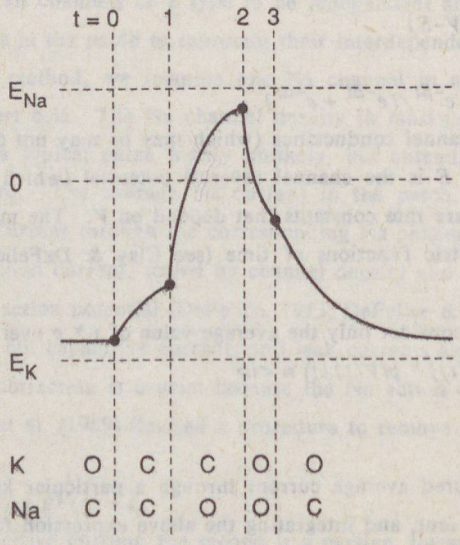

Fig. 1 A qualitative representation of current and voltage in a membrane containing a leak conductance, which is always open, and one K and one Na channel that open and close at different times (adapted from DeFelice et al., 1989).

At t = 0 the K channel has been in the open state for a long time, and the voltage is given by the solution to the equation:

$$C(dV/dt) + \gamma_L V + \gamma_K(V - E_K) = 0$$

which, evaluated at t = 0, gives:

$$V = \gamma_K E_K/(\gamma_L + \gamma_K)$$

Solving similar equations for the various states of the two channels gives the following results (the leak channel is always open): At t = 0 the K channel closes and the voltage decays toward zero according to:

$$V(t) = E_K\gamma_K/(\gamma_L + \gamma_K) * \exp(-\gamma_L t/C)$$

At t = 1 the Na channel opens and the voltage decays toward:

$$V = E_{Na}\gamma_{Na}/(\gamma_L + \gamma_{Na})$$

with time constant:

$$\tau = -C/(\gamma_L + \gamma_{Na})$$

At t = 2 the K channel opens and the voltage decays toward:

$$V = (\gamma_K E_K + \gamma_{Na}E_{Na})/(\gamma_L + \gamma_K + \gamma_{Na})$$

with time constant:

$$\tau = - C/(\gamma_L + \gamma_K + \gamma_{Na})$$

At t = 3 the Na channel closes and the voltage heads toward its original value. The voltage in Fig. 1 is a primitive action potential composed of two channels and a leak conductance.

In Fig. 2 we created an excitable membrane from a probabilistic interpretation of the Hodgkin-Huxley equations (see Clay and DeFelice, 1983; DeFelice and Clay, 1983). 500 Na channels and 50 K channels are placed in 1 um^2 of membrane and allowed to free-run. The result of these calculations in a reduced Hodgkin-Huxley model, in which the Na kinetics are *mh* and the K kinetics are *n*, is spontaneously active. The diastolic depolarization represents random openings of Na channels which, upon reaching a critical value, cause the precipitous opening of Na and K channels that generate action potentials. Since the number of channels is relatively small, the action potentials are stochastic. Figure 3 shows the same calculation for a cm^2 of membrane using the same model: the action potentials are the same shape, and they appear with regular frequency.

No experiments on Na or K action currents exist for nerve membranes; however, a series of articles using the action potential patch clamp have appeared (Fischmeister et al., 1984; Levi & DeFelice, 1986; Mazzanti & DeFelice, 1987a,b; Mazzanti & DeFelice, 1988; Wellis et al., 1989). Figures 4 and 5 plot results adapted from these experimental papers.

Figure 4 shows an action potential (upper trace) from spontaneously beating 7-day chick ventricle cell isolated in tissue culture. The Na action current (leak and capacitive current subtracted) is shown on an expanded time scale below. In this experiment the dynamic reversal potential for the Na current was 8.4 mV, which gives an outward component of the Na current following the upstroke of the action potential. The inset in Fig. 4 is the expected Na action

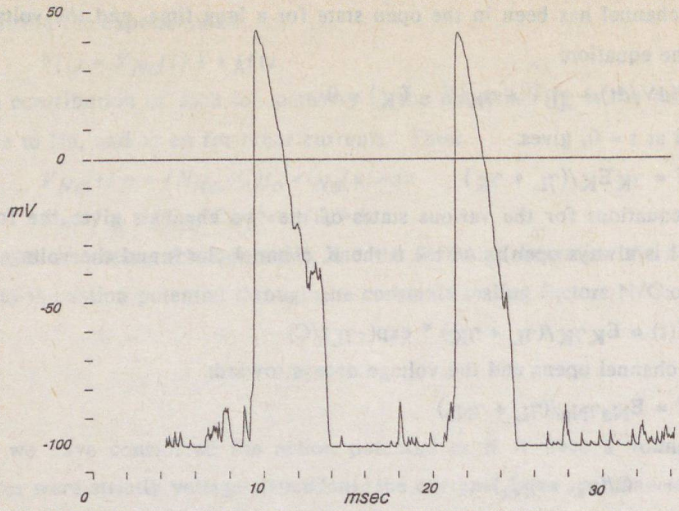

Fig. 2. Simulated action potentials constructed by using 500 Na channels and 50 K channels, whose properties are interpreted from a reduced version of the Hodgkin & Huxley model in which the Na channels are governed by *mh* kinetics and the kinetics channels by *n* kinetics (see DeFelice et al., 1986, for details).

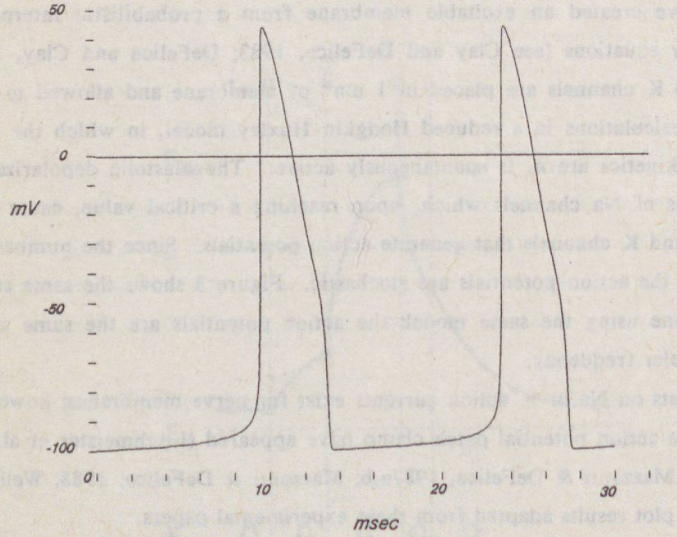

Fig. 3. A simulated action potential using a very large number of Na and K channels in the same proportion as in Fig. 2.

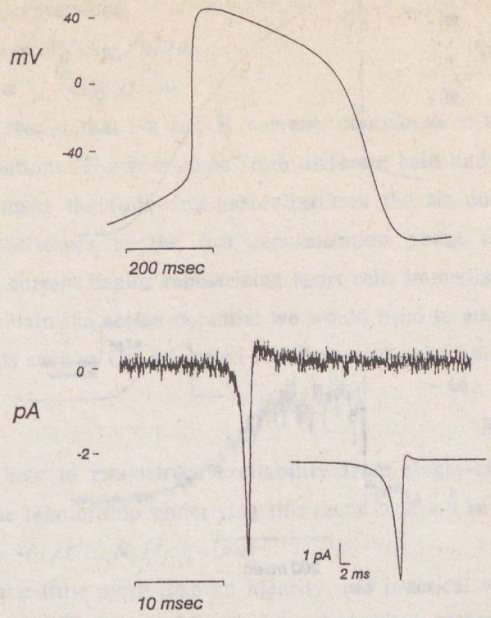

Fig. 4. The Na action current during a heart beat with normal Na concentrations in the bath and the patch pipette (see Wellis et al., 1989, for more details). The inset is a calculation of the expected Na action current from the Ebihara & Johnson (1980) model adapted to our approximate experimental conditions: 24°C and a dynamic reversal potential for Na of of 10 mV (courtesy of W. N. Goolsby).

current from the Ebihara-Johnson model with a Na reversal at 10 mV, the approximate experimental value; a substantial outward current exists in agreement with experiment. The inverted integral of the Na action current in Fig. 4, multiplied by a scaling factor, N_{Na}/C, is the voltage the Na current contributes to the action potential.

Figure 5 shows an action potential (upper trace) from spontaneously beating 7-day chick ventricle cell isolated in tissue culture. (It is not identical to the action potential in Fig. 4, which is consistent with the development stage of our preparation.) The K action current (leak and capacitive current subtracted) is shown on the same time scale below. In this experiment the dynamic reversal potential for the K current was -75 mV. Although the voltage during the action potential dips below this value, there is virtually no inward current through the pathway because the open-channel probability is essentially zero at these times. The inset in Fig. 5 is the expected K action current from the Shrier-Clay model with the K reversal potential at -75 mV. The inverted integral of the K action current in Fig. 5, multiplied by a scaling factor, N_K/C, is the voltage the K current (in this case the delayed-rectifier) contributes to the action potential.

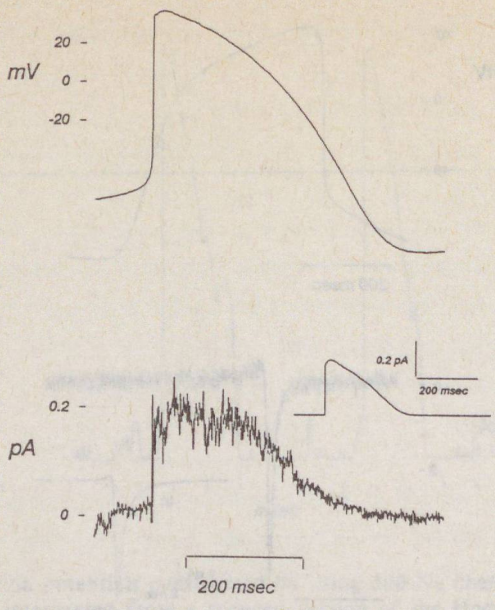

Fig. 5. The K action current during a heart beat with normal K concentrations in the bath and the patch pipette (adapted from DeFelice et al., 1989). This K current is the delayed-rectifier. The inset in the lower right hand corner is a calculation of the expected K action current from the Shrier & Clay (1987) model adapted to our experimental conditions (courtesy of W. N. Goolsby).

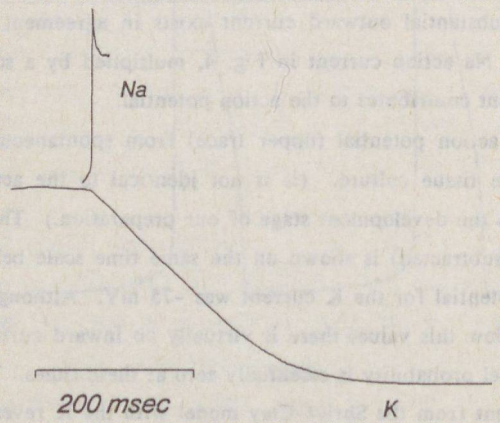

Fig. 6. The time integrals of the Na and K action currents shown in Figs. 4 and 5, inverted and normalized to the same nominal value (adapted from Wellis et al., 1989 and DeFelice et al., 1989).

Figure 6 shows the expressions

$$V_{Na}(t) \propto -\int_0^t \langle i_{Na}(u) \rangle du$$

$$V_K(t) \propto -\int_0^t \langle i_K(u) \rangle du$$

in which we see the *shapes* that Na and K currents contribute to the action potential, but not their absolute contributions. The data come from different cells and are not strictly comparable, nevertheless we can make the following generalizations: the Na current depolarizes heart cells but unexpectedly contributes to the fast repolarization phase following the upstroke; the (delayed-rectifier) K current begins repolarizing heart cells immediately after the upstroke at its maximum rate. To obtain the action potential we would need to add these two wave forms, and those of other currents such as Ca, all scaled for channel density and membrane capacitance.

Summary

We have shown how to reconstruct excitability from single-channel data obtained during action potentials. The relationship underlying this reconstruction is:

$$V(t) = -(1/C)\Sigma_i N_i \int_0^t \langle i(u) \rangle dt$$

This equation, which is little more than an identity, has practical value since $\langle i(u) \rangle$ is directly measurable. Ultimately we wish to relax the assumptions of uniform channel density and non-propagating membrane potentials. We will eventually consider propagation by extending the calculations to saltatory conduction between channels, where patches of channels may be separated by regions of low channel density. In this way we hope to form a complete picture of excitability and channel kinetics in the free-running membrane.

Acknowledgements

We wish to acknowledge the National Institutes of Health (1-PO1-HL27385) for supporting this work. This article is equivalent to the author's contribution to a chapter co-authored with Dr. Rodolphe Fischmeister to be published in French. We are grateful to Dr. Isabelle Gourdon for critical reading of the manusript.

References

Brennecke R, Lindemann B (1974) Theory of a membrane voltage clamp with discontinous feedback through a pulsed current clamp. Rev Sci Instr 45:184-188

Brennecke R, Lindemann B (1974) Design of a fast voltage clamp for biological membranes using a discontinous feedback. Rev of Sci Instr 45: 656-661

Clay JR, DeFelice LJ (1983) Relationship between membrane excitability and single channel open-close kinetics. Biophys J 42:151-157

DeFelice LJ (1983) Reconstructing action potentials from channel fluctuations. Am Physical Soc Symposium on *Noise in Biophysical Systems* Los Angeles

DeFelice LJ, Clay J (1983) Membrane channel and membrane potential from single-current kinetics. In: *Single-Channel Recording*, Sakmann B, Neher E (eds) Plenum Press, New York)

DeFelice LJ, Levi R (1984) Reconstructing the cardiac action potential from single-channel kinetics. IUPAB 8th International Biophys Congress Bristol

DeFelice, LJ, Goolsby WN, Huang D (1986) Membrane noise and excitability. In *Noise in Physical Systems*, D'Amico A, Mazzetti, P (eds) Elsevier, New York

DeFelice LJ, Goolsby WN, Mazzanti M (1989) K channels and the repolarization of cardiac cells. In *Embryonic Origins of Defective Heart Development*, Kirby M, Bockman D (eds) Annals NYAS (accepted)

DiFrancesco D, Noble D (1985) A model of cardiac electrical activity incorporating ionic pumps and concentration changes. Phil Trans (Royal Soc) B307:353-398

Ebihara L, Johnson EA (1980) Fast Na current in cardiac muscle. Biophys J 32:779-790

Fischmeister R, DeFelice LJ, Ayer RK, Jr, Levi R, DeHaan RL (1984) Channel currents in embryonic chick heart cells. Biophys J 46:267-272

Hodgkin AL, Huxley AF (1952) A qualitative description of membrane current and its application to conduction in nerve. J Physiol 117:440-544

Levi R, DeFelice LJ (1986) Na-conducting channels in cardiac membranes in zero Ca. Biophys J 50:11-19

McAllister RE, Noble D, Tsien RW (1975) Reconstruction of electrical activity of cardiac Purkinje fibres. J Physiol 251:1-59

Mazzanti M, DeFelice LJ (1987a) Regulation of the Na-conducting Ca channel during the cardiac action potential. Biophys J 51:115-121

Mazzanti M, DeFelice LJ (1987b) Na channel kinetics during the spontaneous heart beat in chick ventricle cells. Biophys J 52:95-100

Mazzanti M, DeFelice LJ (1988) K channel kinetics during the spontaneous heart beat in chick ventricle cells. Biophys J 54:1139-1148

Mazzanti M, DiFrancesco D (1989) Intracellular Ca modulates K-inward rectification in cardiac myocytes. Pflug Arch 413:322-324

Shrier A, Clay J (1987) Repolarization currents in embryonic chick atrial heart cell aggregates. Biophys J 50:861-874

Wellis D, DeFelice LJ, Mazzanti M (1989) An outward Na current in beating cells Biophys J (submitted)

10th Int.Conf. on Noise in Physical Systems
1989 Budapest, Hungary

NOISE SPECTRA OF A KINETIC MODEL OF CHANNEL GATING, BASED ON AN ELECTRORHEOLOGICAL MODEL OF THE PHYSICAL PROCESS

M.E. GREEN

Department of Chemistry, City College of the City University of New York
New York N. Y. 10031, USA

I. INTRODUCTION

A model for ion-channel gating (Green, 1989), involves (1) protein motion, (2) water in the "vestibule" region of the channel. This water is considered to be "frozen" (by an electroviscous effect) when the channel is closed, "unfrozen" when open. A kinetic model based on this physical idea has one "inactivated" state for each "closed" state. Water may be effectively "frozen" in different orientations in closed and inactivated states. The model therefore has two closed, two inactivated, and one open state.

Noise power spectra come from the kinetic model; its limitations include: (1) with several parameters, a range of spectra is consistent with the model (2) additional physical assumptions are incorporated in the choice of values (3) the physical model may, upon revision, allow for other states.

Some kinetic models in the literature are derived from physical ideas or physiological data; best known is the Hodgkin-Huxley (1952) model, for which, assuming linearity at constant voltage (as we will), Chen and Hill (1972, 1973), and Stevens (1972), determined the noise spectra.

Experimental noise spectra have been reported, primarily for nerve and epithelia, by, among others, Siebenga et al. (1973), Conti et al. (1975), van den Berg et al. (1977), Zeiske and van Driessche (1983), Lewis et al. (1984). Most experimental spectra show one or two Lorentzian components, and 1/f noise, apparently unrelated to channel gating. The Lorentzian components dominate the spectrum and are reproducible at potentials at which channels can be expected to open and close, especially in the -30 mV to +10 mV range. The overall intensity of the dominant component was typically one to two orders of magnitude greater at these potentials than at strongly polarized potentials; the various measurements covered, generally, 1 Hz to 1 kHz.

II. THE MODEL

A) Description: The kinetic model can be most easily described by reference to Fig. 1, which also shows the twelve non-zero rate constants.

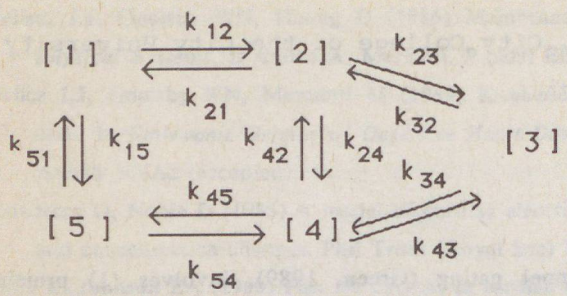

FIGURE 1. Non-zero rate constants for the model: state [3] is open (conducting), [4] and [5] inactivated, and [1] and [2] closed. Protein conformation change corresponds to transitions from states [1] to [2] , and [5] to [4], water rearrangements to the transitions among states [2], [3], and [4]. Rate constants increase to the right with depolarization.

States: [1] Closed, polarized potentials. Protein is in its closed conformation, the water "frozen" (viscous), as determined at least in part by the field.

[2] Closed, less polarized potentials: Protein has had a conformational change.

[3] Open, conducting: Protein is in the same state as [2], water is "unfrozen".

[4] Inactivated, less polarized potentials: Protein about as in [2], with water "refrozen" at low field; mean orientation differs from that in states [1] and [2].

[5] Inactivated, fully polarized potentials: The protein configuration as in state [1] with water like that in state [4]. At sufficiently polarized potentials, transitions back to state [4] should be slow; transitions to state [1] may be difficult, requiring a change in average water orientation, so that state [5] may have a fairly long lifetime (high probability of occupancy).

Protein and water motions are treated independently for kinetic purposes.

B. The rate constants: The 12 rate constants fall into three groups: (1) k_{12}, k_{21}, and k_{54}, k_{45}: rates of voltage dependent protein transitions (2) k_{23}, k_{32} and k_{43},k_{34}: rate of water "unfreezing", "freezing", for closed and inactivated states (3) k_{15},k_{51} and k_{24},k_{42}: direct closed $\rightleftarrows$ inactivated

transitions. Microscopic reversibility requires that rates around each loop in Fig 1 be the same in each direction, leading to eqs (1)

$$k_{12}k_{24}k_{45}k_{51}/k_{21}k_{42}k_{54}k_{15} = 1 \qquad \{1a\}$$

$$k_{23}k_{34}k_{42}/k_{32}k_{43}k_{24} = 1 \qquad \{1b\}$$

Let

$$g = 0.95*sc*(v-v_0)/(v_1-v_0) \qquad (v<v_1) \qquad \{2a\}$$

$$g1 = 0.95*sc1*(v-v_{01})/(v_{11}-v_{01}) \qquad (v>v_{01}) \qquad \{2b\}$$

Set v_0=-100mV, v_{11}=10mV; the scale factors sc, sc1 set the overall rates, while the factors of 0.95 keep the reverse rates from going to zero. Outside the range defined in eqs (2), take g, g1=1. The rate constants in s^{-1}, are: $k_{45}=k_{12}$=g; $k_{54}=k_{21}$=sc-g; $k_{23}=c_{23}$*g1; k_{32}=2*(sc1-g1); $k_{24}=c_{24}$; k_{42}=0.2*k_{24} or 0.002*k_{24}; k_{34}=sc1-g1; k_{43}=0.1*c_{23}*g1 or 0.001*c_{23}*g1; $k_{15}=c_{15}$ or 10*c_{15}; k_{51}=0.2*c_{15} or 0.02*c_{15}. I have examined principally a range of sc, sc1, v_0, and v_{01} values. The values after the "or" must all be used together, and imply slow inactivation; these are used for Fig 2. The c_{ij} are constants.

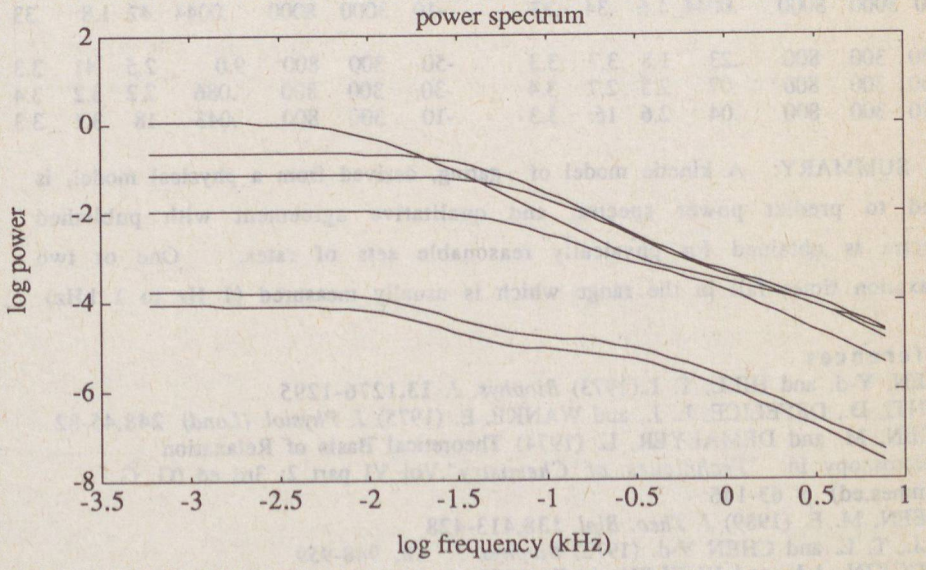

FIGURE 2: Example of power spectra. Parameters: v_1=-30 mV, v_{01}=-60 mV, c_{24}=100, c_{23}=30, c_{15}=10, sc=7000, sc1=700. For these values only 35% of the channels are open at +10mV. Spectra are at 20 mV intervals, from -90 mV, and appear in order of voltage at the lowest frequencies, with -90 mV lowest.

III. CALCULATION OF SPECTRA: The spectra were calculated as in Eigen and de Maeyer (1974). Linear rate equations give the matrix of rates; we diagonalize to obtain the four relaxation times, and calculate the power spectra, adding the sums of squares of the contributions of the four reactions. Computations were done on a MAC II computer, using MATLAB (The Mathworks, Inc). Table I and Fig. 2 show typical results.

TABLE I

Parameters for six cases, three voltages each. The relaxation times found for noise are shown. All are for the case of nearly irreversible inactivation (v_1,v_{01} are the two voltages defining rate constants between states [1], [5], and [2], [4], and between [2], [4], and [3], respectively; voltages are in mV. sc and sc1 are constants used to determine the rate constants: left, v_1=-55, v_{01}=-30; right, -47, -37)

v	sc	sc1	relaxation times (ms)				v	sc	sc1	relaxation times (ms)			
-50	10000	5000	.034	.47	.12	.10	-50	10000	5000	7.6	.10	.066	.10
-30	10000	5000	.012	.44	.10	.10	-30	10000	5000	.014	.39	.13	.10
-10	10000	5000	.0070	.10	2.6	.10	-10	10000	5000	.0069	.13	2.8	.10
-50	3000	8000	.023	.55	.20	.33	-50	3000	8000	6.8	.32	.04	.33
-30	3000	8000	.0074	.27	.34	.34	-30	3000	8000	.0087	.44	.23	.34
-10	3000	8000	.0044	1.6	.34	.33	-10	3000	8000	.0044	.42	1.8	.33
-50	300	800	.23	1.8	3.7	3.3	-50	300	800	9.0	2.5	.41	3.3
-30	300	800	.07	2.5	2.7	3.4	-30	300	800	.086	2.2	3.2	3.4
-10	300	800	.04	2.6	16.	3.3	-10	300	800	.043	18	3.1	3.3

IV. SUMMARY: A kinetic model of gating, derived from a physical model, is used to predict power spectra, and qualitative agreement with published spectra is obtained for physically reasonable sets of rates. One or two relaxation times fall in the range which is usually measured (1 Hz to 1 kHz).

References

CHEN, Y-d, and HILL, T. L.(1973) *Biophys. J.* **13**,1276-1295

CONTI, D., DEFELICE, L. J., and WANKE, E. (1975) *J. Physiol. (Lond)* **248**,45-82

EIGEN, M. and DEMAEYER, L. (1974) Theoretical Basis of Relaxation Spectroscopy in *"Techniques of Chemistry"*,Vol VI part 2; 3rd ed (G. G. Hammes,ed) p 63-146

GREEN, M. E. (1989) *J. Theo. Biol.* **138**,413-428

HILL, T. L. and CHEN Y-d. (1972) *Biophys. J.* **12**, 948-959

HODGKIN, A.L. and HUXLEY, A. F. (1952) *J. Physiol.* (Lond) **117**, 500-544

LEWIS, S. A., IFSHIN, M. S., LOO, D. D. F. and DIAMOND, J. M. (1984) *J. Memb. Biol.* **80**, 135-151

SIEBENGA, E., MEYER, A. and VERVEEN, A. A. (1973) *Pflugers Arch.* **341**, 87-96

STEVENS, C. F. (1972) *Biophys. J.* **12**, 1028-1047

VAN DEN BERG, R. J., SIEBENGA, E., and DE BRUIN, G. (1977) *Nature (Lond)* **265**, 177-179

ZEISKE, W. and VAN DRIESSCHE, W. (1983) *J. Memb. Biol.* **76**, 57-72

SESSION 7

THEORIES OF 1/f NOISE

10th Int.Conf. on Noise in Physical Systems
1989 Budapest, Hungary

SOME RECENT THEORIES OF 1/f NOISE

L.B. KISS

Institute of Experimental Physics, József Attila University
Dóm tér 9, H-6720 Szeged, Hungary

ABSTRACT

A new 1/f noise model (of fractal nature) is presented which does not require any distribution of time-constants and seems to have several applications.

General remarks on some recent models applying distributed time-constants are noted and the correct noise spectrum in the two-dimensional model of self-organized criticality is presented.

1. INTRODUCTION

Most of self-consistent 1/f noise models are based on systems with a large number of elementary fluctuators. Moreover, an appropriate distribution of fluctuator time-constants is required. Although these models have helped to understand the origin of 1/f noise in some special systems, such as surface noise (Uren et al. 1985; Karwath and Schulz 1988; Jäntsch 1987) and some thermally activated bulk 1/f noises (Dutta and Horn 1981), a satisfactory explanation of this phenomenon in most of the observed cases is still missing. Important examples for that are the general 1/f noise phenomena in physical and non-physical systems but, in the author's belief, many 1/f noise

---

Work carried out at: University of Cologne, Institute for Theoretical Physics, Zülpicher-Str. 77, D-5000 Köln, F.R.G.

processes found in the conductance of solids (Hooge this conference; Kleinpenning this conference; Hooge et al. 1981; Kiss 1988) belong to this set.

This talk is organized as follows:

i) We present a possible new frame for 1/f noise models without distributed time-constants.

ii) The results are demonstrated by computer simulations.

iii) Some possible physical and non-physical applications are mentioned.

iv) We make some comments on pictures applying distributed time-constants.

v) As a demonstration, the correct (that is, measured) noise spectrum in the two-dimensional model of self-organized criticality is flashed.

2. TRANSIENT-DIFFUSION 1/f NOISE MODEL

Diffusion, that is, random-walk of independent particles (or that of the value of physical quantities) is a very general process in nature. For that reason, one may conjecture that, in many cases, the origin of the ubiquitous 1/f noise is the general occurrence of the random walk.

On Diffusion Noise

Diffusion noise theories (Richardson 1950; van Vliet and Fassett 1964) were the first attempts to explain conductance 1/f noise by a stationary diffusion. To see what the stationary diffusion noise is, imagine a great number of particles which can freely (and independently) diffuse in the space (disregarding whether they are in

the sample or not) with a diffusion constant D . A particle may influence the sample resistance R through a coupling function $K(\underline{r})$, where $\underline{r}$ is the coordinate of the particle and $K(\underline{r})$ is determined also by the geometry of the sample. In the stationary limit, where the particles are uniformly distributed in the space (including also the sample volume), the "noisy" diffusion equation holds (Richardson 1950):

$$\partial c(\underline{r},t)/\partial t = D \nabla^2 c(\underline{r},t) + z(\underline{r},t) \quad , \qquad (1)$$

where $c(\underline{r},t)$ is the instantaneous concentration fluctuation and $z(\underline{r},t)$ is a delta-correlated random driving term. The spontaneous concentration fluctuation is transformed in a resistance fluctuation R(t) due to the coupling:

$$R(t) = \int c(\underline{r},t)\, K(\underline{r})\, d\underline{r} \quad . \qquad (2)$$

The power density spectrum $S_R(f)$ of the resistance noise can be obtained by calculations based on (time-space) Fourier transformation.

While practical 1/f noises seem to be unexplainable in terms of this stationary diffusion noise theory, an interesting result is obtained for the simplest case where $K(\underline{r})$ is a "theta-function" (Van Vliet and Fassett 1964). This is the universal (geometry-independent) $f^{-3/2}$ law in the high-frequency limit:

$$S_R(f) \propto f^{-3/2} \qquad (3a)$$

for frequencies higher than the reciprocal diffusion times through the sample, provided:

$K(\underline{r})=K$, if the particle is in the sample; (3b)

$K(\underline{r})=0$, if the particle is out of the sample. (3c)

At the sufficiently low frequency limit, this theory predicts a white spectrum.

We note that, regarding a frequency-independent multiplication factor (in the order of 10^{10}), there is a contradiction between experiments on superionic conductors and this simple theory, as it was shown by Dr. Brophy, at this conference. To solve this discrepancy, one should perhaps notice that this strong noise may be interpreted in terms of the random-walk of the height of potential barriers rather than the random-walk of ions.

Transient-Diffusion 1/f Noise (Kiss and Hajdu 1989)

Consider N independent particles executing one-dimensional discrete random-walks $x_n(t)$, $(n=1,2,\ldots,N)$, with step length l , waiting time T_0 , and initial conditions $x_n(0)=x_{n0}$. Assume that the motion $x_n(t)$ is coupled to the time-dependent part of an observed physical quantity R(t) by:

$$R(t) = \mathbf{N}(t)R_0 \quad , \tag{4}$$

where $\mathbf{N}(t)$ is the number of particles having, at time t, their initial positions x_{n0} . The function $\mathbf{N}(t)$ is a non-stationary series of pulses with random heights and random initial times. In the limit $N\to\infty$ and $t >> T_0$, $\mathbf{N}(t)$ can be expressed by the probability

$$g(X_n,t) = (2\pi Dt)^{-1/2} \exp(-X_n^2/2Dt) \tag{5}$$

of finding a particle with displacement $x_n-x_{n0}=X_n$ at time t , where the diffusion constant is given by $D=l^2/T_0$. Taking $X_n=0$ we get:

$$\mathbf{N}(t) = Ng(t) = (T_0/t)^{1/2}(1/2\pi)^{1/2}N \ . \tag{6}$$

As is well-known (e.g. Ambrózy and Kiss 1986), the $t^{-1/2}$ transient signal yields a 1/f energy density spectrum. Accordingly, the energy density spectrum E(f) of $\mathbf{N}(t)$ is of 1/f shape:

$$E(f) = T_0N^2/4f \ . \tag{7}$$

Regarding the validity of Eq.(7), an obvious upper frequency limit is given by:

$$f_2' = 1/T_0 \qquad (8)$$

due to the limitation of the diffusion approximation and Eqs (5)-(6). Another, possibly more restrictive condition for the upper frequency limit f_2 originates from the fact that, for a given frequency f and a noise sample of duration t_o , Eq.(7) is only valid as long as the total number of pulses within the Fourier time period 1/f is large compared to unity, even at the end of the noise sample : $(1/f)(N/T_0)(T_0/t_o)^{1/2} >> 1$. Thus, we get:

$$f_2 = (T_0/t_o)^{1/2}N/T_0 = (T_0/t_o)^{1/2}Nf_2' \quad . \qquad (9)$$

In other words, at $f=f_2$, the phase variance of the pulses exceeds π and a white noise spectrum sets in, for $f > f_2$, due to Campbell's theorem. This white noise energy spectrum is in accordance with the stationary diffusion noise theory (Van Vliet and Fassett 1964) for a sample of length 1 . However, in a fixed frequency range, the 1/f spectrum obtained by this transient diffusion phenomenon can be preserved by assuming that the particle number decays in the long time limit. If, for example,

$$N(t) = N\cdot\exp(-t/T) \quad , \qquad (10)$$

we get (by replacing in Eq.(9) t_o by T)

$$f_2 = (T_0T)^{-1/2}N \quad . \qquad (11)$$

However, Eq.(10) obviously implies that the 1/f spectrum will have also a low-frequency cut-off at

$$f_1 = 1/T \quad . \qquad (12)$$

Consequently, the number of decades of the 1/f spectrum is given either by

$$f_2'/f_1 = T/T_0 \quad , \qquad (13)$$

or by: $f_2/f_1 = (T/T_0)^{1/2}N$. (14)

It is interesting to note that, in the infinite T limit, Eqs (13)-(14) predict an infinite number of decades of 1/f spectrum, even in the one-particle limit.

Till now, we dealt with the energy density spectrum of the diffusion transient (Eqs (4), (6)). To get a stationary noise with 1/f power density spectrum, we apply Campbell's theorem. Let us now consider, instead of one N-particle random-walk process, a set of independent processes of this kind: $x_{kn}(t)$; $n=1,\ldots,N_k$; with initial conditions $x_{kn}(t_k)=x_{kn0}$, where the set of initial times t_k is an ordered random time series generated by a Poisson process of rate ν. Then, according to Campbell's theorem the sum of these processes is a stationary noise process with a 1/f power density spectrum, in the range $f_1 < f < f_2$ (or f_2') :

$$S(f) = \nu \; <E(f)> \; = (\nu T_0/4) <N_k^2> (1/f) \quad . \qquad (15)$$

Obviously, the physical quantity R(t) coupled to N(t) (Eq.(4)) has also a 1/f noise spectrum $S(f)R_o^2$.

It is interesting to note that according to Mandelbrot (1977) the set of time instants at which a random-walk occupies its initial position (so-called "zero-set") is a fractal. That is, this model is a 1/f noise model of fractal nature which may turn out to be interesting to study.

3. COMPUTER SIMULATIONS

In the paper describing the transient-diffusion 1/f noise model (Kiss and Hajdu 1989), we presented some results obtained from computer simulations, which illustrate the above results. (We have flashed the relevant figures at the oral presentation of this material at this conference, but we do not publish the figures here, only outline the results).

In our paper we presented some energy density spectra obtained by simulations for N=100 and N=1 , respectively. The total length of the

processes, t_o/T_0 or T/T_0 , was choosen to extend over 1500 steps. Correspondingly, the Fourier limitation of the total range of investigation was 1/1500 . For N=100 the range of the 1/f noise was limited by this Fourier limit, that is, by the duration of the simulation. However, for N=1 , it is limited also by the small particle number and above f=40 a white spectrum sets in, in accordance with Eq.(9) .

As a function of the dimension d=1,2,3 the random process (4) and Eq.(5) yield $1/t^{d/2}$ transients. Consequently, for d=2,3 a spectrum less steep than 1/f is expected. Computer simulations clearly indicate that, under our conditions, the transient existing at d=1 has not only the highest energy but also the highest energy density at low frequencies to provide a 1/f spectrum.

Finally, regarding computer simulations, I would like to note that natural antecedent of our model were the computer simulations of coordinate-transformed random-walks (with symmetrized power-function transformation) carried out by Gingl and coworkers (1989, and this conference). In that case, the 1/f spectrum data have a rather small scattering which is useful at 1/f noise generation (Ambrózy et al., this conference).

4. APPLICATIONS

A typical application of the transient-diffusion model is the diffusion of some kind of defects created at the surface of a three-dimensional sample into the bulk of the sample. This random-walk process gives rise to a 1/f noise in the resistance since the difference between the surface and the bulk scattering contributions is proportional to the number **N**(t) of defects at the surface and Eqs (4)-(7) apply. (The one-dimensional random-walk coordinate $x(t)-x_0$ is the distance of the defect from the surface). It is interesting to note that for ionized defects **N**(t) is proportional to the Debye length L_D , because a surface layer of depth in the order of L_D have to be considered for the surface scattering of the defects. Then, according to Eq.(7), the 1/f noise spectrum is proportional to L_D^2, that is, it

is proportional to the reciprocal concentration of free carriers in the sample. In conclusion, this effect can be a natural explanation of the factor 1/n in the Hooge formula (see Kiss and Kleinpenning 1987). However, the explanation of the factor 1/V, that is, the surface-induced bulk noise, requires the existence of interfaces between small subvolumes within the sample.

A very similar application is to explain the 1/f noise in the heat current flowing from current-carrying metal wires to the environmental gas (Klausgrete and Storm 1985). Then, the gas atoms are executing three-dimensional random-walks into the bulk of the wire and the heat-transfer from the wire to the gas is influenced by the number N(t) of gas atoms at the surface. The one-dimensional random-walk coordinate is the same as above.

Other possible applications are the random-walk of potential levels in solids (Hajdu 1989, Canel 1989). A relevant example is the hopping of particles in a periodic potential coupled to a heat bath (with bosonic or fermionic excitations). The model also applies to fluctuating double-well systems and to chemical reactions triggered by surface contact of supplied reagents. Another application is an explanation how the motion of single defects can lead to a 1/f noise in terms of the Feng-Lee-Stone model (1986) of universal conductance fluctuations (Feng this conference, Forgacs this conference).

Regarding the 1/f noise in music (Voss 1979), one can realize that a piece of music consists of several motifs repeated several times. If the set of time instants of the repetition-beginnings of a given motif has the same statistics as the "zero-set" of a one-dimensional random-walk then this motif gives rise to a low-frequency 1/f spectrum in the pitch and loudness of the music.

5. ON MODELS WITH DISTRIBUTED TIME-CONSTANTS AND NOISE IN THE MODEL OF SELF-ORGANIZED CRITICALITY

There is a wide-spread opinion that the only realistic way of the explanation of the 1/f noise to look for models applying distributed time-constants. It can be seen from the above considerations that this

belief is not correct. The transient-diffusion phenomena considered above seem to be much more general than 1/f noise phenomena with distributed time constants.

Another well-known point is that the 1/T distribution of independent processes of time constant T can give a 1/f spectrum provided:

i) The elementary processes have a Lorentzian (-like) spectrum;

ii) The elementary processes are normalized, that is their power (integral spectrum) is independent of T.

While elementary fluctuations with property i) are generally occurring in nature, those with property ii) can very seldom be found, because the normalization condition is a very strong restriction. This restriction is rather limiting the applicability of "1/T models" based on lognormal distribution (Montroll and Shlesinger 1983; Shlesinger and West 1988). Let us consider two well-known elementary Loretzian signals as examples. **1:** A random telegraph signal is normalized, if its amplitude and filling factor is independent of T. **2:** A sequence of randomly repeated single square-wave pulses (with mean repetition frequency independent of T) is normalized, if the square of the pulse-amplitude is inversely proportional to the pulse-duration (normalized pulse-energy).

As further illustration, we consider two physical examples. **a:** tunnelling between symmetrical potential wells satisfies both conditions i) and ii), and may give rise to a McWorther-type 1/f noise. **b:** A generation-recombination noise originating from distributed traps satisfies condition i) , but does not satisfy condition ii) due to the exponentially varying filling factor determined by the Fermi-Dirac probability of state occupation.

A further, very relevant example is the Bak-Tang-Wiesenfeld model of Self-Organized Criticality (1988) which initiated a new direction in the research of critical phenomena. In this model, the critical state is provided by independent, randomly starting avalanches on

every length-scale and time-scale. Here we shall concern only one point: the noise spectrum. Bak et al. (1988) conclude that "1/f noise is intimately related to the underlying spatial organization". This conclusion is based on an erroneous calculation of the resultant current spectrum of avalanches (incorrect weighting of elementary avalanche spectra). We repeated their computer simulations for the two-dimensional model, moreover, the power density spectrum of the avalanche current was measured (Kertesz and Kiss 1989). Some of the results: the elementary avalanche (energy) spectrum is Lorentzian-like; the time-constant distribution is a power function proportional to $T^{-1.15}$; the total spectrum of avalanches is also a power function (in the critical range), but it is almost a $1/f^2$ spectrum instead of 1/f.

ACKNOWLEDGMENT

I thank Eric Canel, Shecao Feng, Gabor Forgacs, Zoltan Gingl, Janos Hajdu, Janos Kertesz, Theo Kleinpenning and Dietrich Wolf (Cologne) for valuable discussions. The work was supported by the Deutsche Forschungsgemeinschaft (SBF 341, Germany), the OTKA and the FKP (Hungary) foundations.

REFERENCES

Ambrozy A. and Kiss L.B. 1986, Noise in Physical Systems and 1/f Noise-1985, eds. A. D'Amico and P. Mazzetti, North-Holland, Amsterdam

Bak P., Tang C. and Wiesenfeld K. 1988, Phys.Rev.A 38, 364

Canel E. 1989, private communication

Dutta P. and Horn P.M. 1981, Rev.Mod.Phys. 53, 497

Feng S., Lee P.A. and Stone D. 1986, Phys.Rev.Lett. 56, 1960

Gingl Z., Kiss L.B. and Vajtai R. 1989, Sol.State Comm., in press

Hajdu J. 1989, private communication

Hooge F.N., Kleinpenning T.G.M. and Vandamme L.K.J. 1981, Rep.Prog.Phys. 44, 479

Jantsch O. 1987, IEEE Trans.Electr.Dev. ED-34, 1100

Karwath A. and Schulz M. 1988, Appl.Phys.Lett. 52, 634

Kertesz J. and Kiss L.B. 1989, to be published

Kiss L.B. and Hajdu J. 1989, Sol. State Comm., in press

Kiss L.B. and Kleinpenning T.G.M. 1987, Physica 145B, 185

Kiss L.B. 1988, Rev.Sol.St.Sci. 2, 659

Klausgrete D. and Storm L. 1985, Z.Phys. B61 1

Mandelbrot B.B. 1977, Fractals: Form, Chance and Dimension, p.90, Freeman, San Francisco

Montroll E.W. and Shlesinger M.F. 1983, J.Stat.Phys. 32 209

Richardson J.M. 1950, Bell Syst.Tech.J. 29, 117

Shlesinger M.F. and West B.J. 1988, Random Fluctuations and Pattern Growth: Experiments and Models, NATO ASI Series E: Appl.Sci.157, eds. H.E. Stanley and N. Ostrowsky

Uren M.J., Day D.J. and Kirton M.J. 1985, Appl.Phys.Lett. 47, 1195

van Vliet K.M. and Fassett J.R. 1964, in Fluctuation Phenomena in Solids, ed. R.E. Burgess, Academic, New York

Voss R.F. 1979, Proc. of the 33rd Ann. Symp. on Frequency Control, Atlantic City

10th Int.Conf. on Noise in Physical Systems
1989 Budapest, Hungary

SIMULATION OF 1/f NOISE

K. ANTON, D. WOLF

Institut für Angewandte Physik der Universität Frankfurt
Robert-Mayer-Str. 2-4, D-6000 Frankfurt/Main, FRG

A special stochastic process has been investigated which yields an 1/f-spectrum over a wide range of frequency f. This process introduced by Ambrozy [1] is generated by Gauss-Poisson square-waves (GPSW) with an autocorrelation function $\Psi(\vartheta) = \Psi_0 e^{-2|\vartheta|/\tau_0}$ and a Lorentzian spectrum

$$S(\omega) = \frac{4\Psi_0\tau_0}{4+(\omega\tau_0)^2} \quad , \omega = 2\pi f \, , \tag{1}$$

where Ψ_0 is the second moment of the amplitude distribution. The GPSW is a process with Gaussian amplitude distribution and Poisson distributed zero-crossings.
The 1/f-spectrum results [1-3] from replacing the time constant τ_0 by the variable τ obeying a specific distribution function of time constants τ. Two distribution density functions

$$p_1(\tau) = \frac{1}{\ln(\tau_2/\tau_1)\,\tau} \quad , \tau_2 \geq \tau \geq \tau_1 > 0 \, , \tag{2}$$

and

$$p_2(\tau) = \frac{e^{-\beta\tau}}{Ei(\beta\tau_1)\,\tau} \quad , \qquad \tau \geq \tau_1 > 0 \tag{3}$$

were considered. Ei denotes the exponential integral and $1/\beta$ a specific time constant. The resulting power spectra are

$$S_1(\omega) = \frac{4\,\Psi_0}{\omega \ln(\tau_2/\tau_1)} \left(\arctan(\omega\tau_2) - \arctan(\omega\tau_1)\right) \tag{4}$$

or

$$S_2(\omega) = \frac{4\,\Psi_0}{Ei(\beta\tau_1)\,\omega} \left(Ci(2\beta/\omega)\sin(2\beta/\omega) - si(2\beta/\omega)\cos(2\beta/\omega)\right) \, , \tag{5}$$

resp. Spectrum Eq.(4) obeys an 1/f-law if $\omega\tau_1 \ll 1 \ll \omega\tau_2$, while the second one Eq.(5) shows the 1/f-characteristic in the range $\omega > 2\beta/100$ up to infinity. The 1/f-range of these spectra can be varied by changing the parameters τ_1 and τ_2 and the mean $E\{\tau\}$ of time length τ.

Both processes were implemented on a computer system and analysed experimentally in simulations. The block diagramm in Figure 1 illustrates the generating procedure of the process.

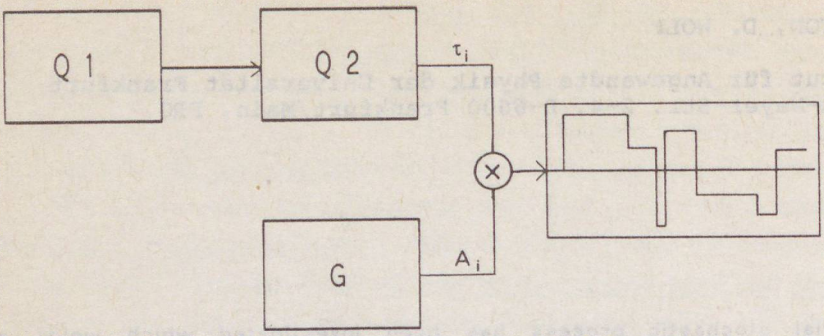

Figure 1 *Block diagram for generating the process*

Q2 is a random source with exponential distribution density while Q1 generates random numbers with density function p_1 or p_2 . The influence of Q1 causes a variation of the parameter of the exponential density of Q2.The amplitude of the process is determined by white Gaussian noise (G). Figure 2 shows a typical section of the signal.

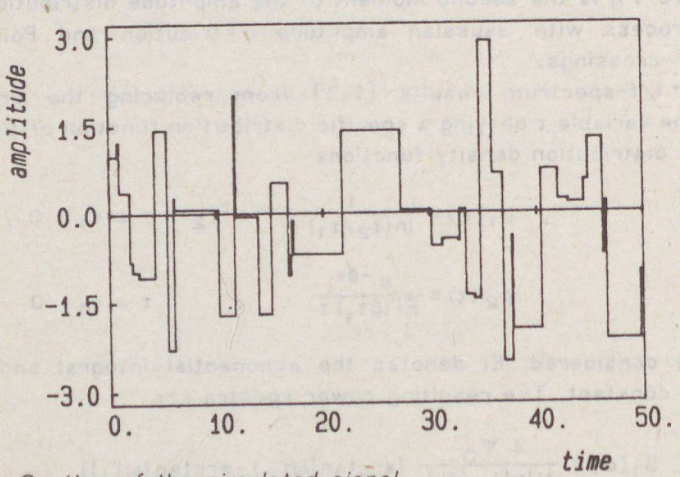

Figure 2 *Section of the simulated signal*

Applying Carson's Theorem the signal analysis was based on the measurements of the distributions of the signal amplitudes and of the time-lengths τ. From these results the power spectra were evaluated .
Some of the calculated and measured spectra with different parameters are shown in Figure 3-5. The solid lines show the theoretical curves while the experimental results are indicated by the symbols (+++). The parameter x is the ratio $x=\tau_2/\tau_1$.

Figure 3

Spectrum S_1 with $x = 10^{10}$ and $E\{\tau\} = 1$

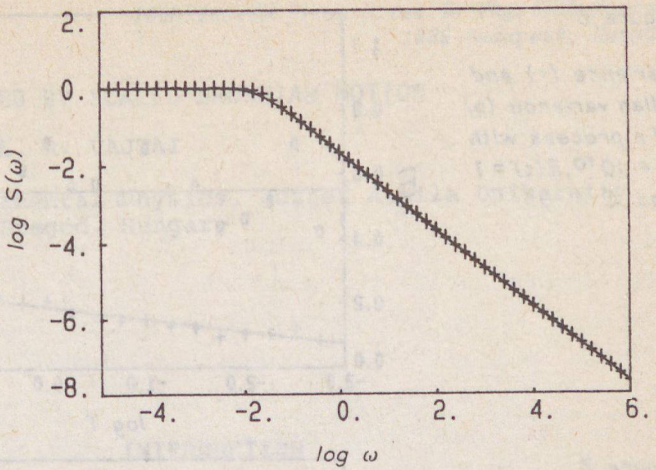

Figure 4

Spectrum S_1 with $x = 10^{18}$ and $E\{\tau\} = 100$

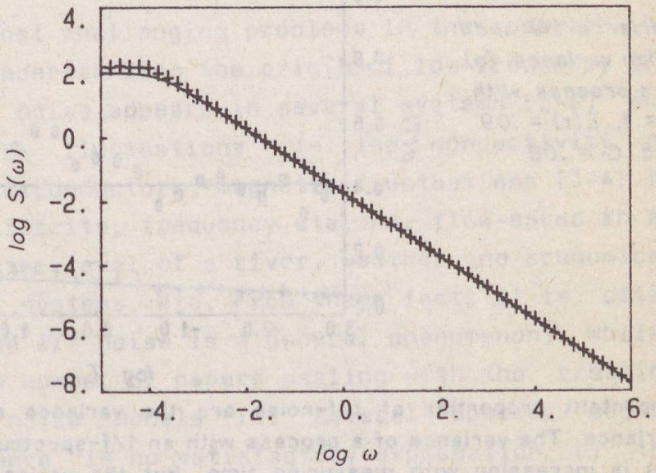

Figure 5

Spectrum S_2 with $\beta = 1$, $\tau_1 = 10^{-5}$ and $E\{\tau\} = .09$

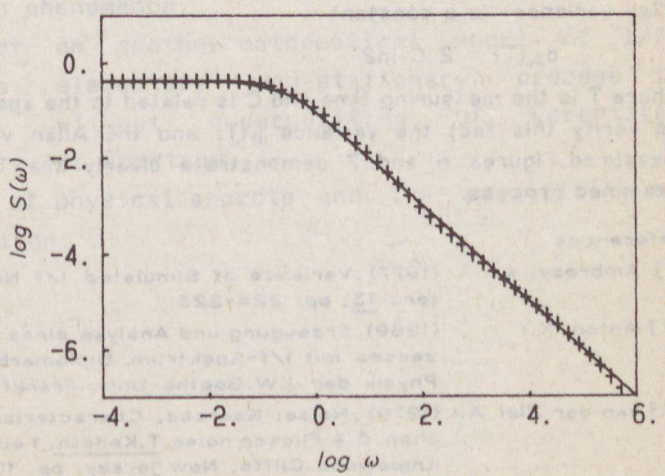

Figure 6

Variance (+) and Allan variance (o) of a process with $x = 10^{10}, E\{\tau\} = 1$ and $C = .05$

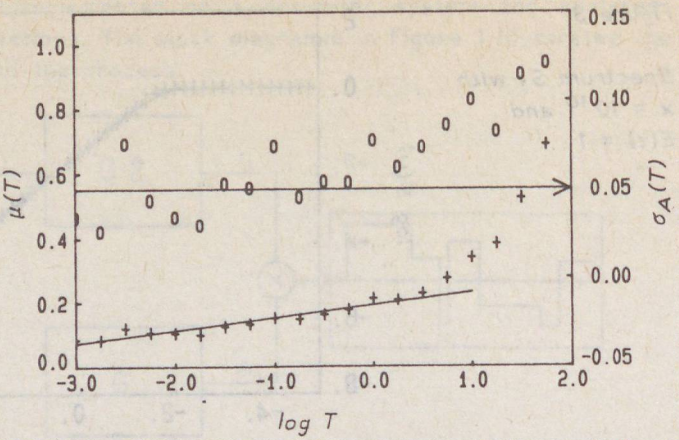

Figure 7

Variance (+) and Allan variance (o) of a process with $\beta = 1$, $E\{\tau\} = .09$ and $C = .08$

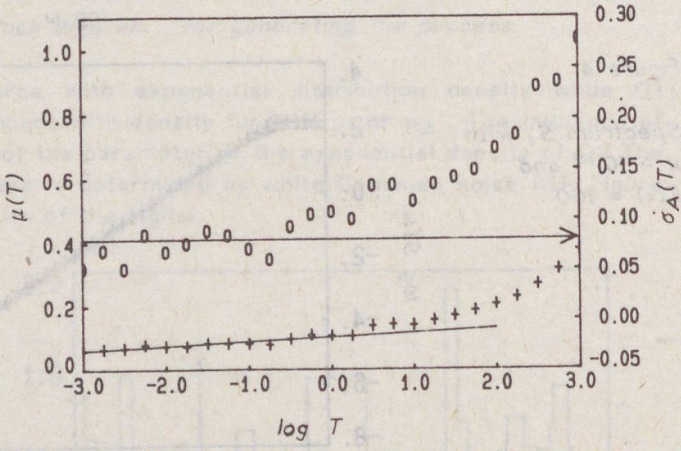

Important properties of 1/f-noise are the variance and the variance of variance. The variance of a process with an 1/f-spectrum is not a constant but is increasing with measuring time. But the variance of variance -the Allan variance- is a constant

$$\sigma_A(T) = 2\ C\ \ln 2 \qquad (6)$$

where T is the measuring time and C is related to the spectrum by $S(\omega)=C/\omega$. To verify this fact the variance $\mu(T)$ and the Allan variance $\sigma_A(T)$ were measured. Figures 6 and 7 demonstrate clearly the 1/f-behavior of the examined process.

References

[1] Ambrozy, A.: (1977), Variance of Simulated 1/f Noise; Electron. Letters 13, pp. 224-225

[2] Anton, K.: (1989), Erzeugung und Analyse eines stochastischen Prozesses mit 1/f-Spektrum, Diplomarbeit, Inst. für Angew. Physik der J.W.Goethe-Univ. Frankfurt am Main

[3] van der Ziel, A.: (1970), Noise: Sources, Characterization, Measurement; chap. 6.4 Flicker noise, T.Kailath, 1 ed., Prentice-Hall Inc., Englewood Cliffs, New Jersey, pp. 106-109

10th Int.Conf. on Noise in Physical Systems
1989 Budapest, Hungary

$1/f^k$ NOISE GENERATED BY SCALED BROWNIAN MOTION

Z. GINGL, L.B. KISS, R. VAJTAI

Institute of Experimental Physics, József Attila University
Dóm tér 9, H-6720 Szeged, Hungary

INTRODUCTION

One of the most challenging problems in the research of fluctuations is understanding the origin of low-frequency 1/f noise[1]. The 1/f noise appears in several systems [2-6] and quantities such as fluctuations in the conductivity of conductors and semiconductors, magnetic fluctuations [3-4] in spin-glasses and ferrits, frequency etalons, flow-speed in an hourglass, the water-level of a river, weather and economical data, biological systems, etc. From these facts it is often concluded that the 1/f noise is a general phenomenon. While, there is a large number of papers dealing with the creation of several 1/f noise models for several special cases, unfortunately, there is no satisfactory explanation of the generality of this phenomenon.

Now we report on another mathematical model of $1/f^k$ noises. A simple elementary non-stationary process is described which, without superposition of Lorentzian fluctuations, has a 1/f spectrum.

We take note of physical aspects and the possibility of technical application.

THE MODEL

It is well known that the position coordinate x(t) of the Brownian motion has a $1/f^2$ power density spectrum, because it is the time-integral of the velocity v(t). Naturally, any modification of the Brownian motion can strongly modify its properties. We investigated how transformations of the displacement modify the spectrum.

Let y(t) be the displacement of a coordinate-transformed Brownian motion. The coordinate-transformation is given by $y(t)=g[x(t)]$ where g(x) is an odd real function and x(t) is the original position coordinate (see Fig.1.). Obviously, the character of the spectrum S(f) of y(t) depends on the scaling function g(x).

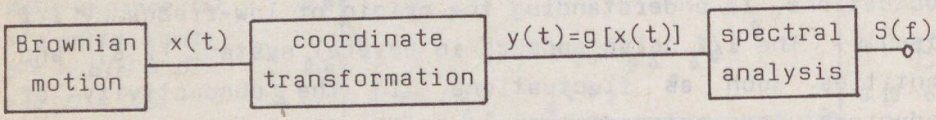

Fig.1

Several g(x) functions were tested. We found that it is interesting to choose a symmetrized power-function with various exponents **c**:

$$g(x)=\begin{cases} x^{c} & \text{if } x>0 \\ 0 & \text{if } x=0 \\ -|x|^{c} & \text{if } x<0 \end{cases} \qquad (1)$$

By this transformation, the spectrum S(f) according to computer modelings is proportional to $1/f^{k}$ over the total frequency range of investigations (five decades, see Fig.2). The connection of **c** and **k** can be seen in Fig.3.

This result can be important even in respect of 1/f noise, because this approach can serve as a possible frame for a new set of 1/f noise models without distribution of time constants.

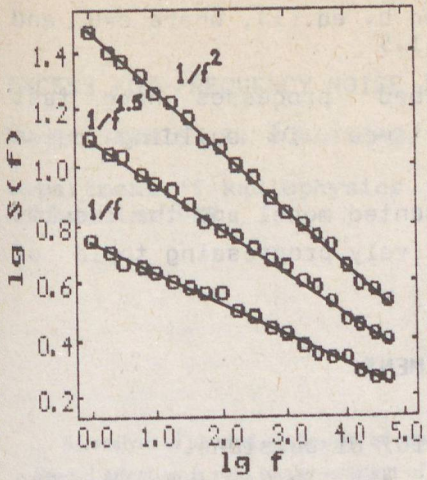

Fig.2

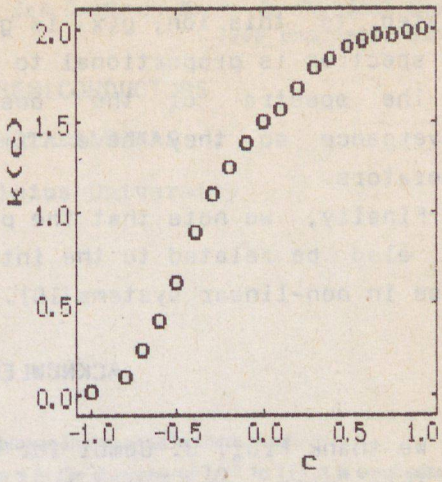

Fig.3

We note that a quasistationary process can be built up by superposition of non-correlated this-type transient elementary processes.

PHYSICAL ASPECTS

If one continuously measures a macroscopic scalar quantity y(t) (for example a voltage) then observes a quantity fluctuating around its mean value. This fluctuation can often be considered as a kind of transformed Brownian motion. So, one gets a spectrum different from $1/f^2$. One may assume that, in a number of physical cases, a hidden physical quantity x(t) can be defined which is fluctuating around its mean value by an ordinary Brownian motion and causing the fluctuation of y(t) due to a non-linear coupling $y(t)=g[x(t)]$.

As a demonstrating example, we refer to the well-known diffusion noise[9]. Then x(t) is the distance of a chosen ion from the contact-interface (where the ion can leave the sample); y(t) is the "fractional" conductance of the sample

related to this ion; g(x) is given by eq.(1), where c=0 and the spectrum is proportional to $1/f^{1.5}$.

The spectra of the described processes have fast convergence so they have importance in building noise generators.

Finally, we note that the presented model and the results can also be related to the intensively progressing topic of noise in non-linear systems [10].

ACKNOWLEDGEMENT

We thank Prof. J. Dombi for useful discussions.

This work was supported by the OTKA and the FKP foundations.

REFERENCES

[1] L.B. Kiss, Rev. of Solid State Sci. 2 (1988) 659

[2] R.F. Voss, Proc. of the 33rd Annual Symp. on Frequency Control (Atlantic City 1979)

[3] P. Svedlindh, P. Norblad and L. Lundgren, Phys.Rev.B 37 (1988) 2383

[4] M.S. Keshner, Proc. of the IEEE 70 (1982) 212

[5] F.N. Hooge, T.G.M. Kleinpenning and L.K.J. Vandamme, Rep.Prog.Phys. 44 (1981) 479,
D.A. Bell, J.Phys.C: Sol.Stat.Phys. 13 (1980) 4425

[6] T. Musha, K. Awata, A. Nakajima and H. Akabane, in "Noise in Physical Systems", edited by C.M. van Vliet (World Scientific, Singapore 1987) p.319.

[7] F. Grüneis, Physica 123A (1984) 149

[8] O. Jäntsch, IEEE Trans. Electr. Dev. ED-34 (1987) 1100

[9] J.J. Brophy, J.Appl.Phys. 61 (1987) 500

[10] "Noise in Nonlinear Dynamical Systems", Vol.1, edited by F. Moss and P.V.E. McClintock (Cambridge University Press, Cambridge 1989)

10th Int.Conf. on Noise in Physical Systems
1989 Budapest, Hungary

EXCESS LOW-FREQUENCY NOISE IN SEMICONDUCTORS

V. PALENSKIS, Z. ŠOBLICKAS, A. STADALNIKAS

Department of Radiophysics, Vilnius University
Lithuanian SSR

An analysis of physical mechanisms of semiconductors flicker noise has been done.

Special attention is paid to the variation of index γ in the specrrum of $1/f^{\gamma}$. In [1] it is emphasized that the dimensions must be given attention, i. e. that one must first be sure that equation

$$S_U/U^2 = (\alpha/N)f^{-\gamma}, \tag{1}$$

describing the phenomenon of flicker noise, includes all the relevant variables. An obvious weakness of the Eq. (1) is that in many cases $\gamma \neq 1$ and it does not deal with the experiment error. The formal assumption must be that parameter α incorporates a complex function of the variables, which will account for the fractional index γ, but this assumption has no physical explanation. Thus, dimensional analysis shows that the equation, describing the physical nature of flicker noise, could not be presented in the form of (1). It has been concluded that an excess current noise with spectrum $1/f^{\gamma}$ type is due to superposition of relaxation-like and burst random processes:

$$S_U/U^2 = \sum_i a_i \tau_i/(1 + \omega^2 \tau_i^2), \tag{2}$$

where a_i is the dimensionless parameter which causes the intensity of flicker noise; τ_i is the relaxation time, and $\omega = 2\pi f$. As it follows from comparing Eq. (2) with Eq. (1), the collection of parameters a_i, τ_i and its number i allows to obtain the proportionality of spectrum $f^{-\gamma}$ type ($0 \leqslant \gamma \leqslant 2$) at any frequency interval without including the fractional dimensions. In addition, the spectrum of type (2) has no uncertainty when frequency approaches to zero. As it is well known, in many cases flicker noise is the stationary random process [2, 3]. For any stationary random process x(t) autocorrelation function $k_x(\tau) = k_x(-\tau)$ and by using Leibniz's theorem one can find the asymptotic behavior of power spectral density $S_x(\omega)$ for $\omega \to 0$ [4]:

$$\lim_{\omega \to 0} \frac{dS_x(\omega)}{d\omega} = \lim_{\omega \to 0} \int_{-\infty}^{\infty} \frac{\partial}{\partial \omega} [k_x(\tau) e^{-j\omega\tau}]\, d\tau = -j \int_{-\infty}^{\infty} \tau k_x(\tau) d\tau = 0, \tag{3}$$

i. e. for the stationary process the power spectral density $S_x(\omega)$ must flatten at $\omega \to 0$; in other words, there is no physical stationary noise with the spectrum $f^{-\gamma}$ type without the restriction of frequency interval. Hence, we come to the description of the flicker noise spectrum in the form (2) again. According to the above arguments and Eq. (2), it is worth noting, that the experimentally observed change in the exponent γ of the noise spectrum has no additional information.

On the basis of our results obtained from the noise spectroscopy of impurities and point defects in silicon, it has been shown that relaxation times of charge carriers vary in a wide range from 10^{-6} to 10 s and more [5]. On the ground of these results it was interesting to model the noise caused by the random processes

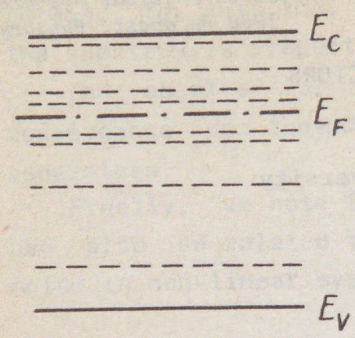

Fig. 1. Homogeneous band model of the semiconductor with impurities.

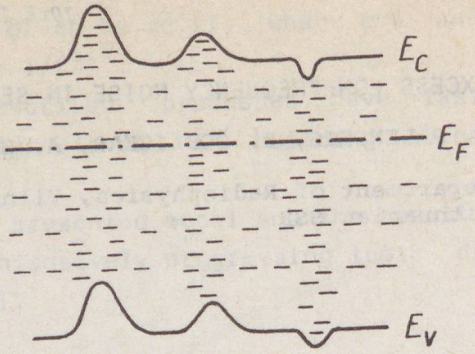

Fig. 2. Nonhomogeneous band model of the semiconductor with impurities and defects.

of Lorentzian type and to study its peculiarities in the formation of 1/f type spectrum. It has been shown that independent on the trap distribution in the band gap (either homogeneous, exponential or any other) with constant capture cross-sections there is no 1/f type noise formed. The superposition of generation-recombination noise gives the noise of 1/f type in any range of frequency, if a wide distribution of charge carriers capture cross-section (or recombination coefficients) for different impurities or point defects with approximately equal activation energies are present. Moreover, coefficient α in the empirical Hooge's relation for the 1/f noise does not exceed 10^{-2} for any parameters of impurities and point defects. It has been concluded that experimentally observed values exceeding 10^{-2} are not due to the large densities of deep impurities and cannot be explained on the ground of a homogeneous band model of semiconductors (Fig. 1). In order to explain α values greater than 10^{-2}, defects leading to the distortion of the band structure of semiconductor should be taken into account (Fig. 2), such as clusters of point defects, dislocations, mechanical damages, precipitates, etc. Having in mind the homogeneous semiconductor band model the explanation of 1/f type spectrum at low frequencies (about 1 Hz an less) requires to assume an electron (or hole) capture cross-section being by several order of magnitude smaller than that of atom, which is difficult to understand.

The interval of relaxation time distribution, required to explain the spectrum of low-frequency noise as well as the dispersion of noise intensity are caused by various relict (or frozen-in) defects and by surface, which induce large-scale distortion of the band gap (Fig. 3). For simplicity let us take a region with the symmetric potential energy barriers (humps) as shown in Fig. 4. The potential energy barrier height φ_B of the defect depends on the electric charge value, localized in the defect. When the characteristic size l (2l is the distance between two potential energy barriers) is much greater than the depletion depth w (Fig. 4), the onedimensional resistance fluctuations of a tested piece of material in the direction perpendicular to the pattern plane due to the fluctuations of the depletion depth may be expressed as $\Delta R_i/R_i \sim \Delta w/(l - w)$. The depletion depth value is caused by the free carrier density n in conduction band: $w \approx [2\epsilon\varphi_B/(en)]^{1/2}$, where ϵ is the dielectric constant, e is the electric charge of the free electron. The fluctuations of the number of occupied traps ΔN_t deal with the fluctuations of the number of free electrons $\Delta N(\Delta N_t = -\Delta N)$, and lead to the fluctuations of the depletion depth w. Having such simplified assumptions we can write that the onedimensional resistance fluctuations due to the fluctuations Δw may be described ty the following proportionality:

$$\frac{\langle \Delta R_i^2 \rangle}{R_i^2} \sim \frac{\langle \Delta N_t^2 \rangle}{n^2 V_i^2} \frac{w^2}{(l-w)^2}, \tag{4}$$

where V_i is the volume of the tested specimen piece. It is obvious that the resistance fluctuations from all non-overlapping fluctuators (potential energy barriers) of the entire specimen are proportional to the total number of those fluctuators N_f. In addition, the random process when occupying the localized states by electrons in the same potential energy barrier is, in general, not an independent process, as it is shown in submicrometer specimens [6, 7]. Hence, thermally activated capture and emission of individual electrons by the traps of the fluctuators lead to switching on and off of discrete resistance increments. We may imagine the resistance fluctuation process as a field-effect transistor (FET) channel's resistance random modulation by an accidental gate voltage, i. e. every fluctuator acts as FET's gate, the voltage of which randomly changes in the electron capture and emission process. This explanation is in good agreement with the results of low-frequency noise in submicrometer specimens [6, 7] and MOSFET's [8]. According to the factor $[w/(l-w)]^2$ in Eq. (4) the most noisy sites of semiconductor are those where depletion regions of fluctuators come into contact. Thus, empirical parameter α may be many times more or less than $2 \cdot 10^{-3}$, it depends on both the location and the number of fluctuators. As far as to the proportionality $S_u \sim 1/N$ (where N is the total number of free charge carriers), it must be considered only as inverse proportionality to the sample volume due to the independent fluctuations of separate fluctuators. This effect explains the dispersion of low-frequency noise intensity too. On the other hand, the greater density of free charge carriers in the homogeneous (uniform) plane of conductivity band (Fig. 3), the less relative volume fluctuations of the fluctuators and, thus, the less intensity of excess noise. Usually, such reduction of 1/f noise level with the increase of free-carrier density (or with the increase of density of ionized impurities) was explained by the assumption of mobility fluctuations as the origin of 1/f noise. In other words, if the number of the

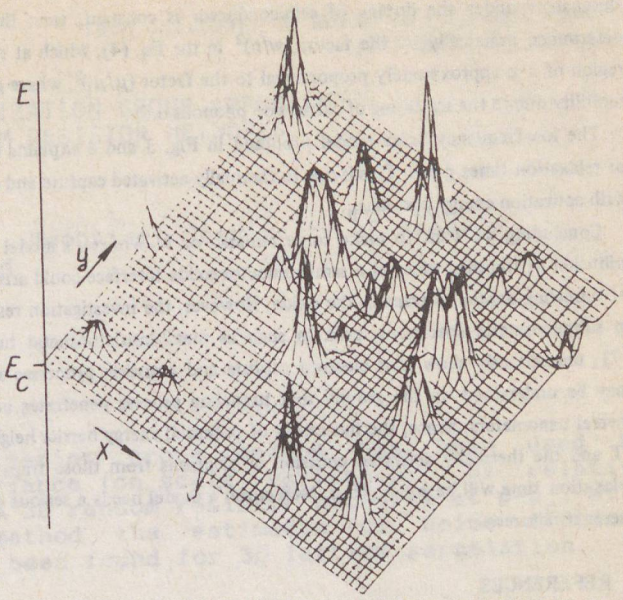

Fig. 3. Schematic conduction band of the semiconductor with large-scale distortions.

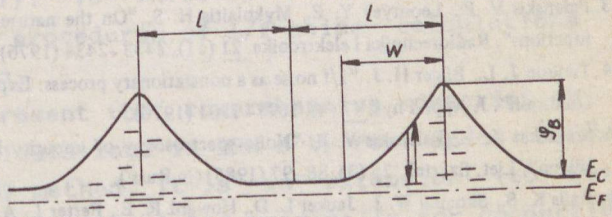

Fig. 4. Potential energy diagram for two symmetric fluctuators.

fluctuators under the doping of semiconductor is constant, then the intensity of low-frequency noise is determined practically by the factor $(w/n)^2$ in the Eq. (4), which at room temperature in the corresponding region of n is approximately proportional to the factor $(\mu/\mu_1)^2$, where μ is the free carrier mobility, μ_1 is the mobility due to the scattering of carriers on phonons only.

The low-frequency noise model proposed in Fig. 3 and 4 explains the large values and broad distribution of relaxation times τ too. This is due to thermally activated capture and emission of electrons in the fluctuators with activation energy $\varphi(x) \leqslant \varphi_B$.

Concluding we want to make some remarks on McWhorter's model [9], in which the required broad distribution of trapping times at a semiconductor-oxide interface could arise from a spatially uniform distribution of tunneling depths to traps in the oxide. However, the investigation results of the low-frequency noise nature in submicrometer specimens, even in such as metal-insulator-metal tunnel junctions [10] and MOSFET's [7], unanimously show that electron capture and emission processes are thermally activated. This situation may be understood on the ground that tunneling process penetrates into the potential energy barrier about several nanometers; hence, the increment of potential energy barrier height $\Delta\varphi(x)$ at that distance will be about kT and the thermally activated emission of electrons from those traps will be very rapid, and the resultant relaxation time will be small. Thus, McWhorter's model needs a serious corroboration, especially in submicrometer structures.

REFERENCES

1. Bell D. A. "A survey of 1/f noise in electrical conductors". J. Phys. C: Solid State Phys. 13 (24), 4425–4437 (1980).
2. Voss R. F., Clarke J. "Flicker (1/f) noise: Equilibrium temperature and resistance fluctuations". Phys. Rev. B. 13 (2), 556–573 (1976).
3. Palenskis V. P., Leontyev Y. E., Mykolaitis H. S. "On the nature of 1/f noise in linear resistors and pn junctions". Radiotechnika i elektronika. 21 (11), 2433–2434 (1976) (in Russ.).
4. Tandon J. L., Bilger H. J. "1/f noise as a nonstationary process: Experimental evidence and some analytical condition". J. Appl. Phys. 47 (4), 1697–1701 (1976).
5. Šoblickas Z. L., Palenskis V. P. "Noise spectroscopy of impurity levels and 1/f noise in high resistance silicon". Liet. fiz. rink. 25 (3), 88–97 (1985) (in Russ.).
6. Ralls K. S., Skocpol W. J., Jackel L. D., Howard R. E., Fetter L. A., Epworth R. W., Tennant D. M. "Discrete resistance switching in submicrometer silicon inversion layers: Individual interface traps and low-frequency (1/f) noise". Phys. Rev. Lett. 52 (3), 228–231 (1984).
7. Uren M. J., Day D. J., Kirton M. J. "1/f and random telegraph noise in silicon metal-oxide-semiconductor field-effect transistors". Appl. Phys. Lett. 47 (11), 1195–1197 (1985).
8. Mutoh N., Teranishi N. "New empirical relation for MOSFET 1/f noise unified over linear and saturation regions". Solid State Electron. 31 (12), 1675–1680 (1988).
9. McWhorter A. L. "1/f noise and germanium surface properties". Semiconductor surface physics. Ed. by R. H. Kingstone. Univ. of Pensilvania Press. 1957, p. 207–228.
10. Rogers C. T., Buhrman R. A. "Composition of 1/f noise in metal-insulator-metal tunnel junctions". Phys. Rev. Lett. 53 (13), 1272–1275 (1984).

10th Int.Conf. on Noise in Physical Systems
1989 Budapest, Hungary

A REAL SPACE RENORMALIZATION GROUP APPROACH TO 1/f NOISE IN RANDOM RESISTOR NETWORKS

A. KOLEK, A. KUSY

Electrical Department, Technical University of Rzeszów
35-959 Rzeszów, Poland

Real space renormalization group method has been used to demonstrate the invariance (on scale variations) of relative noise distribution in 2D random resistor networks at $p=p_c$. With the help of this method the estimates of noise critical exponent κ have also been found for 3D lattice percolation.

1. INTRODUCTION

Recently it has been shown that the magnitude of relative 1/f noise in random resistor networks (RRN's) diverges as $(p-p_c)^{-\kappa}$ near the percolation threshold p_c, where κ is a new critical exponent [1]. To investigate this effect more closely the effective procedures of 1/f noise calculations in RRN's are still needed.

In this paper we present the comprehensive description of relative 1/f noise calculations in RRN's by real space renormalization group (RSRG) method. It is an extension (to noise problem) of the technique formulated originally for conductivity by Stinchcombe and Watson [2]. Up to date the RSRG method has been used for noise calculations only in 2D RRN's by Luck [3] and Rammal [4]. Luck's approach is, however, different from ours, since he used the truncated transform while our transform renormalizes the full joint probability density function. On the other hand, Rammal applied the RSRG method in the range of $p>p_c$. He estimated critical exponent κ by approximation of the data near critical point. Our calculations are done strictly at p_c. We demonstrate here for the first time the scale invariance of the probability density function of the RRN relative 1/f noise. We also present the new estimates of critical exponent κ in 3D RRN's obtained with the help of our RSRG technique.

2. RENORMALIZATION GROUP FORMULATION

Let us define RRN in which bonds or sites are occupied (unoccupied) with probability p (1-p). Conductance of any occupied bond α is a sum: $g_\alpha=g+\delta g_\alpha$ where g is its mean (in time) value and δg_α its fluctuating part. All δg_α are assumed to have the following properties: (i) $\overline{\delta g_\alpha}=0$; (ii) $\overline{\delta g_\alpha \delta g_{\alpha'}}=0$ for $\alpha\neq\alpha'$ (spatial uncorrelation); (iii) $\overline{(\delta g_\alpha)^2}=\Delta f\varphi_g(f)$ where $\varphi_g(f)$ is power spectral density (PSD) of bond conductance fluctuations. The relative PSD is defined as $s=\varphi_g(f)/g^2$ (relative noise). Fluctuations, δG, of RRN conductance, G, are given by $G=\overline{G}+\delta G$, with $\overline{\delta G}=0$, $\overline{(\delta G)^2}=\Delta f\Psi_G(f)$ and relative noise, $\Psi=\overline{(\delta G)^2}/(G^2\Delta f)$. It is often more convenient to consider (instead of G and Ψ) conductivity ($\sigma=GL^{2-d}$ where d is dimensionality) and relative noise multiplied by RRN volume ($S=\Psi L^d$). These quantities are independent of RRN size L over scales grater then correlation lenght ξ.

In RSRG method the probability that RRN percolates, RRN conductance, and relative noise are evaluated in successive renormalization steps. Given probability p of bond occupation and elementary cell of size b, the probability p_1 that the cell percolates is given by the transformation R(p). p_1 is then probability that a bond in the new, decimated RRN is occupied. In the result of the renormalization step N=1 we also form the new joint distribution of cell conductivity and relative noise, $\tilde{P}_1(\sigma,S)$. This distribution can be estimated from the original joint probability density $\tilde{P}_0(\sigma,S)$ and as $\tilde{P}_0(\sigma,S)$, can be divided into two parts:

$$\tilde{P}_N(\sigma,S)=\tilde{W}[\tilde{P}_{N-1}(\sigma,S)] = p_N P_N(\sigma,S) + (1-p_N)\delta(\sigma,S), \quad (1)$$

where $P_N(\sigma,S)$ is also normalized and is conditional joint probability density under the condition that the cell percolates. For $p=p_c=p^*$, $p_1=p_2=\ldots p_N=p^*$. Let us assume that

$$P_N(\sigma,S)=\lambda_t\lambda_\kappa P_{N-1}(\lambda_t\sigma,\lambda_\kappa S). \quad (2)$$

From Eq.(2) the marginal distributions can be found as:

$$P_N^\sigma(\sigma) = \int P_N(\sigma,S)dS = \lambda_t P_{N-1}^\sigma(\lambda_t\sigma), \quad (3)$$

$$P_N^S(S) = \int P_N(\sigma,S)d\sigma = \lambda_\kappa P_{N-1}^S(\lambda_\kappa S). \quad (4)$$

it can be shown from Eqs (3) and (4) that

$$\lambda_t = \langle\sigma\rangle_{N-1}/\langle\sigma\rangle_N \quad (5)$$

$$\lambda_\kappa = \langle S\rangle_{N-1}/\langle S\rangle_N \quad (6)$$

where $\langle\rangle$ denotes ensemble average. The critical exponents t and κ and size dependence exponents β_L and y can be found from

$$-\ln\lambda_t/\ln b = \beta_L + 2 - d = -\frac{t}{\nu} \quad (7)$$

$$-\ln\lambda_\kappa/\ln b = -y + d = \frac{\kappa}{\nu} \quad (8)$$

where ν is correlation length exponent.

3. RESULTS

In Fig.1 the distributions $P_5^S(S)$, $P_6^S(S)$ and $P_7^S(S)$ are shown for square lattice and b=2 cell. Scale invariance has been

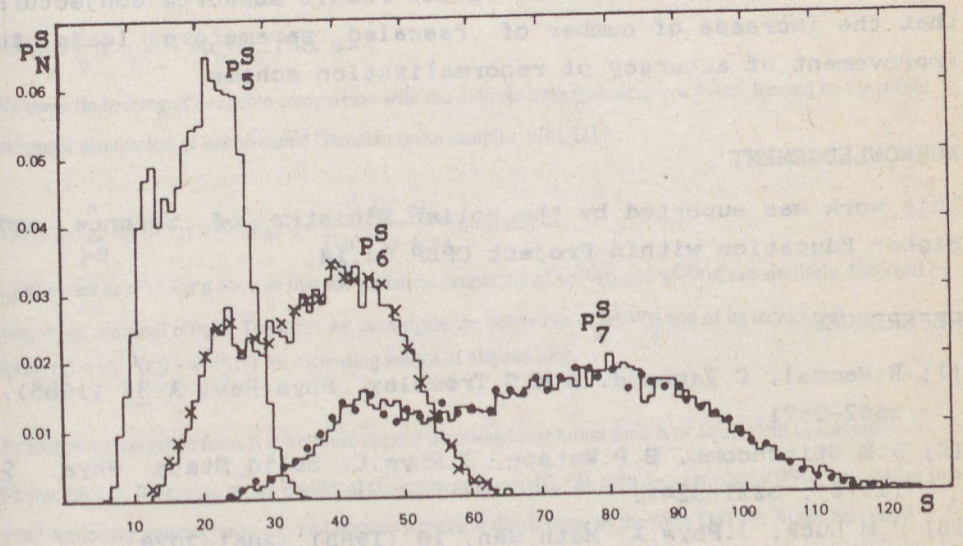

Fig.1. Distributions $P_N^S(S)$ of network relative noise S multiplied by RRN volume obtained as a result of renormalization steps N=5,6,7 done at critical point. To show the scale invariance of $P_N^S(S)$ the points from $P_5^S(S)$ are rescaled, according to eq.(4), to give $P_6^S(S)$ (crosses); similarily $P_6^S(S)$ is rescaled to $P_7^S(S)$ (dots). Calculations were done for the "iterated Wheatstone bridge" [5] at p_c=0.5, b=2 for λ_κ=0.532.

demonstrated by rescaling the points from $P_5^S(S)$ and $P_6^S(S)$ according to equation $W[P_N^S(S)]=\lambda_\kappa P_N^S(\lambda_\kappa S)$. In the result of rescaling the points on $P_6^S(S)$ (crosses) and $P_7^S(S)$ (dots) have respectively been found verifying the relation $P_{N+1}^S(S)=\lambda_\kappa P_N^S(S)$. The value of λ_κ used in rescaling is $\lambda_\kappa = 0.532$. This value was accepted as final result when λ_κ values calculated in successive renormalization steps became constant (within an error of 0.0001). In Eq.(6) different procedures of mean calculations (arithmetic, geometric, harmonic) were used obtaining always the same value $\lambda_\kappa=0.532 \pm 0.0001$. We also applied the described RSRG scheme to estimate critical exponent κ. In 3D RRN's we have used the elementary cell and transformations R(p) previously utilized by Bernasconi [5] and Yuge and Hori [6]. We have obtained $\kappa=1.88$ (t=2.14) for Bernasconi bond percolation case, and $\kappa=2.43$ (t=2.21) for Yuge and Hori site percolation. We also have used originally evaluated (for 3D cell) two parameter transformation, according to Nakanishi and Reynolds [7,8], and obtained $\kappa=1.83$ (t=2.06). The latter result supports conjecture that the increase of number of rescaled parameters leads to improvement of accuracy of renormalization scheme.

ACKNOWLEDGEMENT

This work was suported by the Polish Ministry of Science and Higher Education within Project CPBP 02.14.

REFERENCES

[1] R.Rammal, C.Tannous, A.M.S.Tremblay, Phys.Rev. A 31 (1985), 2662-2671.

[2] R.B.Stinchcomb, B.P.Watson, J.Phys.C: Solid State Phys. 9 (1976), 3221-3247.

[3] J.M.Luck, J.Phys.A: Math.Gen. 18 (1985), 2061-2078.

[4] R.Rammal, J.Physique Lett. 46 (1985), L129-L136.

[5] J.Bernasconi, Phys.Rev. B 18 (1978), 2185-2191.

[6] Y.Yuge, M.Hori, J.Phys.A: Math.Gen. 20 (1987), 3523-3531.

[7] H.Nakanishi, P.J.Reynolds, Phys. Lett. 71A (1979), 252-254.

[8] A.Kusy, A.Kolek, Physica A 157 (1989), 130-134.

10th Int.Conf. on Noise in Physical Systems
1989 Budapest, Hungary

TIME- AND FREQUENCY-DOMAIN MODELS FOR FRACTIONAL NOISES

M.L. MEADE

Faculty of Technology, Open University
Milton Keynes, UK

Elementary models are described for a class of noises $w^{(\mu)}(t)$ generated by the finite fractional integral of white noise. Statistical results are presented in support of a discrete-time technique which simulates the behaviour of the 1/f-type process $w^{(1/2)}(t)$ over an arbitrarily wide range.

CONTINUOUS-TIME MODELS

The class of random process $w^{(\mu)}(t)$ is defined by the finite fractional integral of unit-variance white noise w(t):

$$w^{(\mu)}(t) = \int_0^t (t - t_0)^{\mu-1} w(t_0)\, dt_0 / \Gamma(\mu), \quad \mu > 0$$

We use a finite integral to enable comparison with the discrete-time realizations $w^{(\mu)}[n]$, formed by the μ-fold fractional summation of uncorrelated Gaussian noise samples w[n], [1] :

$$w^{(\mu)}[n] = \sum_{j=0}^{n} h_\mu [n - j]\, w[j] \; ; \; h_\mu[n] = \frac{\Gamma(\mu + n)}{\Gamma(\mu)\, \Gamma(1 + n)} u[n], \quad \mu > 0$$

$h_\mu[n]$ varies as $n^{\mu-1}$ for $n >> 1$ so that the statistical properties of $w^{(\mu)}(t)$ and $w^{(\mu)}[n]$ are similarly disturbed by long-range transient effects. To begin, we investigate the behaviour of $w^{(\mu)}(t)$ and of its increments $d_\mu(t_1, t_2) = w^{(\mu)}(t_2) - w^{(\mu)}(t_1)$ for increasing values of elapsed time.

To ensure convergence for $\mu \leq \frac{1}{2}$ we must impose a notional resolution time Δ or equivalent observation bandwidth $1/\Delta$. Reference to the fractional Gaussian noise $w_H(t)$, [2], then suggests that $w^{(\mu)}(t)$ will evolve to a quasi-stationary process for $\mu < \frac{1}{2}$, and possess a spectral distribution of the form $|\omega|^{-2\mu}$. At the boundary $\mu = \frac{1}{2}$ the band-limited variance increases as ln t and, for observations carried out on a time-scale $\Delta << |\tau| << t$, $w^{(1/2)}(t)$ is described by the covariance distribution

$$k_{1/2}\left(t - \frac{\tau}{2}, t + \frac{\tau}{2}\right) \approx \left[\frac{1}{2} \ln 4 \left| t - \frac{\tau}{2} \right| + \frac{1}{2} \ln 4 \left| t + \frac{\tau}{2} \right| - \ln |\tau|\right]/\pi$$

The covariance of the increments of $w^{(\mu)}(t)$ is given by

$$k_{d\mu}(t_1,t_2) = \int_{-\infty}^{\infty} \int_{-\infty}^{\infty} k_\mu(t_1 - u, t_2 - v)\, h(u)h(v)\, du\, dv$$

where $h(t) = \delta(t) - \delta(t - T)$ is the weighting function of an ideal differencing system. For the case $\mu = \frac{1}{2}$, we obtain :

$$k_{d1/2}(\tau) = [\ \ln|\tau + T| + \ln|\tau - T| - 2 \ln|\tau|\ ]/\pi,\ \ \Delta << |\tau| << t$$

The short-range increments appear stationary and we have the spectral model

$$P_{d1/2}(\omega) = F\{\ k_{d1/2}(\tau)\ \} = [2 \sin \omega T]^2\, \omega^{-1} \operatorname{sgn} \omega,\ \ 1/t << \omega << 1/\Delta$$

from which we conclude that the time-averaged spectrum of $w^{(1/2)}(t)$ is of the form $\omega^{-1} \operatorname{sgn} \omega$.

When $\mu > \frac{1}{2}$, the finite variance of $w^{(\mu)}(t)$ increases as $t^{2\mu-1}$. We define $A_\mu = [(2\mu - 1)\, \Gamma^2(\mu)]^{-1}$, and write the covariance as :

$$k_\mu(t_1,t_2) = \frac{1}{2} A_\mu (t_1^{2\mu-1} + t_2^{2\mu-1}) - \frac{1}{2} \langle d_\mu^2(t_1,t_2) \rangle$$

The variance of the increments can be expressed in the form

$$\langle d_\mu^2\left(t - \frac{\tau}{2}, t + \frac{\tau}{2}\right) \rangle = - B_\mu |\tau|^{2\mu-1} + C_{\mu 1}\, \tau^2\, t^{2\mu-3} + C_{\mu 2}\, \tau^4\, t^{2\mu-5} + ...$$

where $B_\mu = [\ \Gamma(2\mu) \cos \mu\pi\ ]^{-1}$, $2\mu \neq 3,5...$

$A_1 = B_1$ and the coefficients $C_{1n} = 0$ for the Brownian motion $w^{(1)}(t)$, when the increments form a stationary process. Otherwise, the increments are quasi-stationary for $\mu < \frac{3}{2}$, with $\langle d_\mu^2 \rangle$ being independent of t only when $\tau^2\, t^{2\mu-3} << 1$. Under this condition, the output of a first-difference filter will behave in a self-similar fashion with spectral distribution $P_{d\mu}(\omega) = F\{\ k_{d\mu}(\tau)\ \} = [2 \sin \omega T]^2\, |\omega|^{-2\mu},\ \ \frac{1}{2} < \mu < \frac{3}{2}$.

$w^{(3/2)}(t)$ is the time-integral of $w^{(1/2)}(t)$. Its covariance has the limiting form

$$k_{3/2}\left(t - \frac{\tau}{2}, t + \frac{\tau}{2}\right) \approx [\ 2t^2 - \frac{1}{2}\tau^2 \ln|4t| + \frac{1}{2}\tau^2 \ln|\tau|\ ]/\pi$$

Suppose now that $w^{(3/2)}(t)$ is applied to a stable filter with weighting function h(t). Writing $\phi(t) = h(t) * h(-t)$, the output variance will be

$$\sigma^2(t) = \int_{-\infty}^{\infty} k_{3/2}\left(t - \frac{\tau}{2}, t + \frac{\tau}{2}\right) \phi(-t)\, d\tau$$

If the zero- and second-order moments of $\phi(t)$ are zero, the time-dependent components in $k_{3/2}$ will be suppressed. For example, choosing $h(t) = \delta(t) - 2\delta(t - T) + \delta(t + T)$, gives the Allan variance $\sigma^2(T) = (4/\pi)\, T^2 \ln 2$, in agreement with the van Vliet-Handel results for the time-integral of 1/f-noise [3]. Equivalently, any system with the power-transfer function property $\phi(0) = \phi''(0) = 0$ will provide a stabilizing measure and give results in accordance with a time-averaged spectrum $|\omega|^{-2\mu}$ for $\mu < \frac{5}{2}$.

LONG-RANGE APPROXIMATIONS TO $w^{(1/2)}(t)$

The short-run properties of $w^{(1/2)}(t)$ can be investigated experimentally by forming the convolution of white-noise samples with a truncated version of $h_{1/2}[n]$. Alternatively, the behaviour of $w^{(1/2)}[n]$ and $w^{(1/2)}(t)$ can be simulated with minimal computational effort and over an arbitrarily wide range by forming a sum of *equally-weighted* processes of the type p[j,n] shown in Figure 1. The values of p[j,n] over successive intervals of duration L^j samples are taken from a unit variance, zero-mean Gaussian process, w[j,n]. p[j,n] therefore has covariance $k_p[j,m] = 1 - |m|/L^j$, $0 \le |m| < L^j$, and spectral density $S_p(j,\theta) = L^{-j}\,[\sin L^j\,\theta/2]^2/\sin^2\theta/2$.

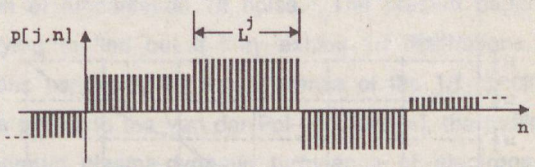

Fig. 1 Component process p[j,n].

The summation $f_N[n] = \sum_{j=0}^{N} p[j,n]$ is a stationary process with covariance $k_N[m]$ and variance $k_N[0] = N + 1$. Due to its structure, a component p[j,n] makes negligible contribution to the fluctuation of $f_N[n]$ over an interval less than L^{j-1}. Thus, if we form the increments, $d_N[m] = f_N[n + m] - f_N[n]$, the variance $\langle d_N^2[m]\rangle$ increases with m in quasi-logarithmic fashion, one unit being added to the variance whenever $m = L^j$, j = 0,1,2... This trend continues up to lags of the order $m = L^{N-1}$ beyond which $\langle d_N^2[m]\rangle$ approaches a constant value of 2(N + 1). We therefore define the 'range' of $f_N[n]$ to be $R = L^{N-1}$. For lags |m| within the range, the increments have variance

$$\langle d_N^2[m]\rangle \approx 2\,V(m) + 2\,|m|\,L^{1-V(m)}/(L - 1),\ |m| < R = L^{N-1} \qquad (1)$$

V(m) is an integer variable given by the logarithmic 'staircase' function V(m) = 0, m = 0; V(m) = 1 + int { log |m|/log L }, |m| > 0.

The behaviour of $f_N[n]$ is consistent with the idea that the sum of spectra of the type $S_P(j,\theta)$ gives a spectral distribution approximating to the form $|\theta|^{-1}$ over a spectral range of the order L^{N-1}. For a 'good'

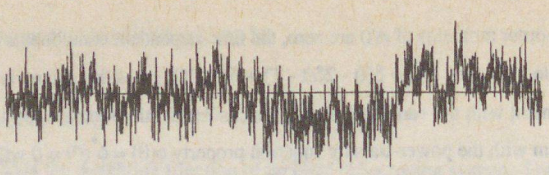

Fig. 2 10 000-point sample function of $f_N[n]$; L = 4, N = 11.

approximation we require $L \leq 4$. If L = 4, as in the 10 000-point realization shown in Figure 2, a sum of 11 components gives a range of 10^6.

The growth of $\langle d_N^2[m] \rangle$ can be extended indefinitely by ignoring the fixed limit, N, and re-defining p[j,n] to be zero for $n < L^j$. At any instant n, the new process f[n] will then be formed by the sum of V(n) components and have variance $\langle f^2[n] \rangle = V(n)$. f[n] thus evolves on a logarithmic time-scale, the variance increasing by one unit at epochs $n = L^j$, when the range $R(n) = L^{V(n)-1}$ increases by a factor L to L^j. The overall effect is to create a non-stationary process for which the temporal and spectral range is determined by the time available for measurement, rather than being artificially constrained.

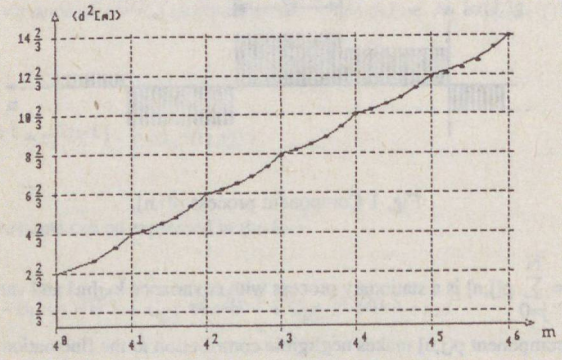

Fig. 3 Variance of increments as function of lag, m.

To demonstrate the properties of f[n], we used L = 4 and measured the variance of the increments, operating on a continuous data stream to simulate conditions in a real-time measurement. The values of $\langle d^2[m] \rangle$ are plotted in Figure 3 against a solid curve drawn from equation (1). The maximum lag of 4^6 was chosen for convenience, since the extension to longer lags simply continues the persistent logarithmic growth at the expense of time required for data collection and processing.

ACKNOWLEDGEMENTS

Data generation and analysis was carried out by Calvin Stanfield.

REFERENCES

1 BARNES, JA and ALLAN, DW: *Proc IEEE*, **54**, 1966, pp 176-178
2 MANDELBROT, BB and VAN NESS, JW: *SIAM Rev*, **10**, 1968, pp 422-437
3 VAN VLIET, CM and HANDEL, PH: *Physica*, **113A**, 1982, pp 261-276

10th Int.Conf. on Noise in Physical Systems
1989 Budapest, Hungary

ANALYTICAL AND NUMERICAL STUDY OF FLUCTUATIONS IN ACTIVE NONLINEAR SYSTEMS

B. WEBER, D. WOLF, P.H. HANDEL*

Institut für Angewandte Physik, Universität Frankfurt
D-6000 Frankfurt a.M., FRG
*Physics Department, University of Missouri
St. Louis, MO 63121, USA

It is well known that some nonlinear systems [1,2] are characterized by fluctuations exhibiting a 1/f spectrum. Nonlinearity of classical [1] and quantum [2] systems with no characteristic scale (with sliding scale) has been recognized in general [3] as the universal origin of fundamental 1/f noise. The present paper examines a few nonlinear systems, trying to find out if they exhibit 1/f fluctuations, and attempts to determine the conditions necessary for the existence of the 1/f spectrum. The systems considered include one similar to the Van der Pol oscillator [4], the traffic fluctuations on a highway [5], the magnetic plasma-dynamic turbulence of electrons and holes in a symmetric semiconductor [1], the similar turbulence of electrons in a metal [1], and the same fundamental turbulence-like behaviour governing all processes in quantum electrodynamics [2]. These processes also provide examples of classical and quantum chaos, generated by the instability of the corresponding laminar flow solutions.

We have first reexamined arbitrary fluctuations around the steady solution $X_0 = (-\alpha/\beta)^{1/2}$ of the *Van der Pol type nonlinear Langevin equation*

$$dX/dt = -\alpha X - \beta X^3 + f(t), \qquad (1)$$

where $\alpha>0$ is a damping constant, β a nonlinear coefficient, and $f(t)$ a random force with a white spectrum. Kawakubo [1] had developed a self-consistent method for calculating the power spectrum of fluctuations in this system, obtaining a lorentzian for small β and a $1/\omega$ spectum at large β. We found that Kawakubo's method is identical with an iterative calculation of the motion of the oscillator in the absence of a random force, following an instantaneous impulse described by Dirac's $\delta(t)$. We then solved the equation analytically, showing that without actual random function input, Kawakubo's self-consistent iterations should have led to steeper spectra, at least in the limit of low frequencies. The same result was obtained by us also numerically, by retracing the steps followed by Kawakubo. Our solution was obtained by substituting $X = X_0 + x$ and solving the resulting equation

$$dx/dt = 2\alpha x - 3\,(-\alpha\beta)^{1/2}\,x^2 - \beta x^3 + 2\pi g\delta(t) \qquad (2)$$

where g is a constant determining the initial displacement $x(0) = 2\pi g = x_0$. With the

notations $\xi=x(\beta/\alpha)^{1/2}$, $2\alpha t=-\tau$, and $\xi_o=2\pi g(\beta/-\alpha)^{1/2}$, $A=\xi_o(\xi_o+2)/(\xi_o+1)^2<1$, we obtain by straightforward integration of Eq. (2)

$$\xi = -1 + [1 - Ae^{-\tau}]^{-1/2}, \qquad (3)$$

and its Fourier transform

$$\xi(\omega) = [-1 + 1/i\omega + (1/2)(1+i\omega)^{-1}(A/1!) + (1/2)(3/2)(2+i\omega)^{-1}(A^2/2!) + (1/2)(3/2)(5/2)(3+i\omega)^{-1}(A^3/3!) + ...]/(2\pi i\omega). \qquad (4)$$

For $\omega\to 0$, $|\xi(\omega)|^2 \sim \omega^{-4}$; for $\omega\to\infty$, $|\xi(\omega)|^2 \sim \omega^{-2}$; if we would excite the system with a sequence of pulses $2\pi g_i\delta(t-t_i)$ randomly distributed, but further apart than $t_o=-1/2\alpha$, this would also be the limiting behaviour of the spectral density of the resulting random process, according to Carson's Theorem. This result, however, does not yet exclude the possibility of 1/f power spectra which could be generated in certain frequency domains, by a more general random source term, which would correspond to a superposition of continuously overlapping and compounded pulses. However, our extended numerical simulations of Eq. (2) with a random white noise imput replacing the delta function, have not produced any extended 1/f-like regions either. An example of a resulting spectrum is shown in Fig. (1). We conclude that this system does not exhibit a fundamental 1/f spectrum in general, lacking scale invariance.

The next system we have examined was *highway traffic*. We used the model of Musha and Higuchi [5], based on a postulated linear dependence of the average traffic speed v on the linear concentration of cars n(x,t) on the road, $v=v_o(1-n/n_s)$. Musha writes the traffic current J as a sum of drift and diffusion currents

$$J = nv - D\partial n/\partial x = nv_o - (v_o/n_s)n^2 - D\partial n/\partial x, \qquad (5)$$

where D is a diffusion coefficient. The equation of continuity is

$$0 = \partial n/\partial t + \partial J/\partial x \equiv (\partial/\partial t + v_o\partial/\partial x)n - 2(v_o/n_s)n\partial n/\partial x - D\partial^2 n/\partial x^2. \qquad (6)$$

This is Musha's fundamental equation of traffic dynamics, which also was written in a system of reference defined by $x' = -x + v_o t$, $t' = t$, in the final form [5,6]

$$\partial n/\partial t' + an\partial n/\partial x' = D\partial^2 n/\partial x'^2, \qquad (7)$$

where $a \equiv 2v_o/n_s$. We normalize the concentration to $n_s/2$, the coordinate x along the road to D/v_o, and the time to D/v_o^2, thereby obtaining the dimensionless form of the fundamental traffic-dynamical equation

$$\partial n(x,t)/\partial t + n(x,t)\partial n(x,t)/\partial x = \partial^2 n(x,t)/\partial x^2. \qquad (8)$$

Expanding in a Fourier series over the interval L, we obtain

$$\partial n/\partial t + i\Sigma_{k'}n(k')n(k-k')k = -k^2 n(k,t). \qquad (9)$$

Defining the autocorrelation function

$$A(\xi,\tau) \equiv \langle n^*(x,t)n(x+\xi,t+\tau)\rangle = \Sigma_k\langle n^*(k,t)n(k,t+\tau)\rangle e^{ik\xi} = \Sigma_k U(k,\tau)e^{ik\xi}, \qquad (10)$$

as a turbulent ensemble average $\langle\ldots\rangle$, in quasistationary homogeneous conditions we obtain by multiplication of Eq. (10) with $n^*(k, t-\tau)$, after ensemble averaging,

$$\partial U/\partial\tau + k^2 U(k,\tau) + i\Sigma_{k'k'}\langle n^*(k, t-\tau)n(k',t)n(k-k',t)\rangle = 0. \qquad (11)$$

Linking the complex function $U(k,\tau)$ to a third-order correlation function, this is the first equation of an infinite chain of equations connecting the Nth order to the order N+1 correlation function. Applying the operator $-\partial/\partial\tau + k^2$ to Eq. (11), and using the complex conjugate of Eq. (9) to define the action of this operator on the first factor inside the averaging brackets in Eq. (11), we obtain

$$-\partial^2 U/\partial\tau^2 + k^4 U = -i\Sigma_{k'}k'\langle[i\Sigma_{k''}k''n^*(k'',t-\tau)n^*(k-k'',t-\tau)]n(k',t)n(k-k',t)\rangle$$

$$\approx\Sigma_{k',k''}k'k''[U(k'',0)U(k',0)\delta_{k,0}+U(k',\tau)U(k-k',\tau)\delta_{k''k'}+U(k',\tau)U(k-k',\tau)\delta_{k'',k-k'}]. \quad (12)$$

The last form was obtained by approximating the fourth-order correlation function with its expression in terms of the second-order correlation applicable for Gaussian processes:

$$\langle ABCD\rangle = \langle AB\rangle\langle CD\rangle + \langle AC\rangle\langle BD\rangle + \langle AD\rangle\langle BC\rangle. \quad (13)$$

This approximation [1] was used by Heisenberg in his turbulence theory, and was successfully verified in its practical applicability by Uberoi and Batchelor.

In the limit $L\to\infty$, setting $U(k,\tau)L/2\pi = u(k\tau)$, we write for $k\neq 0$ Eq. (12) as

$$-\partial^2 u/\partial\tau^2 + k^4 u = \int[k'^2 u(k',\tau)u(k-k',\tau) + k'(k-k')u(k',\tau)u(k-k',\tau)]dk', \quad \text{or}$$

$$-\partial^2 u(k,\tau)/\partial\tau^2 + k^4 u(k,\tau) = k\int k'u(k',\tau)u(k-k',\tau)dk'. \quad (14)$$

This is our fundamental dynamical equation of traffic turbulence. All unspecified limits on integrals in the present paper are from $-\infty$ to ∞. From the symmetry $A(\xi,\tau) = A(-\xi,-\tau) = A^*(\xi,\tau)$ we see that a physically acceptable solution of this equation must satisfy the conditions $u(k,\tau) = u(-k,-\tau) = u^*(-k,-\tau) = u^*(k,-\tau)$. A solution of the form

$$u(k,\tau) = V(k)e^{-imk\tau}, \text{ with } V(k) = V(-k) = V^*(k), \quad (15)$$

where m is a real constant, substituted into Eq. (14), yields

$$k(m^2 + k^2)V(k) = \int k'V(k')V(k-k')dk'. \quad (16)$$

In the low wave number region $k<<m^2$ (i.e., $k<<m^2 v_0/D$) we neglect the k^2 term which arises from diffusion, get scale invariance, and try a solution $V(k) = C|k|^{\varepsilon-1}$, with arbitrarily small $\varepsilon>0$. Substitution into Eq. (16) yields the value of C, independent of k only in the limit of $\varepsilon\to 0$: (17)

$$m^2/C = \int_{-\infty}^{\infty} k'|k'|^{\varepsilon-1}|1-k'/k|^{\varepsilon-1}dk'/k = |k|^{\varepsilon}\int_{-\infty}^{\infty}\kappa|\kappa|^{\varepsilon-1}|1-\kappa|^{\varepsilon-1}d\kappa = |k|^{\varepsilon}\int_{0}^{2}|\kappa|^{\varepsilon}|1-\kappa|^{\varepsilon-1}d\kappa \approx 2/\varepsilon = l,$$

where we used the substitution $k'/k=\kappa$. The divergence at $\varepsilon=0$ disappears when we return to a finite value of the maximal road length L, which corresponds to a minimal k (or k') value $k_0=2\pi/L$, and transforms the integrals back into sums.

Eq. (17) establishes a proportionality between the level of the turbulence,described by C, and the magnitude of the small parameter ε as in earlier turbulence calculations [1]. The same fundamental feature is more clearly expressed, without the pseudo-singularities present here, in the quantum 1/f theory [2], where ε becomes the infrared exponent αA known from quantum electrodynamics. Indeed, αA is present there, just as we see it come in here, both as a factor in front of the final result, and as a small defect in the exponent of f

We can rewrite Eq. (10) in the form

$$A(\xi,\tau) \equiv \langle n^*(x,t)n(x+\xi,t+\tau)\rangle = \Sigma_k U(k,\tau)e^{ik\xi} \equiv \int dk\ u(k,\tau)e^{ik\xi}$$
$$= C\int e^{ik(\xi-m\tau)}|k|^{\varepsilon-1}dk = |\xi-m\tau|^{-\varepsilon}(m^2/I)\int e^{i\kappa}|\kappa|^{\varepsilon-1}d\kappa \approx m^2|\xi-m\tau|^{-\varepsilon}. \qquad (18)$$

Here we have used the substitution $k|\xi-m\tau|=\kappa$, and we have taken the limit $\varepsilon\to 0$ in the integral and in I, noting that they exhibit the same divergence, and therefore can be simplified in the limit. Since only the limit $\varepsilon=0$ satisfies the fundamental dynamical equation of traffic turbulence, Eq. (18) means that the autocorrelation function is a constant. It also indicates that the constant has to be interpreted as the limit of a slowly decreasing power law which depends only on $|\xi-\tau|$; therefore the spectrum in wave numbers is the same as the spectrum in frequencies. The Fourier transform with respect to τ is the spectral density (19)

$$S_n'(\xi,\omega)=\int\langle n^*(x,t)n(x+\xi,t+\tau)\rangle e^{i\omega\tau}d\tau = C\iint(dk/|k|^{1-\varepsilon})e^{ik(\xi-m\tau)+i\omega\tau}d\tau \to 2\pi C[m/\omega]^{1-\varepsilon}$$

for $(\xi\to 0)$. The current fluctuations have the same 1/f spectrum, multiplied by v_o^2.

The fundamental dynamical equation of turbulence in the plasma of electrons and holes of *a semiconductor* is, for the magnetic correlation scalar $u(k,\tau)=k^{-3}v(k,\tau)=\langle \mathbf{B}(\mathbf{k},t)\mathbf{B}(\mathbf{k},t+\tau)\rangle$

$$\frac{\partial v(k,x)}{\partial|x|} + v(k,x) = -\frac{1}{2}v(k,x)\int\frac{d^3k'}{k'^3}\frac{k^2+\mathbf{k}\cdot\mathbf{k}'}{(\mathbf{k}+\mathbf{k}')^2}\left[1-\left(\frac{\mathbf{k}\cdot\mathbf{k}'}{kk'}\right)^2\right]v(k',0), \qquad (20)$$

where $x = \mu\tau k^2$ is a dimensionless variable replacing τ. We see that the integral is independent of k, provided v(k,x) does not depend on its first argument, by setting $\mathbf{k}'/k\equiv\kappa$. This yields a solution. However, with $v=e^{-m|x|}$ we get a logarithmic divergence at $\kappa=0$. We look for an exact solution of the form $v(k,x)=hk^{\varepsilon}e^{-|x|m(k)}$, or $u(k,x)=(h/k^{3-\varepsilon})e^{-|x|m(k)}$, where m(k) is very close to a positive real constant, almost independent of k, and h is a constant proportional to the intensity of the turbulence, or the turbulence level. We get

$$u(\omega) = \int_0^\infty k^2dk\int_0^\infty d\tau k^{-3}v(k,\tau)\cos\omega\tau = h\int_0^\infty\frac{mkdk}{\omega^2+m^2k^2} = \frac{\pi}{4}\frac{h}{\omega} \qquad (21)$$

In metals, the resulting dynamical equation[1] for homogeneous, isotropic, stationary turbulence, which replaces Eq. (20), with the same notations, is

$$-\frac{\partial^2 v(k,x)}{\partial x^2} + v(k,x) = -\frac{1}{2}\int\frac{d^3\kappa}{\kappa^3}\frac{1+\boldsymbol{\kappa}\cdot\mathbf{e}_3}{|\mathbf{e}_3+\boldsymbol{\kappa}|^3}\left[1-\frac{(\boldsymbol{\kappa}\cdot\mathbf{e}_3)^2}{\kappa^2}\right]v(\kappa k,\kappa^2 x)v(k|\mathbf{e}_3+\boldsymbol{\kappa}|,x|\mathbf{e}_3+\boldsymbol{\kappa}|^2). \qquad (22)$$

This also admits, in the $\varepsilon=0$ limit of weak turbulence, a solution v(k,x) which does not depend on the first argument, and $u(k,x) = k^{-3}e^{-xm(x)}$, this time with an x-dependent m. With the change of variables $t=\omega\tau$ and $k'=k/\sqrt{\omega}$ in the second (middle) form of Eq. (21), x remains invariant, and a factor $1/\omega$ will appear in front of the integrals which themselves will yield a constant factor independent of ω or k. We obtain again a universal 1/f spectrum.

REFERENCES

[1] P.H. Handel: "Turbulence Theory for the Current Carriers in Solids and a Theory of 1/f Noise", Phys. Rev. A3, 2066 (1971); Z. Naturforschung 21a, 579-593 (1966).

[2] P.H. Handel: "1/f Noise - an 'Infrared' Phenomenon", Phys. Rev. Letters 34, p.1492 - 1494 (1975); "Quantum Approach to 1/f Noise", Phys. Rev. 22A, p. 745 (80).

[3] P.H. Handel: "Quantum and Classical Nonlinear Dynamics, Quantum Chaos and 1/f Fluctuations of Physical Cross Sections" submitted to the Physical Review.

[4] T. Kawakubo, Phys. Lett. 64A, 5 (1977).

[5] T. Musha and H. Higuchi, Jap. J. Appl. Phys. 15 1271 (1976); 17, 811 ('78).

AN ALTERNATIVE THEORY FOR QUANTUM 1/f NOISE BASED ON QUANTUM ELECTRODYNAMICS

C.M. Van VLIET

Centre de Recherches Mathématiques, Université de Montréal
Montréal, Québec, H3C 3J7, Canada

1. INTRODUCTION

The theory of quantum $1/f$ noise has been with us for over a decade, since Handel (1975) pointed out that infrared divergent coupling of electrons in nonuniform motion with the electromagnetic field causes radiative damping of the cross-sections involved in scattering, as well as a $1/f$ noise component in the spectrum of the associated carrier-flux fluctuations. Handel's original article is in quantum-field language, which is undoubtedly the path to be followed (though the precise nature of his operators Ψ and $\Psi^\dagger$, acting on photon-mode occupancy states, but associated with electron-current density, remains a mystery to us). His cross-section correction caused by radiative damping (effect in first order of the fine structure constant, $\alpha = e^2/4\pi\hbar c$) is in accord with the fundamental paper by Yennie et al. (1965), based on diagrammatic summation techniques. Handel later gave more popular ("gemeinverständliche") versions, based on stochastic one-particle dynamical states $\psi(\mathbf{r},t)$, among several others, his well-known Phys. Rev. paper (Handel 1980). These versions met with much criticism, see Kiss-Heszler (1986) and N-F-vK (1987). An extensive reply by Handel (1986) ("Answer to Objections Against my Theory"), containing second quantization arguments, as well as a much improved "stochastic Schrödinger field" theory, which in contrast to his 1980 paper, employs explicitly the interaction term $\mathbf{p}\cdot\mathbf{A}$, ($\mathbf{p}$ = electron momentum, $\mathbf{A}$ = vector potential), where the vector potential of the EM field is a sum of modes $a_{\mathbf{q}\lambda}\ \cos(\omega_q t + \gamma_{\mathbf{q}\lambda})$, was unfortunately never published. Yet, in our opinion, this formulation, which is patterned after the Kroll-Watson paper for differential cross-section corrections (1973), is Handel's most illuminating exposition within a one-electron many-photon framework and without reference to classical bremsstrahlung results. To finish this brief introduction, we still mention that van der Ziel and coworkers did many $1/f$ noise experiments in recent years, mainly involving micron-dimension modern semiconductor devices, which are in close agreement with the predicted quantum $1/f$ results. For an extensive review paper, see van der Ziel (1988).

2. FORMALISM BASED ON QUANTUM ELECTRODYNAMICS (QED)

After the Montreal Ninth Conference on Noise in Physical Systems (Van Vliet 1987), which contains many contributions and controversies on the quantum $1/f$ noise subject, we felt that an attempt should be made to devise a rigorous quantum field theory of radiative interaction effects, using for the noise, *as called for by van Kampen*, a correlation function based on the Heisenberg operator $\mathbf{J}$ in the

interaction picture and being bilinear in the dynamical state $|\psi\rangle$. Two basic procedures would be at our disposal in principle: a Keldish-Schwinger diagrammatic expansion, as in standard for this type of problem (Heitler 1954; Tremblay 1977), or the approach based on the Van Hove limit for the Heisenberg operators in the interaction picture, as developed by the author and her coworkers in recent years in a convergent re-formulation of linear response theory (Van Vliet et al. 1978-1984). The main results of this approach are that for asymptotic times t and interactions of strength λH^1, with $(\lambda^2 t)^n = \text{finite}$, n any power ≥ 1, the Heisenberg operator for the flux of B, $J_B(t)$, and the stationary current operator J_B are reduced to

$$J_B(t) = \lim_{\lambda,t} e^{i\mathcal{L}t} J_B^S = e^{-(\Lambda_d - i\mathcal{L}^0)t} J_B, \tag{1}$$

$$J_B = \lim_{\lambda,t} J_B(0+) = J_B^S - \Lambda_d B. \tag{2}$$

Here Λ_d and $\mathcal{L}$ are the master and Liouvillian superoperators, respectively ($\mathcal{L}^0$ its equivalent in the interaction picture), while $J_B^S = \dot{B}$ is the Schrödinger form of the flux operator.

More specifically, we consider a Fock space containing all electrons of the sample, $\{n_\zeta\}$, and the occupancies of all photon modes of the universe, $\{N_{\mathbf{q}\lambda}\}$, where λ is the polarization index. The occupation-form many-body states are then $|\gamma\rangle = |\{n_\zeta\}, \{N_{\mathbf{q}\lambda}\}\rangle$. To obtain quantization, we take the volume of the sample to be Ω_0 and of the photon box Ω; both drop out of the final results and, in particular, we let $\Omega \to \infty$. For the Hamiltonian involving electrons scattered by μV ($V = \sum_i v_i(\mathbf{r})$) and in interaction with the EM field via λH^1 we now have,

$$H = H_{\text{el}} + H_{\text{ph}} + \mu V + \lambda H^1 \equiv H^0 + \lambda H^1 \tag{3}$$

where

$$H^0 = \sum_\zeta \mathbf{n}_\zeta \varepsilon_\zeta + \sum_{\mathbf{q}\lambda} \underset{\sim}{N}_{\mathbf{q}\lambda}\, \hbar\omega_{\mathbf{q}}; \tag{4}$$

here $|\zeta)$ is a one-electron state involving scattering by $v(\mathbf{r})$, $\mathbf{n}_\zeta = c_\zeta^\dagger c_\zeta$ is the occupancy operator; similarly for $\mathbf{N}_{\mathbf{q}\lambda} = a_{\mathbf{q}\lambda}^\dagger a_{\mathbf{q}\lambda}$. For the interaction Hamiltonian, we derived earlier the result (Van Vliet 1988)

$$\begin{aligned} \lambda H^1 = \sum_{\zeta\zeta'\mathbf{q}\lambda} \frac{e}{mc} \left(\frac{\hbar c^2}{2\omega_{\mathbf{q}}\Omega}\right)^{1/2} c_\zeta^\dagger c_{\zeta'} [a_{\mathbf{q}\lambda}(\zeta\,|\mathbf{p}\cdot\hat{\boldsymbol{\epsilon}}_{q\lambda} e^{i\mathbf{q}\cdot\mathbf{r}}|\,\zeta') \\ + a_{\mathbf{q}\lambda}^\dagger(\zeta\,|\mathbf{p}\cdot\hat{\boldsymbol{\epsilon}}_{\mathbf{q}\lambda} e^{-i\mathbf{q}\cdot\mathbf{r}}|\,\zeta')], \end{aligned} \tag{5}$$

where we used rationalized Gaussian units and the radiation gauge (Messiah 1960). In (5), $\mathbf{p}$ is the electron momentum and $\hat{\boldsymbol{\epsilon}}_{\mathbf{q}\lambda}$ a unit vector in the direction of polarization and perpendicular to $\mathbf{q}$. The diagonal master operator, associated with transitions $\gamma \to \gamma''$ under the influence of λH^1, is now (Van Vliet et al. 1978-1984):

$$\Lambda_d B = -\sum_{\gamma\gamma''} |\gamma\rangle\langle\gamma|\, W_{\gamma''\gamma} [\langle\gamma''|B|\gamma''\rangle - \langle\gamma|B|\gamma\rangle] \tag{6}$$

where $W_{\gamma''\gamma} = W_{\gamma\gamma''}$ is given by the golden rule,

$$W_{\gamma''\gamma} = \frac{2\pi\lambda^2}{\hbar}|\langle\gamma''|H^1|\gamma\rangle|^2\delta(\mathcal{E}_{\gamma''} - \mathcal{E}_\gamma). \tag{7}$$

For the current density associated with particle transport ($\dot{\mathbf{r}} = \mathbf{v}$), we have in accord with (2), adding the nondiagonal part,

$$\mathbf{J}(\mathbf{r}) = \frac{1}{\Delta^3 r}\left[\sum_\zeta \mathbf{n}_\zeta(\zeta|\mathbf{v}|\zeta) - \sum_{\zeta\zeta'}(\Lambda_d - i\mathcal{L}^0)\, c_\zeta^\dagger c_{\zeta'}(\zeta|\mathbf{r}-\mathbf{r}_0|\zeta')\right], \tag{8}$$

where $\Delta^3 r$ is a small volume in the neighbourhood of $\mathbf{r}$ and where $\mathbf{r}_0$ is a suitable origin for the single electron states $|\zeta)$ (notice that we use round brackets for single particle states matrix elements and angular brackets for many-body scalar products). The first part of $\mathbf{J}$ is the "bare particle" flux; the second part is the radiative damping effect sought for.

3. EVALUATION AND RESULTS OF THE THEORY

The normalized electron wave functions of Bloch electrons scattered by $\mu v(\mathbf{r})$ are in the effective mass approximation, with $|\zeta) \to (\mathbf{r}|\zeta) \equiv \zeta_\mathbf{k}(\mathbf{r})$:

$$\begin{aligned}\zeta_\mathbf{k}(\mathbf{r}) &= \Omega_0^{-1/2}\left[e^{i\mathbf{k}\cdot\mathbf{r}} + \int d^3r\; G(\mathbf{r},\mathbf{r}')\,\mu v(\mathbf{r}')\,\zeta_\mathbf{k}(\mathbf{r}')\,\Omega_0^{1/2}\right] \\ &= \Omega_0^{-1/2}e^{i\mathbf{k}\cdot\mathbf{r}} + \frac{m^*}{4\pi^3\hbar^2}\Omega_0^{1/2}\int d^3k'\,\mu v_{\mathbf{k}'\mathbf{k}}\frac{e^{i\mathbf{k}'\cdot\mathbf{r}}}{k^2 - k'^2}.\end{aligned} \tag{9}$$

Notice that $|\zeta) = |\mathbf{k}) + |\psi_s)$, or $\zeta_\mathbf{k}(\mathbf{r}) = \varphi_\mathbf{k}(\mathbf{r}) + \psi_{s\mathbf{k}}(\mathbf{r})$, i.e. the sum of the incoming normalized Bloch wave and the scattered wave. The second line in (9) is the first Born approximation, $v_{\mathbf{k}\mathbf{k}'} = (\mathbf{k}|v|\mathbf{k}')$. In order for (9) to yield the outgoing scattered wave, the poles of the Green's function must be chosen as $k' = -k - i0$ and $k + i0$, so the denominator is more properly written as $k^2 - k'^2 - 0$, see Akhiezer and Berestetskii (1965); a contour integration then yields the standard spherical wave $\{\exp[ik\,|\mathbf{r}-\mathbf{r}_0|]\}/|\mathbf{r}-\mathbf{r}_0|$, see also Fig. 2 of Kousik et al. (1985).

The particle flux ("probability density current") has the operator form

$$\mathbf{j}(\mathbf{r}) = \frac{1}{2}\left[\delta(\mathbf{r}-\mathbf{r}')\frac{\mathbf{p}}{m^*} + \frac{\mathbf{p}}{m^*}\delta(\mathbf{r}-\mathbf{r}')\right] \tag{10}$$

where $\mathbf{p} = (\hbar/i)\nabla$. Then for the one particle state matrix element if $|\mathbf{r}-\mathbf{r}_0| \sim r$

$$(\zeta|\mathbf{j}|\zeta) \simeq (\Delta^3 r)^{-1}(\zeta|\mathbf{v}|\zeta) = \frac{\hbar\mathbf{k}}{m^*} + \mathbf{k}'\frac{m^*\Omega_0}{4\pi^2\hbar^3 r^2}\mu^2|v_{\mathbf{k}'\mathbf{k}}|^2, \tag{11}$$

where $\mathbf{k}'$ points into the direction $\boldsymbol{\Omega}$ of the scattering process. The first term can be omitted since it does not contribute to $\langle \mathrm{d}I^{\mathrm{d}}_{\mathrm{bare}}\rangle_{\mathrm{eq}}$ defined below. The current scattered within $(\boldsymbol{\Omega},\ \boldsymbol{\Omega}+\mathrm{d}\boldsymbol{\Omega})$ is $|\mathbf{j}|\,r^2\mathrm{d}\boldsymbol{\Omega}$ and will be denoted by $\mathrm{d}i(\boldsymbol{\Omega})$. For the cross section, we have

$$\sigma_{\mathrm{av}}(\boldsymbol{\Omega})\,\mathrm{d}\boldsymbol{\Omega} = (\psi_s|j|\psi_s)\,r^2\mathrm{d}\boldsymbol{\Omega}(m^*\Omega_0/\hbar k). \tag{12}$$

Note that analogous to (10), we can associate *an operator* with the cross-section, so that $\sigma_{\rm av} = (\psi_s\,|\sigma|\,\psi_s)$. For the many-body diagonal "bare particle" current operator in the direction interval $(\mathbf{\Omega},\ \mathbf{\Omega}+\mathrm{d}\mathbf{\Omega})$ we have $\mathrm{d}\,I^{\rm d}_{\rm bare} = \sum \mathrm{d}i(\tilde{\Omega})$, where the sum is over all electrons. Or, in second quantization form, we have from the first part of (8) and the above,

$$\mathrm{d}\,I^{\rm d}_{\rm bare} = \sum_{\mathbf{k}} \mathbf{n}_{\mathbf{k}} k' \frac{m^*\Omega_0}{4\pi^2\hbar^3}\mathrm{d}\mathbf{\Omega}\,\mu^2|v_{\mathbf{k}'\mathbf{k}}|^2, \tag{13}$$

where we still note that $k' \approx k$, while $\mu^2|v_{\mathbf{k}'\mathbf{k}}|^2\mathrm{d}\mathbf{\Omega} \propto \sigma_{\rm av}(\mathbf{\Omega})\,\mathrm{d}\mathbf{\Omega}$. Taking an additional average over a canonical ensemble, we have

$$\langle \mathrm{d}\,I^{\rm d}_{\rm bare}\rangle_{\rm eq} = Tr(\rho_{\rm eq}\,\mathrm{d}\,I^{\rm d}_{\rm bare}) = \sum_{\mathbf{k}} \langle n_{\mathbf{k}}\rangle_{\rm eq} k \frac{m^*\Omega_0}{4\pi^2\hbar^3}\mathrm{d}\mathbf{\Omega}\mu^2|v_{\mathbf{k}'\mathbf{k}}|^2. \tag{14}$$

We now turn to the interaction matrix element. From (9), we find up to first order in μv,

$$\begin{aligned}(\zeta_{\mathbf{k}}\,|\mathbf{p}\cdot\hat{\boldsymbol{\epsilon}}_{\mathbf{q}\lambda}\,e^{-i\mathbf{q}\cdot\mathbf{r}}|\,\zeta'_{\mathbf{k}}) &= (\varphi_{\mathbf{k}}\,|\mathbf{p}\cdot\hat{\boldsymbol{\epsilon}}_{\mathbf{q}\lambda}\,e^{-i\mathbf{q}\cdot\mathbf{r}}|\,\psi_{s\mathbf{k}}) + hcj \\ &= \frac{2m^*}{\hbar}\mu v_{\mathbf{k}\mathbf{k}'}\frac{(\mathbf{k}-\mathbf{k}')\cdot\hat{\boldsymbol{\epsilon}}_{\mathbf{q}\lambda}}{k'^2-k^2}.\end{aligned} \tag{15}$$

From this we find λH^1, $W_{\gamma''\gamma}$, $\Lambda_{\rm d}$, and finally $\mathbf{J}^t_{\rm rad}$; the latter is the total particle flux in $(\mathbf{\Omega},\ \mathbf{\Omega}+\mathrm{d}\mathbf{\Omega})$ due to interaction ($\mathcal{L}^0$ part) and radiative damping ($\Lambda_{\rm d}$ part), as given by the second part of (8). A lengthy but straightforward computation yields

$$\begin{aligned}\mathbf{J}^t_{\rm rad} = {} & \frac{1}{\Delta^3 r}\sum_{\gamma}\sum_{\mathbf{k}\mathbf{k}'\mathbf{q}\lambda}|\gamma\rangle\langle\gamma|\frac{2\pi}{\hbar}\left(\frac{2e}{\hbar c}\right)^2\left(\frac{\hbar c^2}{2\omega_{\mathbf{q}}\Omega}\right)\mu^2|v_{\mathbf{k}'\mathbf{k}}|^2 \\ & \times\left[\frac{(\mathbf{k}-\mathbf{k}')\cdot\hat{\boldsymbol{\epsilon}}_{q\lambda}}{k'^2-k^2}\right]^2(\zeta_{\mathbf{k}}\,|\mathbf{r}-\mathbf{r}_0|\,\zeta_{\mathbf{k}})\{(1-n_{\mathbf{k}})\,n_{\mathbf{k}'}[(N_{\mathbf{q}\lambda}+1)\,\delta(\varepsilon_{\mathbf{k}}-\varepsilon_{\mathbf{k}'}+\hbar\omega_{\mathbf{q}}) \\ & + N_{\mathbf{q}\lambda}\delta(\epsilon_{\mathbf{k}}-\epsilon_{\mathbf{k}'}-\hbar\omega_{\mathbf{q}})] - (1-n_{\mathbf{k}'})\,n_{\mathbf{k}}[(N_{\mathbf{q}\lambda}+1)\,\delta(\varepsilon_{\mathbf{k}}-\varepsilon_{\mathbf{k}'}-\hbar\omega_{\mathbf{q}}) \\ & + N_{\mathbf{q}\lambda}\delta(\epsilon_{\mathbf{k}}-\epsilon_{\mathbf{k}'}+\hbar\omega_{\mathbf{q}})]\} + \mathcal{L}^0\text{-part}.\end{aligned} \tag{16}$$

We note that the two terms within the curly brackets are as in a Boltzmann operator. However, the second term is a flux associated with the outgoing waves $\mathbf{k}\to\mathbf{k}'$, while the first term is a flux associated with the incoming waves $\mathbf{k}'\to\mathbf{k}$. One can show that by a proper choice of poles, the first part is to be deleted and the second part doubled[1]. Next, we confine ourselves to the "vacuum" state $|\gamma_0\rangle = |\{n_{\mathbf{k}}\},\ \{0\}\rangle$ in which no photons are present *ab initio* (remember that in the interaction picture $|\gamma\rangle$ are the eigenstates of H^0); thus in (16), we set $N_{\mathbf{q}\lambda} = 0$[2]. Thus, for the expectation

[1] Conversely, the first term can be carried over into the second one whereby its sign is changed since $\mathbf{r}-\mathbf{r}_0 \propto \pm\mathbf{k}'$ for the two parts.

[2] If there is a radiation background, one obtains a $1/\omega^2$ spectral component, which by renormalization leads to a white spectrum, as shown in a very recent paper by Handel (1988).

value in the state $|\gamma_0\rangle$, taking also the average over a canonical ensemble, we find [noticing also that the $\mathcal{L}^0$-part does not contribute to $\langle\gamma_0|\ldots|\gamma_0\rangle$],

$$\langle J^t_{\rm rad}\rangle_{\rm eq} = -\frac{1}{\Delta^3 r}\sum_{\mathbf{k}\mathbf{k}'q\lambda}\frac{4\pi}{\hbar}\left(\frac{2e}{\hbar c}\right)^2\left(\frac{\hbar c^2}{2\omega_{\mathbf{q}}\Omega}\right)\mu^2|v_{\mathbf{k}'\mathbf{k}}|^2$$
$$\times\left[\frac{(\mathbf{k}-\mathbf{k}')\cdot\hat{\boldsymbol{\epsilon}}_{\mathbf{q}\lambda}}{k'^2-k^2}\right]^2(\zeta_{\mathbf{k}}|\mathbf{r}-\mathbf{r}_0|\zeta_{\mathbf{k}})\langle n_{\mathbf{k}}(1-n_{\mathbf{k}'})\rangle_{\rm eq}\delta(\epsilon_{\mathbf{k}}-\epsilon_{\mathbf{k}'}-\hbar\omega_{\mathbf{q}}). \tag{17}$$

The final evaluation is rather simple. We consider a nondegenerate electron gas, i.e., $1-n_{\mathbf{k}'}\approx 1$, and write

$$\sum_{\mathbf{k}'}\to\frac{\Omega_0}{8\pi^3}\int\frac{\mathrm{d}\varepsilon_{\mathbf{k}'}\mathrm{d}S_{\mathbf{k}'}}{\hbar v_{\mathbf{k}'}}=\Omega_0\int\mathrm{d}\varepsilon_{\mathbf{k}'}\frac{k'm^*}{8\pi^3\hbar^2}\mathrm{d}\boldsymbol{\Omega}, \tag{18}$$

whereby we notice that the spin is usually conserved in scattering. Further, for the position matrix element associated with $\Delta^3 r$, we find for the contribution of $\psi_{sk}(\mathbf{r})$, $(\zeta|\mathbf{R}|\zeta)\to\frac{1}{2}\Delta\mathbf{R}$ and we multiply with $\mathrm{d}\mathbf{S}_R\cdot$ to convert to $\langle\mathrm{d}I_{\rm rad}\rangle_{\rm eq}$. The integration of the factor $[\ \ ]^2$ over the delta function then leaves a term $1/\omega_{\mathbf{q}}^2$. Noticing also

$$\sum_{\mathbf{q}\lambda}\to(\Omega/\pi^2c^3)\int\omega_{\mathbf{q}}^2\mathrm{d}\omega_{\mathbf{q}},\quad[(\mathbf{k}-\mathbf{k}')\cdot\hat{\boldsymbol{\epsilon}}_{\mathbf{q}\lambda}]^2=\frac{1}{3}\Delta k^2, \tag{19}$$

we easily obtain

$$\langle\mathrm{d}\,I^t_{\rm rad}\rangle_{\rm eq}=-\sum_{\mathbf{k}}\langle n_{\mathbf{k}}\rangle_{\rm eq}\left(\frac{e^2}{4\pi\hbar c}\right)\left(\frac{2\hbar^2\Delta k^2}{3\pi m^{*2}c^2}\right)\left(\frac{km^*\Omega_0}{4\pi^2\hbar^3}\right)\mu^2|v_{\mathbf{k}'\mathbf{k}}|^2$$
$$\times\,\mathrm{d}\boldsymbol{\Omega}\int_{\omega_0}^{\omega_{\max}}\mathrm{d}\omega/\omega. \tag{20}$$

The first two factors ( ) yield αA; comparing further with (14), the result for the total current in $(\boldsymbol{\Omega},\ \boldsymbol{\Omega}+\mathrm{d}\boldsymbol{\Omega})$ is

$$\langle\mathrm{d}\,I\rangle_{\rm eq}=\langle\mathrm{d}\,I^{\rm d}_{\rm bare}\rangle_{\rm eq}\left[1-\alpha A\int_{\omega_0}^{\omega_{\max}}\frac{\mathrm{d}\omega}{\omega}\right]. \tag{21}$$

For the cross-section of a single scattering event, we simply omit $\sum_{\mathbf{k}}\langle n_{\mathbf{k}}\rangle_{\rm eq}$. Hence, also

$$\langle\sigma(\boldsymbol{\Omega})\rangle_{\rm eq}=\sigma_0(\boldsymbol{\Omega})\left[1-\alpha A\int_{\omega_0}^{\omega_{\max}}\frac{\mathrm{d}\omega}{\omega}\right], \tag{22}$$

in accord with Yennie et al. (1961).

Finally, we must compute the noise. Since $\sigma(\boldsymbol{\Omega})$ could be defined as an operator (see below (12)), we can compute the Heisenberg operator correlation function. Space does not allow us to do this here. So we give a heuristic argument. For the

variance, we have $\langle \Delta\sigma^2 \rangle_{\rm eq} = \langle \sigma^2 \rangle_{\rm eq} - \langle \sigma \rangle_{\rm eq}^2$. Now one can expect that $\langle \sigma^2 \rangle_{\rm eq} = \sigma_0^2 + 0(\alpha A)^2$. Thus up to order $0(\alpha A)$ from (22),

$$\langle \Delta\sigma(\mathbf{\Omega})^2 \rangle_{\rm eq} = [\sigma_0(\mathbf{\Omega})]^2 \int_{\omega_0}^{\omega_{\max}} 2\alpha A \frac{{\rm d}\omega}{\omega} + 0(\alpha A)^2, \tag{23}$$

which is Handel's result. A more correct computation of the spectrum $S_{\Delta\sigma}$ based on the correlation function, to be published shortly, also yields the radiative corrections to all higher orders so that the spectrum goes as $(1/\omega)^{1-\alpha A}$; so we can let $\omega_0 \to 0$. Naturally, $\omega_{\max} \sim 1/\tau_c$, where τ_c is the collision relaxation time. We further note that $\langle \Delta\sigma^2 \rangle_{\rm eq}$ implies equilibrium fluctuations in the transition rates $w_{\mathbf{k}\mathbf{k}'}$ of the scattering process, see Kousik et al. (1985).

4. DISCUSSION AND CONCLUSIONS

We have given the briefest possible outline of an exact QED theory for quantum $1/f$ noise. The following aspects are to be noted.

(i) Quantum $1/f$ noise is a many-electron effect, as is evidenced by the occurrence of the factor $\langle n_{\mathbf{k}}(1-n_{\mathbf{k}'}) \rangle_{\rm eq}$. For metals, both carrier densities are to be evaluated at the Fermi surface. Then $\langle n_{\mathbf{k}}(1-n_{\mathbf{k}'}) \rangle_{\rm eq} \approx \langle \Delta n_{\mathbf{k}}^2 \rangle_{\rm grand\ can} \simeq \langle n_{\mathbf{k}}(\varepsilon_F) \rangle_{\rm eq}(2kT/3\varepsilon_F)$. An effective one-electron result analogous to (22) and (23) for the cross-section fluctuations, can be given with αA replaced by $\eta\alpha A$, $\eta \simeq 2kT/3\varepsilon_F$. This means that quantum $1/f$ noise in metals is strongly suppressed and generally not observable.

(ii) The above derivation is foremost tailored for impurity scattering, in which case $\mu v(\mathbf{r})$ is a screened Coulomb potential (Brooks-Herring approach). However we believe the derivation can be extended and adapted to electron-phonon scattering, in which case the phonon population, say $\{M_{\mathbf{Q}}\}$, also enters into the picture through the rates $w_{\mathbf{k}'\mathbf{k}}$. The extension to cross-sections not associated with scattering (capture in traps, etc.), or processes like α-particle decay, is not warranted by the theory presented in this paper. As to vacuum tubes: bremsstrahlung due to deflection by nuclei in the anode does occur (continous X-ray spectrum, see Heitler 1954), but the linear acceleration of the transit *yields no matrix element* for λH^1, since $\Delta\mathbf{p} \cdot \hat{\boldsymbol{\epsilon}}_{q\lambda} = 0$. The present theory, therefore, deals with condensed matter only and has no bearing on quantum $1/f$ noise in vacuum tubes, if such noise exists.

(iii) The coupling considered here is with infrared photons. Though criticists of quantum $1/f$ noise have been sceptical of, say, 1 hz photons, we emphasize that infrared divergence in QED *is an established fact* (Yennie et al. 1961; Heitler 1954) indeed, there is no limit to the low frequency end of the electromagnetic spectrum even in the renormalized formalism. The same is not true for other excitations, not associated with the vacuum state (phonons, magnons, rotons, etc); moreover, λH^1 has a different structure for these interactions. Thus, e.g., electron-phonon interaction associated with intraband scattering gives a Lorentzian, of which the "low" frequency tail is ordinary white Nyquist noise.

(iv) The current ${\rm d}I(\mathbf{\Omega})$ of this paper, even when multiplied by the electron charge and integrated over the scattering angles, is *not the terminal electrical current.* The latter could be obtained in principle if the trace over a nonequilibrium ensemble in an external field were taken, as in linear response theory. However, this is a superfluous many-body exercise, since the equilibrium average of ${\rm d}I(\mathbf{\Omega})$ yields directly the cross-section and its spectrum yields the cross-section $1/f$ noise. The

latter then yields the mobility-fluctuation $1/f$ noise; the precise computation goes as in the paper of Kousik et al. (1985). The present theory is therefore a *model for mobility fluctuations*, and the only one we know of today. Since the mobility is a complicated functional of $\sigma(\mathbf{\Omega})$ or of the scattering rates $w_{\mathbf{kk'}}$, we have $\langle \Delta\mu^2 \rangle / \langle \mu \rangle^2 \neq \langle \Delta\sigma(\mathbf{\Omega})^2 \rangle / \langle \sigma(\mathbf{\Omega}) \rangle^2$. Remains valid: $[\langle \Delta I^2_{\text{electr}} \rangle / \langle I^2_{\text{electr}} \rangle]_{\mathbf{E}\to 0} = \langle \Delta\mu^2 \rangle / \langle \mu \rangle^2$.

(v) From the above, it follows that $2\alpha A$ *is not the Hooge parameter of the electrical current noise*, even when (Δk^2) is weighted over the conduction or valence band, or when multiplied with $\exp(-\theta_D/2T)$ (with θ_D the Debye temperature) for umklapp processes, as in the paper by van der Ziel-Handel-Zhu-Duh (1985). While heuristically their approach may have its merits, our present treatment upholds the Kousik-Van Vliet method. As to the calculated Hooge parameters, the two methods yield at 200–300 Kelvin the same order of magnitude ($\alpha_H \sim 10^{-8} - 10^{-9}$), perhaps by coincidence.

(vi) Handel's basic result for the spectrum, as expressed by Eq. (23), has been fully vindicated. As to his method, we note that stochastic states $\{\psi(\mathbf{r},t)\}$ are presently widely used in problems on quantum chaos. Space is not available, however, to make a detailed comparison of the steps in his approach and the route followed in this paper.

REFERENCES

Akhiezer, A.I. and Berestetskii, V.B. (1965), "Quantum Electrodynamics", Interscience N.Y., Chapter V. Also in Russian original edition.

Handel, P.H. (1975), Phys. Rev. Lts **34**, 1492.

Handel, P.H. (1980), Phys. Rev. **A22**, 745.

Handel, P.H. (1986), unpublished.

Handel, P.H. (1988), Phys. Rev. **A38**, 3082.

Heitler, W. (1954), "The Quantum Theory of Radiation", 3rd Ed., Oxford University Press.

Kiss, L.B. and Heszler, P. (1986), J. Phys. **C19**, L631.

Kousik, G.S., Van Vliet, C.M., Bosman, G. and Handel, P.H. (1985), Adv. in Physics **34**, 663; also Physica Status Solidi (b) **154**, in press.

Kroll, N.M. and Watson, K.M. (1973), Phys. Rev. **A8**, 804.

Messiah, A. (1960), "Mécanique quantique", Tome II, Dunod, Paris, 870.

Nieuwenhuizen, Th. M., Frenkel, D. and van Kampen, N.G. (1987), Phys. Rev. **A35**, 2750.

Tremblay, A.-M. (1977), Ph.D. Thesis, Yale University.

van der Ziel, A., Handel, P.H., Zhu, X. and Duh, K.H. (1985), IEEE Trans. Electron Dev. **ED-32**, 667.

van der Ziel, A. (1988), Proc. IEEE **76**, 233.

Van Vliet, C.M. and coworkers (1978-1984), J. Math. Phys. **19**, 1345; **20**, 2573; **23**, 318; **25**, 1391.

Van Vliet, C.M. (1987), Proc. Ninth Conf. Noise in Physical Systems (Ed.), World Scientific Public., Singapore.

Van Vliet, C.M. (1988), Physica **A150**, 244.

Yennie, D.R., Frautchi, S.C. and Suura, H. (1961), Ann. Physics (N.Y.) **13**, 379.

10th Int.Conf. on Noise in Physical Systems
1989 Budapest, Hungary

CHARACTERISTIC FUNCTIONAL OF PHYSICAL THERMAL NOISE WHICH INCLUDES EQUILIBRIUM 1/f NOISE

D. WOLF, P.H. HANDEL,* M. SEKINE**

Institute of Applied Physics, University of Frankfurt, FRG
*Physics Department, University of Missouri, St. Louis, Mo 63121, USA
**Department of Applied Electronics, Tokyo Institute of Technology, Japan

I. INTRODUCTION

In a previous paper [1] the characteristic functional of quantum 1/f noise was derived. This result was applicable to quantum 1/f noise in any cross-section or process rate, and in currents or voltages. In another paper [2] the application of quantum 1/f noise to thermal equilibrium noise was performed, and the quantum 1/f Nyquist theorem was formulated. Deviations from the Gaussian form of thermal noise were expressed [2],[3] in terms of the characteristic function.

The present paper performs the final step in the study of thermal noise with infrared radiative corrections, by calculating the characteristic functional of physical thermal noise. We call it "physical" because we refer to the actually observed thermal equilibrium (Johnson) noise, rather than to the strictly Gaussian noise expected from the Nyquist formula without infrared radiative corrections. The small quantum 1/f contributions come in as time-dependent infrared radiative corrections, required by the interaction of the current carriers with the electromagnetic field, or by the reaction of the bremsstrahlung back on the current which has produced it. Knowing the characteristic functional of a process is the best we can do, the highest level and most comprehensive and complete description possible for a random process.

II. AMPLITUDE DISTRIBUTION AND CHARACTERISTIC FUNCTION

In terms of current fluctuations in equilibrium, to derive the characteristic function of the physical thermal noise variable ξ, we express it in terms of the unmodulated theoretical Nyquist noise variable x:

$$\xi = x(G/G_o)^{1/2} = x + xy, \qquad (1)$$

where $y=\delta G/G$ is the fractional fluctuation in the conductivity $G=G_o+\delta G$ of the conductor whose thermal equilibrium current fluctuations we are considering. Let the quantum 1/f

noise variable y obey a Gaussian amplitude distribution of dispersion σ_2, and x one of dispersion σ_1. We prove now that in terms of the zero-order Bessel function of imaginary argument, the product $z=xy$ will have an amplitude distribution $P(z)=(1/\pi\sigma_1\sigma_2)K_o(z/\sigma_1\sigma_2)$ which has an elementary characteristic function

$$X(v) = (1 + \sigma_1^2\sigma_2^2v^2)^{-1/2}. \qquad (2)$$

In order to derive the amplitude distribution of $z = xy$, we introduce $\eta = \ln z$, $\alpha = \ln x$ and $\beta = \ln y$. From $\eta = \alpha + \beta$ we obtain the distribution

$$P''(\eta)d\eta = d\eta\int P'_1(\alpha)P'_2(\eta-\alpha)d\alpha$$

$$= (2d\eta/2\pi\sigma_1\sigma_2)\int\exp[-(e^{2\alpha})/2\sigma_1^2+\alpha]\exp[-e^{2(\eta-\alpha)}/2\sigma_2^2+(\eta-\alpha)]d\alpha$$

$$=(e^{\eta}\, d\eta/2\pi\sigma_1\sigma_2)\int_{-\infty}^{\infty}\exp\{-[e^{\eta}/\sigma_1\sigma_2]\cosh\varepsilon\}d\varepsilon = (e^{\eta}\, d\eta/\pi\sigma_1\sigma_2)K_o(e^{\eta}/\sigma_1\sigma_2), \qquad (3)$$

where $P'(\alpha)$ and $P'_2(\beta)$ are derived from Gaussians of dispersion σ_1 and σ_2 respectively, $\varepsilon = 2\alpha - \eta + \ln(\sigma_2/\sigma_1)$, and K is the modified zero-order Bessel function. Returning to the real variable z, we obtain from $P''(\eta)d\eta = P(z)dz$

$$P(z) = (1/\pi\sigma_1\sigma_2)K(z/\sigma_1\sigma_2). \qquad (4)$$

The corresponding characteristic function is elementary:

$$X(v) = (1 + \sigma_1\sigma_2v^2)^{-1/2}. \qquad (5)$$

This is just what we wanted to prove.

Our next step is the calculation of the characteristic function of ξ. Due to the mutual dependence of x and z, the characteristic function of ξ differs from the product of the characteristic functions of x and z. We obtain instead the amplitude p.d.f.

$$I(\xi) = \int_{-\infty}^{\infty}P_1(x)P_2(\xi/x - 1)(1/|x|)dx$$

$$= [\exp(-1/2\sigma_2^2)/2\pi\sigma_1\sigma_2]\int_{-\infty}^{\infty}\exp[-x^2/2\sigma_1^2 - \xi^2/2x^2\sigma_2^2 + \xi/x\sigma_2^2]dx/|x|$$

$$= [\exp(-1/2\sigma_2^2)/2\pi\sigma_1\sigma_2]\int_{0}^{\infty}\exp[-x^2/2\sigma_1^2 -\xi^2/2x^2\sigma_2^2]\cosh(\varepsilon/x\sigma_2^2)dx/x, \qquad (6)$$

which we have written down directly, but which can also be obtained by substituting $(e^{\alpha} - 1)^2$ for $e^{2\alpha}$ in Eq. (3). This distribution tends to a Gaussian in the limit $\sigma_2\to 0$, but differs slightly from a Gaussian in general. The skewness is zero, but the kurtosis exhibits a small deviation from the Gaussian amplitude p.d.f..

By performing a Fourier transform of Eq. (6) we find again that the characteristic function of the total physical thermal noise is elementary

$$X(k) = (1 + k^2\sigma_1^2\sigma_2^2)^{1/2}\ \exp[-k^2\sigma_1^2/2(1 + k^2\sigma_1^2\sigma_2^2)]. \qquad (7)$$

while the amplitude distribution itself can not be expressed in elementary functions.

In the remaining part of the paper we derive the characteristic functional of thermal noise including thermal equilibrium quantum 1/f noise. We first familiarize the reader with characteristic functionals in general.

III. CHARACTERISTIC FUNCTIONAL

The complete characterization of a random process j(t) is given by its characteristic functional [4]

$$H[x(t)] = \langle e^{i(j,x)} \rangle. \qquad (8)$$

where j(t) is in our case the relative (or fractional) current (or voltage) fluctuation j(t) = $[J(t) - \langle J \rangle]/\langle J \rangle$, x(t) is the argument function of the functional, and the scalar product in Hilbert space is defined as

$$(j,x) = \int_0^T j^*(t)x(t)dt. \qquad (9)$$

Here T is the interval of observation of the fluctuations, i.e., the length of the sample considered from the stationary random process at hand. For instance, the characteristic functional of a Gaussian process is

$$H_G[x(t)] = \exp[-(1/2)\langle (j,x)^2 \rangle]. \qquad (10)$$

In particular, for thermal short-circuit current fluctuations in a resistor of conductance G described by the simple Nyquist formula with $\sigma_1^2 = 4kTGB$, where B is the bandwidth, the characteristic functional is

$$H[x] = \exp[-2\int k_B T G |x_f|^2 df] = \exp[-2k_B T G B \int_{-\infty}^{\infty} |x(t)|^2 dt], \qquad (11)$$

where x_f is the Fourier-transformed argument function. Here the two-sided frequency integral is limited to the allowed bandwidth B, and the time integral to the interval T of observation. Since $B \to \infty$, $k_B T$ must be replaced by $hf/[e^{hf/kT} - 1]$ and included in the frequency integral, while the time integral must also include the Fourier-transformed Planck kernel.

The characteristic functional of quantum 1/f noise affecting the current j has been shown [1] to be

$$H[x(\varepsilon)] = \exp[-2\pi\alpha_A (I^2/N) \int (\varepsilon/\varepsilon_o)^{\alpha_A} |x(\varepsilon)|^2 d\varepsilon/\varepsilon]. \qquad (12)$$

Here α_A is the infrared exponent $\alpha_A = (4\alpha/3\pi)\langle (\Delta v/c)^2 \rangle$, which is known to enter the expression of both the basic quantum 1/f noise formula and the characteristic functional of quantum 1/f noise in two ways: as a coefficient and as an additional exponent of the frequency f. Sommerfeld's fine structure constant $\alpha = e^2/\hbar c = 1/137$ is well known, and so is the Boltzmann constant k_B. Eq. (12) gives the characteristic functional of 1/f noise for a sample containing N current carriers with an average velocity change $\langle (\Delta v)^2 \rangle$ in the scattering processes which determine their mobility.

For each value of the frequency we now use Eqs. (11) and (12), repeating the steps which led to the derivation of Eq. (5). This yields the characteristic functional of the term z=xy in Eq. (1)

$$X[v(f)] = \exp[-(1/2)\int \ln(1 + \sigma_1\sigma_2 v^2)df]$$
$$= \exp\{-(1/2)\int \ln[1 + 8k_BTG(\alpha A/fN)(f/f_o)^{\alpha A}v^2(f)df]. \quad (13)$$

According to Eq. (1) we now have to add the Nyquist term x. Repeating for every frequency f the steps which led us to Eq. (7) we, obtain now the characteristic functional of physical thermal noise ζ in the form

$$F[k(f)] = \exp\{-(1/2)\int \ln[1 + 8k_BTG(\alpha A/fN)(f/f_o)^{\alpha A}k^2(f)]df\}$$
$$\exp\{-2k_BTG\int k^2(f)[1 + 8k_BTG(\alpha A/fN)(f/f_o)^{\alpha A}k^2(f)]^{-1}df\}. \quad (14)$$

Eq. (14) gives the characteristic functional of physical thermal noise for a sample containing N current carriers with an average velocity change $\langle(\Delta v)^2\rangle$ in the scattering processes which determine their mobility, resulting in a well-defined infrared exponent αA.

One of the authors (PHH) would like to thank Prof. T. Musha for his help in many ways, and to acknowledge the hospitality of the Tokyo Institute of Technology in 1987.

REFERENCES

[1] P.H. Handel and D. Wolf, Phys. Rev. A26, 3727 (1982)

[2] P.H. Handel, C.M. Van Vliet and A. van der Ziel, "Derivation of the Nyquist-1/f Noise Theorem", Proc. 7th Int. Conf. on Noise in Physical Systems and 3rd Int. Conf. on 1/f Noise, Montpellier, May 17-20, 1983, M. Savelli, G. Lecoy and J.P. Nougier Editors, North Holland Publ. 1983, p. 93

[3] P.H. Handel, D. Wolf and K.M. Van Vliet: "Non Gaussian Amplitude Distribution of Thermal Noise in a resistor with 1/f Noise", Proc. 6th Int. Conf. on Noise in Physical Systems. P.H.E. Meijer, R.D. Mountain and R.J. Soulen Editors, NBS Special Publication 614, p. 196 (1981)

[4] See, e.g., J. L. Lumley, Stochastic Tools in Turbulence (Academic, New York, 1970), p. 48.

10th Int.Conf. on Noise in Physical Systems
1989 Budapest, Hungary

SIMPLE INTERPRETATION OF 1/f NOISE PHENOMENON

A.M. ZAKLIKIEWICZ

ITE
02-668 Warszawa, Poland

1. Introduction

All electronic materials and devices investigated up to date show 1/f noise during d.c.current flow. There is no information about any element free of 1/f noise in d.c.current flow conditions. 1/f noise is sometimes named structural noise. It seems to be a pertinent definition. It is commonly known that 1/f noise level in semiconductors and semiconductor devices depends mainly on technological defects, density and quality. However, 1/f noise in polycrystals and grainy materials is related mainly to the grain boundaries *). Thus it is very difficult to estimate 1/f noise level by means of one, generalized relation.

2. 1/f noise generation

The author proposes to introduce the elementary cell of 1/f noise, consisting of current noise source i_n and two resistors - serial R_s and parallel R_p (Fig. 1). Any considered object contains defined number of such cells. We must remember that the

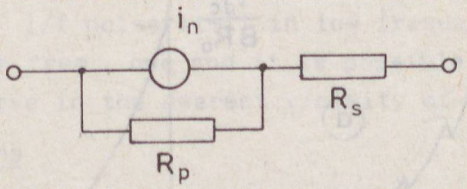

Fig.1. Scheme of the elementary 1/f noise cell

*) E.Kuźma, A.M.Zaklikiewicz, Nonpublished results of investigation.

noise measured at external leads of the object is not the whole noise generated inside this object. It seems that 1/f noise may be well generated in metal as in semiconductor or resistor material. The metal structure is often more imperfect than semiconductor or even resistor structure but in this case 1/f noise internal sources are shortened by a low resistance of material.

General equation of 1/f noise spectral density S may be given in the form:

$$S(f) = \alpha I^{\beta} f^{-\gamma},$$

where I - d.c.current, f - frequency.

In most cases the exponent $\gamma \approx 1$. The coefficient α depends on a density and detailed structure of the introduced elementary 1/f noise cells. The structure is determined by the quantity of cell elements i_n, R_s and R_p. The exponent β should be dependent mainly on R_s to R_p ratio. Not whole d.c.energy supplied from outside takes part in 1/f noise generation.Many years ago the author had investigated 1/f noise in resistors and stated that $\beta \approx 2$. Subsequent investigations of diodes gave β value from 0.7 to 4.1 and this value depended on the sample case and was a function of d.c. current density [1] .

3. Spectrum near null frequency

As the second proposal, the author suggests to consider 1/f noise as a null frequency spectrum. The 1/f noise phenomenon shows the existence of another specific phenomenon in the nature. It is null frequency signal. The spectrum investigation close to f = 0 frequency is obviously more complicated than for

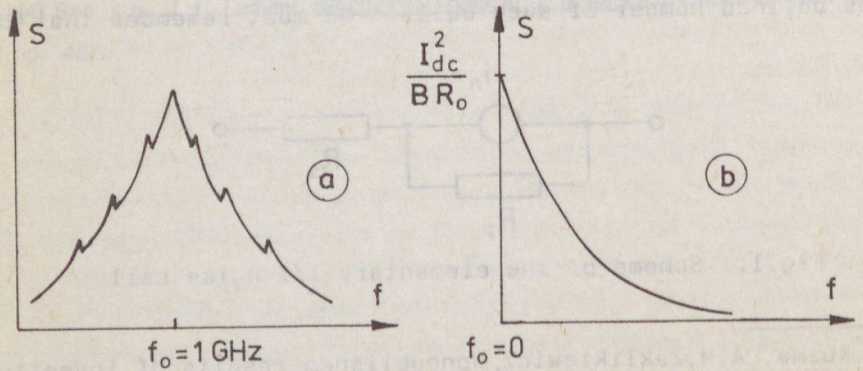

Fig.2.The signal spectra for f = 1 GHz (a) and for f = 0 (b)

example at f = 1 GHz. It is even difficult to draw such a spectrum. We need use linear frequency scale to show signal at f = 0. The signal spectra for f = 1 GHz (a) and for f = 0 (b) are presented only demonstratively in Fig. 2.

Simple example is presented to make clear the difficulties of experimental investigation of 1/f noise at very low frequencies. Let us take that the current I_{dc} = 2 mA is flowing through the resistor R_o = 1 kΩ with 1/f noise above thermal noise level from the 1 kHz frequency. We assume that both direct current power and noise power are defined for the bandwith B = 1 Hz and that 1/f noise law is valid in the whole frequency region.

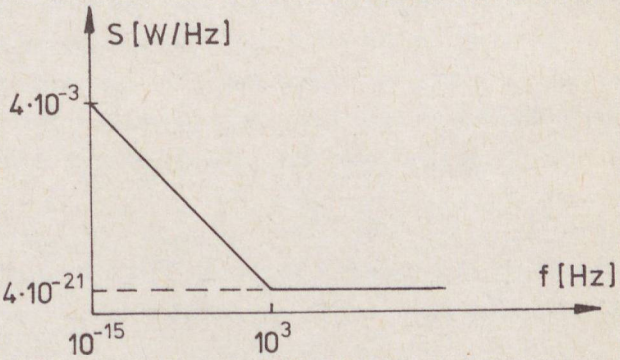

Fig.3. Simplified calculation of very low frequency 1/f noise limit

Simple calculation shows that 1/f noise reaches direct current level at the frequency f = 10^{-15} Hz (Fig. 3). This involves the time period T approximately equal to 10^{10} days.

The calculation presented here gives only approximative estimation of the 1/f noise limit in low frequency range. Exponent γ may differ from one and it is possible to flatten the 1/f noise curve in the nearest vicinity of null frequency.

4. Conclusions

The consideration of 1/f noise generation on the basis of proposed elementary cells may be helpful to solve the problem of that noise mechanism, especially in the case of resistors noise investigation.

I would like to underline once more that we can observe only a part of 1/f noise generated inside investigated object and that only a part of d.c. power supplied to investigated object takes part in the 1/f noise generation mechanism.

Acknowledgements

The author is indebted to Prof. A.Kobus and Prof.J.Kolodziejski for extremely helpful comments on the manuscript.

Reference

1. Zaklikiewicz A.M., Some results of low frequency noise measurements in Schottky barrier diodes, Archiwum Elektrotechniki, 17, pp. 215-219, PWN Warszawa 1968 (in Polish)

SESSION 8

1/f NOISE IN PHYSICAL SYSTEMS
(e.g. MATERIALS)

10th Int.Conf. on Noise in Physical Systems
1989 Budapest, Hungary

IS THERE A SIMPLE EMPIRICAL RELATION FOR 1/f NOISE?

F.N. HOOGE

Department of Electrical Engineering,
Eindhoven University of Technology
Eindhoven, The Netherlands

It is now 20 years ago that a paper entitled "1/f noise is no surface effect" appeared in Physics Letters [1]. Contrary to the then current opinion the author concluded that 1/f noise did not originate at the surface because of the validity of a relation that summarized experimental findings on 1/f noise in homogeneous semiconductors. That relation was

$$\frac{S_R}{R^2} = \frac{\alpha}{Nf} \qquad (1)$$

The total number of free electrons N appeared in the denominator, but not the thickness or other dimensions of the sample. The last point excluded surface effects.

The introduction of N was not based on a theoretical model. At that time we did not know what the electrons were doing while producing 1/f noise. Even today that is a problem. But we may follow the naïve reasoning that, whatever the electrons do, they do it independently. Then for purely statistical reasons, we may expect the factor 1/N. In this paper I shall discuss whether this naïve reasoning is essentially correct.

Considering relation (1) as the relative noise of an ensemble of N electrons, α is nothing else but a measure of the noise normalized to one electron and a frequency of 1 Hz. The surprising fact was that the 1969 collection of experimental data suggested that α was a constant with the value 2×10^{-3}. Therefore relation (1) could be considered as a clear summary of a multitude of experimental results obtained on many materials, metals and semiconductors. It made possible a comparison of 1/f noise in the conductivity, Hall effect and thermo e.m.f., from which it followed that the number of free electrons does not fluctuate with a 1/f spectrum, but that it is the mobility of the electrons that fluctuates [2].

We could go one step further. The noise is in the mobility, but are all scattering mechanisms effective in producing 1/f noise? By comparing samples with varying mixtures of scattering mechanisms we concluded that only lattice scattering produces the 1/f noise with $\alpha_{latt} = 2 \times 10^{-3}$. When other scattering mechanisms are also active we must use

$$\alpha = \left(\frac{\mu}{\mu_{latt}}\right)^2 \alpha_{latt} \qquad \text{since} \qquad \frac{1}{\mu} = \frac{1}{\mu_x} + \frac{1}{\mu_{latt}} \qquad (2),(3)$$

In highly doped or in very thin samples, α will be strongly reduced by a factor of 100 or more. If mechanisms other than lattice scattering are present relation (2) must be used. It is not a possibility for correction for use if needed, and ignored on the other hand, if α already had the desired order of magnitude.

There has always been severe scattering in α-values reported. This was not too alarming so long as deviating α-values could be blamed on faulty contacts, inhomogeneous material or ill-understood devices. But when silicon samples made by modern I.C. technology were studied, α-values of a quite different order of magnitude were found.

Modern technology means two things:

(i) higher quality of the lattice, because of epitaxial growth techniques

(ii) very small dimensions, sometimes even submicron.

Measurements on noise in samples of different size made on the same wafer, showed that small dimensions brought no extra complications [3] (see fig. 1). Measurements on samples in which the quality of the lattice was changed, showed a very systematic variation in α. The results of Vandamme and Oosterhoff on silicon are shown as one example [4]. Radiation damage was partly repaired by annealing. Values of α, measured at room temperature, showed an exponential dependence on the inverse of the temperature at which the sample had been annealed. See fig. 2.

The results of the many applications of relation (1) to metals [5,6] can be summarized in two statements.

(i) The value of α in metals decreases systematically with the degree of perfectness of the sample.

(ii) The range of α-values is narrower than in semiconductors. The vertical axis of the plots of the systematic deviations of α usually is in units 10^{-3}.

The success of relation (1) is greater in metals than in semiconductors. But the fact that α is no constant is often taken as proof of the absolute failure of relation (1) in metals.

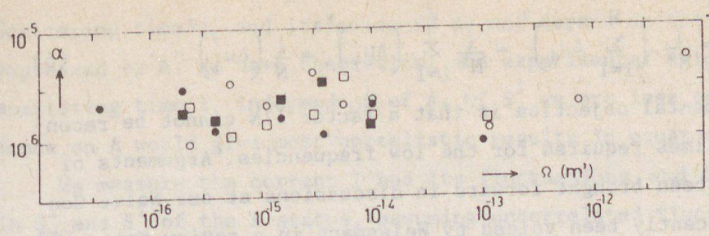

Figure 1: α as a function of the effective noise volume for p-Si at 300 K (•) and 77 K (■) for n-Si at 300 K (o) and 77 K (□). Ref. [3].

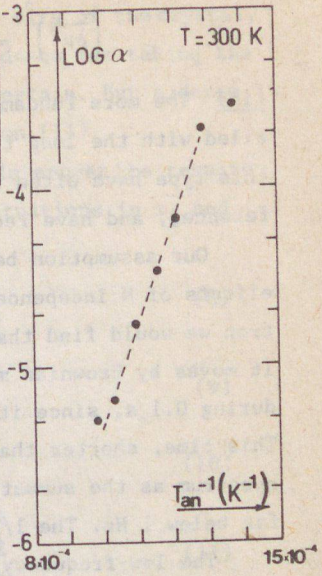

Figure 2: Experimentally observed α-values at T = 300 K as a function of the reciprocal anneal temperature. Ref. [4].

1/N ?

Up to here we have discussed the observed variation in the value of the parameter α, that originally looked like a constant. Apart from the disappointing fact that α scatters wildly, there is the much more fundamental question whether a relation with a factor 1/N makes any sense at all [7]. Some people think it is absurd even to try a relation of this type [5].

The objections raised against the factor 1/N are twofold: (i) statistical arguments, (ii) arguments of more physical nature based on the long characteristic times needed for the low-frequency part of the spectrum.

(i) There has been a long discussion on statistical arguments against the factor 1/N. This discussion has been definitely settled 7 years ago [8-11].

Making a theoretical model for 1/f noise, means making the calculations for an electron i which is representative for the electrons in the sample. One thus discusses the behaviour of this "average" electron, finds μ_i and $\Delta\mu_i$, and no factor N appears in the analysis.

In the experiments one always observes a group of N electrons. The experimental findings on N electrons (e.g. $\overline{\mu}^N$) can be expressed as properties of one electron. The essential steps are

$$\overline{\mu}^N = \frac{1}{N}\sum_{i=1}^{N}\mu_i = \mu_i \qquad \overline{\Delta\mu}^N = \frac{1}{N}\sum_{i=1}^{N}\Delta\mu_i \qquad (4),(5)$$

$$\left(\overline{\Delta\mu^N}\right)^2 = \frac{1}{N^2}\left(\sum_{i=1}^{N}\Delta\mu_i\right)^2 = \frac{1}{N^2}\sum_{i=1}^{N}\left(\Delta\mu_i\right)^2 = \frac{1}{N}\left(\Delta\mu_i\right)^2 \qquad (6)$$

(ii) The more fundamental objection is that a factor 1/N cannot be reconciled with the long times required for the low frequencies. Arguments of this type have often been brought forward in discussions at our Noise Conferences, and have recently been voiced by Weissmann in a review paper [5].

Our assumption behind the factor 1/N is that we add the uncorrelated effects of N independent electrons. If we could follow one individual electron we would find that it stays in the sample only for a short time. When it moves by Brownian motion it will stay in a sample with a length of 1 cm during 0.1 s, since its diffusion coefficient D is of the order of 10^{-3} m^2/s. This time, shorter than 1 s, creates great problems if we consider the 1/f spectrum as the summation of Lorentzian spectra. The spectrum is still 1/f, far below 1 Hz. The 1/f dependence has been observed even at 10^{-6} Hz [12].

The low-frequency contributions require slow processes with very long time constants τ and statistical weight $1/\tau$

$$\int_{\tau_1}^{\tau_2} \frac{1}{\tau}\cdot\frac{\tau}{1+\omega^2\tau^2}\,d\tau = \frac{\pi}{2}\cdot\frac{1}{\omega} \quad \text{for} \quad \frac{1}{\tau_2} < \omega < \frac{1}{\tau_1} \qquad (7)$$

The problem is now, how can electrons that are present for only such short times contribute to fluctuations with those very long time constants ?

These arguments have been countered by pointing out that the slow processes are in the crystal lattice. We have good evidence that the 1/f noise is in the lattice scattering. Somehow the cross-sections for the electrons fluctuate slowly with a 1/f spectrum. There are always N electrons to probe the cross-sections of the lattice modes. We do not follow individual electrons. But the group of - on the average - N electrons that is continuously present, measures the slowly varying lattice properties. Individual electrons may move in and out, the lattice is permanent.

However, if we try to reformulate these verbal arguments in mathematical language we shall find it difficult to end up with a factor 1/N. Even a crude model suffices to show that N is not the obvious choice for normalizing the noise power. Our model is a crystal containing A atoms, and therefore having A electron states in the conduction band. We neglect the differences in energy of these states. Therefore they all have the same probability of being occupied by an electron, given by the Fermi function ϕ. The total number of free electrons is then given by $N = \phi A$. We assume equal scattering probability for each electron i, given by $1/\tau_i$. The noise in τ_i is given by S_τ^i.

Scattering time τ_i and its noise S_τ^i do not depend on the size of the crystal, expressed by A. We have theoretical and experimental evidence for taking the scattering time τ_i independent of A. Of S_τ^i we are less certain. But a dependence on A would give most unrealistic results in equation (11).

We measure the current I and its fluctuations, and interpret the results in S_ϕ^i and S_τ^i of the A states, assuming uncorrelated fluctuations in τ_i and in ϕ_i.

$$I = c \sum_{i=1}^{A} \phi_i \tau_i = cA\phi_i\tau_i = cN\tau_i \tag{8}$$

$$\Delta I = c\phi_i \sum_{i=1}^{A} \Delta\tau_i + c\tau_i \sum_{i=1}^{A} \Delta\phi_i \tag{9}$$

$$S_I = c^2\phi_i^2 A S_\tau^i + c^2\tau_i^2 A S_\phi^i \tag{10}$$

$$\frac{S_I}{I^2} = \frac{1}{A} \cdot \frac{S_\tau^i}{\tau_i^2} + \frac{1}{A} \cdot \frac{S_\phi^i}{\phi_i^2} = \frac{1}{A} \cdot \frac{S_\tau^i}{\tau_i^2} + \frac{1}{N} \cdot \frac{S_\phi^i}{\phi_i} \tag{11}$$

The redistribution of the electrons over the states is a fast process. S_ϕ will be white up to very high frequencies. If S_τ is 1/f, we find 1/f fluctuations in I, proportional not to 1/N but to 1/A. If S_τ^i were to depend on A we would not have found the factor 1/A. We have experimental proof that the noise goes either with 1/A or 1/N; there is no question of $1/A^n$ where n differs appreciably from 1.

Of course we do not claim to have proved here that, in expressions for 1/f noise, the number of electrons N must be replaced by the number of atoms A. But since N had been used without much in the way of theoretical or experimental arguments we now have sufficient reason to try A and see what the results will be. There is really not much experimental evidence that proves that the noise is proportional to 1/N. In older summaries, the noise of samples of different materials, sizes, doping levels, etc. was plotted versus N. The results could be summarized by one simple factor α/N. In later studies, samples of different size were made on one homogeneous wafer. Figure 1 shows the result of such a study. This work demonstrated that the noise is inversely proportional to the volume. Since all samples have the same electron concentration volume can be translated into total number of electrons. But these experiments do not show whether the volume or the number is the essential parameter.

A good proof would be an experiment in which the number is varied by varying the concentration in the same volume. Photoconductivity would be a

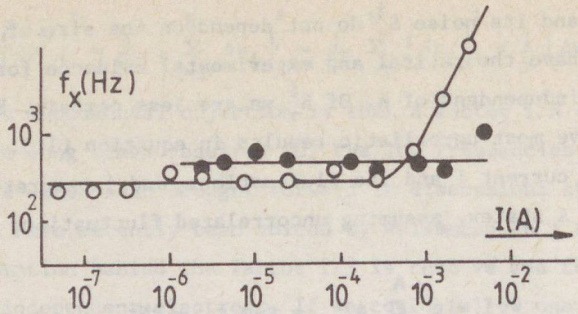

Figure 3: Corner frequency as function of current for long diodes. Ref.[13]

nice example if it could be realized without too many disturbing effects, such as inhomogeneity, contact potentials, etc. that would complicate the outcome.

The only demonstration that N is the essential factor comes from Kleinpenning's analysis of the forward diode [13]. In general one must prefer homogeneous samples to complicated devices, but the analysis of this simple device is so straightforward that it seems to me that we run no great risk by accepting it as good evidence.

Now let us consider a simplified model that shows all the essential features. Kleinpenning's more detailed analysis leads to changes in numerical factors only.

We consider a p^+-n junction in forward bias. The current I injects holes into the N region. There they recombine with recombination time τ. A concentration of holes builds up in the N region. The total number of holes P is given by

$$\frac{I}{q} = \frac{P}{\tau} \tag{12}$$

The diode shows 1/f noise and shot noise

$$S_I = \frac{\alpha}{Pf} I^2 + 2qI \tag{13}$$

The frequency of the crossing point f_x is given by

$$f_x = \frac{\alpha I^2}{P} \cdot \frac{1}{2qI} = \frac{\alpha I^2}{I\tau/q} \cdot \frac{1}{2qI} = \frac{\alpha}{2\tau} \tag{14}$$

f_x is independent of I. This was confirmed by the experiments. From the measurements followed $\alpha = 1.2 \times 10^{-3}$. If α/P were replaced by γ/A then f_x would go with I. Figure 3 shows the result of Kleinpenning's measurements. Similar experimental results were obtained by Kleinpenning on Si single-injection diodes [14], by Fang et. al. on Si p-i-n power diodes [15] and by

Wu, Anderson and Van der Ziel on long diodes of $Cd_xHg_{1-x}Te$ [16]. In all cases α-values of several times 10^{-3} were found.

1/A ?

All in all, the evidence for N being the essential parameter is meagre. We could try the other candidate A as well. The choice of A as the relevant parameter can be justified by several arguments.

1. The experiments with samples of different size and the same dope, demonstrated not so much the dependence on N, but rather on the volume of the sample. Volume can be expressed by the number of atoms A.
2. If the noise is in the lattice mobility, the fluctuating entities are phonon modes. Their number equals the number of atoms.
3. With metals, it is difficult to estimate the effective number of valence electrons. Here one has always used A as an approximation of N.

In order to avoid old α's based on N and new α's based on A we now introduce a quantity γ, honoring the tradition followed in noise research on metals.

Definitions of α and γ:

$$\frac{S_R}{R^2} = \frac{\alpha}{Nf} \qquad (1) \qquad \left| \qquad \frac{S_R}{R^2} = \frac{\gamma}{Af} \qquad (15)$$

$$\frac{\gamma}{\alpha} = \frac{A}{N} = \frac{5 \cdot 10^{22}\ \mathrm{cm}^{-3}}{n} \qquad (16)$$

The numerical value $5 \cdot 10^{22}\ \mathrm{cm}^{-3}$ is sufficiently accurate for most semiconductors and metals. This value is used for constructing the framework of fig. 4.

In fig. 4 we have plotted experimental results obtained in homogeneous materials. They were published since the Rome conference 4 years ago. We included all published data without discrimination. Some older data are included, mainly from systematic investigations of the dependence of α on volume or on N. The values of α derived from data of devices are not included in the figure. Their derivation is much too indirect, requiring too complicated reasoning and too much interpretation. The general impression of this plot is that α is better than γ. There is a clustering around $\alpha \sim 10^{-3}$ and around $\gamma \sim 10^{3}$.

Several groups of materials are worth mentioning.

Semiconductors. We must keep in mind that α-values may be reduced by a factor of 10^3 or so in high-quality silicon. When the quality of the lattice has been improved by annealing in a series of experiments, then we use the α-value of the lowest quality material of this series.

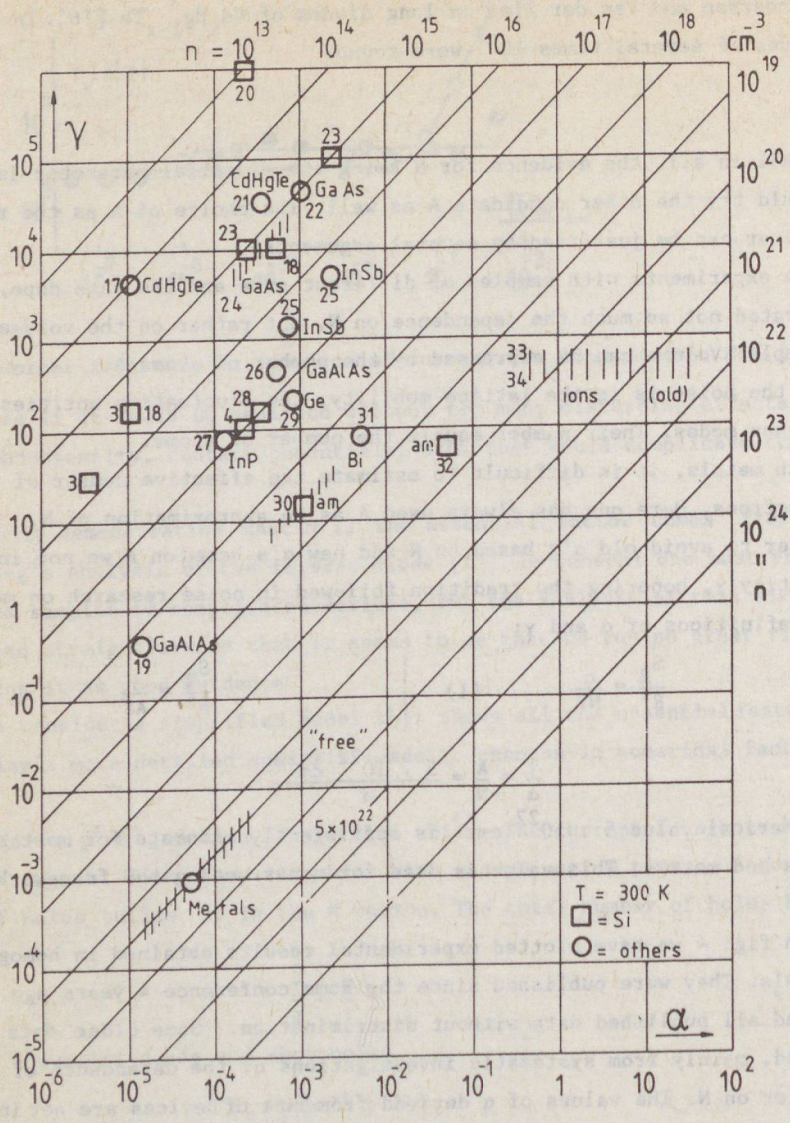

Figure 4: Values of γ and α at T = 300 K. The numbers refer to the List of References.

Several materials other than silicon are represented in the plot. The quality of their crystal lattice is that of silicon before the I.C. era. Here we see a return to $\alpha \sim 10^{-3}$ that was normal for silicon long ago.

Metals. In old publications, α-values were calculated using the number of valence electrons per atom. Those old α's will now be called γ's in our new notation. The number of electrons that effectively takes part in the conduction is smaller than the number of valence electrons. It is the group of electrons that are within a few kT of the Fermi-level. For a calculation of α, we must use the effective number of free electrons. Calculations on simple band models show that the reduction factor is about 20 [35].

Ions. There are old reports on α-values of aqueous solutions of ions [33,34]. However, in recent work on ultra-pure solutions, no 1/f noise has been observed at all [36,37]. If we still attach value to the old measurements it is noteworthy that already in the first publication [33] it was mentioned that α was found to be proportional to the ion concentration. We can express those old results, in which α varies, by one single value $\gamma = 500$.

CONSEQUENCES

In view of the meagre evidence for α/N, one may doubt the correctness of the empirical relation (1). The question is then, what happens to the conclusions drawn from its application to thermo e.m.f., Hall effect, etc? From those experiments we concluded that 1/f noise is in the mobility not in number fluctuations, and that lattice scattering is the only noise source.

Most of these conclusions remain valid. The experiments showed that 1/f noise is inversely proportional to the volume. Perhaps volume can be replaced by number of electrons. If the last step is incorrect it does not matter here. Thermo e.m.f., Hall effect, etc. were studied on samples with fixed volume and number, by measuring the effects of external fields or temperature gradients. Incorrect values of α would have no influence on the ratio of the effects with and without fields. Conclusions regarding Δn and $\Delta\mu$ remain valid.

We concluded from measurements on samples thinner than the electron free path, that surface scattering had no 1/f noise. The reasoning here was based on geometrical arguments, depending on the ratio of thickness and free path. The argument stays correct, whether the noise is written as α/N or as γ/A.

Problems arise with conclusions regarding impurity scattering. We compared the noise of highly doped and weakly doped samples [2]. Since the impurity scattering was increased by high doping, dominating impurity scattering goes together with high electron concentrations. If it is correct

to use α/N, as was assumed in the original work, then $\alpha_{\text{low dope}} > \alpha_{\text{high dope}}$ because of the factor $(\mu/\mu_{latt})^2$. But if γ/A is correct fig. 4 shows that $\alpha_{\text{low dope}} < \alpha_{\text{high dope}}$, which could be counteracted by the factor $(\mu/\mu_{latt})^2$. In any case we are no longer certain of the correctness of the factor $(\mu/\mu_{latt})^2$ in relation (2). First we must decide on α/N or γ/A.

IS THERE A SIMPLE EMPIRICAL RELATION ?

The straight answer is "No". This does not mean that we do not know anything at all. A classification is possible between normal and extremely high-quality material; the difference being a factor of 10^3 or so in α or γ.

The relative noise can be normalized in two ways. Either the noise is expressed per free electron, which leads to α-values, or the noise is expressed per atom, which leads to γ-values. From a theoretical point of view we should prefer γ/A rather than α/N. But fig. 4 shows that α is more successful.

The factor α/N still is a useful parameter. Perhaps it should not be, but it is ! However, by no means we can conclude that a theoretical model for 1/f noise could only be correct, if its result contains a factor 1/N.

REFERENCES

[1] F.N. Hooge., Phys. Lett. 29A, 139-140 (69).
[2] F.N. Hooge, T.G.M. Kleinpenning and L.K.J. Vandamme., Rep. Prog. Phys. 44, 479-532 (81).
[3] R.H.M. Clevers., Physica B154, 214-224 (89).
[4] L.K.J. Vandamme and S. Oosterhoff., J. Appl. Phys. 59, 3169-3174 (86).
[5] M.B. Weissman., Rev. Mod. Phys. 60, 537-571 (88).
[6] N. Giordano., Crit. Rev. Sol. State and Mat. Sc. In press.
[7] L.B. Kiss and T.G.M. Kleinpenning., Physica 145B, 185-189 (87).
[8] K.M. van Vliet and R.J.J. Zijlstra., Physica 111B, 321-322 (81).
[9] A. van der Ziel and K.M. van Vliet., Physica 113B, 15-17 (82).
[10] F.N. Hooge., Physica 114B, 391-392 (82).
[11] A. van der Ziel, C.M. van Vliet, R.J.J. Zijlstra and R.P. Jindal., Physica 121B, 420-422 (83).
[12] T.G.M. Kleinpenning and A.H. de Kuijper., J. Appl. Phys. 63, 43-45 (88).
[13] T.G.M. Kleinpenning., Physica 98B, 289-299 (80).
[14] T.G.M. Kleinpenning., Physica 94B+C, 141-151 (78).
[15] P. Fang, L. He, A.D. van Rheenen, A. van der Ziel and Q. Peng., Solid State El. 32, 345-348 (89).
[16] X. Wu, J.B. Anderson and A. van der Ziel., IEEE Trans. Electron Devices, ED33, 1971-1977 (87).
[17] N. Oda and T. Yamagata., Int. J. Infrared and Millimeter Waves 8, 133-153 (87).
[18] R.H.M. Clevers., Physica 147B, 305-310 (87).
[19] S. Kugler., J. Appl. Phys. 66, 219-222 (89).
[20] E.G. Guk, N.V. D'yakonova, M.E. Levinshtein., Sov. Phys. Semicond. 22, 707-708 (88).
[21] I.S. Bakshi, M.Z. Kodalashvili, E.A. Sal'kov and B.I. Khizhnyak., Sov. Phys. Semicond. 22, 1377-1380 (88).
[22] S.N. Vainshtein, M.E. Levinshtein and S.L. Rumyantsev., Sov. Tech. Phys. Lett. 13, 267-268 (87).
[23] J. Luo, W.F. Love and S.C. Millar., J. Appl. Phys. 60, 3196-3198 (86).
[24] N.V. D'yakonova, M.E. Levinshtein and S.L. Rumyantsev., Sov. Phys. Semicond. 22, 661-663 (88).
[25] S.A. Alekperov, N.Ya. Guseinov, Ch.O. Kadzhar and E.Yu. Salaev., Sov. Phys. Semicond. 20, 973-974. (86).
[26] M. Tacano, Y. Sugiyama and H. Soga., Solid State El. 32, 49-55 (89).
[27] M. Tacano, K. Oigawa and Y. Sugiyama., Solid State El. 31, 1243-1245 (88).
[28] R.H.M. Clevers., J. Appl. Phys. 62, 1877-1881 (87).
[29] N.P. Garbar et. al., Sov. Phys. Semicond. 21, 245-249 (87).
[30] F.Z. Bathaei and J.C. Anderson., Phil. Mag. B55, 87-100 (87).
[31] J. Bisschop and A.H. de Kuijper., J. Appl. Phys. 55, 1353-1358 (84).
[32] A. D'Amico, G. Fortunato and C.M. van Vliet., Solid State El. 28, 837-844 (85).
[33] F.N. Hooge and J.L.M. Gaal., Philips Res. Repts. 26, 77-90 (71).
[34] T. Musha and K. Sugita., J. Phys. Soc. Japan 51, 3820-3825 (82).
[35] T.G.M. Kleinpenning and J. Bisschop., Physica 128B, 84-87 (85).
[36] A. de Vos, R.J. van den Berg and J. de Goede., Phys. Lett. A102, 320-322 (84).
[37] S.M. Bezrukov, A.I. Izkhin and A.J. Sibilev., Phys. Lett. A123, 477-480 (87).

10th Int.Conf. on Noise in Physical Systems
1989 Budapest, Hungary

FLUCTUATIONS OF BRILLOUIN SCATTERED LIGHT INTENSITY WITH QUARTZ SPECIMEN

T. MUSHA, G. BORBÉLY, M. SHOJI

Department of Applied Electronics,
Tokyo Institute of Technology
Nagatsuta, Midoriku, Yokohama 227, Japan

1/f resistance fluctuations were observed in thermal equilibrium as fluctuations of variance of thermal voltage noise by Clarke and Voss (1974). Later, Kleinpenning (1976) and Vaes and Kleinpenning (1977) suggested that mobility fluctuations were one of the possible origins of 1/f resistance fluctuations. Moreover, phonon scattering only among others was found by Hooge and Vandamme (1978) to be generating 1/f mobility fluctuations. Recently Mihaila (1986, 1987) found that in bipolar transistors mobility fluctuations have the 1/f spectrum in which the 1/f coefficient showed singularities corresponding to phonon energies. Apart from electric conductors, 1/f fluctuations of the imaginary part of the dielectric constant of triglycine sulfate were observed by Musha et al. (1988) near the critical temperature for ferroelectric-paraelectric transition. Based on these findings we tried to directly observe phonon number fluctuations of a quartz specimen in thermal equilibrium by means of laser light scattering, and we have obtained evidence that phonon number fluctuations have 1/f spectrum.

EXPERIMENT

When a laser light is passed through a transparent specimen, a small part of it is scattered in all directions by thermal fluctuations in dielectric constant of the material. Since fluctuations in the dielectric constant are caused by lattice vibrations, it can be said that the laser light is scattered by "phonons" in the specimen. Conservation of the wave momentum and energy gives $f_p = 2f_i(u/c)v\,sin(\theta/2)$ where f_p is the phonon frequency, f_i frequency of the incident light, u the acoustic velocity within the specimen, c the speed of light in free space,

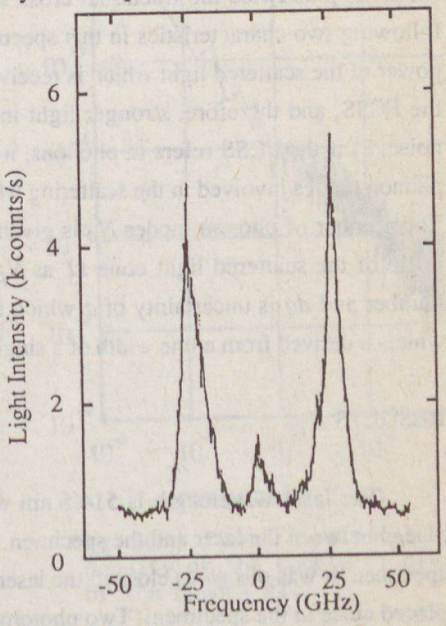

Fig.1 Brillouin spectrum of a quartz specimen.

v the refractive index and θ the scattering angle. The Brillouin spectrum measured with an etalon is shown in Fig.1, where the Rayleigh component with the same frequency as the incident light is very weak and a pair of phonon components are 25 GHz apart from the Rayleigh component. An etalon was not used in the present experiment because it was not stable for a long measurement (20 - 30 hours). As the light scattering cross section by phonons is proportional to the phonon number, the light intensity into a certain direction is proportional to the phonon number involved in the scattering.

Since the laser intensity in general is fluctuating, the scattered light intensity contains fluctuations of the incident light intensity (and beam position) and of the scattering cross section. The incident light intensity fluctuations have been removed by taking a ratio of outputs, I_{s1} and I_{s2}, of two photomultipliers receiving the scattered light. As $I_s + \delta I_s = a(I_i + \delta I_i)(g + \delta g)$ where I_s is the output of a photomultiplier (the number of photon counts per second), I_i is the incident light intensity, g is the cross section, a is a proper constant and δ indicates increment. Therefore, one has

$$\frac{I_{s1}}{I_{s2}} = \frac{(I_{i1}+\delta I_{i1})(g_1+\delta g_1)}{(I_{i2}+\delta I_{i2})(g_2+\delta g_2)} = 1 + \frac{\delta I_{i1}}{I_{i1}} - \frac{\delta I_{i2}}{I_{i2}} + \frac{\delta g_1}{g_1} - \frac{\delta g_2}{g_2} \qquad (1)$$

Here it has been assumed that $I_{i1} \approx I_{i2}$ and $I_{s1} \approx I_{s2}$. If fluctuations of the cross sections are not correlated to each other, the psd of I_{s1}/I_{s2} equals twice the fractional photon shot noise spectrum (FPSNS) plus twice the fractional cross section spectrum (FCSS). Therefore, there are the following two characteristics in this spectrum; 1) the FPSNS is inversely proportional to the power of the scattered light which is received by the photomultiplier while this does not affect the FCSS, and therefore, stronger light intensity enhances the FCSS above the photon shot noise; 2) if the FCSS refers to phonons, it should be inversely proportional to the number of phonon modes involved in the scattering while it is not sensitive to the scattered light intensity. The number of phonon modes N_p is given in terms of the scattering volume V and the solid angle of the scattered light cone Ω as $N_p = 2V\Omega q^2 dq/(2\pi)^3$, where q is the phonon wave number and dq is uncertainty of q which is equal to uncertainty of photon wave number dk which is derived from a line width of a single mode laser light, 3 MHz.

RESULTS

The laser wavelength is 514.5 nm with 100 mW (single mode), and an ND filter was placed between the laser and the specimen. To minimize laser beam displacements within the specimen, it was placed as close to the laser as possible (15 cm). A slit of 0.1 mm in width was placed close to the specimen. Two photomultipliers were placed at $90° \pm 8°$ with the incident laser light and the photon counting technique was used. A typical example of the count by the

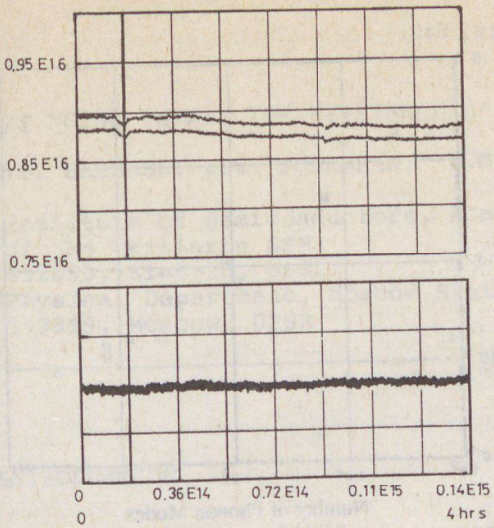

Fig.2 The photocounts/s of two photomultipliers (above) and their ratio.

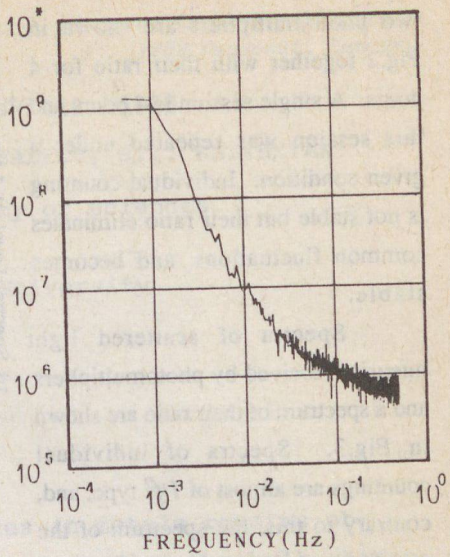

Fig.3(a) Power spectral density of the counts (photomultiplier #1).

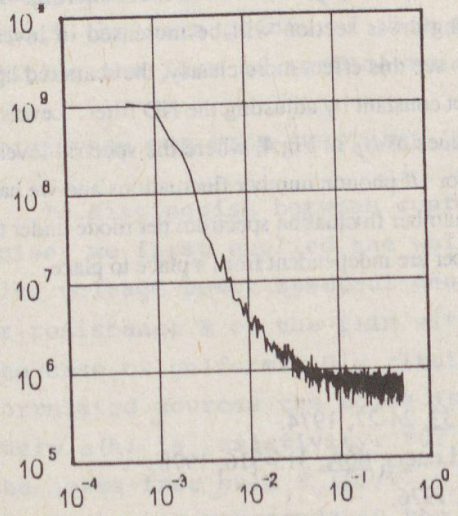

Fig.3(b) Power spectral density the counts (photomultiplier #2).

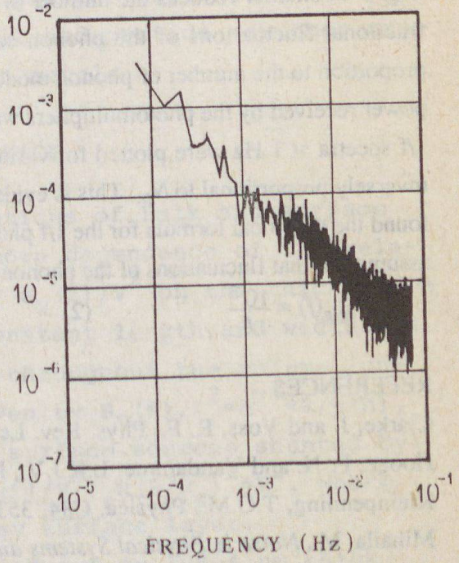

Fig.3(c) Power spectral density of the counts #1 divided by the counts #2.

two photomultipliers are shown in Fig.2 together with their ratio for 4 hours. A single session is 4 hours and this session was repeated under a given condition. Individual counting is not stable but their ratio eliminates common fluctuations, and becomes stable.

Spectra of scattered light intensity received by photomultipliers and a spectrum of their ratio are shown in Fig.3. Spectra of individual countings are almost of $1/f^2$ type, and, contrary to this, the spectrum of the counting ratio is of $1/f$ type. Evidence for that this spectrum is attributed to phonon number fluctuations was obtained in the following fashion.

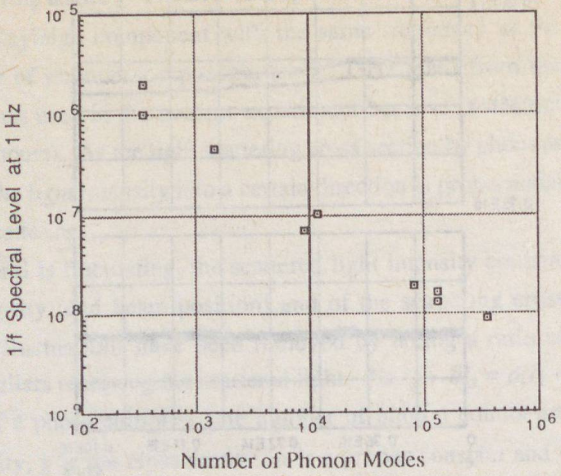

Fig.4 Dependence of the 1/f spectral level at 1 Hz on the number of phonon modes involved in the scattering.

Two identical diaphragms with a hole were placed in front of the lenses to limit the scattering angle. A smaller reduces the number of phonon modes (N_p) involved in the scattering. The fractional fluctuations of the phonon scattering cross section will be increased in inverse proportion to the number of phonon modes. To see this effect more clearly, the scattered light power received by the photomultipliers was kept constant by adjusting the ND filter. Levels of 1/f spectra at 1 Hz were plotted for various values of N_p in Fig.4, where the spectral level is inversely proportional to N_p. This is evidence for 1/f phonon number fluctuations and we have found the empirical formula for the 1/f phonon number fluctuation spectrum per mode under the assumption that fluctuations of the phonon number are independent from a place to place.

$$S_{\delta g/g}(f) = \frac{10^{-3}}{f} \qquad (2)$$

REFERENCES

Clarke, J. and Voss, R. F., Phys. Rev. Letters, 33, 24-27, 1974.

Hooge, F. N. and Vandamme, L.K.J.V., Phys. Letters, 66A, 315-316, 1978.

Kleinpenning, T.G.M., Physica, C84, 353-361, 1976.

Mihaila, M., *Noise in Physical Systems and 1/f Noise, ed. by A. D'Amingo and P. Mazetti, Elsevier, 433, 1986.*

Mihaila, M.,*Noise in Physical Systems, ed. by C.M.Van Vliet, World Scientific, 343, 1987.*

Musha, T., Nakajima, A. and Akabane, H., Jap. J. Appl. Phys., 27, L311-313, 1988.

Vaes, H.M.J. and Kleinpenning, T.G.M.K., J. Appl. Phys., 48, 5131-5234, 1977.

1/f NOISE IN Al: THE EXISTENCE OF SURFACE NOISE

I.S. BAKSHEE, V.V. POTEMKIN,* E.A. SALKOV, B.I. KHIZHNYAK

Institute of Semiconductors, Academy of Sciences
of the Ukrainian SSR
252650, Kiev-28, USSR
*Physical Department, Moscow State University
119899, Moscow, USSR

INTRODUCTION

The location of 1/f noise sources in metals remains obscure. On the one hand, in a number of studies the bulk character of noise has been established (1). On the other hand, the evidence was obtained that noise arises at grain boundaries (2) and, presumably, at film-substrate interface (3). The first direct proof of the existence of "surface" noise in metals has been published recently (4). In the present paper we briefly report the main points of this result and provide new ones supporting the idea of surface noise in metals.

NOISE FROM THE FILM-SUBSTRATE INTERFACE

To distinguish between contributions of bulk and surface noise, we first applied the well-known dependence of the relative voltage power spectral density $S_V(f)/V^2$ on the thickness h or resistance R of the film with constant length and width. In the case of uniformly distributed, throughout the volume uncorrelated sources the noise is given by $S_V(f)/V^2 \propto h^{-1} \propto R/\rho(h)$, where $\rho(h)$ is resistivity. For the surface sources shunted by the noise-free bulk $S_V(f)/V^2 = [S_V(f)/V^2]_s \times (R/R_s)^2 \propto R^2$, where the index s corresponds to the noisy surface layer.

The experiments have been carried out on 108 ± 4 nm thick aluminium films deposited by electron beam evaporation onto oxidized silicon substrate in vacuum of $5 \times 10^{-4} \div 10^{-3}$ Pa. Then the plate was divided into two parts and one of them was

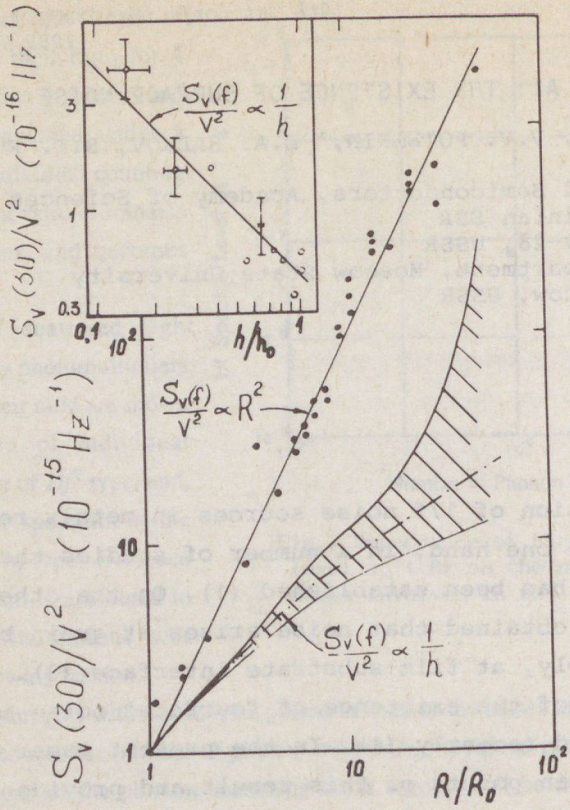

Fig. 1. $S_V(30)/V^2$ vs. R/R_o (where R_o is the initial resistance) for 2.3 mm x 40 μm samples made from annealed film. Inset: $S_V(30)/V^2$ vs. h/h_o (where h_o is the initial thickness) for 2.2 mm x 43 μm sample made from unannealed film.

annealed for 1 h at 450°C in H_2 atmosphere. It was found by SEM investigation that the diameter of grains was roughly 200 nm in both the prepared and annealed films.

The thickness of the films was decreased by anodic oxidation (5). In order to check the composition of oxidized layers, the depth profiles were made using Auger electron spectroscopy. The thickness of aluminium layer was shown to decrease proportionally to the voltage applied to the electrolytic cell, as expected. The extraction rate was found to be 8.9 ± 0.4 Å/Volt. The thickness dependence of resistivity and its temperature coefficient agreed well with the Fuchs-Sondheimer theory (5).

The excess noise measurements were performed using four-probe bridge-type specimens cut with a steel blade. In each step of thinning the spectral density followed the expression $S_V(f) \propto f^{-\gamma} V^2$ with $\gamma = 1.10 \pm 0.03$. Figure 1 represents typical noise intensity versus resistance for annealed film. The observed $S_V(f) \propto R^2$ dependence implies surface mechanism of the noise. The disagreement between the experiment and the curve for bulk noise is obvious in spite of considerable uncertainty (shown as hatched area) due to errors in thickness calculations. The samples made from unannealed part of the plate were one or two orders of magnitude quieter and exhibited the usual $S_V(f)/V^2 \propto h^{-1}$ law in good agreement with bulk effect prediction (see the inset in Fig. 1). One can infer from this fact that (i) the film-anodic oxide interface weakly contributes to the total noise, (ii) the observed surface noise source is located at the film-substrate interface, and (iii) this source was formed during the annealing procedure. We speculate that Si added to aluminium film with the reduction of SiO_2 by Al is responsible for the observed surface noise in this case.

NOISE FROM THE TOP OF THE FILM

The next manifestation of the surface noise we have found in the 330 nm thick aluminium film prepared with the help of modified evaporation technique providing coarse-grained films with an average grain size about 1.1 μm. We found this film to be very noisy, but we were able to suppress the noise magnitude by anodic oxidation. For instance, $S_V(30)/V^2$ for two of the prepared samples (3.3 mm long, and 13 μm wide) were 2.4×10^{-17} Hz^{-1} and 4.2×10^{-18} Hz^{-1}. After removing a ~10 nm thick surface layer, $S_V(30)/V^2$ was reduced to approximately 9×10^{-19} Hz^{-1} in both samples. It is well known that coarse-grained films are obtained as soon as the conditions of a film growth approach the thermal equilibrium ones. These conditions favour also the impurity segregation at peripheries of grains that supposedly result in appearance of the observed noise.

Finally, we have found that the immersion samples made from another film in distilled water for some minutes increase the

noise magnitude by a factor of roughly 10, while the subsequent anodic oxidation to ~10 nm in depth completely eliminates this additional noise. Thus this source also can be treated as a "surface" one. The grain size in this film was about 300 nm; the film thickness was 250 nm; the typical value of $S_V(30)/V^2 \cong 1 \times 10^{-16}$ Hz^{-1} for samples prepared with dimensions 2.2 mm x 10 μm. It should be noted that the noise in the two above-mentioned films was not affected by the contact with water. At the present time we are unable to answer the question why water does produce surface noise in one film and does not in the other. New experiments are needed to clear the situation. But it is worth noting that the photolithographic technique, which is conventional in a noise sample patterning, should be used with more care.

In conclusion, it has been shown experimentally that both surface and bulk sources are involved in 1/f noise generation in metals.

REFERENCES

1. Zimmerman, N.M., Scofield, J.H., Mantese, J.V., Webb, W.W., Phys. Rev. B34 (1986) 773-7, and references therein.
2. Verbruggen, A.H., Koch, R.H., Umbach, C.P., Phys. Rev. B35 (1987) 5864-7.
3. Rodbell, K.P., Ficalora, P.J., Koch, R., Appl. Phys. Lett. 50 (1987) 1415-6.
4. Bakshee, I.S., Potemkin, V.V., Salkov, E.A., Khizhnyak, B.I., Zh. Techn. Fiz., Pisma 14 (1988) (see English transl. in JTP Lett.), 1202-7.
5. Bakshee, I.S., Litvinenko, V.V., Potemkin, V.V., Salkov, E.A., Khizhnyak, B.I., Yakubtsov, D.A., Pribory i Techn. Eksp. 1989, No. 2, 212-215 (see Engl. transl. in Instrum. and Exper. Techn.).

1/f NOISE IN QUARTER-MICRON FILAMENTS OF GaAs AND InP MADE BY FOCUSED ION-BEAM IMPLANTATION

M. TACANO, T. KANAYAMA, Y. SUGIYAMA, S. HASHIGUCHI*

Electrotechnical Laboratory
Umezono 1-1-4, Tsukuba, 305, Japan
*Department of Electronics Engineering,
Yamanashi University
Takeda 4-3-11, Kohfu, 400, Japan

Introduction

Typical 1/f noise was excited in quarter-micron filaments of both GaAs and InP which were successfully made by a focused ion-beam implantation. Their noise levels were observed to vary exactly as $f^{-1.0}$ and increased in proportion to the square of the terminal voltages. The GaAs filament has a generation-recombination(GR) noise bulge at around 500 Hz, corresponding to the deep level activation energy of 0.6 eV. The noise levels of the InP filament, on the other hand, decreased monotonically throughout the frequency ranges from 0.1 Hz to 100 KHz, indicating much less deep levels. The Hooge's noise parameters were evaluated exactly by the carrier numbers derived from the Hall measurement and 1/f noise levels to be 4.5×10^{-6} in the GaAs filament and 6.1×10^{-6} in the InP one. These values are the smallest ones ever reported in these materials, and are in good agreement with the quantum theory for 1/f noise. The noise parameter of various compound semiconductor device substrates is compared especially at low total carrier numbers.

Fabrication and Characteristics of Devices

Focused ion-beam(FIB) implantation is a powerful tool that has been developed for delineating submicron patterns directly onto semiconductor substrates. This technology, in addition to providing an efficient means for fabricating ultra-large-scale integrated circuits, can be used to prepare new device structures previously unattainable by conventional technologies. We have used this technology to fabricate a Greek-cross Hall device with dimensions of 1/4x1/4 μ m, which, to our knowledge, is the smallest ever made. Simultaneous measurements of f^{-1} noise levels and

carrier consentrations in a Hall device make it possible to evaluate the Hooge's parameter exactly. The structure of the device is indicated schematically in Fig.1(a). A 120KeV Si ion beam was implanted in a GaAs filament of area 6x0.25 μ m to a total dose of $5x10^{8}$ cm^{-2}, and a rapid thermal annealing at 900 ^{o}C for one minute activated the sheet carrier concentration of $7.3x10^{12}$ cm^{-2} with the mobility of $3.7x10^{3}$ cm^{2}/VS. Current-voltage characteristics of the device is shown in Fig. 1(b). Unlike those of the conventional epitaxial layers, the current saturates at electric field above 10 KV/cm and at current densities of 10^{6} A/cm^{2}. The total carrier number within the 6x0.25 μ m filament is evaluated to $N=6.9x10^{4}$, corresponding to a terminal resistance of 12 kΩ . Fig. 2 shows the electric field dependence of the carrier concentration and the mobility. The total carrier number and the carrier mobility does not change with the electric field. Similar process to the same area of InP made an InP filament with the concentration of $4.0x10^{12}$ cm^{-2} and the mobility of $3.6x10^{3}$ cm^{2}/VS. The total carrier number within the filament is $N=6.0x10^{4}$ in InP.

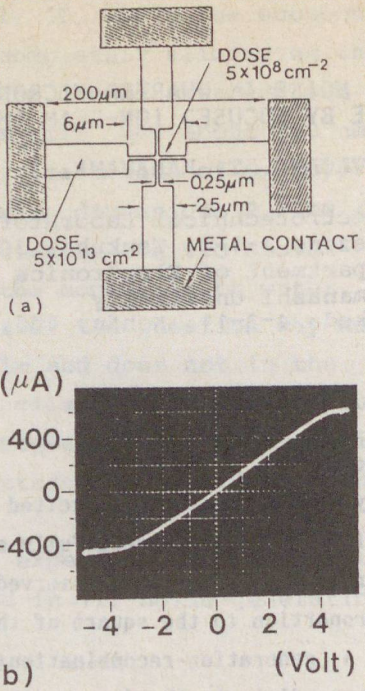

Fig. 1 Schematic structure of (a) quarter-micron Hall device, (b) current-voltage characteristics

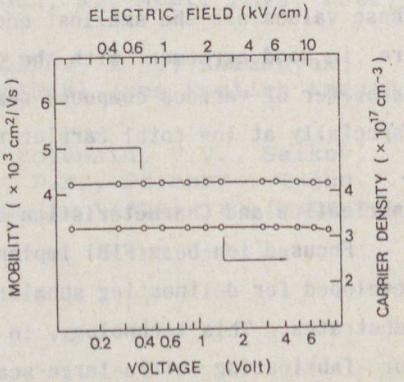

Fig. 2 Mobility and carrier concentration of GaAs Hall device

1/f Noise Characteristics

The noise measurement system was

the same as described elsewhere.[1] Noise spectra of the quarter-micron filament of GaAs are shown for a variety of current terminal voltages in Fig. 3, indicating an f^{-1} behaviour below 10 Hz and a bulge at around 500 Hz corresponding to the Lorenzian shaped GR noise. The Hall terminal noise was about 15 dBV/$\sqrt{\ }$ Hz lower than the noise across the current electrodes. The 1 Hz f^{-1} noise levels of the filaments, plotted as a function of terminal voltage in Fig. 4, show a V^2 dependence for terminal voltages below 2 V(E=3.3KV/cm). The Hooge's parameter α_H can be derived experimentally as $\alpha_H = S_V f N/V^2 = 4.5\times10^{-6}$, where S_V is the noise level. These parameters can be larger than 10^{-5} at higher electric fields, as indicated in Fig. 4. Taking into account the effects of the inter-valley scattering process of the electrons, quantum f^{-1} noise theory predicts a value of 7×10^{-6} for n-GaAs.[2] This agrees amazingly well with our experimental result.

Noise spectra of the InP filament are shown for a variety of current terminal voltages in Fig. 5. Noise levels decrese linearly with the frequency exactly at the rate of $f^{-1.0}$ throughout the ranges observed. This is a typical characteristics of ion-implanted InP layers[3] and the results evidently indicate far small-

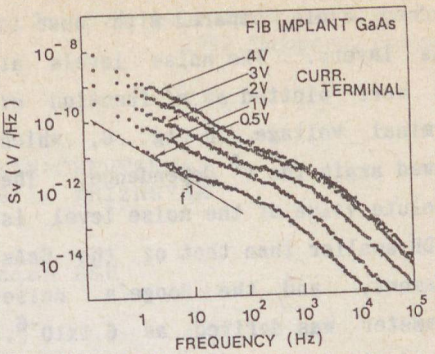

Fig. 3 Low-frequency noise spectra of GaAs across current terminals

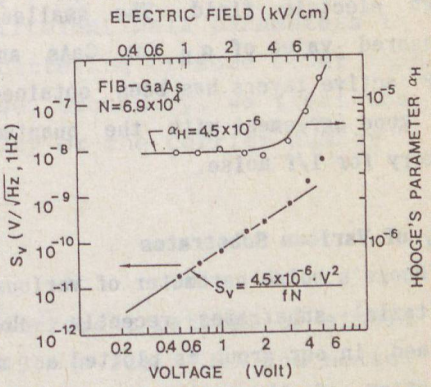

Fig. 4 Noise levels and Hooge's parameter of GaAs

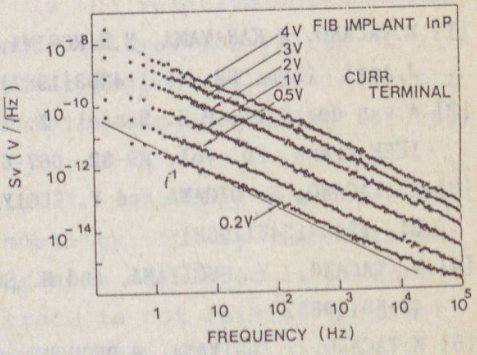

Fig. 5 Low-frequency noise spectra of InP across current terminals

er deep levels compared with those in GaAs layers. The noise levels at 1Hz were plotted as a function of terminal voltage in Fig. 6, which showed again the V^2 dependence. The absolute value of the noise level is 3 DB smaller than that of the GaAs filament, and the Hooge's noise parameter was derived as 6.1×10^{-6}. Our device can be characterized by the extraordinarily small numbers of carriers(about$(6\text{-}7)\times 10^4$) carrying very large currents (10^5 A/cm)in a high electric field. The smallest measured value of α_H for GaAs and InP active layers has been obtained in good agreement with the quantum theory for 1/f noise.

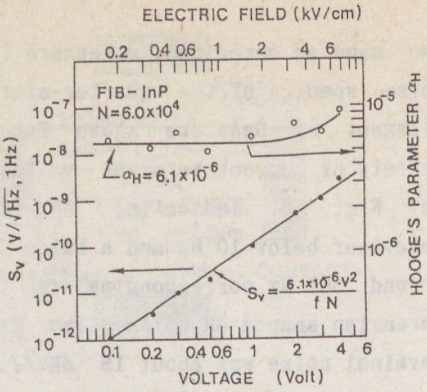

Fig. 6 Noise levels and Hooge's parameter of InP

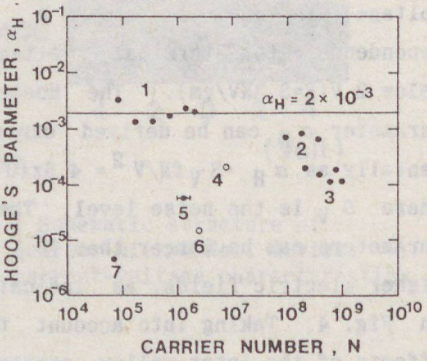

Fig. 7 α_H vs carrier number of various compound device substrates

α_H of Various Substrates

Hooge's noise parameter of various epitaxial substrates recently obtained in our group is plotted as a function of the rather low total carrier number within the sample;[4], [5].

References

[1] M.TACANO, M.KANAYAMA, H.HIROSIMA, M.KOMURO and Y.SUGUYAMA; J.Appl. Phys, **62**, 4301-4303(1987)

[2] A.van der Ziel, P.H. Handel, X. Zhu and K.H. Duh; IEEE trans. ED, vol. **ED-32**, 667-671(1985)

[3] M. TACANO, K. OIGAWA and Y. SUGIYAMA; Solid-State Electronics, **31**, 1243-1245(1988)

[4] M. TACANO, Y. SUGIYAMA, and H. SOGA; Solid-St. Electronics, **32**, 49-55(1989)

[5] M.TACANO, Y.SUGIYAMA, S.DEGUCHI, S.UEKUSA and H.SOGA; IECE of Japan, **ED88-87**(1988), in Japanese

10th Int.Conf. on Noise in Physical Systems
1989 Budapest, Hungary

1/f NOISE IN n-$Cd_xHg_{1-x}Te$

I.S. BAKSHEE, V.F., GRIN', L.A. KARACHEVTZEVA,
M.Z. KODALASHVILI, E.A. SALKOV, B.I. KHIZHNYAK

Institute of Semiconductors,
Academy of Sciences of the Ukrainian SSR
252650, Kiev-28, USSR

In this report we present the summary of two recent papers (1, 2) concerning 1/f noise in $Cd_xHg_{1-x}Te$. Firstly, we consider noise data for the samples with different Hall parameters in order to search whether lattice scattering or some other mechanisms are responsible for 1/f noise. Secondary, we treat the problem whether the carrier mobility or the carrier number fluctuations cause 1/f noise.

INFLUENCE OF DEFECT CONCENTRATION

We have examined a number of different batches of single-crystal n-type $Cd_xHg_{1-x}Te$ (x = 0.19 - 0.22). Hall and noise measurements performed on the same samples at 85 K yielded Hall mobility μ_H of $(0.94 \div 4.4) \times 10^5$ cm^2/V sec, carrier concentration n of $(0.8 \div 10) \times 10^{14}$ cm^{-3} and Hooge parameter $\alpha = [S_V(f)/V^2]fn\,\Omega$ of $3 \times 10^{-6} \div 4 \times 10^{-4}$. Here $S_V(f)/V^2$ is the relative voltage power spectral density and Ω is the sample volume. The values of α for the samples cut out from adjacent regions of crystals were found to be independent of sample thickness suggesting the bulk character of the noise.

The results are plotted in Fig. 1. Note that the noise decreases rapidly with increasing mobility. It was demonstrated by optical microscopy taken on surfaces developed to produce dislocation etch pits that this trace is not related to dislocation and low-angle grain boundary density.

It is known that the electron mobility in n-$Cd_xHg_{1-x}Te$ at ~80 K is mainly determined by charged centre, polar-optical

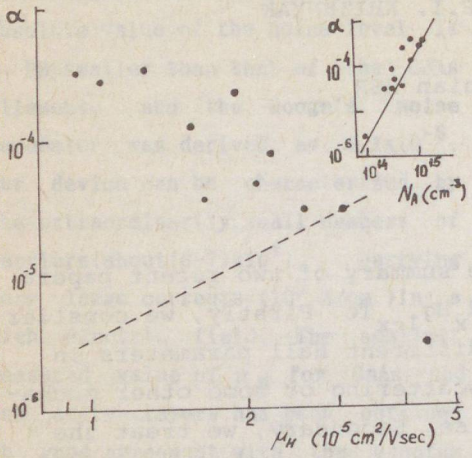

Fig. 1

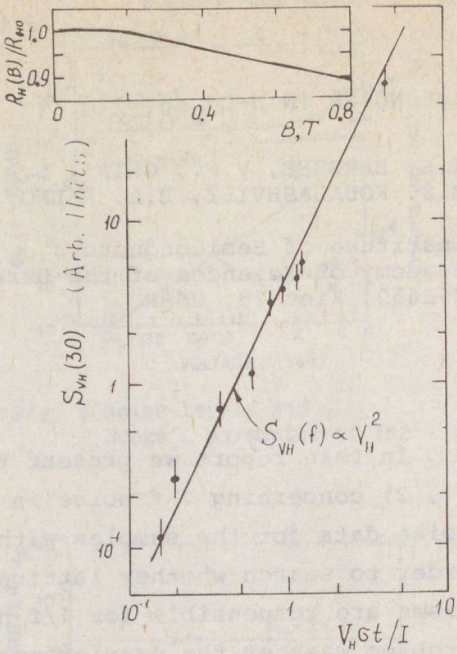

Fig. 2

Fig. 1. Log-log plot of Hooge parameter α versus Hall mobility μ_H. The dashed line has slope 2, which is the prediction of the Hooge-Vandamme model. Inset: α versus N_A. The solid line $\alpha \propto N_A^2$ is drawn as a guide to the eye.

Fig. 2. Spectral density of Hall effect noise as a function of normalized Hall voltage, $V_H\sigma t/I = [R_H(B)/R_{HO}]\,\mu_H B$, where σ is the conductance, and R_{HO} is the Hall coefficient value at low magnetic inductions. Inset: relative Hall coefficient versus magnetic induction.

phonon and alloy scattering (3). The temperature dependence of the mobility studied in the range of 4.2 to 200 K has shown that it is the charge centre density that determines the variation in the mobility values measured at 85 K and presented in Fig. 1. If the noise could arise only from lattice scattering, as was originally supposed by Hooge and Vandamme (4), α would be given by $\alpha \propto (\mu/\mu_1)^2$. As seen in Fig. 1, the experimental data clearly contradict this prediction, but are well consistent with the idea that 1/f noise is generated by point defects. We have estimated acceptor and donor concentration from

the measurements of μ_H and n using calculations in ref. (5). The acceptor concentration N_A was found to correlate with the noise magnitude, while the donor concentration does not. The data shown in the inset of Fig. 1 indicate that α scales approximately as N_A^2.

At the present time we can only speculate on the observed scaling law. Perhaps some interference terms (like that suggested by Robinson (6)) are involved to produce the quadratic dependence of α on the concentration N_f of "fluctuators", N_f being proportional to N_A. However, it is quite possible that $\alpha \propto N_f$, while $N_f \propto N_A^2$. The last law would be realized, if e.g. the fluctuators were acceptor pairs. Further study is required to distinguish between these possibilities.

HALL EFFECT 1/f NOISE

Kleinpenning and Bell (KB) (7) have shown that fluctuations in Hall voltage $V_H = (r/nq)\,(IB/t)$ could arise not only from fluctuations in carrier concentration n, as it was assumed previously, but also from fluctuations in parameter r. (Here B is the magnetic induction, I is the current, t is the sample thickness, and q is the elementary charge.) According to KB, parameter r fluctuates due to the fluctuations in mobility $\mu(E)$ of carriers with kinetic energy E, since for low magnetic inductions $r = \langle\mu^2(E)\rangle / \langle\mu(E)\rangle^2$. Here $\langle\ \rangle$ means the average taken over all energies in the conduction band.

It is widely known that in the limit of strong (in a classical sense) magnetic inductions $(\mu_H B)^2 \gg 1$ the parameter $r \to 1$, and susceptibility of r to scattering mechanisms and relaxation times disappears (8). We point out that for this reason the Hall noise magnitude should vanish, if the noise comes from KB mechanism. Really, extending the KB approach to the limit of $(\mu_H B)^2 \gg 1$ for relative spectral density of Hall noise one may obtain:

$$S_{VH}(f)/V_H^2 \propto B^{-4}\left[\int_0^\infty \mu^{-4}(E)E^2 n(E)dE - 2\langle\mu^{-1}(E)\rangle \int_0^\infty \mu^{-3}(E)E^2 n(E)\right.$$

$$\left. xdE + \langle\mu^{-1}(E)\rangle^2 \int_0^\infty \mu^{-2}(E)E^2 n(E)dE\right] \Big/ \left[\int_0^\infty En(E)dE\right]^2,$$

where n(E)dE is the concentration of carriers with energy between E and E+dE. Thus, $S_{VH}(f)$ should scale as V_H^{-2}.

Experimentally, we have investigated the Hall effect noise at magnetic inductions in the range $0.02 \leq (\mu_H B)^2 \leq 20$.

Experiments have been carried out at 85 K on two similar samples with $x \cong 0.21$, $n \cong 2.5 \times 10^{14}$ cm^{-3}, $\mu_H \cong 1.0 \times 10^5$ cm^2/V sec and $\alpha \cong 3.1 \times 10^{-4}$. Figure 2 represents the results for Hall effect noise and Hall coefficient $R_H(B) = r/nq$ in the constant current experiment. As seen in the Figure, the Hall noise magnitude follows the $S_{VH}(f) \propto V_H^2$ law at both low and classically strong magnetic inductions that contradicts the extended KB model prediction which has been made above. On the other hand, the experimentally obtained values of the ratio $\gamma_H = [S_{VH}(f)/V_H^2]/[S_V(f)/V^2]$ were 1.0 ± 0.1 and well consistent with the predictions from carrier concentration fluctuations model.

REFERENCES

1. Bakshee, I.S., Grin', V.F., Karachevtzeva, L.A., Kodalashvili, M.Z., Salkov, E.A., Khizhnyak, B.I., Fiz. Tekh. Poluprov. 23 (1989) 571-3.
2. Bakshee, I.S., Kodalashvili, M.Z., Salkov, E.A., Khizhnyak, B.I., Fiz. Tekh. Poluprov, 22 (1988) 2182-6.
3. Dubowski, J.J., Dietl, T., Szymańska, W., Gałazka, R.R., J. Phys. Chem. Sol. 42 (1981) 351-62.
4. Hooge, F.N., Vandamme, L.K.J., Phys. Lett. 66A (1978) 315-6.
5. Gorokhovskii, I.R., Laurinavichus, A.K., Pozhela, Yu. K. et al. Fiz. Tekh. Poluprov. 21 (1987) 1998-2001.
6. Robinson, F.N.H., Phys. Lett. 97A (1983) 162-3.
7. Kleinpenning, T.G.M., Bell, D.A., Physica 81B (1976) 301-4.
8. Smith, R.A., Semiconductors. Cambridge University Press, London 1964.

10th Int.Conf. on Noise in Physical Systems
1989 Budapest, Hungary

DYNAMICS OF DISORDERED FRONTS: DIFFUSION AND INVASION NOISE

J.F. GOUYET,* B. SAPOVAL,* Y. BOUGHALEB,*,** M. ROSSO*

*Laboratoire de Physique de la Matière Condensée,
Ecole Polytechnique
F-91128 Palaiseau, France
**Groupe de Physique Théorique, Faculté des Sciences II,
Ben M'Sik, Université Hassan II
Casablanca, Maroc

ABSTRACT : Whenever fractal interfaces are obtained by particles diffusion or fluid invasion, they may present geometry fluctuations with an anomalous $1/f^{\alpha}$ power spectrum.

I. INTRODUCTION

It has recently been realized that diffusion creates fractal structures [1,2] which are closely related to the geometry of percolation clusters. The *geometrical* fluctuations of such structures are related to the fluctuations of connection and disconnection of the clusters. It is in general possible to define a front of a diffused distribution of particles, which is associated to a given physical property. For instance in the case of an electrical contact, diffusion of metallic atoms generates a front [3] which is the external surface of the set of metallic particles electrically linked to the metallic source. One very particular characteristic of such fronts is their instability during the diffusion process : A diffusion front fluctuates at a frequency much higher than the inverse of the particles average jump time θ^{-1}. A system which may be otherwise considered as quenched due to an extremely large jump time could present interface fluctuations at observable frequencies. These geometrical fluctuations could induce impedance fluctuations, different from the flicker noise studied by Rammal et al.[4]. In addition the fractal character of these interfaces leads to a $1/f^{\alpha}$ behaviour for the noise spectrum.

II. STRUCTURE OF A DIFFUSION FRONT

Consider particles diffusing on a lattice following a simple diffusion equation

$$\partial p(\vec{r},t)/\partial t = D\,\Delta p(\vec{r},t)$$

with a concentration $p(x,t)$ subjected to fixed boundary conditions along the x axis $p(x=0,t)=p_M$ (the source) and $p(x=L,t)=p_m$ (the sink). A stationary state is reached for which the concentration varies as $p(x,t) = -\dfrac{p_M - p_m}{L}\,x + p_M$.

A diffusion interface is then defined. We simply consider here clusters of first neighbour connected particles. If p_M is large enough (close to one for example) a large cluster exists connected to the source. The diffusion front is defined as the external surface of this cluster.

The geometrical characteristics of this front are well known[5]: In two dimensions the front is entirely located around the percolation threshold p_c of the associated percolation problem and has a width σ_{ft} which varies as a power law of the local concentration gradient ∇p. In three dimensions, the front is extended on a wide concentration range (see Ref.[6]). Around p_c there exists a critical region of width σ_{ft} (the width of the front tail) with the same power law behaviour as in the 2d case,

$$\sigma_{ft} \propto |\nabla p|^{-\nu/(1-\nu)}$$

ν is the critical exponent of the percolation connection length (ν=4/3 in 2d, and $\nu \approx 0.88$ in 3d).

Fluctuations are located in the critical region, which is fractal with a fractal dimension D_f (which we proved to be equal to the fractal dimension d_H of the percolation hull).

We have considered here the fluctuations of the interface (length in 2d or surface in 3d) but depending on the physical problem considered, other kind of fluctuations could be considered (fluctuations of mass...). This is in particular the case for the slow injection of a non-wetting fluid in a porous medium in presence of gravity[7]. In the next section we describe the theoretical behaviour of the fluctuations and compare it to 2d numerical simulations.

III. FLUCTUATIONS OF THE FRONT

A film[8] showing a computer simulation of the diffusion process reveals the erratic character of the diffusion fronts. The frequency of events τ_1^{-1} on the front is much higher than the inverse hopping time of the activated jump process : $\theta^{-1} = \nu_o \exp -\Delta E/kT$.
(ΔE being the barrier height). The frequency τ_1^{-1} depends on the number of particles N_f close to or on the front which can connect or disconnect a part of it : $\tau_1^{-1} = N_f/\theta$. To determine the fluctuations of length or surface of the front we calculate the mean square fluctuation of $\Delta N_f(t) = N_f(t) - N_f(0)$. The general behaviour of the fluctuations as a function of time shows that for small time intervals the average square fluctuations increase; they saturate for a cross-over time interval t_c. The fluctuations follow the law,

$$\langle \Delta N_f(t)^2 \rangle = \langle (N_f(t) - N_f(0))^2 \rangle \propto t^{2H}.$$

where H is the Hurst exponent [9]. For short time H=1/2 corresponding to a $1/f^2$ brownian noise, while for longer time H becomes zero and a 1/f noise is observed. This behaviour is shown in Fig.1, for different values of the gradient of concentration, $\nabla p=(p_M-p_m)/L$.

At low frequency the dependence on the concentration gradient is determined by considering that the dominant events are the connection or disconnection of clusters of linear size of order σ_{ft} [11-13]. One finds in a d-dimensional space,

$$\langle \Delta N_f(t)^2 \rangle = (\sigma_{ft})^{2D_f - d+1}.$$

When d=2, the corresponding exponent of ∇p is -10/7 (the numerical value is -1.48).

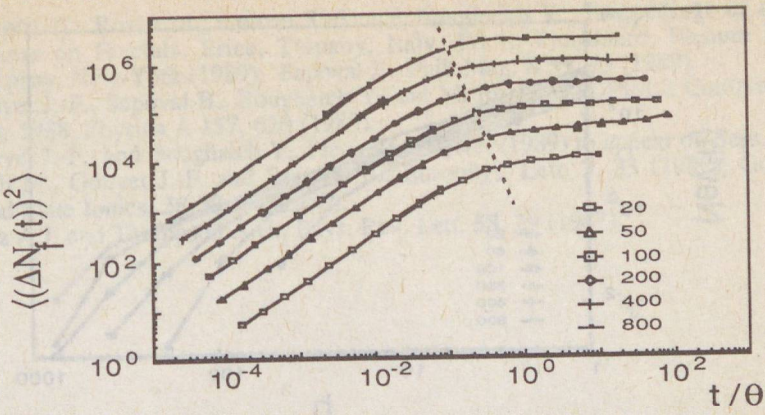

Fig.1 The mean square fluctuation $\Sigma^2 = \langle \Delta N_f(t)^2 \rangle$ as a function of t for various values of the inverse concentration gradient.The small time behaviour corresponds to a $1/f^2$ noise. Above a gradient dependent threshold t_c diffusion generates a 1/f noise.

At high frequency ($t<t_c$), $\langle \Delta N_f(t)^2 \rangle = \mathcal{A}t$, and it can be shown that the prefactor $\mathcal{A}$ is the product of three terms : The size of the individual dominant fluctuations $(\sigma_{ft})^{2D_f}$, the number [5] of sites on the front $N_f \equiv L(\sigma_{ft})^{D_f-d+1}$ and the probability Π to connect or disconnect a typical cluster. The crucial point is to remark that Π is proportional to the number of "red-bonds" or "cutting-bonds" in a domain of linear size σ_{ft}, the "red-bonds" [10] being the bonds which, when cut, disconnect opposite sides of a given domain (here of size σ_{ft}). Their number determined by Coniglio [10] varies as a power law of the size of the domain, and then $\Pi \propto (\sigma_{ft})^{1/\nu}$. So that finally

$$\mathcal{A} \propto (\sigma_{ft})^{2D_f - d+1+1/\nu}.$$

In two dimensions the corresponding exponent of ∇p is -13/7 (the numerical value is -1.83).

The cross-over time between the $1/f^2$ and 1/f regime is easily found : $t_c \propto |\nabla p|^{1/(1+\nu)}$. The smaller the gradient of concentration, the larger the crossover frequency.

IV. STATISTICS OF THE EVENTS

Another important quantity of the dynamics of diffusion fronts is the number of events $N_{ev}(h)$ of a given size h. The detailed calculation of $N_{ev}(h)$ has been given elsewhere [11-13], and we will only give here the final result. The number of events varies as

$$N_{ev}(h) = L^{d-1} h^{1/\nu D_f - 2} (\sigma_{ft})^{D_f-d+1} K(h/h_M)$$

where K is a cutoff function (large clusters are truncated due to the concentration gradient). The corresponding 2d simulation is shown in Fig. 2 below.

CONCLUSION

We have shown that macroscopic objects obtained by diffusion can present, even if they look quenched, $1/f^\alpha$ fluctuations due to the incomplete quenching of atomic diffusion. Here only the

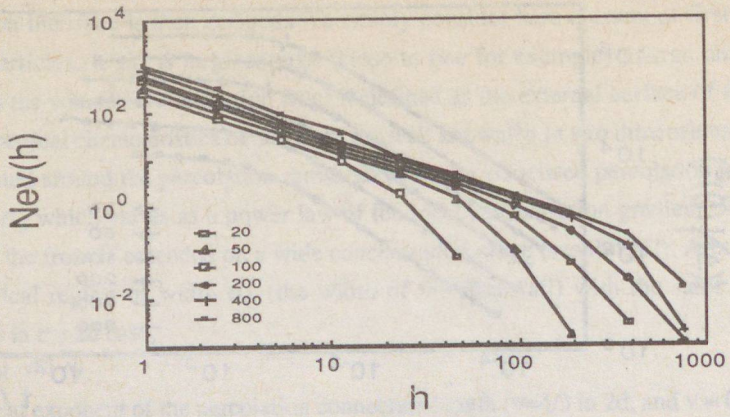

Fig.2 Number of events of size h as a function of h and of the inverse concentration gradient. The slope extracted from numerical calculations is 1.42±0.05, while the theoretical value is 1.57. A cutoff is observed for large values of h, due to the concentration gradient.

case without interaction (except exclusion of double occupancy of a site) has been studied, but under certain conditions, diffusion of interacting particles should present a similar character.[14] A similar behaviour is expected in the slow invasion of a porous medium by a non wetting fluid[4], and experiments on flux fluctuations of injected fluids would be very interesting to perform : if the static properties are now well understood, no experiment has been made on the fluctuations of flux or of pressure; fluctuations of conductivity during invasion [15] also exhibits an erratic character and scaling laws in qualitative agreement with the above model, however, they correspond to a more complicated situation which is at present not completely understood.

REFERENCES

[1] Mandelbrot B., The fractal geometry of Nature, W.H. Freeman and Cy, San Francisco (1982); Feder J., Fractals, Plenum Press, New-York (1988).
[2] Sapoval B., Rosso M. and Gouyet J.-F., J. Phys. Paris Lett. **46**, 149 (1985).
[3] Sapoval B.,Rosso M., Gouyet J.-F., and Colonna J.-F., Solid States Ionics **18&19**, 232 (1986).
[4] Rammal R., Tannous C., Breton P. and Tremblay A.-M.S., Phys. Rev. A **54**, 1718 (1985).
[5] Sapoval B., Rosso M., Gouyet J.-F., Fractal interfaces in diffusion, invasion and corrosion in "*The fractal approach to the chemistry of disordered systems, polymers, colloid and surfaces*". Ed. D. Avnir. John Wiley & Sons Ltd (1989).
[6] Rosso M., Gouyet J.-F., and Sapoval B., Phys. Rev. Lett. **57**, 3195 (1986); Gouyet J.-F., Rosso M. and Sapoval B., Phys. Rev. B **37**, 1832 (1988).
[7] Hulin J.P., Clément E., Baudet C., Gouyet J.-F. and Rosso M., Phys. Rev. Lett. **61**, 333 (1988).
[8] Sapoval B., Rosso M., Gouyet J.-F. and Colonna J.-F., *Fractal structure of a Diffusion Front,* (Imagiciel, 1985).
[9] Mandelbrot B. and Van Ness J.W., SIAM Review **10**, 422 (1968).
[10] Stanley H.E., J. Phys. A **10**, L211 (1977); Coniglio A., J. Phys. A **15**, 3829 (1982).

[11] Sapoval B., Rosso M., Gouyet J.-F. and Boughaleb Y., Proceedings of the special seminar on Fractals, Erice, Trapany, Italy. Ed L. Pietronero, Plenum Publishing Company, New-York (1989); Sapoval B., Phil. Mag. B **59**, 75 (1989).
[12] Gouyet J.-F., Sapoval B., Boughaleb Y. and M. Rosso, ETOPIM 2 Conference, Paris, Sept. 1988, Physica A **157**, 620 (1989).
[13] Gouyet J.-F. and Boughaleb Y., Phys. Rev. B, **40**, (1989) to appear on Sept. 1st.
[14] Kolb M., Gouyet J.-F. and Sapoval B., Europhys. Lett. **3**, 33 (1987); Gouyet J.-F., Solid State Ionics, **28-30**, 72 (1988).
[15] Katz A.J. and Thompson A.H., Phys. Rev. Lett. **58**, 29 (1987).

10th Int.Conf. on Noise in Physical Systems
1989 Budapest, Hungary

DISORDER-INDUCED FLICKER NOISE

Yu.M. GAL'PERIN, V.L. GUREVICH, V.G. KARPOV, V.I. KOZUB

A.F. Ioffé Physico-Technical Institute
Leningrad, USSR

A significant progress in the study of flicker noise has been achieved in recent years which to a great extent was due to a series of experiments carried out on small-size systems (see, e.g. (1, 2)). It has appeared that low-frequency noise observed in such systems can be decomposed into a sum of contributions from separate objects, the so-called "fluctuators", each of them exhibiting Lorentzian noise spectrum. These results are consistent with the hypothesis (3) that the flicker noise originates from a system of scatterers with internal degrees of freedom possessing exponentially broad relaxation time distribution. It is well known that such a scatter of relaxation times necessary for the flicker noise formation is an inherent property of disordered systems, where the transitions between metastable states are due to tunnelling or activation processes. On the other hand, the slowest processes in solids are usually connected with atomic motion. The motions of such a type are possible in structurally disordered materials, where atoms (or group of atoms) move in effective two-well potentials forming specific low-energy excitations - so-called two-level systems (TLS). Kogan and Nagaev (4) were the first to suggest that TLS can provide a source of the flicker noise. The detailed theory of the corresponding phenomenon for tunnel junctions and point contacts (the surroundings of which are disordered) was developed by one of the authors (5). Note that an essential role of the structural disorder for flicker noise formation was pointed out by the experiments (6), where the introduction of a weak disorder (producing no significant resis-

tivity increase) leads to an essential increase of noise. However, one should keep in mind that the TLS concept in the form used in (4, 5) is valid only for the low-temperature region. We have demonstrated that the two-well potential concept is fruitful and allows one to explain the existing experimental data for the high-temperature region as well.

We have used the soft-potential model (7), according to which the defect we are interested in is an atom or a group of atoms with a mass M moving in the potential

$$V(x) = \varepsilon(\eta(x/a)^2 + t(x/a)^3 + (x/a)^4) \qquad (1)$$

where x is some generalized coordinate, ε is a characteristic atomic energy scale, a is interatomic spacing. Note that the low-frequency processes are dominated by the objects with small relaxation rates, i.e. those with high and wide barriers. The fact that a given well can contain many levels is of no importance for the low-frequency noise, because intrawell transitions correspond to small time scale, while at large time scales each well can be described by the parameters averaged over the intrawell levels. It is obvious that the fluctuator relaxation related with changes of the well's occupation numbers can be due to tunnelling or activation. The relaxation time τ is generally expressed as $\tau = \tau_o \exp(-\lambda(\varepsilon, T))$, where τ_o^{-1} is an attempt rate (for a soft potential with small η $\tau_o \sim 10^{-13}$ s), while λ is the tunnelling or activation probability. One can express λ in terms of the model's parameters taking into account that the characteristic barrier height is $\sim(W/4)(\eta/\eta_L)^2$ while its strength is $\sim 0.5(|\eta|/\eta_L)^{1/2}$, where $\eta_L = (\hbar/2Ma^2\varepsilon)^{1/3} \sim 10^{-2}$, $W \sim \varepsilon\eta_L^2 \sim (10 \div 30)$ K. As a result, one gets an estimate for the cross-over temperature between tunnelling and activation regimes:

$$T_{cr} \sim 0.3\ W\ (|\eta|/\eta_L)^{1/2} \sim (3/8)^{4/3}\ W \log^{1/3}(\tau/\tau_o) \qquad (2)$$

The transitions between the wells of i-th defect lead to changes of a cross-section for an electron scattering on the defect

$\Delta\sigma_i \sim a^2(2n_i(\tau))^{1/2}$; so they generate the sample's resistance fluctuations. For their spectral density one can obtain (5)

$$(\delta R^2)_\omega / R^2 = (1/V)^2 \sum_i (\Delta\sigma_i)^2 n_0^i (1-n_0^i)\tau_i |1+(\omega\tau_i)^2|^{-1} \qquad (3)$$

where l is the electron mean free path, V is the sample's volume, n_0 is the equilibrium occupation number of one of the wells. It is obvious that for a small contact the noise spectrum is determined by a small number of fluctuators and is a "fingerprint" of the contact. For large contacts, the noise spectrum is of flicker type due to the broad scatter of the soft potential relaxation rates. The details of the Hooge constant α behaviour appear to be sensitive to the character of the parameter distribution function P. As a rule, α contains only logarithmic frequency dependence, although appearance of power corrections to the flicker law is possible (if $P(|\eta|)$ decreases at large $|\eta|$ as Gaussian or more quickly). At low temperatures T (tunnelling regime) $\alpha \sim T$ which is due to an increase of the number of activated fluctuators with an increase of temperature. At higher temperatures α (T) can exhibit a maximum (8). As for quantitative estimates of α, one obtains $\alpha \sim 10^{-2} \div 10^{-3}$ for fluctuator densities characteristic of amorphous materials; it agrees with upper experimental values of α. So we believe that our model allows to explain general features of the flicker noise in bulk samples.

Let us compare the theoretical predictions with the experimental data (1, 2). The authors of (1, 2) observed the transition from tunnel to activation relaxation for a given fluctuator at 15÷20 K which is in excellent agreement with (2). Ralls and Buhrman (2) studying the noise from the copper point contact have also estimated the cross-section for a given fluctuator (1÷30 Å^2), the activation barrier's height (70÷300 meV) and the attempt rate ($\sim 10^{-13}$ s). These values are also in good agreement with the theory. So, in our opinion, the existing experiments on small-size contacts provide evidence that the soft interatomic potentials generated by structural disorder are responsible for flicker noise in metals.

Now let us discuss the relation of purely classical fluctuations considered above to the universal quantum fluctuations of conductance (the latter can be due to the same two-well potential). Similarly to the estimates (9) one can show that in 3-dimensional case the quantum contribution dominates only if $(\lambda/l)^2 > (l/L)^3$ where L is the sample dimension, λ is the electron wavelength. In this estimate one supposes $L < L_T = (lV_F\hbar/T)^{1/2}$, otherwise one should replace $L \to L_T$. Thus one can see that at least for 3-dimensional contacts the conditions for observation of the quantum effects are rather restricted and the classical effects dominate for many typical experimental situations.

REFERENCES

1. Rogers, C.T., Buhrman, R.A., Composition of 1/f noise in metal-insulator-metal tunnel junctions. Phys. Rev. Lett., 1984, 53, 1272-1275.
2. Ralls, K.S., Buhrman, R.A., Defect interactions and noise in metallic nanoconstrictions. Phys. Rev. Lett., 1988, 60, 2434-2437.
3. Bernamont, J., Ann. Phys., 1937, 7, 71.
4. Kogan, S.M., Nagaev, K.E., On the low-frequency current 1/f noise in metals. Sol. St. Commun., 1984, 49, 387-389.
5. Kozub, V.I., Low-temperature properties of a tunnel junction with an amorphous layer. Sov. Phys. - JETP, 1984 59, 1303-1311; Properties of superconducting S-I-N, S-I-S and S-L-S structures..., 60, 810. Sov. Phys. - Solid State, 1984, 26; Low-frequency noise in Josephos structures with amorphous weak links, 26, 1121-1122; Low-temperature properties of point and bridge microcontacts..., 1186-1191.
6. Pelz, J., Clarke, J., Dependence of 1/f noise on defects induced in copper films by electron irradiation. Phys. Rev. Lett., 1985, 55, 738-741.
7. Karpov, V.G., Kligger, M.I., Ignat'ev, F.I., Atomic tunnelling states and low-temperature anomalies... . Sol. St. Commun., 1982, 44, 333-337.
8. Gal'perin, Yu.M., Karpov, V.G., Kozub, V.I., Zh. Eksper. Teor. Fiz., 1989, 95, 1123-1135.
9. Feng, S., Lee, P.A., Stone, A.D., Sensitivity of the conductance of a disordered metal on the motion of a single atom... Phys. Rev. Lett., 1988, 56, 1960-1967.

10th Int.Conf. on Noise in Physical Systems
1989 Budapest, Hungary

1/f NOISE IN VARIABLE CARBON GRANULE RESISTORS

E.J.P. MAY, S.H. AL-CHARCHAFCHI*

Department of Engineering Science,
University of Exeter
North Park Road, Exeter EX4 4QF, Devon, UK
*Department of Electronic System Design,
Cranfield Institute of Technology
Cranfield MK43 0AL, UK

ABSTRACT

A variable resistance consisting of a carbon-loaded polyurethane strip between two aluminium plates has been used to determine the ratio of the time varying component of the resistor to the value of the resistance itself for various values of the resistor. The values of the resistance were altered by varying the pressure between the plates. Measurements were also made on similar resistors having two or more strips of polyurethane separated by aluminium foil. The results support the new diffusion-surface state theory [1,2] as well as the work on 'augmented 1/f noise' [3].

1. INTRODUCTION

It has been shown that carbon-loaded polyurethane resistors produce 1/f noise and $1/\Delta f$ noise when direct current or alternating current flows through them [4]. These resistors can be varied by subjecting them to mechanical pressure so that the contact between the granules can be varied. The capability of varying the resistance affords an experimental investigation into the validity of the mathematical theory published recently [1].

This paper presents practical results which indicate that the ratio $\langle(\frac{\Delta R}{R})^2\rangle$ remains constant irrespective of the value of R where ΔR is the time varying component of the actual value of the resistor. A model based on the recently proposed origin of 1/f noise [1,2] and the work on augmented 1/f noise [3] predicts this result.

2. EXPERIMENTAL PROCEDURE

2.1 Description of Sample

Carbon-loaded polyurethane is realised in the form of a high density foam and is usually used for shorting out the electrodes of semiconductor devices in storage. A piece of this foam, 5mm thick, was cut into a rectangular shape with dimensions 5.8cms x 7.0cms. This piece of foam was sandwiched between two aluminium plates which formed the electrodes. The resistance of the sample was found to vary with pressure conveniently within the range 200-2000 ohms.

A modified form of the sample described above was also fabricated; in this case, the foam strip was replaced by two identical foam strips separated by aluminium foil.

2.2. Measurement of 1/f Noise

A block diagram of the measuring equipment is shown in Fig. 1. The resistance R_s was chosen to be very much larger than R, the resistance of the sample, so that the d.c. current, I, can be regarded as a constant-current source. The noise voltage across R was amplified using a low-noise amplifier having 60 dB gain, and taken to a wave analyser (type 2010 B&K). Throughout the measurements the bandwidth of the analyser was 3.16Hz.

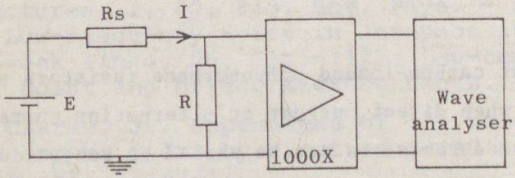

FIG. 1. Block diagram of measuring equipment.

Measurements of noise power versus frequency were made on the sample consisting of one piece of foam. These were made on the sample with pressure between the plates to give a resistance of 250 ohm, 500 ohm and 1000 ohm. The current in all cases was 0.5mA. The results are plotted in Fig 2.

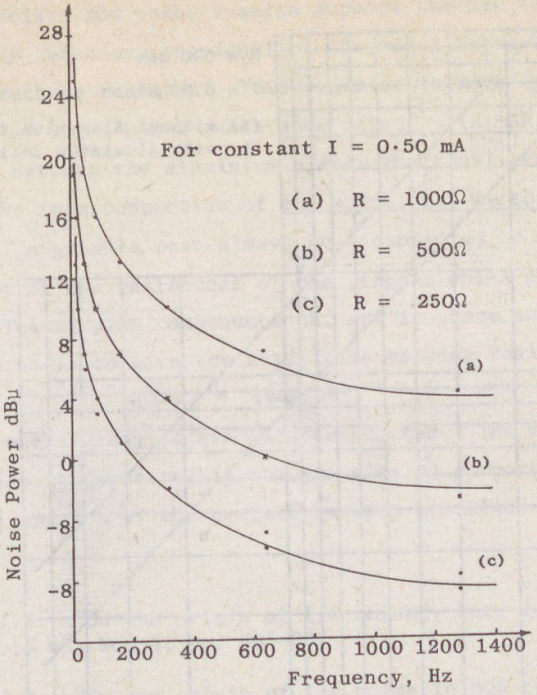

FIG 2. Effect of R on $\frac{1}{f}$ noise spectra.

The measurements were repeated using the sample with two layers of foam adjusted to have a resistance of 500 ohm. The current was 0.5mA. These measurements were taken with and without the aluminium foil. The results are shown in Fig 3.

3. DISCUSSION AND CONCLUSIONS

The curves of Fig 2 show that when the resistance is doubled, by adjusting the pressure between the plates of the sample, the mean-square noise voltage $\langle(\Delta V)^2\rangle$ increases by 6dB; that is, it increases by a factor of four. One can conclude that the ratio $\langle(\frac{\Delta R}{R})^2\rangle$ is constant for all values of R, provided the variations of R are obtained by changing the pressure between the plates. During the experimental work, two strips of carbon-loaded polyurethane samples were inserted between the two aluminium plates. It was found that the noise voltage for a given value of R was exactly the same whether there were two strips of the above

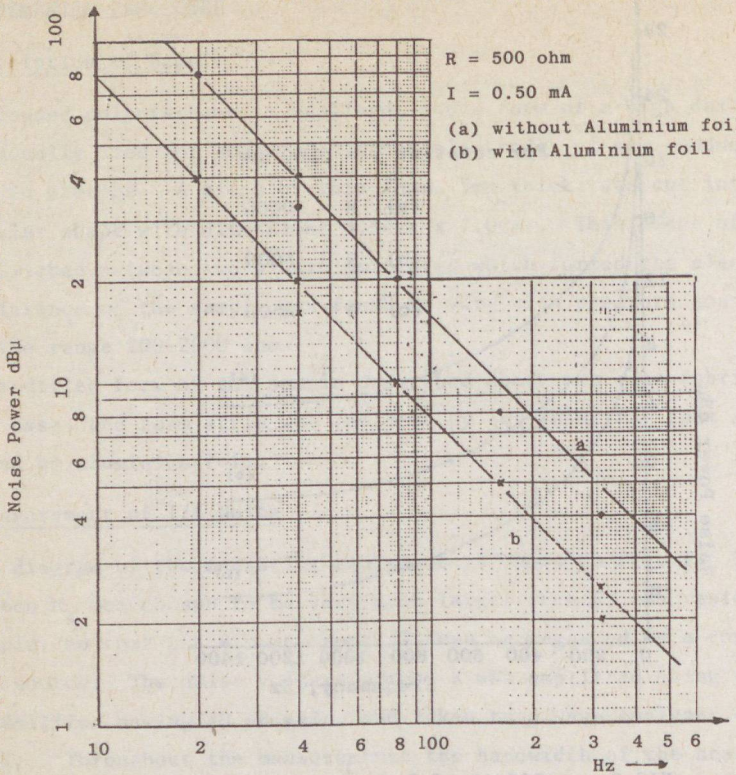

FIG. 3. Noise Power versus Frequency
2 layer sample.

mentioned sample or simply one strip. This can be seen by comparing 'curve a' in Fig. 3 with 'curve b' in Fig. 2. Further work (not reported) revealed that increasing the number of strips between the aluminium plates did not affect the noise voltage for any given value of resistance. However, when the samples of foam were separated by aluminium foil, the noise power dropped by 3dBμ; in Fig. 3 the 'curve b' lies 3dBμ below the 'curve a'. Again it was noted (not reported) that by having four foam samples separated by three pieces of aluminium foil the noise power drops by 6dBμ provided the total resistance remains 500 ohm. The obvious conclusion is that the noise voltage contributions are in phase unless the foam samples are separated by aluminium foil. It is believed that the noise pulses trigger each other off. This could be regarded as the augmented noise effect [3].

To appreciate how these results support the new theory mentioned earlier, it is necessary to visualize the model representing the carbon-loaded polyurethane resistor. This resistor is made up of granules of carbons each of which has a resistance given by $(R_o+\Delta R_o)$. By adjusting the pressure between the aluminium plates the total resistance, R, is made up by the interconnection of the granules. R_o, the fixed value of resistance of a granule, must always be accompanied by ΔR_o, the time varying component of the resistance of the granule which gives rise to the 1/f noise. The varying components ΔR_o are in phase and hence combine on a voltage basis to give the total time varying resistance ΔR. Hence

$$\frac{\langle \Delta R^2 \rangle}{R^2} = \text{constant}$$

no matter how the granules are interconnnected. The main conclusion is that the noise is generated in the granules as purported by the new theory [1,2] and not by the contact between granules.

REFERENCES

1. MAY, E.J.P. "On the origin of 1/f noise", Int. J. Electronics, 1988, Vol. 65, No. 4, pp. 805-807

2. MAY, E.J.P., "On the origin of 1/f noise in MOS transistors", Proc. 18th European Solid State Device Research Conference, J. de Physiques, Sept. 1988. pp. 161-163.

3. MAY, E.J.P., AL-CHARCHAFCHI, S.H., "The generation of augmented 1/f and 1/Δf noise in resistors by the injection of short duration pulses", Journal of the Institution of Electronic and Radio Engineers, 57 (3) 1987, pp. 125-128.

4. MAY, E.J.P., AL-CHARCHAFCHI, S.H. and MEHDI, H.H. "1/f and 1/Δf noise on carbon-loaded polyurethane", Proceedings of 4th International Conference on 1/f Noise, Sept. 1985, North-Holland Physics Publishing, The Netherlands.

10th Int.Conf. on Noise in Physical Systems
1989 Budapest, Hungary

1/f NOISE IN CARBON AND ASBESTOS WETTED BY SALINE SOLUTIONS

E.J.P. MAY

Department of Engineering Science, University of Exeter
North Park Road, Exeter EX4 4QF, Devon, UK

ABSTRACT

Noise measurements were made on damp carbon particles and asbestos fibres. These measurements afforded a method of assessing the effect of surface states on 1/f noise. This led to important implications regarding the role of asbestos as a carcinogen.

1. INTRODUCTION

1/f noise is a special case of a family of low frequency noises produced by surface states. Such 1/f noise is produced when the fast states predominate [1]. Slow states which give rise to pulses rather than impulses result in a departure from the 1/f law as is the case with gallium arsenide. In general, it can be shown by using the convolution theorem that the noise produced by a pulse is given by $|F(\omega)|^2$ 1/f where $F(\omega)$ is the Fourier transform of the pulse.

To prove these ideas, noise measurements were made on both dry and moist activated carbon particles. The results indicated that for the moist particles there was a departure from the 1/f law, but it was not clear whether this noise was made in the carbon or the saline solution with which it was wetted. This is why in the second experiment moist asbestos fibres were used. The results showed that saline solutions, which normally do not exhibit low frequency noise, do so when asbestos is added to them; these results have implications regarding the toxicity of the carcinogenic asbestos.

2. MEASUREMENT PROCEDURE

The measurements were made using techniques which have been described in a previous paper at this conference [2]. The test samples were activated carbon particles (100 mesh) and asbestos fibres which were obtained by carefully filing a piece of asbestos. The carbon/asbestos material was

placed in a shallow dish of diameter 1.5 inch. Stainless steel electrodes were placed in the dish and made contact with the carbon/asbestos. The noise voltages between the electrodes were measured using a constant current source [2]. The bandwidth was 3.12 Hz.

The noise frequency characteristic for dry carbon, with a constant current of 1 mA, is shown in curve a of Fig. 1. Curve b shows the results after the carbon was exposed to the atmosphere for 24 hours (relative humidity 54%). In curve c, the sample consisted of 1.52g of saline solution added to 3.58g of carbon. The saline solution was prepared using 5.7g of sodium chloride in one litre of distilled water. Noise measurements were made on the saline solution by itself; these are not recorded because the readings were too low to measure with the available equipment. The values of the index n in $1/f^n$ were 1.008, 1.305 and 3.5 for the curves a, b and c in Fig. 1.

The measurements on the asbestos fibre were made using a sample of 1.5 g of fibre added to 3g of the saline solution. The results are given in Fig. 2.

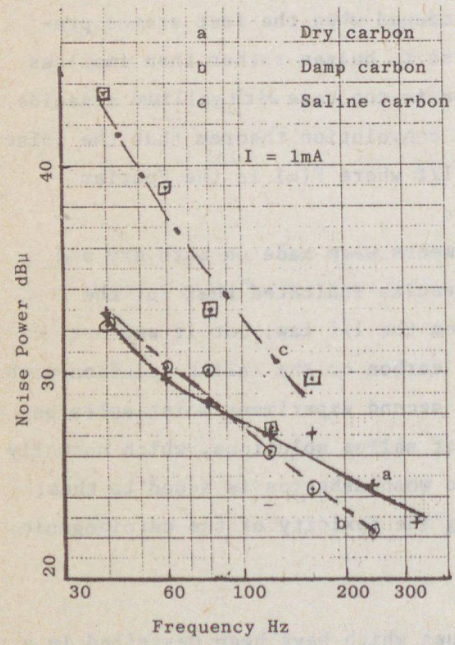

Fig 1. Noise Power Characteristics (Carbon)

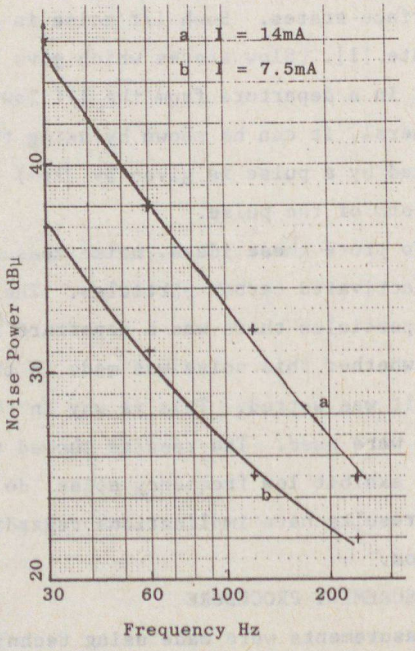

Fig 2. Noise Power Characteristics (Asbestos)

3. IMPLICATIONS AND CONCLUSIONS

The noise measurements on carbon particles, as seen in Fig. 1, support the idea that surface states are responsible for the creation of 1/f noise. Curve a in Fig. 1 represents the dry carbon particles; the frequency index is found to be 1.0, as one would expect. Measurements made in the laboratory using carbon exposed to the atmosphere are shown in curve b Fig. 1. The index rose to 1.3 because the slow surface states became predominant. However, when a saline solution was added to the carbon the diffusion of 'inter-surface states' charges into the saline solution may have been responsible for a time varying component in the resistivity of the solution. From curve c in Fig. 1 it is seen that the frequency index rises to 3.5.

Asbestos when dry is an insulator but when moistened with a saline solution it becomes a conductor either because of the mobile ions in the electrolyte or it may act as an ion exchanger in which the counter ions are mobile. From Fig. 2, it is seen that it also generates low frequency noise which may be due to the diffusion of charge in accordance with the surface state diffusion theory [1]. This implies that adsorption has a small time varying component.

Asbestos is known to be a carcinogen; but the underlying cause of toxicity has evaded explanation because asbestos is chemically inert [3]. This property of inertness is an essential feature of a new model of the toxicity effect based on the work described in this paper.

In this model the asbestos may be regarded as the hardware or the electronic system which produces a current with a frequency spectrum which has very strong low frequency components which include the range 50 - 60 Hz. An asbestos fibre lodged in living tissue of the lung would produce local electromagnetic fields because of the natural electric potentials in the body. These fields are not unlike those produced by the 50 - 60 Hz power distribution lines. There have been reports that the latter produce carcinogenic effects [4,5]. This implies that the underlying causes of toxicity for asbestos and power lines are shared. It should be noted that the electromagnetic fields adjacent to fibres lodged in living tissue are only 0.1 μm away from the current source. The culpable electric currents in power distribution lines are often 40m away [4,5]. This means that the currents in the fibres need only be 10^{-9} of those in the distribution system to produce the same effect. The durability of the electronic system (the asbestos) is paramount, but the shape and size of the fibre is obviously important for two reasons. It must be long so as to produce the

effective magnetic field, but its length must not prohibit it from entry through the nose to the lungs. Also the diameter must be small enough to ensure that it adheres to the tissue. This fact has been recognised for some time. The notion that size and shape is all important is known as the Stanton hypothesis [3]. The optimum size has been determined and seems to be 0.2μm diameter and 6μm length.

It should be noted that the earth's magnetic field could also contribute to this effect. What is more, the alternating 50 - 60 Hz power line systems have magnetic fields which would produce $1/\Delta f$ noise; these would include strong components at the low end of the frequency spectrum. Asbestos may well be the co-factor some workers have been looking for [4]. Also radio frequency electromagnetic fields produce 1/f noise [6,7] and may also be culpable.

Other carcinogenic particles, for example, the carbon particles discussed in this paper, may behave in a similar manner. Further work in this field is in progress; the effect of adding carbon particles to the asbestos seems to promote electrolysis within the electrolyte which gives off chlorine. This in itself may be a source of toxicity.

REFERENCES

1. May, E.J.P., 'On the origin of 1/f noise', International Journal of Electronics, 1988, Vol. 65, No 4, pp 805-807.
2. May, E.J.P., and Al-Charchafchi, S.H., '1/f Noise in variable carbon granule resistors', Proceedings 10th International Conference on Noise in Physical Systems, 1989, Budapest.
3. Zurer, P.S., 'Asbestos', Special Report, Chemical & Engineering News, 1985 March 4, pp28 - 41.
4. Wertheimer, N., and Leeper, E., 'Electrical wiring configuration and childhood cancer', American Journal of Epidemiology, 1979, Vol. 109, No 3, pp273-282
5. Wertheimer, N., and Leeper, E., 'Adult cancer related to electrical wires near the home', International Journal of Epidemiology, 1982, Vol. 11, No 4, pp345-355.
6. May, E.J.P., and Horwood, J.M.K., '1/f Noise Produced by Radio Frequency Current in Thin Films of Gold, Silicon and Lead Sulphide'. Proceedings of the Symposium on 1/f Fluctuations, Tokyo Institute of Technology, July 1977, pp.124-131.
7. May, E.J.P., and Sellars, W.D., '1/f Noise Produced by Radio-frequency Current in Resistors'. Electronic Letters I.E.E. Vol.11, Oct 1975, pp 544-545.

10th Int.Conf. on Noise in Physical Systems
1989 Budapest, Hungary

NYQUIST 1/f NOISE IN SEMICONDUCTOR-TUNNELING DIELECTRIC-SEMICONDUCTOR STRUCTURES

L.N. NEUSTROEV, V.V. OSIPOV, O.N. PANASHCHENKO

Moscow, USSR

This paper predicts the possible occurrence of a thermodynamic-equilibrium fluctuating voltage with a 1/f spectrum across the ends of an open circuit semiconductor heterostructure. It is shown that the real part of the admittance can increase in proportion to the frequency, $\sigma(f) \sim f$, in a semiconductor-(tunneling-thin-insulator)-semiconductor structure (Fig. 1) over a wide frequency range. The real part of the impedance varies in accordance with $\mathrm{Re}\, Z(f) = \sigma(f)[\sigma^2(f) + (2\pi Cf)^2]^{-1}$, where C is the capacitance of the structure, and the spectral density of the fluctuations in the voltage across the ends of an open structure of this sort has a spectrum $S_V(f) = 4kT\, \mathrm{Re}Z(f) \sim 1/f$ according to the Nyquist theorem.

Let us consider the case in which the conductivity of the structure is determined by the trapping and ejection of carriers by trapping centers in the insulator. In this case the physical reason for the increase in $\sigma(f)$ with increasing frequency is as follows: When the electron is trapped at a trapping center in the insulator (process r_n in Fig. 1) a charge qa_n/a is transferred in the external circuit, while in the trapping of a hole (r_p in Fig. 1) a charge qa_p/a is transferred, where q is the charge of an electron, a_n and a_p are the size of the space charge region in the n-type and p-type semiconductors, and $a = a_n + a_p$ (it is assumed here that the thickness of the insulator is $d \ll a_n + a_p$). When an electron or hole is ejected from a trapping center in the insula-

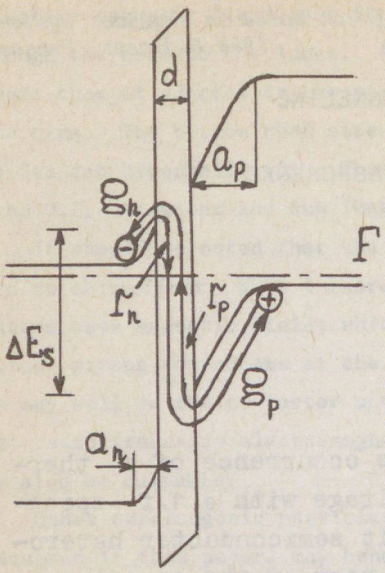

FIG. 1. Energy band diagram of a semiconductor-(tunneling-thin-insulator)-semiconductor structure; schematic diagram of the trapping and ejection of carriers by trapping centers in the oxide film; F - Fermi level.

tor (g_n and g_p in Fig. 1), a charge - qa_n/a or - qa_p/a, respectively, is transferred in the external circuit. Let us put all possible generation-recombination processes involving trapping centers in four groups: trapping of an electron with trapping of a hole (r_n-r_p); ejection of an electron with ejection of a hole (g_n-g_p); trapping of an electron with ejection of an electron (r_n-g_n); and trapping of a hole with ejection of a hole (r_p-g_p). Since the area under the pulse corresponding to the process (r_n-g_n) or (r_p-g_p) by itself is zero, these processes do not contribute to the static conductivity. We denote by ν_n the average frequency of the r_n and g_n processes (at thermodynamic equilibrium, the frequencies of these processes are equal), and we denote by ν_p the average frequency of processes r_p and g_p. The average frequency of processes which determine the conductivity, (r_n-r_p) and (g_n-g_p), is determined by the smaller of the frequencies ν_n and ν_p. If the frequencies are nonzero, the processes (r_n-r_p) and (g_n-g_p) will be accompanied by (r_n-g_p) and (r_p-g_p) in contributing to the conductivity. The average frequencies of the latter two processes are ν_h and ν_p, respectively. The frequencies ν_n and ν_p may differ in magnitude by an exponentially great amount, especially in wide-gap semicon-

ductors. Since the static conductivity of a heterojunction is determined by the smaller of the frequencies ν_n and ν_p, while the rf conductivity is determined by the larger, then if $\max(\nu_n, \nu_p) \gg \min(\nu_n, \nu_p)$ there must exist a frequency range in which the real part of the conductivity of the structure will increase with increasing frequency. If the tunneling transparency of the insulator is close to unity, there will be a single time scale for the charge exchange of the trapping centers in the insulator, and the real part of the conductivity of the heterostructure will increase in accordance with $\sigma(f) \sim f^2$. If, on the other hand, the tunneling transparency of the insulator is quite small, then there will be a set of time scales for the charge exchange of trapping centers of the insulator. The calculations below show that in this case the real part of the conductivity increases in accordance with $\sigma(f) \sim f$.

To calculate the admittance of a semiconductor-(tunneling thin-insulator)-semiconductor structure we used the method which was developed by Van Vliet for a p-n junction with trapping centers in the space-charge region. The results of the calculation are

$$\sigma(f) = \frac{q^2 A}{kT} \sum_i \frac{N_{ti}}{(2\pi f)^2 + \tau_{ti}^{-2}} \left[\frac{\alpha_{ni}\alpha_{pi} n_{s1} p_{s2}}{\tau_{ti}} + \right.$$

$$\left. + \left(\frac{2\pi f}{a}\right)^2 \left(\frac{\alpha_{ni} n_{s1} n_{i1} a_n^2}{n_{s1} + n_{i1}} + \frac{\alpha_{pi} p_{s2} p_{i2} a_p^2}{p_{s2} + p_{i2}} \right) \right], \quad (1)$$

$$C(f) = \frac{\varepsilon\varepsilon_0 A}{a} + \frac{q^2 A}{kTa} \sum_i \frac{N_{ti}}{(2\pi f)^2 + \tau_{ti}^{-2}} \left[\alpha_{ni}^2 n_{s1} n_{i1} a_n^2 + \right.$$

$$\left. \alpha_{pi}^2 p_{s2} p_{i2} a_p^2 - 2\alpha_{ni}\alpha_{pi} n_{s1} p_{s2} a_n a_p \right]. \quad (2)$$

Here A is the area of the insulator, N_{ti} is the density of trapping centers in the insulator at a distance x_i from the interface between the insulator and the first semiconductor; $\alpha_{ni} = \alpha_{no} \exp(-x_i/\lambda_n)$ and $\alpha_{pi} = \alpha_{po} \exp(x_i - d)/\lambda_p$ are the trapping coefficients for electrons and holes at trapping center i, λ_n and λ_p are the electron and hole tunneling lengths in the insulator at energies corresponding to the bot-

tom of the conduction band at the surface of the first semiconductor and the top of the valence band at the surface of the second semiconductor, $\tau_{ti}^{-1} = \alpha_{ni}(n_{s1}+n_{i1})+\alpha_{pi}(p_{s2}+p_{i2})$, n_{s1} and p_{s2} are the densities of electrons in the first semiconductor and of holes in the second semiconductor, at the heterojunction, $n_{i1} = n_{s1}\exp(E_i-F)/kT$, $p_{i2} = p_{s2}\exp(F-E_i)/kT$, E_i is the energy of trapping center i, F is the Fermi level, ε is the dielectric constant of the semiconductors, ε_o is the permittivity of free space, and T is the temperature. The summation in (1), (2) is over all the trapping centers in the insulator.

Analysis of (1), (2) shows that under the conditions $\max(f_{no},f_{po}) \gg \min(f_{no},f_{po})$ and $\exp(d/\lambda_n)$, $\exp(d/\lambda_p) \gg 1$, where $f_{no} = \alpha_{no}n_{s1}(2\pi)^{-1}$ and $f_{po} = \alpha_{po}p_{s2}(2\pi)^{-1}$, there is always a frequency range in which the real part of the impedance varies a $\mathrm{Re}\, Z(f) \sim 1/f^{\gamma}$, where γ is some number which is close to unity. We turn now to the results of a calculation of sums (1), (2) for the very simple case in which the tunneling length of the electrons and holes are equal ($\lambda_n = \lambda_p = \lambda$). Expressions (1), (2) are symmetric with respect to the frequencies f_{no} and f_{po}. For definiteness we set f_{no} f_{po}, and we analyze one limiting case of (1), (2): $D_T^{-1}f_{po}$ f_{no}. This inequality would be most likely to hold in semiconductor-(tunneling-thin-insulator)-semiconductor structures which use widegap semiconductors, in which the values of n_{s1} and p_{s2} may differ by many orders of magnitude. From (1), (2) we then find the following expression for the spectral density of the thermodynamic-equilibrium fluctuating voltage across the ends of the open-circuit structure:

$$S_V(f) = 4kT\,\mathrm{Re}\,Z(f) = \frac{q^2kTA\lambda N_t(F)}{f d C_n^2} \quad \text{for } f_{no} > f > D_T f_{no} \qquad (3)$$

where $C_n = \varepsilon\varepsilon_o A/a_n$. Let us look at some numerical estimates. We assume $n_{s1}p_{s2} = 10^{10}$ cm^{-6}, corresponding to T = 300 K and to an energy gap $\Delta E_s = 1.5$ eV between the bottom of the conduction band at the surface of the first semiconductor and the

top of the valence band at the surface of the second semiconductor. Choosing $n_{s1} = 10^{8}$ cm^{-3}, $p_{s2} = 10^{2}$ cm^{-3}, $\alpha_{no} \sim \alpha_{po} \sim 10^{-8}$ cm^{3}/s and $D_T = 10^{-5}$, we find $D_T^{-1} f_{po} \ll f_{no}$, and an equilibrium 1/f noise exists over the frequency range from 0.1 to 10^{4} Hz.

10th Int.Conf. on Noise in Physical Systems
1989 Budapest, Hungary

NOISE IN THE TUNNELING CURRENT THROUGH THIN SiO_2 FILM AT 77 AND 295 K

Z.M. SHI, M. DUTOIT, M. ILEGEMS

Institute for Micro- and Optoelectronics,
Swiss Federal Institute of Technology
CH-1015 Lausanne, Switzerland

ABSTRACT

The noise in the tunneling current through polysilicon gate capacitors was measured as a function of frequency and time at constant voltage at 77 and 295 K. We found that this noise contains two components. One, reflecting shot noise, is related to direct band-to-band tunneling and dominates at high frequencies (1 - 10 kHz). Its power spectral density (PSD) is proportional to the current and independent of temperature and charge trapping. The other, indicating flicker noise, is due to trapping/detrapping and dominates at lower frequencies (1 Hz - 1 kHz). Its PSD is proportional to I^2/f^n, where n varies during charge injection and is related to the spatial location of charge trapping.

1. Introduction

As is well known from fundamental physical laws, thermal noise and shot noise in solid state devices are unavoidable whatever method of device preparation is used. But low-frequency noise (LFN) strongly depends on device fabrication and thus has received intensive attention in recent years[1]. $1/f^n$ noise (where $0.7 < n < 1.2$) in MOS devices is related to dynamic charge trapping/detrapping in the oxide[2,3]. Steady state charge trapping in thin SiO_2 film was studied by many investigators[4-6].

This work was motivated by earlier observations of fluctuations in the tunneling current through thin SiO_2 films[7,8]. We set up an experimental system to simultaneously measure DC-tunneling current and noise on MOS capacitors (MOSC) at constant voltage.

2. Experimental procedures

A. Sample preparation

The samples were n^+-poly-Si/SiO_2/n-Si MOSC whose area was 6.4×10^{-5} cm^2. The gate oxide was grown in dry O_2 at 900 °C to 97 ± 3 Å. The polysilicon was then deposited by LPCVD at 620 °C and doped at 1000 °C using $POCl_3$. The samples were manufactured at the Centre Suisse d'Electronique et de Microtechnique (CSEM) in Neuchâtel. They were packaged in TO-18 sockets. High-frequency C-V measurements

were done on all samples. Only samples with undistorted C-V curves, without leakage current (< 10 μA/cm^2 at 8 MV/cm) and with clean noise were considered.

B. Measurement system

A schematic of the measurement system is shown in Fig.1. A low noise voltage source (LNVS) provided a stable constant voltage to perform charge injection. The current through the sample was converted to a voltage by an ultralow-noise amplifier (ULNA). The DC-voltage and tunneling current were measured by two digital volt meters (DVM) through buffers. The power spectral density (PSD) was measured by a HP3562A dynamic signal analyzer (1 Hz - 10 kHz).

C. Experimental results

(1) DC-tunneling current

During constant-field stressing, the tunneling current decreases with charge injection due to net electron trapping. From Fig.2 we observe that the current decreases much faster at 295 K than at 77 K. This indicates that the trapping rate increases with temperature. After prolonged charge injection at 295 K, the current suddenly increases and dielectric breakdown follows.

(2) Noise in the tunneling current

Simultaneous noise measurements were started as soon as the applied voltage stabilized. Two typical noise power spectra are shown in Fig.3.

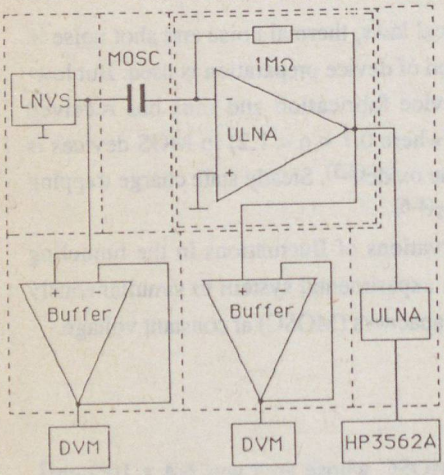

Figure 1. Block-diagram of our experimental system.

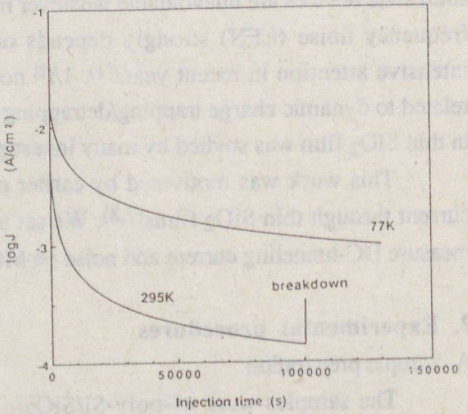

Figure 2. Tunneling current across n$^+$-poly-Si/SiO_2(97 Å)/n-Si capacitors at constant field (10.5 MV/cm, positive gate) at 77 and 295 K. Area: 6.4x10^{-5} cm^2.

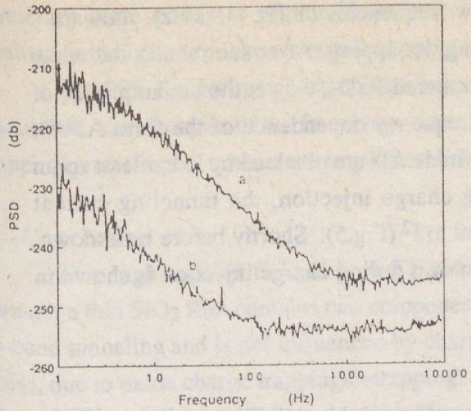

Figure 3. Total noise power spectra of the tunneling current at constant applied field (10.5 MV/cm) at 77 K after injecting (a) 28 C/cm^2 (I = 670 nA) and (b) 250 C/cm^2 (I = 67 nA).

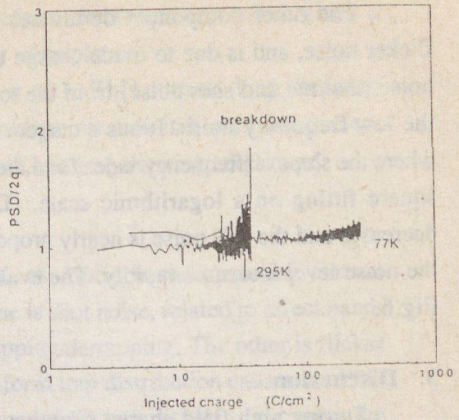

Figure 4. The PSD of shot noise in the tunneling current at constant applied field (10.5 MV/cm) at 77 and 295 K normalized by 2qI (I = 10 nA - 2 μA).

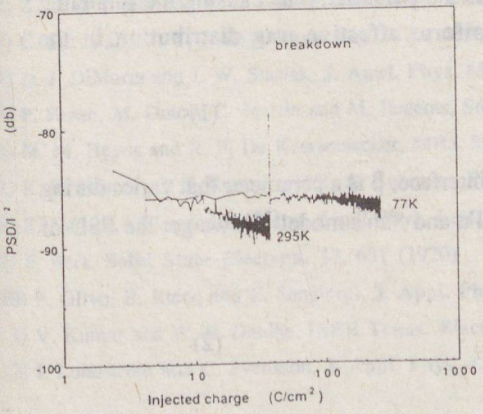

Figure 5. The PSD of low-frequency noise (at 1 Hz) in the tunneling current at constant applied field (10.5 MV/cm) at 77 and 295 K.

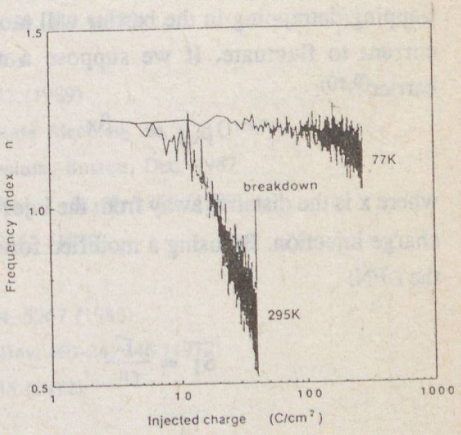

Figure 6. Frequency index n of low-frequency noise in the tunneling current at constant applied field (10.5 MV/cm) at 77 and 295 K.

In addition to thermal noise (4kT/R) from the sampling resistor (1MΩ in Fig.1), the measured noise contains two components. One dominates at high frequencies (1 - 10 kHz), reflecting shot noise and is related to direct band-to-band Fowler-Nordheim tunneling. Subtracting the thermal noise from the total high frequency component, we get the net amplitude of the shot noise. It is proportional to the current (I). The net PSDs of shot noise normalized to 2qI are independent of temperature and charge trapping (Fig.4).

The other component dominates at low frequencies (1 Hz - 1 kHz), indicating flicker noise, and is due to oxide charge trapping/detrapping. After subtracting the white noise (thermal and shot noise) from the total measured PSDs, we get the net amplitude of the low frequency noise. It has a current and frequency dependence of the form AI^2/f^n, where the slope n (frequency index) and the amplitude AI^2 are obtained by linear least mean square fitting on a logarithmic scale. During charge injection, the tunneling current decreases and the $1/f^n$ noise is nearly proportional to I^2 (Fig.5). Shortly before breakdown, the noise level increases rapidly. The evaluation of n during charge injection is shown in Fig.6.

3. Discussion

During high field charge injection, the traps which have the largest capture cross section are filled first. Then the traps which have a smaller capture cross section will be filled, and so on. The total electron trapping rate decreases with charge injection and the decrease of tunneling current becomes slower and slower (Fig.2).

It is well known that the tunneling current is a function of the barrier potential, which depends on the actual configuration of charges in the barrier. Random charge trapping/detrapping in the barrier will modulate the potential, thus causing the tunneling current to fluctuate. If we suppose a nonuniform effective trap distribution in the barrier[9,10]:

$$\rho_{ox} \propto e^{\beta x}, \qquad (1)$$

where x is the distance away from the injecting interface, β is a parameter that varies during charge injection. By using a modified form of Fu and Sah's model[11], we get the PSD of the LFN:

$$S_I \propto \frac{I^2}{f^n}, \qquad (2)$$

where,

$$n = 1 + \frac{\beta}{2\alpha}. \qquad (3)$$

α is the tunneling decay constant (0.6 Å^{-1}, for the Si/SiO_2 barrier)[12].

From relations (1-3) we find that, if the effective trap density has a uniform distribution ($\beta = 0$), the noise PSD follows a 1/f law (n =1). When the effective traps are close to the injecting interface ($\beta < 0$), then $n < 1$. When the effective traps are located deep in the oxide ($\beta > 0$), then $n > 1$. From a physical point of view, deeper tunneling corresponds to larger time constants, which correspond to lower frequencies, shallow

tunneling corresponds to higher frequencies. Therefore, the frequency index gives a qualitative indication of where electron trapping mainly takes place.

At 295 K, during short charge injection, $n > 1$. This means deep trapping dominates. The decrease of the frequency index with charge injection indicates that shallow trapping gradually becomes more important. When $n < 1$, shallow trapping takes over.

4. Conclusion

At a high applied field at both 77 and 295 K, the noise in the tunneling current through a thin SiO_2 film contains two components. One is shot noise, related to direct band-to-band tunneling and is not influenced by charge trapping/detrapping. The other is flicker noise, due to oxide charge trapping/detrapping. A uniform trap distribution causes the PSD of the LFN to follow a 1/f law. A nonuniform (exponential) trap distribution causes the PSD to follow a $1/f^n$ law. Its frequency index n provides information about the spatial location of charge trapping.

References

(1) M. B. Weissman, **Rev. of Mod. Phys. 60**, 537 (1988)

(2) Z. Celik-Butler and T. Y. Hsiang, **Solid State Electron. 30**, 419 (1987)

(3) C. Surya and T. Y. Hsiang, **Phys. Rev. B 33**, 4898 (1986)

(4) D. J. DiMaria and J. W. Stasiak, **J. Appl. Phys. 65**, 2342 (1989)

(5) P. Fazan, M. Dutoit, C. Martin and M. Ilegems, **Solid State Electron. 30**, 829 (1987)

(6) M. M. Heyns and R. F. De Keersmaecker, **MRS Symposium, Boston,** Dec. 1987

(7) K. R. Farmer, C. T. Rogers and R. A. Buhrman, **Phys. Rev. Lett. 58**, 2255 (1987)

(8) B. Neri, P. Olivo and B. Ricco, **Appl. Phys. Lett. 51**, 2167 (1987)

(9) F. Berz, **Solid State Electron. 13**, 631 (1970)

(10) P. Olivo, B. Ricco and E. Sangiorgi, **J. Appl. Phys. 54**, 5267 (1983)

(11) V. Kumar and W. E. Dahlke, **IEEE Trans. Electron Dev. ED-24**, 146 (1977)

(12) I. Lundström and C. Svensson, **J. Appl. Phys. 43**, 5045 (1972)

10th Int.Conf. on Noise in Physical Systems
1989 Budapest, Hungary

1/f NOISE AND QUANTUM 1/f APPROACH IN FERROELECTRICS AND FERROMAGNETICS

P.H. HANDEL

Physics Department, University of Missouri
St. Louis, MO 63121, USA

1/f fluctuations were measured by Musha [1] in the relaxation rate of ferroelectric triglycine sulphate (TGS) and were also sought in ferromagnetic samples. However, while in a ferroelectric such as TGS the results were positive [1], in ferromagnetics no 1/f noise was found by Musha. We present here first a calculation of the expected quantum 1/f effect in TGS.

In ferroelectrics, and in general in piezoelectrics, the infrared exponent αA which otherwise describes the interaction of electric charges with photons, is replaced by the corresponding quantity gA for the interaction with piezophonons [2],[3]. The fine structure constant $\alpha = e^2/\hbar c$ is replaced by

$$g = \pi C^2 (e^2/\varepsilon\hbar v_s)(Q^2/\varepsilon\rho v_s^2), \qquad (1)$$

where ε is the static dielectric constant, Q the piezoelectric constant, v_s the speed of transversal sound waves, ρ the crystal density, and C a constant of the order of the unity depending on the crystal structure. The factor A in the infrared exponent becomes now

$$A = 2(\mathbf{k}' - \mathbf{k})^2/3\pi k_s^2, \qquad (2)$$

where k_s corresponds to a Compton wave number $M'v_s/\hbar$ defined, however, with the speed of sound v_s, while $\mathbf{k}'$ and $\mathbf{k}$ are the wave vectors of the outgoing and incoming charge carriers in the reorientation process whose quantum 1/f noise we calculate.

For TGS we take [4] $Q^2 = 3\ 10^{11}$ dyn/cm^2, $\rho = 1.68$ g/cm^2 at room temperature, $\varepsilon = 1000$, $v_s = 3\ 10^5$ cm/s, and C =1. This yields

$$g = 5\ 10^{-3}. \tag{3}$$

The elementary process whose quantum 1/f noise is of interest for us is the reorientation of a group of atoms in the TGS molecule containing nitrogen, and involving a mass M' of about 10 % of the molecular mass M=230 of TGS, during polarization reversal. This happens in an electric field E which accelerates the group over a distance of the order of d=10Å. We obtain

$$A = 2(\mathbf{k}' - \mathbf{k})^2/3\pi k_s^2 = 2\hbar^2(\mathbf{k}' - \mathbf{k})^2/3\pi M'^2 v_s^2, \tag{4}$$

Taking E=1V/cm, and the charge of the group q =e = 4.8 10^{-10} e.s.u., we find

$$qEd = \hbar^2(\mathbf{k}' - \mathbf{k})^2/2M'; \quad A = (4/3\pi)(qEd/M'v_s^2) = 4\ 10^{-8}. \tag{5}$$

The fractional spectral density of the corresponding rate r fluctuations, or relaxation time τ fluctuations, is therefore

$$r^{-2}S_r(f) = \tau^{-2}S_\tau(f) = 2gA/f = 4\ 10^{-10}/f. \tag{6}$$

In general, we can cast this result in the universal form

$$r^{-2}S_r(f) = (4\ 10^{-10}/f)(q/e)(E/1V/cm)(d/10Å)((23/M')(1000/\varepsilon)^2. \tag{7}$$

In ferromagnetics we expect only the rotation of a spin, or spin-flip, in the magnetic field, rather than acceleration of electric charges in a force field, and therefore a much smaller infrared exponent is expected and negligible 1/f noise should be obtained in ferromagnetic materials.

The author would like to thank Prof. Toshimitsu Musha for his help and for his hospitality at the Tokyo Institute of Technology. The author also thankfully acknowledges the invitation of the Tokyo Institute of Technology in 1987.

REFERENCES

1. T. Musha, A. Nakajima and H. Akabane, Jap. Journ. Appl. Phys. 27, L-311 (1988).

2. P.H. Handel and T. Musha, Noise in Physical Systems and 1/f Noise, M. Savelli, G. Lecoy and G. Nougier Eds., p. 101. Amsterdam, NY, Elsevier, 1983.

3. P. H. Handel and T. Musha, Z. Physik B70, 515 (1988)

4. Y. Tsujimi, T. Yagi and I. Tatsuzaki, J. Phys. Soc. Japan 52, 1469 (1982).

MEASUREMENTS OF THE EQUILIBRIUM MAGNETIC NOISE OF A SHORT-RANGE ISING SPIN GLASS

K. GUNNARSSON, P. SVEDLINDH, P. NORDBLAD, L. LUNDGREN,
H. ARUGA,* A. ITO*

Department of Solid State Physics, Institute of Technology,
Uppsala University
S-751 21 Uppsala, Sweden
*Department of Physics, Faculty of Science,
Ochanomizu University
Bunkyo-ku, Tokyo 112, Japan

INTRODUCTION

During the last decade, the spin glass relaxation has been zealously studied experimentally, theoretically and by simulations. In this paper we focus on the dynamics of the short-range Ising spin glass $Fe_{0.5}Mn_{0.5}TiO_3$. Experimental results from real Ising spin glass systems can be directly compared to Monte Carlo (MC) simulations, which are mostly based on Ising models. In order to investigate a larger time interval of the relaxation, several techniques must be combined. Together, time dependent magnetization and ac susceptibility measurements cover more than nine decades in time, $2x10^{-5}$ s< t <$3x10^4$ s. Here, we present results from another experimental method, viz. measurements of *the equilibrium magnetic noise* (Svedlindh et al. 1989). Unlike the two former techniques, it can be performed in zero magnetic field. Therefore, the non-linear field dependence of the relaxation near T_g is effectively avoided.

MEASUREMENTS

The measurements were performed on a single crystal of $Fe_{0.5}Mn_{0.5}TiO_3$ using a Superconducting QUantum Interference Device (SQUID) magnetometer. At constant temperature, the SQUID signal was sampled at a given rate. By varying the sampling frequency, 0.2 Hz < f_s < 200 Hz, a frequency interval of 5 x 10^{-3} Hz < f < 1 x 10^2 Hz of the noise power spectra was covered. For each sampling frequency an anti-aliasing filter, with a cut off frequency set equal to the Nyqvist frequency (f_s/2), was used. The data were transformed by a standard FFT algorithm to get the the noise power spectra.

From ac susceptibility measurements, the dynamic susceptibility $\chi(\omega) = \chi'(\omega) + i\,\chi''(\omega)$ is obtained (ω is the angular frequency of the field).The *fluctuation dissipation theorem* (Kubo

1966) relates the imaginary part of $\chi(\omega)$ to the magnetic noise power, $S(\omega)$, by :

$$S(\omega) = 4\,kT\,\frac{\chi''(\omega)}{\omega} \qquad (1)$$

where k is the Boltzmann constant. Fig. 1 shows the magnetic fluctuations of the $Fe_{0.5}Mn_{0.5}TiO_3$ spin glass vs time at three different temperatures. An increase in the noise amplitude as the temperature decreases towards T_g is apparent.

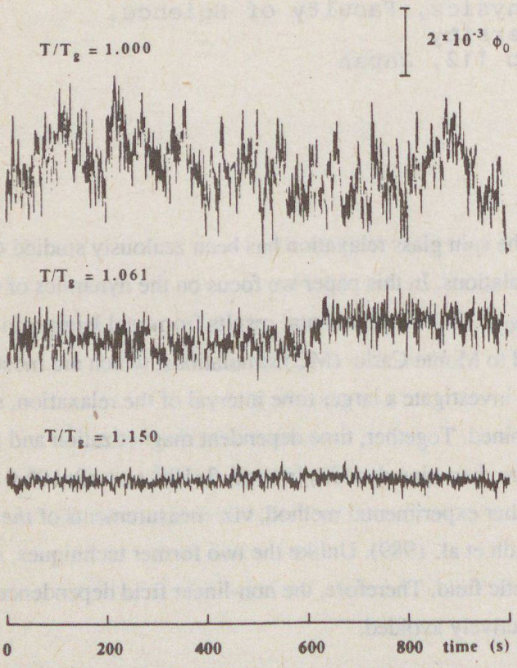

Fig. 1. Magnetic-flux noise vs time for $Fe_{0.5}Mn_{0.5}TiO_3$ at three different temperatures. A relative flux change in the SQUID sensor of 2 x 10-3 ϕ_0 is indicated (ϕ_0 = 2.07 x 10-15 Vs). The sampling frequency is 2 Hz.

Fig. 2 displays the Fourier transformed data, log $S(\omega)$, vs log ω at some temperatures above T_g (unfilled symbols). Close to T_g, the spectra exhibit a 1/f behaviour, indicating a weak frequency dependence of $\chi''(\omega)$. At higher temperatures, however, a deviation from the 1/f line and a convergence to plateaus is apparent. The frequency dependence of $S(\omega)$ in the zero frequency limit indicates the low frequency behaviour of $\chi''(\omega)$, viz. $\chi''(\omega) \rightarrow \omega$ as $\omega \rightarrow 0$. These features of $\chi''(\omega)$ have been verified through ac susceptibility measurements (Gunnarsson et al. 1988) and the fluctuation dissipation theorem has been shown to be valid for the $Fe_{0.5}Mn_{0.5}TiO_3$ spin glass (Svedlindh et al.1989).

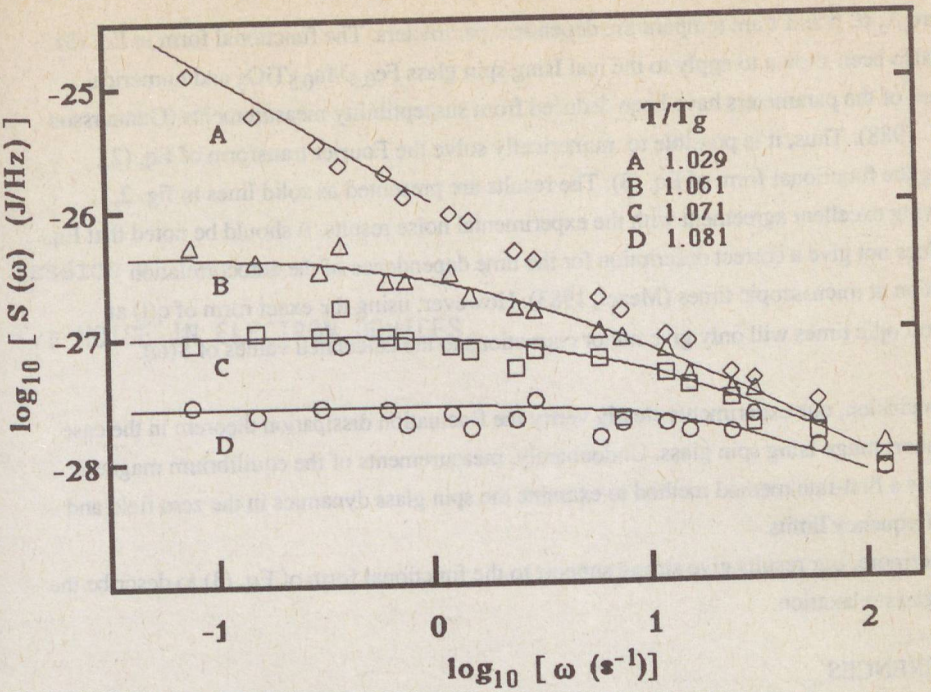

Fig. 2. $\log_{10}[S(\omega)]$ vs $\log_{10}[\omega]$ for $Fe_{0.5}Mn_{0.5}TiO_3$ at four different temperatures above T_g (unfilled symbols). The solid lines show $\log_{10}[S(\omega)]$ obtained from Wiener-Khintchines theorem, using the functional form of Eq. (3) for the integration. To scale the calculated values of $S(\omega)$ to the measured noise power, a factor of 2×10^{-26} was used.

DISCUSSION

It is also possible to relate the measured noise power to the relaxation function, which at thermal equilibrium is directly related to the autocorrelation function, q(t). According to the theorem of Wiener-Khintchine (van Kampen 1965), S(ω) is equal to the Fourier transform of q(t), i.e.

$$S(\omega) = \frac{2}{\pi} \int_0^\infty q(t) \cos \omega t \, dt \qquad (2)$$

Based on results from MC simulations, Ogielski (1985) has proposed the following empirical formula to describe q(t):

$$q(t) = A \frac{\exp[-(t/\tau)^\beta]}{t^\alpha} \qquad (3)$$

where A, α, β and τ are temperature dependent parameters. The functional form in Eq. (3) has also been shown to apply to the real Ising spin glass $Fe_{0.5}Mn_{0.5}TiO_3$ and numerical values of the parameters have been deduced from susceptibility measurements (Gunnarsson et al. 1988). Thus, it is possible to numerically solve the Fourier transform of Eq. (2), using the functional form of Eq. (3). The results are presented as solid lines in fig. 2, showing excellent agreement with the experimental noise results. It should be noted that Eq. (3) does not give a correct description for the time dependence of the autocorrelation function at microscopic times (Mezei, 1983). However, using the exact form of q(t) at microscopic times will only give minor corrections to the calculated values of $S(\omega)$.

In conclusion, our experiments clearly verify the fluctuation dissipation theorem in the case of a short range Ising spin glass. Undoubtedly, measurements of the equilibrium magnetic noise is a first-rate method method to examine the spin glass dynamics in the zero field and zero frequency limits.
Furthermore, our results give strong support to the functional form of Eq. (3) to describe the spin glass relaxation.

REFERENCES

Gunnarsson, K., Svedlindh, P., Nordblad, P., Lundgren, L., Aruga, H. and Ito, A. Phys. Rev. Lett. 61, 754-757 (1988)

Kampen, N.G. van, "Fluctuations in nonlinear systems", Fluctuation phenomena in solids, R. E. Burgess (ed.), 1st ed., Academic Press Inc., New York, 142-144 (1965)

Kubo, R., Rep. Prog. Phys. 29, 255 (1966)

Mezei, F., J. Magn. Magn. Mater. 31-34, 1327-1330 (1983)

Ogielski, A. T., Phys. Rev. B 32, 7384-7398 (1985)

Svedlindh, P., Gunnarsson, K., Nordblad, P., Lundgren, L., Aruga, H. and Ito, A. accepted for publication in Phys. Rev. B (1989)

SESSION 9

1/f NOISE IN ELECTRON DEVICES

10th Int.Conf. on Noise in Physical Systems
1989 Budapest, Hungary

1/f NOISE IN ELECTRONIC DEVICES

T.G.M. KLEINPENNING

University of Technology
Eindhoven, The Netherlands

INTRODUCTION

The aim of the present paper is to review the literature of the last years on 1/f noise in electronic devices. The 1/f noise of most of the devices is discussed in terms of the Hooge parameter α. It should be noted that we restrict ourselves to a discussion of experimental facts. A comparison of experimental α-values with existing quantum theories of 1/f noise has been omitted, as such a comparison is to be found in an extensive review paper by Van der Ziel [1].

P-N DIODES

Relations for the 1/f current noise in several types of p-n diodes based on the mobility-fluctuation model have been derived by Kleinpenning, with the following results.

For a diffusion-current-dominated long p^+-n diode, Kleinpenning [2] found

$$S_I(f) = \frac{\alpha q I}{4 f \tau}\left[1 - \frac{\ln(1+a)}{a}\right] \qquad (1)$$

with $a = I/I_o = \exp(qV/kT) - 1$, τ the hole lifetime in the n-type base, I_o the saturation current and V the applied voltage. Van der Ziel's result [1] was somewhat different as he used the transmission-line analog. However, he neglected the effect that hole mobility fluctuations in the base at spot x lead to fluctuations in the gradient dp(x)/dx. An increase in the mobility results in a decrease of the gradient, thus there is a negative feedback and $\Delta I_p/I_p < \Delta\mu_p/\mu_p$. This negative feedback has been neglected by Van der Ziel. For a generation-recombination-current dominated diode we have [3,4]

$$S_I(f) = \frac{2\alpha q I}{3 f \tau_j}\left[1 - e^{-qV/2kT}\right] \qquad (2)$$

with τ_j the lifetime of carriers in the junction. An alternative calculation

based on fluctuations in the capture cross-section of the traps is given by Van der Ziel [1].

For a diffusion-current-dominated short p^+-n diode the current noise is [5]

$$S_I(f) = \frac{\alpha q I D_p}{fW^2(1 + D_p/sW)^2} \cdot \ln\left[\frac{1 + sW/D_p}{1 + (sW/D_p)\exp(-qV/kT)}\right] \qquad (3)$$

Here W is the width of the base, D_p the hole diffusivity in the base, and s the contact-recombination velocity of holes.

In p-i-n diodes, the current noise is found to be [5]

$$S_I(f) = \frac{2\alpha q I}{3f\tau_i}\left(\frac{W_i}{2L}\right)^4\left[1 - e^{-qV/2kT}\right] \qquad (4)$$

with τ_i the carrier lifetime in the i-region, W_i the width of the i-region and L the average diffusion-recombination length. Equation (4) is derived for p-i-n diodes with $W_i < L$. Van der Ziel et al. [6] argue that for p-i-n diodes with $W_i < L$ there is no carrier density gradient and hence no diffusion, so that one would not expect mobility 1/f noise. This is incorrect. However, for diodes with $W_i/2L \ll 1$, the 1/f noise becomes low.

Recent experimental data

The 1/f noise in n^+-p HgCdTe diodes presented by Van der Ziel et al. [6,7] can be described in terms of Eq. (1). The experimental α-values are in the range of 10^{-4} - 10^{-2}. For p-i-n HgCdTe diodes with $W_i < L$ they found a much lower 1/f noise level. This can be ascribed to the factor $(W_i/2L)^4$ in Eq. (4). Wu et al. [8] have investigated the 1/f noise in long n^+-p $Hg_{0.7}Cd_{0.3}Te$ diodes at 193 K. Near zero bias and at reverse bias the noise obeys Eq. (1) with $\alpha \cong 10^{-2}$. The bias dependence of the noise at high forward bias may be explained by a decrease of τ, due to an increase in the hole-and-electron density. Vandamme and Orsal [9] have investigated the 1/f noise in short p^+-n diodes made of $Hg_{0.56}Cd_{0.44}Te$. At forward bias in the low-injection case the current is diffusion-dominated and the 1/f noise obeys Eq. (3). Using W = 1 μm, D_p = 2 cm^2/s, L_p = 5 μm and s = 10^4 cm/s, they found $\alpha \cong 2 \times 10^{-4}$. A short discussion of earlier 1/f noise results on Si diodes can be found elsewhere [5,10].

BIPOLAR JUNCTION TRANSISTOR (BJT)

During recent years the 1/f noise in BJTs has been discussed mainly in terms of mobility fluctuations. Here we shall present a summary of the

important equations describing the 1/f mobility noise in BJTs. For a pnp transistor, where the collector current I_C is determined by diffusion in the base, we have, according to Kiss and Kleinpenning [11]

$$S_{I_C}(f) = \frac{\alpha q I_C D_p}{f W_B^2 (1 + D_p/W_B s_p)^2} \ln(1 + s_p W_B/D_p) \tag{5}$$

Here W_B is the base width and s_p the recombination velocity of holes at the end of the base. The base current can be written as the sum of several components $I_B = I_{B1} + I_{B2} + I_{B3}$, where I_{B1} is due to electrons injected from the base into the emitter ($\sim \exp(qV_{EB}/kT)$), I_{B2} to carriers recombining in the space-charge region between emitter and base ($\sim \exp(qV_{EB}/2kT)$), and I_{B3} to holes injected from the emitter into the base and recombining there ($\sim \exp(qV_{EB}/kT)$). For the noise in current I_{B1} we have a result similar to that given in Eq. (5)

$$S_{I_{B1}} = \frac{\alpha q I_{B1} D_n}{f W_E^2 (1 + D_n/W_E s_n)^2} \ln(1 + s_n W_E/D_n) \tag{6}$$

where W_E is the emitter width, D_n the electron diffusivity in the emitter and s_n the recombination velocity of electrons at the end of the emitter. The 1/f noise in the recombination current I_{B2} is given by [4,12]

$$S_{I_{B2}} = 2\alpha q I_{B2}/3f\tau_j \tag{7}$$

This relation is equivalent to Eq. (2) for $qV_{EB} >> kT$. The noise in current I_{B3} is found to be [12]

$$S_{I_{B3}} = \frac{\alpha q I_{B3}}{2f\tau_p} \ln\left[\frac{p(0)}{p(W_B)}\right] = \frac{\alpha q I_{B3}}{2f\tau_p} \ln(1 + s_p W_B/D_p) \tag{8}$$

Apart from the factor $\ln[p(0)/p(W_B)]$, Van der Ziel [1] found the same result. However, his calculations are based on assuming fluctuations in the capture cross-section of the traps in the base.

An additional 1/f noise source in bipolar transistors is due to mobility fluctuations in the intrinsic base resistance r_b. For a transistor with a circular emitter we have [12]

$$S_{r_b} = 4\alpha r_b^2/3fN \tag{9}$$

Here, N is the number of electrons in the base. For a rectangular emitter, the factor 4/3 in Eq. (9) must be replaced by 18/5.

The total 1/f noise of a transistor in the common-emitter configuration can be calculated with the help of Eqs. (5)-(9).

We now have the equivalent noise circuit shown in Fig. 1. Here $g_m = dI_C/dV_{EB}$

is the transconductance, $r_\pi = dV_{EB}/dI_B$ the input resistance and R_B the external base resistance. It is assumed that R_B has no 1/f noise. For the usual situation that $r_\pi >> r_b + R_B$, the total 1/f current noise in the short-circuit current I is (see Fig. 1)

$$S_I = g_m^2(r_b+R_B)^2\left[\frac{I_B^2 S_{r_b}}{(r_b+R_B)^2} + S_{I_B}\right] + S_{I_C} = g_m^2(r_b + R_B)^2 S_{I_B}^{eq} + S_{I_C} \qquad (10)$$

Van der Ziel [13] has recently claimed that the noise cannot be described as mobility 1/f noise if S_I is not proportional to the current I_C or I_B. From Eq. (10) we see that this claim is incorrect.

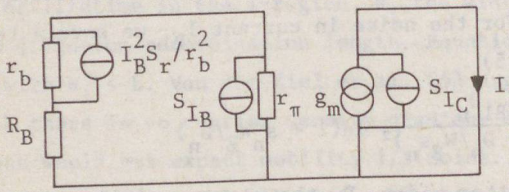

Fig. 1. Equivalent circuit of common-emitter configuration

Recent experimental data

Pawlikiewicz et al. [14,15] have studied the 1/f noise in silicon bipolar transistors. The 1/f collector current noise can be described by Eq. (5) with $\alpha \cong 10^{-8}$. The 1/f base current noise shows a current dependence as predicted by Eq. (10). This is illustrated in Fig. 2 where $S_{I_B}^{eq}/I_B$ is plotted versus I_B. One part of the noise can be described by Eq. (6) with $\alpha \cong 3 \times 10^{-9}$, the other by base resistance noise (Eqs. 9,10) with $\alpha/N \cong 3 \times 10^{-13}$. Taking $N = nAW_B \cong 10^8$, then we have $\alpha = 3 \times 10^{-5}$

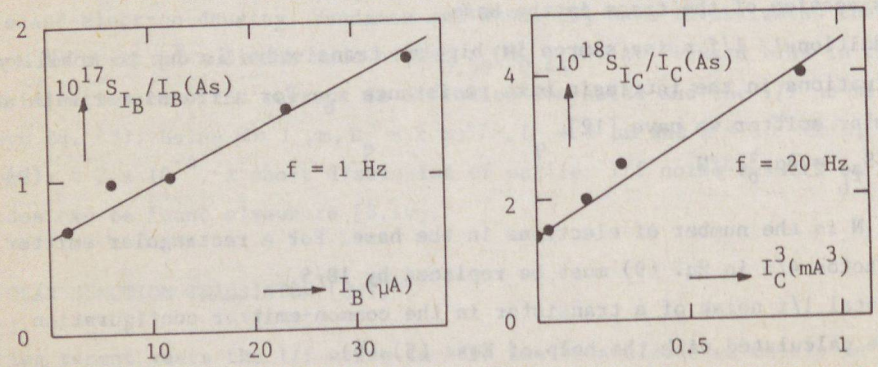

Fig. 2. S_{I_B} vs. I_B (see table 2 in [14]) and S_{I_C} vs. I_C (see Fig. 4 in [18])

Pong-Fei Lu [16] has investigated the low-frequency noise in self-aligned bipolar transistors made by means of different technologies. He found $S_{I_B} \sim I_B^n$ with $1 < n < 2$, which is not in contradiction to Eq. (10). However, owing to lack of detailed data, an analysis of his presented results is not possible. The location of 1/f noise sources in BJTs was discussed by Van der Ziel et al. [17]. They introduced an additional noise-current generator between the base and the collector. The 1/f noise of this generator is of the so-called partition-noise type (see also [1]). However, Van der Ziel et al. did not take into account the mobility 1/f noise in the recombination current, Eq. (7), nor the noise in the internal base resistance, Eq. (9). Zhu et al. [18] have investigated the 1/f noise in npn microwave transistors. The noise in the base current was measured with an a.c. open-circuited base and was found to be of the $1/f^\gamma$ type with $\gamma \cong 1$. At f = 1 kHz they found $S_{I_B}/I_B \cong 6 \times 10^{-19}$ As for the excess noise, and according to Eq. (6) one has $\alpha \cong 10^{-6}$. The collector noise was obtained with a.c. short-circuited base. Experimentally they found $S_I >> g_m^2 r_b^2 S_{I_B}$. According to Eq. (10) one then has

$$S_I = g_m^2 I_B^2 S_{r_b} + S_{I_C} = aI_C^4 + bI_C$$

In Fig. 2 we have plotted $S_I(20\,\text{Hz})/I_C$ vs I_c^3. Consequently, one part ($\sim I_C$) can be interpreted with Eq. (5) and $\alpha \cong 3 \times 10^{-9}$, the other ($\sim I_C^4$) with base-resistance noise, where $S_{r_b}(20\ \text{Hz}) = 2 \times 10^{-8}\ \Omega^2\text{s}$. Similar results are obtained by Kilmer et al. [19]. They found $S_{I_B} \sim I_B$, whereas S_I was found to be more than porportional to I_C.

MOST

The 1/f noise in MOSTs has been extensively discussed both in terms of mobility fluctuations and in terms of number fluctuations (McWhorter). At the moment the source of the noise is still in dispute. Here we shall present the noise formulas and a survey of the recent literature.

Mobility fluctuations

For mobility fluctuations, the 1/f current noise in the source-drain current below saturation is given by [20]

$$S_{I_d} = \frac{\alpha q \mu I_d V_d}{fL^2} = \frac{\alpha q I_d^2}{fCV_G^*(1 - \eta/2)} = \frac{\alpha I_d^2}{fN(1 - \eta/2)} \qquad (11)$$

Here L is the channel length, μ the mobility of the carriers, C the oxide capacitance, V_G^* the gate voltage minus the threshold voltage, $\eta = V_d/V_G^*$,

and $N = CV_G^*/q$ the number of carriers at $V_d = 0$. The equivalent gate voltage noise is given by

$$S_{V_G} = S_{I_d}/g_m^2 = \alpha q V_G^*(1 - \eta/2)/fC \qquad (12)$$

Above saturation ($V_d \geq V_G^*$) the noise can be described by Eqs. (11,12) with I_d replaced by the saturation current I_{sat} and η by 1.

The following observations have to be made with respect to the mobility fluctuation model.

- The electric fields in a MOST are often high. Due to its field dependence, α becomes dependent on V_G^* and V_d [21].
- If the channel is degenerated, then only a fraction of the carriers is available for fluctuations [22].
- If the mobility is determined by several scattering mechanisms, then the magnitude of α can be reduced.

Number fluctuations

Below saturation ($\eta < 1$) the 1/f noise relations are given by [23]

$$S_{I_d} = \frac{q^2 I_d^2 \lambda N_t}{C^2 V_G^{*2} zf} \cdot \frac{\ln(1 - \eta)^{-1}}{\eta(1 - \eta/2)} \qquad (13)$$

and

$$S_{V_G} = \frac{q^2 \lambda N_t}{C^2 zf} \cdot \frac{(1 - \eta/2)\ln(1 - \eta)^{-1}}{\eta} \qquad (14)$$

where λ is a tunnelling parameter of the order of 10^{-10} m, z the thickness of the gate oxide and $N_t = N_t(E_F)kT$ the number of effective traps in the oxide at the Fermi level. Comparing Eqs. (11) and (13) one can define a Hooge parameter for the McWhorter model with

$$\alpha = \frac{q\lambda N_t}{CV_G^* z} \cdot \frac{\ln(1 - \eta)^{-1}}{\eta} \qquad (15)$$

Here the variance of the carriers in the channel is assumed to be $\overline{\Delta N^2} = N_t << N$. However, at weak inversion, where $N < N_t$ (thus $V_G^* < qN_t/C$) we have $\overline{\Delta N^2} = N$. In that case, for $\eta << 1$ we obtain

$$S_{I_d} = \frac{qI_d^2\lambda}{CV_G^* zf}, \quad S_{V_G} = \frac{q\lambda V_G^*}{Czf}, \quad \alpha = \lambda/z \qquad (16)$$

From Eqs. (13,14) it follows that both S_{I_d} and S_{V_G} go to infinity for $\eta = 1$. However, these relations are not exact. For $\eta = 1$ the carrier density n near the drain is so low that $n < n_t$. Taking this effect into account, for the case $\eta \leq 1$, Kleinpenning [24] found the same relations as in Eqs. (13,14) provided that term $\ln(1-\eta)^{-1}$ has been replaced by $\ln[(1+N_t/N)/(1+N_t/N-\eta)]$.

At very weak inversion, the 1/f noise relations for number fluctuations have to be multiplied by a reduction factor [1]

$$C_n^2/(C_d + C_{ss} + C + C_n)^2 \sim [V_G^*/(V_G^* + V_o)]^2$$

Here $C_n = q^2N/kT$ is the channel charge capacitance, C_d the depletion capacitance and C_{ss} the surface-state capacitance. Note that $C_n/C = qV_G^*/kT$. For $V_G^* >> V_o \cong kT/q$ the reduction factor is equal to unity. The calculated S_{I_d} vs V_G^* behaviour for $\eta << 1$ is shown in Fig. 3.

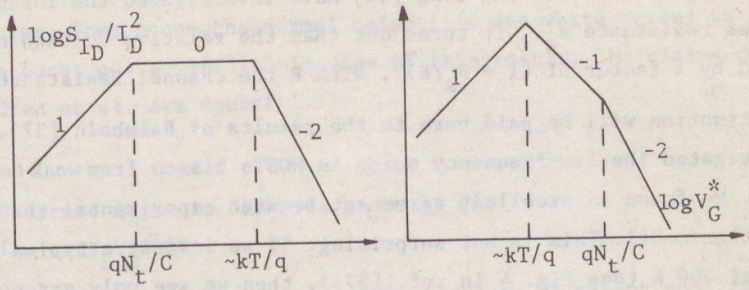

Fig. 3. S_{I_D} vs V_G^* of a MOST according to the McWhorter model

Recent experimental data

Here we shall present a survey of experimental results obtained from both n- and p-MOSTs during recent years.

In n-MOSTs one often finds $\alpha \sim 1/V_G^*$ as predicted by the McWhorter model [25-31]. The observed α-values are in the range from 10^{-5} to 10^{-3}. Some investigators have found α to be independent of V_G^* in n-MOSTs [23,32], which is an indication for mobility fluctuations. In p-MOSTs one found both α independent of V_G^* [25,33] and $\alpha \sim 1/V_G^*$ [27], the magnitude of α being found to be in the range 10^{-5} to 10^{-4}. For a number of p- and n-MOSTs, Maes et al. [34] found S_{V_G} to be exactly proportional to $N_t(E_F)$ over the two-orders-of-magnitude variation of both quantities, which is evidence of the validity of McWhorter's model. Stegherr [35] investigated the 1/f noise in short-channel MOSTs where artificial states were generated by hot carriers. The longer the device is stressed, the more 1/f noise is measured. This can be explained in terms of mobility noise. An increase in crystal defects can result in an increase in α. An explanation in terms of number fluctuations is also possible, here we have $S_{V_G} \sim N_T$.

Vandamme [25], Celik and Hsiang [32] and Peng et al. [36] have studied the 1/f noise in p- and n-MOSTs as a function of channel length L. Accor-

ding to Handel's quantum theories one would expect $\alpha \sim \overline{\Delta v^2}/c^2 = (L/c\tau)^2$ where $\Delta v = L/\tau$ with $\tau = m^*\mu/q$ is the collision time and Δv the change in electron velocity. For n-MOST, Peng obtains $\alpha \sim L^2$ up to $L = 50$ μm at 300 K. However, in this case we find $\Delta v = 2 \times 10^8$ m/s, much higher than the thermal velocity ($\sim 10^5$ m/s) and higher than the velocity of light in silicon ($\sim 9 \times 10^7$ m/s)! Here it should be noted that their spectra have a frequency dependence of $S(f) \sim f^{-1.3}$. Vandamme [25] did not find any L-dependence, Celik and Hsiang [32] found $\alpha \sim L^4$.

Hayat et al. [27] and Tsai and Gong [29] have investigated the influence of a series resistance R_s. It turns out that the relative voltage noise is reduced by a factor of $(1 + R_s/R)^2$, with R the channel resistance.

Special attention will be paid here to the results of Reimbold [37], who has investigated the low-frequency noise in MOSTs biased from weak to strong inversion. He found an excellent agreement between experimental results and the McWhorter model. This is not surprising. If we inspect a typical noise spectrum at 300 K (see Fig. 4 in ref. [37]), then we see only g-r noise and white noise, but no 1/f noise. In Fig. 4 we have reproduced Reimbold's Fig. 4. For the measured g-r spectra at 300 K he found $S_{I_d}/I_d^2 \sim 1/V_G^{*2}$ at high V_G^* and $S_{I_d}/I_d^2 \sim$ const. at low V_G^*, which is in accordance with number fluctuations (see Fig. 3). At 77 K he did not find a plateau at weak inversion. Moreover, at 77 K he observed S_{I_d}/I_d to be almost independent of V_G at fixed V_d, which points to mobility fluctuations (see Eqs. (11) and (13)). However, he did not present spectra measured at 77 K, so that the question arises: did he measure 1/f or g-r noise at this temperature.

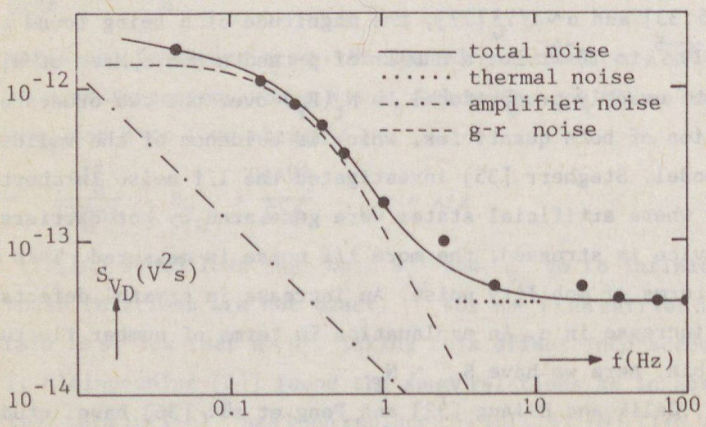

Fig. 4. Typical drain voltage noise spectrum of a MOST (see Fig. 4 in [37])

Restle [38] and Uren et al. [39] have investigated the low-frequency noise in submicron silicon MOSTs. They found the spectra to be dominated by random telegraph-signal noise. Such RTS fluctuations have a Lorentzian spectrum. They claimed that the 1/f noise in large devices is the result of a superposition of RTS noise due to individual carrier-trapping events. On looking at the fluctuating signals observed by Restle and by Uren et al., what one observes is just a normal fluctuating signal with bursts. Strasilla and Strutt [40] have described a measurement method which allows the separate measurement of the power spectra of the normal noise superimposed on the burst noise. They found the normal noise (1/f and white noise) to be lower than the burst noise ($1/f^2$). In view of this result, the claims of Restle and of Uren et al. are doubtful.

JFET

The 1/f current noise in JFETs is given by [1]

$$S_{I_D} = \alpha q \mu I_D V_D / L^2 f \qquad (17)$$

so long as the device is not saturated. A survey of recent publications on 1/f noise in JFETs will now be presented.

Pawlikiewicz et al. [41,42] have investigated the low-frequency noise in n- and p-channel silicon JFETs. The presented spectra did not show 1/f noise, only $1/f^\gamma$ noise with $\gamma \cong 2$. It is therefore impossible to obtain values for α. The only conclusion is $\alpha < 10^{-8}$. However, they discussed the low-frequency noise in terms of α and in terms of Handel's quantum 1/f noise theory. The claim that the data are in full agreement with this theory is incorrect, the theory predicts 1/f and the experiment gives $1/f^2$. Duh and Van der Ziel [43] have discussed the Hooge parameter α in a short-channel Si JFET. They found $\alpha \cong 2.5 \times 10^{-8}$. However, the spectra (see Fig. 7 in [43]) did not show an obvious 1/f component, thus $\alpha < 2.5 \times 10^{-8}$.

Bhatti and Jones [44] have made noise measurements in ohmic silicon JFETs. They found $S_V \sim 1/f^\gamma$ with $0.3 < \gamma < 2.0$ and γ a function of temperature T and of frequency f. Their results suggest that the noise is a sum of 1/f and g-r components. Generally they obtain $10^{-8} < \alpha < 10^{-7}$, both for n- and p-channels. They concluded that the noise cannot be ascribed to mobility fluctuations because $\alpha << 10^{-3}$.

GaAs MESFET

Peransin et al. [45] have investigated the noise in the gate current of a MESFET. They found only $1/f^2$ noise and white noise, but no 1/f noise. Vandamme

et al. [46], however, found 1/f noise in the gate current with $S_{I_g} \sim I_g^2$. They found that devices with slight differences in $S_{I_{DS}}$ can have great differences in S_{I_g}. They concluded that 1/f noise study in I_g is a better diagnostic tool than in I_{DS} for characterising the quality of the device.
Hughes et al. [47] have studied the low-frequency noise in GaAs MESFETs. Their spectra are often dominated by g-r noise. They interpreted the spectra as a sum of g-r components. The distribution of relaxation times τ is ascribed to a variation of temperature across the FET because τ is assumed to be a function of temperature.
Hashiguchi et al. [48] have investigated the 1/f noise in epitaxial GaAs MESFETs. The 1/f current noise in the conducting channel can be described with Eq. (17). Then α is found to be sensitive to the gate voltage in the range of 10^{-4} - 10^{-2}. The current noise in the gate was found to be proportional to I_g^2/f. The fluctuations in I_{DS} and I_g are found to be uncorrelated.
Duh and Van der Ziel [43] found that the 1/f noise in the channel can be described by Eq. (17) with $\alpha \cong 3 \times 10^{-4}$ independently of the gate voltage.

SCHOTTKY BARRIER DIODES

A rough estimate of the magnitude of the 1/f noise in Schottky barrier diodes in terms of mobility fluctuations has been given by Kleinpenning [49] in 1974. Recently, Luo et al. [50] have presented an exact calculation of the 1/f noise in such diodes. At forward bias they obtained $S_I \sim I$. From experimental data of commercial diodes from HP they found α to be of the order of 10^{-8}.

JOSEPHSON TUNNEL JUNCTIONS (JTJ)

Savo et al. [51] investigated the 1/f noise in Nb-Al_2O_3-Nb JTJs. Their results can be characterized by

$$\gamma = [S_{I_o} A/I_o^2]^{\frac{1}{2}} \sim 10^{-11} \text{ m/Hz}^{\frac{1}{2}} \quad \text{at } f = 1 \text{ Hz}$$

with I_o the critical current and A the area of the junction. Kleinpenning [52] interpreted the noise in terms of modulation of the transmission coefficient of the barrier due to Nyquist noise. Savo et al. [53] believed that trapping and detrapping of electrons in the barrier cause the 1/f noise. Matsuda et al. [54] found the 1/f noise to be dependent on the barrier materials used. Their results can be explained by the two above-mentioned interpretations.

ACKNOWLEDGEMENT

This work was supported in part by the European Economic Community in the ESPRIT Basic Research Action.

REFERENCES

1. Van der Ziel, A., Proc. IEEE, 76, 233-258 (1988).
2. Kleinpenning, T.G.M., Physica B 145, 190-194 (1987).
3. Kleinpenning, T.G.M., Physica B 121, 81-88 (1983).
4. Kleinpenning, T.G.M., Physica B 132, 364-366 (1985).
5. Kleinpenning, T.G.M., Physica B 154, 27-34 (1988).
6. Van der Ziel, A., Fang, P., He, L., Wu, X.L., Van Rheenen, A.D. and Handel, P.H., J. Vac. Sci. Technol. A7, 550-554 (1989).
7. Van der Ziel, A., Handel, P.H., Wu, X.L. and Anderson, J.B., J. Vac. Sci. Technol. A4, 2205-2216 (1986).
8. Wu, X.L., Anderson, J.B. and Van der Ziel, A., IEEE-ED34, 1971-1977 (1987).
9. Vandamme, L.K.J. and Orsal, B., IEEE-ED35, 502-506 (1988).
10. Kleinpenning, T.G.M., J. Vac. Sci. Technol. A3, 176-182 (1985).
11. Kiss, L.B. and Kleinpenning T.G.M., Physica B145, 181-184 (1987).
12. Kleinpenning, T.G.M., Physica B 138, 244-252 (1986).
13. Van der Ziel, A., Solid-St. Electron. 32, 91-93 (1989).
14. Pawlikiewicz, A.H., Van der Ziel, A., Kousik, G.S. and Van Vliet, C.M., Solid-St. Electron. 31, 831-834 (1988).
15. Pawlikiewicz, A.H. and Van der Ziel, A., IEEE-ED34, 2009-2012 (1987).
16. Pong-Fei Lu, J. Appl. Phys. 62, 1335-1339 (1987).
17. Van der Ziel, A., Zhang, X. and Pawlikiewicz, A.H., IEEE-ED33, 1371-1376 (1986).
18. Zhu, X.C., Pawlikiewicz, A.H. and Van der Ziel, A., Solid-St. Electron. 28, 473-477 (1985).
19. Kilmer, J., Van der Ziel, A. and Bosman, G., Solid-St. Electron. 28, 287-288 (1985).
20. Vandamme, L.K.J. and Penning de Vries, R.G.M., Solid-St. Electron. 28, 1049-1056 (1985).
21. Kleinpenning, T.G.M. and Vandamme, L.K.J., J. Appl. Phys. 52, 1591-1595 (1981).
22. Kleinpenning, T.G.M. and Bisschop, J., Physica B 128, 84-87 (1985).
23. Hendriks, E.A. and Zijlstra, R.J.J., Solid-St. Electron. 31, 1105-1111 (1988).
24. Kleinpenning, T.G.M., to be published.
25. Vandamme, L.K.J., paper 913, these proceedings.
26. Jones, B.K. and Russell, P.C., Semicond. Sci. Technol. 4, 82-86 (1989).

27. Hayat, S.A., Jones, B.K. and Russell, P.C., Semicond. Sci. Techn. 3, 919-925 (1988).
28. Mutoh, N. and Teranishi, N., Solid-St. Electron. 31, 1675-1680 (1988).
29. Tsai, C.Y.H. and Gong, J., IEEE-ED35, 2373-2377 (1988).
30. Celik-Butler, Z. and Hsiang, T.Y., Solid-St. Electron. 30, 419-423 (1987).
31. Hendriks, E.A., Zijlstra, R.J.J. and Middelhoek, J., Physica B147, 297-304 (1987).
32. Celik, Z. and Hsiang, T.Y., IEEE-ED32, 2797-2801 (1985).
33. Surya, C. and Hsiang, T.Y., Solid-St. Electron. 31, 959-964 (1988).
34. Maes, H.E., Usmani, S.H. and Groeseneken, G., J. Appl. Phys. 57, 4811-4813 (1985).
35. Stegherr, M., Solid-St. Electron. 27, 1055-1056 (1984).
36. Peng, Q., Birbas, A.N., Van der Ziel, A., Van Rheenen, A.D. and Amberiadis, K., J. Appl. Phys. 64, 907-912 (1988).
37. Reimbold, G., IEEE-ED31, 1190-1197 (1984).
38. Restle, P., Appl. Phys. Lett. 53, 1862-1864 (1988).
39. Uren, M.J., Day, D.J. and Kirton, M.J., Appl. Phys. Lett. 47, 1195-1197 (1985).
40. Strasilla, U.J. and Strutt, M.J.O., Proc. IEEE 62, 1711-1713 (1974).
41. Pawlikiewicz, A.H., Van der Ziel, A., Kousik, G.S. and Van Vliet, C.M., Solid-St. Electron. 31, 233-236 (1988).
42. Pawlikiewicz, A.H. and Van der Ziel, A., IEEE-EDL6, 500-501 (1985).
43. Duh, K.H. and Van der Ziel, A., IEEE-ED32, 662-666 (1985).
44. Bhatti, G.S. and Jones, B.K., J. Phys.D.: Appl. Phys. 17, 2407-2422 (1984).
45. Peransin, J-M., Vignaud, P., Rigaud, D. and Dumas, J.M., Electron. Lett. 25, 439-440 (1989).
46. Vandamme, L.K.J., Rigaud, D., Peransin, J.-M., Alabedra, R. and Dumas, J.-M., IEEE-ED35, 1071-1075 (1988).
47. Hughes, B., Fernandez, N.G. and Gladstone, J.M., IEEE-ED34, 733-741 (1987).
48. Hashiguchi, S., Aoki, N. and Ohkubo, H., Solid-St. Electron. 29, 745-749 (1986).
49. Kleinpenning, T.G.M., Solid-St. Electron. 22, 121-128 (1979).
50. Luo, M.-Y., Bosman, G., Van der Ziel, A. and Hench L.L., IEEE-ED35, 1351-1356 (1988).
51. Savo, B., Wellstood, F.C. and Clarke, J., Appl. Phys. Lett. 50, 1757-1759 (1987).
52. Kleinpenning, T.G.M., Appl. Phys. Lett. 52, 2001 (1988).
53. Savo, B., Wellstood, F.C. and Clarke, J., Appl. Phys. Lett. 53, 2001-2002 (1988).
54. Matsuda, M., Matachi, A., Kuriki, S. and Hasegawa, H., J. Appl. Phys. 65, 692-696 (1989).

LOW-FREQUENCY NOISE IN THIN GaAs LAYERS

A. AMBRÓZY, P. GOTTWALD,* B. SZENTPÁLI*

Department of Electronics Technology,
Technical University of Budapest
*Research Institute for Technical Physics,
Hungarian Academy of Sciences
Budapest, Hungary

INTRODUCTION

The greater part of modern microwave active devices are fabricated on thin conducting layers of GaAs deposited onto semi-insulating GaAs substrates. Typical parameters of such an n-type layer suitable for preparing MESFET's or MMIC's are: thickness in the range of 0.2...0.5 μm, and the doping concentration values of $5 \times 10^{16} \ldots 2 \times 10^{17}$ cm^{-3}.

This active layer is an inherent component of the devices and all its electrical fluctuations, instabilities have a significant influence on the final noise behavior of he circuit, so the choice of the proper layer-building technique is an important point of view.

Because the noise behaviors of the microwave devices depend strongly also on the device technologies, it seems advantageous to investigate the properties of the layers on the simplest possible structures. Therefore the low frequency noise characteristics of planar resistors fabricated on these layers have been measured. Hellums and Rucker [1] and Belan [2] have described the results obtained on layers made by ion implantation. Tacano et.al. [3] investigated the low frequency noise in layers fabricated by Molecular Beam Epitaxy (MBE). In the present paper we are going to report the measurements of layers grown by Vapour Phase Epitaxy (VPE).

METHOD

For the measurements planar resistors have been prepared by standard microelectronic technology. Figure 1 shows the layout of the chip.

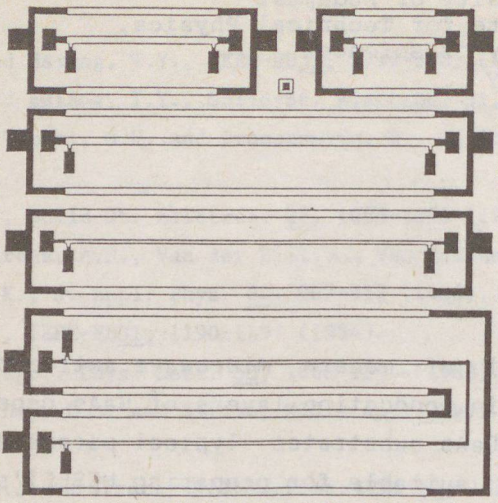

Figure 1

The layout of the chip has 3x3 mm^2 dimensions. Each chip contains five resistor structures having different lenght/width ratios (200,100,50,20,10.).The resistors have four electrical contacts making possible four-point measurement and each of them are surrounded by a guard-ring to avoid the surface leakage currents.

The active n-GaAs layers were grown by vapour phase epitaxial method in a hot wall open system (EPIGAR 2) using S as dopant material from SF_6 source. The layer thickness was 0.3 μm and the doping concentration $1x10^{17}/cm^3$. The doping profile was flat according to the profile measurements. The ohmic contacts were fabricated by evaporated Au:Ge:Ni:Au metallization alloyed at 400 C^o [4]

The noise measurements were carried out by a computer-controlled Brüel Kjaer Digital Frequency Analyser in the frequency range of 1.6Hz...20kHz [5] .

RESULTS

Figure 2 shows typical noise spectra obtained on bare samples exposed to different atmospheres and on protected ones. As can be seen, during the strorage the magnitude and the slope of the curve had increased; the same effect can be caused by the absorption of water or acetone vapour on the free semiconductor surface. The lowest noise was obtained in the case of N_2 atmosphere, but a superposition of G-R noise appears in the spectrum. It should be noted, that an increase of resistance of about 10% was also observed in connection with the increase of noise levels.

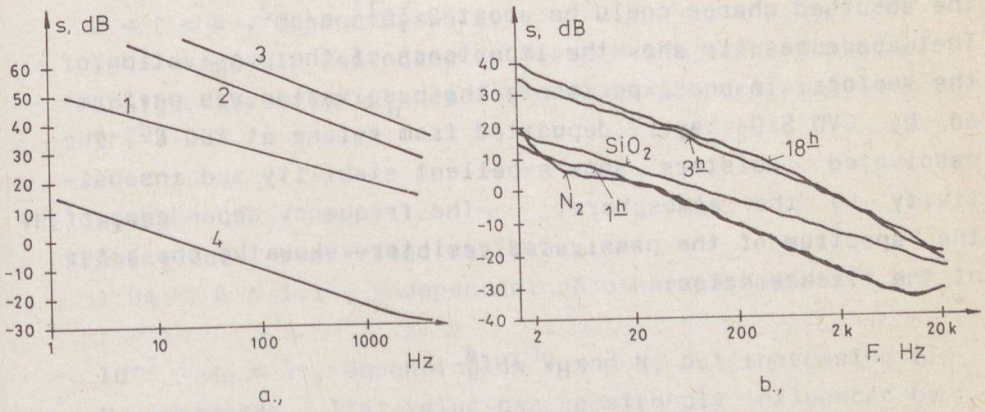

Figure 2

a./Curve 1 was measured after processing. Curve 2 represents the noise spectrum of the same resistor after a long storage (3 months) of the sample in free atmosphere, while curve 3 was obtained after introducing water vapour to the surface of the sample. Curve 4 shows the noise spectrum of a similar sample prepared from the same wafer but protected by SiO_2.

b./The effect of acetone atmosphere. Curve 1 was measured in N_2 atmosphere after stabilization, curves 2,3 and 4 were obtained on the same resistor, 1,3, and 18 hours later on after saturating the N_2 atmosphere with acetone vapour. Curve 5 belongs to the sample having SiO_2 protection on the surface.

The effect can be interpreted as an extra depletion of mobile charge carriers due to the absorption of ions onto the free surface. The formation of the usual surface barrier is assumed, it is formed by trapping electrons in the surface states [6] . Taking into account the doping concentration and the usual height of this barrier - for GaAs it is about 0.9 eV, a space charge width of 0.11 μm and a surface charge density of 1.1×10^{12} q/cm^2 can be deduced (q=number of elementary charges). From the measured resistances - assuming the drift mobility value of 3700 cm^2/Vs which had been obtained on similar samples by other measurements - the width of the space charge layer under the surface can be estimated as 0.13 μm and so the average value of the absorbed charge could be about 2×10^{11} q/cm^2.

The above results show the importance of the passivation of the surface. In our experiments the passivation was performed by CVD SiO_2 layer, deposited from silane at 400 C^o. The passivated resistors show excellent stability and insensitivity to the atmosphere. The frequency dependence of the spectrum of the passivated resistors shows the character of the flicker noise:

$$\alpha_H V^\Gamma / N f^\beta$$

where $\beta = 1.05 \ldots 1.1$. Some series of wafers show the presence of G-R noise as well, but there were found also series having flat characteristics in the investigated frequency range.

The bias dependence of the noise levels was, however, much stronger than expected from the theory. Γ values about 3 have been obtained instead of 2. At higher biases a systematic increase of resistance was observed, e.g. an increase of 10% occurred by changing the bias from 2.5 V to 10 V. The reason of this effect is not understood yet.

COMPARISONS

Finally, the following brief summary of experimental data can be made for layers prepared by different technologies:

Ion-Implanted layers:

Hellums and Rucker, 1984 [1]:

$0.5 < \beta < 1.5$, the value depends on V and f.

Belan, 1988, [2]:

$0.024 < \alpha_H < 0.52$, depending on the annealing process.

MBE layers:

Tacano al., 1988 [3]:

$0.5 < \beta < 1.5$, depending on V and f.

$2 < \Gamma < 4$, depending on f.

$10^{-2} < \alpha_H < 1$ depending on V and N, the total number of charge carriers; α_H was found to be proportional to $N^{-2.2}$.

VPE layers:

Present work, passivated resistors:

$1.04 < \beta < 1.1$, independent of other parameters.

$\Gamma > 3$

$10^{-2} < \alpha_H < 1$, depending on V and N, but increasing if N increases. Its value can be strongly influenced by the condition of the free surface.

It should be emphasized, that the value of α_H can be treated only as a characteristic amplitude in cases when $\Gamma > 2$, because it is not dimensionless any more..

Duh and van der Ziel [7] have published α_H values in the order of magnitude of 10^{-5} measured on GaAs FET's. Comparing this fact with the measurements of resistors we can conclude also to the importance of the surface conditions, which can be influenced by materials commonly used in semiconductor technologies.

REFERENCES:

[1] Hellums, G.R., Rucker, L.M: Low frequency noise in GaAs structures. Solid State Electronics. Vol.27, 1984/8, pp.949-952

[2] Belan,J.: 1/f Noise in GaAs Ion-Implanted Resistance Structures. Solid State Electronics Vol.31, 1988/12, pp. 1711-1713

[3] Tacano,M. et al.: Low frequency noise in GaAs layers. Solid State Electronics Vol.31, 1988/7, pp.1215-1219.
Proc. 5th School on Microwave Physics and Engineering. 28. Sept.-3.Oct.1987. Varna, Bulgaria. Ed. by A.Spanov.pp. 269-304.

[5] Ambrózy,A.: Noise measurements on thick film resistors. Noise in Physical Systems and 1/f Noise, 1985 Elsevier, pp. 65-69.

[6] Weber, E.R. et al.: The Mechanism of Fermi Level Pinning at Schottky Contacts on GaAs.
Proc. ICPS-19, Warsaw, 1988, pp.705-709.

[7] Duh, K.H. and van der Ziel,A.: Hooge Parameters for Various FET Structures. IEEE Trans. on El.Dev. ED-32, 1985/3. pp. 662-666.

This work was supported by contract No. 622 of OTKA (National Scientific Research Found).

CONNECTION BETWEEN THE 1/f NOISE AND THE NOISE OF GENERATION-RECOMBINATION TYPE IN SEMICONDUCTORS

N.B. LUKYANCHIKOVA, M.V. PETRICHUK, N.P. GARBAR, A.P. SASČIUK

Institute of Semiconductors, Academy of Sciences of the Ukrainian SSR
Kiev-28, USSR

Discovery of empirical Hooge relation has initiated a lot of experimental and theoretical investigations of 1/f noise. As a result, many new physical ideas have appeared. Their development has extended our knowledge concerning the possible reasons for occurence of 1/f noise as well as has provided new information about the complex and multiform physical processes in solids.

The following idea by Ngai /1/ seems to be of peculiar interest. He supposed that the 1/f noise is one of the exhibitions of slow relaxation of the exited states of a lattice which states appear as a result of capture and release of the charge carriers by the local centres.

These processes of carrier capture and release are known to be accompanied by the generation-recombination (GR) noise with a Lorenzian-type spectrum. The characteristics of such a spectrum are determined by the parameters of corresponding centres including the relaxation time τ which defines the rate of the electron density change on such centres. Thus, if the same GR process is accompanied both by GR noise and 1/f noise, hence, characteristics of these two types of noise may be connected with each other.

It appears that such a connection takes place indeed. The present work includes the results of experimental observation and investigation of this effect.

Thin ground n-Ge plates (ρ = 40 Ohm·cm, 1,2x(0,05-0,2)x(0,12-0,36) cm^3 in size) have been investigated. Noise spectra have been measured by the probe method in the frequency

range from 20 Hz to 100 kHz at temperatures T = 150-300 K. The following results were obtained.

The noise spectra have a 1/f region followed by the GR plateau at higher frequency and then this plateau is followed by the f^{-2} or $f^{-3/2}$ dependence. From the 1/f noise the Hooge coefficients α_H have been determined and, using the GR noise, the values of τ and $\overline{\Delta n^2}/n$ have been obtained where n is the free electron density, and Δn^2 is the dispersion of fluctuations of this density.

The analysis of temperature dependences of τ and $\overline{\Delta n^2}/n$ shows that, at $300 \geqslant T \geqslant 250$ K, the observed GR noise is connected with the recombination (r-) level, i.e. the process of carrier exchange between this level and both c- and v-band is accompanied by such GR noise. At lower temperatures the GR noise is due to electron trapping, i.e. to the electron exchange between the c-band and shallow t-level.

Measurements carried out at T = 300 K on samples with different thickness d show that $\alpha_H \sim d^2$ and $\tau \sim d^2$ so one may suppose that $\alpha_H(d) \sim \tau(d)$ (Fig.1).

Here α_H is increased with d from the value $\alpha_H = 1{,}7 \cdot 10^{-3}$ to $2{,}8 \cdot 10^{-2}$. Note that in this case the electron-hole recombination takes place at the sample surface and τ is determined by the carrier diffusion to the surface.

The analysis of the noise spectra measured at different temperatures shows that the temperature dependences of α_H and τ are similar (Fig.2): $\alpha_H(T) \sim \tau(T)$ both in the region of carrier exchange with the r-level and in the region of carrier exchange with the t-level.

Note that in the region of the exchange with the r-level the contribution of electron-hole diffusion to the surface is decreased with decreasing temperature and, as a result, the equality $\tau = \tau_\Omega$ appears to be fulfilled where τ_Ω is the electron-hole pair lifetime in the sample volume.

It is seen from Fig.2 that in the region of the exchange with the r-level α_H is decreased with decreasing temperature, but in the region of carrier exchange with the t-level α_H is increased with decreasing T. Thus, the dependence $\alpha_H(T)$ has a minimum at T = 250 K, and the minimum value of α_H is about

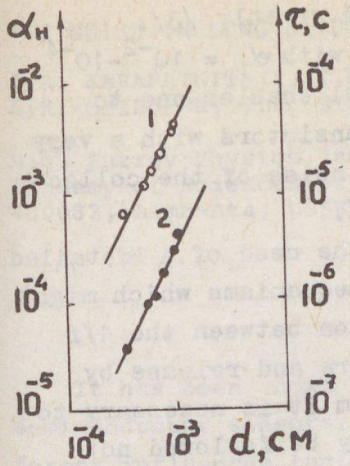

Fig.1. Dependences of α_H (1) and τ (2) on d at T = 300 K.

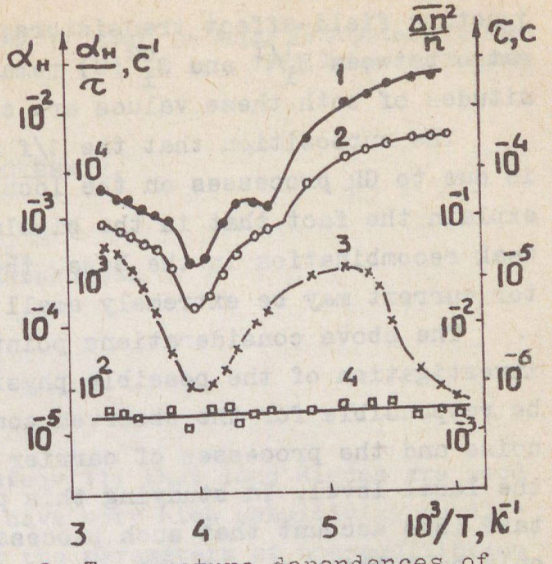

Fig.2. Temperature dependences of α_H (1), τ (2), $\overline{\Delta n^2}/n$ (3) and α_H/τ (4) for the sample with d = $1{,}25 \cdot 10^{-1}$ cm.

10^{-4}. At T < 200 K the value of α_H may be as large as $2 \cdot 10^{-2}$.

It is found that the value of α_H at low T is increased with increasing density of t-levels.

Thus, the intensity of 1/f noise is proved to be connected both with the rate of change of electron density on the local centres (which centres capture and emit electrons and have the single level in the energy gap of the semiconductor) and with the density of such centres. This is true, no matter where these centres are located in the sample, what is their nature and with which band the carrier exchange occurs.

It is important that we have observed these phenomena in the other semiconductors as well. For example, an increase of α_H with increasing τ we have observed, too, on InSb plates at T = 77 K /2/. In this case the values of α_H and τ have been varied by changing the sample thickness as well as by placing the samples in the crossed electric and magnetic fields. Besides, the connection between the levels of 1/f and GR noise in the region of the plateau of the noise spectrum $S_i^{GR}(0)$ (where $S_i^{GR}(0) \sim \tau$) we have also observed in the silicon

junction field-effect transistors; it has been found that the ratio between $S_i^{1/f}$ and $S_i^{GR}(0)$ remains constant when the magnitudes of both these values are changed greatly /3/.

The supposition that the 1/f noise with $\alpha_H = 10^{-2}$-10^{-4} is due to GR processes on the local level enables one to explain the fact that in the bipolar transistors with a very weak recombination in the base, the 1/f noise of the collector current may be extremely small /4,5/.

The above considerations point to the need of a detailed investigation of the possible physical mechanisms which might be responsible for the observed connection between the 1/f noise and the processes of carrier capture and release by the local level. In studying this problem it is necessary to take into account that such processes may be followed not only by lattice polarization but also by the other effects relating to the great variety of different lattice relaxation phenomena.

References

1. K.L.Ngai. Unified theory of 1/f noise and dielectric response in condensed matter. Phys. Rev. B22, No.4, pp.2066-2077, 1980.
2. N.B.Lukyanchikova, N.P.Garbar, V.K.Malutenko, G.I.Teslenko. Fluctuations of InSb conductivity in the crossed electric and magnetic fields. Fizika i technika poluprovodnikov 15, No.2, pp.336-344, 1981.
3. N.B.Lukyanchikova, N.P.Garbar, A.P.Sasčiuk, D.I.Kropman, M.V.Petrichuk. Connection between the levels of 1/f and GR noises. In: Fluctuation phenomena in physical systems. Vilnus, 1988, pp.141-143 (in Russian).
4. C.M. Van Vliet, A. Van der Ziel. Summary of the 2nd quantum 1/f noise conf. 1986. Solid-State Electron. 30, No.7, pp.777-778, 1987.
5. N.B.Lukyanchikova, N.P.Garbar, M.V.Partika, et al. Sources of the excess noise in transistor elements of microcircuits. Radiotechnika i electronika 33, No.2, pp.400-408, 1988.

10th Int.Conf. on Noise in Physical Systems
1989 Budapest, Hungary

1/f NOISE IN LONG Si DIODES

I.A. KARAPATNITSKI, I.N. SYRGABEKOV,
L.K. OSIPCHUK, V.I. STAFEEV

High Energy Physics Institute,
Academy of Sciences of the Kazakh SSR
480082, Alma-Ata, USSR

It has been shown by Stafeev (1) that long diodes are good semiconductor sensors. They have very high sensitivity to different influences that alter the parameters of non-equilibrium conductivity of base region. At a high-level injection the forward current-voltage characteristics of long diodes are determined considerably more by minority-carrier mobility and lifetime than by their concentration. Therefore a long diode is a proper model both for experimental check of known hypotheses for mechanism of 1/f noise and for study of noise of a large class of semiconductor sensors.

The results of low-frequency noise ($f \leq 1$ kHz) analysis in high-ohmic p-Si long diodes are presented in this paper. The devices with parallelepiped geometry had a cross-section of $A = 0.5 \times 0.5$ mm^2. The lengths were made d = 0.6;1.0 mm. The alloyed and antibarrier contacts were situated on opposite sides with cross-section A. Diodes worked in high-injection conditions in the base. The value of forward current (I) varied from 1.0 to 3.0 mA. As it was shown by Karakushan et al. (2) effective minority-carrier lifetime (τ) in the devices of such kind was about 5×10^{-6} s, ambipolar diffusion length (L) was about 10^{-2} cm, the ratio d/L = 10. The main contribution to τ was made by recombination process on a surface because the bulk lifetime exceeded 300×10^{-6}s. Numerical solution of nonlinear differential equation for non-equilibrium carrier concentration in base of long diodes shows that if injection coefficients of both contacts are equal to unity, diffusion approximation be-

comes acceptable with current density greater than 0.4 A/cm^2. Potential distribution along the base of our diodes investigated experimentally shows that the above approximation can be used to estimate the sample properties with d = 1 mm and forward bias voltage about 6 V under J = 1.2 A/cm^2. It is interesting to estimate the noise voltage value of the long diodes which can be caused by carrier mobility fluctuation in case it is transferred mostly by diffusion.

Long diode voltage fluctuations were estimated as follows. One-dimensional nnp$^+$ structure was considered with the junction injection coefficients equal to unity. We considered a thin layer in base that extends from $x = x_1$ to $x = x_2$. Fluctuations in the diffusion length δL in this layer lead to redistribution of charge carriers in the whole base. Therefore (I is constant), we have voltage fluctuation in long diode such as $\delta U = F(d/L, \delta L/L, x_1, x_2)$. To calculate δU, we divided the base into three parts with coordinates: 0, x_1, x_2, d. The diffusion length in the layer between points x_1 and x_2 was assumed to be $L_2 = L_1 \pm \delta L$, where L_1 is ambipolar diffusion length $L_1 = \sqrt{\frac{2}{b+1}\frac{KT}{q}\mu_n \tau}$. Boundary conditions in contacts are assumed to be $J_n(0) = 0$, $J_p(d) = 0, n'(0) = -\frac{I}{2qD_p}$, $n'(d) = \frac{I}{2qD_n}$. In this case it was also assumed that the function n(x) and the derivative n'(x) are continuous in sections $x = x_1$ and $x = x_2$. Further the function:

$$K(d/L, \delta L/L, x_1, x_2) = \lim_{\delta L/L \to 0} \lim_{x_2 - x_1 \to 0} \frac{\delta U}{\delta L/L\,(x_2 - x_1)} \qquad (1)$$

describing the "amplifying capacity" of long diode for diffusion length change in a limited layer of base was determined. The integral noise of long diode has been calculated assuming that the mobility fluctuations are independent in reference to each other and the system under consideration was linear and noninertial in reference to the fluctuations in different sections of the device. When deriving the final expressions for S/V^2 we have allowed for the fact that the concentrations of

free holes and electrons are practically equal and connected with the electrical field intensity by the following expression:

$$E(x) \cong \frac{I\,b}{q\mu_n (b+1) n(x)} \qquad (2)$$

For long diodes with d/L = 5-10, b = 3, μ_n = 1500 $cm^2/V\,s$

$$S/V^2 \cong 5.4\times10^{-19}\,\frac{\alpha}{I\times f\times L^2}\exp\frac{d}{2L} \qquad (3)$$

Our experimental results are presented below.

1. Samples with d = 0.1 cm; d/L = 10.6; L = 95×10^{-4} cm

In the frequency range f≤1 kHz, S/V^2 was described by $S\sim f^{-\gamma}$ with γ = 0.9-1.0. If f = 1 Hz, I = 1 mA then S/V^2 = = $(2.0-3.5)\times10^{-12}$ s, i.e. 1.5-2.5 times higher as compared to the calculated value with $\alpha = 2\times10^{-3}$. The increase of direct bias current up to 3 mA reduced S/V^2 by approximately 10-20%. According to our estimations charge carrier concentration in the base increased 2.3-2.5 times. Since long diodes possess high magnetosensitivity, the estimations of low-frequency noise in samples were in magnetic fields with induction B = 0.3-0.5 T. During that there was observed inconsiderable increase of γ which within fields was equal to B = 0.5 T up to 5% with I = 1 mA and to 12% with I = 3 mA. The S/V^2 in the magnetic fields gives a steep rise, the increase rate of S/V^2 being more than the value of a forward bias voltage.

2. Samples with d = 0.06 cm; d/L = 7; L = 87×10^{-4} cm

For f = 1 Hz, I =1 mA, S/V^2 = $(0.8-3.0)\times10^{-12}$ s. The calculated value is $S/V^2 = 5\times10^{-13}$ s. So the visible decrease of base length has not changed the expected effect of S/V^2 in most samples. This fact as well as a considerable increase of noise in devices within magnetic fields means probably that there are some noise marks with a spectrum 1/f in the diodes studied.

3. Irradiated samples

Small-dose nuclear radiation which uniformly alters practically only volume lifetime of non-equilibrium charge carriers in the base (p-30 MeV, α-50 MeV) reduced S/V^2. This effect is more remarkable in diodes with higher initial value of excess noise. This fact from our point of view can be explained by a decrease of influence of noise caused by surface recombination processes.

Introduction of recombination centres into a narrow base layer adjoining antibarrier contact decreased the S/V^2 value in samples with relatively high initial noise, but caused some increase of the value mentioned among samples which before irradiation were characterized by values of noise similar to the calculated ones. Our estimations show that such behaviour of S/V^2 can be observed only if 1/f noise is caused by mobility fluctuations. We used uniform introduction of radiation defects also for the confirmation of hypotheses that the diode noise in the magnetic field is caused mainly by surface fluctuation processes. Initially noise was measured in the magnetic field with B = 0.3 T. Then the diode was irradiated by flux F in such a way that the forward bias voltage with B = 0 was equal to that with B = 0.3 T before irradiation. Then we repeated the noise measurement. It was shown that $S/V^2 \cong (F = 0, B = 0.3\ T) = (5\text{-}10) \times S/V^2 (F, B = 0)$. These facts confirm the results of Karapatnitski et al. (3) which show that recombination process on the surface of the base influences greatly the formation of magnetosensitivity of long diodes with diffusional charge carrier transport.

In conclusion we note that these results do not contradict the theory of 1/f noise caused by mobility fluctuations in semiconductor volume. Moreover, some results of less noisy samples could be satisfactorily explained by that very theory.

REFERENCES

1. Stafeev, V.I., Modulation of diffusion displacement as a new principle of action of semiconducting devices. Sov. Solid State Physics, V.I, N6, (1959), pp. 841-847.

2. Karakuchan, E.I., Karapatnitski, I.A., Stafeev, I. I., Effective lifetime of minority charge carriers in magnetodiodes. Sov. Phys. Tech. Semicond., V.16, N7, (1982), pp. 1190-1193.

3. Karapatnitski, I.A., Karakuchan, E.I., Isaev, N.U., Stafeev, V.I., Investigation of the irradiation effect on Si magnetodiode characteristics. Proc. Conf. on Radiat. Physics of Semicond. and Related Materials, Tbilisi, 1980, pp. 850-853.

10th Int.Conf. on Noise in Physical Systems
1989 Budapest, Hungary

EVIDENCE OF 1/f BULK NOISE SOURCES IN SOS DEVICES

G. DIMOPOULOS,* A. CHOVET

Lab. P.C.S. (ura CNRS), Institut National Polytechnique
de Grenoble, E.N.S.E.R.G., BP 257
38016 Grenoble Cedex, France

Abstract: The 1/f noise of double-injection p^+nn^+ Silicon-On-Sapphire (SOS) gated diode is studied. It appears to be due to bulk noise sources related to local conductance fluctuations. As a consequence, and in agreement with theoretical calculations, the current fluctuation spectral density S_I is proportional to V^3 where V is the diode forward bias. Moreover, it is shown how these bulk noise sources can be activated or not under the gate voltage action.

1. INTRODUCTION

The 1/f noise in semiconductor devices appears to have several possible causes [1-3]: while in bipolar structures its bulk origin (usually related to mobility fluctuations) seems established [3-5], it is proved that in MOSFET's, microMOST's and MISFET's, 1/f noise is due to surface trapping effects [3,6-10].

Here is presented a clear experimental evidence of bulk noise sources which can be controlled by an electrical parameter, namely a gate voltage. Devices under investigations are gated Silicon-On-Sapphire p^+nn^+ structures. These "long" diodes (where the length L of the "base", i.e. the n-region between p^+ and n^+ contacts, is several times the carrier diffusion length) are designed so that a double-injection regime (holes and electrons) is easily reached for a forward bias. Due to their sensitivity to a magnetic field, such structures are often called "magnetodiodes" [11]. Their noise behaviour is an important parameter in order to define their resolution as a sensor.

The new feature is the gate electrode, superimposed on the n-region (see insert Fig.2); it allows to control, among other parameters, the current in the device, more precisely the current density i_x in each point and therefore, as it will be shown, the noise associated with bulk sources.

2. 1/f NOISE IN DOUBLE-INJECTION STRUCTURES

Among works related to noise in injection devices [4,11,12], few papers are devoted to 1/f noise in double-injection diodes. From studies on such diodes with different geometries, it was shown [11] that 1/f noise probably originates from bulk fluctuations. The best confirmation will be given by calculating the

---

* Alexander Onassis Foundation Scholar

current fluctuation spectral density $S_I(f)$ for a diode forward biased by a voltage V. We first recall that the static I-V relation is given, in the "semiconductor" double-injection regime (i.e. with a negligible space charge) by the following quadratic relation [12], deduced from a simple one-dimensional analysis :

$$i_x = \sigma(x)\, E_x(x) \simeq q(\mu_n + \mu_p)\, n(x)\, E_x(x)$$
$$= (9/8)\, q\mu_n\mu_p\, |n_o - p_o|\, \tau V^2/L^3 \qquad (1)$$

with $i_x = I/A$, the current density and A the cross-section; τ, the carrier effective lifetime; n_o and p_o the majority and minority equilibrium carrier concentrations (before injection); $n(x) = p(x)$ are the injected carrier concentrations :

$$n(x) = \frac{3}{4}\,\frac{\mu_n\mu_p}{\mu_n+\mu_p}\,|n_o - p_o|\,\frac{\tau V}{L^2}\,\left(\frac{L}{x}\right)^{1/2} = n(L)\left(\frac{L}{x}\right)^{1/2} \gg |n_o - p_o| \qquad (2)$$

The low-frequency ($\omega\tau \ll 1$) 1/f bulk noise, due to any conductivity fluctuation, can be deduced from the HOOGE relation $S_I/I^2 = S_V/V^2 = S_R/R^2(x) = \alpha_H/fN(x)$ applied to each homogeneous volume element; $N(x) = n(x)\, A\, dx$. After integrating, we obtain :

$$S_I(f) = g_d^2\, S_V(f) = \frac{18}{5}\,\frac{\alpha_H}{f}\,\frac{A}{L}\,\frac{i_x^2}{n(L)} \qquad (3)$$

where g_d is the low-frequency dynamic conductance of the structure: $g_d = \partial I/\partial V$. If $n_o \gg p_o$, from eq.(1), $i_x \propto n_o V^2$ and from eq.(2), $n(L) \propto n_o V$, so that :

$$S_I(f) \propto A\, n_o\, V^3/f \qquad (4)$$

$$S_I(f) \propto I^{3/2}/f(A\, n_o)^{1/2} \qquad (5)$$

Such variations of S_I with the external bias parameters, V or I, is a basic feature resulting from the bulk noise source hypothesis and the non-linear (quadratic) I-V characteristic of a double injection device.

3. 1/f NOISE IN GATED DOUBLE-INJECTION DIODES

Our investigations were performed on SOS p^+nn^+ devices processed by Thomson-DMS (Grenoble): <100> n-type low-doped ($n_o \simeq 5.10^{15}cm^{-3}$) silicon epitaxial layers, 0.62 µm thick, were provided with ion implanted p^+ and n^+ contacts (~ $10^{20}cm^{-3}$), according to a self-aligned process with p^+ polysilicon gates deposited on a 65 nm gate oxide (see insert Fig.2).

3.1. Diode characterization : From the I-V characteristics shown in Fig.1, it is clear that the double injection phenomenon is influenced by the gate voltage. We have shown recently [13] that in such a structure, double-injection takes place as if the equilibrium carrier concentrations (n_o and p_o in eq.(1)) were $n_o(y)$ and $p_o(y)$ resulting from the field-effect due to the gate voltage V_G. This is the reason why, if the quadratic I-V law is always reached for highest voltages V, this regime seems to be "delayed", as V increases, under positive V_G : indeed the conjugated action of V and V_G limits the current increase when a part of the film is progressively depleted (when $V \sim V_G$).

As far as the noise is concerned, a 1/f noise was observed in the whole frequency range under investigation (0 - 100 kHz). Figures 2 and 3 show the V_G and V influences on the current-fluctuation spectral density S_I : the 1/f bulk noise dependences on V and I for double-injection devices (eqs.(4) and

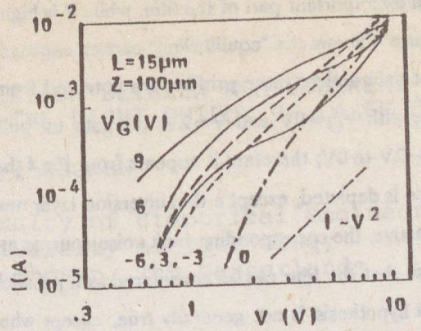

Fig.1 : Current-voltage forward characteristics of a gated SOS double-injection p^+nn^+ diode, with the gate to cathode (n^+) voltage V_G as a parameter (Z is the diode width).

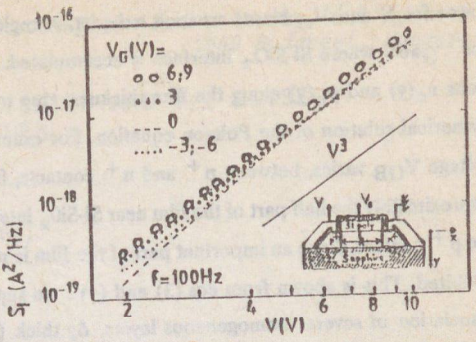

Fig.2 : Measured power spectral density of 1/f current fluctuations (at f = 100 Hz) as a function of the diode forward bias V, with the gate voltage V_G as a parameter (for the device in Fig.1).

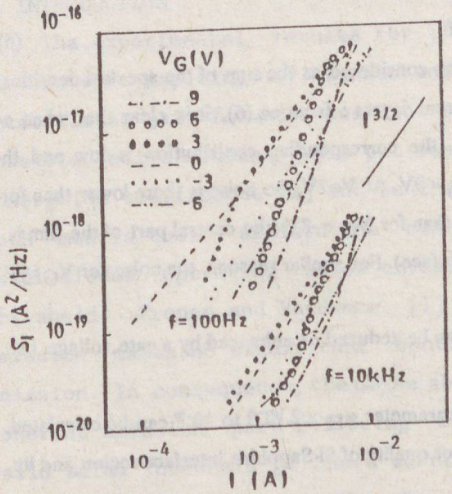

Fig.3 : Measured power spectral density of 1/f current fluctuations (at f = 100 Hz and f = 10 kHz) as a function of the current I in the diode, with the gate voltage V_G as a parameter (for the device in Fig.1).

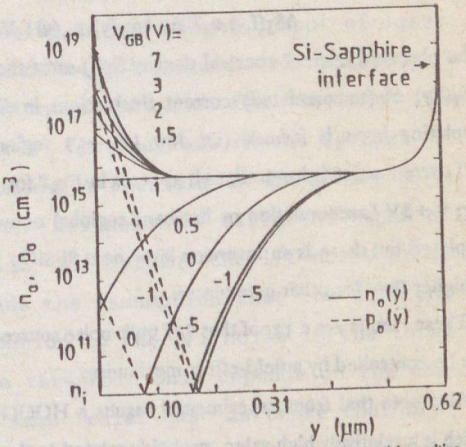

Fig.4 : Carrier "equilibrium" concentrations $n_o(y)$ or $p_o(y)$, resulting from the gate action, in each plane x ; y is the depth inside the silicon film. The parameter is the gate to "bulk" potential $V_{GB} = V_G - V(x)$, so that at the p^+ contact $V_{GB} = V_G - V$, and at the n^+ contact $V_{GB} = V_G$. Interface parameters for this simulation: surface state N_{SS}(cm⁻²eV⁻¹) and fixed charge N_f(cm⁻²) densities = 10^{10} at the Si-SiO_2 interface, and 5.10^{12} at the Si-Sapphire interface.

(5)) are very well observed. The $S_I(I)$ curves, however, show a greater dispersion (Fig.3), due to the complex $I(V,V_G)$ relations (Fig.1). This also means that the physically pertinent parameters for an easier device analysis are V and V_G rather than I and V_G. But it is worth noticing from Fig.3 that the best $S_I \propto I^{3/2}$ relations are observed for $V_G \leq 0V$; they correspond to gate biases for which the $I \propto V^2$ double-injection law is verified in the widest range of the I-V characteristics in Fig.1. Also note that no surface trapping effect of carriers in an accumulation or inversion layer (as in MOS structures) could explain the observed 1/f noise behaviour with V and V_G.

All these results already confirm the bulk origin of 1/f noise in our double-injection gated diodes.

3.2. Bulk noise source control : Figure 2 shows that the current noise does not strongly depend on V_G. Several properties are however apparent : e.g. the 1/f noise is systematically

lower for V and V_G biases creating a depletion region in an important part of the film, while it is higher for $V_G \geq 6V$ where Si-SiO_2 interface is accumulated. Figure 4 shows the "equilibrium" carrier concentrations $n_o(y)$ and $p_o(y)$ along the film thickness due to the gate action; these profiles are obtained from a numerical solution of the Poisson equation. For example, with $V_G = 0V$ and $V = 2V$, the gate to "bulk" voltage V_{GB} varies, between p^+ and n^+ contacts, from -2V to 0V; therefore it appears from Fig.4 that approximately the half part of the film near Si-SiO_2 interface is depleted, except a thin inversion layer near the p^+ contact. Since an important part of the film is not active, the corresponding bulk noise sources are inhibited. This is shown from eqs.(3) and (4) : we suppose that the film can be considered as a parallel-association of several homogeneous layers, Δy thick (this hypothesis is not generally true, except when $|V_G| \gg V$, but allows to get a good first-order picture). Each layer exhibits current fluctuations $\Delta S_I(f,y)$ given by eq.(3), with $A = Z\,\Delta y$ and corresponding values for $i_x(y)$ and $n(L,y) \propto |n_o(y)-p_o(y)|$ (eq.(2)). This leads to an expression similar to eq.(4) :

$$\Delta S_I(f,y) \propto Z\,\Delta y\,|n_o(y)-p_o(y)|\,V^3/f \qquad (6)$$

The observed current spectral density $S_I(f)$ must then be considered as the sum of the spectral densities $\Delta S_I(f,y)$ of (uncorrelated) current fluctuations in different layers ; from eq.(6), it is clear that when a depletion layer is formed (i.e. low $|n_o-p_o|$ region) , the corresponding contribution is low and the 1/f current noise is lowered, as it appears in Fig.2 for $V_G = 0V$. At $V \simeq 2V$, the noise is there lower than for $V_G = +3V$ (accumulation or flat-band regions) or even than for $V_G = -3V$ (the central part of the film is depleted but there is an inversion layer near Si-SiO_2 interface). For similar reasons, the noise for $V_G \geq 6V$ is higher than for other gate biases.

These results are a proof that 1/f bulk noise sources can be reduced or enhanced by a gate voltage, i.e. can be controlled by a field-effect mechanism.

Also note that from experimental results a HOOGE parameter $\alpha_H \sim 2.10^{-4}$ to 10^{-3} can be calculated, which is a relatively high value, probably related to the poor quality of Si-Sapphire interface region and its strong carrier scattering process.

REFERENCES

[1] F.N. HOOGE, T.G.M. KLEINPENNING, L.K.J. VANDAMME, Rep. Progr. Phys. 44 (1981), 479.

[2] O. JANTSCH, IEEE Trans. Electron Devices ED34 (1987), 1100.

[3] A. VAN DER ZIEL, Proc. IEEE 76 (1988), 233.

[4] T.G.M. KLEINPENNING, Physica 98B (1980), 289.

[5] T. G. M. KLEINPENNING, Noise in Physical Systems and 1/f Noise 1985 , A. D'Amico and P. Mazzetti (Eds.), North-Holland, Amsterdam, 1986, p.389 and 393.

[6] G. REIMBOLD, P. GENTIL, A. CHOVET, Noise in Physical Systems and 1/f Noise 1983, M. Savelli, G. Lecoy and J.P. Nougier (Eds.), North-Holland, Amsterdam, 1983, p.295.

[7] G. REIMBOLD, IEEE Trans. Electron Devices ED31 (1984), 1190.

[8] M.J. UREN, D.J. DAY, M.J. KIRTON, Appl. Phys. Lett. 47 (1985), 1195.

[9] Z.H. FANG, S. CRISTOLOVEANU, A. CHOVET, IEEE Electron Device Lett. EDL7 (1986), 371.

[10] A. CHOUJAA, Thesis Doctorat-es-Sciences, ECL and UCB Lyon (1989).

[11] A. CHOVET, S. CRISTOLOVEANU, A. MOHAGHEGH, A. DANDACHE, Sensors and Actuators 4 (1983), 147 ; and ibid. ref.[6], p.257.

[12] M.A. NICOLET, H.R. BILGER, R.J.J. ZIJLSTRA, Phys. Stat. Sol.(b) 70 (1975), 9.

[13] G. DIMOPOULOS, F. BALESTRA, A. CHOVET, M. BENACHIR, J. BRINI, Solid State Devices 1987 (Proc. 17th ESSDERC), North-Holland, Amsterdam, 1988, p.611.

RELATION BETWEEN NON-COHERENT EMISSION AND 1/f NOISE IN THE LIGHT OUTPUT OF LASER DIODES

R.J. FRONEN

Faculty of Electrical Engineering,
University of Technology
Eindhoven, The Netherlands

1. INTRODUCTION

The experimental results for 1/f noise in the light output of laser diodes were explained by Fronen and Vandamme [1] in terms of spatially uncorrelated gain fluctuations and spontaneous emission fluctuations. Two possible noise sources were put forward; fluctuations in the optical absorption coefficient [2] and in the number of carriers in the cavity [3]. Both models could explain the observed 1/f noise of different types of laser diodes operating below threshold. To explain the 1/f noise above threshold, Fronen and Vandamme [1] made the assumption that the coherent emission makes no significant contribution to the 1/f noise in the total emission. In consequence, the noise above threshold only depends on the non-coherent emission part following the same relations as those that are valid below threshold [4]. Here we present an experimental study of the 1/f noise at different wavelengths of a monomode Hitachi HLP 1400 laser diode. These experiments are shown to support the above assumption. The 1/f fluctuations in the light output at different wavelengths are correlated or uncorrelated, depending on the operating region.

2. 1/f NOISE AT FIXED OPTICAL BANDWIDTH ($\Delta\lambda$ fixed; λ variable)

The emission of a Hitachi HLP 1400 laser diode is collimated and projected, with a cylindrical lens, on the entrance slit of a monochromator with a focal length of 1 m, and a resolution of about 0.1 Å. To prevent the onset of modes due to external cavity reflections, we used an optical isolator composed of a Fresnel and Glan-Thompson prism. The light leaving the exit slit is collected with a large area PIN detector which is short-circuited by a low-noise current amplifier.

The light-current plots at three different central wavelengths λ with

the same optical bandwidths $\Delta\lambda$ are presented in figs. 1a,b. The emission at λ = 825.75 nm contains the single lasing mode and shows a linear dependence between collected power measured as detector current I_d, and laser current I_L, fig. 1b. The power in this mode is mainly coherent laser emission. The light at all other wavelengths is noncoherent emission i.e., emission with random phase. The threshold current is 54.5 mA. The lasing operating region for shorter wavelengths (below 825.75 nm) shows perfect saturation or even oversaturation of the power with increasing current. For longer wavelengths the emission continues to increase with current, indicating nonperfect saturation. At low current in fig. 1a the average power increases with current as $\langle P \rangle \propto I_L^2$. In this LED operating region the emission is due to spontaneous emission, resulting in a smooth light spectrum. Just below threshold, in the so-called superradiation region, the output power abruptly increases due to stimulated emission. The light spectrum is peaked at every longitudinal mode at spaces of 0.42 nm.

The 1/f noise has been investigated as a function of the collected power at five different wavelengths. The results for three wavelengths are presented in fig. 2.

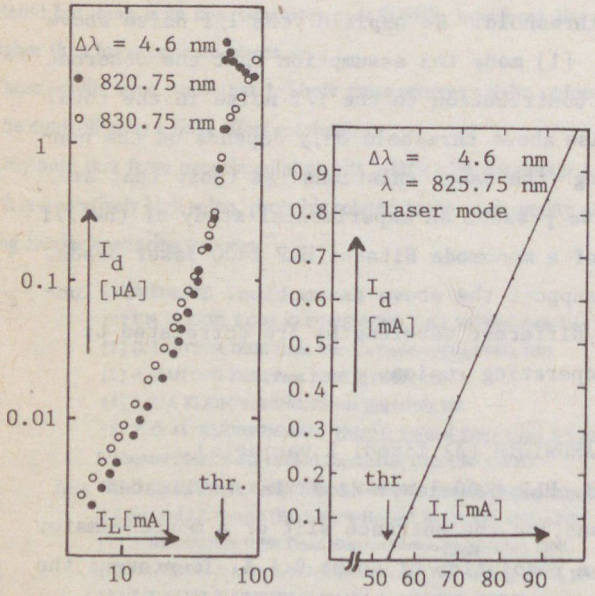

Figure 1a,b. Detector current vs. laser current at different wavelengths with the same optical bandwidth. The arrow marked "thr" denotes the threshold current.

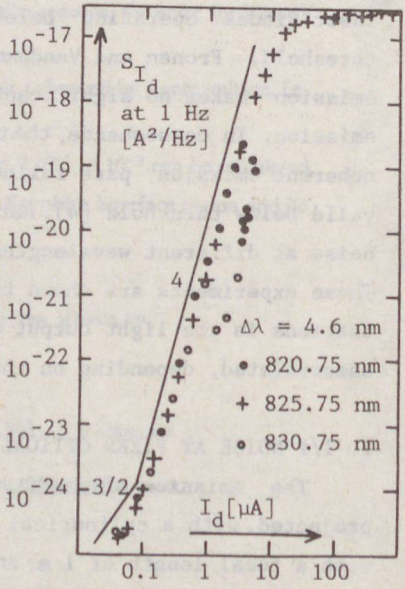

Figure 2. Experimental 1/f noise results at the same wavelengths as in fig. 1. The full lines correspond to $S_p \propto P^{3/2}$ and $S_p \propto P^4$.

Below threshold the noise is the same at all five wavelengths. The spectral noise density S_p increases with the power as $S_p \propto \langle P \rangle^{3/2}$ in the LED region and as $S_p \propto \langle P \rangle^4$ in the superradiation region, in agreement with the models in ref. [1]. The threshold is at different power for every wavelength. At the threshold the noise abruptly changes for some bands (815.75, 830.75 and 835.75 nm) and smoothly varies for the other bands as can be seen in fig. 2. This is not yet understood. Above threshold the relation $S_p \propto \langle P \rangle^4$ holds at the four wavelengths not containing the lasing mode. At the two longer wavelengths the power and the noise increase. At λ = 815 nm both are constant. At 820.75 nm the power and its noise level even decrease. As stated earlier, all the coherent light is concentrated at 825.75 nm. The behaviour of the noise at this wavelength agrees perfectly with our assumption that the coherent emission makes no significant contribution to the 1/f noise. The non-coherent emission and the noise (vertical axis of fig. 2) is saturated but the detector current (horizontal axis) increases due to an increasing coherent emission.

3. 1/f NOISE AS A FUNCTION OF OPTICAL BANDWIDTH ($\Delta\lambda$ variable; λ fixed)

For the three operating regions (LED, superradiation and laser region) the 1/f noise has also been investigated as a function of optical bandwidth. The collected power $\langle P \rangle$ can be considered as a sum of equal power $\langle P_1 \rangle$, $\langle P_2 \rangle$, ..., $\langle P_N \rangle$ in N spectral subbands.

$$\langle P \rangle = \sum_{n=1}^{N} \langle P_n \rangle = N \langle P_1 \rangle \qquad (1)$$

Assuming the spectral density of the fluctuations in every subband equal, yields

$$\langle \Delta P_n^2 \rangle = \sigma_{P_1} \qquad n = 1, 2, \ldots N \qquad (2)$$

in which $\Delta P_n = P_n(t) - \langle P_n(t) \rangle$ is the fluctuation in the power and σ the variance. Two simple cases are considered here.

i) The fluctuations in the subbands are completely correlated in time, with eq. (2), it follows that

$$\Delta P_n = \Delta P_1 \qquad n = 1, 2, \ldots N \qquad (3)$$

hence with eqs (1,2,3), we have

$$\frac{\sigma_P}{\langle P \rangle^2} = \frac{\left\langle \left(\sum_{n=1}^{N} \Delta P_n \right)^2 \right\rangle}{N^2 \langle P_1 \rangle^2} = \frac{N^2 \langle \Delta P_1^2 \rangle}{N^2 \langle P_1 \rangle^2} = \frac{\sigma_{P_1}}{\langle P_1 \rangle^2} \qquad (4)$$

ii) The fluctuations in the subbands are completely uncorrelated in time, so that

$$\langle \Delta P_n \Delta P_m \rangle = 0 \qquad m \neq n \qquad (5)$$

In this case, with eqs (1,2,5), it follows that

$$\frac{\sigma_p}{\langle P \rangle} = \frac{\langle \sum_{n=1}^{N} \Delta P_n^2 \rangle + \langle \sum_{n=1}^{N} \sum_{m=1}^{N} \Delta P_n \Delta P_m \rangle}{N \langle P_1 \rangle} = \frac{\sigma_{P_1}}{\langle P_1 \rangle} \qquad m \neq n \qquad (6)$$

Fig. 3 shows the detector current as a function of the optical bandwidth for the superradiation region. In the LED region the collected power is a linear function of bandwidth while in the superradiation region it is a typical staircase curve. The height of every step is two times the power within a mode (except for the first step) because λ remains and $\Delta\lambda$ increases symmetrically around λ. The steps are 0.42 nm apart, corresponding to the distance between the modes. The noise results show $S_p/\langle P \rangle$ to be constant for the LED region and $S_p/\langle P \rangle^2$ constant for the superradiation region. Which, with eqs (4,6) means that the noise is uncorrelated for every subband in the LED region and correlated for the superradiation region. The 1/f noise in the collected power above threshold is independent of the bandwidth. Hence the main noise contribution is due to the noncoherent emission within a small optical band around the laser mode.

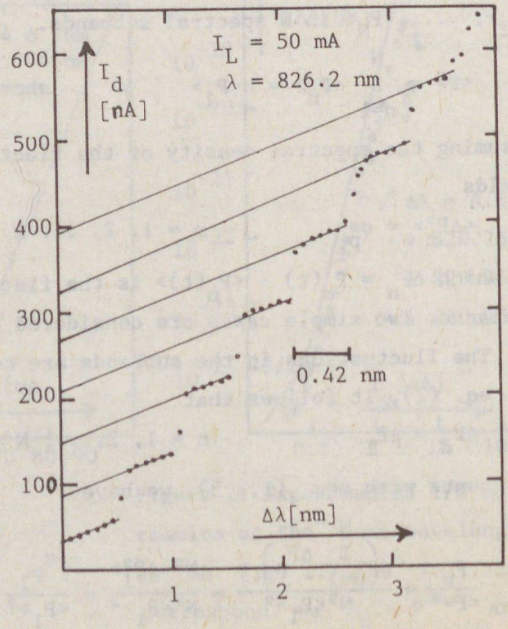

Figure 3. Detector current at fixed wavelength as a function of optical bandwidth for the superradiation region at I_L = 50 mA.

4. LITERATURE

[1] IEEE J.Q.E., vol. 24, p. 724 (1988).

[2] Proc. 8th Int. Conf. Noise phys. syst., p. 381 (1986).

[3] Proc. 9th Int. Conf. Noise phys. syst., p. 187 (1987).

[4] J. Appl. Phys., 51(4), p. 1932 (1980).

10th Int.Conf. on Noise in Physical Systems
1989 Budapest, Hungary

1/f NOISE, DEGRADATION AND RELIABILITY OF GaAsP LED's

J. ŠIKULA, B. KOKTAVÝ, P. VAŠINA, A. ČERMÁKOVÁ*

Department of Physics, Technical University
Barvičova 85, 662 37 Brno, Czechoslovakia
*Electrical Testing Institute
Pod lisem 129, 181 02 Praha, Czechoslovakia

1. INTRODUCTION

An ideal p-n junction makes a source of shot noise which is in order of magnitude comparable to the thermal noise [2]. On the other hand, p-n junctions containing structure defects exhibit an excess noise the magnitude of which is related to the imperfectness of the technology [3].

It has been experimentally verified that in the course of operation of LED´s structure defects are generated. A proof of existence of these defects has been given, e.g., by TSC measurements.

As noise makes, in general, an indicator of structure defects, particularly of those developing in the course of the device operation, it is advantageous to use it for the degradation evaluation and also, to a certain extent, reliability prediction.

2. EXPERIMENT AND RESULTS

Our study has been carried out on 4 groups of 50 experimental GaAsP LED s, aiming at finding relations between the noise, U-I, C-U curves, and the luminescence degradation. We measured the noise spectral density S_u in the forward direction, where we evaluted the maximum value S_{uM}, which is the value of the spectral density measured across a 10 kΩ load resistor.

In the reverse direction we evaluated the voltage U_s at which the spectral density of the voltage fluctuations measured across a load resistor of 100 kΩ surpassed twice the corresponding value of the thermal noise of this resistor.

As a measure of the degradation we take the decrease of luminescence in the course of the LED operation. We have also carried out structure and metallographic analysis of the defects in the samples. A part of the chip has been ground away, which made it possible to trace the emission and the potential profiles along the p-n junction by optical and electron scanning microscopes. We have found that the built-in potential is not constant along the section plane. Furthermore we observed many dislocation lines going out into the section plane. The dislocations are mostly a direct consequence of the lattice constant misfit.

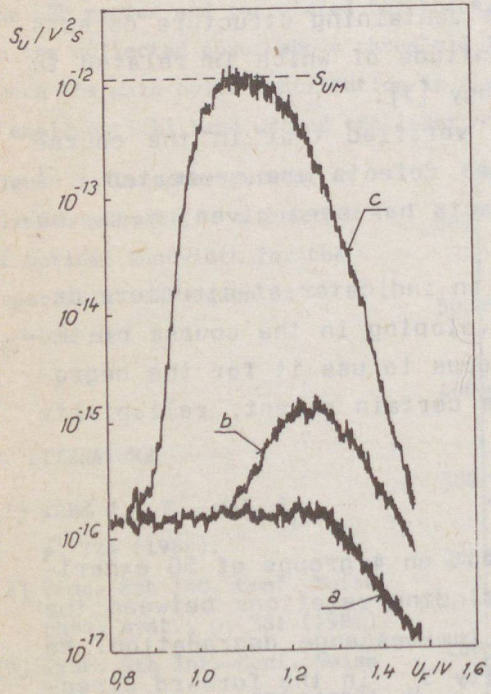

Fig.1 S_U vs. U_F plot: a) background + shot noise, b) initial state, c) after 4000 hours

In order to influence the structure defects due to the misfit and their evolution we have tested various ageing procedures.

From the point of intentional defect evolution and the consequent degradation the most effective procedure has been found which ran as follows: exposition to steady temperature of 80°C for 60 minutes; temperature drop to -40°C during 90 minutes; 60 minutes exposition to - 40°C; temperature increase to 80°C during 90 minutes. Evaluation of the ageing test after 4000 hours has shown that the noisy diodes

have the probable life-time by one order of magnitude lower than those having low noise. Furthermore, we have found that during the ageing process the noise of some diodes has increased (curve c) in Fig.1), while for some others it did the contrary. A substantial decrease of noise has been observed in about 10% of the samples.

The ensemble of low-noise diodes proved to be relatively stable their noise spectral density being kept low during the entire test.

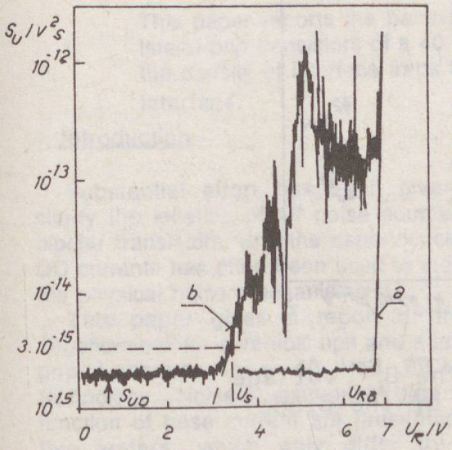

Fig.2 Reverse bias spectral density S_U vs. DC voltage U_R plot. At $U_R = U_S$ the spectral density $S_U = 2S_{UO}$

Fig.2 illustrates a behaviour under reverse bias of good and noisy diodes (curves a) and b), respectively). It is to be noted that the ensembles having high forward and reverse noise coincide.

Fig.3 demonstrates the effect of ageing on the diode parameters. On the horizontal axis the slope g_1 of the C^{-2} vs U_R plot is designated, while the vertical axis designates the voltage U_S as defined above. It is seen that after 4000 hours of the test some diodes exhibit a great deterioration of this parameter.

CONCLUSION

Our analysis confirms that the source of the luminescence degradation lies in structure defects and technology imperfections. These defects cause increase in number of the non-radiative transitions which in their turn bring about the luminescence deterioration. Noise measurements in combination

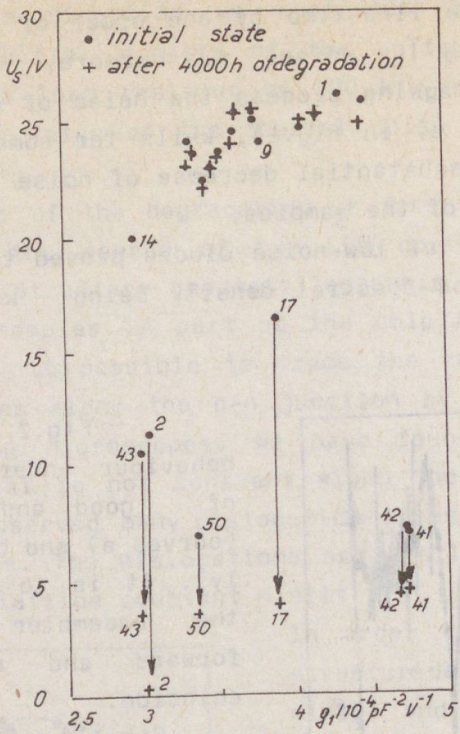

Fig.3 Variation of the U_S voltage during ageing of the diode ensemble

with transport characteristics measurements thus have proved to be an efficient tool for non-destructive analysis of the technology and reliability prediction.

REFERENCES

[1] J. ŠIKULA et al., Czech. Journ. of Physics, A 37, 140, (1987)

[2] P.O. LAURITZEN, Trans IEEE ED - 15, 770, (1968)

[3] T.G.M. KLEINPENNING, Physica 98 B, 289, (1980)

10th Int.Conf. on Noise in Physical Systems
1989 Budapest, Hungary

INFLUENCE OF THE DENSITY OF INTERFACE TRAPS ON THE BASE 1/f NOISE IN VERTICAL NPN AND LATERAL PNP TRANSISTORS

S. DECOUTERE, L. DEFERM, C. CLAEYS, G. DECLERCK

IMEC
B-3030 Leuven, Belgium

This paper reports the behaviour of the base 1/f noise of vertical npn and lateral pnp transistors of a 40 Volt BiCMOS process. The noise is related to the density of interface traps and identified as recombination at the Si-SiO_2 interface.

1. Introduction

Substantial effort has been given to clarify the location of 1/f noise sources in bipolar transistors, and the dependence on DC currents has often been used to identify the physical noise mechanisms [1].

This paper gives a report of these dependences for a vertical npn and a lateral pnp transistor in a 40 Volt BiCMOS technology. Noise measurement data as a function of base current are presented for five wafers, which only differ by the metallization process, giving a different density of interface traps (D_{it}), ranging approximately from 4.10^9 to 10^{11} #/cm^2eV, as determined by a charge pumping technique, which is known to give accurate results even for very low values of the D_{it} [2]. The D_{it} was measured on field MOS transistors. Wafer numbers and the corresponding values of Dit are summarized in table 1, with a short description of the metallization processes. The process changes for obtaining the differences in interface trap density are such that they do not influence the impurity profiles. It can be assumed that the diffusion current components are not influenced and that all measured changes are related to a change in the Si-SiO_2 surface characteristics, due to the presence of hydrogen in the different used process steps and the subsequent temperature treatments, resulting in a different D_{it}.

It will be shown that in our devices, the base 1/f noise was related to the density of interface traps. The dependence of the 1/f base noise on DC base current and on D_{it} identifies the noise as due to recombination at the Si-SiO_2 interface, for the total base current range.

TABLE 1

Wafer nr.	Dit [/cm^2eV]	Metallization
W40	$9.2\ 10^{10}$	Single metal
W56	$4.6\ 10^{10}$	Double metal+Ti barrier+nitr.+P
W54	$3.8\ 10^{10}$	Double metal+Ti barrier+P
W08	$1.5\ 10^{10}$	Single metal+P
W36	$3.7\ 10^{10}$	Double metal+P

(P means a passivation layer)

2. Experimental set-up

The common emitter measurement set-up was based on the insertion of a large series resistor Rs between the base contact and supply voltage Vs, in order to discriminate between the base and collector 1/f noise current generators, meanwhile providing an easy DC biasing. Figure 1 shows the small signal circuit, indicating the location of the 1/ f noise sources, as proposed by [1].

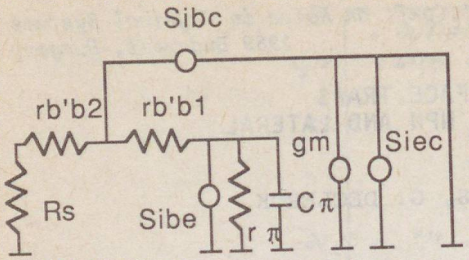

Figure 1. Small signal model indicating the location of the 1/f noise sources.

Because of Vs (=9Volt) >> kT/q, for all bias points the relation holds that Rs >> rπ. The large value of Rs allows one to approximate the spectrum measured at the collector and to refer it back to the base by the next equation:

$$S(f) = S_{ibe}(f)+S_{ibc}(f)+S_{ibc}(f)/\beta^2 + S_{iec}(f)/\beta^2 \qquad (1)$$

For β^2 substantially larger than unity and neglecting $S_{iec}(f)/\beta^2$ [1] , this expression simplifies further to :

$$S(f) = S_{ibe}(f) + S_{ibc}(f) \qquad (2)$$

3. Discussion of the noise data

The noise spectra of the vertical npn transistors, evaluated at 10 Hz, have a slope of 1.3 on a double logarithmic plot as a function of the base current (figure 2). This behavior can be explained by considering the base recombination current at the surface of the emitter/base space charge region (Ib_{recscl}) as the noise source, which means that the noise spectra S(f) are proportional to $[\exp(qVbe/mkT)]^2$, with m equal to 1.5. The distinct influence of the D_{it} is due to its influence on the surface parameters. Similar results were reported in [1,3] where a slope between 1 and 2 was attributed to recombination in the emitter/base space charge region at the surface.

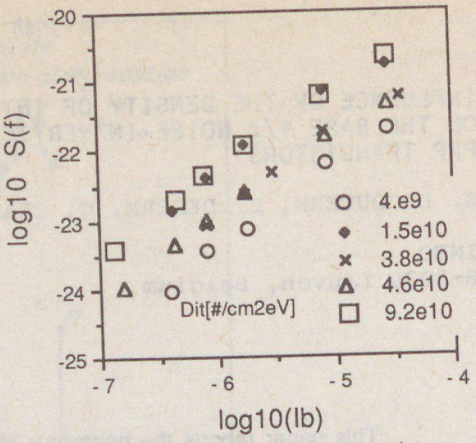

Figure 2. Spectra of the npn transistors evaluated at 10 Hz versus base current.

In figure 3, the spectrum evaluated at 10 Hz and 1 μA base current, is plotted versus the D_{it}, showing a pronounced increase in noise for increasing D_{it}. A strong correlation between D_{it} and degradation of the common emitter current gain is shown in figure 4, which is in favor of our identification of the noise as due to recombination in the emitter/base space charge region at the surface. All spectra are $1/f^{\gamma}$ with $\gamma \approx 1$ in the range 1 to 100 Hz.

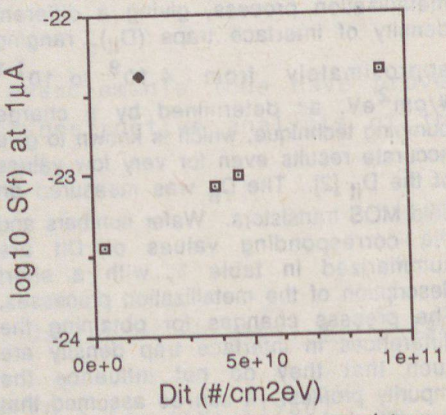

Figure 3. Spectra of the npn transistors, evaluated at 10 Hz and 1 μA base current, versus D_{it}.

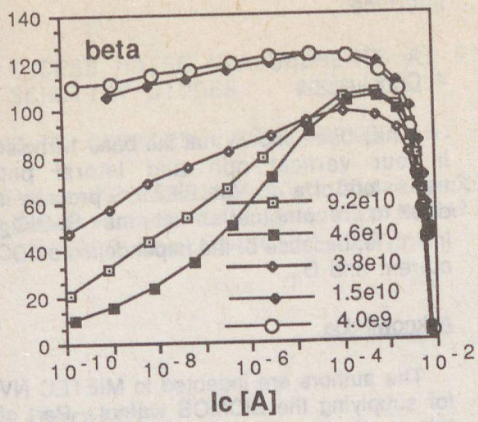

Figure 4. Degradation of the common emitter current gain of the npn transistors.

The noise spectra, evaluated at 10 Hz, of the lateral pnp transistors, are shown in figure 5 for the five process options. Figure 5 clearly indicates that two current regions can be distinguished. Expressions of the form $S(f) = K_f\, Ib^a/f$ have been fitted to both the low current region (index 1) and the high current region (index 2). For all process options, the value of a_1 was very close to 1 and the value of a_2 was very close to 2.

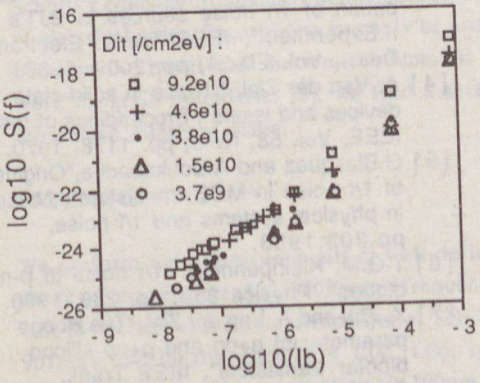

Figure 5. Spectra of the pnp transistors evaluated at 10 Hz versus base current.

To identify the noise in the low current region, one has to consider two possible physical noise mechanisms which result in a proportionality between noise spectrum and base current. First, noise from recombination at the surface of the emitter/base space charge region shows a dependence on bias expressed as $S(f) \propto \exp(2qV_1/kT)$. For a symmetric junction, $V_1 = V_{be}/2$ [4], what leads to the proportionality $S(f) \propto I_b$, when the diffusion current is higher than Ib_{recscl}. The p+ emitter in our pnp devices is extended with the base of the npn devices to provide a good lateral action, resulting in a more symmetric junction compared to our npn devices. Secondly, diffusion noise shows also a dependence $S(f) \propto I_b$. Diffusion noise can be due to collisions of carriers with the lattice (which we will call here fundamental 1/f noise) or due to scattering and/or trapping at defects and interface traps [5]. Because of the dependence of K_{f_1} on D_{it} (figure 6), the diffusion noise increases for increasing D_{it}. Using Kleinpennings model for long diodes [6], the Hooge parameter extracted from our data for the lowest value of the Dit, was estimated as $\alpha_H = 16\ 10^{-8}$. According to [7], this value is slightly higher than their prediction for fundamental diffusion noise.

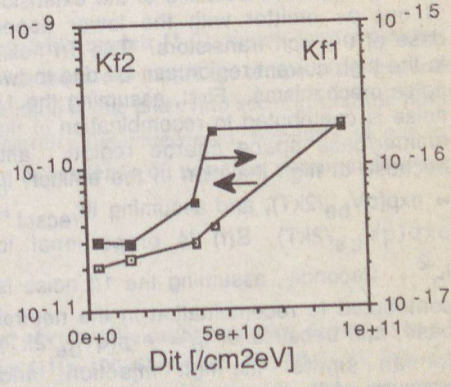

Figure 6. Dependence of the noise factors Kf_1 and Kf_2 on the D_{it}.

To identify the 1/f noise in the pnp transistors for low currents, the degradation of the common emitter current gain

for increased D_{it} (figure 7) as well as the presence of recombination 1/f noise in our npn devices, are in favor for a identification of the 1/f noise in our pnp devices as due to recombination in the emitter/base space charge region at the $Si-SiO_2$ interface.

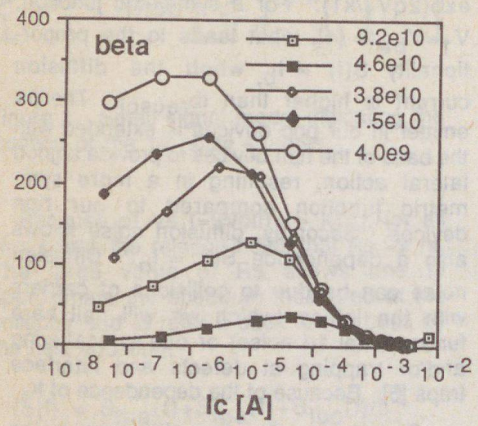

Figure 7. Common emitter current gain versus collector current for the pnp transistors.

At the transition between the low and the high current regions, the base enters into high injection. For higher currents, probably also part of the emitter enters into high injection because of the extension of our p+ emitter with the lower doped base of the npn transistors. The 1/f noise in the high current region can be due to two noise mechanisms. First, assuming the 1/f noise is contributed to recombination in the emitter/base space charge region, and because of high injection in the emitter, $I_b \propto \exp(qV_{be}/2kT)$, and assuming $Ib_{recscl} \propto \exp(qV_{be}/2kT)$, S(f) is proportional to I_b^2. Secondly, assuming the 1/f noise is contributed to recombination in the neutral base, and because of $I_b \propto \exp(qV_{be}/2kT)$ for an emitter in high injection, and because of $Ib_{surfrec} \propto \exp(qV_{be}/2kT)$ for a base in high injection , S(f) is proportional to I_b^2.

The dependence of the 1/f noise factors K_f on the D_{it} as shown in figure 6 suggests that the recombination is at the $Si-SiO_2$ interface.

4. Conclusions

It has been shown that the base 1/f noise in our vertical npn and lateral pnp transistors of a 40 Volt BiCMOS process is due to recombination at the $Si-SiO_2$ interface, because of the dependence on DC current and D_{it}.

Acknowledge

The authors are indebted to MIETEC NV for supplying the BiCMOS wafers. Part of this work was financially supported by "Fonds voor industrieel onderzoek in Vlaanderen".

Noise measurements were performed by G. Vanhorebeek.

REFERENCES

[1] A. Van der Ziel, X.Zhang and A. Pawlikiewicz, "Location of 1/f noise sources in BJT's and HBJT's - I. Theory", IEEE Trans. Electron. Dev., Vol. ED-33,pp. 1371, 1986.

[2] G.Groeseneken, H.Maes, N.Beltran and R.Dekeersmaecker, " A reliable approach to charge-pumping measurements in MOS transistors", IEEE Trans. Electron. Dev., Vol. ED-31, pp. 42, 1984.

[3] A.Pawlikiewicz and A.Van der Ziel,"Location of 1/f noise sources in BJT's - II.Experiment", IEEE Trans. Electron. Dev. , Vol. ED-34, pp. 2009, 1987.

[4] A. Van der Ziel, " Noise in solid-state devices and lasers", Proceedings of the IEEE, Vol. 58, No.8, pp. 1178, 1970.

[5] G.Blasquez and A.Boukabache,"Origins of 1/f noise in MOS transistors", Noise in physical systems and 1/f noise, pp.303,1983.

[6] T.G.M. Kleinpenning, "1/f noise in p-n diodes", Physica 98B, pp. 289, 1980.

[7] X. Zhu and A. Van der Ziel, "The Hooge parameter of n+pn and p+np silicon bipolar transistors", IEEE Trans. Electron. Dev. , Vol. ED-32, pp. 658, 1985.

10th Int.Conf. on Noise in Physical Systems
1989 Budapest, Hungary

EXCESS NOISE MEASUREMENTS AT SILICIDE/SILICON SCHOTTKY DIODES

H.H. GÜTTLER, J.H. WERNER, H. STOLL*

Max-Planck-Institut für Festkörperforschung
*Max-Planck-Institut für Metallforschung
D-7000 Stuttgart 80, FRG

ABSTRACT

Electronic properties of Schottky diodes are sensitive to inhomogeneities at the metal/semiconductor interface. As an empirical law, we discover that excess noise increases drastically when the standard deviation σ_s of the spatial distribution of Schottky barrier heights exceeds the critical threshold value of 2kT. Schottky barrier fluctuations are analyzable by a combination of current/voltage curves and capacitance/voltage data.

INTRODUCTION

Noise at Schottky contacts is not completely understood: Hsu [1] explained 1/f-noise at frequency f by carrier fluctuations and multistep tunnelling processes within the space charge region of the semiconductor. Luo et al. [2] ascribed noise to mobility fluctuations and used Handel's [3,4] theory of infra-quanta emission; this model quantitatively described room temperature noise of commercially available diodes.

Our contribution demonstrates that presently available models [1,2], which tacitly assume that Schottky contacts are spatially homogeneous, are inadequate to model the temperature dependence of electrical noise. Excess noise can only be understood if one takes into account that the interface between the metal and the semiconductor is *spatially inhomogeneous*. Similarly to our earlier work on grain boundaries [5], we find a severe dependence of noise on potential fluctuations within the interface plane.

EXPERIMENTAL

We perform noise measurements at well-defined abrupt silicide/Si Schottky diodes over a wide range of temperatures (50-350K) and frequencies (1Hz-100kHz). $CoSi_2$/Si, Pd_2Si/Si, PtSi/Si, and IrSi/Si-diodes with (room temperature) Schottky barriers Φ_{B_0} of 664meV, 723meV, 853meV, 901meV and ideality factors of 1.02, 1.06, 1.04, and 1.04, respectively, are investigated. These diodes are prepared by evaporating 10-100nm of the respective metal on Si single crystals followed by an anneal to form the silicide; an ohmic backside contact is achieved by phosphorous implantation and metallization. In addition to these silicide/Si contacts, we also investigate a commercially available low-noise diode from Hewlett Packard (HP).

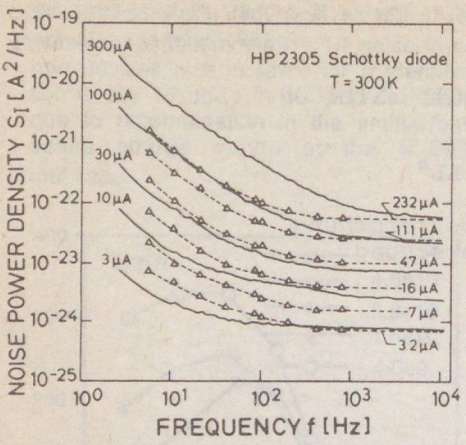

Fig.1: Measured noise power density of a HP 2305 Schottky diode at room temperature. Our results (heavy lines) agree with those from Luo et al. [Ref.2] (dashed lines).

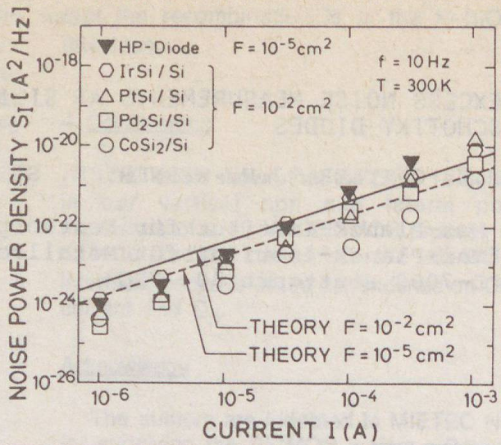

Fig.2: Room temperature noise (f=10Hz) for the HP diode (Fig.1) and several silicides/Si contacts with a different area in comparison with the theory of Luo et al. [Ref.2] .

In order to enable a comparison with earlier investigations we characterize first the same commercially available diode as Luo et al. [2] with an area $F=1\times10^{-5}cm^2$ and a doping of $3\times10^{16}cm^{-3}$. Figure 1 demonstrates that our measurements (1600 data points from 1Hz to 125kHz) for the frequency-dependent current noise $S_I(f)$ agree with the results of Luo et al. at temperature T=300K. For frequencies $f<10^3$Hz we observe 1/f-noise which exceeds the high-frequency (thermal) noise by orders of magnitude. Similar behavior is found for our silicide/Si diodes ($CoSi_2$/Si, Pd_2Si/Si, PtSi/Si, and IrSi/Si) with an area $F=1\times10^{-2}cm^2$ and a Si doping of $2\times10^{15}cm^{-3}$; the noise depends only weakly on the metal which is used for silicide formation.

Figure 2 compares our results to the mobility fluctuation theory of Luo et al. (Eq. (30) in Ref. [2]). The overall noise behavior and, in particular, the *linear* increase of the noise $S_I(f)$ with increasing current I seems to be well described. Our result for the Hooge parameter $\alpha_{HP}^{MPI}=2\times10^{-9}$ is in good agreement with the value $\alpha_{HP}^{Luo}=4.2\times10^{-9}$ of Luo et al. [2]. For the silicide/Si contacts we find $\alpha_{Silicides}^{MPI}$-values which range between 3×10^{-10} ($CoSi_2$/Si) and 2×10^{-9} (IrSi/Si). It is, however, interesting to note that all these α-values deviate by up to two orders of magnitude from the theoretical value $\alpha_{theory}\approx6\times10^{-8}$ which Kousik et al. [4] predicted for the room temperature value of n-type silicon. Values for α below 10^{-8} could theoretically only be understood if one required that intervalley scattering in Si was absent!

The discrepancy between theoretical predictions and experiments becomes even more pronounced if we discuss the temperature dependence of the noise: The model of Hsu [1] predicts that noise is independent of temperature T. Following Luo et al. [2] one should expect that the current noise $S_I(f)$ at constant current I *decreases* upon cooling because the electron mobility increases and the Hooge parameter α (Fig. 16 in Ref.[4]) decreases for lower T. Figure 3 reveals that for our silicide/Si diodes, contrary to theoretical predictions, the noise *increases* drastically upon cooling. We also find similar behavior for the HP 2305 diode and for all bias currents I.

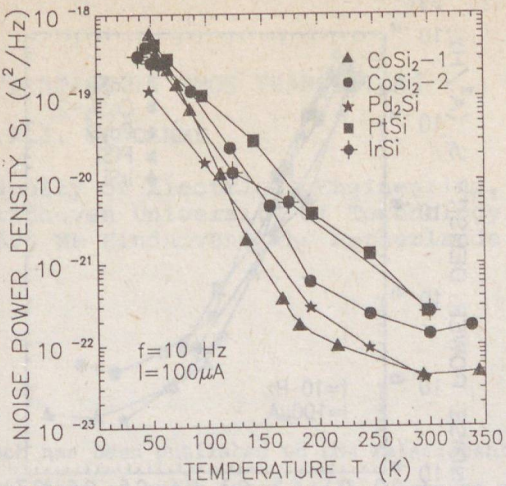

Fig.3: Contrary to theoretical predictions [Ref.2,4], the noise of all Schottky diodes increases upon cooling. These data are better understandable on the basis of Fig.5.

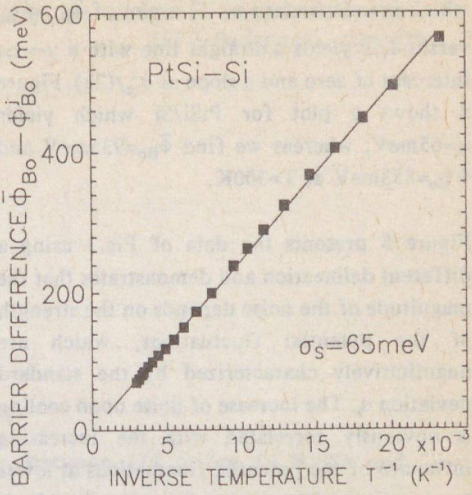

Fig.4: A plot of the difference of Schottky barriers from C/U and I/U-data versus 1/T after Eq. (2) yields the standard deviation σ_s from the slope.

POTENTIAL FLUCTUATIONS MODEL

At present we cannot offer a perfect quantitative model for the observed temperature and frequency dependence of the electrical noise at Schottky diodes. However, we show here that the magnitude of the observed noise is correlated with the strength of potential fluctuations. The current I across a Schottky contact with Richardson constant A^*, area F, and ideality n under bias U is usually described within the thermionic emission theory

$$I = A^* F T^2 \exp\left(\frac{-\Phi'_{Bo}}{kT}\right)\left\{\exp\left(\frac{qU}{nkT}\right) - 1\right\} \qquad (1)$$

and the Schottky barrier Φ'_{Bo} is derived from I/U-data [6]. Equation (1) shows that any fluctuations of the Schottky barrier result in strong fluctuations of the current I. It is, in fact, reasonable to assume that the Schottky barrier fluctuates *spatially*. Most silicides grow for example, not epitaxially but polycrystalline on Si; the interfaces are therefore not atomically flat but rough with the result of local variations of the electric field and consequently also of the band bending and effective Schottky barrier. Similarly to our work on grain boundaries [5] we model the spatial fluctuations of the barriers by a Gaussian distribution $P(\Phi_{Bo})$ with a mean barrier $\bar{\Phi}_{Bo}$ and a standard deviation σ_s at zero bias. Integrating Eq.(1) over the potential distribution $P(\Phi_{Bo})$ one finds [7] that the Schottky barrier height Φ'_{Bo} which controls current/voltage curves is related to the mean Schottky barrier $\bar{\Phi}_{Bo}$ by

$$\Phi'_{Bo} = \bar{\Phi}_{Bo} - \frac{\sigma_s^2}{2kT}. \qquad (2)$$

The barrier Φ'_{Bo} is always *lower* than the mean barrier $\bar{\Phi}_{Bo}$ because the current flows preferentially through the lower barriers in the potential distribution. The mean barrier $\bar{\Phi}_{Bo}$ can, on the other hand, be deduced from capacitance (C) data [7]. Equation (2) predicts that (for a distribution

which is independent of T) a plot of $\bar{\Phi}_{Bo}-\Phi'_{Bo}$ versus 1/T yields a straight line with a y-axis intercept of zero and a slope of $\sigma_s^2/(2k)$. Figure 4 shows a plot for PtSi/Si which yields σ_s=65meV, whereas we find $\bar{\Phi}_{Bo}$=935meV and Φ'_{Bo}=853meV at T=300K.

Figure 5 presents the data of Fig.3 using a different delineation and demonstrates that the magnitude of the noise depends on the strength of the potential fluctuations, which are quantitatively characterized by the standard deviation σ_s. The increase of noise upon cooling is obviously correlated with the increasing influence of the potential fluctuations at lower temperatures. The noise for all samples is drastically enhanced for $kT<0.5\sigma_s$. Vice versa, we find therefore as an empirical law that noise due to interfacial inhomogeneities is low as long as the 'strength' of potential fluctuations is small compared to the thermal energy, i.e. for $\sigma_s<2kT$.

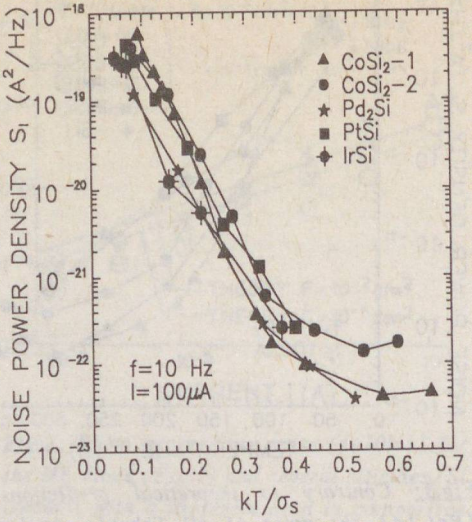

Fig.5: The current noise $S_I(f)$ increases when the thermal energy kT of the carriers becomes smaller than $0.5\sigma_s$.

CONCLUSIONS

The theory of Luo et al. [2] is appropriate to describe room temperature noise of Schottky diodes if and only if one adjusts the Hooge parameter. Presently available models [1,2] for Schottky barrier noise are, however, in contradiction to the increase of noise at low temperatures. We propose that this effect is correlated with potential fluctuations; the noise increases drastically when the standard deviation σ_s exceeds the critical threshold value of 2kT.

ACKNOWLEDGEMENTS

We gratefully acknowledge the continuous support of H.J. Queisser and A. Seeger.

REFERENCES

1 S. T. Hsu, IEEE Trans. Electr. Dev. **ED-18**, 882-887 (1971)

2 M.-Y. Luo, G. Bosman, A. Van der Ziel, and L. L. Hench, IEEE Trans. Electr. Dev. **ED-35**, 1351-1356 (1988)

3 P. H. Handel, Phys. Rev. A **22**, 745-757 (1980)

4 G. S. Kousik, C. M. Van Vliet, G. Bosman, P. H. Handel, Adv. Phys. **34**, 663-702 (1985)

5 A. J. Madenach and J. H. Werner, Phys. Rev. Lett. **55**, 1212-1214 (1985); Phys. Rev. B **38**, 13150-13161 (1988)

6 E.H. Rhoderick and R.H. Williams, *Metal Semiconductor Contacts*, Second Edition, (Clarendon Press, Oxford 1988), chapters 3,4

7 J. H. Werner and H. H. Güttler (unpublished)

10th Int.Conf. on Noise in Physical Systems
1989 Budapest, Hungary

1/f NOISE IN CMOS TRANSISTORS

L.K.J. VANDAMME

Faculty of Electrical Engineering,
Eindhoven University of Technology
5600 MB Eindhoven, The Netherlands

Much has been published on the relationship between 1/f noise in MOSTs and interface or oxide traps [1-3]. Observed spectra are sometimes erroneously interpreted [1,2] as pure 1/f noise, while the spectrum is the sum of a generation-recombination and 1/f component. Such results are explained by the McWhorter model. It has been demonstrated that 1/f and G-R noise have sources differing in spatial distribution and hence in physical origin [4]. The main problem still remains the bulk or surface origin, in other words, the concept of mobility fluctuation or number fluctuation. The observation as to the summation of G-R and 1/f noise should also be taken seriously by those [5-7] who believe that 1/f noise consists of a summation of discrete switchings of the current. Strasilla and Strutt demonstrated that burst noise consists of a random telegraph signal superimposed on 1/f noise and both are independent phenomena [8].

Here the 1/f noise in CMOS transistors will be investigated in terms of the empirical relation [9,10]

$$S_V/V^2 = S_I/I^2 = S_{I_s}/2I_s^2 = \alpha/Nf \qquad (1)$$

where N is the number of free carriers in the inversion layer and V is the applied drain source voltage biasing the MOST in the ohmic region. At a fixed gate voltage, the relative current fluctuations in saturation are twice those observed in the ohmic region [10] as can be seen from the factor 1/2 in eq. (1).
The dependence of the 1/f noise on channel length ℓ has been recently presented [11]. This $\alpha \propto \ell^2$ dependence provides arguments for the fundamental postulate of Van der Ziel's acceleration 1/f noise theory which is based on Handel's quantum 1/f noise theory.

The purpose of the present work on enhancement p- and n-MOSTs made on the same chip with 2 μm ≤ ℓ ≤ 100 μm and 3 μm ≤ W ≤ 300 μm is:

(i) to study the geometry and scaling effects on 1/f noise at a fixed effective gate voltage $V_G^* = V_G - V_T$ in view of Vand er Ziel's acceleration noise theory,

(ii) to compare the α versus V_G^* dependence with the outcomes of the Δn- and the Δμ-model, and

(iii) to calculate better parameters for device and CMOS circuit modeling.

Calculations based on [10] give the noise S_{I_s} (A^2/Hz) at saturation, so that

$$S_{I_s} = \alpha q \mu_e^2 C_o V_G^{*3}(W/\ell^3)/2f \propto \alpha \mu_e^2 (W/\ell^3) \qquad (2)$$

where μ_e is the mobility at $V_D = V_G$, C_o is the gate oxide capacitance per unit area and W the channel width. We are interested in the dependence on W and ℓ. Comparing CMOS transistors with different ℓ at a fixed bias V_G^*, we should expect $S_{I_s} \propto W/\ell^3$ if α is ℓ-independent. The acceleration noise theory with $\alpha \propto \ell^2$ results in a proportionality $S_{I_s} \propto W/\ell$. In contrast to results published by others [11-12] we do not find experimental arguments for Van der Ziel's theory.

Figure 1 shows $S_{I_s} \propto W/\ell^3$. We see that α is ℓ-independent and also that p-MOSTs are less noisy than n-MOSTs on the same chip. It is essential to keep V_G^* constant when comparing α-values from MOSTs with different lengths, as can be seen from fig. 2. The upper line in fig. 1 fits the n-MOST results and is calculated from eq. (2) using the observed values $\mu_e = 515\ cm^2/Vs$ and an α-value of 10^{-4} independent of length. The p-MOST line (through the circles) is calculated with $\mu_e = 160\ cm^2/Vs$ and $\alpha = 6 \times 10^{-6}$.

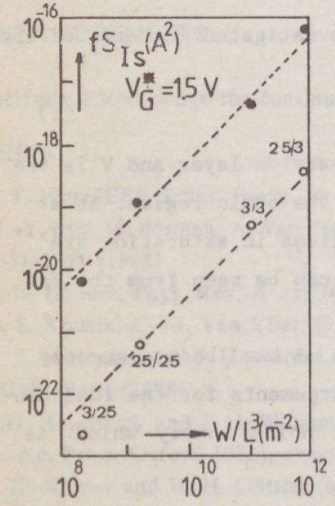

If there is no appreciable mobility degradation with increasing V_G^* and if the 1/f noise source is spatially uniform under the SiO_2 then α must be considered as independent of V_G^* according to the Δμ model [9].

Fig. 1: The experimentally observed normalised 1/f noise in saturation current fS_{IS} at $V_G^* = 1.5$ V versus W/ℓ^3 of four n (dots) and four p (circles) MOSTs in CMOS technology (on the same chip). The numbers indicate the channel width and lengths respectively. Equation (2) holds, which means that α is length-independent.

The p-MOSTs in fig. 2 obey the straightforward $\Delta\mu$ model for $V_G < 5$ V. If the 1/f noise is due to trapping in uniformly distributed oxide traps then α becomes inversely proportional to V_G^* [3] according to the McWhorter Δn model

$$\alpha_{\Delta n} = x_o D_o kTW\ell(x_o/x_2)/N \propto V_G^{*-1} \qquad (3)$$

where x_o is a characteristic decay length of the wave function ($\cong$ 1 Å) and x_2 = 30 Å. The n-MOSTs in fig. 2 obey the straightforward Δn model for low V_G^*.

In device modeling (SPICE programs), the coefficients K and m are used as defined by the expression

$$S_{I_s} = KI_s^m/f \qquad (4)$$

The exponent x of the α versus V_G^* dependence determines what values for K and m must be used. In these investigations we found x = 1, x = 0 and x = -1. The table shows the m and K values which must then be used in the device and circuit modeling.

Table: The exponent x in $\alpha \propto V_G^{*x}$ and the calculated K and m values

x = - 1	m = 1	$K = \alpha_r V_G^* q\mu_e/\ell^2$
x = 0	m = 3/2	$K = \alpha q(2\mu_e/C_o W\ell^3)^{\frac{1}{2}}$
x = 1	m = 2	$K = 2\alpha_r q/(W/\ell)^2 C_o$

The value of α_r is obtained from $\alpha \propto V_G^{*x}$ at V_G^* = 1 V and α is the value when no V_G^* dependence occurs.

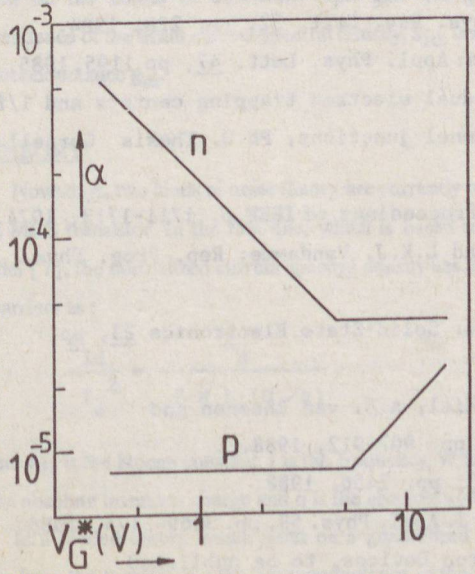

Fig. 2: α versus $V_G^* = V_G - V_T$ obtained from either the ohmic region fS_v/V^2, μ and R or saturation fS_{I_s}/I_s^2. The solid lines represent the average values of α at a given V_G^* of at least five MOSTs of different ℓ on one and the same chip. The results can be summarised with $\alpha \propto V_G^{*x}$ with x = -1 for n-MOSTs and x = 0 for p-MOSTs at low V_G^* and x = 1 at high V_G^* and x = 0 for n-MOSTs at high V_G^*.

Comparing enhancement n- to p-MOSTs on one and the same chip shows that p-MOSTs are less noisy than n-MOSTs. This has been found for two different CMOS technologies (MIETEC and IMEC).

The dependence of α on V_G^* in $\alpha = \alpha_r V_G^{*x}$ with $x = 0, -1$, and 1 can be explained by the mobility model, taking into account the spatial distribution of α [4], [14]. The implantations used in CMOS technologies to adjust the threshold voltage result in defect and α-profiles [13][14].

We have demonstrated that the V_G^* dependence of α unambiguously determines the m and K parameters in SPICE modeling.

The parameter α at a fixed V_G^* is no function of channel length and hence our results give no experimental support to Van der Ziel's acceleration 1/f noise theory.

Acknowledgement: The author gratefully acknowledges Herman Casier from Mietec and Claeys from IMEC for providing the samples. This work has been supported partially by an ESPRIT Basic Research action of the EEC.

References

[1] C.T. Sah and F.H. Hielscher: Phys. Rev. Lett. 17, pp. 956-958, 1966.

[2] G. Reimbold: IEEE Trans Electron Devices ED-31, pp. 1190-1198, 1986.

[3] L.K.J. Vandamme and R. Penning de Vries: Solid State-Electronics 28, pp. 1049-1056, 1985.

[4] L.K.J. Vandamme: IEEE Trans Electron Devices, ED-36, pp. 987-992, 1989.

[5] K.S. Ralls, W.J. Skocpol, L.D. Jackel, R.E. Howard, L.A. Fetter, R.W. Epworth and D.M. Tennant: Phys. Rev. Lett. 52, pp. 228, 1984.

[6] M.J. Uren, D.J. Day and M.J. Kirton: Appl. Phys. Lett. 47, pp.1195, 1985.

[7] C.T.Jr. Rogers: A study of individual electron trapping centers and 1/f noise in metal-insulator-metal tunnel junctions, Ph.D. Thesis Cornell University, 1987.

[8] U.J. Strasilla and M.J.O. Strutt: Proceedings of IEEE p. 1711-1713, 1974.

[9] F.N. Hooge, T.G.M. Kleinpenning and L.K.J. Vandamme: Rep. Prog. Phys. 44, pp. 479-532, 1981.

[10] L.K.J. Vandamme and H.M.M. de Werd: Solid-State Electronics 23, pp. 325-329, 1980.

[11] A.N. Birbas, Q. Peng, A. van der Ziel, A.D. van Rheenen and K. Amberiadis, J. Appl. Phys. 64, pp. 907-912, 1988.

[12] A. van der Ziel, J. Appl. Phys. 63, pp. 2456, 1988.

[13] L.K.J. Vandamme and S. Oosterhoff: J. Appl. Phys. 59, pp. 3169-3174, 1986.

[14] L.K.J. Vandamme, IEEE Trans Electron Devices, to be published.

10th Int.Conf. on Noise in Physical Systems
1989 Budapest, Hungary

FLICKER NOISE IN MOS TRANSISTORS FROM LIQUID HELIUM TO ROOM TEMPERATURE

G. GHIBAUDO, I.M. HAFEZ, F. BALESTRA

Laboratoire de Physique des Composants à Semiconducteurs,
UA-CNRS 840, ENSERG
BP 257, 38016 Grenoble, France

1. INTRODUCTION

In recent years, much work has been devoted to flicker noise in MOS (Metal-Oxide-Semiconductor) transistors [1-3]. It is now accepted that the carrier number fluctuation model is the most adequate to interpret the noise transfer characteristics of a MOS transistor at room temperature [1,2]. However, very few studies have dealt with flicker noise in MOS devices operating at very low temperature [4-6]. More specifically, it is not evident whether or not the carrier number fluctuation model is still applicable at liquid Helium temperature.

In this paper, we show experimentally that the carrier number fluctuation model is indeed suitable for explaining the noise features of MOS devices throughout a wide range of temperature i.e. from liquid Helium to room temperature. In particular, we demonstrate using a proper formulation of noise based on the notion of equivalent input gate voltage spectral density S_V that the gate voltage dependence of the drain current spectral density, S_{Id}, is strongly correlated to that of the square of the transconductance g_m.

2. THEORY

Nowadays, two kinds of noise theory are currently available for the interpratation of the 1/f noise in a MOS transistor. In the first one, which is based on the well-known Hooge mobility fluctuation model [7], the normalized current spectral density has to be inversely proportional to the total number of carriers as :

$$\frac{S_{Id}}{I_d^2} = \frac{\alpha_H}{f\,W\,L\,(Q_i/q)} \qquad (1),$$

where α_H is the Hooge constant, f is the frequency, W is the channel width, L is the channel length, Q_i is the absolute inversion charge and q is the absolute electron charge.

In a second theory, which relies on a generalized McWorther's model, the current fluctuations arise from the transfer, via the transconductance of the inversion charge fluctuations induced by those

of the interface charge [8]. Therefore, the normalized drain current spectral density can be represented by the expression [8,9] :

$$\frac{S_{Id}}{I_d^2} = \left(\frac{g_m}{I_d}\right)^2 S_V \qquad (2),$$

where $g_m = dI_d/dV_g$ is the device transconductance and S_V is the equivalent input gate voltage spectral density which, in fact, can be shown to be equal to the flat band voltage spectral density associated with the fluctuations of the oxide interface charge Q_{ss} such as [8,9] :

$$S_V = \frac{S_{Qss}}{W\,L\,C_{ox}^2} \qquad (3),$$

where C_{ox} is the gate oxide capacitance.

At room temperature, assuming that $S_{Qss} = A/f$ and substituting g_m and I_d by their analytical expressions yields the so-called Reimbold's relation [10] :

$$\frac{S_{Id}}{I_d^2} = \frac{A}{f} \frac{q^2}{\alpha^2 W\,L\,kT^2 (C_{ox} + C_d + C_{it} + C_i)^2} \frac{\mu_{eff}^2}{\mu_o^2} \qquad (4),$$

where α is numerical constant ($\alpha = 1$-2 from weak to strong inversion), kT/q is the thermal voltage, μ_{eff} is the effective mobility, μ_o is the low field mobility and C_d, C_{it} and C_i are the depletion, interface state and inversion charge capacitances respectively.

At very low temperature ($T \leq 25$ K), the same treatment can be done but using an appropriate mobility law versus inversion charge [11,12]. The normalized drain current spectral density takes therefore the form :

$$\frac{S_{Id}}{I_d^2} = \frac{A}{f} \frac{C_i^2}{W\,L\,(C_{ox} + C_d + C_{it} + C_i)^2} \frac{\mu_{eff}^2}{\mu_m^2} \frac{Q_m^2}{Q_i^4} \qquad (5),$$

where $\mu_{eff} = 2\mu_m (Q_i/Q_m + Q_m/Q_i)^{-1}$ is the effective mobility, μ_m is the maximum mobility and Q_m is the corresponding inversion charge [11-13].

2. RESULTS AND DISCUSSION

Experiments have been carried out on standard N channel MOS devices fabricated at the LETI-LIR (Grenoble). The current-voltage characteristics have been measured using a semiconductor parameter analyser HP 4145 and the transconductance was deduced numerically by a further derivation of the $I_d(V_g)$ curves. The drain current noise has been measured using a digital spectrum analyzer TAKEDA RIKEN 9405A within a frequency range 1Hz-1kHz and using a standard biasing circuit [1].

Fig. 1 a-c displays in a synthetic manner the results of our measurements for three temperatures (T=4K, 77K and 300K). The left-hand scale refers to the normalized drain current spectral density S_{Id}/I_d^2 while the rigth-hand scale corresponds to $(g_m/I_d)^2$. It is worth mentioning that, instead of plotting these quantities as a function of gate voltage, they have been plotted as a function of drain current in order to magnify the weak inversion region and also to avoid the use of the gate voltage in a logarithmic scale.

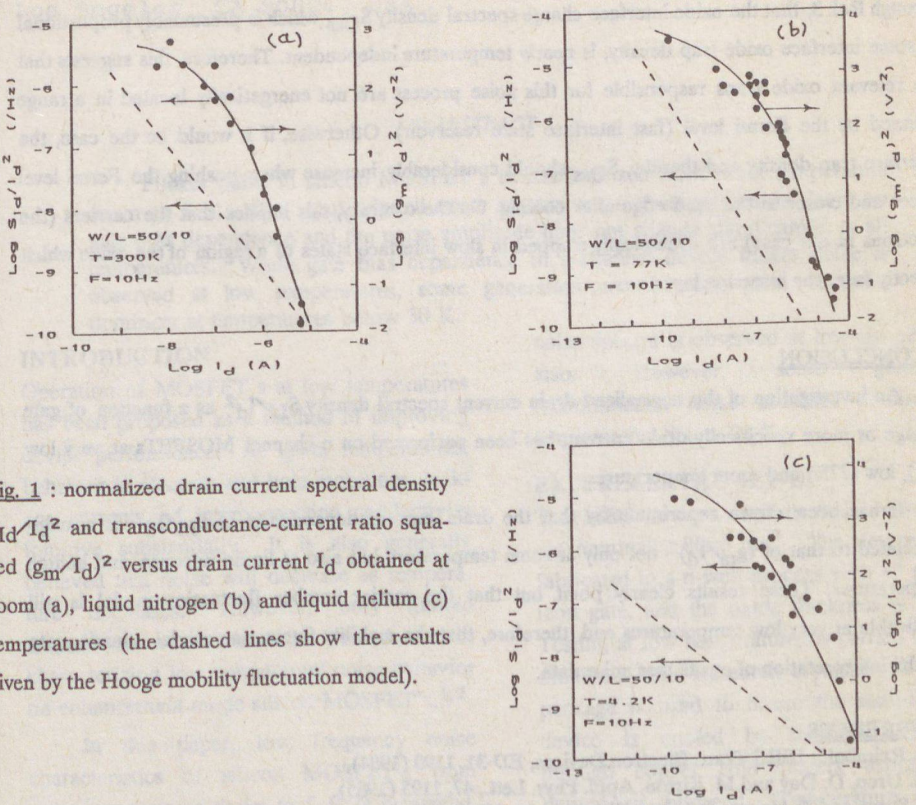

Fig. 1 : normalized drain current spectral density S_{Id}/I_d^2 and transconductance-current ratio squared $(g_m/I_d)^2$ versus drain current I_d obtained at room (a), liquid nitrogen (b) and liquid helium (c) temperatures (the dashed lines show the results given by the Hooge mobility fluctuation model).

On the same figures are also plotted the theoretical curves obtained using the mobility fluctuation model (Rel. 1). For room and liquid nitrogen temperatures, the inversion charge has been obtained using classical analytical equations [14], whereas at liquid helium temperature, Q_i has been calculated using a quantized inversion layer model [11]. Therefore, since for T=77 and 300 K, the effective mobility below threshold is nearly constant, the inversion charge is proportional to the drain current (Fig. 1 a and b). In contrast, at liquid helium temperature, the effective mobility at low drain current varies as Q_i [11-13] and, in turn, the inversion charge is proportional to the square root of the drain current (Fig. 1 c).

The examination of Fig. 1 a-c clearly shows that, only the carrier number fluctuation model in

which the drain current spectral density S_{Id} has to be proportional to g_m^2 is appropriate for the interpretation of our room, low and very low temperature noise data. In contrast, the mobility fluctuation model is inadequate to provide neither a qualitative nor a quantitative fit of our data throughout the whole studied drain current range (10^{-10} to 10^{-4} A).

It should also be noted that the coefficient of proportionality between S_{Id}/I_d^2 and $(g_m/I_d)^2$ namely, according to Rel. 2, the equivalent input gate voltage spectral density S_V, deduced from Fig. 1 a-c, is practically independent of temperature and lies around $5x10^{-9}V^2/Hz$ (+ 20%). This means, through Rel. 3, that the oxide interface charge spectral density S_{Qss} which is presumably proportional to some interface oxide trap density, is nearly temperature independent. Therefore, this suggests that the relevant oxide traps responsible for this noise process are not energetically located in a range scanned by the Fermi level (fast interface state reservoir). Otherwise, if it would be the case, the interface trap density and thereby, S_{Qss} should considerably increase when pushing the Fermi level closer and closer to the band edge after cooling. On the contrary, this implies that the carriers (the electrons in our case) are dynamically trapped in slow interface states of a region of the oxide which directly faces the inversion layer..

3. CONCLUSION

An investigation of the normalized drain current spectral density S_{Id}/I_d^2 as a function of gate voltage or more specifically drain current, has been performed on n channel MOSFETs at very low (4K), low (77K) and room temperatures.

It has been shown experimentally that the drain current dependence of S_{Id}/I_d^2 is strongly correlated to that of $(g_m/I_d)^2$ not only at room temperature but also at liquid nitrogen and helium temperatures. These results clearly point out that the carrier number fluctuation model is still applicable at very low temperatures and, therefore, that the mobility fluctuation model is inadequate for the interpretation of our flicker noise data.

REFERENCES

1. G. Reimbold, IEEE Trans Electron Devices, ED-31, 1190 (1984).
2. M. Uren, D. Day and M. Kirton, Appl. Phys. Lett., 47, 1195 (1985).
3. C. Surya and T. Hsiang, Sol. Stat. Electron., 31, 959 (1988).
4. R. Voss, J. Phys. C, 11, L923 (1978).
5. C. Adkins and R. Koch, J. Phys. C, 15, 1829 (1982).
6. E. Hendriks and J. Zijlstra, Sol. Stat. Electron., 31, 1105 (1988).
7. F. Hooge, Physica B, 83, 14 (1976).
8. G. Ghibaudo, Phys. Stat. Solidi (a), 104, 917 (1987).
9. G. Ghibaudo, Phys. Stat. Solidi (a), in press (1989).
10. G. Ghibaudo, Sol. Stat. Electron., 30, 1037 (1987).
11. G. Ghibaudo and F. Balestra, Sol. Stat. Electron., 31, 105 (1988).
12. G. Ghibaudo and F. Balestra, Sol. Stat. Electron., 32, 221 (1989).
13. F. Balestra, I. Hafez, G. Ghibaudo, ESSDERC, Montpellier (France), J. Phys., C4, 817 (1988).
14. G. Ghibaudo, Phys. Stat. Solidi (a), 95, 323 (1986).

10th Int.Conf. on Noise in Physical Systems
1989 Budapest, Hungary

LOW-FREQUENCY NOISE IN CMOST'S AT CRYOGENIC TEMPERATURES

J. CHANG, C.R. VISWANATHAN

Electrical Engineering Department, UCLA,
University of California
Los Angeles, CA 90024, USA

ABSTRACT

Flicker noise in silicon MOSFET's is characterized from room temperature down to 5 K. The input-referred noise spectra for n-channel devices show no gate bias dependence and the noise amplitude does not change significantly, at all temperatures. While gate bias dependence in p-channel device flicker noise is observed at low temperatures, some generation-recombination noise becomes dominant at temperatures below 30 K.

INTRODUCTION

Operation of MOSFET's at low temperatures has been proposed as a method of improving device performance. At lower temperatures, behavior in electron and hole mobilities, leakage current and interconnection conductivity improve substantially. It is also generally believed that noise will decrease as temperature decreases. However, only limited amount of work has been carried out in characterizing low temperature noise behavior on enhancement mode silicon MOSFET's.[1,2]

In this paper, low frequency noise characteristics of silicon MOSFET's from room temperature down to 5 K is presented. At room temperature, it has been shown that the input-referred noise spectra for n-channel FET's show no gate voltage dependence, while gate bias dependence is observed in p-channel devices.[3] At low temperatures, the input-referred noise spectra for n-channel devices show no gate bias dependence and the noise amplitude does not change in any significant order of magnitude, at all temperatures down to 5 K. In p-channel transistors, the gate bias dependence in the input-referred noise spectra is observed at low temperatures also. However, some generation-recombination noise becomes dominant at temperatures below 20 K.

EXPERIMENTAL SET-UP

The MOS devices used in this investigation are nominally 80×6 μm^2. The devices were fabricated in a n-well process with n^+ polysilicon gate, and the oxide thickness is 775 Å. Testing at low temperatures is carried out in a modified Janis Research cryostat. A 68 pin package is used to house the sample. The device is cooled by thermal conduction through copper cold fingers using liquid helium or nitrogen. Temperature can be varied from room temperature down to 5 K utilizing a LakeShore DRC 82C temperature controller. The low frequency noise spectra are characterized by an automated noise measurement setup described elsewhere.[4,5]

When carrying out measurements at temperatures below 20 K, care was taken to make sure the device is operating in equilibrium before measurements are carried out. Transient measurements[6] indicate that our n-channel samples have response times of over

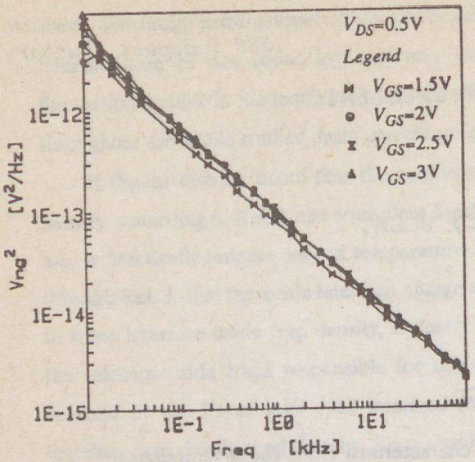

Fig. 1 : Input-referred noise spectra of the 80×6 μm^2 n-channel FET at room temperature with different gate voltages.

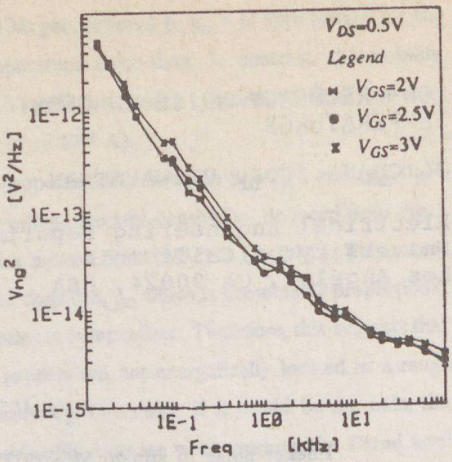

Fig. 2 : Input-referred noise spectra of the n-channel FET at 30 K with different gate voltages.

5 minutes, due to freezeout at low temperatures. Since the transient caused by the delay in the ionization of the dopants is much faster at slightly higher temperatures, the process can be speeded up by biasing up the test sample at higher temperatures, such as 20 K, to reach equilibrium, and then lowered to the testing temperature.

EXPERIMENTAL RESULTS

Low frequency noise for surface channel NMOS devices has been characterized from room temperature down to 5 K. Figures 1 and 2 show some typical noise spectra at room temperature and 30 K respectively. The input-referred noise spectra presented show no bias dependence for all temperatures. The noise spectra show a increase in slope at lower temperatures. This peculiar behavior is found in devices from this particular fabricator, and is probably due to a generation-recombination noise source at low frequency. Figure 3 summarizes the change in flicker noise with temperature. Contrary to common belief, flicker noise at low temperatures does not decrease in any significant order of magnitude.

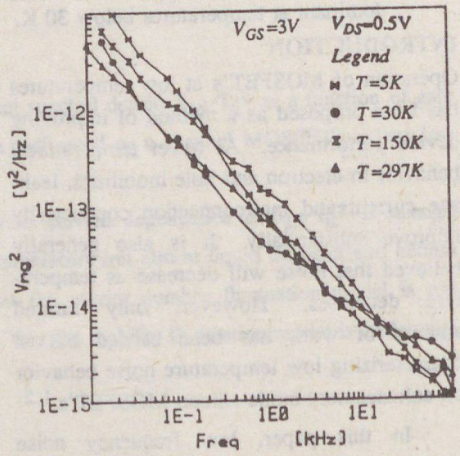

Fig. 3 : Comparison of the NMOS input-referred noise spectra at temperatures from 5 to 297 K.

Noise was measured at low temperatures in PMOS devices as a function of gate voltage. At a given temperature, noise showed gate bias dependence similar to what is observed at room temperature (Fig. 4). Figure 5 shows the low frequency noise plotted as a function of frequency at 5 K for several gate voltages. It can be seen that the noise amplitude increases significantly. To

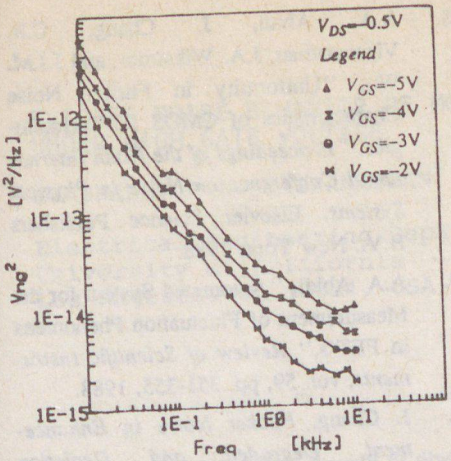

Fig. 4 : Input-referred noise spectra of the 80×6 μm^2 p-channel FET at room temperature with different gate voltages. Gate bias dependence is observed.

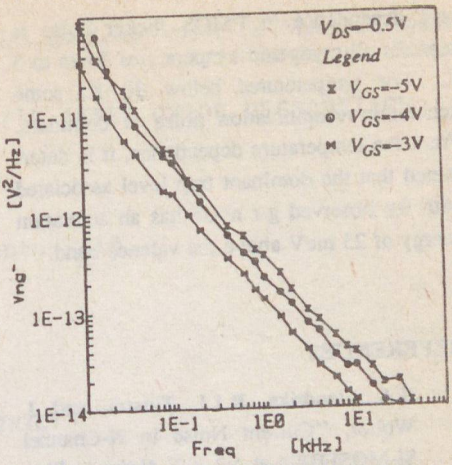

Fig. 5 : Input-referred noise spectra of the p-channel FET at 5 K. Gate voltage dependence is observed.

compare the noise behavior versus temperature, the noise measured at a fixed drain voltage of –0.5 V and a drain current of 0.2 mA in the p-channel transistor is plotted in Fig. 6. The noise goes down at 150 K from the room temperature value and the slope of the spectra shows practically no change. However, at 30 K, the noise goes up and around 1 kHz, the slope becomes very small. At 20 K, the noise definitely displays a generation-recombination (g-r) characteristics. At 5 K, the peak due to the g-r noise appears to have moved to much lower frequencies. This dominant trap level that causes the g-r noise can be characterized by an Arrhenius' plot. It is determined that the trap level has an activation energy of 0.025 eV above the valence band. This energy level is very close to the energy level of oxygen impurity and the boron acceptor.

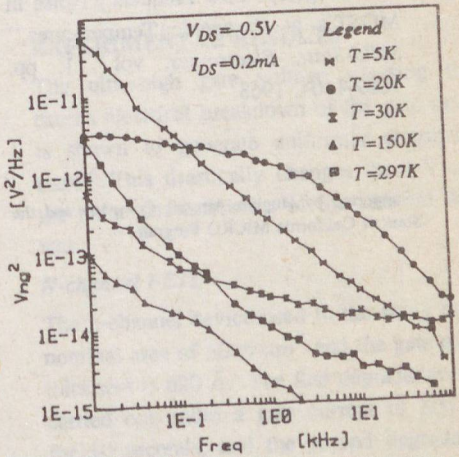

Fig. 6 : Comparison of the PMOS input-referred noise spectra at temperatures from 5 to 297 K at a fixed I_{DS} of 0.2 mA.

DISCUSSION

The input-referred noise spectra in surface channel NMOS devices are independent of bias point, both in the linear and saturated regions of operations, for all temperatures. Their amplitude varies only slightly over a wide range of temperatures. This gives credence to a tunneling model such as McWhorter's carrier-density fluctuation model, [7] which is temperature-independent to the first order.

In p-channel FET's, the usual gate vol-

tage dependence in PMOS flicker noise is seen for all cryogenic temperatures down to 5 K. For temperatures below 30 K, some generation-recombination noise is dominant. From the temperature dependence, it is determined that the dominant trap level associated with the observed g-r noise has an activation energy of 25 meV above the valence band.

REFERENCES

1. E.A. Hendriks, R.J.J. Zijlstra, and J. Wolter, "Current Noise in N-Channel Si-MOSFET's at 4.2 K," *Noise in Physical Systems and 1/f Noise 1985*, pp. 175-180, Elsevier Science Publishing Co., Inc., New York, 1986.
2. C.G. Rogers, "Low Frequency Noise in MOST's at Cryogenic Temperatures," *Solid-State Electronics*, vol. 11, pp. 1099-1104, 1968.
3. A.A. Abidi, J. Chang, C.R. Viswanathan, J.A. Wikstrom, and J.J.M. Wu, "Uniformity in Flicker Noise Characteristics of CMOS IC Technologies," *Proceedings of the Ninth International Conference on Noise in Physical Systems*, Elsevier Science Publishers B.V., New York, 1988.
4. A.A. Abidi, "Automated System for the Measurement of Fluctuation Phenomena in FET's," *Review of Scientific Instruments*, vol. 59, pp. 351-355, 1988.
5. J. Chang, *Flicker Noise in Enhancement, Degraded and Depletion MOSFET's*, M.S. Thesis, UCLA, 1988.
6. M. Grupen, *The Transient Current Phenomenon in MOSFET's Below 30 K*, M.S. Thesis, UCLA, 1989.
7. A.L. McWhorter, *Semiconductor Surface Physics*, p. 207, University of Pennsylvania Press, Philadelphia, 1956.

*Supported by Hughes Aircraft Company and the State of California MICRO Program.

10th Int.Conf. on Noise in Physical Systems
1989 Budapest, Hungary

FLICKER NOISE BEHAVIOR OF MOSFET'S AFTER OXIDE DEGRADATION UNDER HIGH GATE VOLTAGE

J. CHANG, C.R. VISWANATHAN

Electrical Engineering Department, UCLA,
University of California
Los Angeles, CA 90024, USA

ABSTRACT

A significant amount of divergence of ideas exists as to the origin of flicker noise in MOS transistors. Insights into the physical mechanism of the low frequency noise is obtained by deliberately introducing traps in the oxide by high gate voltages. Our experimental results seem to support the McWhorter's tunneling model.

INTRODUCTION

The flicker noise in MOS transistors has been the object of study in a number of research laboratories. A significant amount of divergence of ideas exists as to the origin of the flicker noise. Park and van der Ziel[1] have tried to discriminate between the carrier-density fluctuation [2] and mobility fluctuation [3] models, but the results are inconclusive.[4] In this paper, we report results of studies of low frequency noise in n- and p-channel devices in which traps have been introduced deliberately. The results offer a better insight into the origin of the noise.

EXPERIMENTAL SET-UP

The virgin samples are first characterized by measuring the I_D–V_{GS} and subthreshold curves using the HP 4145A semiconductor parameter analyzer with the HP 16058A test fixture. The low-frequency noise spectra are characterized by an automated noise measurement set-up using a custom-made low-noise amplifier.[5] Then, the devices are stressed by applying a high gate voltage of approximately 80 V on the gate, in a dark test fixture with a limiting gate current. The post-stress characteristics are recorded similar to those obtained under pre-stress conditions.

EXPERIMENTAL RESULTS

The ultra-high gate voltage stressing that causes electrical breakdown of the gate oxide is shown to generate uniformly distributed traps.[6] This drastically changes the I-V and the noise characteristics of the stressed devices.

N-channel FETs

The n-channel device used in the study has a nominal area of 50×6 μm^2 and the gate oxide thickness is 620 Å. The first degradation was carried out under a gate current of 300 pA for 10 seconds, and the second degradation was performed under the same condition for another 10 seconds. Figures 1 and 2 show the change in I_D–V_{GS} and the subthreshold slopes in the undegraded (virgin) n-channel device and the behavior after the first and second degradation. The change in slope in the I-V and the subthreshold slope indicates the generation of interface traps. The the input-referred noise spectra of the n-channel virgin sample are shown in Fig. 3. As can be seen, not too much gate bias dependence is observed in the n-channel samples. Fig. 4 shows the noise spectral change after

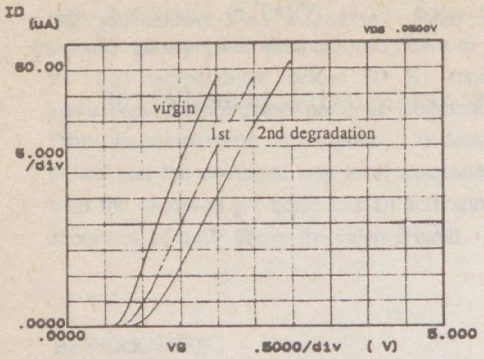

Fig. 1 : Changes in the I_D–V_{GS} curves for the n-channel MOSFET after successive degradations.

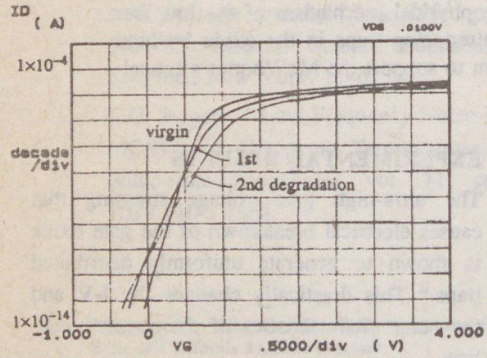

Fig. 2 : Changes in the subthreshold curves for the n-channel MOSFET after successive degradations.

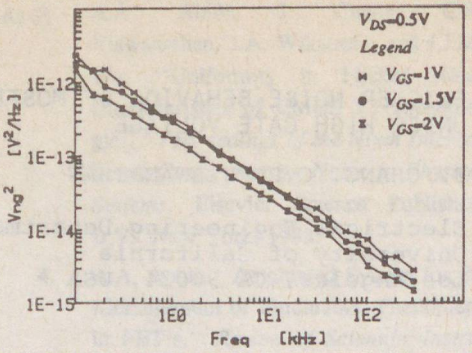

Fig. 3 : The input-referred noise spectra for the virgin n-channel FET.

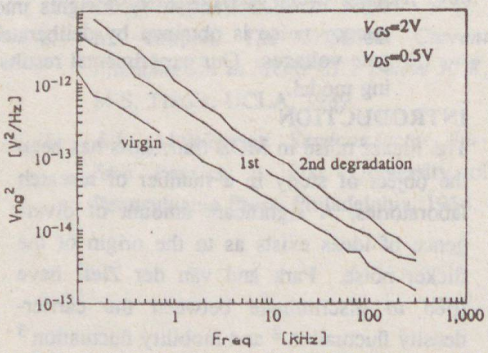

Fig. 4 : Comparison of the input-referred n-channel noise spectra after successive degradations.

successive degradations. Besides the increase in noise, the slope of the spectra changes from 0.8 to 1.

P-channel FETs

The p-channel device used in the study is nominally 50×7 μm^2 and the gate oxide thickness is 620 Å. The first degradation was carried out under a limiting gate current of 300 pA for 15 seconds. Since negligible degradation was observed after the first stressing, the second degradation was carried out with a larger limiting gate current for another 15 seconds. Figures 5 and 6 show the changes in the I_D–V_{GS} and the subthreshold curves of the p-channel device. There is practically no difference in the I-V characteristics after the first degradation. Figure 7 shows the noise characteristics of the virgin p-channel sample in the linear region of operation. Gate voltage dependence is obvious in the p-channel noise spectra. It can be shown that as the magnitude of the gate bias increases, the noise amplitude of the virgin p-channel device increases and saturates at a level that coincides remarkably with the noise amplitude of the n-channel device of the same dimension on the same chip.

Figures 8 and 9 compare the noise of

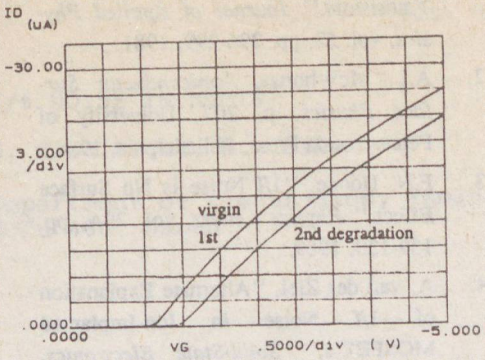

Fig. 5 : Changes in the I_D–V_{GS} curves for the p-channel MOSFET after successive degradations.

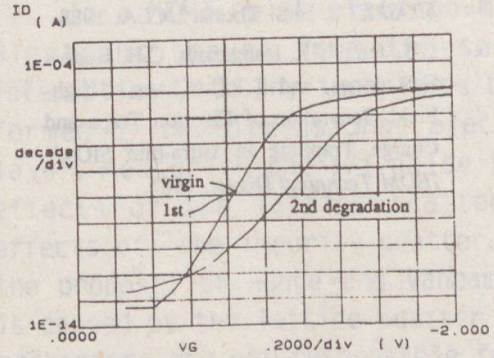

Fig. 6 : Changes in the subthreshold curves for the p-channel MOSFET after successive degradations.

the p-channel device after successive degradations. The gate bias is adjusted (0.3 V) to account for the threshold voltage shift due to the formation of the fixed positive oxide charges after the second stressing.

It is clear from Fig. 9 that the noise increases little with successive degradations but the gate voltage dependence disappears approaching a behavior similar to that of the n-channel devices.

Similar results were obtained in both the n- and p-channel devices of area $12\times3\ \mu m^2$ from a second fabricator with a gate oxide thickness of 450 A.

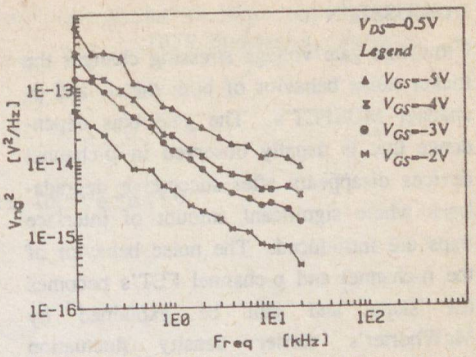

Fig. 7 : The input-referred noise spectra for the virgin p-channel FET.

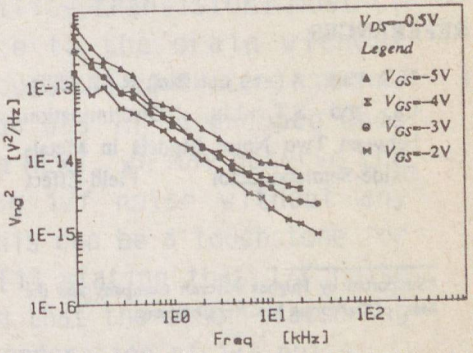

Fig. 8 : The input-referred noise spectra for the p-channel device after first degradation.

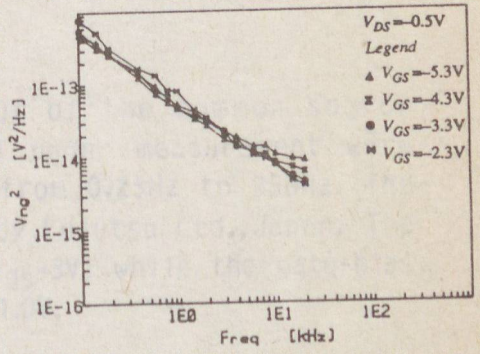

Fig. 9 : The input-referred noise spectra for the p-channel device after second degradation. Gate voltage dependence disappeared.

DISCUSSION

Ultra-high gate voltage stressing changes the flicker noise behavior of both the n- and p-channel MOSFET's. The gate bias dependence that is usually observed in p-channel devices disappears after successive degradations where significant amount of interface traps are introduced. The noise behavior of the n-channel and p-channel FET's becomes the same and can be explained by McWhorter's carrier density fluctuation model.

REFERENCES

1. H.S. Park, A. van der Ziel, R.J.J. Zijlstra, and S.T. Liu, "Discrimination between Two Noise Models in Metal-Oxide-Semiconductor Field-Effect Transistors," *Journal of Applied Physics*, vol. 52, pp. 296-299, 1981.
2. A.L. McWhorter, *Semiconductor Surface Physics*, p. 207, University of Pennsylvania Press, Philadelphia, 1956.
3. F.N. Hooge, "1/f Noise is No Surface Effect," *Physics Letters*, vol. 29A, pp. 139-130, 1969.
4. A. van der Ziel, "Alternate Explanation of 1/f Noise in Ion-Implanted MOSFET's," *Solid-State Electronics*, vol. 26, pp. 927-928, 1983.
5. J. Chang, *Flicker Noise in Enhancement, Degraded and Depletion MOSFET's*, M.S. Thesis, UCLA, 1988.
6. C.S. Jenq, T.R. Ranganath, C.H. Huang, H.S. Jones, and T.T.L. Chang, "High-Field Generation of Electron Traps and Charge Trapping in Ultra-thin SiO_2," *IEDM Technical Digest*, 1981.

*Supported by Hughes Aircraft Company and the State of California MICRO Company.

10th Int.Conf. on Noise in Physical Systems
1989 Budapest, Hungary

1/f NOISE IN HEMTS

S. HASHIGUCHI, H. IRIE

Department of Electronics, Yamanashi University
Kofu 400, Japan

INTRODUCTION

In a HEMT (high electron-mobility transistor) most of electrons travel from the source to the drain without interacting with any impurities through the conducting channel formed by two-dimensional electron gas in an undoped GaAs layer. Measuring the 1/f noise in a HEMT, we may observe the effects of the lattice scatter on 1/f noise without any effects of the impurity scatter. This can be a touchstone for the proposal of Hooge and Vandamme[1] stating that 1/f noise is caused by the lattice scatter and that the other scattering mechanisms are not responsible for generation of 1/f noise.

We report here the experimental results of the gate-bias dependence of 1/f noise in a HEMT.

MEASUREMENTS

Spectra of the noise output of the common source configuration including the HEMT under measurement were observed in the frequency range from 0.25Hz to 250Hz. The sample HEMT is FHX01FH supplied by Fujutsu Ltd.,Japan. The drain voltage was held constant (V_{ds}=3V) while the gate-bias voltage was varied from +0.1V to -1.0V.

RESULTS AND DISCUSSIONS

Figure 1 shows the noise spectral density at 1Hz. All the obtained spectra were strictly proportional to 1/f in the

frequency range of the present measurement. The lower two traces show the drain current noise spectral density $S_i(1Hz)$ at 300K and at 77K, respectively. $S_i(1Hz)$ at 300K gradually increases as the gate-bias decreases from +0.1V, reaches its peak at about -0.4V, and then sharply decreases. $S_i(1Hz)$ at 77K is almost constant for the gate-bias more than -0.5V and slowly decreases below -0.5V. $S_i(1Hz)$ is higher at 77K than at 300K at the gate-bias below -0.7V.

The upper two traces show the gate noise voltage spectral density $S_i(1Hz)/g_m^2$, where g_m is the transconductance. Two traces coincide with each other both below -0.9V and above 0V. The noise output at 77K is attributable to the noise generated at the gate portion. The spectral density of the noise generated at the gate portion is estimated as about -110dbV/Hz at 1Hz. The difference between $S_i(1Hz)/g_m^2$ at 300K and 77K is attributable to the noise generated in the conducting channel.

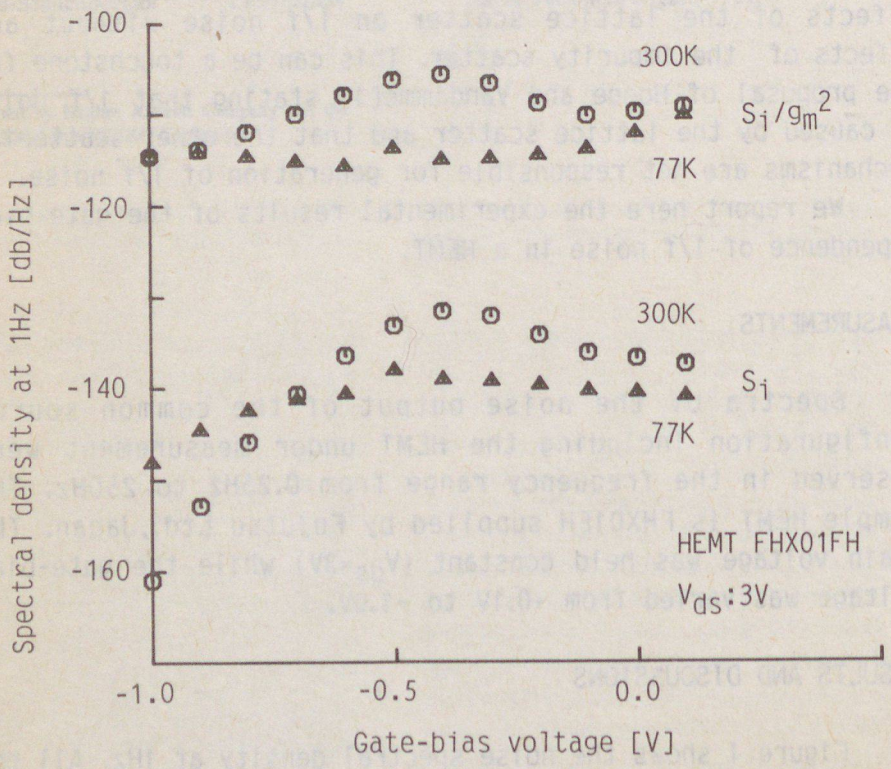

Fig.1 Gate-bias dependence of the noise spectra

Figure 2 shows the relative fluctuation of the drain current S_i/I_d^2 at 1Hz. S_i/I_d^2 at 300K gradually increases with the decrease of the gate-bias voltage above -0.5V, and it is almost constant below -0.5V. This behavior is understood by using a simple model of the conducting channel in the HEMT as follows.

With the decrease of the gate-bias voltage the conducting channel at first becomes narrower until the portion next to the drain electrode reaches its narrowest state, and then the length of this narrowest portion grows towards the source. As a result the drain current decreases monotonically with the decrease of the gate-bias voltage, while the noise current increases at first because of the reduction of the effective volume of noise generation and then it decreases because of the increase of the effective volume. At the gate-bias voltage below -0.8V the contribution of the noise voltage generated at the gate predominates over the contribution of the drain current noise. This effect appears at the leftmost part of the plots of S_i/g_m^2. S_i is higher at 77K than at 300K at the gate-bias below -0.7V because g_m is larger at 77K than at 300K, and accordingly the contribution of the noise voltage generated at the gate portion is larger at 77K than at 300K.

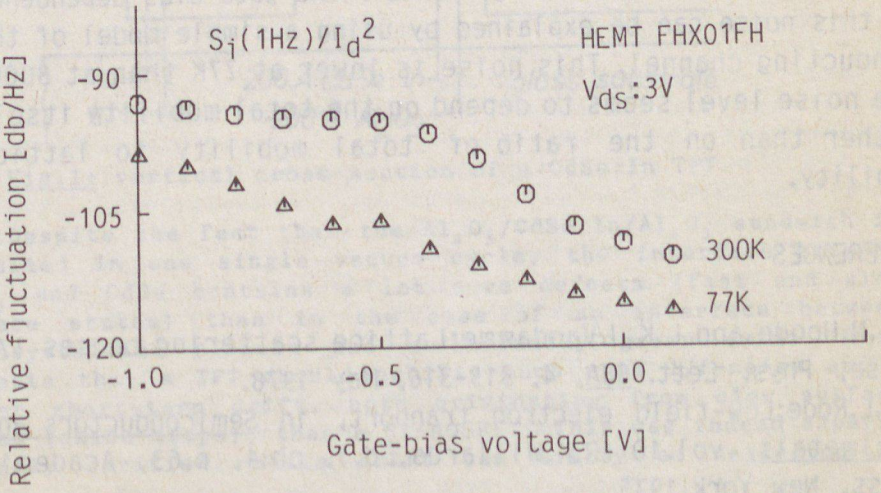

Fig.2 Relative fluctuation of the drain current

The difference between the noise levels at 300K and 77K might be attributed to the difference either in the contact potential or in the carrier mobility. Because of the difference between the contact potential at 77K and at 300K the effective volume responsible for noise generation is larger at 77K than at 300K. The impurity density in the conducting channel is $10^{14}cm^{-3}$. At 300K the lattice scatter predominates over the impurity scatter and the mobility is determined by the lattice scatter[2], while at 77K the impurity scatter cannot be neglected and the mobility is affected by the impurity scatter.

The difference between the measured noise levels at 77K and at 300K is not inconsistent with the proposal of Hooge and Vandamme stated above, but the fact that the MESFET with a conducting channel doped at $10^{18}cm^{-3}$ generates noise higher by 10db than the HEMT cannot be explained by the proposal. The noise level seems to depend on the magnitude of the total mobility itself rather than on the ratio of total mobility to lattice mobility.

CONCLUSIONS

The noise in HEMTs biased between -0.7V and -0.1V originates in the conducting channel. The gate-bias dependence of this noise can be explained by using a simple model of the conducting channel. This noise is lower at 77K than at 300K. The noise level seems to depend on the total mobility itself rather than on the ratio of total mobility to lattice mobility.

REFERENCES

1)F.N.Hooge and L.K.J.Vandamme;Lattice scattering causes 1/f noise, Phys. Lett. 66A, 4, 315-316, May 1978.

2)D.L.Rode;Low-field electron tranport, in Semiconductors and Semimetals, vol.10 (R.K.Willards,Ed.), ch.1, p.63, Academic Press, New York,1975.

10th Int.Conf. on Noise in Physical Systems
1989 Budapest, Hungary

A CORRELATION BETWEEN 1/f-NOISE AND SHORT-TERM DRIFT IN POLY-CdSe: In THIN FILM TRANSISTORS

J. DOUTRELOIGNE,* J. De BAETS, I. De RYCKE, H. De SMET,**
A. Van CALSTER, J. VANFLETEREN

Laboratory of Electronics, Ghent State University
Sint-Pietersnieuwstraat 41, B-9000 Gent, Belgium

A thin film transistor (TFT) is basically a field effect device, made on a glass substrate by physical vapour deposition, used as pixel transistor in active matrix displays or as active element in integrated display drivers. Its operation is analogous to that of a silicon MOSFET. A vertical cross-section of a TFT, based on the polycrystalline n-type In-doped CdSe semiconductor, is depicted in fig.1.[1]

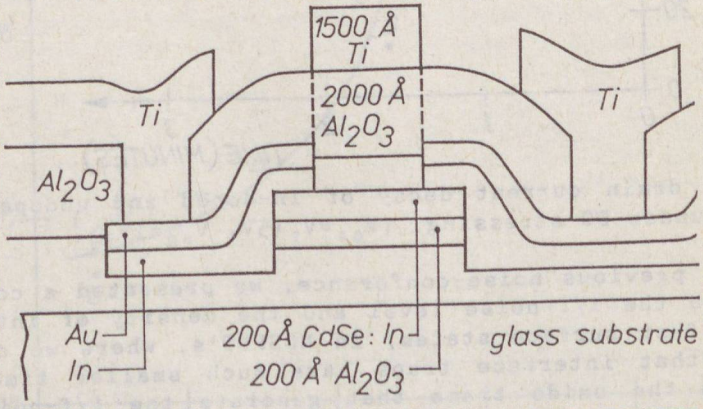

Fig.1: vertical cross-section of a CdSe:In TFT.

Despite the fact that the Al_2O_3/CdSe:In/Al_2O_3 sandwich is deposited in one single vacuum cycle, the interface between Al_2O_3 and CdSe contains a lot more defects (fast and slow surface states) than in the case of an interface between monocrystalline silicon and a thermally grown oxide. This suggests that a TFT should exhibit much more 1/f-noise and a larger short-term drift, both originating from slow surface states (oxide traps), than a Si-MOSFET. This was indeed experimentally verified. While drift can mostly be neglected in

*is supported by the NFWO. **is supported by the IWONL

MOSFET's, a drain current decay of more than 40% in 3 minutes was found in some lightly-doped CdSe:In TFT's. The spectral density of the equivalent input noise voltage was 2 to 5 orders of magnitude larger for TFT's than for Si-MOSFET's. It should be noted, however, that more heavily-doped CdSe:In TFT's (0.8 Å In) are considerably more stable than the lightly-doped ones, having a short-term drift as low as 4% in 3 minutes, which is extremely good compared to other TFT types. An example of experimentally obtained drift curves is given in fig.2.

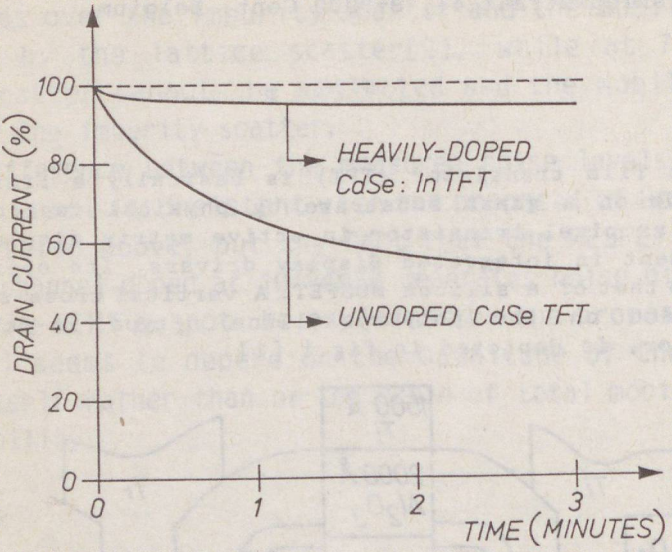

Fig.2: drain current decay of In-doped and undoped CdSe TFT's under DC stressing. ($V_{GS}=V_T+5V$, $V_{DS}=1V$)

At the previous noise-conference, we presented a correlation between the 1/f-noise level and the density of interface traps N_{it} (fast surface states) in MOSFET's, where we clearly underlined that interface traps have much smaller time constants than the oxide traps that generate the 1/f-noise.[2] In the present paper, we want to examine a potential correlation between the 1/f-noise level and the short-term DC drift of a CdSe:In TFT. It should be clear that the time constants of the oxide traps that cause the drain current decay (measured during 3 minutes) are larger than those of the oxide traps that generate the 1/f-noise (measured at 5 Hz). Therefore, such a correlation is far from obvious. The experimental results are shown in fig.3. The horizontal axis represents the short-term drift of the ON-current under DC stressing. During 3 minutes, a DC voltage $V_{GS}=V_T+5V$ was applied while the drain voltage was kept at $V_{DS}=1V$. The drain current decay during these 3 minutes was determined. The 1/f-noise level was measured, using the experimental set-up shown in fig.4 [2,3], at $V_{DS}=10V$, $V_{GS}=V_T+2V$ and f=5Hz, and was normalized as follows:

$$\overline{v_i^2} = \frac{C}{f \cdot W \cdot L}$$

where C is the normalized noise level, $\overline{v_i^2}$ the equivalent input noise voltage spectral density, W the channel width and L the channel length. Fig.3 clearly indicates that the measured data corresponding to samples, processed in the very same run (samples A,B,C,D), indeed obey a direct correlation between the 1/f-noise level and the drift, which means that the densities

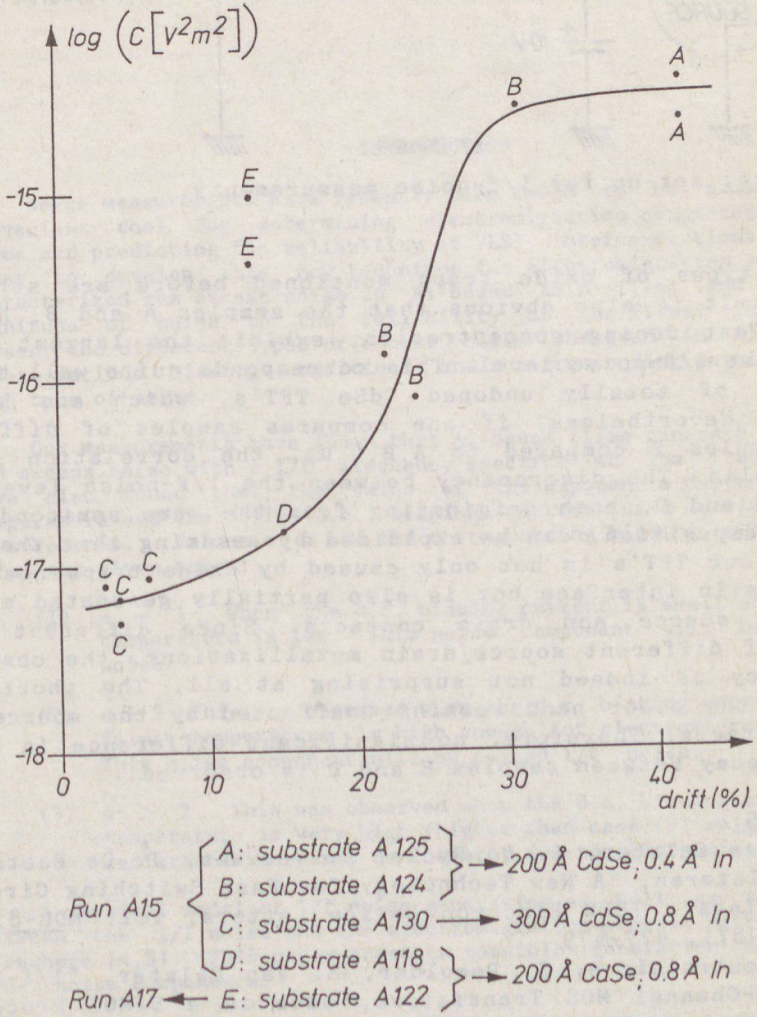

Fig.3: normalized equivalent input noise voltage spectral density ($V_{GS}=V_T+2V$, $V_{DS}=10V$, f=5Hz) vs. the short-term DC drift ($V_{DS}=1V$, $V_{GS}=V_T+5V$ during 3 minutes) of a CdSe:In TFT.

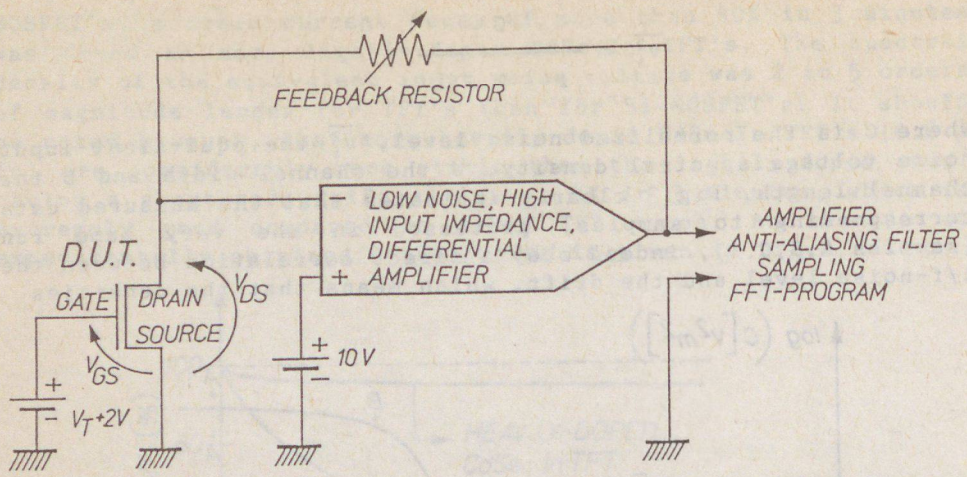

Fig.4: set-up for 1/f-noise measurements.

of both types of oxide traps mentioned before are strongly related. It is also obvious that the samples A and B, having the smallest doping concentration, exhibit the largest drift and highest 1/f-noise level. This corresponds quite well to the situation of totally undoped CdSe TFT's, which are highly unstable. Nevertheless, if one compares samples of different runs (samples E compared to A,B,C,D), the correlation is no longer valid. The discrepancy between the 1/f-noise levels of samples E and D, both originating from the same semiconductor sandwich deposition, can be explained by assuming that the 1/f-noise in our TFT's is not only caused by oxide traps near the Al_2O_3/CdSe:In interface but is also partially generated at the CdSe/InAu source and drain contacts. Since different runs consist of different source/drain metallizations, the observed discrepancy is indeed not surprising at all. The short-term drift on the other hand remains unaffected by the source and drain contacts. Therefore, no significant difference in drain current decay between samples E and D is observed.

REFERENCES:

[1] A. Van Calster, I. De Rycke, A. Vervaet, J. De Baets, J. Vanfleteren, "A New Technology for Fast Switching Circuits on Glass", IEEE Electron Device Letters, vol. EDL-8, No. 10(1987), 477-479

[2] J. Doutreloigne, S. Demolder, A. Van Calster, "1/f-Noise in P-Channel MOS Transistors, made in a BIMOS Process", Proceedings 9th Int. Conf. on Noise in Physical Systems (1987), 461-464

[3] S. Demolder, M. Vandendriessche, A. Van Calster, "The Measuring of 1/f-Noise of Thick and Thin Film Resistors", J. Phys. Sci. Instr. vol.13(1980), 1323-1327

10th Int.Conf. on Noise in Physical Systems
1989 Budapest, Hungary

ELECTROMIGRATION AND $1/f^{\alpha}$ NOISE IN Al-BASED THIN FILMS*

T.M. CHEN, P. FANG, J.G. COTTLE

Department of Electrical Engineering,
University of South Florida
Tampa, Florida 33620, USA

INTRODUCTION

Noise measurements have recently been found to be a sensitive and convenient tool for determining electromigration parameters of Al-based films and predicting the reliability of VLSI interconnections [1-3]. In order to develop this new technique for electromigration study, we have characterized the excess noise in Al-based thin films and related the magnitude of noise to the reliability of the films. This paper will present the different types of excess noise observed in Al-based films under various biasing conditions and a corresponding physical model for each type of noise.

Our measurements have shown that Al-based films generate thermal noise and excess noise with a $1/f^{\alpha}$ frequency spectrum at low frequencies. We have also found that the value of the exponent α depends on the film temperature and the film d.c. biasing current used during the noise measurements. Values of α and the corresponding biasing conditions of the films are given below:

(1) $\alpha = 1$ When the d.c. biasing current is small and/or the film temperature is low. This noise component will be called 1/f noise.

(2) $\alpha = 2$ This was observed when the d.c. biasing current and/or the films temperature is high enough for electromigration to occur. This noise component will be called $1/f^2$ noise.

(3) $\alpha > 2$ This was observed when the d.c. biasing and/or the film temperature is very high (higher than case (2) so that the film resistance increases nonlinearly due to electromigration.

A physical model of 1/f noise generation as well as a relationship between the 1/f noise and the electromigration process have been reported elsewhere [4,5]. This paper presents possible generation models of the other noise components.

* This work was supported by SRC Contract # 89-SJ-124 and DARPA Grant # MDA 972-88-J-1006.

$1/f^2$ NOISE DUE TO THE VACANCY FLUCTUATION OF VACANCY DIFFUSION

We have shown experimentally that the magnitude of the $1/f^2$ noise and the electromigration rate of the Al-films have a similar temperature and current density dependence. In addition, the activation energy determined from the $1/f^2$ noise measurements often has a value close to the grain boundary activation energy, E_a, of the film. Based on these facts, we have developed a physical model of the $1/f^2$ noise generation associated with the grain boundary electromigration process of the film as follows:

Let us consider a small volume of grain near a grain boundary in a film. Let n_s be the total number of vacancies contained in the grain under a unit surface area on the grain boundary. Since most of the vacancies in a grain are contained in the region close to the grain boundary, n_s, mainly includes vacancies in the volume only several atomic distances under the grain boundary. The vacancy density changes from the grain boundary into (or out of) the grain. The vacancy flux associated with this diffusion process can be expressed as

$$J_v = \frac{dn_s}{dt} = J_{vo} + H(t) \tag{1}$$

where J_{vo} is the average value of the vacancy flux, H(t) represents fluctuation of the vacancy flux around its average value. The total number of vacancies in the grain per unit surface area at the grain boundary is

$$n_s = (J_{vo}t + A_o) + \delta n_s(t) \tag{2}$$

where A_o is the initial value of n_s at t=0, $\delta n_s(t)$ represents the fluctuations of n_s around its average linear rate of increase and

$$\frac{d}{dt}\,\delta n_s(t) = H(t) \tag{3}$$

Solving Eq. (3) by standard method [6], one can easily prove that the spectral density of n_s, $S_{ns}(f)$ is related to the spectral density of H(t), $S_H(t)$, by

$$S_{ns}(f) = \frac{S_H(f)}{\omega^2} = \frac{S_H(o)}{\omega^2} = \frac{2J_{vo}}{\omega^2} \tag{4}$$

Since H(t) is a white noise source, $S_H(f) = S_H(o)$. Here we assume that H(t) has a shot noise fluctuation, thus $S_H(o) = 2J_{vo}$.

Eqs (1) and (2) give $$\frac{dn_s}{dt} = J_{vo} + \frac{d}{dt}\,\delta n_s(t) = J_{vo} + H(t) \tag{5}$$

The first term of this equation represents the average flux of vacancies flowing through a grain boundary and the second term represents the fluctuation of the vacancy flux which has a shot noise fluctuation. If we divide the grain boundary in a sample into a large number of small boundary elements, the fluctuations of the rate of vacancies flowing through each boundary element are expected to be independent. Therefore each small boundary element should have a positive contribution to $S_{\delta ns}(f)$. On the other hand, J_{vo} in Eq. (5) represents the average vacancy flux density flowing through a grain boundary element. Since vacancies flow into grains (positive J_{vo}) through some grain boundaries but out of grains (negative J_{vo}) through other grain boundaries, the average value of the vacancy flux density over all the grain boundaries (to be represented by Q) should be much less than the magnitude of J_{vo}; that is

$$Q = \frac{1}{M\Delta S}\sum_{i=1}^{M} J_{voi}\Delta S << \frac{1M}{M1}\sum_{i=1}^{M}|J_{voi}| \tag{6}$$

where M represents the total number of grain boundary elements of area ΔS in the sample and J_{voi} is the density of vacancy flux flowing through the ith element. As will be explained later that ($J_{vo}t + A$) term in Eq. (2) will result in a resistance change of the film. From the above analysis one can see that a large fluctuation of vacancy flux, $S_{\delta ns}(f)$ could exist before a significant resistance change is noted during the noise measurement process. Thus

$$S_{ns}(f) \doteq S_{\delta ns}(f) = \frac{2J_{vo}}{\omega^2} = \frac{2J}{\omega^2} \tag{7}$$

since the vacancy flux J_{vo} and the ion flux J have the same magnitude. To relate vacancy scattering to noise, a convenient parameter to be used in equation is the density of vacancies, n, inside the grain. n is much smaller than the density, n_s, of vacancies under a unit surface area since most vacancies are located near the surface. Hence, one may write $n = \alpha n_s$ where α is a constant much less than unity. Consequently

$$S_n(f) = \alpha^2 S_{ns}(f) = \frac{2\alpha^2 J}{\omega^2} \tag{8}$$

The ion flux J associated with electromigration has an expression [7]

$$J = N_a Z^* e \ell j \left[\frac{D_o}{k_B T}\right] \exp\left[\frac{-Ea}{k_B T}\right] \tag{9}$$

where N_a is the atomic concentration, Z^*e is the ion effective charge, D_o the infinite temperature diffusion coefficient, E_a the activation energy, ℓ the resistivity of the metal and j is the current density. Thus

$$S_n(f) = \frac{2\alpha^2 N_a Z^* e \ell j}{\omega^2}\left[\frac{D_o}{k_B T}\right] \exp\left[\frac{-Ea}{k_B T}\right] \tag{10}$$

To give the relation between $S_n(f)$ and the current fluctuation in a metal film, the current, I, in the metal film of length L_1 is related to the electron mobility, μ, by

$$I = q\mu N_e \frac{V}{L_1^2} \tag{11}$$

where q is electron charge, V is the dc voltage to the sample and N_e is the total number of electrons in the sample. A fluctuation of mobility will cause a corresponding fluctuation in current. The electron mobility will cause a corresponding fluctuation in current. The electron mobility μ is related to the mobility μ_v due to scattering by vacancies and the mobility μ_e due to all other scattering processes by

$$\frac{1}{\mu} = \frac{1}{\mu_e} + \frac{1}{\mu_v} \tag{12}$$

Let us examine the effect due to fluctuation of μ_v by ignoring the fluctuations of μ_e. If the vacancies scatter independently, $1/\mu_v = cn$ where c is a constant, then

$$\Delta\mu = -\frac{\mu^2}{\mu_v n}\Delta n = -c\mu^2\Delta n \tag{13}$$

This mobility fluctuation will give rise to a current fluctuation

$$\Delta I = - \frac{qcVN_e\mu^2}{L_1^2} \Delta n \qquad (14)$$

The spectral density of the current fluctuation is therefore

$$S_I(f) = \left[\frac{qcN_e\mu^2 V}{L_1^2}\right]^2 S_n(f) \qquad (15)$$

The voltage fluctuation across the film can be represented by

$$S_v(f) = R^2 S_I(f) \qquad (16)$$

Combining Eqs (10), (15) and (16), one can obtain

$$S_v(f) = \frac{Aj^3}{Tf^2} \exp\left[-\frac{Ea}{k_B T}\right] \qquad (17)$$

where A is a constant for a given film. Eq. (17) clearly shows that $S_v(f)$ is proportional to $\exp[-Ea/k_BT]$ and has a $1/f^2$ frequency dependence as was found experimentally [3].

We now turn to the effect of resistance drift on $S_v(f)$. The $J_{vp}t$ term in Eq. (2) will give rise to an increase of the film resistance when the biasing parameters are such that the film resistance exhibits a change during noise measurements. One can show that the resistance drift will cause $S_v(f)$ to be proportional to $\exp[-2Ea/k_BT]$. If the resistance increases linearly, one will again see $S_v(f)$ has $1/f^2$ frequency dependence. However if $R(t)$ increases nonlinearly, a similar analysis can show that $S_v(f)$ has $1/f^\alpha$ components with $\alpha > 2$. Due to the page limitations, the detailed analysis of the effect of resistance drift on $S_v(f)$ will be presented elsewhere.

REFERENCES

(1) J. G. Cottle and T. M. Chen, "Characterization of Excess Noise in VLSI Interconnects", Proc. IEEE 1987 Southeastcon., Vol. 1, pp. 166-170, Tampa, Fl. (1987).

(2) B. Neri, A. Diligenti and P. E. Bagnoli, IEEE Trans. on Electron Dev., Vol. ED-34, No. 11, 2317 (1987).

(3) J. G. Cottle and T. M. Chen, "Excess Noise and Its Relationship to the Activation Energies Associated with Electromigration in Thin Al and Al-Si Films," Proc. of 4th Int. IEEE VLSI Multilevel Interconnection Conference, pp. 449-455, Santa Clara, Ca. (1987).

(4) P. Dutta and P. M. Horn, "Low Frequency Fluctuations in Solids: 1/f noise", Rev. Mod. Phys., 53, 3 (1981).

(5) R. H. Koch, J. R. Lloyd and J. Cronin, "1/f Noise and Grain Boundary Diffusion in Aluminum and Aluminum Alloys", Phys. Rev. Lett., 55, 22 Nov. (1985).

(6) A. van der Ziel, Noise in Solid State Devices and Circuits, Chapter 2, John Wiley & Sons (1986).

(7) J. R. Black, "Physics of Electromigration", Proc. of 1974 Ann. Symp. Rel. Phys., 142 (1974).

10th Int.Conf. on Noise in Physical Systems
1989 Budapest, Hungary

DETERMINATION OF Al-BASED METAL FILM LIFETIMES USING EXCESS NOISE MEASUREMENTS*

M.I. SUN, J.G. COTTLE, T.M. CHEN

Department of Electrical Engineering,
University of South Florida
Tampa, Florida 33620, USA

INTRODUCTION

Low frequency excess noise measurements have been previously suggested by several researchers as a potential tool for determining metal film quality [1-4]. The same physical processes which have been associated with film damage and failure due to electromigration (EM) also have a profound influence on the magnitude of the excess noise spectrum at frequencies below 10 Hz [2]. It is possible to predict metallization failure in an accelerated EM constant current test by observing noise generated by the film. These predictions may be made with a high degree of confidence if the excess noise with a $1/f^2$ frequency dependence between 1 and 10 Hz is consistently stimulated.

The asymptotic behavior of the excess noise component of the current noise spectrum may be described by $f^{-\alpha}$. For an aluminum or aluminum alloy film with relatively small film current densities ($J \leq 10^6$ A/cm^2), and temperatures below 500 K, the slope of the spectrum is $1/f$ and closely follows the thermally activated behavior published by Dutta and Horn [5]. Dutta et al. do not predict a $1/f$ magnitude. Most often however, the microstructural variations in the film cause an additional magnitude above that predicted by Hooge's empirical formula for bulk metals [6].

At current densities and temperatures commonly used for accelerated EM testing, $\alpha \approx 2$. There are several conditions which may produce an erroneous f^{-2} slope to a power spectrum plot. It is important to discriminate between these sources of data corruption and the fluctuations which correlate to film lifetime. Although data trends, d.c. offset and aliasing may cause a f^{-2} spectrum slope, they are not noise signals and perturb the spectrum as deterministic sources, i.e. with distinctively low variance. Large magnitudes of corrupting sources are sufficient to produce a f^{-2} slope, but their presence is not necessary for a thin film to produce a $1/f^2$ noise spectrum. Valdes [7] has recommended steps to eliminate these erroneous f^{-2} sources.

MEASUREMENT METHOD

The magnitude of $1/f^2$ fluctuations and the rate of vacancy flux in an aluminum film due to electromigration are closely related [8]. This is evident in the experimentally observed $1/f^2$ noise behavior as well as the theoretical derivation for the case of a vacancy

*This work is supported by SRC Contract # 89-SJ-124 and DARPA Grant # MDA 972-88-J-1006

density fluctuation suggested by Chen et al. [9].

$$S_v(f) = \frac{A_n j_n^3}{T_n f^2} \exp\left(\frac{-E_a}{k_B T_n}\right) \tag{1}$$

where the observed values of E_a are closely similar to those in the literature determined from median time to failure (MTF) testing. It is possible therefore to predict a film's lifetime, T_f, if the lifetime is proportional to the inverse of the vacancy flux. This is a deterministic form of the MTF statistical expression.

$$\begin{aligned} T_f &\propto T j^{-n} \exp\left(\frac{E_a}{k_B T_A}\right) \\ &= K_A T_A j^{-n} \exp\left(\frac{E_a}{k_B T_A}\right) \end{aligned} \tag{2}$$

Combining equations (1) and (2), the log failure time may be expressed as follows.

$$\log T_f = b_1 \log S_v + c_1 = b_1 \log \overline{e_n}^2 + a_1 \tag{3}$$

$$b_1 = \frac{-T_n}{T_A} \tag{4}$$

$$a_1 = \log(K_A T_A j_A^{-n}) - \frac{T_n}{T_A} \log\left(\frac{f^2 T_n}{A_n j_n^3}\right) \tag{5}$$

$$\overline{e_n}^2 = \int_{f_1}^{f_2} S_v(f) df = S_v(f_1)\left[f_1\left(1 - \frac{f_1}{f_2}\right)\right] \tag{6}$$

and the subscripts n and A represent quantities taken from the noise measurement and accelerated tests, respectively.

Current densities and temperatures which stimulate $1/f^2$ noise are often the same order of magnitude as those used in accelerated testing. The noise measurement period however, is usually much shorter in duration. Small amounts of resistance drift however, may be encountered during the noise measurement period. When there is a quasi-linear trend comparable to the vacancy-flux noise, the activation energy value will be twice that expected for grain boundary vacancy flux, $2E_a$ [9]. The assumption of a quasi-linear drift in the presence of the vacancy flux leads to

$$S_v(f) = \frac{A_2 j_n^4}{T_n^2 f^2} \exp\left(\frac{-2E_a}{k_B T_n}\right) \tag{7}$$

which when combined with equation (2) yields a log failure time expresssion

$$\log T_f = b_2 \log S_v + c_2 = b_2 \log \overline{e_n}^2 + a_2 \tag{8}$$

$$b_2 = \frac{-1}{2}\frac{T_n}{T_A} = \frac{b_1}{2} \tag{9}$$

$$c_2 = \log(K_A T_A j_A^{-n}) - \frac{T_n}{2T_A} \log\left(\frac{f^2 T_n}{A_2 j_n^4}\right) \tag{10}$$

$$a_2 = c_2 - \frac{T_n}{2T_A} \log f_1 \left(1 - \frac{f_1}{f_2}\right) \tag{11}$$

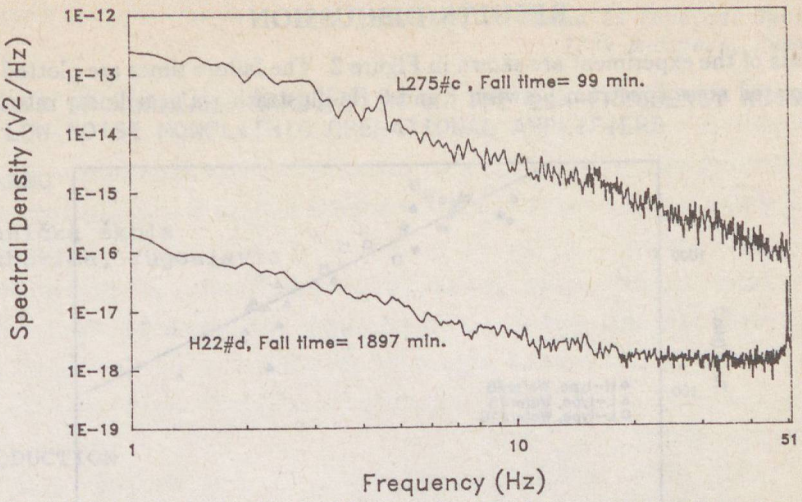

Figure 1: Typical noise spectra for two different main film groups.

If the noise to failure time relationship is fit to a general statistical expression of the form $\log T_f = a + b \log \overline{e_n}^2$, the confidence in using noise measurements as a thin film failure predictor may be experimentally investigated. The above development predicts that $b = -T_n/T_A$ if the $1/f^2$ noise is primarily due to vacancy density fluctuations and $b = \frac{1}{2}(-T_n/T_A)$ if resistance drift is responsible for the $1/f^2$ noise. T_n and T_A refer to the film temperature for the noise measurement and accelerated test, respectively.

EXPERIMENTAL PROCEDURE

Two sets of films were fabricated of pure aluminum(99.99%) sputtered on 10000Åof SiO_2 with different substrate temperatures. These are designated **L-type** and **H-type** corresponding to 125°C and 250°C, respectively. The test structures were $2\mu m \times 0.8\mu m \times 1250\mu m$ with die packaged in a 24-pin dual in-line (DIP) package. TCR measurements for the L and H types yielded average values of 4059 and 3927 ppm/°C, respectively. TEM analysis showed that the two groups of films had different grain sizes and distribution, thereby providing an intentional variation in their expected lifetimes.

Noise measurements were performed at a current density of 1.9×10^6 A/cm^2 and a package temperature of 493K. I^2R heat generated by the bias current was measured and found to be 12K above the package temperature ($T_n = 505$K). All spectral slope values for the 36 samples were observed to be approximately $\alpha = 2.0 \pm 0.3$ for the duration of the noise measurement (≈ 4 min.). The magnitude of the spectrum for the films varied several orders of magnitude at 1 Hz. This variation is illustrated in Figure 1.

Following the noise measurements, the films were stressed to failure using a constant current, accelerated EM test. The test current density and ambient temperature were $j_A = 1.25 \times 10^6$A/cm^2 and $T_{ambient} = 426$K, respectively. It was found that the amount of I^2R heat at this current density was negligible ($T_A \approx T_{ambient}$). At these test parameters, the lifetime of the films varied from 99 to 3575 minutes.

RESULTS/DISCUSSION

The results of the experiment are shown in Figure 2. The failure times are plotted versus the integrated noise spectrum between 1 and 6 Hz illustrating a near linear relationship

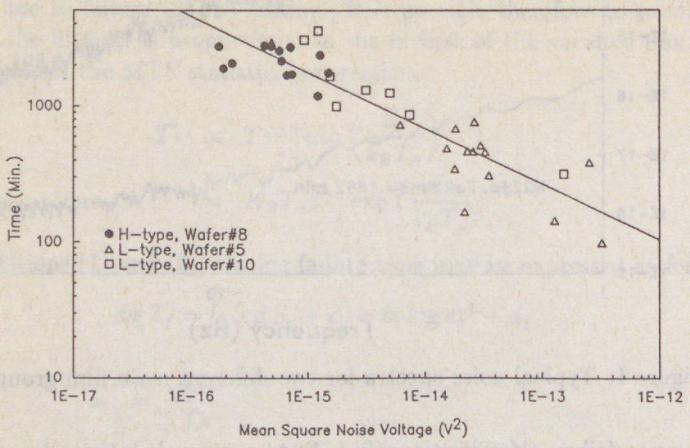

Figure 2: Film time to failure versus pre-test mean squared $1/f^2$ noise voltage

for the measurement parameters used. For this set of films and measurement parameters, the line drawn in the figure describes 83.4% of the correlated data indicating that the $1/f^2$ noise measurements were an accurate predictor of individual failure times. The line corresponds to a regression model of $\log T_f = a + b \log \overline{e_n}^2$ with $a = -2.902$ and $b = -0.410$. The value of b indicates that this $1/f^2$ noise data was predominantly the vacancy fluctuation superimposed on a small drift component.

In addition to discriminating a poor film (L-type) from a better fabricated one (H-type), the noise measurements were also useful in predicting the reliability differences in two wafers fabricated in the same group.

REFERENCES

1. J. L. Vossen, Appl. Phys. Lett., **23**, pp.287-289 (1973).
2. T. M. Chen, T. P. Djeu and R. D. Moore, Proc. of 23rd Intl. Rel. Phys. Symp. (1985).
3. R. H. Koch, J. R. Lloyd and J. Cronin, Phys. Rev. Lett., **55**, pp.2487-90 (1985).
4. A. Diligenti, et. al., Elec. Dev. Lett., **EDL-6**, pp.606-608, (1985).
5. P. Dutta and P. M. Horn, Rev. Mod. Phys., **53**, pp.497-516 (1981).
6. F. N. Hooge, Phys. Lett., **29A**, pp.139-140 (1969).
7. J. Valdes, 1st Intl. Symp. on Meas. of Elec. Quant., Como, Italy June 19-21, 1986.
8. J. G. Cottle and T. M. Chen, J. Elec. Matls., **17**, no. 5, pp.467-471 (1988).
9. T. M. Chen, P. Fang and J. G. Cottle, 10th Intl. Conf. on Noise in Phys. Sys. (this conference), Budapest, Aug.21-25, 1989.

10th Int.Conf. on Noise in Physical Systems
1989 Budapest, Hungary

THE EFFECTS OF NUCLEAR IRRADIATION ON THE LOW-FREQUENCY NOISE OF SOME LOW NOISE MONOLITHIC OPERATIONAL AMPLIFIERS

I. ŠOŠTAREC

Viša tehnička škola
24000 Subotica, Yugoslavia

1. INTRODUCTION

The topic of this work belongs to a large multidimensional field, which lies on the boundary between irradiation (IR) effects and noise (N). Knowing the great research efforts and hundreds of published articles every year in each of the mentioned ranges it is surprising that in the IR-N field only few articles have been published (in the open literature) since 1963 when I began my work in this field (1). The field has many important implications as follows:

- Noise is limiting parameter in many electronic circuits at nuclear power plants, accelerators, space vehicles, which are steadily exposed to irradiations.
- The noises caused by atomic explosions.
- The effects of ion implantations on the noise of fabricated devices and the annealing techniques used to cancel them.

It would be of great importance to investigate the noise thoroughly in all electronic devices exposed to various irradiations of various energies, doses and dose rates. The collection of a large amount of reliable data could lead us to laws which connect the noise and irradiation parameters. In this way predictions could be done about the behaviour of devices in various IR fields, and new hardened devices could be developed.

Low noise OP-s which benefit the recent clean MOS technologies are very convenient experimental devices as they can be free from pseudonoise (2).

In my research I tried to get answers to the following questions:

- At which threshold level of irradiation is excess noise noticeable?
- Is there a dose rate effect in γ irradiation?
- What is the efficiency of mixed (γ after neutron) irradiation?
- How do the noise parameters change with received dose?
- What is the relative efficiency of neutron vs. γ irradiation at different types of OP-s?

2. EXPERIMENTAL

The measurements were carried out on the following operational amplifiers (OP): AD OP-07EH/1-7; PMI OP-27EJH/1-10; *PMI OP-37EJH/1-10; *AD 517KH/1-6; FμA 725HC/1-11. They all are in metal TO99 encapsulation with 8 leads. The irradiation of OP-s was performed in three steps at the Institute "RUDJER BOŠKOVIĆ" in Zagreb. There is a neutron-generator which gives 14.6 MeV monoenergetic neutrons from a D-T reaction and two Co^{60} facilities (one with nominal 300 Gy(30 kRad)/h(Low) and the other with 3 kGy/h(High) dose rate).

At the first step the OP-s with the lowest noise were irradiated to $5x10^{9}n/cm^{2}$ (07/2, 27/8, 37/8, 517/5, 725/8) and three others (27/4, 27/9, 37/4) to $10^{11}n/cm^{2}$. At the second step 07/1, 07/7, 25/5, 27/7, 27/10, 37/1, 37/7, 517/2, 517/6, 725/4 and 725/II got $5x10^{11}n/cm^{2}$ and 27/3, 37/3, 37/6 received 400 Gy (slow rate). At the third step 27/1, 37/10 and 517/1 obtained 124.4 Gy (slow); 07/5, 517/3, received 400 Gy (slow); 07/6, 517/4, 517/5, 725/1, 725/3 got 400 Gy (fast); 27/3 and 37/3 1.2 kGy (fast); 27/9, 725/6, 725/8 $5x10^{11}n/cm^{2}$ and 07/1, 27/7, 27/10, 37/1, 37/10, 517/6, 725/4 received additional $15x10^{11}n/cm^{2}$.

The 07/3, 07/4, 27/6, 37/2, 725/5, 725/7, 725/9 devices were rejected due to their instable behaviour or burst noise. The other devices which were not irradiated served for checking

*Gift of the Precision Monolithics Inc.

the stability of the measurement setup and reproducibility of the results.

During all irradiations the OP-s were placed on styropore boards their leads shorted with thin copper wire. The neutron doses were measured with an α-counter and amplitude analyser and the peaks in energy spectrum were integrated with a computer. The possible sources of error were carefully analysed and we believe that in the worst case error in neutron dose estimation has been within 15%. The situation in γ-dose estimation is not so clear since it had been done in kRads and the real energy deposition from Compton electrons in Si, SiO_2 has not yet been known.

On all devices U_o, dU_o/dT; $\pm I_{in}$, A_o, CMRR, PSRR and $\pm I_{supply}$ were measured with a Tektronix 577/178 L.I.C. parameter analyser. We used the storage capability of this instrument to check carefully (at least 0.5 hour each) the devices to be free from burst noise and instable behaviour. As only permanent effects of irradiation were investigated, the devices rested at least 30 days after irradiation, and the measurements followed afterwards.

The noise voltage and current were measured in Budapest at the Department of Prof. Ambrózy. The measurement setup and the problems connected with reliable low-frequency noise measurements are described in detail elsewhere (3, 4, 5). I will give a short explanation here. The first measurements on unirradiated devices were carried out with two self-made preamplifiers from which the first one used the device under test (DUT). After the first irradiation the second amplifier was not used any more, thus the early noise spectra at higher frequencies have additional uncertainties. The transfer function of the first amplifier with the DUT was measured with a Hewlett-Packard noise generator (NG) HO1-3722 A, a 100 kΩ: 100 Ω divider and the digital analyser (DA) 2131 from Brüel and Kjaer. The analyser itself was also calibrated with the NG after averaging 96 spectra, each of 128 s duration. The analyser had 0.1 dB resolution and 42 frequency channels from 1.6 Hz to 20 kHz in logarithmic order. The calibration constants have a statistical uncertainty ranging from 0.57 dB at 1.6 Hz to 0.11 dB

at 40 Hz. The noise spectra of devices were measured 4 times each of 512 s duration. After that AVG and STD were calculated. All in all some 450 such averaged spectra were collected during a period of 14 months. From the raw data the noise voltage and current spectra were carefully calculated and yielded the excess noise spectra above plateau level and the excess noise spectra introduced by irradiation. The results are graphically presented on 55 cm x 37 cm mm paper sheets so the fine details can be recognized. Until now more work on numerical evaluation of fine details have not been carried out. Annealing experiments have been also done at 120°C on a limited number of devices.

3. MAIN RESULTS

At this place I shall present some selected results from the large amount of collected data.

The effects of $5x10^{9}n/cm^{2}$ IR were within experimental uncertainties at 27/8, 37/8 and 07/2 OP-s. At 725/8 the excess noise current density(ENCD)introduced was 31% at 2 Hz and 40% at 10 Hz from the initial value. In noise voltage density (NVD) there was no measurable effect. Contrary to this, at 517/5 NVD increased 1.8 dB at 2 Hz and 1.4 dB at 10 Hz and the ENVD was 71% and 62% of the initial value (at 2 Hz and 10 Hz). In NCD of 517/5 there was no measurable effect.

The $10^{11}n/cm^{2}$ dose gave noticeable effects in the NCD of 27/4, 27/9 and 37/4. The NCD increased 2.5 dB, 1.61 and 1.54 dB at 2 Hz and 3.3, 1.97 and 1.45 dB at 10 Hz. The respective ENCD values were 0.878; 0.775; 0.652 times at 2 Hz and 1.068; 0.872; 0.63 times at 10 Hz of the initial value. The NVD-s increased only 0.388; 0.495 times at 2 Hz and 0.187; 0.364 at 10 Hz for 27/4 and 37/4. At $5x10^{11}n/cm^{2}$ there were very pronounced effects at all devices. The ENCD-s at devices of the same type were very close to each other. For example for 27/5, 27/7 and 27/10 ENCD was 12.97; 12.1; 12.14 $pA/Hz^{0.5}$ at 2 Hz and 6.05; 5.63; 5.62 $pA/Hz^{0.5}$.

At the left side of Table 1 the initial values of NCD, then the excess NCD introduced by $5x10^{11}n/cm^{2}$ and at 27/7, 27/10,

TABLE 1

	$5 \cdot 10^{11}$ n/cm^2							400Gy(low dose rate)					
	$(NCD)_o$ (pA/$\sqrt{Hz}$)		ENCD (pA/$\sqrt{Hz}$)		ENCD/$(NCD)_o$			$(NCD)_o$ (pA/$\sqrt{Hz}$)		ENCD (pA/$\sqrt{Hz}$)		ENCD/$(NCD)_o$	
	2Hz	10Hz	2Hz	10Hz	2Hz	10Hz		2Hz	10Hz	2Hz	10Hz	2Hz	10Hz
27/5	4.68	2.0	12.97	6.07	2.77	3.03	27/3	4.96	2.23	9.51	3.97	1.92	1.78
27/7	6.36	2.54	12.1	5.63	1.9	2.21				11.23	4.75	2.26	2.13
			31.06	12.8	4.89	1.98	37/3	11.8	5.12	32.86	13.45	2.93	2.63
27/10	4.89	1.98	12.14	5.62	2.48	2.84				26.38	10.19	2.36	2.13
			19.73	9.68	4.03	4.88	37/6	11.3	5.07	38.03	12.17	3.36	2.4
37/1	10.7	5.05	26.35	10.4	2.46	4.06	07/5	1.59	.677	1.98	.835	1.3	1.33
			56.24	23.9	5.26	4.73	517/3	.328	.152	.86	.385	2.61	2.53
37/7	11.4	4.9	27.01	10.3	2.38	2.1				400Gy(high dose rate)			
07/1	1.59	.67	3.67	1.64	2.31	2.45	07/6	1.99	.757	1.18	.564	.59	.745
			5.31	2.58	3.84	3.86	517/4	.175	.041	.107	.038	.61	.94
07/7	1.38	.54	3.37	1.52	2.45	2.84	517/5	.143	.073	.32	.123	2.11	1.69
517/2	.13	.034	.43	.198	3.31	5.89	725/1	1.68	.634	4.53	1.81	2.7	2.86
517/6	.205	.096	.456	.314	2.22	2.23	725/3	2.06	.653	4.15	1.72	2.02	2.63
			.541	.245	2.64	2.55							
725/II	2.75	1.08	28.22	12.8	10.2	11.9							
725/6	.589	.221	5.75	2.75	9.77	12.4							
725/8	.9	.34	5.37	2.48	5.97	7.28							

37/1, 07/1, 517/6 ENCD values from additional 15×10^{11} n/cm^2 are given. The effects are not linear with dose, and β in $1/f^{\beta}$ (at least in this limited part of spectrum) with a few exception goes lower as we can see from the fourth column. At the right side of Table 1 results after 400 Gy (low and high dose rate) and for additional irradiation with 1.2 Gy (high dose rate!) the 27/3 and 37/3 samples are given. The effects at low dose rates are substantially higher than at the high dose rate with the exception of 517/5 which was preirradiated with 5×10^9 n/cm^2 and the old 725 series which was highly vulnerable also at neutron irradiation. A table similar to Table 1 was also prepared for NVD and ENVD after twofold correction. The correlation resistance R_C calculated as ENVD/ENCD steadily decreases at all devices tending to R_B of input bipolar transistors at 27/37 series. That means also that irradiation effects in NDV in 27/37 series are not so pronounced as in NCD. The results

mentioned above were selected at 2 Hz and 10 Hz as characteristic frequencies. The whole spectra (42 values which were shown at the Conference) give naturally more information and provide the possibility to extract data about β in $1/f^{\beta}$, G-R noise, 1/f corner frequency, etc.

4. CONCLUSIONS

1. Until now the changes in low frequency (excess) noise parameters of electronic devices due to irradiation have not been predictable.

2. The IR-N field is only slightly explored. A thorough investigation would be of great importance. An appeal is given now to do so.

3. The effects of $5x10^{9} n/cm^{2}$ are clearly visible at 517 series (which has very high correlation resistance (1 MΩ)) in NVD and at 725 series in LF NCD.

4. There are pronounced dose rate effects; low dose rate being more effective.

5. The preirradiation with $5x10^{9} n/cm^{2}$ greatly enhanced the effect of high dose rate gammas.

6. The changes in NCD although very close for the same type and dose, considerably differ from type to type, the old 725 series being the most vulnerable. The change of NCD is sublinear with the received dose in all devices.

7. Concerning NCD at 27, 07 and 725 series $5x10^{11} n/cm^{2}$ are more efficient than 400 Gy (low dose rate) but at 37 series 400 Gy is somewhat more efficient.

ACKNOWLEDGMENT

I am greatly indebted to Prof. Dr. A. Ambrózy, head of the Department of Electronics Technology, Technical University Budapest, for his great help in my work. The stimulating discussions with him helped me to clarify many undefined problems. He placed also at my disposal his laboratory of noise measurements, and his rich collection of articles from the whole world.

There were also many people from his Department and from the Institute Rudjer Bošković in Zagreb whose support was of great value for me. For lack of space their names cannot be listed here.

REFERENCES

1. Šoštarec, I., The noise figure of LF transistors after irradiation with 14.6 MeV neutrons. Proc. IXth Conf. ETAN, Bled 1964, pp. 371-377 (in Serbo-Croatian).
2. Šoštarec, I., Pseudonoise in low level DC and VLF measurements. 2nd Symposium of the IMEKO Technical Committee on Metrology-TC8, Theoretical and practical limits of measurement accuracy, Budapest 1983, pp. 249-259.
3. Šoštarec, I., The characteristics of new L.I.C-s (OP-27/37) and their importance in low level measurements. Proc. VIIth Scientific Symposium Kandó Kálmán VMF, Budapest 1982, pp. 203-208 (in Hungarian).
4. Šoštarec, I., About some problems at LF noise measurements on L.I.C-s. Proc. Xth JUKEM Budva 1982, pp. 999-1006 (in Serbo-Croatian).
5. Šoštarec, I., LF. noise of modern monolithic L.I.C-s. Proc. XXVIth Conf. ETAN, Subotica 1982, pp. I. 537-I. 544 (in Serbo-Croatian).

EXCESS NOISE AS AN INDICATOR OF DIGITAL INTEGRATED CIRCUIT RELIABILITY

B.K. JONES, P.C. RUSSELL, Y.Z. XU

University of Lancaster
Lancaster, LA1 4YB, United Kingdom

Abstract

The intensity of excess noise, here 1/f noise, is used as a measure of the 'quality' of a CMOS digital integrated circuit. It is found that this measure correlates well with other electrical measurements of quality.

Introduction

For some applications, such as satellites and submarine cables, it is necessary to use high reliability devices. Such high quality devices are normally produced using a conservative process and by rigorous monitoring during manufacture. Some tests are performed on the finished device. The main test is a functional test, which may be incomplete on a very complex integrated circuit. The present work is a small part of a large study with the aim to devise and assess a series of sensitive electrical tests which could be used on finished devices to assess their quality of manufacture. The challenge was to be able to detect one or more weak devices within a VLSI integrated circuit which would pass a functional test. The assumption is that this would be a test of incipient failure through some failure modes. A full report will be produced elsewhere.

The system used was CMOS digital technology and mainly the 4013 dual flip-flop which is small enough for complete simulation but large enough that there was confidence that the tests could be extrapolated in scale. Even for a special quality device a test needs to take only a short time. There is an inherent conflict between the need to perform a rapid evaluation and the desire to detect the smallest departure from the ideal behaviour. In a large scale integrated circuit there is a problem of scale. If the measurement was of the total circuit properties then very high discrimination would be needed to detect a single weak device but the test would be rapid. If, however, each element of the circuit could be tested separately only low sensitivity is needed but the test would be slow.

In a digital integrated circuit there are few external connections to the large number of devices, these are the input and output terminals and the power supply terminals. There is another problem in digital circuits that a binary circuit is largely self-healing so that a degraded output from one gate is restored to its full level by the next gate so that the degradation is not propagated to the output.

The method adopted in most of the tests to obtain adequate discrimination was to monitor the supply current and subdivide the total circuit into smaller sections by turning parts on or off. There are two approaches: to study the static supply current with different combinations of gates on or off and to study the dynamic supply current as a few of the gates are switched.

The methodology of the study to verify the value of the tests is rather special. A sample of devices were taken and subjected to the tests. They were then subjected to accelerated aging by a dynamic exercise at an elevated temperature. At intervals the devices were retested. A quantity derived from each test was then taken and its variation used as a measure of the departure of the device from its normal conditions. In the study many devices showed degradation but only a small minority failed to pass a functional test.

NOISE EXPERIMENTS

Noise measurements were chosen for some of the tests because excess noise has been shown many times to be large in "poor quality" devices. The generation-recombination noise or 1/f noise has been shown to increase with increases in various defective properties: oxide charge density after hot electron damage, surface state density, deep level and trapping centre density, electromigration damage, low gain, leaking junctions and surface channels.

In the first test the noise in the static leakage current of the device was studied. In a CMOS digital circuit the only current flowing when the gates are fixed in one configuration is the leakage current through the particular junctions which are reverse biased by the power supply. Different junctions are involved in different gate states. A weak junction will then produce a large supply current in those states in which that junction is reverse biased. In one of the tests this was used but the noise in that current was also studied.

For the devices used the current is typically 10^{-10} A and the noise circuit used was a modification of that used by Stocker (1984) and had a noise level corresponding to the shot noise of a current of 8×10^{-12} A (Xu 1986).

Typical results are shown in Figure 1. In Figure 1(a) the noise of a normal device is shown. It has a white spectrum corresponding with the shot noise due to the measured leakage current shown by the solid line. In Figure 1(b) is shown a typical spectrum of a device which has shown abnormal behaviour after stressing. Other properties have changed detectably and the noise also shows a 1/f component in excess of the shot noise. The drop in intensity at very low frequencies is an experimental artifact. There was clear evidence that the excess noise intensity increases with the deterioration of the device as measured by the results on the other tests which increase as the stress continues.

In the second test the circuit is switched between different configurations of the internal gates. As a gate switches a pulse of supply current passes through the gate which is switching. This current thus gives a measure of the conduction properties of that small part of the total device. If it is defective one might expect the current pulse to be noisy.

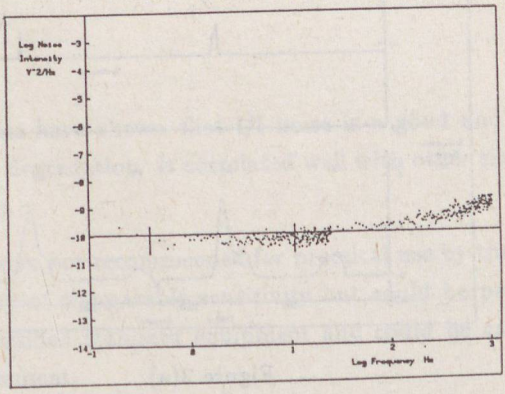

Figure 1(a)

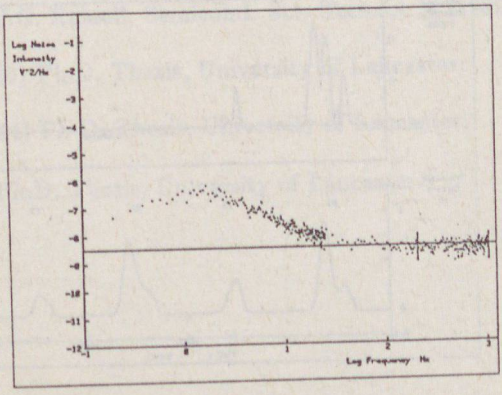

Figure 1(b)

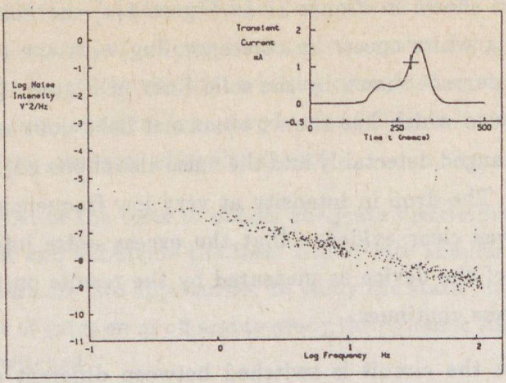

Figure 2

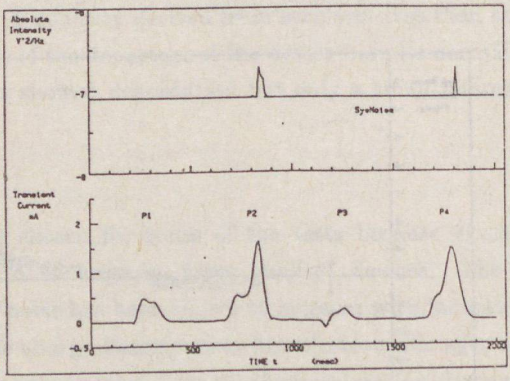

Figure 3(a)

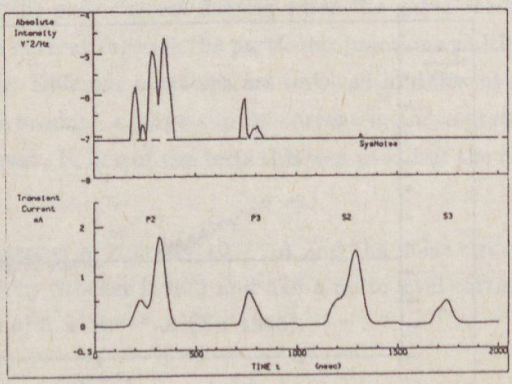

Figure 3(b)

The method used was to investigate the amplitude fluctuation of a current pulse through successive repetitions. This was achieved by using a 10 ns boxcar integrator. The amplitudes were then Fourier analysed. The details are given by Russell (1986), Xu (1986) and Jones and Russell (1989). A typical spectrum for a defective device is shown in Figure 2 together with an inset showing the position on the pulse where the data were taken. The noise shows a clear 1/f spectrum larger than the measurement system noise.

Figure 3 shows the noise intensity at 1 Hz scanned through a cycle of operation of the 4013 flip-flop. The four peaks correspond to different stages of the cycle. The results for a normal device are shown in Figure 3(a) and is only just above the system noise. For the defective device shown in Figure 3(b) noise is shown for only two of the peaks. Inspection of the data reveals that the noise is the differential of the current peaks so that it corresponds to jitter noise due to fluctuations in the internal timing of the circuit. Again correlation was found between the noise test and other measures of the device quality.

CONCLUSIONS

The measurements have shown that 1/f noise is a good and sensitive indicator of device quality or degradation. It correlated well with other similar tests and showed similar sensitivity.

The noise tests were not recommended for practical use by the study since the other tests were usually of comparable sensitivity but could be performed more rapidly, with slightly modified standard equipment and could be carried out in a normal industrial environment.

REFERENCES

B.K. Jones and P.C. Russell, Semicond. Sci. Technol. 4 (1989) 82-6.

P.C. Russell (1986) Ph.D. Thesis, University of Lancaster.

J.D. Stocker (1984) Ph.D. Thesis, University of Lancaster.

Y.Z. Xu (1986) Ph.D. Thesis, University of Lancaster.

10th Int.Conf. on Noise in Physical Systems
1989 Budapest, Hungary

INVESTIGATIONS ON THE NOISE OF POWER SUPPLY CURRENT OF CMOS IC-S

P. BÁNLAKI

Department of Electronics Technology,
Technical University
Goldmann György tér 1-3, H-1521 Budapest, Hungary

INTRODUCTION

In the course of our work for quality and reliability control of CMOS integrated circuits used in some space research projects (VEGA, PHOBOS) we were not quite satisfied with our methods and results. We used screening, burn-in and screening processes in a special way. On the basis of the results we tried to estimate the reliability of some given types. However, we had two problems:

- we had reliability information about a lot of a given type but not about specific ones, but we wanted to use highly reliable concrete ones in space research equipment;
- in some cases we had different types in small quantities because of several reasons. It was not possible to use statistical methods in reliability investigation.

We could find only one solution of our problems in theory by noise measurements. It is well known that there is a connection between the reliability and the noise of devices. We can measure the noise parameters of amplifier-like devices and resistors without any problem. However, the method for noise measurements of inner structures in the case of SSI - MSI - LSI CMOS digital integrated circuits is not so obvious. We find the only possibility to get information about the noise of the inner elements of a complex digital circuit through the power supply current. Investigations on the noise content of the power sup-

ply current of CMOS ICs have many aspects and possibilities, including quiescent state and high-speed working, normal and high temperature, etc. In practice we have done the first steps only.

IMPERFECT PHYSICAL STRUCTURE AND NOISE

A relative high noise level in a device is a result of the imperfect physical structure. The imperfect physical structure may be a result of several effects, one or more from the following:

- some problems in the course of the manufacturing process, in technology;
- some electric influence, for example some kind of
  - electrostatic discharge (ESD),
  - latch-up,
  - overload,
- some non-electric influence, for example some kind of
  - radiation,
  - mechanical shock,
  - overheating.

There are several different types of damage, and each of these tends to be typical of specific component technologies and elements. Immediate failure caused by some exposure is easily determined: the device no longer works properly. There are, however, devices which have been exposed to some specific effect, but which have not immediately failed. Unfortunately, there have never been sufficient data dealing with the long-term reliability of devices which have survived some specific effects. However, it is obvious and a practical experience that there can be significant degradation without immediate failure. Damage can manifest itself in either shortening of the devices lifetime, or in electrical performance shifts, many - but not all - of which cause the device to fail electrical test limits, and in noise level.

To justify our theory and to get numerical results we have planned and have begun executing a method which consists of the following phases:

1. to measure the static and dynamic parameters of devices to be observed,
2. to measure the noise characteristics of the devices,
3. to slightly destroy the devices by some specific effects,
4. to measure again the static and dynamic parameters of the devices,
5. to measure again the noise characteristics of the devices,
6. to use a burn-in process at high temperature,
7. to repeat the whole process again several times.

LATCH-UP EFFECT AND NOISE

In the CMOS digital integrated circuits there are parasitic thyristors at each P and N chanel FET pairs, which form an elementary inverter, as shown in Fig. 1.

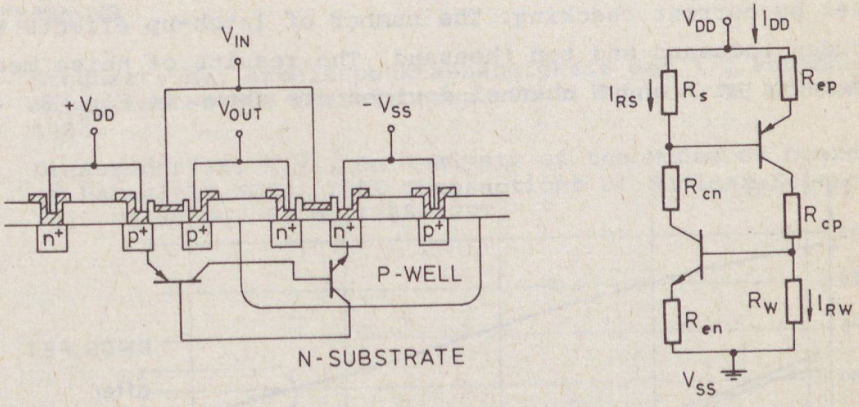

Fig. 1. Cross-section of a standard CMOS section and the lumped equivalent model of pnpn parasitic.

Under normal conditions, the parasitic SCR is in blocking state but, if subjected to a large voltage spike or if exposed to other effects (e.g. ionizing environment), triggering may occur. This may result in device burn-out or loss of state, depending on the power or current damaging the device.

We observed the effect in the case of the simple integrated circuit of CD 4007 B, and its Soviet version K 176 LP 1. The

circuit consists of three pairs of P and N channel FETs and almost every electrode of the transistors is available as a connection of the encapsulated chip, as shown in Fig. 2.

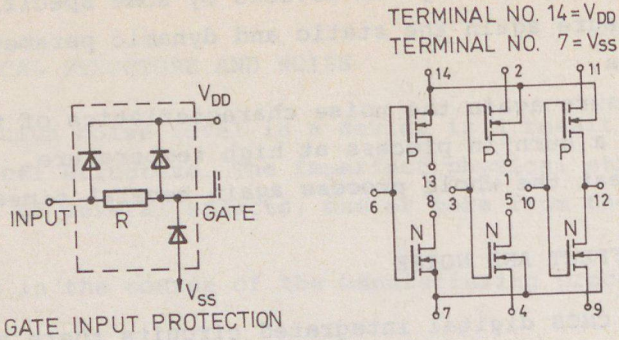

Fig. 2. Scheme for the RCA CD 4007 B

We have forced the devices to latch up at limited power level by current checking. The number of latch-up effects was between thousand and ten thousand. The results of noise measurements at P and N channel devices are shown in Fig. 3.

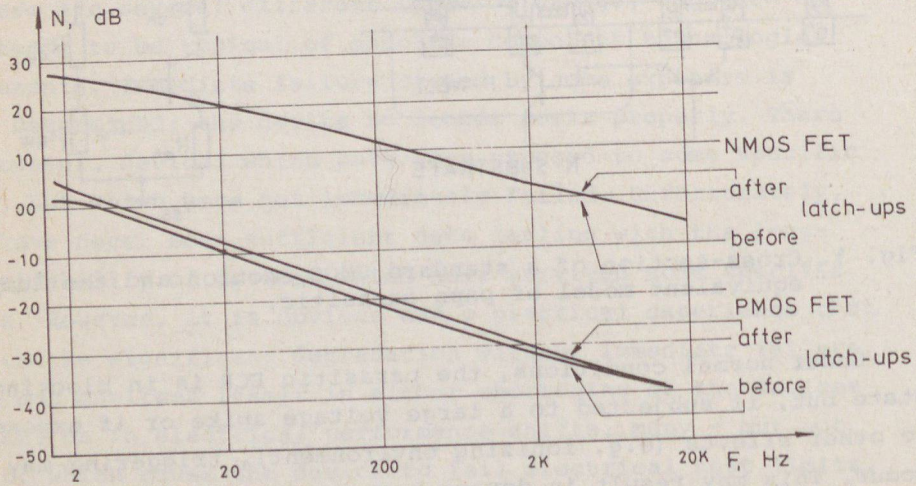

Fig. 3. Noise levels of CMOS FETs before and after forced latch-up effects

It is well known that the noise levels of the P and N channel FETs are different. By our measurements, the noise level of the N-channel devices is higher by about 30 dB than that of the P channel devices. After forced latch-up effects we could not measure any change of the noise level in the case of the N channel devices, but there was a 2-3 dB growing at the P channel devices. It is possible that the extra noise in N channel devices is overlapped by the other noise sources having higher noise levels originally. It is very important that we could not observe any other change in the parameters and working of the devices.

As a summary, we can state that there is a relatively well-measurable change in the noise level of damaged devices even if the damage is not detectable by other methods only when the reliability of the device is decreased.

REFERENCES

1. Stegherr, M., Arbeitspunktabhängigkeit des 1/f Rauschens integrierter MOS Transistoren. Ph.D. Thesis, TU München 1984.

2. Dressendorfer, P.V., An Analysis of the Modes of Operation of Parasitic SCRS. IEEE Transactions of Nuclear Science, Vol. NS-28 No. 6, p. 4288-4291.



10th Int.Conf. on Noise in Physical Systems
1989 Budapest, Hungary

LOW-FREQUENCY NOISE CORRELATIONS IN SUPERLATTICE DUAL-DRAIN MAGNETIC SENSORS

H.P. BALTES, A. NATHAN, R. CASTAGNETTI

Physical Electronics Laboratory, Institute of Quantum Electronics, Swiss Federal Institute of Technology (ETH) 8093 Zürich, Switzerland

Abstract

We present measurement results of low frequency noise in modulation-doped AlAs/GaAs superlattice dual-drain magnetic sensors. In particular, we investigate the degree of coherence between drain noise voltages for various device currents. We observe that at low frequencies, f < 100 Hz, the correlation is higher and decreases with decreasing device currents. At frequencies above 1 kHz, however, the correlation increases with decreasing currents. This may be attributed to different noise mechanisms predominating at different frequency ranges.

Introduction

Highly sensitive Hall devices based on the modulation-doped AlAs/GaAs superlattice structure have been fabricated recently using molecular beam epitaxy (MBE) technology. The motivation is the relatively high electron Hall mobility, μ_n^* in the very thin (~ 10 nm) two-dimensional electron gas (2DEG) close to the AlAs/GaAs heterojunction. A high Hall mobility is crucial for a high output response to magnetic fields. The device exhibits a sensitivity of 1200 V/AT for fields perpendicular to the device surface and its temperature coefficient is –0.1 %/K [1]. Based on this superlattice structure, dual-drain devices with a geometry which is reminiscent of the split-drain MOSFET [2], were realised. The high Hall mobility (~ 6400 cm^2/Vs) yields at 1 tesla, a relative current imbalance of 48 % [3]. This is an order of magnitude larger than the counterpart MOSFET sensors which have a N-channel Hall mobility of about 700 cm^2/Vs.

For most applications, the signal-to-noise ratio (SNR) controls the minimum field detection limit B_{min}, and thus knowledge of the noise behaviour in such devices is of major interest. Investigations of low frequency noise in heterojunction-based magnetic sensors show that both flicker (1/*f*) and generation-recombination (G-R) noise mechanisms are present in the 2DEG [4]. In GaAlAs/GaAs heterojunction Hall plates with SnAu as contact material, the noise power at very low frequencies ($f < 10$ Hz) appears to follow a 1/*f* type behaviour and at frequencies higher than 10 Hz, there is superposition of G-R noise. With AuGe as the contact material, a $f^{-1.5}$ behaviour was observed at frequencies below 10 Hz and at frequencies above this, G-R noise predominates. The G-R noise around 10 Hz corresponds to a trap level of 0.8 eV which is expected to be introduced by a Ga vacancy in the GaAs due to the diffusion of Ge into GaAlAs/GaAs heterojunction [4]. It was

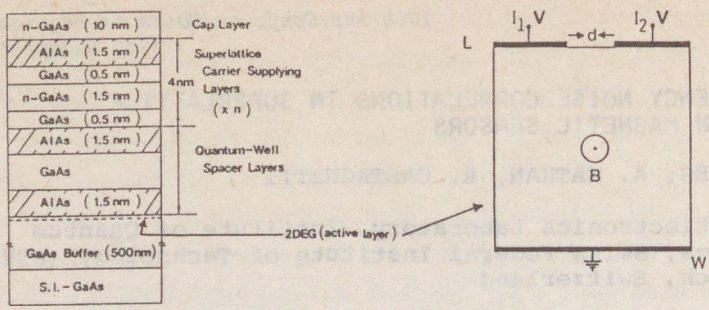

Fig. 1 Cross-sectional view [1] of the modulation-doped AlAs/GaAs superlattice and top view of the active device region.

observed for both devices, that the flicker noise is independent of the contact resistance but the G-R noise levels increased with increasing contact resistance. Noise measurements performed for the modulation-doped AlAs/GaAs superlattice Hall structures [1] showed similar results.

In this paper, the noise behaviour in modulation-doped AlAs/GaAs superlattice dual-drain magnetic sensors (see Fig. 1) is presented for various device geometries (d/W, L/W) and operating currents. We confirm our previous findings [5] of a positive correlation in drain noise voltages, based on measurements performed for square geometries ($L = W$) and for a limited span of frequencies ($f \leq 100$ Hz). We now extend our measurements to geometries, $L < W$ and in particular, investigate the dependence of the correlation on device operating current for a larger span of frequencies, $f \leq 100$ kHz.

Measurement Procedure

The samples used for the noise experiments were fabricated at the Electrotechnical Laboratory, Japan, using MBE. Ohmic contacts were made with AuGe/Ni/Au film. The device fabrication details are described in [1]. The device operation is as follows: the presence of a magnetic field perpendicular to the device surface, results in an imbalance in the current between the drains. This imbalance is a function of the total device current, the Hall mobility in the 2DEG, the magnetic induction, and the device geometry. For not too large Hall angles, the magnetic sensitivity can be expressed in the form $S = \Delta I_D / (I_D.B) = k\,\mu_n{}^*$, where $k = f(L/W, d/W)$ is a geometric factor and depends on device length L, width W, and drain separation d.

We measure in single-ended operation, the individual drain noise voltage power spectral densities (PSDs), $S_{xx}(f)$ and $S_{yy}(f)$, as well as the cross spectral density $S_{xy}(jf)$. In differential operation, the measured differential noise voltage PSD is denoted by $S_d(f)$. The degree of coherence between drain noise voltages is evaluated as follows

$$\gamma(jf) = S_{xy}(jf) / [S_{xx}(f) \cdot S_{yy}(f)]^{1/2}. \qquad (1)$$

In all structures and frequencies considered here, the imaginary part of $\gamma(jf)$ was found to be negligible. Under these conditions, we note that $\gamma(f)$ can be evaluated from knowledge of just $S_{xx}(f)$, $S_{yy}(f)$, and $S_d(f)$, since the

real part of $S_{xy}(jf)$ can be retrieved using the relation

$$S_d(f) = S_{xx}(f) + S_{yy}(f) - 2\,\mathrm{Re}S_{xy}(jf). \qquad (2)$$

We assume that the thermal noise generated by load resistors, R_L used in the measurement is negligible, and that it is uncorrelated with the drain noise current, and correspondingly with the drain noise voltages. Measurements indicate that the noise is unaffected by the presence of the magnetic field for $|B| \leq 1$ T. Details of the noise measurement set-up and specifications of pertinent measurement equipment are given in [5].

Results and Discussion

Noise spectral densities for the device with L/W = 100 μm/200 μm and d = 10 μm are shown in Fig. 2 for frequencies up to 100 kHz. The individual spectra are almost identical, $S_{xx}(f) \sim S_{yy}(f)$ and for f < 100 Hz, $S_d(f) < S_{xx}(f)$ as a result of a positive correlation. This can be noted from the corresponding cross spectral density, where $S_{xy}(f) \sim S_{xx}(f)$. At higher frequencies, however, $S_{xy}(f) < S_{xx}(f)$ and consequently, $S_d(f) > S_{xx}(f)$ due to the decreased coherence in the drain noise voltages. The spectra follow an $f^{-\alpha}$ type spectrum with $\alpha \sim 2$, indicating that the predominant mechanism is G-R noise. The same was also observed in [4] for 2 DEG Hall devices with AuGe contacts. Based on the power spectra $S_{xx}(f)$ and $S_{yy}(f)$, there are two corner frequencies; the first one at frequencies below 1 Hz and the next occurs at f > 10 kHz, which would correspond to two distinct trap levels. The same behaviour was observed for geometries, L = W [5].

The value α appears to be dependent on bias conditions and this is illustrated in Fig. 3 where the single-ended PSD is shown for various device currents. For device currents greater than 0.5 mA and for frequencies less

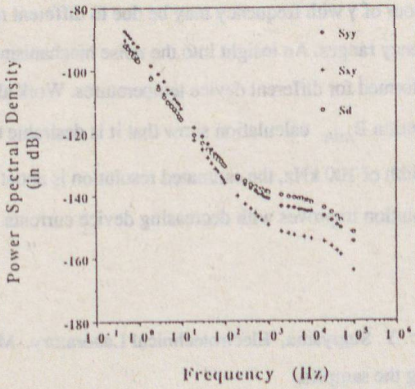

Fig. 2 The single-ended drain noise voltage PSDs, the differential PSD, and the cross spectral density for L/W = 100 μm/200 μm and d = 10 μm.

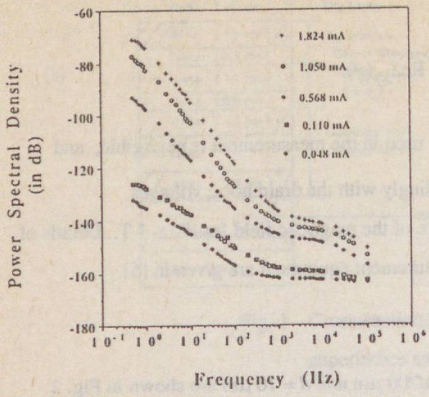

Fig. 3 The individual drain noise voltage PSDs for various device currents. The device geometry as in Fig. 2.

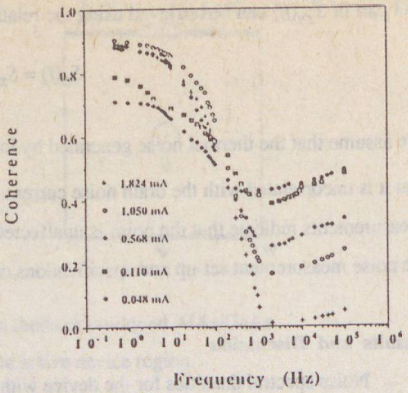

Fig. 4 The coherence as a function of frequency for various device currents. The device geometry as in Fig. 2.

than 1 kHz, α is approximately 2. In this regime, the noise power appears to follow an I^{β} dependence with $\beta \sim 4$. On the other hand, a 1/f type behaviour (for $f < 1$ kHz) is observed for currents less than 0.5 mA, with the dependence on current such that $\beta \sim 2$.

The degree of coherence, $\gamma(f)$ is higher for $f < 100$ Hz and increases with increasing device currents (Fig. 4). In fact, γ appoaches a saturation value of 0.9 at 1 Hz for currents grater than 0.5 mA. At frequencies higher than 1 kHz, however, the dependence of γ on device current is reversed. The degree of coherence is higher with lower device currents (saturating at a value of 0.5 at 100 kHz for $I < 0.5$ mA) and decreases with increasing currents. This anomalous behaviour of γ with frequency may be due to different noise mechanisms predominating at different frequency ranges. An insight into the noise mechanisms involved can perhaps be obtained with measurements performed for different device temperatures. Work along these lines is in progress.

In terms of the field resolution B_{min} calculation show that it is desirable to operate the device in differential mode. Over a bandwidth of 100 kHz, the estimated resolution is about 3 μT for a device current of 1 mA and $R_L = 10$ kW. The resolution improves with decreasing device currents.

Acknowledgements

It is a pleasure to thank Dr. Y. Sugiyama, Electrotechnical Laboratory, Ministry of International Trade and Industry, Japan for providing the samples.

References

[1] Y. Sugiyama, H. Soga, and M. Tacano, "Highly-sensitive Hall element with quantum-well superlattice structures", *Journal of Crystal Growth*, vol. 95, 1989, pp. 394-397.

[2] D. R. Briglio, A. Nathan, and H. P. Baltes, "1/f noise in magnetic-field-sensitive dual drain MOSFET's", in : Noise in Physical Systems, C. M. Van Vliet, Ed., Singapore: World Scientific, 1987, pp. 453-456.

[3] Y. Sugiyama, H. Soga, M. Tacano, and H. P. Baltes, "Split-contact magnetoresistor made of AlAs/GaAs superlattice", *Tech. Dig., 7th Sensor Symp.*, 1988, pp. 47-50.

[4] M. Tacano, Y. Sugiyama, and H. Soga, "Device process dependence of low-frequency noise in GaAlAs/GaAs heterostructure", *Sol.-St. Electron.*, vol. 32, 1988, pp. 49-55.

[5] A. Nathan, H. P. Baltes, R. Castagnetti, Y. Sugiyama, and D. R. Briglio, "Low frequency noise in modulation-doped AlAs/GaAs superlattice dual-drain magnetic sensors", *Sensors and Actuators*, in press.

SESSION 10

MEASUREMENT TECHNIQUES

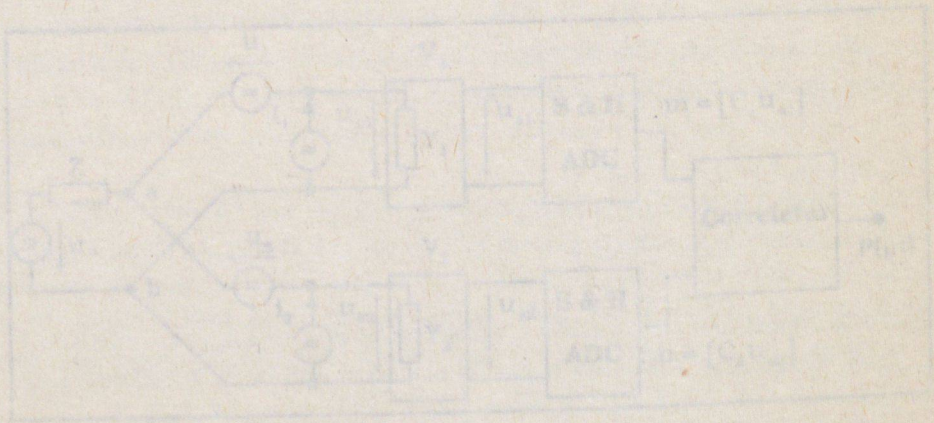

ERRORS ASSOCIATED WITH THE MEASUREMENT OF POWER SPECTRA BY THE CORRELATION TECHNIQUE

L. STORM

Institut für Angewandte Physik
4400 Münster, FRG

1) Introduction

For the precise measurement of noise power spectra the correlation method is best suited, because it allows to eliminate the major part of the amplifier noise. Fig. 1 shows the equipment. The unknown noise source u_x with internal impedance Z, autocorrelation function R_x and power spectrum S_x is connected to two channels in parallel. Each consists of amplifiers with total gain V, an input admittance Y, a sample and hold and an ADC with conversion factor C, which samples the output voltage u_a with sampling period τ at time instants $k\tau$. The output integers m, n are stored in the correlator and the numbers

$$P(\mu\tau) = \frac{1}{N}\sum_{k=1}^{N} m(k\tau)n((k+\mu)\tau), \qquad -M \le \mu \le M \tag{1}$$

are calculated for a lot of time shifts $\mu\tau$ simultaneously.

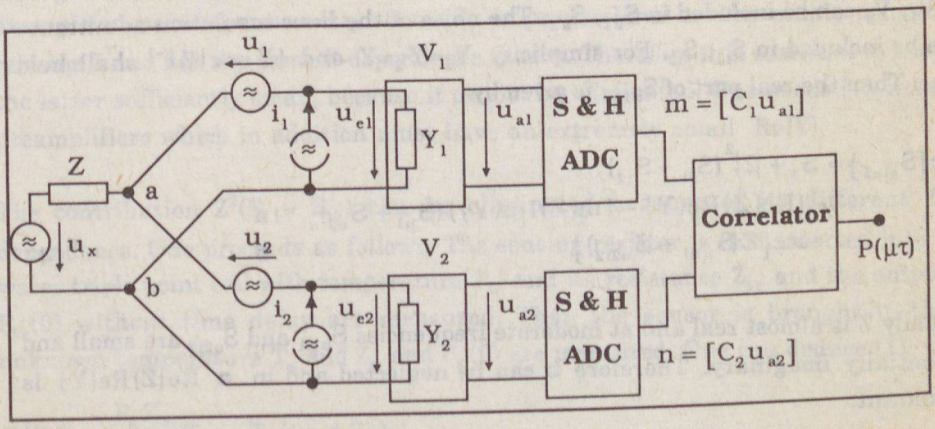

Fig. 1 Principle of the measuring equipment
$m=[C_1 u_{a1}]$ means the integer closest to $C_1 u_{a1}$

If we neglect the quantization, we have $m=C_1 u_{a1}$ and $n=C_2 u_{a2}$. Then the expected value $\langle P \rangle$ of P is given by

$$\begin{aligned}\langle P(\mu\tau)\rangle &= C_1 C_2 \langle u_{a1}(k\tau)\ u_{a2}((k+\mu)\tau)\rangle \\ &= C_1 C_2 R_{a1a2}(\mu\tau) \\ &= C_1 C_2 \int_{-\infty}^{+\infty} S_{a1a2}(f)\exp(i2\pi f\mu\tau)\,df \\ &= C_1 C_2 \int_{-\infty}^{+\infty} S_{e1e2}(f)\,V_1^*(f)\,V_2(f)\exp(i2\pi f\mu\tau)\,df \end{aligned} \tag{2}$$

R_{a1a2} (S_{a1a2}) means the crosscorrelation function (cross power spectrum) of u_{a1}, u_{a2}; S_{e1e2} is the cross power spectrum of the input voltages u_{e1}, u_{e2} and V_1^* means the conjugate complex of V_1. By inversion of Eq. (2) one obtains

$$\mathrm{Re}\{S_{e1e2}(f)\,V_1^*(f)\,V_2(f)\} = \frac{1}{C_1 C_2}\int_{-\infty}^{+\infty}\langle P(t)\rangle\cos 2\pi ft\,dt \tag{3}$$

Our aim is to obtain S_x by a discrete Fourier transform of P(t). The different errors associated with the measuring and mathematical procedure are discussed in the following section.

2) Error estimation

2.1 Error due to amplifier noise

The noise of the amplifiers can be taken into account by voltage sources u_1, u_2 and current sources i_1, i_2 with power spectra S_{u1}, S_{u2}, S_{i1}, S_{i2} and cross power spectra S_{u1i1} and S_{u2i2}. The noise of the lines resistance from points a, b (Fig. 1) to V_1, V_2 can be included in S_{u1}, S_{u2}. The noise of the lines insulation admittance can be included in S_{i1}, S_{i2}. For simplicity $Y_1=Y_2=Y$ and $|Y|\ll|Z|^{-1}$ shall hold true. Then the real part of S_{e1e2} is given by

$$\begin{aligned}\mathrm{Re}\{S_{e1e2}\} \approx\ & S_x + |Z|^2(S_{i1}+S_{i2}) \\ & -(\mathrm{Re}\{Z\}\mathrm{Re}\{Y\} - \mathrm{Im}\{Z\}\mathrm{Im}\{Y\})(S_{u1}+S_{u2}) \quad \textbf{a} \\ & +\mathrm{Re}\{Z(S_{u1i1}+S_{u2i2})\} \quad \textbf{b}\end{aligned} \tag{4}$$

Usually Z is almost real and at moderate frequencies S_{u1i1} and S_{u2i2} are small and essentially imaginary. Therefore **b** can be neglected and in **a** $\mathrm{Re}\{Z\}\mathrm{Re}\{Y\}$ is dominant.

The noise of well designed differential amplifiers is mainly determined by its two input transistors. One has

$$S_u = 2k_B T(2R_{eq} + R_l + R_f) + 1/f \text{ noise}; \qquad Y_t R_{eq} \approx 1$$
$$S_i = \text{shot noise} + 2k_B T \mathrm{Re}\{Y\} + 1/f \text{ noise}$$

Y_t is the transductance of the input transistors. The lines resistance R_l and a certain feedback resistor R_f depending on the construction of the amplifiers must be added to $2R_{eq}$. If FETs are used, the shot noise can commonly be neglected. For a gate bias current of 5pA and T=290K the thermal noise of $\mathrm{Re}\{Y\} \approx 10^{-10}\,\Omega^{-1}$ already equals the shot noise. By feedback the gate-source and gate-drain admittances of the input transistors can be eliminated. One is left with the insulating admittance. But even in this case such a low value of Re{Y} can hardly be obtained, especially at higher frequencies when dielectric losses of the insulating material become important. Therefore in most cases the thermal noise of Y is by far the dominant part, if FETs are used. Then, disregarding the 1/f noise, $Z\,\mathrm{Re}\{Y\}\,S_u$ equals $Z^2 S_i$, if $Z = 2R_{eq} + R_l + R_f$. For larger values of Z the contribution $Z^2 S_i$ is dominant.

The imaginary part of S_{e1e2} is commonly very small and does not depend on S_x. It vanishes, if the amplifiers have equal noise. If the two channels cannot be distinguished with regard to noise and input admittance, $S_{e1e2} = S_{e2e1} = S^*_{e1e2}$ must hold true. One can eliminate $\mathrm{Im}\{S_{e1e2}\}$ by equalizing the phase shifts of V_1 and V_2. Then $V_1^* V_2$ becomes real and only $\mathrm{Re}\{S_{e1e2}\}$ inters into Eq. (3).

The above considerations are important in high precision measurements, for example in noise thermometry. Here S_x is proportional to the ohmic sensing resistor Z and has the same Z-dependence than **a**. Therefore it is essential to keep the latter sufficiently small, because it cannot be eliminated. One needs low noise preamplifiers which in addition must have an extremely small Re{Y}.

The contribution $Z^2(S_{i1} + S_{i2})$ can be eliminated because of its different Z-dependence. One proceeds as follows: The sensing resistor is first inserted into a water triple point cell with temperature T_{tr} and its resistance Z_{tr} and the output $P_{tr}(0)$ without time delay are measured. Then the sensor is brought to the unknown temperature T_x and Z_x and $P_x(0)$ are measured. One can deduce [1]

$$F(Z_x) := \frac{P_x Z_{tr}}{P_{tr} Z_x} T_{tr} \approx T_x(1 + AZ_x)$$

The factor A only depends on the temperatures, but not on Z_x. If now the procedure is repeated with different values of Z_x, one obtains the straight line in Fig. 2 and T_x is obtained by extrapolation. The relative error of about 10^{-4} is equal to that of the best gasthermometric measurements [2]. Such a small error can only be obtained if the input circuit is designed according to [1].

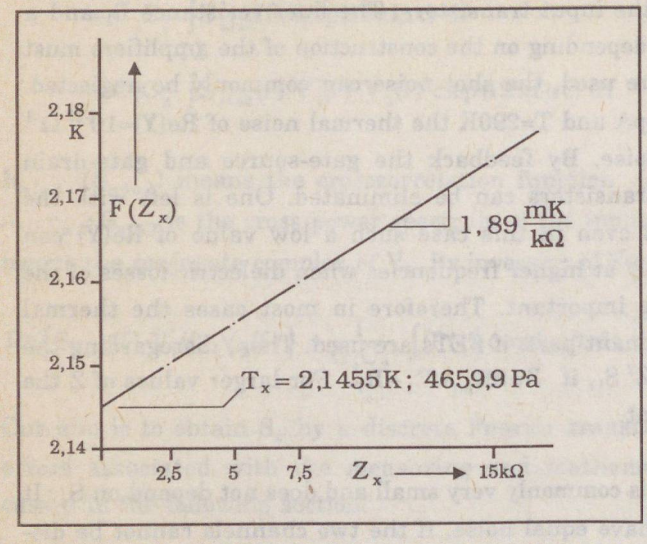

Fig. 2 $F(Z_x)$ at 2,1455 K

2.2 Quantization error

Due to quantization by the ADCs a systematic error occurs, which clearly depends on the statistical properties of u_{a1} and u_{a2}. The relative quantization error

$$\varepsilon = \frac{\langle mn \rangle - C^2 \langle u_{a1} u_{a2} \rangle}{C^2 \langle u_{a1} u_{a2} \rangle}$$

has been computed with the following assumptions:

a) The ADCs have equal conversion factors, $C_1 = C_2 = C$, and have a characteristic as shown in Fig. 3.

b) $\langle u_{a1}^2 \rangle = \langle u_{a2}^2 \rangle = \langle u_a^2 \rangle$

c) u_{a1} and u_{a2} are jointly normally distributed with correlation coefficient $r(\mu\tau) = R_{a1a2}(\mu\tau) / \langle u_a^2 \rangle$

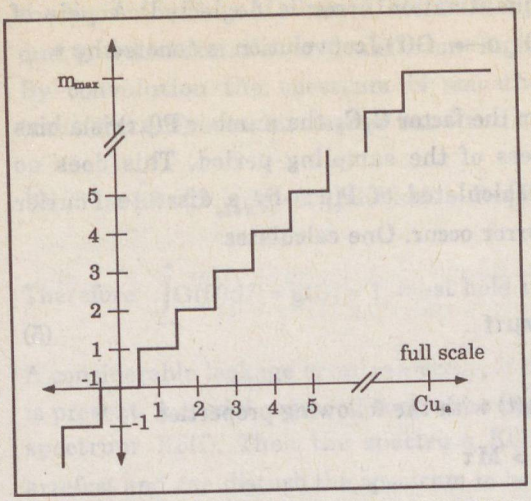

Fig. 3

Characteristic of an ideal ADC
steps localized exactly at $Cu_a = \pm 0{,}5; \pm 1{,}5; \ldots$

Fig. 4 shows the result for 12 bit ADCs. The relative error is positive for small input voltages, for high input voltages it becomes negative due to clipping. For all values of r the relative error is less than 1 ppm, if the input voltages $\sqrt{\langle u_a^2 \rangle}$ are properly adjusted. They should at least correspond to 300 LSB and should not exceed 19% of full scale. The quantization error can be neglected, generally the error due to the integral nonlinearity - usually a few LSBs - is larger. For this reason it can be necessary to use ADCs with a larger bit number.

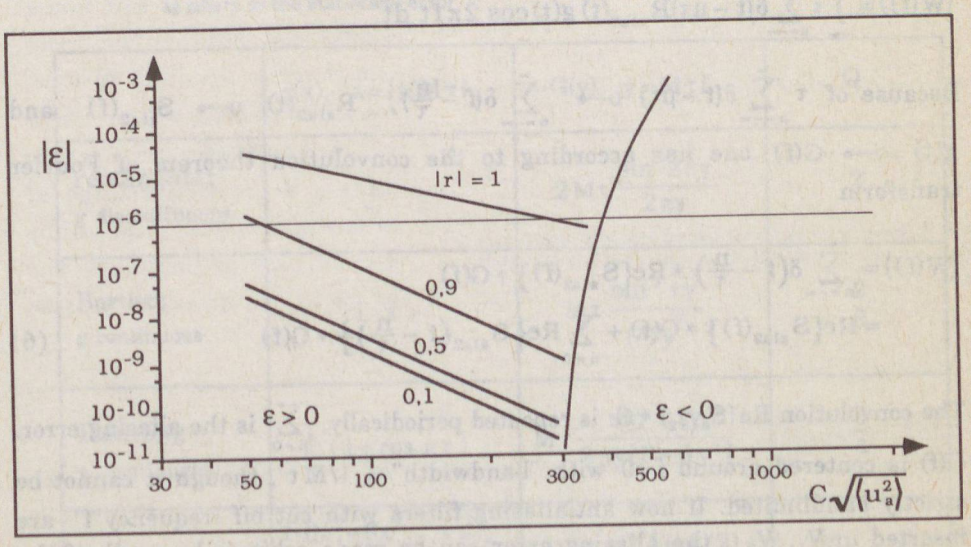

Fig. 4 Relative quantization error for 12 bit ADCs

2.3 Errors due to discrete Fourier transform

In all further considerations the quantization error is neglected. A pair of Fourier transforms is denoted by $g(t) \circ\!\!-\!\!\bullet\, G(f)$, convolution is denoted by *.

From Eq. (2) it follows, that apart from the factor C_1C_2 the number $P(\mu\tau)$ is a bias free estimator of $R_{a1a2}(\mu\tau)$, regardless of the sampling period. This does no longer hold true, if a spectrum is calculated of $P(\mu\tau)$ by a discrete Fourier transform. Two kinds of systematic error occur. One calculates

$$W(f) = \frac{1}{C_1C_2}\,\tau \sum_{\mu=-M}^{M} P(\mu\tau)\, g(\mu\tau) \cos 2\pi\mu\tau f \tag{5}$$

$P(\mu\tau)$ is multiplied by a time window $g(t)$ with the following properties

$g(t)=g(-t)$; $g(0)=1$; $g(t)=0$ if $|t| > M\tau$

The expected value of W is

$$\langle W(f)\rangle = \tau \sum_{\mu=-M}^{M} R_{a1a2}(\mu\tau)\, g(\mu\tau) \cos 2\pi\mu\tau f$$

With Dirac's δ-function this can be rewritten as

$$\langle W(f)\rangle = \int_{-\infty}^{\infty} \tau \sum_{\mu=-\infty}^{\infty} \delta(t-\mu\tau) R_{a1a2}(t)\, g(t) \cos 2\pi f t\, dt$$

Because of $\tau \sum_{\mu=-\infty}^{\infty} \delta(t-\mu\tau) \circ\!\!-\!\!\bullet\, \sum_{n=-\infty}^{\infty} \delta(f-\frac{n}{\tau})$, $R_{a1a2}(t) \circ\!\!-\!\!\bullet\, S_{a1a2}(f)$ and $g(t) \circ\!\!-\!\!\bullet\, G(f)$ one has according to the convolution theorem of Fourier transform

$$\begin{aligned}\langle W(f)\rangle &= \sum_{n=-\infty}^{\infty} \delta\left(f-\frac{n}{\tau}\right) * \mathrm{Re}\{S_{a1a2}(f)\} * G(f) \\ &= \mathrm{Re}\{S_{a1a2}(f)\} * G(f) + \sum_{n\neq 0} \mathrm{Re}\left\{S_{a1a2}\left(f-\frac{n}{\tau}\right)\right\} * G(f)\end{aligned} \tag{6}$$

The convolution $\mathrm{Re}\{S_{a1a2}\} * G$ is repeated periodically. $\sum_{n\neq 0}$ is the aliasing error. $G(f)$ is centered around $f=0$ with "bandwidth" $\approx 1/M\tau$, though it cannot be strictly bandlimited. If now antialiasing filters with cut off frequency f' are inserted in V_1, V_2, the aliasing error can be made arbitrarily small, if the Nyquist condition $\tau^{-1} > 2(f' + 1/M\tau)$ is met.

The remaining convolution is not a bias free estimation. This holds true only in the limit of infinite M, then G(f) tends to $\delta(f)$. The error - called leakage error - is due to truncation. Power "leaks" from high power regions to low power regions. By convolution the spectrum is smoothed. For very large M the Fourier transform G(f) becomes narrow band and

$$\langle W(f)\rangle = \int_{-\infty}^{\infty} \mathrm{Re}\{S_{a_1a_2}(f-f')\}G(f')df' \approx \mathrm{Re}\{S_{a_1a_2}(f)\}\int_{-\infty}^{\infty} G(f')df'$$

Therefore $\int_{-\infty}^{\infty} G(f')df' = g(0) = 1$ must hold true.

A considerable leakage error can occur, if a strong noise at infralow frequencies is present. A trivial source of such noise is an offset at the amplifier outputs with spectrum $K\delta(f)$. Then the spectrum KG(f) is generated which is merely an artefact and can disturb the spectrum to be measured at the low frequencies. One needs a time window with a strong decay of G(f). Table 1 shows some frequently used time windows and their Fourier transforms. The discontinuous rectangular window is not suitable, g(t) should at least be continuous, which leads to $G(f) \sim f^{-2}$. If derivatives of g(t) are also continuous, the decay is stronger.

Table 1 Time windows g(x) and their Fourier transforms G(y)
Q refers to the statistical error

	g(x), $x = \lvert t/M\tau \rvert$	G(y), $y = M\tau f$	Q
rectangular g discontinuous	1	$2M\tau \dfrac{\sin 2\pi y}{2\pi y}$	2
Bartlett g continuous	$1-x$	$M\tau \dfrac{\sin^2 \pi y}{(\pi y)^2}$	$\dfrac{2}{3}$
Hanning g' continuous	$\dfrac{1}{2}(1+\cos \pi x)$	$M\tau \dfrac{\sin 2\pi y}{2\pi y[1-4y^2]}$	$\dfrac{3}{4}$
Parzen g" continuous	$1-6x^2+6x^3$; $x \le \frac{1}{2}$ $2-6x+6x^2-2x^3$; $\frac{1}{2} \le x \le 1$	$\dfrac{3M\tau}{4} \dfrac{\sin^4(\pi y/2)}{(\pi y/2)^4}$	$\dfrac{151}{280} \approx 0{,}54$

2.4 Error due to a drift of ambient temperature

If the 1/f-noise of a dc-current-carrying sample is measured, a drift of the ambient temperature can produce a strong infralow frequency noise, if the resistance of the sample is temperature dependent. The noise should be suppressed by high pass filters within V_1 and V_2. If the Fourier transform is carried out with different time windows, the result must remain unchanged. The temperature drift can cause a large error, if it has Fourier components within the measuring range. Suppose for example that the noise of a copper whisker with diameter 2μm and length 2mm is measured. The number of carriers is about $5*10^{14}$, and according to Hooges formula in the frequency range 0,1 Hz to 1 Hz

$$\frac{\langle(\Delta U)^2\rangle}{U^2} = \frac{\langle(\Delta R)^2\rangle}{R^2} = \frac{2*10^{-3}}{5*10^{14}} \ln 10 \approx 10^{-17}$$

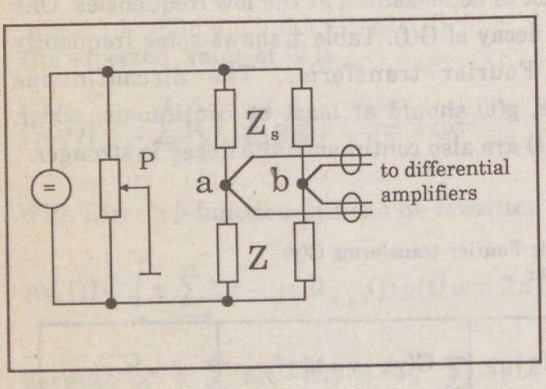

Fig. 5

Bridge circuit for suppression of ambient temperature fluctuations. By P the dc-potential at a, b is adjusted to zero.

If now $\Delta R = R\beta\Delta T$ and $\beta T \approx 1$, which is a good approximation for pure metals, one has $\Delta R/R \approx \Delta T/T$ and $\Delta T_{rms}/T < 3*10^{-9}$ is required. This severe condition can be moderated, if a bridge circuit is used, see Fig. 5. Two equal samples Z together with two equal series resistors Z_s form an adjusted bridge. Now a drift of the ambient temperature causes a common voltage at points a, b, which is rejected by the differential amplifiers. The noise of the dc-source is also suppressed.

2.5 Statistical error

The numbers $P(\mu\tau)$ are random variables. As all $P(\mu\tau)$ are obtained from the same temporal segment of the noise voltages, the $P(\mu\tau)$ are clearly statistically dependent. In order to calculate the error of any function of $P(\mu\tau)$, one needs the full covariance matrix

$$C^{P}_{\mu\nu} := \langle (P(\mu\tau) - \langle P(\mu\tau)\rangle)\,(P(\nu\tau) - \langle P(\nu\tau)\rangle)\rangle$$

The following result can be deduced

$$C^{P}_{\mu\nu} \approx \frac{(C_1 C_2)^2}{N\tau} \sum_{n=-\infty}^{+\infty} \cos(\mu-\nu)\,n\pi \cdot \int_{-\infty}^{+\infty} \Big[S_{a1a2}\Big(f+\frac{n}{2\tau}\Big) S_{a1a2}\Big(f-\frac{n}{2\tau}\Big) \cos 2\pi f(\mu+\nu)\tau + S_a\Big(f+\frac{n}{2\tau}\Big)\, S_a\Big(f-\frac{n}{2\tau}\Big) \cos 2\pi f(\mu-\nu)\tau \Big]\, df \qquad (7)$$

conditions: $S_{a1}=S_{a2}=S_a$; S_{a1a2} real, even; $N>>M>>1$;
$(N\tau)^{-1}$ << bandwidth of S_a, S_{a1a2};
u_x=normal process.

If the Nyquist condition for the sampling rate is met, all terms with $n\neq 0$ vanish. The remaining result holds also true for continuous signal processing. An insufficient sampling rate leads to an increase of all variances because of the loss of information. Because of $S_a=S_{a1a2}+S_v$, wherein S_v denotes the amplifiers contribution to S_a, the amplifiers noise strongly enters into $C^{P}_{\mu\nu}$, especially if $S_v > S_{a1a2}$.

Using the law of error propagation one can calculate the variance C^{W}_{ff} of W(f). The result is

$$\frac{C^{W}_{ff}}{S^2_{a1a2}(f)} \approx \left(1 + \frac{S_v(f)}{S_{a1a2}(f)} + \frac{S^2_v(f)}{2S^2_{a1a2}(f)}\right)\frac{M}{N}\,Q \qquad (8)$$

$$Q = \frac{1}{M\tau}\int_{-M\tau}^{M\tau} g^2(t)\,dt \approx \frac{1}{M}\sum_{\mu=-M}^{M} g^2(\mu\tau)$$

The conditions are the same as in Eq. (7). In addition the Nyquist condition must be met and $f > 1/M\tau$. The variance C^{W}_{00} is twice as large. Table 1 gives the values of Q for the different time windows. By $S_{a1a2}=S_a$ and $S_V=0$ one obtains the single channel versions of Eq. (7) and Eq. (8). The $P(\mu\tau)$ and consequently W(f) are almost normally distributed. This follows from the central limit theorem.

Summary

For the precise measurement of noise power spectra the correlation technique is best suited. In order to obtain the desired spectrum several operations must be carried out, each operation is associated with its specific error. In table 2 the

$P(\mu\tau)$	
$\Downarrow$	$\rightarrow$ statistical error
$\langle P(\mu\tau)\rangle$	
$\Downarrow$	$\rightarrow$ quantization error
$R_{a1a2}(\mu\tau)$	
$\Downarrow$	$\rightarrow$ aliasing and leakage error
$Re\{S_{a1a2}\}$	
$\Downarrow$	$\rightarrow V_1^* V_2$ = real
$Re\{S_{e1e2}\}$	
$\Downarrow$	$\rightarrow$ error due to amplifier noise
S_x	

Table 2

List of operations and associated errors

operations and errors are listed up. Additional errors occur due to nonlinear distortion and drifts of V_1, V_2, C_1, C_2. Such errors are difficult to estimate and have not been treated here.

Acknowledgement

Dipl. Phys. U. Springer has kindly computed the quantization error.

References

[1] H.-H. Klein, G. Klempt, L. Storm: Metrologia 15, 143-154 (1979)

[2] K. H. Berry: Document CCT / 76-27

10th Int.Conf. on Noise in Physical Systems
1989 Budapest, Hungary

AN IMPROVED TECHNIQUE OF MEASURING THE CONTACT NOISE IN THICK FILM RESISTORS

A. MASOERO, B. MORTEN,* M. PRUDENZIATI,* A. STEPANESCU**

Istituto Elettrotecnico Naz. 'Galileo Ferraris', Torino
*Dipartimento di Fisica, Università di Modena
**Dipartimento di Fisica del Politecnico, Torino
Unità GNSM-CISM di Torino e Modena, Italy

INTRODUCTION

The interest in knowledge of excess noise in thick film resistors stems from the desire to optimize the performance of hybrid components and sensors as well as to correlate the processes of preparation of pastes and layers with their electrical properties [1].

A correct evaluation of the noise should allow a discrimination between the "bulk" component due to electrical transport into the resistor volume and that due to transport across or near the resistor/termination interface, viz. the so-called "contact noise". This latter can be responsible for a significant fraction of the total noise [2].

The term "bulk noise" does not imply equal noise levels into the whole volume of the resistive layer; e.g. the noise may change at various depths in the film (thickness dependent noise [3]) as a consequence of interactions between the resistor and the substrate. In this context bulk and contact noise are differentiated by the fact that only the second one can be varied by changing the preparation of resistor terminations.

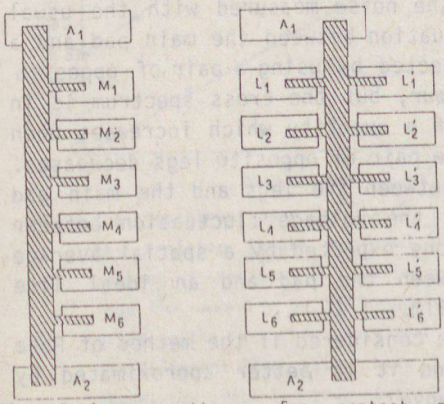

Fig.1-Resistor patterns for contact noise measurements. Left: after [2]; Right: configuration used for the cross-correlated method.

In order to measure the contribution of contact noise to the total noise Rhee and Chen [2] suggested an elegant method which makes use of a resistor configuration where, besides the two standard contacts (A1 and A2 in Fig. 1), several side contacts are prepared (M1-M6 in Fig.1) for the measurement of noise as a function of resistor length. The main idea is to provide the resistive film with very narrow legs, which should introduce no deformation of the current stream, since they are very fine and do not carry any current. The plot of the noise power spectrum integrated

over a suitable frequency range v_f^2 vs the distance x of each leg from a main pad will give an intercept at x=0 representing the contact noise generated at the interface between the resistive strip and a main contact A.
In this work we show that this method overestimates the noise taken at short distances from the main pad, while an accurate measurement is obtained by taking the cross spectrum of the noise on the pairs of opposite side contacts prepared along the resistor. Moreover, as an application of this method we show that Ag diffusion from terminations in the resistors is responsible for high levels of contact noise.

2. SAMPLES AND METHODS

RuO_2-based resistors have been prepared on 96%-alumina substrates (Hechst, CeramTec 708), starting from inks of model systems whose composition, preparation and characterization have been reported previously [4]. In particular the results here reported deal with samples prepared by an ink made with a glass frit containing $PbO:SiO_2:Bi_2O_3:Al_2O_3$ in the relative percentage 55.5:10.5:22.0:12.0 by weight and RuO_2 powder having 75 m^2/g (BET measurements) in 9% wt with respect to the glassy content. Inks were screen printed on prefired terminations based on PdAg and PtAu thick film conductors. Firing cycles used lasted 30 min, with 850°C peak temperature and 3 min dwell time. Different patterns were prepared for various measurements: 1x1 mm^2 layers for four probe point measurements (without contacts), a series of 2 mm wide resistors with lengths from 1 mm to 10 mm for evaluation of size effect (actual sheet resistance as a function of resistor length), and the pattern shown in Fig. 1 (right) for the measurement of contact noise. The main pads A_1 and A_2 carry the d.c. biasing current, provided by a regulated d.c. supply. Voltage fluctuations are measured with a spectrum analyzer (Nicolet 660A).

3. RESULTS

Fig. 2 compares the power spectrum of the noise measured with the usual procedure (i.e. taking the voltage fluctuation between the main pad and a single leg) with the cross spectrum detected by using a pair of opposite legs. Both spectra exhibit a 1/f behaviour, but the cross spectrum is in general lower than the power spectrum of a quantity which increases when the distance between the main pad and the pair of opposite legs decreases. The reason is that, when the distance between the legs and the main pad becomes comparable with the film width, the voltage fluctuation between the pad and each leg is larger than the one expected by a spatial average over different current flux lines between the pad and an ideal line joining the two opposite legs across the film.
This last quantity is the right one to be considered if the method of Rhee and Chen should correctly be applied and it is better approximated by taking the cross-spectrum as described above.
Fig.3 shows the cross-spectrum power density $\Phi_{12}(\omega)$ at 1 kHz vs the distance x of the legs, for samples with PdAg and PtAu-based terminations. In both cases Φ_{12} exhibits the expected linear dependence on x; the intercepts

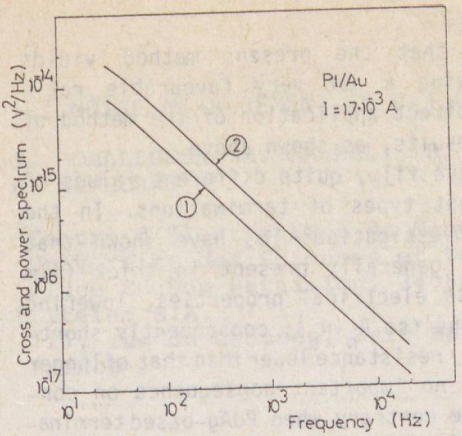

Fig.2-(1) Cross spectrum of the current noise signals between a main contact A and a pair of opposite legs L_1, L_1'; for the specimen Pt/Au (R=20.18 KΩ) at I = 1.7x 10^{-3} A (see fig. 3) - (2) Power spectrum of the current noise between A and each of the previous legs for the same specimen and the same bias current.

of the straight lines at x = 0 evidence that the contact noise is negligible in samples with PtAu-based terminations, while it is considerable in the case of PdAg terminations. Finally Fig.4 illustrates the effective sheet resistance R_n (i.e. the ratio between the actual resistance and the aspect ratio n) normalized to the "bulk sheet resistance" R_b measured with the 4-point probe method. It is notable that with both types of terminations, even 10 mm long samples exhibit a sheet resistance some percent different from the value of the bulk. Moreover a "direct size effect" (e.g. $R_n < R_b$) is observed with PdAg-based terminations [5].

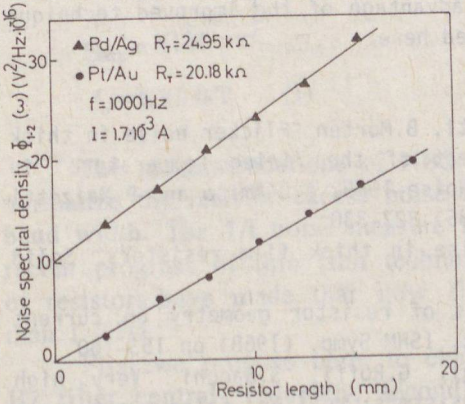

Fig.3-Cross-spectrum power density $\Phi_{1-2}(\omega)$ vs. the resistor length measured with the present technique, in samples obtained from the same ink on different contacts. Owing to the fact that cross spectra taken at different leg pairs have the same shape, the cross spectrum power density at each analysis frequency and the cross spectrum integral are proportional.

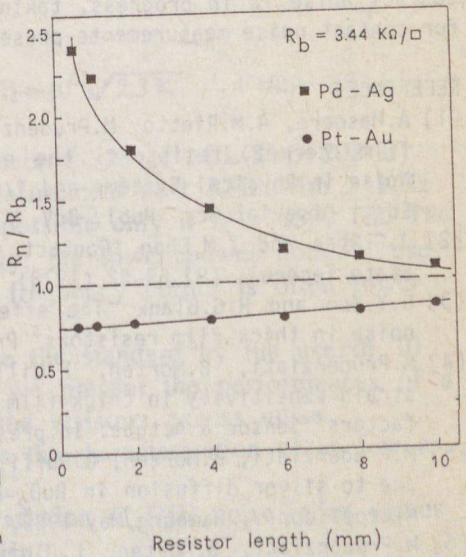

Fig.4-Effective sheet resistance of samples of various length normalized to the bulk value.

4. DISCUSSION AND CONCLUSIONS

The curves reported in fig. 3 show that the present method yields reasonable results even with films having a not very favourable ratio width to length. In these conditions a direct application of the method of Rhee and Chen would provide uncorrect results, as shown above.

We can observe that, in the same resistive film, quite different values of contact noise are obtained with different types of terminations. In the case of PtAu-based contacts previous investigations [6] have shown that diffusion of bismuth (a "fluxing agent" generally present in thick film conductors) into the resistor affects its electrical properties, lowering the film resistivity near the terminations (so $R_n < R_b$); consequently shorter resistors exhibit an effective sheet resistance lower than that of longer ones, as seen in Fig.4. This effect has no important consequence on contact noise, as observed in Fig. 3. On the contrary when PdAg-based terminations are concerned, the diffusion of Ag from the contacts is the main physico-chemical effect, responsible for an increase of the resistivity of the material; hence the "inverse size effect" is observed (Fig. 4). To the same cause we ascribe the increase of the contact noise. A comprehensive picture of the consequences of Ag diffusion (rearrangement of RuO_2 grains, glass counterdiffusion, etc.) is not available yet; however, it seems reasonable that an increase of resistivity (due to either additional scattering, or lower concentration of charge carriers) is associated with an increase of voltage fluctuations of the film near the terminations. Further investigations devoted to correlate the microstructure of the films with contact noise is in progress, taking advantage of the improved technique for contact noise measurements presented here.

REFERENCES

[1] A.Masoero, A.M.Rietto, M.Prudenziati, B.Morten "Flicker noise in thick film (cermet) resistors: the effect of the firing temperature" in Noise in Physical Systems and 1/f Noise-1985, A.D'Amico and P.Mazzetti Eds., Elsevier Sci. Publ. B.V. (1986) 327-330

[2] J.G.Rhee and T.M.Chen "Contact noise in thick film resistors" Solid State Technol. (9) 59-62 (1978)

[3] C.Y.Kuo and H.G.Blank "The effects of resistor geometry on current noise in thick-film resistors" Proc. ISHM Symp. (1968) pp 153-160

[4] M.Prudenziati, B.Morten, F.Cilloni, G.Ruffi, S.Sacchi "Very high strain sensitivity in thick film resistors: real and false super gauge factors" Sensor & Actuat. In press

[5] M.Prudenziati, B.Morten, G.Ruffi, E.Argentino, C.Iachetti "Size effect due to silver diffusion in RuO_2-based resistors" Proc.7th Europ.Hybr. Microel.Conf., Hamburg May 1989, paper 4.5

[6] M.Prudenziati, B.Morten, L.Olumekor, L.Moro, A.Tombesi "Interaction between terminations and thick film (cermet) resistors: the role of bismuth" J.Phys.D.Appl.Phys. 19, (1986) 275-282

ACKNOWLEDGEMENTS - The authors wish to thank Professor Piero Mazzetti for useful discussion and Mr. S.Rocco for help in the measurements.

1/f NOISE MEASUREMENT IN 0.1 OHM RESISTORS

J. COMALLONGA, M. SAVELLI, R. MARTIN, J. RABARIOELINA, P. MONBLANC*

Centre d'Electronique de Montpellier (UA 391)
Université des Sciences et Techniques du Languedoc
Place Eugène Bataillon, 34060 Montpellier
*Litelec S.A.
121, rue du Caducée, Parc Euromédecine, 34090 Montpellier, France

1- GENERALITIES

Let the frequency corner f_c between 1/f excess noise and thermal noise of resistor R = G-1 and let the noise index of resistor [NI] :

$S_{Th} = 4kGT$

$S_{exc} = KI^2/f$

$\Big\} \quad S_i = 4kGT\,(1+f_c/f)$

$f_c = KVI/4kT$ (1)

$[NI] = 10^6 \sqrt{2.3\,K}$ (2)

The recommendations of NBS (method 308 of MIL-STD 202 B) normalize the resistor excess noise measurement at 1 KHz with 1 KHz band width. The 1/f noise measure is possible only if $f_c > 1500$ Hz. The recent progress of thin film technology, the lower power nominal use of resistors have made that now the frequency corner is often lower than 1 KHz.

First we propose here, to change the standard by the use of 10 Hz filter central frequency, secondly we present the performances of a NM 1500 noise meter which allows the resistors excess noise measurement at 10 Hz and also allows the characterization of as low as 0.1 Ω resistors.

In fig 1 we present the variation of [NI] noise index versus power IV, for f_c=1500 Hz and f_c=10 Hz.

$$[NI] = 3\,10^6 \sqrt{f_c kT/IV} \qquad (3)$$

We see the improvement of measurement field to low excess noise values.

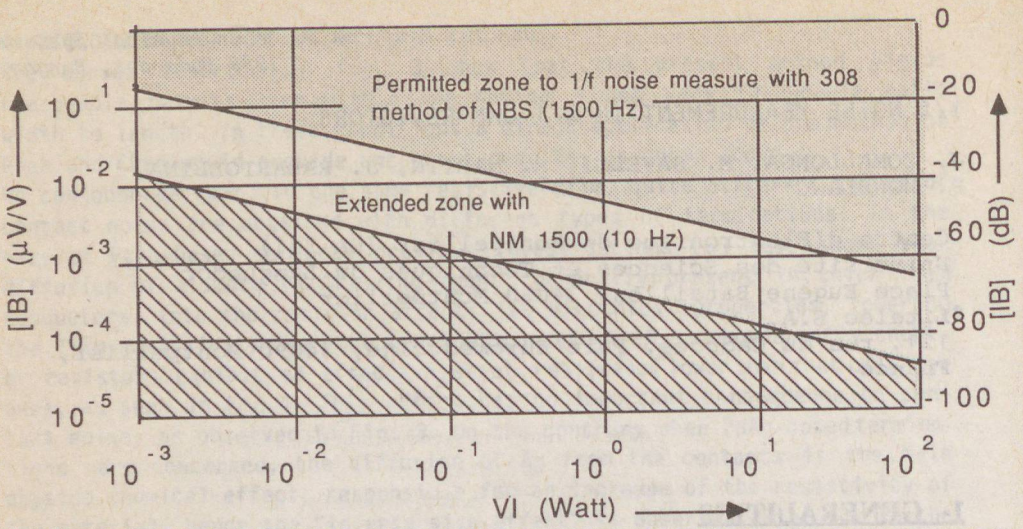

fig-1

2-PRINCIPLE OF MEASUREMENT

The general diagram in fig-2 shows the different parts of the noise meter and the different noise sources: e_E of bias system E, e_G of noise generator, e_o of preamplifier and e_R of the thermal and excess noise of resistor under test R.U.T.

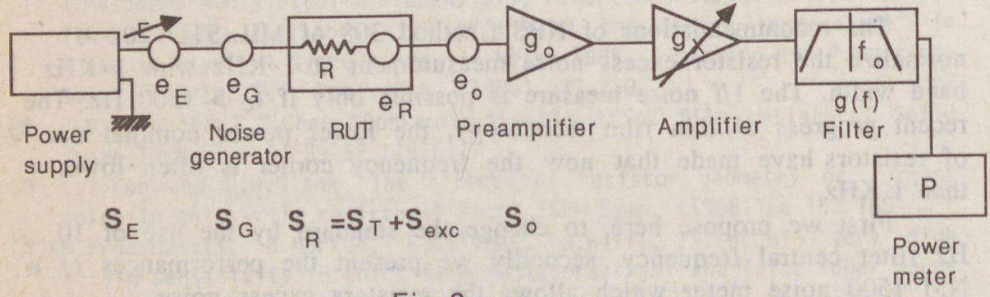

Fig-2

The process includes three measures synthesized in fig 3. The internal noise generator presents a 1/f spectrum, which allows to calculate the excess noise spectral density expression of R.U.T. :

	E	e_G	g_x	P
measure 1	0	1	g_1	P_1
measure 2	0	0	g_2	P_2
measure 3	1	0	g_3	P_3

fig-3

$$S_{exc}(f_o) = S_G(f_o) \frac{P_3/g_3 - P_2/g_2}{P_1/g_1 - P_2/g_2}$$

3-PRINCIPLE OF THE DIGITAL 1/f NOISE GENERATOR

It gives a sampled voltage e_g at sampling frequency f_e (see fig. 4)

$$e_{G_k} = V_G \sum_{p=2}^{p=127} \frac{1}{\sqrt{p}} \left(\sin \frac{2\pi}{256} p \frac{k}{f_e} + \Phi_p \right) \quad \text{with } V_G = 0.088 \text{ V and } \Phi_p = \text{random phase}$$

which presents a 1/f decreased lines spectrum spread between 0.81 Hz and 52 Hz (10 Hz filter), or 81 and 5200 Hz (1 KHz filter). Before attenuation, the voltage spectrum density is 3.84 10^{-4} V/√hz.

filter central frequency f_0	10 hz	1 khz
sampling frequency f_e(hz)	104.16	10,416
frequency step Δ f(hz)	0.407	40.7
minimum frequency f_{min}(hz)	0.81	81
maximum frequency f_{max}(hz)	52	5200
f_{max} / f_{min}	64	64

fig-4

4-PRINCIPLE OF PREAMPLIFIER

It is made up by a transductance amplifier preceded by a step up self-transformer with a ratio n and global gain go (see fig. 5).

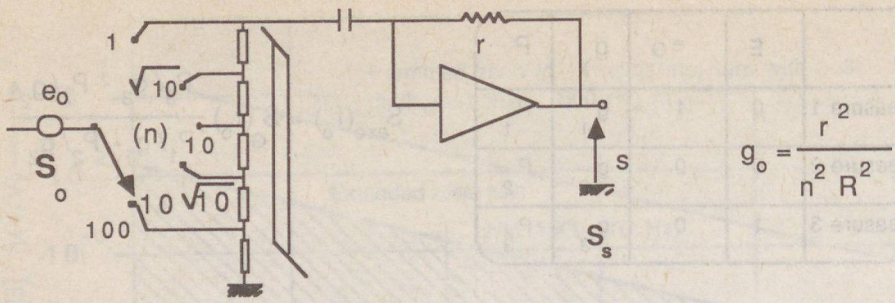

Fig-5

Fig.6 shows for r=1 MΩ the numerical values relative to different range of resistance values. The examination of S_T, S_0, S_G and S_E shows the comfort obtained in the measurement.

Resistance range (Ω)	100K / 10K	10K / 1K	1K / 100	100 / 10	10 / 1	1 / 0.1
n	1	1	$\sqrt{10}$	10	$10\sqrt{10}$	100
g_o range	10^2 / 10^4	10^4 / 10^6	10^5 / 10^7	10^6 / 10^8	10^7 / 10^9	10^8 / 10^{10}
RUT's thermal noise S.D. $\frac{S_T}{1.6}$	10^{-15} / 10^{-16}	10^{-16} / 10^{-17}	10^{-17} / 10^{-18}	10^{-18} / 10^{-19}	10^{-19} / 10^{-20}	10^{-20} / 10^{-21}
Preamplifier's internal noise S_o	10^{-18}	10^{-18}	10^{-19}	10^{-20}	10^{-21}	10^{-22}
Power supply's internal noise S_E	10^{-18}	10^{-18}	3×10^{-22}	3×10^{-22}	3×10^{-22}	3×10^{-22}
Power supply	260 V - 2 mA 22 V - 22mA		22 V - 22 mA 2.2 V - 220mA		2.2 V - 220 mA 50 mV - 500 mA	
Internal source noise S.D. S_G	3.8×10^{-13}	3.8×10^{-14}	3.8×10^{-15}	10^{-16}	10^{-17}	10^{-18}

(S in V^2 /Hz)

Fig.6

DIFFUSION NOISE GENERATORS REALIZED BY ANALOG CIRCUITS

Gy. TREFÁN, L.B. KISS, Z. GINGL, M. TÖRÖK, I. HEVESI, A. AMBRÓZY*

Department of Experimental Physics,
József Attila University
H-6720 Szeged, Hungary
*Technical University
H-1521 Budapest, Hungary

1. A MODEL OF THE DIFFUSION NOISE

Let's consider an electrically charged particle in a certain sample undergoing a one-dimensional Brownian motion! It means that the velocity v(t) of the particle is delta-correlated (v(t) is a white noise) and the displacement X(t) of it is a $1/f^2$ noise. When the particle reaches the border of the sample it steps out, so its contribution Y(t) to the conductivity is zero (if $X(t)>0$ then $Y(t)=0$); but when the particle is inside the sample it has a certain constant contribution Y(t) to the conductivity (if $X(t)<0$ then $Y(t)=1$). Since the Y(t) time-dependent dichotomous function with random switching times characterizes the essential diffusion features of the particle we call the process diffusion noise.

The spectrum of the diffusion noise Y(t) is proportional to $1/f^{3/2}$ as the (macroscopic) analytical [Van Vliet] and (microscopic) computer [Gingl et al.] investigations show. Since all particles move independently from each other, one Y(t) function shows the same spectrum like an ensemble of particles [Gingl et al.].

2. DIFFUSION NOISE MODELLING BY ANALOG CIRCUITS

We realized the above detailed principle by an analog circuit, the block-scheme of which you can see in Fig. 1. A white noise generator provides signal v(t). Then v(t)

is integrated by an active integrator, that gives signal X(t). X(t) drives a comparator which provides the dichotomous noise Y(t). We measured the spectrum S(f) of all signals by a selective nanovoltmeter in 10, logarithmically equidistant points in the 10Hz-10kHz range. The obtained spectra we presented in the appropriate places of Fig. 1. On the measured spectra we fitted a curve proportional to $1/f^k$.

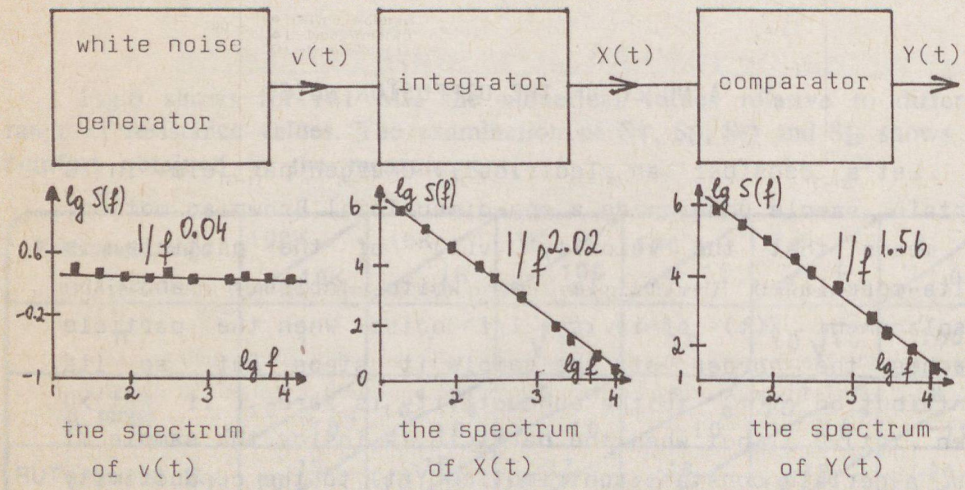

tne spectrum of v(t) | the spectrum of X(t) | the spectrum of Y(t)

Fig. 1.:Diffusion noise modelling by analog circuits and the appropriate spectra.

3. DIFFUSION NOISE GENERATOR GOVERNED BY COLORED NOISE

We investigated the cases when the spectrum of v(t) is not white, so that the spectrum of X(t) is not proportional to $1/f^2$. We colored the noise in the usual way [Keshner].

a;If the spectrum of v(t) is proportional to f^2 then X(t) has white spectrum and Y(t) has constant spectrum as well (Fig. 2.a.).

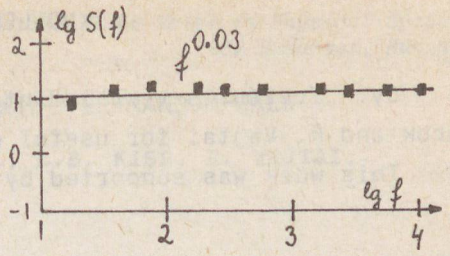

Fig. 2.a. The spectrum of Y(t) if v(t) has an f^2 spectrum.

b;If the spectrum of v(t) is proportional to f then X(t) is a 1/f noise and the spectrum does not change significantly after comparation (Fig. 2.b.).

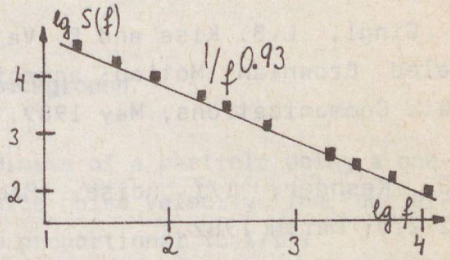

Fig. 2.b. The spectrum of Y(t) if v(t) has an f spectrum.

b;If the spectrum of v(t) is proportional to 1/f then X(t) is $1/f^3$ noise and the spectrum of Y(t) is $1/f^2$-like. (Fig. 2.c.).

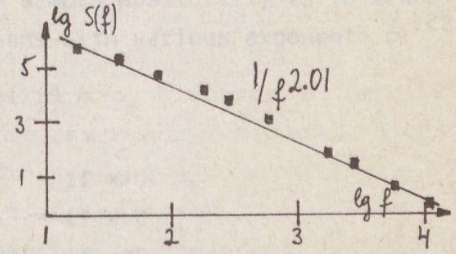

Fig. 2.c. The spectrum of Y(t) if v(t) has a 1/f spectrum.

ACKNOWLEDGEMENTS

Gy. Trefán is very indebted to Z. Gingl, L.B. Kiss, M. Török and R. Vajtai for useful discussions.

This work was supported by the OTKA and the FKP.

REFERENCES

Z. Gingl, L.B. Kiss and R. Vajtai; $1/f^k$ Noise Generated by Scaled Brownian Motion; accepted for publication in Solid State Communications, May 1989.

M.S. Keshner; 1/f noise; Proc. IEEE; 70; No. 3.; pp. 212-218; March 1982.

K.M. van Vliet and J.R. Fassett; Fluctuation Phenomena in Solids; ed. R.E. Burgess; Academic Press Inc.; New York; 1965.

10th Int.Conf. on Noise in Physical Systems
1989 Budapest, Hungary

$1/f^k$ NOISE GENERATORS BASED ON COMPUTER-RANDOM-WALK

A. AMBRÓZY, P. BÁNLAKI, Z. GINGL, L.B. KISS, R. VAJTAI,
Gy. TREFÁN, I. HEVESI

Technical University,
H-1521 Budapest, Hungary
Institute of Experimental Physics, József Attila University
H-6720 Szeged, Hungary

Theoretical background

Let x(t) be the position coordinate of a particle doing a one-dimensional random-walk with a white noise velocity. The Fourier-transform of x(t) yields a spectrum proportional to $1/f^2$.

A well-known approximation of this problem is a one-dimensional random-walk. A non-linear transformation of position coordinates x_i makes the spectrum change. A simple possibility is to transform x_i by symmetrized power functions with various exponents c:

$$y_i = g_c(x_i),$$

where

$$g_c(x) = \begin{cases} x^c & \text{if } x>0 \\ 0 & \text{if } x=0 \\ -|x|^c & \text{if } x<0 \end{cases}$$

In this case the spectrum of new position coordinates y_i strongly depends on the exponent c but, according to computer simulations, stays proportional to $1/f^k$, where k is determined by c ($0<k\leq 2$) [1].

Realization

The discrete random-walk can be easily modelized by computers and the transformation of the position coordinates is simple too. So, if one needs $1/f^k$ noise generators with variable exponent k, it is useful to use a computer. To get analog signals we can apply D/A-converters.

For the realization we used a C-64 microcomputer. The random-walk was simulated by a short and simple program written (by Z.G.) in assembler for satisfying computing speed. The exponent of the transforming power function was variable. The D/A-converter was a 8-bit AD7524 which has suitable parameters.

We used the measuring arrangement outlined here:

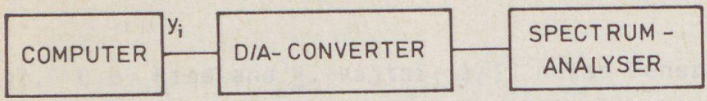

Fig.1

When the random-walk reached the boundary coordinates (127 or -128) then the system was sent back to the initial state (x_i=0). The average repetition frequency of such initialization turned out to be approximately 1 Hz, thus we got a noise stationary for longer times than 1 sec. We found that the spectra were proportional to $1/f^k$ in the frequency range 1.6Hz-8kHz at several values of the exponent of the transforming power-function. If the exponent is less than -0.6 then the above proportionality doesn't exist more. It comes from the limited resolution of the 8-bit D/A-conversion. The results can be seen below:

exponent of $g_c(x)$ c	exponent of the spectrum k
1.0	1.95
0.8	1.95
0.6	1.94
0.4	1.85
0.2	1.70
0.0	1.52
-0.2	1.34
-0.4	1.17
-0.6	1.02

The great advantages of this generator principle are simplicity, high speed and the wide range of the $1/f^k$ spectrum obtained. Fig. 2 shows the spectra generated by computer.

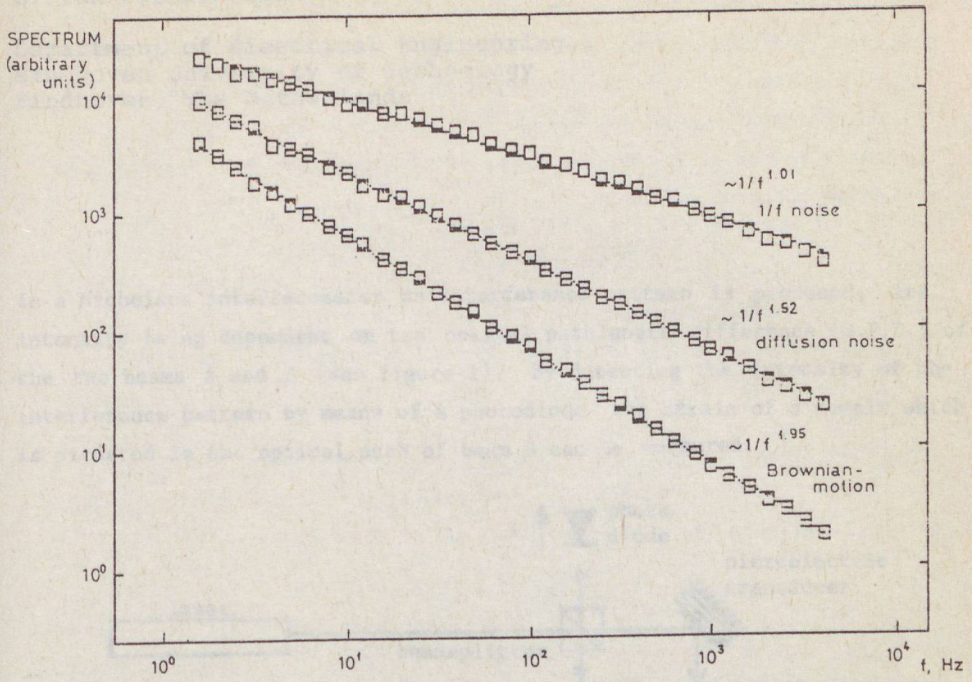

Fig.2

It is important to note that the reachable $1/f^k$ range of frequcncy is proportional to the squared range of the D/A-converter.
Thus, a 16-bit D/A-converter can provide a $1/f^k$ spectrum through more than 7 decades of frequency.

Reference

[1] Z. Gingl. L.B. Kiss, R. Vajtai, '$1/f^k$ Noise Generated by Scaled Brownian Motion', accepted for publication in Solid State Communications, May 1989.

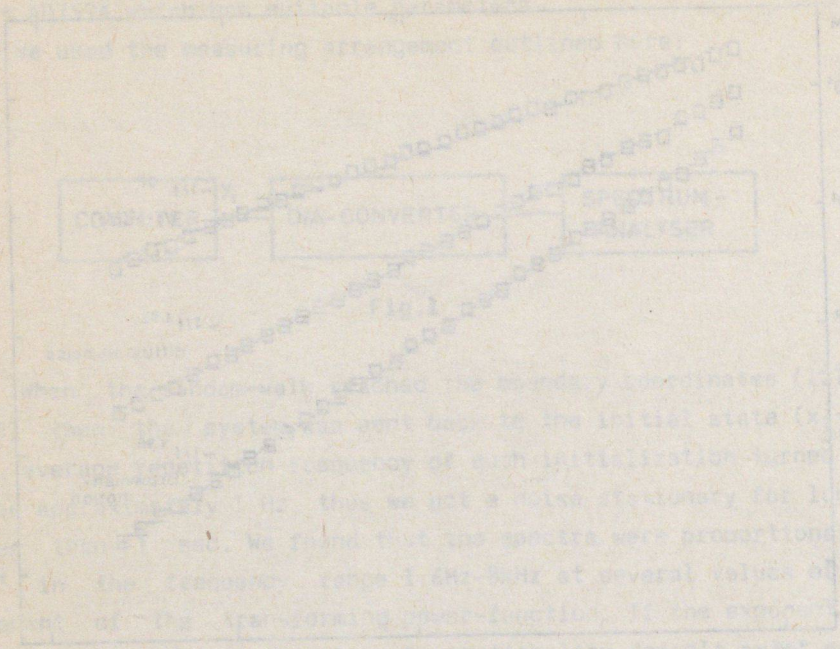

10th Int.Conf. on Noise in Physical Systems
1989 Budapest, Hungary

NOISE LIMITED RESOLUTION OF A MICHELSON INTERFEROMETER

S. van STERKENBURG

Department of Electrical Engineering,
Eindhoven University of Technology
Eindhoven, The Netherlands

In a Michelson interferometer an interference pattern is produced, its intensity being dependent on the optical pathlength difference (O.P.D.) of the two beams A and B (see figure 1). By detecting the intensity of the interference pattern by means of a photodiode the strain of a sample which is situated in the optical path of beam B can be measured.

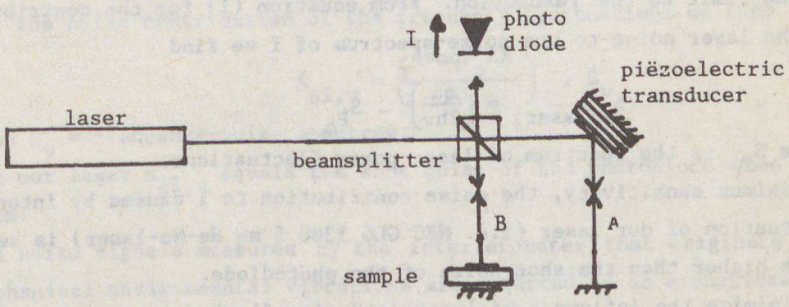

Figure 1: Schematic diagram of a Michelson interferometer

A Michelson interferometer can be used as a dilatometer to measure electrostrictive strains [1].
For certain ionic crystals with very small electrostrictive strains, different values of electrostrictive constants have been measured, which might be explained by a limited resolution and accuracy of the measuring equipment [2],[3].
We analysed the limitations of the resolution of a Michelson interferometer and changed the set-up to obtain an optimum performance.
We found five contributions that deteriorate the resolution.
1. The shot noise in the photodiode used to detect the light intensity of the interference pattern sets the lower resolution limit.

The current I through the photodiode is

$$I = \frac{\alpha q P_o (1 + A \sin \phi)}{2h\nu} \qquad (1)$$

with α = light power loss factor, P_o = laser-light power, ν = frequency of the laser-light, A = contrast factor accounting for the inequality of the power in the two arms, $\phi = 4\pi(X + x)/\lambda$ with λ = wavelength of laser light, X = static O.P.D. and x = dynamic dilatation of sample.
The sensitivity defined as $(\partial I/\partial x)$ has a maximum for $\phi = \pm n\pi$.
For these values of ϕ the shot noise of the photodiode contributes to the noise-spectrum of x with

$$S_x = \frac{2qI}{(\partial I/\partial x)^2} = \frac{hc\lambda}{4\alpha\pi^2 P_o A^2} \quad [m^2/Hz] \qquad (2)$$

with c the light velocity.
For a He-Ne-laser with A = 0.9 and P_o = 5 mW and α = 0.5 we find

$\langle S_x \rangle^{\frac{1}{2}} = 1.3 \cdot 10^{-15}$ m/$\sqrt{Hz}$.

2. The noise caused by intensity fluctuations of the laser light sets a second limit to the resolution. From equation (1) for the contribution of the laser noise to the noise-spectrum of I we find

$$S_{I(laser)} = \left(\frac{q\alpha}{2h\nu}\right)^2 \cdot S_{P_o} \qquad (3)$$

where S_{P_o} is the spectrum of laser-power fluctuations.
At maximum sensitivity, the noise contribution to I caused by intensity fluctuation of our laser (i.e. NEC GLG 5360 5 mW He-Ne-laser) is several times higher than the shot noise of the photodiode.
To minimize the influence of laser-intensity fluctuations we introduce the use of an optical isolator technique (O.I.T.) in our interferometer as has been shown in figure 2.

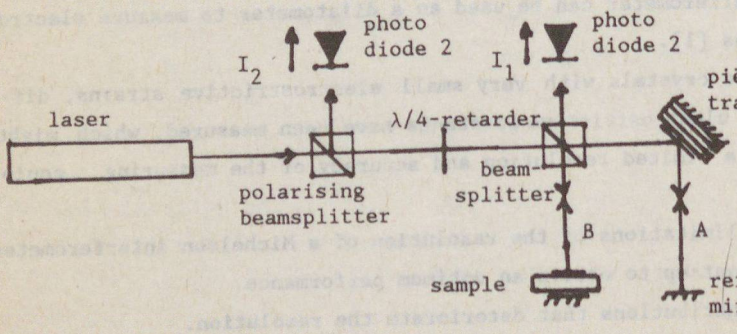

Figure 2: New set-up of Michelson interferometer with O.I.T. to minimize laser-noise influences

By using this O.I.T. one can measure the other half of the interferred beam coming from the beamsplitter. If the currents through the diodes are given by

$$I_1 = \frac{\alpha q P_o (1 + A \sin \phi)}{2h\nu}, \qquad I_2 = \frac{\alpha q P_o (1 - A \sin \phi)}{2h\nu}$$

then the current difference ΔI defined as $\Delta I = I_1 - I_2$ is

$$\Delta I = \frac{\alpha q P_o A \sin \phi}{h\nu} \tag{4}$$

The influence of the laser noise on ΔI is now

$$S_{\Delta I(\text{laser})} = \left(\frac{q\alpha}{h\nu} A \right)^2 \cdot \sin^2\phi \cdot S_{P_o} = 0 \text{ for maximum sensitivity.}$$

Another important advantage of this O.I.T. is an increase of the measured light power by a factor of two, which leads to a decrease in the shot noise contribution to the noise spectrum of x by a factor of two.

3. Frequency fluctuations of the laser light also contribute to noise in the current difference ΔI. In fact, Michelson Interferometers are very suitable for measuring laser frequency fluctuations [4]. From equation (4) for the noise contribution of the frequency fluctuations we find

$$S_{\Delta I,\nu} = \left(\frac{4\pi\alpha q P_o A X}{h\nu c} \right)^2 \cdot S_\nu \tag{5}$$

with S_ν = frequency-noise spectrum.

For our laser $S_{\Delta I,\nu}$ equals the shot noise of the photodiode when X is 1 cm.

4. All noise signals measured by the interferometer that originate from mechanical environmental vibrations are referred to as acoustical noise. This can be minimized by rigid construction of the interferometer and the use of acoustic isolating techniques. Careful design of our interferometer leads to a more or less white noise spectrum owing to acoustic noise in the frequency range between 100 Hz and 1 kHz dominating all other noise sources mentioned. For frequencies above 1 kHz the influence of the acoustic noise decreases rapidly to values below the shot noise level.

5. Beside the four noise sources mentioned there is an important systematic error. In the measurement of electrostrictive strains we found that Coulomb forces from the applied electric field lead to a vibration of the sample holder at the same frequency as the electrostriction signal. The vibration depends strongly on the configuration of the sample holder and electrodes. The amplitude of these dilatations is in the order of 10^{-13} m at a field strength of 10^6 V/m over the sample (which is a usual field

strength for electrostriction measurements). We developed a new double interferometer that measures both the dilatation of the sample and holder, thus making it possible to eliminate the influence of Coulomb forces (see figure 3). The noise of a double interferometer is twice that of a single interferometer, assuming that noise signals of both interferometers are uncorrelated.

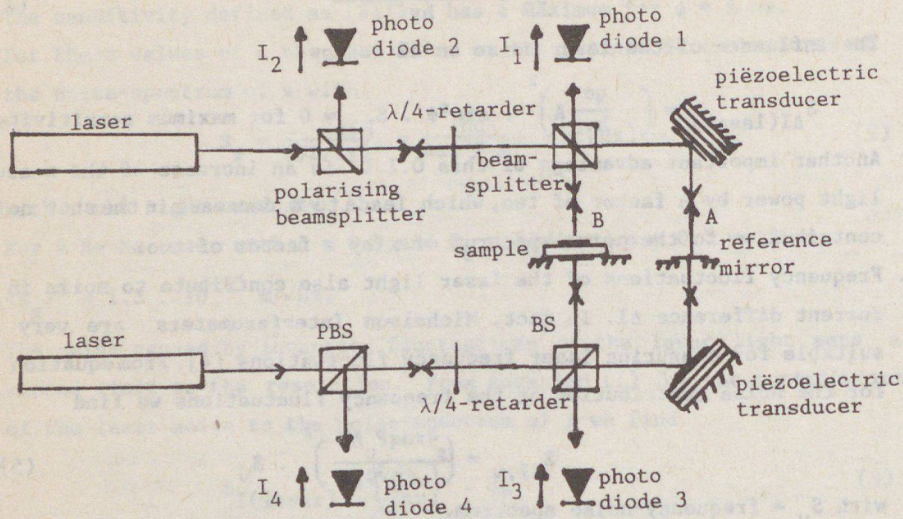

Figure 3: Schematic diagram of a double Michelson interferometer

In conclusion we can state that, in the frequency range between 100 Hz and 1 kHz, acoustic noise is the most important noise source. For frequencies above 1 kHz the shot noise in the photodiodes determines the ultimate resolution. We expect that all measures made to minimize the noise and systematic errors will lead to reliable determinations of the electrostrictive constants of ionic crystals.

REFERENCES

[1] Th. Kwaaitaal, Rev. Sci. Instrum. 45, 39-41 (1974).

[2] G.J. Legg and P.C. Lanchester, J. Phys. E. Sci. Instrum. Vol. 14, 1241 (1981).

[3] Q.M. Zhang, S.J. Jong and L.E. Cross, J. Appl. Phys. 65 (7), 1989.

[4] P. Spano, S. Piazzolla and M. Bamburinni, IEEE J. Quantum Electron. 2E-20, 350 (1984).

10th Int.Conf. on Noise in Physical Systems
1989 Budapest, Hungary

NOISE REDUCTION PRINCIPLES IN SPECTRO-ELLIPSOMETRY

V. NAUMBURGER

Zentrum für Wissenschaftlichen Gerätebau,
Akademie der Wissenschaften der DDR
Seestrasse 82, Berlin-Rahnsdorf, 1166 GDR

The spectro-ellipsometric measurement is an optical method for evaluating very thin films both in thickness and composition used in the field of semiconductor research and production. Modern ellipsometers are required to be very fast still ensuring high accuracy measurement. Thus electronically controlled high-frequency light modulators, photo-multiplier and digital equipment are used.

The required information about the sample to be investigated are encoded in the so-called Stokes-Fourier vector s_o, s_1, s_2 and s_3 of the incident linearly polarized light beam after touching the surface of the sample. Presuming that the angle of incidence and the wavelength of light as well as the Stokes-Fourier vector are known, the film thickness and composition of the sample can be determined.

Our spectro-ellipsometer uses two photo-elastic modulators in order to modulate the incident light beam twice. Only in this case can all components of the Stokes-Fourier vector be estimated. They are proportional to the amplitudes of certain spectral lines of the photo-current i_K (E_q. (1)).

$$i_K = s_o + s_1 \sin[\phi_1(t)] \cos[\phi_2(t)] + s_2 \cos[\phi_1(t)] + s_3 \sin[\phi_1(t)] \cos[\phi_2(t)] \quad (1)$$

Being sinoidal functions of the frequencies f_1 and f_2, $\phi_1(t)$ and $\phi_2(t)$ possess one common subharmonic which represents the fundamental frequency f_o for all spectral lines occurring. Thus

the Stokes-Fourier vector can be yielded by means of Fourier transformation.

Of course the photo-current delivered by the photo-multiplier is more or less superposed by noise which disturbs the measurement. The error e, due the influence of noise, is equal to the square root of the noise power $\tilde{s}_N^2$ in the spectral band ΔF. Presuming that the spectral power density S_N of the interfering noise is known, Eq. (2) is valid:

$$e = \sqrt{\tilde{s}_N^2} = \sqrt{2\Delta F \; S_N(f_i)} \tag{2}$$

whereby f_i represents the frequency of the spectral line in question. From the uncertainty principle it is known that the bandwidth ΔF is indirectly proportional to the observing time ΔT. Under these conditions the shortest observing time can be estimated for any given error e (Eq. (3)):

$$\Delta T = 2 \; S_N(f_o)/e^2 \tag{3}$$

i.e. the noise influence on the accuracy of the result can be reduced by increasing the observing time. But what about the situation in the case of digital signal processing? One of the most important things to be dealt with is the resolution required for the analog to digital conversion. On the one hand, the finite extent of the ADC's smallest step (LSB) leads to the so-called quantizing noise. On the other hand, the resolution required is limited by the noise of the signal source (Eq. (4)):

$$\text{resolution/bit} = \frac{1}{20 \; \lg 2} \; \text{SNR/dB} \tag{4}$$

whereby SNR stands for the logarithmic Signal to Noise Ratio and shall include the signal dynamics here. In this case the quantizing noise power is equal to the noise power of the signal source. The situation becomes critical if the ADC's resolution is smaller than estimated in Eq. (4), because either the subtilities of the signal will be neglected or the peaks of the signal will be truncated. We use in our ellipsometer a fast

video-ADC with 8-bit resolution. But the resolution required should not be less than 10 bit in respect to the dynamics and the SNR of the signal.

This dilemma can be overcome by using one of the most famous methods for reducing the influence of superimposed noise on periodical signals - the so-called "averaging". Averaging in connection with Fourier transformation may be considered as a splitted performance of Fourier transformation. Both averaging and Fourier transformation are time-depending integrals. If the Fourier time interval ΔT is identical with an integer multiple of the fundamental frequency period T_o of the signal to be investigated, and if the signal is stationary in this interval, then the time interval of the Fourier transformation can be reduced to one period of the fundamental frequency without any error, and if the averaging cycle time can also be chosen as equal to the fundamental frequency period T_o, the Fourier transformation can be carried out in two separate steps. First the full-scale averaging is carried out. Then the Fourier transformation follows in a fraction of the original time interval. This is a very effective way to reduce signal processing time and to minimize memory effort. But the main advantage emerges from introducing a "well-determined" interfering signal to improve the resolution of the analog to digital converting process. This interfering signal is superimposed to the signal to be investigated. If u_{LSB} is equal to the voltage extent of the LSB and $p = 2^P$ (P integer) is equal to the number of averaging cycles, then the "well-determined" interfering signal consists of a monotonically increasing direct voltage, which increases in steps of u_{LSB}/p after each averaging cycle. In this way the resolution can be increased by P bit as far as the remaining noise power is bigger than the noise power of the signal to be investigated.

As the averaging process is based on the different properties of coherent and incoherent signals like periodical and stochastic signals, noise also can help to increase the resolution of the analog to digital converting process. Presuming that the interfering noise is Gaussian, the resolution can be improved by P bit after carrying out $p = 2^{2P}$ averaging cycles,

because noise is an incoherent signal. Under this condition the effective resolution will be increased by the square root of p like the SNR.

In contrast to this, the "well-determined" interfering signal is coherent to the signal to be investigated, thus the improvement is more close to P by p averaging cycles. Figure 1 shows the dependence of the effective resolution on the number of averaging cycles under the condition of SNR about 55 dB and a 4-bit ADC.

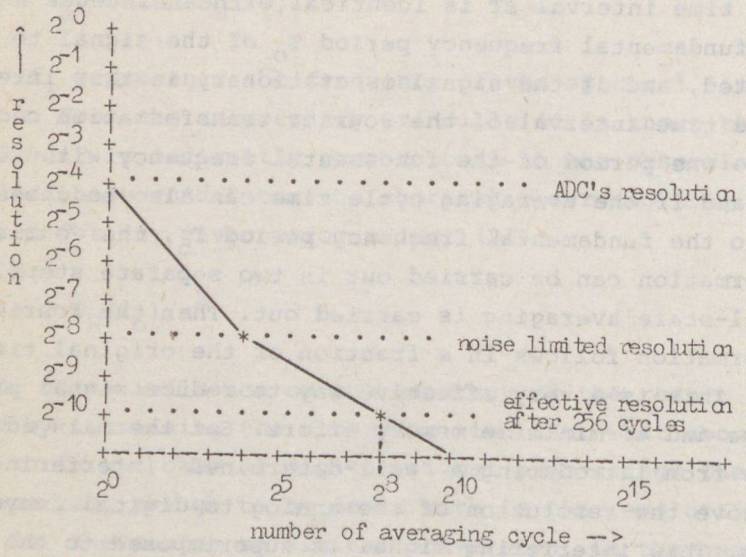

Fig. 1. Resolution versus number of averaging cycles

With respect to this statement the most important work in the field of fast ellipsometry by photo-elastic modulation is to synchronize the periodic signals. For this purpose all frequencies, especially the sampling frequency for the ADC, the feeding frequencies for the light modulators and the fundamental frequency for the Fourier transformation are derived from one single clock generator. Thus it is ensured that the signal components to be investigated are absolutely coherent. The accuracy of the Fourier transformation including the light modulators and the ADC was proved experimentally by means of bandwidth measurement and it was shown that the results yielded are very close to the theoretically predicted ones.

10th Int.Conf. on Noise in Physical Systems
1989 Budapest, Hungary

REAL TIME EXPERIMENTAL MEASUREMENTS OF NOISE SOURCE CORRELATION IN AMPLIFIERS AND TRANSDUCERS

R. ALABEDRA, D. RIGAUD, B. ORSAL, J.M. PERANSIN, M. VALENZA

Centre d'Electronique de Montpellier
(associé C.N.R.S. UA 391),
Université des Sciences et Techniques du Languedoc
34060 Montpellier Cedex, France

Abstract : With the help of a two-channel F.F.T. spectrum analyzer, the coherence function is obtained. The experimental method is applied to active semiconductor devices such as laser diodes or F.E.T.'s. The first experimental results are presented.

I - INTRODUCTION

Generally in active semiconductor devices, two or more noise sources are required for their noise characterization. These sources are correlated.

In order to obtain a better analysis of the behaviour of the devices than a single spectral density measurement, it is necessary to determine the coherence function in real time.

The purpose of this paper is to present firstly the experimental set-up which allows us to reach the coherence values and, secondly, two different applications for semiconductor devices.

II - EXPERIMENTAL SET-UP AND COHERENCE FUNCTION

The equipment includes two independent low noise amplifier channels, for instance two voltage or current amplifiers or a voltage and a current amplifier.

It is possible to reach the noise measurement of an equivalent current as low as 10^{-10} with current amplifiers in the frequency range 1Hz-100KHz ; or an equivalent noise resistor as low as 10Ω in the same frequency range.

The output signals are connected to the channel of the F.F.T. spectrum analyzer (HP 3562A Dynamic signal analyzer). Both the noise spectra and the coherence function are obtained.

Usually if S_{xx} and S_{yy} are the channel 1 and 2 power spectra and S_{xy} is the cross spectrum, the coherence function is defined according to the

following formula [1] :

$$\gamma^2 = \frac{|S_{xy}|^2}{S_{xx} S_{yy}} \qquad (1)$$

III - APPLICATION TO THE LASER DIODES

For laser diodes we present the coherence function between the electrical noise and the optical power fluctuations.

In this case the experimental set-up is shown in figure 1.

In channel 1, we measure the voltage fluctuations across the laser diode. In channel 2, the optical power fluctuations are converted into current fluctuations by means of a standard photodiode.

Equation (1) becomes :

$$\gamma^2_{\text{opt-elec}} = \frac{|S_{I_{ph}V}(f)|^2}{S_{I_{ph}}(f) \cdot S_v(f)} \qquad (2)$$

where $S_{I_{ph}V}(f)$ is the cross spectrum, $S_{I_{ph}}(f)$ and $S_v(f)$ are the spectral densities of the two channels (see figure 1).

The results obtained on an index guided Sharp LMT 10 laser [2] used for optical fibers at wavelength of 0.8µm are reported in figure 2 : the values of the coherence function at 100KHz are shown versus the drive current. In the regions (I) and (III),(see figure 2) corresponding to spontaneous (I_L < 52 mA) and stimulated (I_L < 70 mA) emissions no coherence is observed. Nevertheless, in region (II), between 52 and 70 mA, the coherence increases as the gain and decreases when the optical mode gain becomes saturated [3].

IV - APPLICATION TO FIELD EFFECT TRANSISTORS

For F.E.T.'s the coherence function has been measured between the gate noise $i_g(t)$ and the channel noise $i_d(t)$. The experimental set-up for this application is given in figure 3.

Equation (1) becomes :

$$\gamma^2_{V_1-V_2} = \frac{|S_{V_1-V_2}(f)|^2}{S_{V_1}(f) \cdot S_{V_2}(f)} \qquad (3)$$

where $S_{V_1}(f)$ and $S_{V_2}(f)$ are the spectrum densities of the fluctuations at the outputs of the two amplifiers.

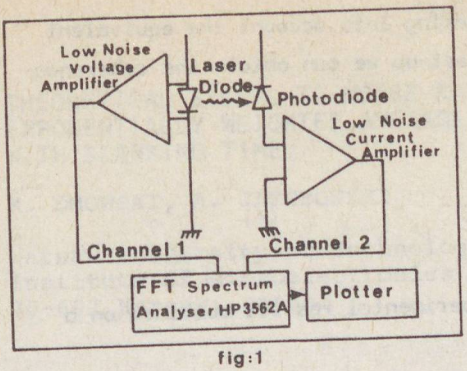

fig:1

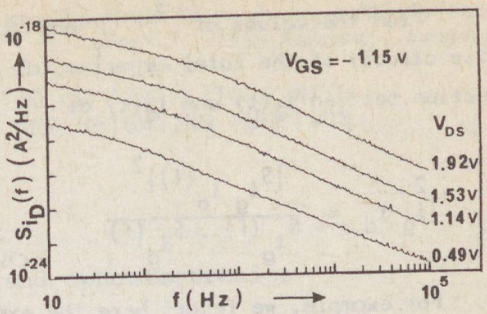

fig:4

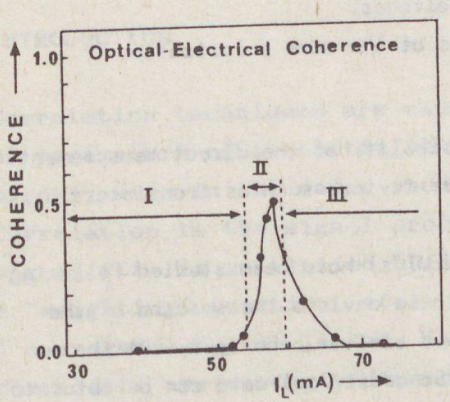

fig:2

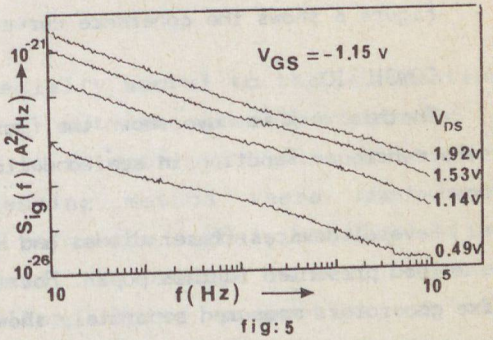

fig:5

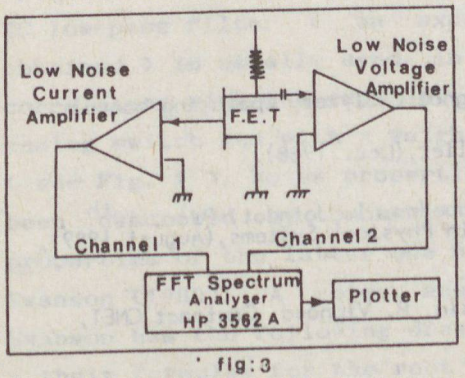

fig:3

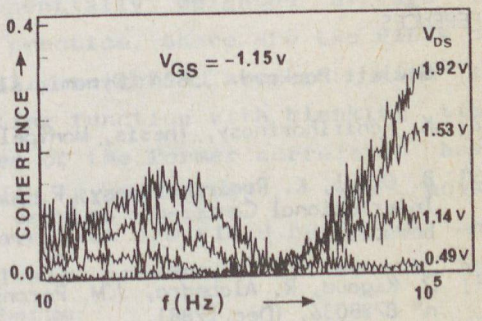

fig:6

From the values of $\gamma^2_{V_1-V_2}$ and taking into account the equivalent noise circuit of the total experimental set-up we can obtain the coherence function between $i_g(t)$ and $i_d(t)$ as :

$$\gamma^2_{i_g-i_d} = \frac{|S_{i_g i_d}(f)|^2}{S_{i_g}(f) \cdot S_{i_d}(f)} \qquad (4)$$

For example, we report here the experimental results obtained on a Ga As HEMT [4].

Figures 4 and 5 show the noise spectra of the channel and the gate measured separately for different bias voltages.

Figure 6 shows the coherence curves at the same polarization.

V - CONCLUSION

In this work we have shown the feasibility of the direct measurement of the coherence function in semiconductor devices such as transistors or transductors.

Several devices (laser diodes and HEMT's) have been studied following the method presented in this paper. For these devices the spectra of the noise generators measured separately showed similar behaviour, but the coherence functions were very different. So additional data can be obtained in order to specify and characterize the semiconductor devices more accurately.

REFERENCES

[1] Hewlett Packard 3562A Dynamic signal analyzer, Operating manual.

[2] K. Raniriharinosy, Thesis, Montpellier, (Dec. 1988).

[3] B. Orsal, K. Raniriharinosy, R. Alabedra, I. Joindot, Proc. 10th International Conference on Noise in Physical Systems, (August 1989), Budapest.

[4] D. Rigaud, R. Alabedra, J.M. Peransin, P. Vignaud, Contract CNET, n° 878B036, (Dec. 1988).

10th Int.Conf. on Noise in Physical Systems
1989 Budapest, Hungary

THEORETICAL SIGNAL-TO-NOISE RATIO OF CORRELATORS WITH EXPONENTIALLY WEIGHTED AVERAGE AND WEIGHTING FUNCTION WITH BLANKING TIME

K. DMOWSKI, A. JAKUBOWSKI

Warsaw University of Technology,
Institute of Microelectronics and Optoelectronics
00-662 Warsaw, Poland

INTRODUCTION

Correlation techniques are especially useful to the estimation of parameters of a repetitive (not necessarily periodic) signal, even in the cases when it is entirely hidden in noise. Correlation is the signal processing method where the input signal f(t) is multiplied by a reference signal, usually called a "weighting" function w(t), and the product is next filtered (averaged) by a linear filter. Noise properties of the correlator are strongly dependent on the weighting function, as well as on the filtering method. As a filter, an integrator [a true (summing or linear) averaging is obtained] or a simple RC low-pass filter (an exponentially weighted average is obtained) is usually used. In practice, there are two kinds of correlators with the exponentially weighted average: with an analog switch and with a weighting function with blanking time (see Fig. 1). Noise properties of the former correlator have been described by Dmowski and Pióro (1987). The noise properties of the latter one have been described by Borsuk and Swanson (1980). A noise analysis presented by Borsuk and Swanson has the following drawbacks:

- their formulas for the root mean square value of the output noise and the output signal-to-noise ratio are limited to case when $T_m \to T_p$ and they have inconvenient forms for calculations,
- those formulas are derived using a mathematical model of white noise which is not preferable considering simplicity and efficiency of calculations,

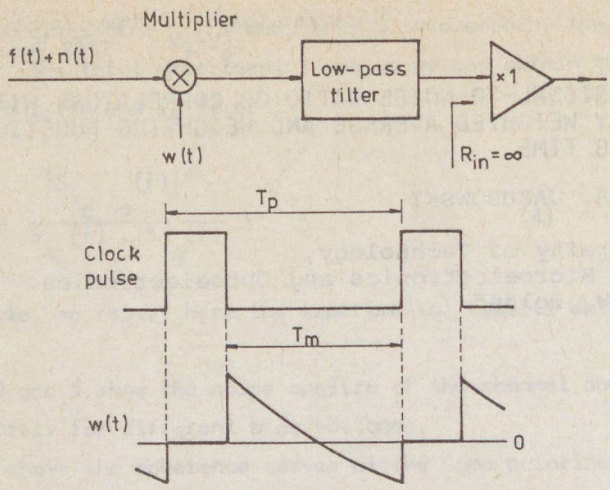

Fig.1. A simplified block diagram of the correlator with an exponentially weighting average and a weighting function with blanking time. The shape of the weighting function in the time interval $[0,T_m]$ is arbitrarily chosen.

- there are not specified assumptions for which those final formulas are satisfied.

This paper presents a new approach to this problem based on the theory of stochastic processes which is free of the drawbacks mentioned above.

THEORETICAL CONSIDERATIONS

We assume that the signal available for analysis has the form

$$g(t) = \begin{cases} f(t) + n(t), & 0 < t < T_p \\ 0, & t < 0 \end{cases} \qquad (1)$$

where $n(t)$ is noise, $f(t)$ is a transient signal which satisfies the following condition

$$f(t + kT_p) = f(t) \quad \text{for } k = 1, 2, \ldots, n, \ldots$$

The correlator output at $t=nT_p$ is given by

(2)

$$E(nT_p) = \int_0^{nT_p} 1/RC \exp[-(nT_p - t)/RC][f(t) + n(t)]w(t)dt$$

where $w(t)$ is an arbitrarily chosen weighting function which must satisfy only Dirichlet's conditions.
The steady state of the signal part, S, of the correlator output is reached within a deviation of less than 1% after the measurement time $t = nT_p$ ($nT_p/RC \geq 5$) and can be expressed as

(3)

$$S = S_{d-c} + S_{a-c}$$

where S_{d-c} is given by

$$S_{d-c} = \exp[-(T_p - T_m)/RC] \frac{1 - \exp(-T_m/RC)}{1 - \exp(-T_p/RC)} \frac{1}{T_p} \int_0^{T_m} f(t)w(t)dt$$

and S_{a-c} - is a sum of a Fourier series. For many applications [as for deep-level transient spectroscopy (DLTS)] the parameters of the transient signal $f(t)$ may be estimated from S_{d-c}. A strong rejection of the ac fluctuation is necessary for unambiguous and precise measurement. It is satisfied for $2\pi RC/T_p \gg 1$. The correlator properties are strongly affected by the shape of the weighting function. Therefore, for the given application it is necessary to match the "optimum" weighting function. The most important problem for such optimization is the calculation of the output signal-to-noise ratio. The calculations similar to those presented by Dmowski and Pióro, can be performed for three mathematical models of white noise. Considering the simplicity and efficiency of calculations, the method based on the theory of stochastic processes proved to be the most preferable. Because of space limitations, we present only an analysis for a mathematical model of white noise based on the theory of stochastic processes. Noise at the correlator output can be described by the process

$$y(t) = \int_0^t 1/RC \exp[-(t-t_1)/RC] n(t_1) w(t_1) dt_1 \qquad (4)$$

The root mean square value of the output noise at instant $t=nT_p$ is given by the variance of the process $y(t)$. After some calculations, it can be shown that for $2\pi RC/T_m \gg 1$ and $2nT_p/RC \geq 5$ the output signal-to-noise ratio $[(S/N)_{out}]$ can be expressed as

(5)

$$(S/N)_{out} = B^* \sqrt{\frac{2RC}{T_p}} \sqrt{\frac{1 - \exp(-T_m/RC)}{1 - \exp(-T_p/RC)} \frac{1 + \exp(-T_p/RC)}{1 + \exp(-T_m/RC)}}$$

$$\text{where} \quad B^* = \sqrt{\frac{2}{N_0}} \int_0^{T_m} f(t) w(t) dt \Big/ \left[\int_0^{T_m} w^2(t) dt \right]^{1/2}$$

Using Schwarc's inequality it can be readily shown that the $(S/N)_{out}$ takes the maximum value when $w(t)$ has the same shape as $f(t)$. In practice, for $T_m/RC \ll 1$ and $T_p/RC \ll 1$ Eq.(5) reduces to the following form

$$(S/N)_{out} = B^* \sqrt{\frac{2RC}{T_p}} \sqrt{\frac{T_m}{T_p}} \qquad (6)$$

The analytical formulas obtained in this paper and those derived by Dmowski and Pióro can be simply used in designing and optimization of correlators with the exponentially weighted average. In our future paper, the calculations of the output S/N ratio and the signal-to-noise improvement ratio, another frequently used noise parameters of the correlators, will be presented in detail.

1. Borsuk J.A. and Swanson R.M 1980, IEEE Trans. Electron Dev. ED-27, pp.2217-2225

2. Dmowski K. and Pióro Z. 1987, Rev. Sci.Instrum. 58, pp.2185-2191

10th Int.Conf. on Noise in Physical Systems
1989 Budapest, Hungary

NOISE PROPERTIES OF NEGATIVE R, C AND L ONE-PORTS BASED ON FOUR-FREQUENCY PARAMETRIC SYSTEMS

V.N. DAMGOV

Space Research Institute, Bulgarian Academy of Sciences
1000 Sofia, Bulgaria

ABSTRACT

A general theory of the noise properties of negative R, C and L one-ports based on four-frequency parametric systems is presented. Conditions for utilization of parametric one-ports with negative parameters in a joint stage are derived.

INTRODUCTION

As it has been demonstrated in our previous works (1-4), by the use of C-, L-, RC- and RL- four-frequency parametric systems the low noise negative C, L and R with constant absolute values can be obtained. The negative C, L and R can exist in a wide video frequency band from 0 Hz up to a limited frequency, equal to (5÷10)% of the pumping frequency of the parametric elements.

Wide-band negative conductances are applied in the design of a new type of parametric amplifiers - regenerative parametric videoamplifiers without conversion of the signal frequencies. Low-noise wide-band negative C and L can be effectively applied to wide-band frequency correction, increasing the sensitivity of various systems.

The purpose of this paper is to present a general theory and an experimental examination of the noise properties of the negative C, L and R one-ports based on four-frequency parametric systems.

EQUIVALENT CIRCUITS

The noise properties of the four-frequency parametric system as a one-port with negative parameters have been studied on the basis of the equivalent circuit, shown in Fig. 1. The signal source, the parametric system (PS) and the load (the next amplifying stage) have been considered as a joint stage. The noise sources considered and the corresponding admittances are clear from Fig. 1, where $Y_s = G_s + jB_s$, $Y_L = G_L + jB_L$, $\overline{i^2_{NL}} = G_{NL}N$, $\overline{u^2_{NL}} = R_{NL}N$, $N = 4kT\Delta f$, Δf is a frequency band, G_{NL} and R_{NL} are respectively the noise effective conductance and the noise effective resistance of the load (the next amplifying two-port). PS is presented by the parametric capacitance C(t) and the parametric conductance G(t), connected in parallel; $\dot{Y}_1 = G_1^0 + jB_1$ is the admittance of the PS input circuit and $\dot{Y}_+$ and $\dot{Y}_-$ present the admittances of the PS oscillating circuit at frequencies $\omega_+ = \omega_p + \omega_s$ and $\omega_- = \omega_p - \omega_s$ where ω_p is the pumping frequency. It is assumed that $\dot{Y}_i = 0$ for all frequencies $\omega \neq \omega_i$, where $i \to s, +, -$.

The internal noise of PS is taken into consideration including the noise sources $\overline{i^2_{Nn}} = N\,\mathrm{Re}(\dot{Y}_n)$, $\overline{i^2_{dn}} = 2qI_0\Delta f_n$, where $n \to 1, +, -$, q is the electron charge, I_0 is D. C. current through the complex parametric element. In the first approxima-

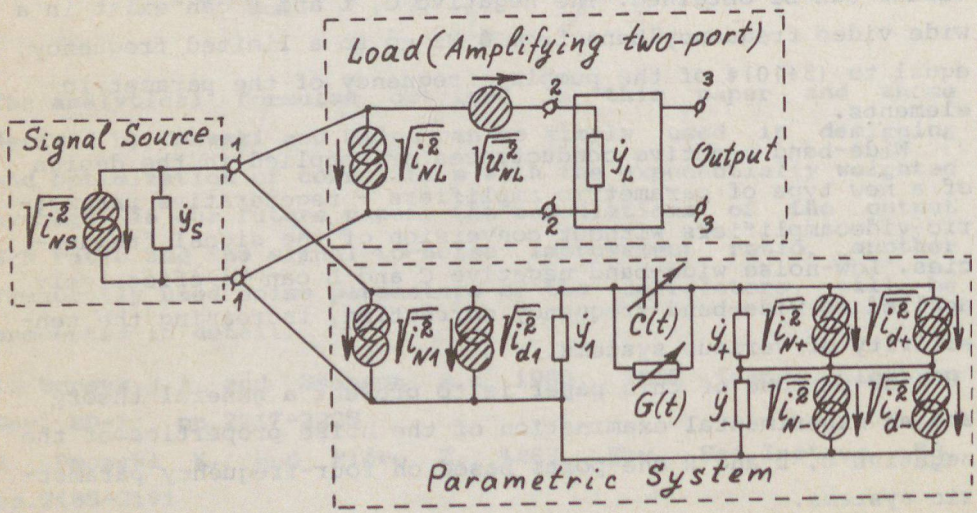

Fig. 1. General equivalent circuit of the joint stage.

tion the flicker noise and the correlation between noise sources $\overline{i^2_{dn}}$ is neglected.

The equivalent input admittance of PS can be presented as $\dot{Y}_{in} = \dot{Y}_1 + \dot{Y}_g$, where $\dot{Y}_g = -G_g - jB_g$; G_g, $B_g > 0$. Besides, PS introduces an additional noise $\overline{i^2_{Na}}$ in the input circuit. Hence the equivalent circuit of Fig. 1 can be presented as it is shown in Fig. 2.

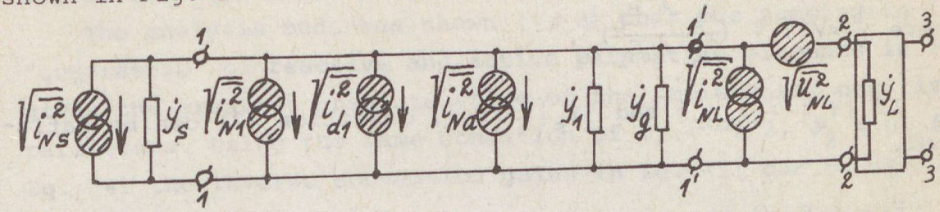

Fig. 2. Equivalent circuit of the system with a negative one-port.

GENERAL ANALYSIS

The noise factor of the system of Fig. 2 can be defined as: $F = 1 + \overline{i^2_{N\Sigma}} / \overline{i^2_{NS}}$, where

$$\overline{i^2_{N\Sigma}} = \overline{i^2_{N1}} + \overline{i^2_{d1}} + \overline{i^2_{Na}} + \overline{i^2_{NL}} + \overline{U^2_{NL}} \left| \frac{\dot{Y}_L (\dot{Y}_s + \dot{Y}_{in})}{\dot{Y}_L + \dot{Y}_s + \dot{Y}_{in}} \right|^2 -$$

$$- 2\dot{Y}_{cor} \overline{U^2_{NL}} (\dot{Y}^*_s + \dot{Y}^*_{in}) \left| \frac{\dot{Y}_L}{\dot{Y}_L + \dot{Y}_s + \dot{Y}_{in}} \right|$$

$\dot{Y}_{cor} = \sqrt{\overline{i^2_{NL}}} \sqrt{\overline{U^2_{NL}}}^* / |\overline{U^2_{NL}}|$, the noise correlation in the load.

We consider that the utilization of PS as a one-port with negative parameters would be reasonable if the following conditions are satisfied (5):

$$M < F_{PC} - 1 \qquad (1)$$

where M is the noise number (6) and F_{PC} is the noise factor of the passive circuit when PS is absent.

Defining the noise factor of PS as $F_{PS} = G_{PS}/G'_g$, where G_{PS} is some equivalent noise conductance of PS and $G'_g = G_g - G^0_1$,

condition (1) can be written as:

$$\{G_{NL} + F_{PS}G'_g + R_{NL}[(G_s - G'_g)^2 - 2\dot{Y}_{cor}(\dot{Y}^*_s + \dot{Y}^*_{in})]\}\times$$

$$\frac{\gamma(G_s + G_L)}{(\gamma - 1)(G_s + G_L) + G'_g} < G_{NL} + R_{NL}(G_s^2 - 2\overline{\dot{Y}_{cor}\dot{Y}^*_s}) \qquad (2)$$

where $\gamma = \sqrt{1 + (\frac{B_s + B_L}{G_s + G_L})^2}$.

If $|\dot{Y}_s| >> |\dot{Y}_{cor}|$ and $|\dot{Y}_s| >> |\dot{Y}_L|$, condition (2) can be satisfied.

$$F_{PS} < R_{NL}G_s \qquad (3)$$

The inequality (3) is suitable for initial practical estimations.

Now we have to determine the PS noise factor F_{PS}.

Presenting the parametric elements in PS (Fig. 1) as

$$C(t) = C_0 + 2C_1\cos(\omega_p t + \psi_1) + 2C_2\cos 2(\omega_p t + \psi_1),$$

$$G(t) = G_0 + 2G_1\cos(\omega_p t + \psi_2) + 2G_2\cos 2(\omega_p t + \psi_2),$$

the process in PS can be described by the following matrix equation:

$$\begin{vmatrix} \dot{I}_1 \\ \dot{I}_+ \\ \dot{I}^*_- \end{vmatrix} = \begin{vmatrix} \dot{Y}_{1\Sigma}; & G_1 e^{-j\psi_2} + j\omega_s C_1 e^{-j\psi_1}; & G_1 e^{j\psi_2} + j\omega_s C_1 e^{j\psi_1} \\ G_1 e^{j\psi_2} + j\omega_+ C_1 e^{j\psi_1}; & \dot{Y}_+; & G_2 e^{2j\psi_2} + j\omega_+ C_2 e^{2j\psi_1} \\ G_1 e^{-j\psi_2} + j\omega_- C_1 e^{-j\psi_1}; & G_2 e^{-2j\psi_2} - j\omega_- C_2 e^{-2j\psi_1}; & \dot{Y}^*_- \end{vmatrix} \begin{vmatrix} \dot{U}_1 \\ \dot{U}_+ \\ \dot{U}^*_- \end{vmatrix} \qquad (4)$$

where $\dot{I}_n$ and $\dot{U}_n$ are, respectively, currents and voltages at frequencies ω_s, ω_+ and ω_-; $\dot{Y}_{1\Sigma} = \dot{Y}_1 + \dot{Y}_s + \dot{Y}_L$.

Considering PS as a resonance circuit with admittances which are specified as $\dot{Y}_+ = G_0[1+2Q(\eta+\xi)]$, $\dot{Y}^*_- = G_0[1-2Q(\eta-\xi)]$, where $\eta = \frac{\omega_p - \omega_0}{\omega_p}$, $\omega_0 = 1/\sqrt{LC_0}$, $Q = 1/(G_0\omega_p L)$, $\xi = \frac{\omega_s}{\omega_p}$, the pro-

duct $F_{PS}G'_g$ can be expressed as:

$$F_{PS}G'_g = G_1^0 + G_0\left(\left|\frac{D_+}{D_1}\right|^2 + \left|\frac{D_-}{D_1}\right|^2\right) + \frac{qI_0}{2kT}\left(1+\left|\frac{D_+}{D_1}\right|^2 + \left|\frac{D_-}{D_1}\right|^2\right); \quad (5)$$

D_1, D_+, D_- are the corresponding algebraic adjuncts of the matrix determinant in Eq. (4).

The analysis made has shown (1, 2) that the pumping in "quadrature" of reactive and active parametric elements in PS gives the greatest absolute value of the implemented negative parameters. Using the same condition of $\psi_1 = -\pi/2$, $\psi_2 = 0$, from Eq. (4) the inverse conversion gains in Eq. (5) can be determined as:

$$\frac{D_+}{D_1} = \frac{M_1 - \xi m_1 Q(1 + 2M_2) + j2Q[m_1\xi Q(\xi_0 - \xi) - M_1(\xi_0 + m_2 - \xi)]}{1 + 2M_2 + 4Q^2(\xi_0^2 + \xi_0 m_2 - \xi^2)} \quad (6)$$

$$\frac{D_-}{D_1} = \frac{M_1 + \xi m_1 Q(1 + 2M_2) + j2Q[m_1\xi Q(\xi_0 - \xi) - M_1(\xi_0 + m_2 + \xi)]}{1 + 2M_2 + 4Q^2(\xi_0^2 + \xi_0 m_2 - \xi^2)} \quad (7)$$

where $m_1 = \frac{C_1}{C_{eff}}$, $m_2 = \frac{C_2}{C_{eff}}$, $M_0 = \frac{G_0}{G_{eff}}$, $M_1 = \frac{G_1}{G_{eff}}$, $M_2 = \frac{G_2}{G_{eff}}$,

$C_{eff} = C_0 - C_2$, $G_{eff} = G_0 - G_2$, $\xi_0 = \eta - \frac{m_2}{2}$, (1, 2).

The estimation made shows that for practical conditions $F_{PS}G'_g \approx 1.5\, G_1^0$.

Taking into account that for being a one-port with negative parameters, PS is to provide $G_g \gg G_1^0$, it is obvious that $F_{PS} \ll 1$.

The numerical examinations as well as our experimental investigation made have shown that the noise factor of PS was in the limits $F_{PS} = 0.005 \div 0.15$. Going back to condition (3), for practical estimations it is suitable to use the inequality $0.1 < R_{NL}G_s$.

The modern transistor amplifiers have $R_{NL} \propto 100\ \Omega$, thus for the condition of reasonable PS utilization as a one-port with

negative parameters we receive the following final inequality:

$$G_s > 10^{-3}\text{Sm}. \qquad (8)$$

The similar analysis made has shown that for the high resistant signal sources ($G_s < 10^{-3}$Sm) it is necessary to use reactive four-frequency PS exhibiting negative wide-band reactances and high positive input conductances. Such reactive PS realize wide-band frequency correction and the corresponding amplification.

CONCLUSION

A general theory of the noise properties of the joint stage with negative G and C based on four-frequency parametric systems (PS) has been developed. Conditions for reasonable PS utilization as one-port with negative parameters have been derived. A general analyis of the noise properties of RL-parametric systems exhibiting wide-band negative R and L has been developed in a similar manner.

REFERENCES

1. Damgov, V.N. (1978). Parametric RC-system as a two-terminal of negative conductance. Bulg. J. Physics, 5, No. 5, pp. 519-534.
2. Damgov, V.N. (1982). Design and application of negative R, C, and L two-poles based on four-frequency parametric systems. Proc. IEEE Int. Symp. on Circuits and Systems, Rome, May 10-12, 1982, Vol. 1, pp. 190-193.
3. Damgov, V.N. (1984). Injection-locked self-oscillating system as a one-port with controlled parameters. IEE Proc., Part G, Vol. 131, No. 1, pp. 1-9.
4. Damgov, V.N. PRB Patents. Int. Cl. G 01 27/26, NoNo 25959, 25960, 25961, 28971, 29260, 29998, 30003, 30009, 45821.
5. Emelyanov, S.L. et al. (1978). Increasing of the small signal amplifier sensitivity used for measuring of the parameters of interplanetar plasma by the modulating method. Radiotechnica, 33, No. 4, pp. 78-79.
6. Van der Ziel, A. (1979). Noise in Measurements. Moscow, Mir, Ch. 6.

10th Int.Conf. on Noise in Physical Systems
1989 Budapest, Hungary

MULTIFUNCTIONAL NOISE MEASUREMENT SYSTEM FOR ELECTRONIC COMPONENT QUALITY EVALUATION

L.Z. HASSE, L. SPIRALSKI

Institute of Electronic Technology,
Technical University of Gdańsk
80-952 Gdańsk, Poland

INTRODUCTION

A number of produced low-noise electronic components must be rejected according to appropriate standards after the preliminary selection due to values of their noise parameters. Material defects and defects introduced during manufacturing cause the increase of noise intensity in elements. Therefore it is possible by noise measurements to estimate the quality of technological operations and to classify devices into groups with a different level of reliability. The presented system enables to execute both noise production testing and detailed investigations.

GENERAL OPERATION

The system can operate in one of the following modes of work:

I. Standard. Testing of noise parameters for data sheets of components, e.g. transistors in the wide frequency band 10-50 Hz or in the narrow band at 1 kHz ($\Delta f \leq 200$ Hz). Time requirements as for the production line.

II. Reliability evaluation. Measurement of noise power in a narrow band at five preliminary settled frequencies in the range to 100 Hz. Every measured element is classified into groups with a different reliability level.

III. Characterization. Estimation of basic statistical functions of noise, specially a power spectral density (PSD)

in the frequency range up to 1 kHz, for a selected population of components.

SYSTEM PERFORMANCE

The functional block diagram of the system is given in Fig. 1.

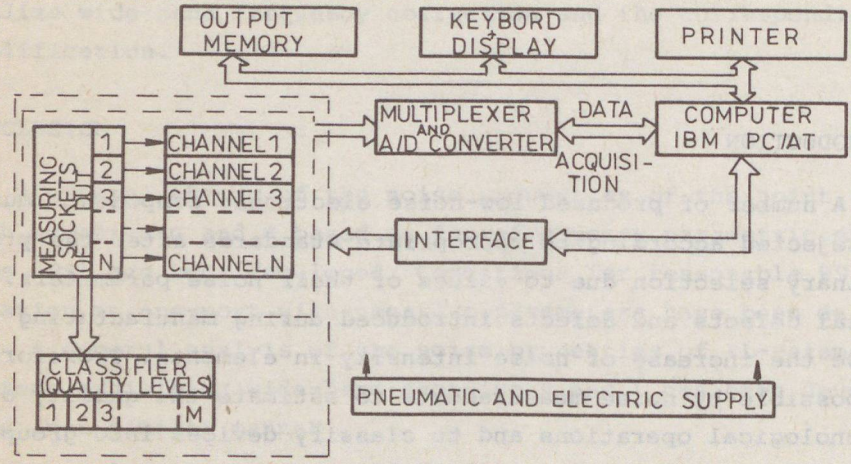

Fig. 1. The functional block diagram of the system

Different types of components are provided to be tested in the system (also power semiconductor devices), so testing circuits and threshold levels of classifying devices depend on a type of components under test. Every measuring channel contains a testing circuit (with special solutions to adjust, stabilize and repeat the bias condition for devices under test rapidly), low-noise preamplifier and amplifiers with anti-aliasing filters (5 Sallen-Key sections each - slope -60 dB per octave, cut-off frequency 1.5 kHz). The setting time of measurement conditions was assumed to be 3 seconds and the total time of noise measurement not longer than 20 seconds. The interface includes some input/output port cards to provide setting of measurement conditions. The flow chart of measurement is shown in Fig. 2.

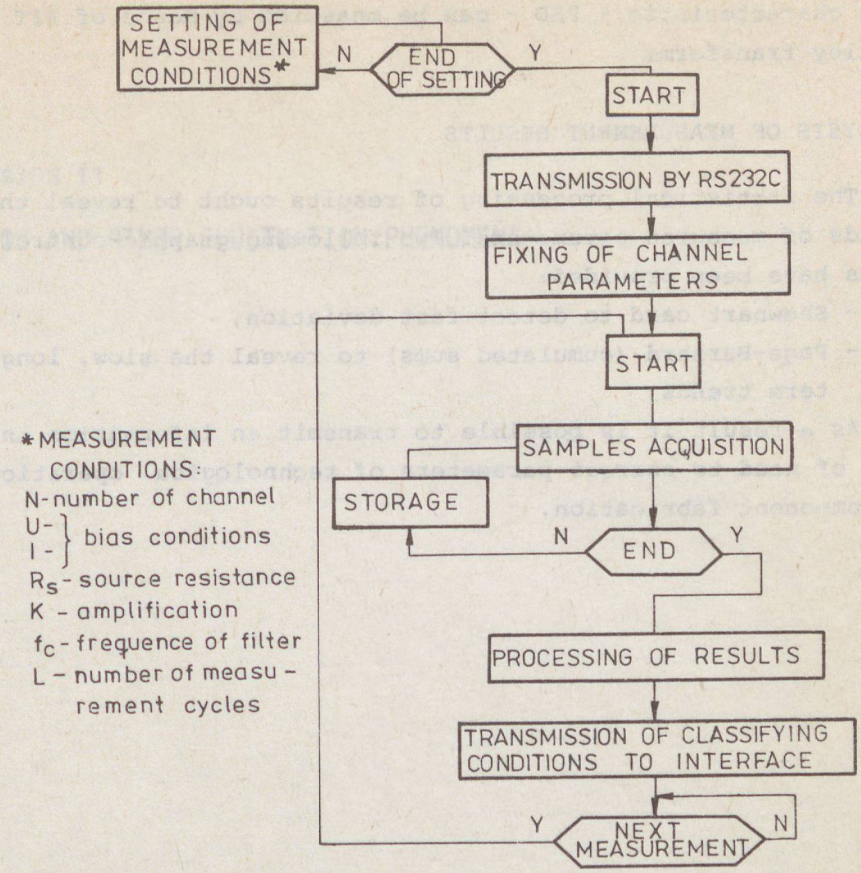

Fig. 2. The flow chart of noise measurements in modes I and II

In the reliability evaluation mode the measurement of noise power in a narrow band is performed by digital filters. As criteria of the selection the a slope of PSD estimated by means of the least-squares method, the value of noise power at the preliminary-selected frequency or a possible occurrence of the burst noise can be chosen (Lorentzian-type component in spectrum). The efficiency of this mode (number of measured devices per hour) is the same as for the standard mode.

In the characterization mode only a small part (e.g. according to MIL-105) of selected components is measured in longer time after the measurements in one of the other modes. The

main characteristic - PSD - can be measured by means of FFT or Hartley transform.

ANALYSIS OF MEASUREMENT RESULTS

The statistical processing of results ought to reveal the trends of measured parameters. Two following graphic-control cards have been provided:

- Shewhart card to detect fast deviation,
- Page-Barnard (cumulated sums) to reveal the slow, long-term trends.

As a result it is possible to transmit an information in case of need to correct parameters of technological operations in component fabrication.

SESSION 11

CHAOS AND OTHER FLUCTUATION PHENOMENA

10th Int.Conf. on Noise in Physical Systems
1989 Budapest, Hungary

CHAOTIC PULSATIONS IN THE SOLAR CORONA

J. KURTHS, A.O. BENZ,* U. BIRKEMEYER,** H. ISLIKER*

Zentralinstitut für Astrophysik, AdW
1501 Tremsdorf, GDR
*ETH, Institute of Astronomy
Zürich, Switzerland
**Humboldt-Universität, Sektion Mathematik
Berlin, GDR

ABSTRACT

A time series analysis of a set of pulsation events suggests that low-dimensional chaos is the typical structure of this kind of solar activity. Estimates of the dimension-like quantities $D(\gamma)$ point to inhomogeneous attractors especially for events characterized by spectra with a power law decay.

INTRODUCTION

Although the energy output of the Sun as a whole is remarkably constant being a main basis of life on the Earth, it is well-known that transient disturbances, involving the release of substantial amounts of energy (e.g. up to some 10^{32} erg/s during flares), occur on the Sun. Coronal pulsations observed in the dm-m wave range of solar radio emission are a typical phenomenon in the course of such solar activity events. The study of these pulsations is a convenient tool to reveal information about plasma processes in the solar atmosphere. To model this kind of solar activity the dynamical properties are of decisive importance (Aschwanden, 1987). Applying modern methods of time series analysis it has been shown recently that the "irregular" behaviour during a special pulsation event is due to low-dimensional chaos (Kurths and Herzel, 1987). The purpose of the present paper is an analysis of 20 pulsation events to discuss the following problems:

1. Is deterministic chaos a usual structure of coronal pulsations?

2. What shapes of power spectra are related to such a behaviour?
3. Are the attractors homogeneous?

POWER SPECTRA

Burg's maximum entropy spectral (MES) estimation chosen on account of its optimal spectral resolution properties (Robinson, 1982) is applied to the data. The power spectra calculated from the pulsations can be classified in three types

A) exponential decay
B) power-law decay at high frequencies ($f^{-\gamma}$, $\gamma = 1.6 - 3$)
C) smeared peaks.

Broadband features in power spectra can arise from stochastic or deterministic processes, but Sigeti and Horsthemke (1987) have shown that the decay in B is typical for systems subject to noise. The shapes A resp. C have been reported for deterministic systems (Brandstater and Swinney, 1987, Isola, 1988). However, it is questionable whether these relations are clear-cut. Therefore, another concept of time-series analysis is taken into account.

ATTRACTOR ANALYSIS

Deterministic chaos is characterized by strange attractors in phase space and exponential instability of trajectories. Recently techniques have been developed that are capable of extracting such geometrical information of nonlinear systems from scalar time series data (cf. the review of Broomhead and Jones, 1989). Instead of a single measurement x_i the vector

$$\underline{x}_i = (x_i , x_{i+\tau} , \ldots , x_{i+(m-1)\tau}) \qquad (1)$$

spanned by delay-coordinates is considered (method of embedding).

Correlation Dimension

To estimate attractor dimensions local densities $n_i(r)$ around points $\underline{x}_i$ can be used

$$n_i(r) = \sum_j \Theta (r - \| \underline{x}_i - \underline{x}_j \|) \qquad (2)$$

(Θ - Heaviside function). The correlation dimension D_2 , as proposed by Grassberger and Procaccia, is calculated by averaging these n_i

$$C(r) = \sum_i n_i(r) \sim r^{D_2} \qquad (3)$$

The application of this procedure to observational data for which the low dimensionality is not known a priori has to be done carefully. Therefore, some noise reduction methods and the calculation of error bars have been included.
From the analysis of the 20 pulsation events we conclude:

- there are relatively large scaling regions for 16 examples indicating a low-dimensional attractor, whereas in the other 4 cases the noise dominates
- we find $\overline{D}_2 = 2 \ldots 5$ at which for the majority $\overline{D}_2 = 3. \pm 0.5$. The error bars are about 0.2 for lower dimensions and reach to 0.8 in the case of $D \approx 5$
- in a few events the attractor dimension increases with time (cf. Kurths and Karlicky, 1989 according to a route to chaos of a special event)
- the three different kinds of power spectra do not relate to the value of D_2 .

Dimensions from Near-Neighbor Information
The procedure to estimate D_2 has limited applicability for inhomogeneous attractors due to restricted scaling regions. Another algorithm, which does not require a scaling region of r, is based on the calculation of distances $r_k(\underline{x}_i)$ to the k-th nearest neighbors of attractor points $\underline{x}_i$. Different ways of averaging over many reference points lead to a set of dimension-like quantities $D(\gamma)$ interrelated with the dimensions D_q

$$\langle r_k^{1/\gamma} \rangle \sim k^{1/D(\gamma)} / G(k, D(\gamma)) \qquad (4)$$

with $G(k, D(\gamma)) = k^{1/D(\gamma)} \Gamma(k) / \Gamma(k+1/D(\gamma))$
(Badii and Politi, 1985 and van de Water and Schram, 1988).

Varying the order of the neighbor k we have estimated $D(\gamma)$ via (4) yielding:

- the corresponding values of $D(\gamma)$ are in good accordance with $\overline{D}_2$
- the significant growth of $D(\gamma)$ with increasing γ gives some evidence for inhomogeneous attractors in particular for events characterized by spectra with a power law decay

References

Aschwanden, M.: 1987, Theory of radio pulsations in coronal loops, Solar Phys. 111, 113-136.

Badii, R. and Politi, A.: 1985, Statistical description of chaotic attractors: the dimension function , J. Stat. Phys. 40, 725-750.

Brandstater, A. and Swinney, H.L.: 1987, Strange attractors in weakly turbulent Couette-Taylor flow, Phys. Rev. A 35, 2207-2220.

Broomhead, D. S. and Jones, R.: 1989, Time-series analysis, Proc. R. Soc. Lond. A 423. 103-121.

Isola, S.. 1988 Resonances in chaotic dynamics, Comm. Math. Phys. 116, 343-352.

Kurths, J. and Herzel, H.: 1987, An attractor in a solar time series, Physica 25D, 165-172.

Kurths, J. and Karlicky, M.: 1989, The route to chaos during a pulsation event, Solar Phys. 119, 399-411.

Robinson, E. A.: 1982, A historical perspective of spectrum estimation, Proc. IEEE 70, 885-906.

Sigeti, D. and Horsthemke, W.: 1987, High-frequency power spectra for systems subject to noise, Phys. Rev. A 35, 2276-2282.

Van de Water, W. and Schram, P.: 1988, Generalized dimensions from near-neighbor in formation, Phys. Rev. A 37, 3118-3125.

10th Int.Conf. on Noise in Physical Systems
1989 Budapest, Hungary

A NEW TYPE OF SPACE-TIME CHAOS

V.V. GAFIJCHUK, B.S. KERNER, V.V. OSIPOV, Z.I. VASYUNYK

Institute for Applied Problems of Mechanics and
Mathematics, Ukrainian SSR Academy of Sciences
Lvov, USSR

Space-time chaos is observed when the system's homogeneous state is layered due to the mechanism of instability of all the inhomogeneous stationary states (1). The present work considers the new mechanism of homogeneous states (strata) spontaneously formed in the electron-hole plasma (EHP) and causing the occurrence of oscillations chaotic in space and time.

Consider the non-degenerate EHP of such density (n=p), that conditions of its quasi-hydrodynamic description are fulfilled. When effective masses of electrons and holes are not very much different due to effective energy exchange between electrons and holes, carriers in the electric field are heated as a single system up to some effective temperature T. Distribution of the temperature and electron concentration in the quasi-neutral EHP are described by the equations

$$\partial n/\partial t = -div\, \vec{j}_e + G_0 + n\nu_i(T) - n/\tau_r, \tag{1}$$

$$3\partial(nT)/\partial t = -div\, \vec{j}_\varepsilon + \vec{j}\vec{E} - n(T-T_l)/\tau_\varepsilon, \tag{2}$$

where densities of electron flow $\vec{j}_e$ and carrier energy $\vec{j}_\varepsilon$ are equal to

$$\vec{j}_e = -(\sigma_e/e\sigma)\vec{j} - \vec{\nabla}(nD), \tag{3}$$

$$\vec{j}_\varepsilon = -(5/2+\alpha)[nD_e(1+b^{-1})\vec{\nabla}T - T(\vec{j}/e + 2\vec{j}_e). \tag{4}$$

Here G_o is the rate of thermo- and photogeneration of carriers; τ_r is the time of their life; ν_i is the rate of interzone collision ionization; τ_ε stands for characteristic time of carriers energy relaxation; D_e and D are factors of electron diffusion and bipolar diffusion; $b = \mu_e/\mu_h$; $\sigma = \sigma_e + \sigma_h$; μ_e, μ_h and σ_e, σ_h stand for mobilities and conductivities of electrons and holes; $\vec{j}$ is the density of full current; T_1 is the lattice temperature; $1+\alpha = \partial \ln D/\partial \ln T$.

When conditions

$$L \gg l, \quad \alpha + S > -1 \tag{5}$$

are fulfilled, the homogeneous state of the EHP becomes unstable, then its temperature $T > T_o = (2+\alpha+S)(1+\alpha+S)^{-1} T_1$ and strata are jumpwise formed in the plasma as layers with high temperature and low concentration of carriers perpendicular to the current line (2). In Eq. (5) $S = \partial \ln \tau_\varepsilon / \partial \ln T$; $L = (D^o \tau_r)^{1/2}$ is the length of bipolar diffusion; $l = [(5/2+\alpha)\tau_\varepsilon^o D_e^o (1+b^{-1})/2]^{1/2}$ stands for the length of electron cooling; $D^o = D(T_1)$, $D_e^o = D_e(T_1)$, $\tau_\varepsilon^o = \tau_\varepsilon(T_1)$. Existence of such strata is connected with an intensive ejection of carriers from the stratum, i.e. from the high-temperature region occurring due to thermodiffusion. Owing to this, the carrier concentration in it and, hence, the plasma conductivity σ, are considerably lower than at the stratum periphery. Therefore power j^2/σ heating the carriers turns out to be the greatest in the stratum centre, which maintains the high temperature in it (2). Thus, the strata existence is directly connected with intensive ejection of hot carriers from these regions. When T exceeds the Debye temperature, Eq. (5) is fulfilled for many semiconductors. In this case stable strata are formed at such parameters of EHP when thermodiffusion is carried out by ejection of the carriers formed in the stratum due to collision ionization (3).

The present work considers the opposite situation when the carriers generated in the centre of the strata due to collision ionization lead to breakdown of the stratum formed. This effect is realized when, due to the exponential dependence of ν_i on T, condition

$$\nu_i(T_m)\,\tau_z(T_m, n_m) \gg 1 \qquad (6)$$

is fulfilled. In its turn, from the strata theory (4) it follows that the greater the allowance with which Eq. (5) is fulfilled, the higher is the temperature T_m in the strata centre. In other words, when Eqs (5) and (6) are fulfilled in an unstable homogeneous EHP, stationary strata cannot be formed. The picture of turbulence arising in this case should present a process of random nucleation of strata in some regions of the EHP, their further breakdown due to the collision ionization when the temperature in the strata centre reaches some critical value, random appearance of new strata in other regions and so on. Just this process was observed in numerical investigations (Fig. 1).

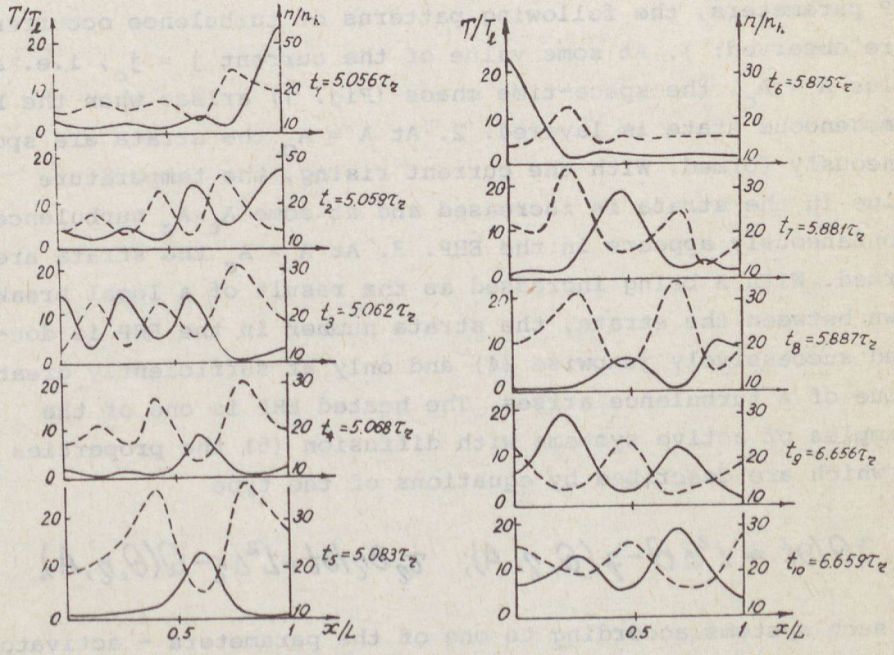

Fig. 1. Space-time chaos in EHP: distributions of Θ (solid lines) and η (dashed lines) in successive time instants for G_e parameters characteristic at T_1 = 300 K, A = 100.

For the sake of simplicity, the case was analyzed when α, S = const and the EHP was heated by high-frequency field with frequency w ($\tau_\varepsilon^{-1} << w << \tau_p^{-1}$, τ_p is the time of the pulse relaxation). Under these conditions it follows from Eqs (1)-(4) that the equations describing the inhomogeneous state in the EHP may be written as:

$$(3/2)\tau_\varepsilon^o \partial(\eta\Theta^{-\alpha})/\partial t = \ell^2\partial^2(\eta\Theta)/\partial x^2 + A\Theta\eta^{-1} - \eta\Theta^{-1-S-\alpha}(\Theta-1), \quad (7)$$

$$\tau_r \partial(\eta\Theta^{-1-\alpha})/\partial t = L^2\partial^2\eta/\partial x^2 + 1 - \eta\Theta^{-1-\alpha}[1-\nu_i(\Theta)\tau_r], \quad (8)$$

where $\Theta = T/T_1$, $\eta = nD/n_h D^o$, $n_h = G_o\tau_r$, $A = (\tau_\varepsilon^o/4e\mu_e^o n_h^2 T_1)\,\overline{j^2}$ stand for the level of EHP heating; $\mu_e^o = \mu_e(T_1)$; $\overline{j^2}$ is the mean value of j^2 during the period of field variation. In the numerical investigations of Eqs (7) and (8), depending on the EHP parameters, the following patterns of turbulence occurrence were observed: 1. At some value of the current $j = j_c$, i.e. at value $A = A_c$, the space-time chaos (Fig. 1) arises when the EHP homogeneous state is layered. 2. At $A = A_c$ the strata are spontaneously formed. With the current rising, the temperature value in the strata is increased and at some $A_t > A_c$ turbulence spontaneously appears in the EHP. 3. At $A = A_c$ the strata are formed. With A being increased as the result of a local breakdown between the strata, the strata number in the EHP is doubled successively jumpwise (4) and only at sufficiently great value of A turbulence arises. The heated EHP is one of the examples of active systems with diffusion (5) the properties of which are described by equations of the type

$$\tau_\Theta \partial\Theta/\partial t = \ell^2\Delta\Theta - q(\Theta,\eta,A); \quad \tau_\eta \partial\eta/\partial t = L^2\Delta\eta - Q(\Theta,\eta,A). \quad 9)$$

In such systems according to one of the parameters - activator (Θ) in some range of existence levels A the positive feedback is carried out, i.e. $q'_\Theta \equiv \partial_q/\partial\Theta < 0$ and according to another parameter - an inhibitor η a negative feedback is carried out, i.e. $Q'_\eta \equiv \partial Q/\partial_\eta > 0$. Equation (6) of strata instability is reduced, as it follows from Eq. (8) that in the strata centre value $Q'_\eta < 0$,

i.e. the strata instability is connected with the fact that in their centre the negative feedback against the inhibitor is changed from the positive one.

REFERENCES

1. Kerner, B.S., Osipov, V.V., Sov. Phys., JETP, 82, 56, 1275; Sov. Phys., Doklady, 83, 28, 485.
2. Kerner, B.S., Osipov, V.V., Sov. Phys., Solid State, 79, 21, 1348.
3. Dubitsky, A.L., Kerner, B.S., Osipov, V.V., Sov. Phys., Semiconductors, 86, 20, 755.
4. Kerner, B.S., Osipov, V.V., Sov. Phys., JETP, 78, 47, 874.
5. Kerner, B.S., Osipov, V.V., UFN (Russ.), 89, 157, 201.

10th Int.Conf. on Noise in Physical Systems
1989 Budapest, Hungary

CHAOS IN SHORT-DISTANCE DOPPLER RADARS WITH SELF-DETECTING OSCILLATORS

V.N. DAMGOV, T.S. HRISTOV

Space Research Institute, Bulgarian Academy of Sciences
1000 Sofia, Bulgaria

ABSTRACT

The possibility for stochastic oscillations arising in short-distance Doppler radars with self-detecting oscillators (autodynes) has been investigated numerically. Cases with constant and variable delay of the reflected signal have been considered. The mechanism of chaos arising has been obtained by determination of the dimension of the strange attractor in the phase space.

INTRODUCTION

The Doppler autodynes are widely used as detecting and emitting modules in short-distance radars (1, 2, 3). Since these systems work at short distances, the reflected signals may be relatively strong and their intensity is comparable with the emitted one. In such cases characteristic relaxation instabilities of the oscillations appear. In certain conditions these instabilities may cause a chaotic behaviour of the system.

The aim of the present work is to investigate the possibilities for the arising of the instabilities with a chaotic character from the most recent point of view. Such instabilities are observed in the modern UHF semiconductor autodyne systems with a negative resistance. A comparison of the conditions for the emergence of chaos in autodynes is done. These autodynes are described by second-order (when current controlled UHF de-

vices as IMPATT are used) and third-order (when voltage-controlled UHF devices as Gunn and tunnelling diodes are used) ordinary differential equations. The coefficient K of the reflected signal is taken as a ruling parameter.

EQUATIONS

The analysis is carried out on the basis of ordinary differential equations, describing with a good precision the real autodyne systems. The processes in the autodyne systems with voltage-controlled devices (with 1.5 degrees of freedom) can be described by the following equations.

$$\frac{d^3x}{dt^3} + (1-\xi)\frac{d^2}{dt^2}[\alpha x - \delta f(x) + \beta f^2(x)] + (1-\xi)^2\frac{d}{dt}[\zeta x + \kappa f(x) + \alpha\beta f^2(x)] + (1-\xi)^3[\gamma f(x) + \zeta\beta f^2(x)] = K\frac{1-\xi}{Q}\left[\frac{d^2 f(x_\tau)}{dt^2} + (1-\xi)\delta_1\frac{df(x_\tau)}{dt}\right] \quad (1)$$

Table 1: Bifurcation values of the refraction coefficient K

	K_o	K_1	K_2	K_3	K_4
System I	0.07	0.19	0.43	0.47	0.53
System II	0.17	0.43	0.97	1.11	1.19
Characteristic frequencies in the spectrum	f_o	f_o, f_1	f_o, f_1, $\frac{f_1}{2}$,	f_o, f_1, $\frac{f_1}{2}$, $\frac{f_1}{4}$	Chaos

where x is dimensionless charge, passing through the active device, $f(x) = x(1 - c_1x - c_2x^2)$ is a function describing both the nonlinearity of the capacitance reactivity in the system and the voltage of the emitted signal. c_1, c_2, α, δ, β, κ, ζ, δ_1, Q are constant coefficients, ξ is the relative disturbance in the system. The right-hand side of Eq. (1), i.e. the active force, is formed by the reflected signal $kf(x_\tau)$, where $x_\tau = x(t - \tau)$, τ is the time delay of the signal, $\tau = \tau_o \pm \varepsilon t$,

$\tau_o = \frac{4\pi L_o}{\lambda}$, $\varepsilon = \frac{\omega_D}{\omega}$, $\omega_D = 2\omega v/c_L$ is Doppler's frequency, λ is the electromagnetic wavelength, L_o is the distance to the object when $t = 0$, v is the velocity of the object, c_L is the speed of light.

The processes in the current controlled systems (with one degree of freedom) are described by the following equation (3):

$$\frac{d^2x}{dt^2} + f(x) = \delta \frac{dx}{dt} - \beta \left(\frac{dx}{dt}\right)^2 + k\frac{df(x_\tau)}{dt} \qquad (2)$$

where x is the total dimensionless magnetic flow through the active device, $f(x) = x(1 + L_1x + L_2x^2)$ is a function describing both the nonlinearity of the inductance reactivity in the system and the voltage of the emitted signal. L_1, L_2, δ, β are constant coefficients and the reflected signal is $kf(x_\tau)$.

NUMERICAL EXPERIMENT

From now on, for simplicity, the systems described by Eqs (1) and (2) will be referred to as systems I and II respectively and superscripts I and II will be used.

For the constant coefficients and characteristics in Eqs (1) and (2) we use values typical for Gunn and IMPATT autodyne systems (1). Changing sequentially the value of the ruling parameter K we investigate the behaviour of the systems.

In the beginning we shall discuss the case with a time-constant delay of the reflected signal, i.e. in case $\tau = \tau_o = 30$. The data of the numerical experiment are presented in Table 1.

When the reflection coefficient K is relatively small ($0 < K < K_o$) in the systems of both types, periodic oscillations with frequency f_o, nearly equal to the eigenmode $f_o = 1/(2\pi) \approx 0.17$ exist. If the reflection coefficient K increases, the limit cycle corresponding to these oscillations loses its stability. In the phase space a two-dimensional torus appears, corresponding to quasiperiodic oscillations with two basic frequencies f_o and $f_1 = 1/\tau_o = 0.029$. The torus is stable if the coefficient K satisfies the condition $K_o < K < K_1$. If the in-

crease of K continues in the interval $K_1 < K < K_2$, a bifurcation of the quasiperiod of the torus is observed. In the narrow interval $K_3 < K < K_4$ one can see a phenomenon resembling a third bifurcation of the torus quasiperiod. On the following increase of the reflection coefficient $K_4 < K$ the background suddenly increases and the separate frequencies become indistinguishable. From this value of the ruling parameter on the system behaves chaotically.

Here we have to mention that the frequencies f_o and f_1 slightly change when the coefficient K changes.

The exact values of parameters K_o and K_1 for which the bifurcations occur to a great extent depend on the delay time τ_o and on the nonlinearity of the function f(x). For example in the case of a relatively low increase of the delay time $\tau = 40$, the bifurcation values for the system of type I become $K_o^I = 0.05$ and $K_1^I = 0.14$. The situation is almost the same when the nonlinearity of the function f(x) increases. For instance if the coefficients c_2 and L_2 increase 10 times, the bifurcation values for K significantly decrease - $K_o^I = 0.0015$, $K_1^I = 0.01$, $K_o^{II} = 0.0023$, $K_1^{II} = 0.025$.

In order to determine the influence of the object's speed, Eqs (1) and (2) have been investigated when $\varepsilon = 0.01$. The values of the other parameters have not been changed. In the case $\varepsilon \neq 0$ the transition to chaos differs from one in the case $\varepsilon = 0$. Even when K is very small, quasiperiodic oscillations with two frequencies $f_o = 0.17$ and $f_D = 0.0017 = \varepsilon f_o$ (f_D is the Doppler's frequency) are generated in the system. That means that in the phase space a two-dimensional torus already exists. With the increase of K ($K^I > K_1^I = 0.13$ and $K^{II} > K_1^{II} = 0.29$) the two-dimensional torus loses its stability and a three-dimensional torus appears, i.e. there are quasiperiodic oscillations with three basic frequencies: f_o, f_D and $f_1 = 0.03$. When K becomes greater, the noise background in the system increases and a chaotic behaviour is observed.

It is clear from the numerical results that the bifurcation values for K are much smaller for systems of type I (Eq. (1)) than those for systems of type II (Eq. (2)). Formally it can be explained with the difference of 1/2 in the degrees of freedom.

From the physical point of view this phenomenon is connected with the regenerating action of the additional aperiodic complex circuit in the system I, leading to potential relaxation instability.

The observed transitions to chaos are characterized by the change of the dimension of the attractor. As the dimension of the attractor we use the correlation index ν (4), computed in the following manner. Since the time dependence of x is available, we can make the sequences $x_i = x(t + iT)$, $i = 0,\ldots,N$ and to construct the d-dimensional phase space with elements $\zeta_i = (x_i, x_{i+1},\ldots,x_{i+d})$. For each d-dimensional phase space we can calculate the following correlation index:

$$\nu_d = \lim_{\varepsilon_\nu \to 0} \frac{\ln C(\varepsilon_\nu)}{\ln \varepsilon_\nu}$$

where $C(\varepsilon_\nu) = \lim_{N\to\infty}(M(\varepsilon_\nu)/N^2)$, $M(\varepsilon_\nu)$ is the number of pairs (ζ_i, ζ_j), $i \neq j$ with the corresponding distance $\rho(\zeta_i, \zeta_j) < \varepsilon_\nu$.

With the increase of d the value of ν_d increases and asymptotically tends to some value ν, nearly equal to the Hausdorph dimension of the attractor. In the case of periodic oscillations $\nu = 1$; in the case of quasiperiodic oscillations $\nu = 2$. If the behaviour is chaotic, with the increase of K ν smoothly increases from the value $\nu = 2$.

CONCLUSION

The results in the present paper allow us to make a conclusion that the chaos in the autodyne system, characterized by its self-influence, appears as a result of a bifurcation in the case of a constant delay time and as a result of two- and three-dimensional torus occurrence in the case of a variable delay time (moving object). The possibility for the existence of the limit cycle, torus or strange attractor in the phase space has been confirmed by the determination of their dimensions.

We have to note that the occurrences of chaos and as a result a whole absence of information from the short-distance

radars have been proved also by the real experiment. As a system of type I a Gunn generator has been used, and as a system of type II an IMPATT generator. The Doppler's shift of the frequency and the delay time have been set with a special imitator. Using the parameters $\tau_o = 20$ $\varepsilon = 10^{-6}$ the bifurcation values $K_4^I = 0.35$ and $K_4^{II} = 0.95$ of the chaos occurrence have been obtained.

REFERENCES

1. Hotuncev, J.L., Tamarchak, D.Y. (1982), Injection-locked oscillators and autodynes on a semiconductor device. Moscow, Radio i svja's (in Russian).
2. Damgov, V.N. (1989), Conversion properties of short-distance Doppler radars with self-mixing oscillators. Proc. SBMO Int. Microwave Symposium, Brasil, São Paulo, 24-27 July, 1989.
3. Damgov, V.N. (1987), Peculiarities in application of the converting properties of the short-distance radars with self-detecting oscillators. Radiotehnika, 1987, 42, No. 5, pp. 6-13.
4. Naymark, J.I., Landa, P.S., Stochastic and chaotic oscillations. Moscow, Nauka, 1987 (in Russian).

10th Int.Conf. on Noise in Physical Systems
1989 Budapest, Hungary

EFFECT OF WEAK NOISE ON CHAOTIC DYNAMIC SYSTEMS

A.R. BULSARA, W.C. SCHIEVE,* E.W. JACOBS

Naval Ocean Systems Center
San Diego, CA 92152, USA

When one considers the response of a nonlinear dynamic system in the real world, the presence of noise in the perturbation cannot be ruled out. Recently, a number of researchers[1–4] have attempted to quantify the effects of weak Langevin noise on the transition to chaos in driven nonlinear systems. In this work, we consider a classical dissipative nonlinear system driven by a deterministic forcing term in the presence of weak noise. Initially, we shall consider the case of weak Langevin noise and its effect on the homoclinic threshold of the system. In the deterministic case the homoclinic threshold may be characterized by the Melnikov function[5–6] whose zeros yield the criterion for a homoclinic tangency in terms of the system and forcing parameters. In the presence of weak noise we introduce a generalization of this function and consider the criterion for homoclinic crossing in the mean. The new test function is an ensemble-averaged Melnikov function which is seen to consist of its deterministic counterpart shifted by a constant amount that depends on the statistics of the noise. The influence of noise on the chaotic attractor and its accompanying multi-maximum probability associated with the deterministic case is also investigated. In this case, the noise is introduced into the dynamics through an ensemble of random initial conditions. The effect of multiplicative noise on the chaotic attractor is also examined (the noise being introduced, once again, as an ensemble of initial conditions) via a computation of the probability density function associated with the maximal Liapounov exponent of the system.

Let us first consider a general nonlinear second-order system driven by *weak* external Langevin noise which we take to be Gaussian and delta-correlated with zero mean and variance σ^2 (the case of multiplicative noise will be discussed later). The state variable $x(t)$ obeys the dynamic equation,

$$\ddot{x} + \beta f(x) = F(t), \tag{1}$$

where β is a parameter that characterizes the strength of the nonlinearity. In the limit of weak noise (i.e. small σ^2), we treat (1) as being approximately conservative. Then, its general solution may be expressed as,

$$x(t) = x_s(t) + \delta x(t), \tag{2}$$

$x_s(t)$ being the solution of (1) in the absence of noise, i.e. the separatrix solution. Substituting (2) in (1) and expanding to leading order in δx we obtain,

$$\ddot{x}_s + f(x_s) = 0, \tag{3a}$$

$$\delta\ddot{x} - \omega^2(t)\,\delta x = F(t), \tag{3b}$$

where $\omega^2(t) \equiv -\left[\frac{d}{dx} f(x)\right]_{x=x_s}$, $x_s(t)$ being the separatrix solution to (3a). For a given model system, this solution may be computed directly from the dynamics.

* Permanent address: Physics Dept. and Ilya Prigogine Center for Statistical Mechanics, Univ. of Texas, Austin, TX 78712.

We now define an extension of the Melnikov function in the presence of the noise (it being assumed that the system is now subject to a deterministic dissipative perturbation $-k\dot{x}$ and a driving $Q\,g(t, t_0)$):

$$\Delta_F(t_0) = -k \int_{-\infty}^{\infty} \dot{x}^2(t)\,dt + Q \int_{-\infty}^{\infty} \dot{x}(t)\,g(t, t_0)\,dt\,. \tag{4}$$

The function Δ_F is a random quantity but by averageing it over the ensemble of the noise we obtain,

$$<\Delta_F(t_0)> = \Delta(t_0) + <\Delta_c(t_0)>, \tag{5}$$

where,

$$<\Delta_c> \equiv -k \int_{-\infty}^{\infty} <\delta\dot{x}^2(t)>\,dt\,. \tag{6}$$

The quantity $<\Delta_F>$ is an ensemble-averaged generalization of the usual Melnikov function for the deterministic case. It is seen to be the deterministic Melnikov function $\Delta(t_0)$ plus a correction term that depends on the second-order statistics of the random part of the solution of (1). For the case of noise having zero mean value, there is no contribution to the averaged correction $<\Delta_c>$ from the mean value $<\delta\dot{x}(t)>$ since we assume that this mean value is zero at time t. This is equivalent to assuming that the mean value of the random displacement $x(t)$ is its separatrix value. Under these conditions, it is evident that the Langevin noise *elevates* the homoclinic threshold, on average. The ensemble-averaged Melnikov function introduced in (5) is similar to the function introduced by Schieve and Petrosky[7] to take into account the effects of small quantum fluctuations on the homoclinic threshold of classical nonlinear systems. We must point out that a significant and formidable question exists regarding the existence of a Birkoff-Smale theorem[6] for solutions of the stochastic differential equation (1). Our work suggests that, under weak noise, there are, following the noisy tangency, multiple crossings for each realization of the ensemble and thus a Cantor-set-like structure in this weak sense.

The quantity $<\Delta_c>$ may be computed[8] for a given model system. The calculations are lengthy and will not be reproduced here. The procedure involves setting up and solving a Fokker Planck equation for the probability density function describing the time-dependent Ornstein-Uhlenbeck process (3b). In order to do so, we must first solve the transport equation, obtained by ensemble-averageing (3b), for the mean values $<\delta x(t)>$, $<\delta\dot{x}(t)>$. This is done using a WKB approximation. Having computed the mean values, one may directly compute the second-order correlation $<\delta\dot{x}^2(t)>$ from the Fokker Planck equation. In terms of the deterministic driving parameters k and Q, we may characterize the homoclinic threshold as,

$$\frac{Q}{k} = \left[\frac{Q}{k}\right]_0 + B\,\sigma^2, \tag{7}$$

where the first term on the right-hand-side characterizes the homoclinic threshold in the absence of noise and the second term may be expressed in the form,[8]

$$B \equiv \left[\int_{-\infty}^{\infty} \dot{x}_s(t)\,g(t, t_0)\,dt\right]^{-1} \frac{1}{2<\delta\dot{x}^2(t_0)>} \int_{-\infty}^{\infty} <\delta\dot{x}(t)>^2 dt\,, \tag{8a}$$

An extension of the above results to the case of multiplicative noise (the parameter β in (1) is assumed to fluctuate) has been done in reference 9. In figure 1 we show the Melnikov function for the rf SQUID ($\beta f(x) \equiv -x + \beta \sin 2\pi x$). The curve and the solid straight line represent the components of the noise-free Melnikov function that arise from the periodic driving term $g(t, t_0) \equiv \sin\Omega(t - t_0)$ and the dissipative term respectively. The oscillator and driving parameters have been chosen so that one is at the homoclinic tangency for the deterministic case. The dotted line represents the effects of weak Langevin noise as embodied in the correction term $<\Delta_c>$. One observes that, in the presence of the noise, a much larger value of the amplitude Q is required to produce homoclinic tangency. It is worth noting that the dynamic potential characterizing the rf SQUID consists of a deep center well flanked by much smaller side wells for the $\beta = 2$ value used in figure 1. Our results in this figure pertain to homoclinic crossing in a *side* well. Hence, the correction shown by the dotted line is relatively small, due to the considerable disparity in well-depths between the side and center wells.

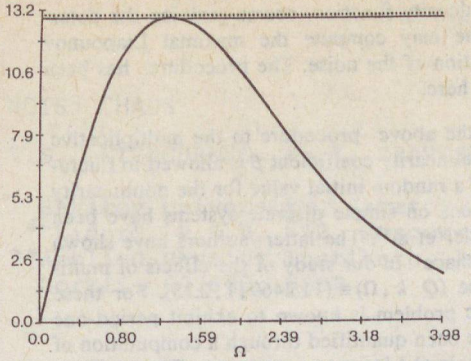

Fig.1: Melnikov function for the rf SQUID; curve and solid line represent the Melnikov function (at the homoclinic threshold) for noise-free case. Dotted line shows the effect of introducing Langevin noise of variance $\sigma^2=0.2$. $(\beta,k,Q,\Omega)\equiv(2,2.24,4,2.25)$.

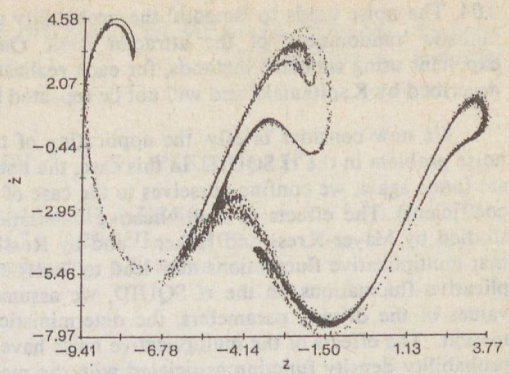

Fig.2: Chaotic attractor for rf SQUID in the presence of Langevin noise. $(\beta,k,Q,\Omega,\sigma^2)\equiv(2,1.1133,10.02,2.25,0.04)$.

We now consider the effect of an ensemble of random initial values on the chaotic attractor that occurs above the homoclinic threshold. Once again, we consider the rf SQUID driven by the dissipative and periodic forcing terms as well as random noise which is assumed to change at time $t=0$ only. This is equivalent to changing the dynamic potential that characterizes the system for each realization of the noise. The stochastic differential equation is integrated up to some final time t for each realization of the noise and the procedure repeated for 40,000 different random initial values of the noise (each such value constitutes a realization of the noise). The chaotic attractor for the deterministic problem has already been plotted, for different (Q,k,Ω) in reference 10. In figure 2 we show the effect, on the deterministic attractor, of noise of variance $\sigma^2=0.04$. The noise results in a greater region of phase space being accessible to the system; at the same time, the self-replication property of the deterministic attractor breaks down with increasing noise. The multi-maximum probability density function corresponding to the displacement variable z $(\equiv 2\pi x-\pi/2)$ may be computed directly from the data of figure 2. In figure 3 we show this probability density over a small range of z for the noise variances $\sigma^2=0$ (deterministic case), as well as $\sigma^2=10^{-5}$ and

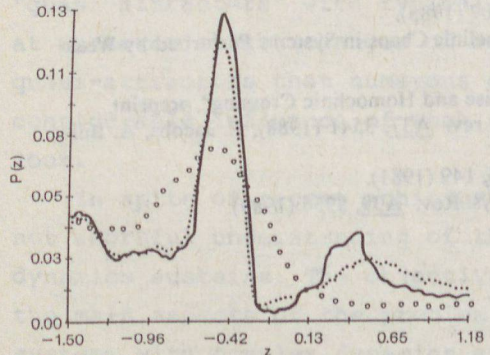

Fig.3: Displacement probability density function over limited range, for rf SQUID with Langevin noise variance $\sigma^2=0$ (solid curve), 10^{-5}, (dotted curve) and 0.04 (data points). Other parameters same as fig. 2.

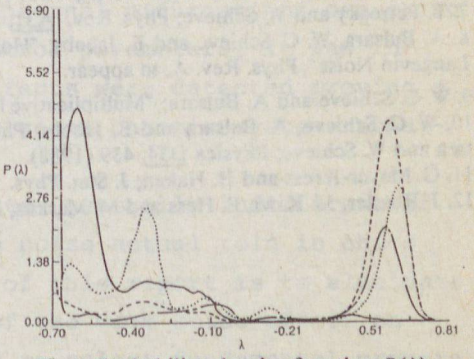

Fig 4: Probability density function $P(\lambda)$ corresponding to the maximal Liapounov exponent λ for multiplicative noise in the rf SQUID. Curves correspond to noise variance $\sigma^2=10^{-5}$ (solid), 0.0005 (dotted), 0.05 (dashed), and 1.976 (dash-dotted).

0.04. The noise tends to 'smooth' the probability density function, coarse-graining the deterministic 'randomness' of the attractor itself. One may compute the maximal Liapounov exponent using standard methods, for each realization of the noise. The procedure has been described by Kapitaniak[2] and will not be repeated here.

We now consider briefly, the application of the above procedure to the multiplicative noise problem in the rf SQUID. In this case, the nonlinearity coefficient β is allowed to fluctuate (once again, we confine ourselves to the case of a random initial value for the nonlinearity coefficient). The effects of multiplicative fluctuations on simple discrete systems have been studied by Mayer-Kress and Haken[11] and by Rossler et al[12]. The latter authors have shown that multiplicative fluctuations may lead to "early chaos". In our study of the effects of multiplicative fluctuations on the rf SQUID, we assume $(Q, k, \Omega) \equiv (11.2469, 1, 2.25)$. For these values of the driving parameters, the deterministic problem is known to exhibit period-one motion. The effects of the multiplicative noise have been quantified through a computation of probability density function associated with the maximal Liapounov exponent. These effects are shown in figure 4. For extremely small $\sigma^2 (\approx 10^{-6})$, the probability density function $P(\lambda)$ has a single peak centered at some negative value of λ. The motion in this case is periodic and is unaffected by the noise. As σ^2 increases, one obtains, for some realizations of the noise, a destruction of the periodic behavior. Hence, in the mean, one obtains a mixture of periodic and chaotic motion. For such a case, the noisy attractor looks similar to that shown in figure 2 for the additive noise case. However, the probability density function $P(\lambda)$ begins to develop a peak at some positive value of λ. This is seen in figure 4. As σ^2 increases, the peak on the positive side grows at the expense of the other one, showing a preponderance of chaotic motion for these high noise-strengths. Ultimately, a limit is reached beyond which the reverse phenomenon occurs, namely the positive peak begins to diminish (with increasing σ^2) until finally one obtains periodic motion once again, at extremely large noise values. This latter effect is exemplified in figure 4 by the curve corresponding to $\sigma^2 = 1.976$. A more detailed description of these effects will be published elsewhere.

REFERENCES

1. J. Crutchfield, J. Farmer and B. Huberman; Phys. Repts. 82, 45 (1982).
2. T. Kapitaniak; "Chaos in Systems with Noise", (World Publishing, N.Y. 1989).
3. L. Carlson and W. C. Schieve; "The Noisy Shift Map', J. Math. Phys., to appear.
4. H. Herzel, W. Ebeling and Th. Schulmeister; Z. Naturforsch, 42A, 136 (1987).
5. V. Melnikov; Trans. Moscow Math. Soc. 12, 1 (1963).
6. J. Guckenheimer and P. Holmes; "Nonlinear Oscillations, Dynamical Systems and Bifurcations in Vector Fields", (Springer-Verlag, N.Y. 1983).
7. T. Petrosky and W. Schieve; Phys. Rev. A31, 3907 (1985).
8. A. Bulsara, W. C. Schieve and E. Jacobs; "Homoclinic Chaos in Systems Perturbed by Weak Langevin Noise", Phys. Rev. A, to appear.
9. W. C. Schieve and A. Bulsara; "Multiplicative Noise and Homoclinic Crossing", preprint.
10. W. C. Schieve, A. Bulsara and E. Jacobs; Phys. rev. A37, 3541 (1988); E. Jacobs, A. Bulsara and W. Schieve; Physica D34, 439 (1988).
11. G. Mayer-Kress and H. Haken; J. Stat. Phys. 26, 149 (1981).
12. J. Rossler, M. Kiwi, B. Hess and M. Markus; Phys. Rev. A39, 5954 (1989).

10th Int.Conf. on Noise in Physical Systems
1989 Budapest, Hungary

NOISY CHAOS

V.S. ANISHCHENKO, Yu.A. KRAVTSOV,* A.S. PIKOVSKII**

Saratov University, Saratov, 410601, USSR
*"Lidar", P.O.B. 512, Moscow-57, 125057, USSR
**Applied Physics Institute, Academy of Sciences
Gorkii, 603600, USSR

1. INTRODUCTION

In the beginning of dynamic chaos investigation it was noticed that some statistic characteristics of strange attractors, e.g. the correlation function, the power spectrum and the one-dimensional probability density are weakly sensitive both to internal and external fluctuations (noises). For example, in 1974 Kifer (1974) has constructed a proof of a theorem which reads that small random perturbations only slightly affect the probability measure of strange attractors. However, later it became clear that the idea of statistical properties being slightly changeable is valid only for the "uniform" hyperbolic attractor, while real chaotic systems are related to so-called "quasi-attractors" with typical internal bifurcations occurring at whatever slight changes of control parameters. It was in quasi-attractors that numerous effects were detected proving a considerable influence of weak noise on chaotic systems behaviour.

In spite of recent achievements, generally indifferent if not scornful understanding of the noise actual role in chaos dynamics sustains. The objective of this report is to elucidate the main aspects of the problem of the weak noise effect on systems with complex dynamics and to select fundamental properties of real chaos which are due to the noise effect.

2. EFFECT OF NOISE ON MAIN CHARACTERISTICS OF CHAOS

2.1. Probability density on attractors is considered to be weakly dependent on noise level, because, supporters of this concept argue, the attractor is an infinite trajectory, and noise induces transitions from one part of the trajectory to another, thus maintaining the invariant measure. But to what extent are these arguments true?

Let $y = \{y_1, \ldots, y_n\}$ be a multidimensional chaotic process, and let $w(y)$ be the probability density of value y, determined through the relative duration of the system's stay within a small Δy interval. If the probability density, $w(y)$, is more or less uniform ($w(y) \cong$ const.) on the attractor, the noise effect on w is weak, indeed. But if there is a "slowdown" region on the attractor, wherein probability density has a noticeable peak, the noise effect is considerable: it reduces duration of stay within the "slowdown" region on the attractor wherein probability density has a noticeable peak, the noise effect is considerable: it reduces duration of stay within the "slowdown" region thus decreasing the height of the w_{max} peak to smoothen the probability density w on the attractor. An example of this pattern are results of two-dimensional density, $w(y_1, y_2)$, digital modelling for an oscillator with inertial nonlinearity (Anishchenko, 1989).

If we represent the noise-induced trajectory rms deviation in the "slowdown" region from the undisturbed state by the symbol σ_s, the condition on which w varies insignificantly can be written as an inequality $\sigma_s |\nabla_y w| << w$.

2.2. The probability density - a fine structure. Fractal dimension. In the presence of noise the attractor's fractal structure breaks down beginning with a certain δy_{min} value determined by noise level, so the notion of fractal dimension, strictly speaking, looses its significance. In practice, the attractor's dimension increases beginning with δy_{min}, which was repeatedly observed in quantitative experiments.

2.3. The Lyapunov index spectrum, the correlation function and the power spectrum. The noise effect primarily shows up in the shift of bifurcation lines in the space of control para-

meters. Sometimes the noise-induced Lyapunov indices are positive (the order-chaos transition), at other times the positive indices disappear (the chaos-order transition, when chaos is dampened by noise). Noise may also induce phase transitions which are not implemented in a purely dynamic system. Qualitative changes of the Lyapunov indices spectrum in the moment of noise-induced phase transitions are followed by a considerable change of the power spectrum and correlation function, as was demonstrated e.g. by Anishchenko and Safonova (1988).

3. NOISE EFFECTS DURING TRANSITION TO CHAOS AND NOISE AFFECTING INTRACHAOS TRANSITIONS

As parameters vary, the quasi-attractor structure may be subject to qualitative changes which are natural to interprete as intrachaos bifurcations. These bifurcations can be induced by low-level noise, and this draws special attention to the problem. The following aspects can be specified here:

- the characteristic noise induced transition to chaos via period doubling, via quasi-periodicity and via intermittence;
- use of the renorm group method for the analysis of transition to chaos;
- effect of chaos threshold lowering;
- noise-induced transitions to chaos in multistable systems with nonattracting homoclinic structures;
- effects of attractor interaction through the separatrix surfaces destroyed by noise;
- noise-induced disappearance of stability islands;
- noise-induced destruction of locking range boundaries;
- chaos-to-chaos transitions;
- effect of noise on static intermittence characteristics;
- modulation intermittence and the chaos-to-chaos intermittence;
- intermittence and flicker-noise.

4. CHAOS PREDICTABILITY

The fundamental role of noise is especially demonstrative when one tackles the problem of chaos behaviour prediction based on hypotetic (model) equations. The time of deterministic behaviour, τ_{det}, can be involved as time of correlation between the observed process y(t) and the model forecasting process, z(t). This time can be prolonged by reducing measurement (instrumental) noise and optimizing the model equation for the z(t) forecast. However, there is a maximum deterministic time, $\tau_{det\ max}$, related wholly to fluctuational forces and naturally identified with the predictability horizon. It is due to this mechanism that a principal limit of predictability for all physical, biological, economic, etc. systems can be set. With regard to these predictability limitations it should be noted that we are dealing with a partly deterministic chaos (rather than a deterministic one) allowing a forecast for maximum deterministic times, $\tau \lesssim \tau_{det\ max}$ (Kravtsov, 1989).

Similar limitations of the τ_{det} value arise when we use an information measure of the y and z process closeness (Shaw, 1981). From the viewpoint of the information theory the chaos unpredictability for long time intervals τ_{det} is due to the fact that noises continuously generate new information lacking in the z(t) deterministic chaos model.

REFERENCES

V.S. Anishchenko, 1989, Dynamical Chaos in Physical Systems. Experimental Investigations of Self-Oscillating Circuits. Teubner-Texte, Leipzig, 210 pp.

V.S. Anishchenko, M.A. Safonova, 1988, Zh. Tekhn. Fiz., 58, N 4, 641.

Yu.I. Kifer, 1974, Russ. Math. Surv., 29, N 3. 205.

Yu.A. Kravtsov, 1989, Randomness, Determinism, Unpredictability. Uspekhi Fiz. Nauk, 158, N 1, 93.

R. Shaw, 1981, Strange Attractors, Chaotic Behaviour and Information Flow. Z. Naturforschung, 36a, N 1, 80.

10th Int.Conf. on Noise in Physical Systems
1989 Budapest, Hungary

CHAOTIZATION OF VIBRATIONS OF A NON-AUTONOMOUS OSCILLATOR AFFECTED BY A NOISE SIGNAL: EXPERIMENTAL STUDY

Yu.A. VOSHCHINSKII, A.S. MAGARSHAK, D.M. SHTEINGRADT

Engineering Centre "LIDAR", Academy of Sciences
P.O.Box 512, Moscow, 125057, USSR

An oscillator in the form of a physical pendulum has a sinusoidal response function, a Q-factor of 10^2 and a natural frequency of 1 Hz. The pendulum's non-autonomous mode of operation is provided by interaction of static magnetic dipole fastened on the pendulum lens with an inductor of alternative (harmonic) magnetic field of 50 Hz localized within a small area around the pendulum's equilibrium point.

The dynamics of the discussed oscillator system has a remarkable feature: amplitudes of stationary oscillations (phase plane limit cycles) are weakly dependent on friction and on the pump amplitude (Bunkin et al. 1988), their number is determined, with respect to the oscillator nonlinearity pattern, only by the pumping field frequency. As to the width of the separate zone of stationary oscillations (limit cycle attraction region), it depends on the pumping field energy excess over oscillator dissipation.

The pendulum dynamics was studied using a two-processor control system for measuring period, amplitude and velocity distribution of the pendulum to an accuracy of 10^{-6}, 10^{-4} and 10^{-4}, respectively, as well as phase relationships of pendulum and pumping field oscillations to within 10^{-3}.

The system of control and data acquisition/processing was constructed using IBM-compatible PC with a special interface consisting of a processor module, a measuring module comprising five parallel time-interval counters with a clock frequency of 10 MHz and a special generator module powering the pumping in-

ductor which allows mixing of an unperturbed harmonic signal (formed with an accuracy not less than 10^{-3}) with a white noise spectrum random telegraph signal occurring in the generator.

Investigation of the oscillator dynamics under the action of an unperturbed pumping field proved that relaxation of a point representing the oscillator behaviour on the phase plane (i.e. the oscillator amplitude - the pump current phase plane) towards the limiting point (wherein the limit cycle path and the given phase plane intercross) has a much less damping factor than that of the oscillator.

The motion of the representing point on the phase plane around the limiting point can be interpreted in terms of simple mechanic motion and effective potential energy: the period of this motion depends solely on the oscillator stationary amplitude and the ratio between the pump current and the minimum necessary one for stationary oscillations. The size of the limit cycle attraction region, wherein the representing point moves, also depends on this ratio. As the pump current decreases to the minimal level this region tends to zero (see Fig. 1).

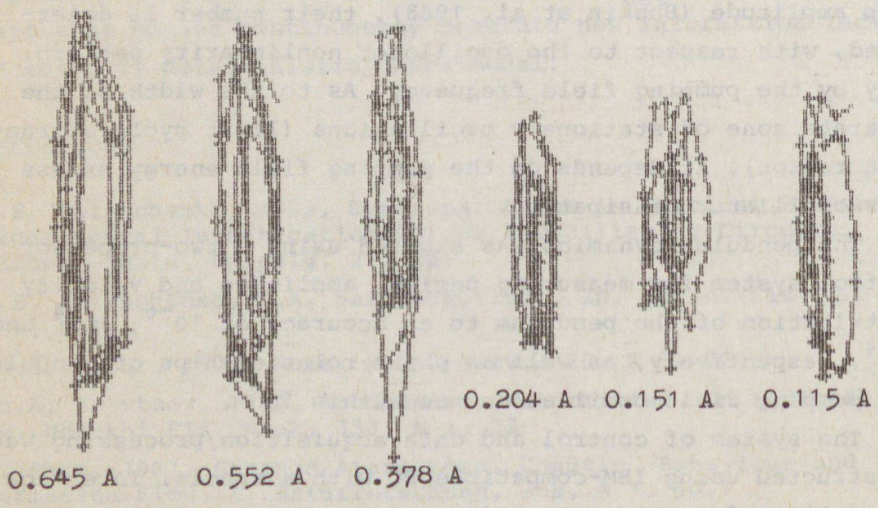

Fig. 1

Since the representing point motion on the phase plane may be identified as some kind of mechanic motion with effective potential energy, one can suppose that the limit cycle attraction region is related to the region of the local minimum of the effective potential, its size depending upon how much the pump current amplitude is higher than the minimum necessary one.

This assumption is supported by the dynamics of the representing point showing up when the oscillator is affected by a single fluctuation causing the point's damping motion along the higher-energy path with a correspondingly higher amplitude but with the same period of revolution around the limiting point as before the fluctuation (see Fig. 2).

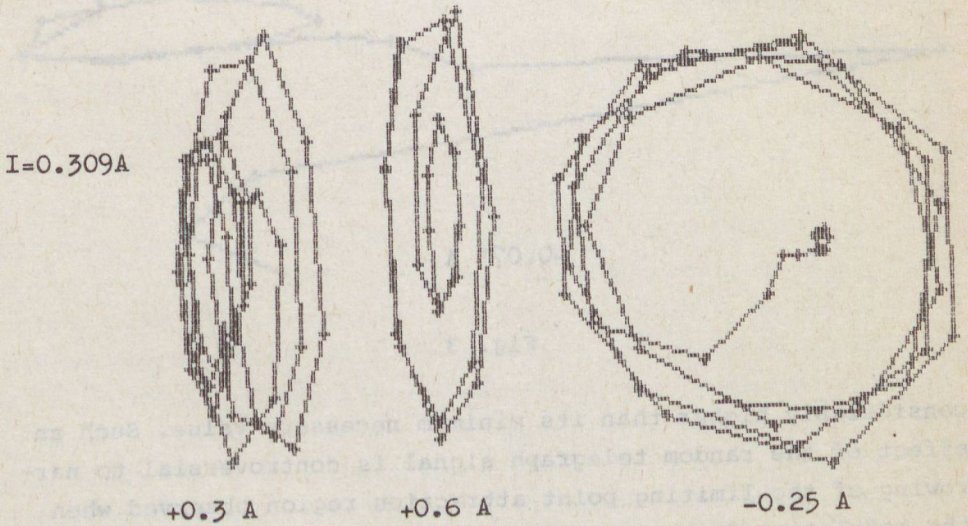

Fig. 2

In the second series of experiments the oscillator dynamics was studied when the oscillator was under the action of harmonic pumping modulated by the white noise spectrum random telegraph signal.

The representing point movement becomes more chaotic as modulation depth increases (see Fig. 3). The stationary oscillations are observed to be destroyed though the pump current is

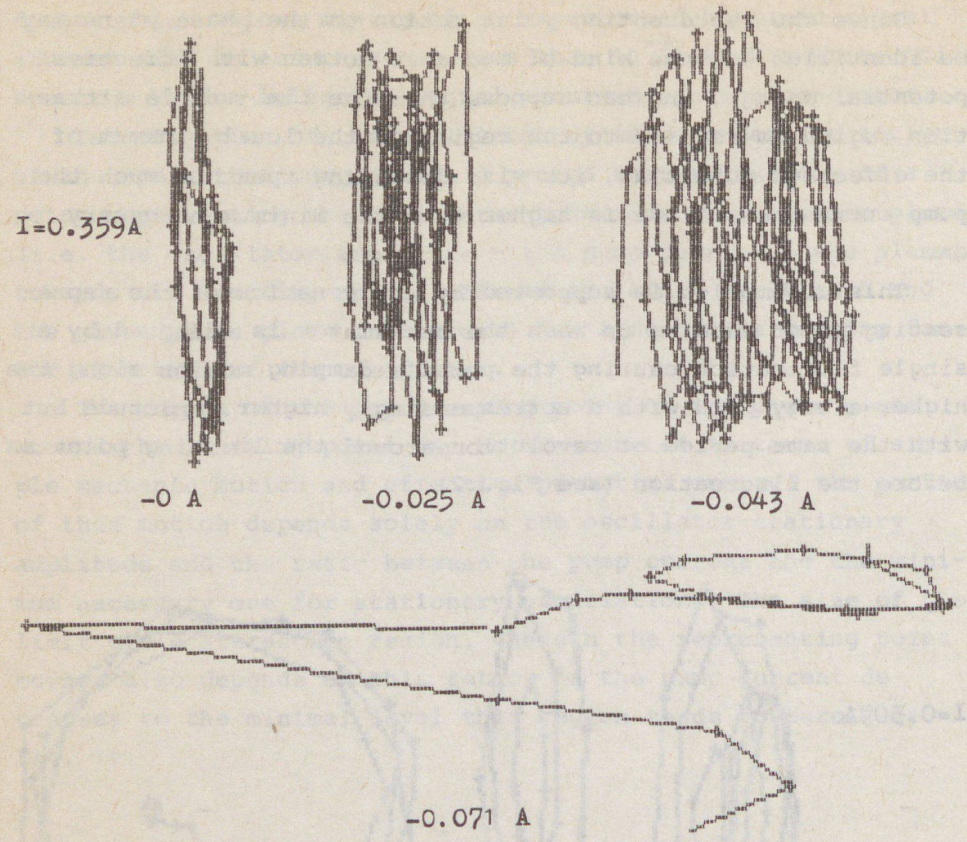

Fig. 3

considerably higher than its minimum necessary value. Such an effect of the random telegraph signal is controversial to narrowing of the limiting point attraction region observed when the modulation depth is increased, and this fact agrees well with reduction of the difference between the maximum and the minimum amplitudes of the representing point showing up when the modulation depth is increased. Therefore modulation of pump current by the random telegraph signal has opposite effects on the attraction region and on the representing point path within this region. The effect of this signal, disregarding chaotization of the representing point path, is equivalent to the pump current reduction. The probability of oscillation destroying must be non-zero due to chaotization even at minor modulation

depths, but since this probability is small, it has never been observed in experiments (in the course of 10,000 oscillations).

Destroying of oscillations observed at a great modulation depth (> 20% of the pump current amplitude value) correlates well with a characteristic lifetime of stationary oscillations (600 periods of the oscillator).

The obtained results allow the evaluation of the effect of a random force on the HF-pumped oscillator behaviour, necessary to estimate accuracy of measurement based on this oscillator system in the future.

REFERENCE

Bunkin, F.V. et al., J. Techn. Phys., v. 58, No. 11, p. 2241, 1988.



10th Int.Conf. on Noise in Physical Systems
1989 Budapest, Hungary

STOCHASTIC RESONANCE: HOW INCREASING THE NOISE CAN RESULT IN MORE ORDER

T. ZHOU,* F. MOSS

Department of Physics, University of Missouri at St. Louis
St. Louis, MO 63121, USA

The statistical phenomenon known as *stochastic resonance* (SR) was first introduced by Benzi et al.[1] and by Nicolis and Nicolis[2] in 1981 as a model for the observed periodicity in the recurrence of the Earth's Ice Ages. It is a property, most often observed in periodically modulated, bistable, noise driven systems, whereby the signal-to-noise ratio of the response passes through a maximum as some externally applied noise level is increased from zero. The response is usually defined as a switching event which carries the system from the neighborhood of one stable state to the other. In the absence of periodic modulation, often called "the signal", such switching events are purely random. However, in the presence of the modulation they become more-or-less correlated with it. At both low and high intensities of the external noise, the modulation and the switching events are not well correlated, but at some intermediate value, i.e. at "resonance", they become better correlated. Obviously, such a characteristic property is of interest in the analysis of the generalized switching process, but its first application was to meteorology. In that view, the Earth's climate is represented by a zero-dimensional bistable system, one stable state of which is a largely ice covered Earth. The external noise derives from short term fluctuations in the solar insolation, and the periodic modulation is supposed to originate from a small observed oscillation in the eccentricity of the Earth's orbit with a 100,000 year period. The first realization of stochastic resonance in a laboratory experiment was provided in 1983 by Fauve and Heslot[3], who periodically modulated a Schmitt trigger (electronic bistable device) while applying white noise. These authors measured the power spectrum of the output of the switch for various levels of input noise intensity while the amplitude of the periodic modulation or "input signal" was held constant. From these measurements, they constructed the signal-to-noise ratio (SNR), which has now become the most frequently studied quantity, and observed better than a factor of 5 increase in the SNR at the resonant value of the noise voltage.

*Permanent address: Institute for Semiconductors, Chinese Academy of Sciences, Beijing.

Renewed interest in stochastic resonance has recently been stimulated by Roy and co-workers who operated a ring laser as the bistable system[4]. This demonstration stimulated a large amount of recent theoretical activity[5-8] and two analog simulations[9,10]. Nearly all of these studies focused on the simple, one dimensional, bistable Langevin equation,

$$\dot{x} = x - x^3 + c\sin\omega_m t + V_n(t), \tag{1}$$

where the modulation has frequency ω_m and amplitude c. We consider only Gaussian noise in the white noise limit, $\langle V_n(t)\, V_n(t+s)\rangle = 2D\delta(t-s)$, where D is the noise intensity. Equation (1) derives from a bistable potential whose unmodulated ($c = 0$) barrier height is $\Delta U = 1/4$, and where the potential minima are located at $x_0 = \pm 1$. When $c > 0$, the potential is "tipped" at the rate ω_m such that each potential minimum is alternately raised and lowered in height relative to the barrier. Bistability is never destroyed, because c is small.

SR can be understood as follows: When $V_n = 0$, no switching is possible. The state of the system is confined to one well or the other depending on initial conditions. However, for $V_n > 0$ there will always be noise induced switching given by the instantaneous Kramers rate $R \propto \exp[-2\Delta U(t)/D]$. With modulation, $\Delta U(t) = \Delta U_0 + u\sin\omega_m t$. Therefore, the switching rate becomes modulated at the frequency ω_m. The output signal is therefore correlated with the noisy modulation, or input signal, and *this correlation has been induced purely by the additive noise.* The power spectrum of the output shows a strong peak at ω_m. An example, measured on our analog simulator, is shown in Fig. 1. The principles of analog simulation have been reviewed previously[11].

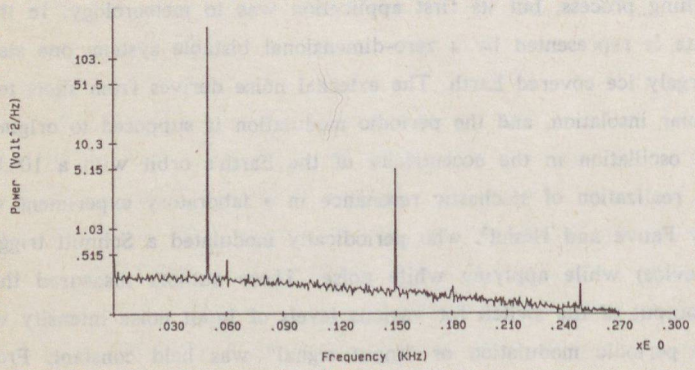

Fig. 1. Power spectrum measured for $\omega_m = 49.8$ Hz, $D = 0.1\ V^2s$, $c = 0.35$ V.

The SNR of the output is defined as the ratio of the height of this peak to the level of the noise background at the signal frequency ω_m. With increasing noise intensity the

output SNR passes through a maximum, and for higher levels of noise, the correlation between input and output becomes increasingly washed out. The maximum SNR occurs when the noise intensity dependent escape time, averaged over the changing potential becomes comparable to the half period of the modulation, behavior which has given rise to the somewhat misleading term *resonance*. An example is shown in Fig. 2, where the SNR in decibels is plotted versus $\sqrt{D}$ which is proportional to the rms noise voltage $\sqrt{\langle V_n^2 \rangle}$. In this figure, the solid curve is a theory given in Ref. 5.

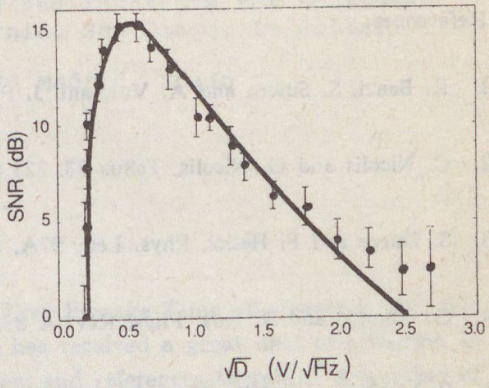

Fig. 2. The SNR in decibels versus the square root of the noise intensity.

A different characterization of SR, which to date has not been used, is the probability density of residence times. The output signal is a noisy switching function which randomly changes state from the neighborhood of one potential minimum to the other. The residence time is defined as the time between barrier crossing events as observed from one well. Because the switching is to some degree random, this density should decay exponentially as for the random telegraph signal. However, because near resonance it is highly correlated with the modulation, it should have a maximum at 1/2 the period of the modulating function. An example measured probability density is shown in Fig. 3.

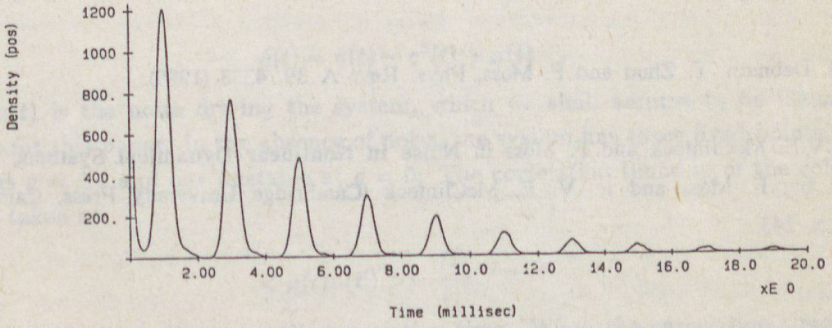

Fig. 3. The probability density of residence times for f_m = 500 Hz. Note the maxima at odd multiples of the half period of 1 ms.

Note that the power spectrum, traditionally used to investigate noisy signals, is no more sensitive to the harmonic content than is this density. Moreover, the density of residence times is more appropriate in some applications, e. g. the ice age models. Note also the peaks at odd multiples of the half period. Similar peaks, due to the same internal symmetries are in the power spectrum shown in Fig. 1. These peaks are the unmistakable signature of SR, and are predicted in only one current theory[6,8].

This work was supported by the U.S. Office of Naval Research and by N.A.T.O.

References

1. R. Benzi, S. Sutera and A. Vulpiani, J. Phys. A **14**, L453 (1981).

2. C. Nicolis and G. Nicolis, Tellus **33**, 225 (1981).

3. S. Fauve and F. Heslot, Phys. Lett. **97A**, 5 (1983).

4. G. Vemuri and R. Roy, Phys. Rev. A **39**, 4668 (1989).

5. B. McNamara and K. Wiesenfeld, Phys. Rev. A **39**, 4854 (1989).

6. P. Jung and P. Hanggi, Europhys. Lett., **8**, 505 (1989).

7. R. Fox, Phys. Rev. A **39**, 4148 (1989).

8. P. Jung, Z. Phys. B., in press.

9. L. Gammaitoni, F. Marchesoni, E. Menichella-Saetta and S. Santucci, Phys. Rev. Lett. **62**, 349 (1989).

10. G. Debnath, T. Zhou and F. Moss, Phys. Rev. A **39**, 4323 (1989).

11. P.V.E. McClintock and F. Moss in **Noise in Nonlinear Dynamical Systems, Vol. 3** edited by, F. Moss and P. V. E. McClintock (Cambridge University Press, Cambridge, 1989) p. 243.

10th Int.Conf. on Noise in Physical Systems
1989 Budapest, Hungary

ESCAPE OVER A POTENTIAL BARRIER DRIVEN BY COLORED NOISE

L. RAMIREZ-PISCINA, J.M. SANCHO, K. LINDENBERG,*
F.J. de la RUBIA**

Department d'Estructura i Constituents de la Materia,
Universitat de Barcelona Diagonal 647, 08028 Barcelona, Spain
*Department of Chemistry, B-040 and Institute for Nonlinear Science, University of California, San Diego, La Jolla, CA 92093, USA
**Física Fundamental, UNED, 28080 Madrid, Spain

The problem of evaluating the Mean First Passage Time of a system with two wells under the influence of colored noise has received a great deal of attention in the past few years (see Ref. 1 for a review and references therein). A number of different theories and techniques (some of them conflictive) have recently appeared in the literature. Most of the conflicts arise on the different interpretations of the numerical or analogical available data.

In order to attain a better understanding of the relations among these various theories and the accuracy of their predictions, we have carried out extensive numerical simulations of the Langevin equations that serve as the model from which all these theories depart [2,3]. By covering extensive ranges of parameter values (in particular the correlation time τ of the noise), we were able to arrive at some definitive conclusions that should help to clarify some of the present uncertainties in the field.

As our system, we shall consider the generic and widely studied bistable model

$$\dot{q}(t) = q(t) - q^3(t) + \mu(t) \tag{1}$$

where $\mu(t)$ is the noise driving the system, which we shall assume to be Gaussian throughout this paper. In the absence of noise, the system has three fixed points, two stable at $q = \pm 1$ and one unstable at $q = 0$. The correlation function of the colored noise is taken as

$$< \mu(t)\mu(t') >= \frac{D}{\tau} e^{-|t-t'|/\tau} \tag{2}$$

where D is the intensity and τ the correlation time. When the correlation time τ is zero, the correlation function becomes a delta, which corresponds to the white noise case.

The analysis of the digital simulation have established some points which gave a better understanding of the present theories and that have clarified the apparent conflicts between them. It is now clear [2] that Kramers's approximation for the white noise limit ($\tau = 0$) should be taken with care due to the important errors introduced for finite intensity. In this sense the relevant quantity to compare the different predictions for the dependence on τ (calculated following Kramers's approximation) is the quotient between the mean first passage times corresponding to $\tau \neq 0$ and $\tau = 0$. This procedure compensates the systematic finite-D errors introduced in the steepest descent calculation. The importance of the boundaries has also been confirmed mainly when the final point is not in the well but at the top of the potential, and the role of the separatrix is now well understood [2]. The behavior of the MFPT for small values of τ (up to 0.2) is explained correctly, but for intermediate τ (from 0.2 to 1) it is imposible to conclude which theory leads to a better τ-dependence due to the uncertainties of the digital simulation and the asymptotic character of the theoretical predictions.

For very large values of τ ($\tau \gg 1$) the fluctuating potential picture of Tsironis and Grigolini [4] leads to a qualitatively correct asymptotic exponential dependence in $2\tau/27D$ in the MFPT, but a very recent analysis of this situation [3] shows that this exponential dependence should be modified by a factor near to 4/3.

In this communication we have explored two new aspects of this problem not discussed in our previous works [2,3]. The first one is the way in which T_{top} (MFPT corresponding to the system starting from the well at q=-1 and reaching the top at q=0) approaches T_{bot} (from q=-1 to the other well at q=1) when τ grows. For white noise and very small D, Kramers's theory predicts $T_{bot}=2T_{top}$. For highly colored noise we have found in our digital simulations that T_{bot} becomes equal to T_{top}. The qualitative explanation is clear. When $\tau=0$ the separatrix is placed at q=0, and when the particle is there it has the same probability to reach the other well than to turn back to the first well. However, when τ is larger, the separatrix moves near the starting point, and if the particle reaches q=0 (now in the attraction region of the second well), the probability of reaching first the second well is larger, and the mean time (T_{bot}) is closer to T_{top}. In Fig. 1 we see that T_{bot}/T_{top} as a function of τ decays exponentially. To date there is only a partial explanation of this behavior. It is known that the dependence of these two quantities to order τ is

$$T_{bot}(\tau) = T_{bot}(0)(1 + \frac{3}{2}\tau) \tag{3}$$

$$T_{top}(\tau) = T_{top}(0)(1 + \alpha\sqrt{\tau} + \frac{3}{2}\tau) \tag{4}$$

with α=1.16519..., [5]. To the same order in τ, and assuming $T_{bot}(0)=2T_{top}(0)$ (which is asymptotically valid for small D) the ratio T_{bot}/T_{top} is

$$\frac{T_{bot}(\tau)}{T_{top}(\tau)} = 2 - 2\alpha\sqrt{\tau} + 2\alpha^2\tau \tag{5}$$

We have interpreted this result as the first terms of an exponential decay

$$\frac{T_{\text{bot}}(\tau)}{T_{\text{top}}(\tau)} - 1 = \exp(-2\alpha\sqrt{\tau}) \tag{6}$$

As we see in Fig. 1 the agreement is very good, mainly for very small values of D, as one can expect from the theoretical analysis.

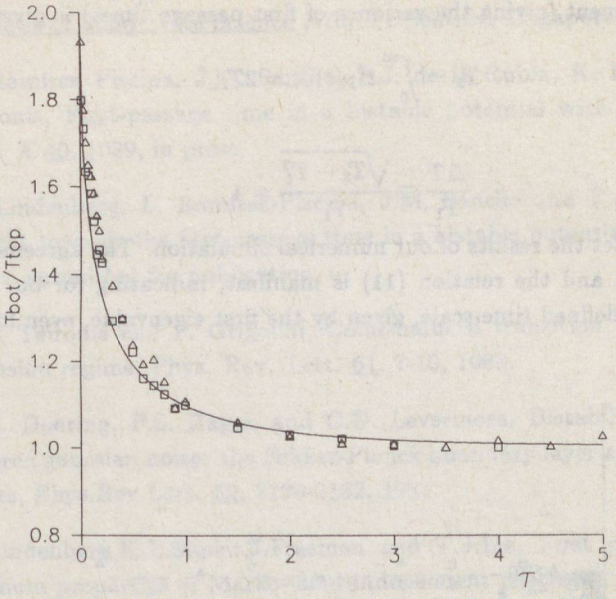

Fig.1. $T_{\text{bot}}/T_{\text{top}}$ vs τ. Squares, $D = 0.083$; triangles, $D = 0.114$. Solid line:theoretical prediction, Eq.(6).

The second aspect we want to discuss in this work is the existence of a single time scale, characterizing the long-time evolution of the system, even for large values of τ.

If the evolution equation for the probability density P characterizing the system is written as $dP/dt = \mathcal{L}P$ where $\mathcal{L}$ is an operator, then the temporal behavior of the system is determined by the spectrum of $\mathcal{L}$. If the lowest eigenvalue of $\mathcal{L}$ is isolated (call it λ_1) then the characteristic time scale at long times is $1/\lambda_1$ (if there is no isolated lowest eigenvalue then the evolution is not characterized by a single time scale). An example of an operator $\mathcal{L}$ that leads to isolated eigenvalues is the Fokker-Planck operator.

If such an isolated lowest eigenvalue exists, then the probability density of the first passage time to reach the well at $q = +1$ (under weak noise conditions) may be written as [6,7]

$$p(t) = T_{\text{bot}}^{-1} \exp(-t/T_{\text{bot}}) \tag{7}$$

the mean first passage time is

$$T_1 = \int_0^\infty tp(t)dt = T_{\rm bot} \tag{8}$$

and is related to the lowest eigenvalue through [2]

$$T_{\rm bot} = 2\lambda_1^{-1} \tag{9}$$

The second moment (giving the variance of first passage times) is given by

$$T_2 = \int_0^\infty t^2 p(t)dt = 2T_1 \tag{10}$$

and therefore

$$\frac{\Delta T}{T_1} \equiv \frac{\sqrt{T_2 - T_1^2}}{T_1} = 1 \tag{11}$$

In Fig.2 we depict the results of our numerical simulation. The agreement between the numerical data and the relation (11) is manifest, indicating for our system the existence of a well-defined time scale, given by the first eigenvalue, even for large τ

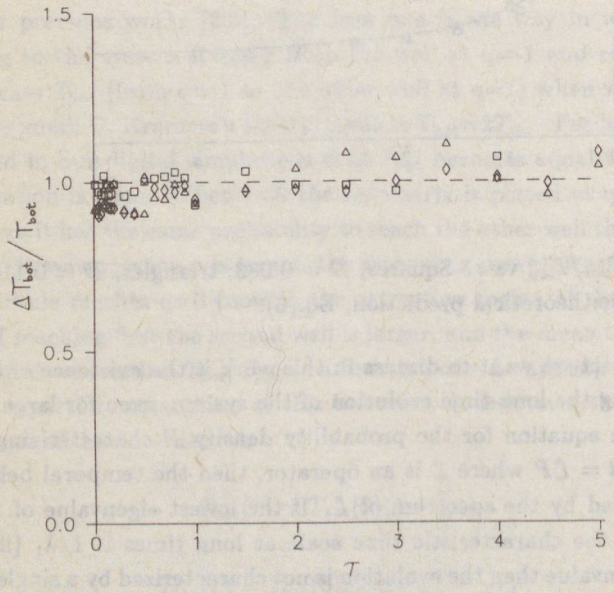

Fig.2. Simulation results for $\Delta T_{\rm bot}/T_{\rm bot}$ vs τ. Squares, $D = 0.083$; triangles, $D = 0.114$; rhombuses, $D = 0.153$.

We acknowledge financial support from the Dirección General de Investigación Científica y Técnica (Spain), Grant Nos. AE87-0035, PB87-0014 (LRP and JMS) and PB85-0024 (FJR). One of us (KL) also acknowledges partial support from U.S. Department of Energy Grant No. DE-FG03- 86ER13606.

REFERENCES

1. K. Lindenberg and B.J. West, Bistable systems driven by colored noise, in Reviews of Solid State Science ,World Scientific, Singapore, 1989, in press.

2. L. Ramírez Piscina, J.M. Sancho, F.J. de la Rubia, K. Lindenberg and G.P. Tsironis, First-passage time in a bistable potential with colored noise, Phys. Rev. A 40, 1989, in press.

3. K. Lindenberg, L. Ramírez-Piscina, J.M. Sancho and F.J. de la Rubia, New insight towards the first-passage time in a bistable potential with highly colored noise, submitted for publication.

4. G.P. Tsironis and P. Grigolini, Color-induced transition to a nonconventional diffusion regime, Phys. Rev. Lett. 61, 7-10, 1988.

5. C.R. Doering, P.S. Hagan and C.D. Levermore, Bistability driven by weakly colored gaussian noise: the Fokker-Planck boundary layer and mean first-passage times, Phys.Rev.Lett. 59, 2129-2132, 1987.

6. K.Lindenberg,K.E.Shuler,J.Freeman and T.J.Lie, First passage time and extremum properties of Markov and independent processes, J.Stat.Phys. 12, 217-251, 1975.

7. P.Talkner, Mean first-passage time and the lifetime of a metastable state, Z.Phys. B. 68, 201-207, 1987.

10th Int.Conf. on Noise in Physical Systems
1989 Budapest, Hungary

FRACTAL DIMENSIONS: PROBLEMS OF CALCULATIONS

D.M. VAVRIV, V.B. RYABOV

Kharkov State University
310077 Kharkov, USSR

It is now an accepted notion that fractal dimension is the universal characteristic of many physical objects with hierarchical structure. Although this quantity is widely used for analysis of different processes and its rigorous definition is rather evident, a number of serious problems related to its direct calculation still exists. We shall dwell upon some of them and outline ways for their solution.

Most real objects with hierarchical structure are multifractals and for their description it was proposed to use a set of generalized dimensions D_q or singularity spectrum $f(\alpha)$ (1). The usual approach to the definition of D_q or $f(\alpha)$ operates with the limit of partition functions $\Gamma(\varepsilon, q, N)$ when $\varepsilon \to 0$ and $N \to \infty$ (ε - characteristic size of partition cells, N - the number of points of fractal). As is known, so far as the real calculations always operate with finite values of N and ε, this, firstly, creates an additional problem of choosing the magnitudes of N and ε and, secondly, leads to systematic errors (2). We demonstrate the seriousness of these problems by the simple example of D_q calculations for two-dimensional region with area S which contains N points randomly distributed on it with the probability density $w = 1/S$. If the area S is subdivided into cells with equal size ε one can analytically derive the generalized entropy

$$\chi_q = \sum_{i=1}^{N} \left(\frac{i}{N}\right)^q C_N^i (S/\varepsilon^2)^{1-i} (1-\varepsilon^2/S)^{N-1}$$

In the limit $\varepsilon \to 0$ and $N \to \infty$ all $D_q = \frac{1}{q-1} \lim \frac{\log \chi_q}{\log \varepsilon}$ coincide and equal 2. However, calculations with any finite values of N and ε result in the whole spectra of D_q and consequently $f(\alpha)$ (see Fig. 1). If $N \to \infty$ then $f(2) = 2$ and $f(\alpha) = 0$ when $\alpha \neq 2$. But in reality $f(\alpha)$ always has finite width even the set investigated is not multifractal. In the case considered here one can estimate the $f(\alpha)$ spectrum width $d^*(N, \varepsilon)$ at the level $f(\alpha) = 0$.

$$d^*(N, \varepsilon) \cong -\frac{4 \log (N\varepsilon^2)}{\log N\varepsilon^2 (1-\varepsilon^2/S)^{N-1}} \quad \text{for } \varepsilon^2 > S(1-N^{-1/(N-1)})$$

We believe that the value of d^* is in a sense the fundamental limit for $f(\alpha)$ calculations with finite N and ε.

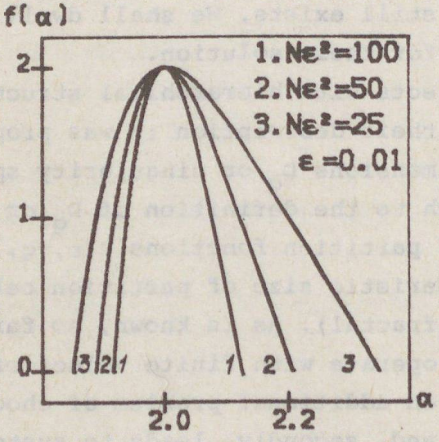

Fig. 1. The $f(\alpha)$ spectrum for uniform distribution on a plane.

Alongside with the problem of ε and N finiteness the accuracy of results is strongly influenced by the lacunarity of fractals (3) which causes the uncertainty in the very definition of D_q as they are usually determined from the slope of corresponding curves in the log-log coordinates. For example, let us consider a Cantor set which is obtained from the interval (0;1) by replacing it by two subintervals of lengths l_1 and

l_2 and by repeating this procedure for each of them self-similarly and so on. We propose the following algorithm of the correlation integral calculation with any degree of accuracy for any scale. It is based on the well-known method of determining the probability distribution function of distances between points randomly situated on the interval. Correlation integral C(l) is calculated by counting the Cantor set elements represented in Fig. 2a inside the strip between straights $y = X \pm 1$. The results of numerical experiments are shown in Fig. 2b.

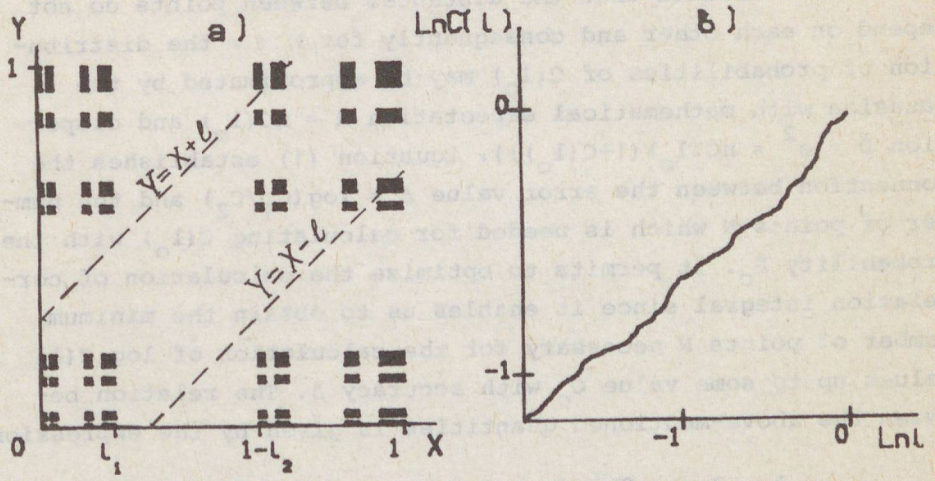

Fig. 2. First three steps of the construction used for C(l) calculations with $l_1 = 0.2$, $l_2 = 0.4$ (a); correlation integral for Cantor set (b).

For real fractals which are not so regular the lacunarity consists of aperiodic oscillations and it seems important to know the behaviour of such curves for all scales (as we know at present, there exists an efficient algorithm of C(l) calculations for small l only (4)). Here we shall develop one of the possible approaches to the solution of this problem.

We make use of the fact that the correlation integral is the probability distribution function of the distances between points situated on fractal. Suppose that we want to calculate C(l) with the accuracy Δ at some $l = l_o$. To do so, having spe-

cified condifence of probability P_c, we calculate the limits of confidence interval $(C_1; C_2)$. Provided $nC^*(l_o)(1-C^*(l_o))>9$ we find

$$C_{1,2} = \frac{2nC^*(l_o)+t^2 \pm t(4nC^*(l_o)(1-C^*(l_o))+t^2)^{1/2}}{2(n+t^2)} \qquad (1)$$

where $C^*(l_o)$ is the value of correlation integral calculated according to its definition; $n = N(N-1)/2$, where N is the number of points of fractal used; t is the half-width of the confidence interval normalized on the root-mean-square deviation σ. (We have assumed that the distances between points do not depend on each other and consequently for $N \to \infty$ the distribution of probabilities of $C(l_o)$ may be approximated by the Gaussian with mathematical expectation $M = nC(l_o)$ and dispersion $D = \sigma^2 = nC(l_o)(1-C(l_o)))$. Equation (1) establishes the connection between the error value $\Delta = \log(C_1/C_2)$ and the number of points N which is needed for calculating $C(l_o)$ with the probability P_c. It permits to optimize the calculation of correlation integral since it enables us to obtain the minimum number of points N necessary for the calculation of log C(l) values up to some value C_c with accuracy Δ. The relation between the above-mentioned quantities is given by the expression

$$C_c \cong 4t^2/(4t^2 + n\Delta^2) \qquad (2)$$

Thus, when C(l) is large (large scales) the number of points necessary for reaching the required accuracy may be reduced.

The optimal algorithm consists of the following. At first it is necessary to calculate C(l) for $l<l_o$ ($l_o<<l_m$, where l_m is maximum scale) with the largest possible number of points N_o (on the basis of computer resources) using the method of Ref. (4). Then we obtain the values of C(l) up to some value of $l_1>l_o$ having determined the number of points N_1 required for calculations and so on. At each such step the number of points required is considerably reduced, that is $N_1<<N_o$, $N_2<<N_1$, etc. Finally it enables us to evaluate C(l) for all scales with slight increase of computation time.

REFERENCES

1. T.C. Halsey et al., Fractal measures and their singularities: The characterisation of strange sets. Phys. Rev., A33 (1986) 1141-1151.

2. P. Grassberger, Finite sample corrections to entropy and dimension estimates. Phys. Lett., A128 (1988) 369-373.

3. B.B. Mandelbrot, The Fractal Geometry of Nature. Freeman, San Francisco 1982.

4. J. Theiler, Efficient algorithm for estimating the correlation dimension from a set of discrete points. Phys. Rev., A36 (1987) 4456-4462.

10th Int.Conf. on Noise in Physical Systems
1989 Budapest, Hungary

EXPERIMENTAL INVESTIGATIONS ON DYNAMICAL CHAOS IN WEAKLY NONLINEAR OSCILLATORS

I.Yu. CHERNESHOV, D.M. VAVRIV

Kharkov State University
310077 Kharkov, USSR

1. The study of the oscillation dynamics of quasilinear oscillators has started as known rapid development of physics of nonlinear oscillations at the beginning of our century. Among the first physical objects which stimulated such investigations the simplest electronic circuits, such as nonlinear RLC-circuits, vacuum-tube oscillator etc., should be mentioned. At the moment we can note returning to the investigation of such circuits realizing that their dynamics is really much more complicated and it may include different regimes of stochastic oscillations.

In order to show the place of the present work among the enormous number of investigations in the field of dynamical chaos, we shall consider for instance forced oscillations of RLC-circuit with nonlinear capacity. It is known that the stochastic oscillations as a result of period-doubling bifurcations (1) may arise in this circuit at high levels of external harmonic drive. In Fig. 1 the experimental phase diagram of regimes in parameter space drive frequency f-normalized drive amplitude $\mu = 10 \lg(U/U_o)$ is shown, where U_o = amplitude of oscillations at which hysteresis in the system occurs. The line of the first period-doubling bifurcation is marked as L^1 and the corresponding region of chaos is represented by shading. Resulting stochastic oscillations are specified by a wide band noise spectrum and for the mathematical description of this case usually essentially nonlinear Duffing's equation has been used. However, it turned out (2, 3) that narrow band-width

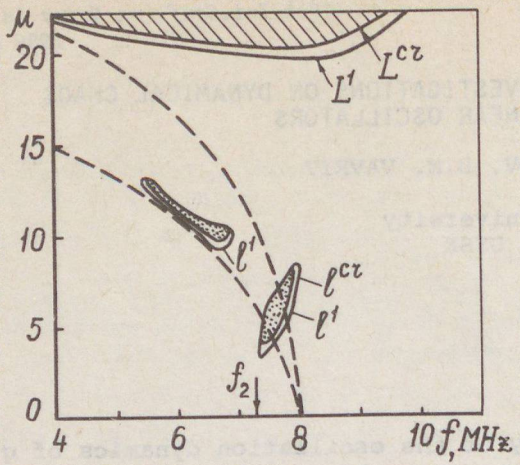

Fig. 1. Phase diagram for harmonically and two-harmonically forced nonlinear RLC-circuit.

chaotic oscillations may also arise in the RLC-circuit if several incommensurate components are present in the spectrum of external drive. In this case additional regions of chaos arise at the phase diagram. For the two-frequency (f and f_2) drive upon the circuit these regions are distinguished by dots. The value of the additional frequency f_2, is shown in Fig. 1 by arrow, and its amplitude $U_2 = 2U_o$. Characteristic peculiarities of chaos arising in these regions consist of the following. Firstly, chaos arises here due to the destruction of quasiperiodic oscillations, for example, as a result of succession of period-doubling bifurcations of differential frequency period $|f - f_2|$ (line of first bifurcations is marked 1^1 in Fig. 1). Secondly, chaotic oscillations arise at considerably lower levels of external signal as those by single-frequency drive. As the chaotization of oscillations is observed there in a weakly nonlinear oscillator, the mathematical simulation is possible with the help of averaged equations of the oscillator (3).

The object of this paper is a systematic study of conditions and routes of transition to chaos arising in single and

coupled quasilinear oscillators by means of experimental investigation.

2. Experiments with the vacuum-tube oscillators permitted the study of stochastization of oscillations in an active oscillator. Here like in RLC-circuits arising of chaos by quasilinear assumption limiting is possible in the presence of external quasiperiodic oscillation only. In Fig. 2 the typical diagram of oscillating regimes of the oscillator on the plane of parameters: the normalized amplitude of external drive

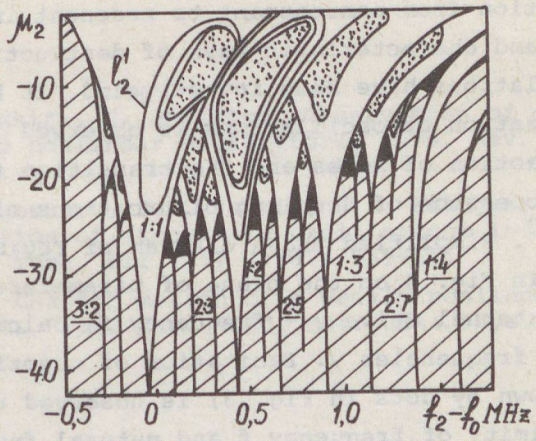

Fig. 2. Phase diagram for the nonautonomous vacuum-tube oscillator.

$\mu = 10 \lg (U_2/U_a)$ - frequency detuning $|f_2 - f_a|$ is shown, where U_a, f_a = amplitude and frequency of autooscillations, f_2 = one of the frequencies of external double-frequency drive. Shading shows the fields of oscillations with three incommensurate frequencies f_1, f_2 and f_a. Three-dimensional invariant torus T^3 corresponds to such a motion of the system in its phase space. As a result of three-frequency combined resonances on T^3, characterized by the rotation number $m/n = |f_a - f_1|/|f_2 - f_1|$ (typical values m/n are shown in the figure), the tongues of synchronization arise. Transition to chaos is performed either as a result of three-frequency or two-frequency oscillations breakdown with the rise of strange torus-attractors AT^3 and AT^2, respectively. The regions of existing AT^2 in Fig. 2 are

marked by dots and AT^3. Taking into account the results of our investigations we should note that the presence of additional spectral components with rather low intensity in the spectrum of synchronizing signal may cause the destruction of synchronous oscillations even in the fundamental region of synchronization.

3. The experimental studies of the two-degree of freedom oscillators allow to supplement the idea of nonautonomous dynamics of coupled quasilinear oscillators in the presence of external harmonic signal. Evolution of oscillating regimes during the transition from nonresonant to resonant interaction has been analyzed and characteristic ways of destruction of quasiperiodic oscillations have been investigated. It has been shown that stochastization of oscillations is observed also by nonresonant interaction of modes and the transition to chaos goes through the succession of doubling bifurcations of three-dimensional torus T^3. Simplified phase diagram of regimes for this case is shown in Fig. 3 on the plane of parameters: normalized amplitude of external drive μ - frequency f, calculated from one of partial frequencies ν. Excitation of chaotic oscillations (area shown by dots in Fig. 3) is observed under the condition of proximity of frequency f and natural frequency f_p of

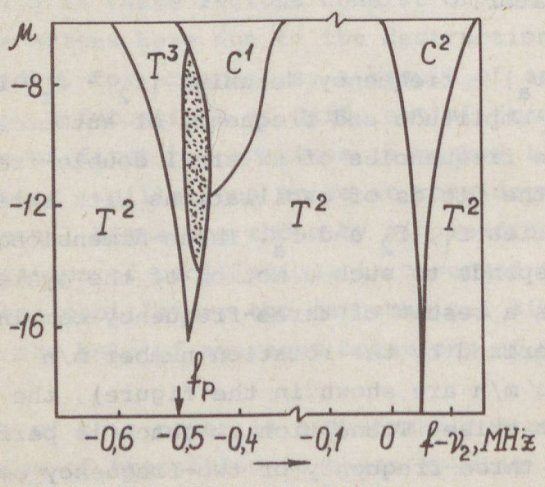

Fig. 3. Phase diagram for the harmonically forced two-degree of freedom system.

passive mode. Regions of existence of synchronous single-frequency oscillations are shown here as C^1 and C^2. In the case of resonant interaction of modes, two main ways of transition to chaos are realized: through doubling bifurcations of two-dimensional torus and through soft destruction of three-dimensional torus.

Experiments with oscillators of different types have demonstrated that disclosed regularities of evolution of chaotic and regular regimes are fairly well general regularities of quasi-linear systems dynamics.

REFERENCES

1. R. Van Buskirk, C. Jeffries, Observation of chaotic dynamics of coupled nonlinear oscillators. Phys. Rev., A31 (1985) 3332-3357.
2. A.B. Belogortsev, D.M. Vavriv, B.A. Kalugin, On conditions of excitation of stochastic oscillations in nonlinear circuit. Zh. Tech. Fiz., 57 (1987) 559-561.
3. J. Miles, Chaotic motion of a weakly nonlinear modulated oscillator. Proc. Nat. Acad. Sci. USA: Phys. Sci., 81 (1984) 3919-3923.

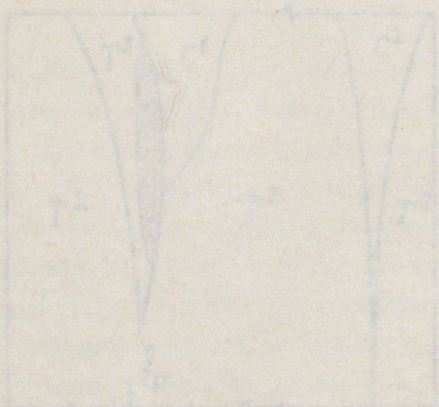

10th Int.Conf. on Noise in Physical Systems
1989 Budapest, Hungary

THE INTERACTION OF RESONANCES AND CHAOS IN QUASILINEAR SYSTEMS

A.B. BELOGORTSEV, D.M. VAVRIV

Kharkov State University
310077 Kharkov, USSR

1. INTRODUCTION

The dynamics of a great number of physical processes is described by the equations of motion of the N coupled quasilinear oscillators

$$\ddot{x}_i + \omega_i^2 x_i = \varepsilon f_i(x_1, \dot{x}_1, x_2, \dot{x}_2, \ldots, x_N, \dot{x}_N), \; i = 1,2,\ldots,N, \qquad (1)$$

where x_i are generalized coordinates of oscillators, ω_i are their natural frequencies, f_i are functions which describe nonlinearity and dissipation, ε is a small perturbation. The main result on stochastic behaviour of Eq. (1) is that solutions have been obtained for the systems $\varepsilon \cong 1$. We have made systematic investigations on chaotic dynamics of system (1) with $\varepsilon << 1$ when its behaviour is adequately described by averaged equations for amplitudes and phases of oscillations. In this case the main scenarios of transition to chaos, which was observed when the number of the interacting oscillators exceeded two, are related to the destruction of the quasi-periodic oscillations. Due to this fact the quasilinear systems proved to be most convenient models particularly for regarding processes of turbulence arising.

Scenarios and mechanisms of chaos appearing in systems (1) depend essentially on each oscillator non-equilibrium parameters G_i, which are determined by parameters (1). For some $G_i = G_{icr}$ the corresponding oscillator undergoes Hopf bifurca-

tion that means transition from the passive into the active state. We study some typical cases when system (1) may exhibit chaotic motion. In order to simplify the analysis we shall take into account that in many real physical situations the parameters G_i considerably differ for different oscillators. This allows us to study the behaviour of passive oscillators as well as active ones, for which the parameters G_i slightly exceed their critical values, without taking into account their reverse influence upon active oscillators with $G_j >> G_{jcr}$ performing developed self-excited oscillations. For the oscillator with cubic nonlinearity this leads to a more simple model (1):

$$\frac{da}{d\tau} = (\alpha - \gamma a^2)a + \sum_{k=1}^{K} S_k \cdot \sin(\phi - (\Delta_k - \Delta)\tau),$$
$$a\frac{d\phi}{d\tau} = (-\Delta + \beta a^2)\, a + \sum_{k=1}^{K} S_k \cdot \cos(\phi - (\Delta_k - \Delta)\tau), \qquad (2)$$

where a and ϕ are amplitude and phase of a certain oscillator, τ is a nondimensional time, S_k are amplitudes of other active oscillators affecting the chosen one, $\Delta_k - \Delta$ is a normalized deturning of their frequencies relative to ω_i, β is a parameter of non-isochronism of the oscillations, $\alpha = (G_i - G_{icr})/G_{icr}$. Below are considered three typical situations: $\alpha \cong 0$, $\alpha < 0$, $\alpha > 0$ for the simplest case $K = 2$.

2. THE INTERACTION OF RESONANCES

When α, γ are small, system (2) close to a Hamiltonian system and chaos may appear as a result of an interaction of resonances (2). We have summarized this mechanism realization conditions specified for system (2) which for $K = 2$ are the following:

$$1 \lesssim 2(\Delta_1 \sqrt{\eta}_1 + \Delta_2 \sqrt{\eta}_2)/|\Delta_2 - \Delta_1| \lesssim 2, \qquad (3)$$

$$0 \leq |\Delta_k - \Delta_o|/(2\Delta_o) \lesssim \sqrt{\eta}_k,\ 2|\alpha|/\Delta_o \cong \eta_k,\ k = 1,2, \qquad (4)$$

where $\Delta_o = \beta|\alpha|/\gamma$, $\eta_k = 2\, S_k\sqrt{\beta}/\sqrt{\Delta_k^3} << 1$. Conditions (3) are the result of applying the classical Chirikov's criterion and relationships (4) impose additional limitations on the dissipation parameters α, γ and on the non-isochronism parameter β. The true character of expressions (3) and (4) is confirmed by the detailed numerical experiments (3). They demonstrate that chaos exists either during long time interval $\tau >> 1/\alpha$ (active oscillator, $\alpha > 0$) or during the finite time $\tau \cong 1/|\alpha|$ (passive oscillator, $\alpha < 0$) depending on the sign of α. As far as the second case is considered, the appearance of chaos which exists on time interval $\tau >> 1/|\alpha|$ is possible due to realization of mechanisms, which differ from resonance interaction.

3. MULTIPLE PASSING THROUGH THE RESONANCE

For chaotization of the oscillations in a passive oscillator the presence of their finite non-isochronism is necessary. As we established, it occurs when

$$\max (S_1, S_2) \cong (S_+ + S_-)/2, \quad \min (S_1, S_2) \cong (S_+ - S_-)/2, \tag{5}$$

where

$$S_{\pm} = \{6\Delta_i(\alpha^2 + \Delta_i^2/9) \pm 2[3(\Delta_i^2/3 - \alpha^2)^3]^{1/2}\}^{1/2}/3\sqrt{\beta}), \quad i = 1 \text{ or } 2.$$

If conditions (5) are satisfied, repeated passing through the resonance (4) is realized. Transition to chaos may take place via two routes: as series of period-doubling bifurcations of oscillations on difference frequency $|\Delta_1 - \Delta_2|$ (5) or as intermittence. As distinct from the case of single-frequency excitation of nonlinear oscillators, the transition to chaos is possible here at any low level of external force. In particular, it demands revising a number of classical results concerning the stability of oscillations in passive resonant electrical circuits and resonators regarding the effect of multifrequency signals.

4. STOCHASTIZATION OF ACTIVE OSCILLATORS

The simplest case of interaction of three active oscillators is described in Eqs (2) by parameter $\alpha > 0$ and $K = 2$. The transition to chaotic dynamics is performed here through a sequence of period-doubling bifurcations of resonance cycle on a three-dimensional torus T^3, through loss of smoothness of T^3 and through intermittence. Our investigations have demonstrated that in contrast with the case of passive oscillators, appearance of stochasticity is possible here in the absence of non-isochronism, i.e. at $\beta = 0$. However, in the case of finite β, the regions of chaos existence and development of chaoticity of oscillations considerably increase. Stochastization occurs in the vicinity of parameter values prescribed at $S_1 = S_2 \equiv S$ by the following relationships:

$$\Delta_{1,2} \cong \Delta_0 \pm \Delta_c, \quad \text{where} \quad \Delta_c \cong S\sqrt{(1 + \beta^2/\gamma^2)\gamma/\alpha}. \tag{6}$$

If every condition (6) is satisfied, the saddle-node bifurcation is realized in the reduced system (2) ($K = 1$). The influence of the third oscillator leads to arising of the strange torus-attractor.

Beside the described results we carry out investigations on more general models (1), taking into consideration effects of mutual influence of oscillators, stability of oscillating modes to perturbations (both regular and noisy). The problems of identification of strange attractors and noisy regular attractors are also discussed.

REFERENCES

1. N.N. Bogoliubov, Yu.A. Mitropolsky, Asymptotic Methods in the Theory of Non-linear Oscillations. Fizmatgiz, Moscow, 1958.
2. B.V. Chirikov, Chaotic dynamics in Hamiltonian systems with divided phase space. Lect. Notes Phys., 179 (1983) 29-46.
3. A.B. Belogortsev, D.M. Vavriv, O.A. Tret'yakov, Stochastic oscillations in quasilinear oscillational systems. Zh. Tech. Fiz., 58 (1988) 284-293.

4. A.B. Belogortsev, D.M. Vavriv, O.A. Tret'yakov, The involvement of a passive mode in turbulent motion. Zh. Eksp. Teor. Fiz., 92 (1987) 1316-1321; Sov. Phys. JETP, 65 (1987) 737-740.

5. J. Miles, Chaotic motion of a weakly nonlinear, modulated oscillator. Proc. Nat. Acad. Sci. USA; Phys. Sci., 81 (1984) 3919-3923.

10th Int.Conf. on Noise in Physical Systems
1989 Budapest, Hungary

ELECTROHYDRODYNAMIC INSTABILITIES IN NEMATICS DRIVEN BY DICHOTOMOUS STOCHASTIC VOLTAGES

U. BEHN, R. MÜLLER

Sektion Physik, Karl-Marx-Universität
7010 Leipzig, GDR

1. INTRODUCTION

The effects of parametric stochastic modulation of control parameters on the onset of dissipative structures are subject of increasing interest [1, 2]. One of the experimental model systems are the electrohydrodynamic instabilities in nematic liquid crystals. Sandwiching a layer of nematics between two parallel electrode plates one observes with increasing strength of an applied electric field a sequence of instabilities similar to the Benard instabilities. A superposition of a slowly fluctuating deterministic and a fast fluctuating stochastic field results in a stabilization of the nematic state. A comprehensive review on recent experimental and theoretical work excited by this phenomenon can be found in [3].

We consider the superposition of a constant field ε_1 with a stochastic dichotomous field ε_t jumping with mean frequency α between $\pm\,\varepsilon$. Supposing that the transition from the nematic phase towards roll cells is smooth (supercritical) we investigate the linear 1d model of Dubois-Violette et al. [4],

$$\dot{\vec{z}} + (\mathbb{A} + \mathbb{B}\,\varepsilon_t)\,\vec{z} = 0 \qquad (1)$$

where $\vec{z} = (q, \Psi)$, q is the space charge density, Ψ is the curvature of the angle between the director and electrode plane. $\mathbb{A}$ and $\mathbb{B}$ are constant 2×2 matrices specific for 1d and 2d theories depending on material parameters, on ε_1, and on the wave numbers k_x and k_z of the test mode.

In this paper we compare within a 1d model different stability criteria: amplitude, energetic, and sample stability. The influence of boundary conditions is investigated analyzing the amplitude stability of a 2d model.

2. STABILITY OF MOMENTS

Since $\varepsilon_t^2 = \varepsilon^2$ =const it is possible to obtain closed equations for the moments of the form [5, 6]

$$(\mathbb{1}\, d/dt + \mathbb{C})(\langle \vec{w} \rangle , \langle \varepsilon_t \vec{w} \rangle)^T = 0 \qquad (2)$$

$\mathbb{C}$ depends on the same parameters as $\mathbb{A}$ and $\mathbb{B}$, and on α. For the first moments (amplitude stability), it is a 4×4 matrix and $\vec{w} = \vec{z}$. For the second moments (energetic stability) it is a 6×6 matrix and $\vec{w} = (q^2, q\Psi, \Psi^2)$. The exponential solutions of Eq. (2) are unstable if the largest exponent has a positive real part. The threshold value of the external field is obtained after minimizing the stable region with respect to the wave numbers (mode selection).

The stability analysis of the first moments (Fig. 1) can qualitatively explain the experimentally observed direct transition towards chaos above a critical strength of the stochastic field as well as the destabilizing effect of the noise if its correlation time is of the order of the characteristic time

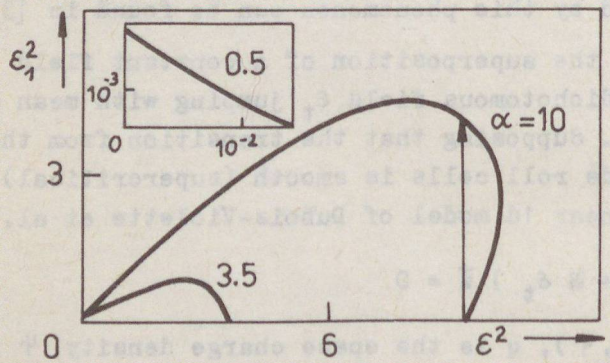

Fig. 1. Amplitude thresholds for different α. Typical cases: (i) Stabilization by noise and direct transition toward chaos (solid arrow) above a critical strength of the noise (α =10). (ii) Destabilization by noise (α =0.5). Helfrichs parameter ζ^2=2.5, arbitrary units.

of the system [5] . The energetic stability criterion gives always a lower threshold with the same qualitative behaviour.

3. SAMPLE STABILITY

Introducing polar coordinates (r, φ) one obtaines from Eq. (1)

$$\dot{r} = g(\varepsilon_t, \varphi)\, r \quad , \quad \dot{\varphi} = h(\varepsilon_t, \varphi) \quad , \tag{3a,b}$$

where g and h are nonlinear functions of ε_t and φ, depending on the same parameters as $\mathbb{A}$ and $\mathbb{B}$. For a given trajectory of the driving process the linear equation (3a) can be solved. This leads to the Lyapunov exponent [7]

$$\lambda = \lim_{t\to\infty} (1/t) \int_0^t d\tau\, g(\varepsilon_\tau, \varphi) = \sum_{\sigma=\pm} \int dP_\sigma(\varphi)\, g(\sigma\varepsilon, \varphi) \, . \tag{4}$$

$P_\sigma(\varphi)$ is the invariant measure of the joint process (ε_t, φ) which can be obtained exactly from Eq. (3b). The threshold from the sample stability criterion is always higher than the second moment's threshold.

In Fig. 2 the thresholds due to the above criteria are compared for the simplest case of pure stochastic excitation.

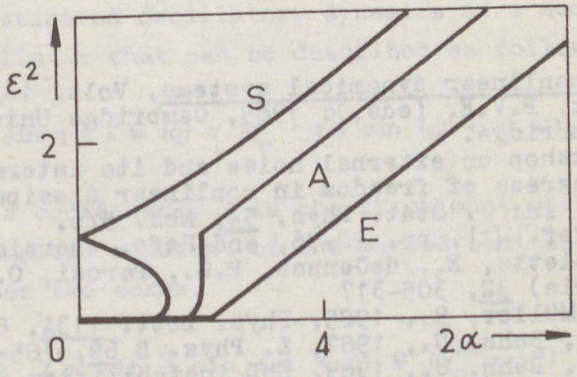

Fig. 2. Pure stochastic excitation. Thresholds corresponding to different criteria against α. Sample (S), amplitude (A), and energetic (E) stability. $\varsigma^2=3$, arbitrary units.

4. INFLUENCE OF BOUNDARY CONDITIONS

Since in the 1d theory no boundary conditions appear we investigate a 2d theory with free boundary conditions [8] which

can be written also in the form of Eq. (1). The amplitude thresholds are slightly above the 1d theory but show the same qualitative behaviour. In qualitative agreement with the experiment the wave number k_x of the roll cells increases with increasing strength of the stochastic field as well as with decreasing correlation time of the stochastic field (in the 1d theory k_x is always constant).

5. CONCLUDING REMARKS

In all considered cases we are able to obtain results which are exact in the frame of the models. Especially, we avoid 'adiabatic' elimination procedures. Full details will be published elsewhere [6].

To investigate the possibility of a hysteretic (subcritical) transition one should treat a nonlinear model.

To explain the appearance of different patterns along the threshold curve (alteration of bifurcation sequence) it would be necessary to test the stability of a 3d theory against the corresponding test modes.

REFERENCES

[1] Noise in nonlinear dynamical systems, Vols. 1-3, Moss, F., McClintock, P.V.E. (eds.), 1989, Cambridge University Press, Cambridge.

[2] Proc. Workshop on external noise and its interaction with spatial degrees of freedom in nonlinear dissipative systems, 1989, in: J. Stat. Phys. 54, Nos. 5/6.

[3] Kai, S., Ref. [1], pp. 22-76, and Refs. therein.

[4] Dubois-Violette, E., deGennes, P.G., Parodi, O., 1971, J. Phys. (Paris) 32, 305-317

[5] Behn, U., Müller, R., 1985, Phys. Lett. 113A, 85-88; Müller, R., Behn, U., 1987, Z. Phys. B 69, 185-192.

[6] Müller, R., Behn, U., 1989, EHD instabilities in nematics driven by dichotomous noise: Stability criteria and influence of boundary conditions, submitted to Z. Phys. B.

[7] Arnold, L., Kloeden, P., 1989, Lyapunov exponents and rotation number of two-dimensional systems with telegraphic noise, to appear in SIAM J. Appl. Math.

[8] Goosens, W.J.A., 1978, in: Advances in liquid crystals, Brown, G.H. (ed.), Vol. 3, pp. 1-39 , Academic Press, New York, San Francisco, London.

10th Int.Conf. on Noise in Physical Systems
1989 Budapest, Hungary

AMPLITUDE STOCHASTIZATION OF OSCILLATIONS OF NONLINEAR OSCILLATOR WITH HIGH-FREQUENCY PUMPING MODULATED BY A TELEGRAPH RANDOM SIGNAL

A.S. MAGARSHAK, A.Yu. SINKEVICH, D.M. SHTEINGRADT

Engineering Centre "LIDAR", Academy of Sciences,
P.O.Box 512, 125057 Moscow, USSR

It has been suggested earlier (Kogan, Nagaev 1984; Kozub 1984) that 1/f-noise is generated by a random telegraph process. In this connection, it is of interest to study stochastization of stable oscillations under the action of a random telegraph signal.

The desire to know what physical processes are responsible for the 1/f-noise and the above suggestion led us to study the random telegraph signal effect on stationary oscillations. The most convenient method was to study the movement of a high-frequency-pumped oscillator.

We investigated oscillatory dynamics of a nonlinear HF-pumped oscillator that can be described as follows:

$$\ddot{q} + \beta\dot{q} + \sin q = 2\, w\, (q)\, V\, (q_o^2 - q^2)\, \sin\, (\omega t + \psi)\, \sin \frac{q}{2} \qquad (1)$$

where q is a coordinate, β is the frictional coefficient and w is the coupling constant of the pumped oscillator. Equation (1) comprises two terms,

$$\beta\dot{q} \quad \text{and} \quad 2\, w \sin \frac{q}{2} \sin\, (\omega t + \psi)\, V\, (q_o^2 - q^2)$$

determining time dependence of the oscillator amplitude. As a zero approximation to Eq. (1), the following equation, omitting these terms, will be considered:

$$\ddot{q} + \sin q = 0. \qquad (2)$$

Solution of this equation contains oscillation energy (E) and related oscillator amplitude (K) as a parameter (e.g. Ahiezer 1970):

$$\sin \frac{q}{2} = ksn\ (t, k);\ \dot{q} = 2\ kcn\ (t, k);\ E = 2k^2;\ 1 \geq k \geq 0$$

The quantity q_o is equivalent to two other ones: s_o, t_o, convenient here:

$$\sin \frac{q_o}{2} = s_o = ksn\ (t_o, k)$$

Let us write the equation describing the oscillator energy change with time (E(t)). To do this we must multiply Eq. (1) by the generalized coordinate time derivative. The sum of the first and the third terms in the left-hand side of the equation equals the oscillator energy time derivative, while the two other terms, as mentioned above, will govern the oscillator dynamics and its energy changes with the time interval larger than the oscillation period of an ideal autonomous oscillator:

$$\dot{E}(t) = -\beta\dot{q}^2 + 2\ w\ \dot{q}\ \sin\ (\omega t + \psi)\ V\ (q_o^2 - q^2) \qquad (3)$$

Deriving Eq. (3) we disregarded the assumption about the smallness of the contributions of terms containing β and ω, i.e. about a very small change of the oscillator energy during one period. With this in mind, let us substitute solution of Eq. (2) into Eq. (3) as a first approximation:

$$\dot{E}(t) = -4\beta k^2 (cn(t,k))^2 + 4wk^2 \sin\ (\omega t + \psi)\ sn\ (t,k)\ cn\ (t,k)\ x$$

$$x\ V\ (s_o^2 - k^2\ (sn\ (t,k)^2).$$

Turning from energy to the amplitude we obtain:

$$\frac{dlnk}{dt} = -\beta (cn(t,k))^2 + wsn(t,k)\ \sin\ (\omega t + \psi)\ x$$

$$x\ V\ (s_o^2 - k^2\ (sn(t,k))^2). \qquad (4)$$

For stationary amplitudes:

$$\left\langle \frac{d\ln k}{dt} \right\rangle_{t\to\infty} = 0.$$

This condition permits calculation of possible stationary amplitudes by averaging over a large number of oscillation periods $\pi/2$

$$T_o = 4 \int_o^{\pi/2} d\alpha [1-k^2 (\sin\alpha)^2]^{-1/2} = 4K(k)$$

Averaging Eq. (4) for time NT ($N\to\infty$) we obtain (after Prudnikov et al. 1981):

$$0 = -\beta(K(k))^{-1} k^{-2} [E(k)-(1-k^2)K(k)] + w\,(4NK(k))^{-1} \times$$

$$\times \sum_{n=0}^{2N-1} \int_{-t_o}^{t_o} dt\, sn(t,k)cn(t,k) \sin[\omega(t + 2nK(k)) + \psi]$$

At $N\to\infty$ the difference between the two terms in the right-hand side of the equation can turn into zero, if the second component sum is proportional to N, which is valid at

$$2\omega K(k) = 2\pi m$$

where m is a natural number (Efimov 1980). This condition determines amplitudes of stationary oscillations (K_m) and therefore the ratio between the oscillation period and the pumping period will be:

$$T_o/T_H = T_o\,\omega/2\pi = 2m$$

Since $s_o \ll K$, let us derive the integral of the second term in the right-hand side. The resultant equation determines the pump current phase necessary to realize stationary oscillations at instants when q equals zero. Due to the ratio of the

oscillator and pumping periods the required pump current phase ψ_m is constant:

$$\cos \psi_m = \frac{\beta\omega^2 [E(k_m) - (1-k_m^2) K(k_m)]}{wk_m^2 \left(\sin \frac{\omega s_o}{K_m} - \frac{\omega s_o}{K_m} \cos \frac{\omega s_o}{K_m}\right)}$$

Since $|\cos \psi_m| < 1$ and since w is in the denominator, stationary amplitude zones show up at $w \geq w_{min}$. At $w = w_{min}$ ($\psi = 0$) the corresponding amplitude is unstable. For $w > w_{min}$ Eq. (4) takes the form describing half-cycle amplitude change

$$\frac{\Delta k}{2k} = -\frac{\beta}{k^2} [E(k) - (1-k^2) K(k)] + \frac{w \cos}{\omega^2} \left(\sin \frac{\omega s_o}{k} - \frac{\omega s_o}{k} \cos \frac{\omega s_o}{k}\right)$$

We take into account the fact that at $K = K_m$; $\psi = \psi_m$ (5)

the left-hand side of Eq. (5) turns into zero:

$$\Delta(k-k_m) = -(k-k_m) \frac{2\beta}{k_m^2} [E(k_m) - (1-k_m^2) K(k_m)] \left[\left(\frac{\omega s_o}{k_m}\right)^2 \left(1 - \frac{\omega s_o}{k_m} \operatorname{ctg} \frac{\omega s_o}{k_m}\right) + \right.$$

$$\left. + \frac{(2-k_m^2) K(k_m) - 2E(k_m)}{E(k_m) - (1-k_m^2) K(k_m)}\right] - (\psi - \psi_m) \frac{2\beta}{k_m} \operatorname{tg} \psi_m [E(k_m) - (1-k_m^2) K(k_m)]. \quad (6)$$

The half-cycle change of pump current phase, i.e. phase change within two successive instances corresponding to $q = 0$, is determined by the duration of additional time necessary for one half-period of oscillations with amplitude $K \neq k_m$ to complete:

$$\Delta(\psi - \psi_m) = 2\omega [K(k) - K(k_m)] \approx (k-k_m) \frac{2\omega}{k_m (1-k_m^2)} [E(k_m) - (1-k_m^2) K(k_m)]. \quad (7)$$

It follows from Eqs (6) and (7) that oscillations are stable in both amplitude and phase at

$$1 > \frac{\omega s_o}{k_m} \operatorname{ctg} \frac{\omega s_o}{k_m}.$$

Therefore, stability is determined by phase relations and pumping region transit time if stationarity of oscillations is provided with regard to an accurate compensation of frictional losses by the applied field.

The results of a computer-based experiment suggest that stationary oscillations with a single limiting amplitude are realized when the applied field is almost as small as the minimal one, determined by the dissipation term value and when there are no fluctuations. If stationary oscillations occur owing to the oscillator interaction with the applied field whose value considerably exceeds that required to compensate for frictional losses, then the amplitude of stationary oscillations within the zone may tend to the double limiting point mode. In this case we observe stationary oscillations with related oscillator amplitudes successively taking two or more values.

It is natural to ask, how strong pumping must be to permit oscillation transfer from the single-limiting-amplitude to the double-limiting-amplitude mode. Portion of energy consumed by the oscillator for the oscillation period depends on phase difference between oscillator moving and pumping, as well as on oscillator-pumping-region transit time, i.e. on oscillator amplitude. Therefore, it is due to the amplitude value and oscillation phase difference that the limiting point value is determined. Then $\vec{U}_i = \begin{pmatrix} \Delta K \\ \Delta\psi \end{pmatrix}_i$; $\Delta\vec{U}_{i+1} = \hat{D}\,\vec{U}_i$

$$\left(\vec{U}_{i+1} - \vec{U}_i\right) = \begin{pmatrix} -A & B \\ -C & 0 \end{pmatrix} \vec{U}_i .$$

The pattern of oscillator relaxation within one zone is obeyed by transition matrix $\begin{pmatrix} -A & B \\ -C & 0 \end{pmatrix}$ and its self-values:

$$\lambda_{1,2} = \frac{A}{2} \pm \frac{1}{2}\sqrt{A^2-4BC}$$

The (A^2-4BC) change of sign corresponds to the relaxation pattern change. Substituting the A, B, C explicit form from Eqs

(6) and (7) one obtains the boundary between two relaxation modes.

The pumping current is supposed to be modulated by the random telegraph signal (see Fig. 1 where the pumping amplitude level K_1 is insignificantly higher than that of frictional loss compensation K_o). With pumping amplitude level K_1 we observe a mode of oscillations when the system relaxes tending to the single-limiting-amplitude, while with pumping amplitude level

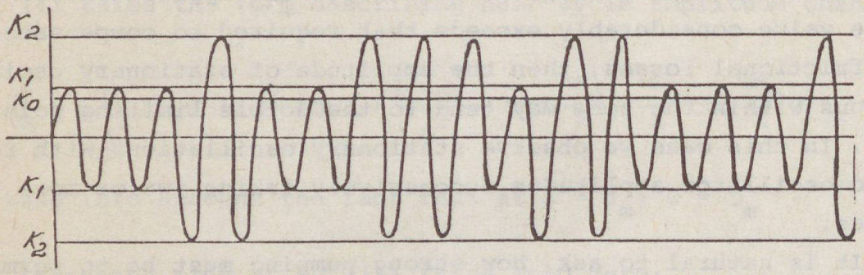

Fig. 1. Pattern of pumping modulation by a random telegraph signal. K_o - pumping level equalling the threshold of frictional loss compensation; K_1 - pumping level slightly exceeding the threshold; K_2 - pumping level considerably exceeding the threshold.

K_2, considerably higher than K_o, the system's amplitude relaxation is towards the double-limiting mode. In this case the stable amplitude of oscillator movement will continuously fluctuate within the stability zone between the single- and double-limiting modes. The proposed model permits tracing the dynamics of stationary oscillation stochastization. The random telegraph signal modulation of the pump current has two fixed levels, K_1 and K_2 (K_o equals the level of frictional compensation threshold). Duration of each level is a random white noise spectrum value. While the pump current amplitude is K_1, the oscillator gradually relaxes tending to the single-limiting amplitude. The process is towards the double-limiting mode when the pump current amplitude is K_2. These two alternative modes (their durations determined by a random value) form certain cross-point distributions on the amplitude-phase plane (Fig. 2).

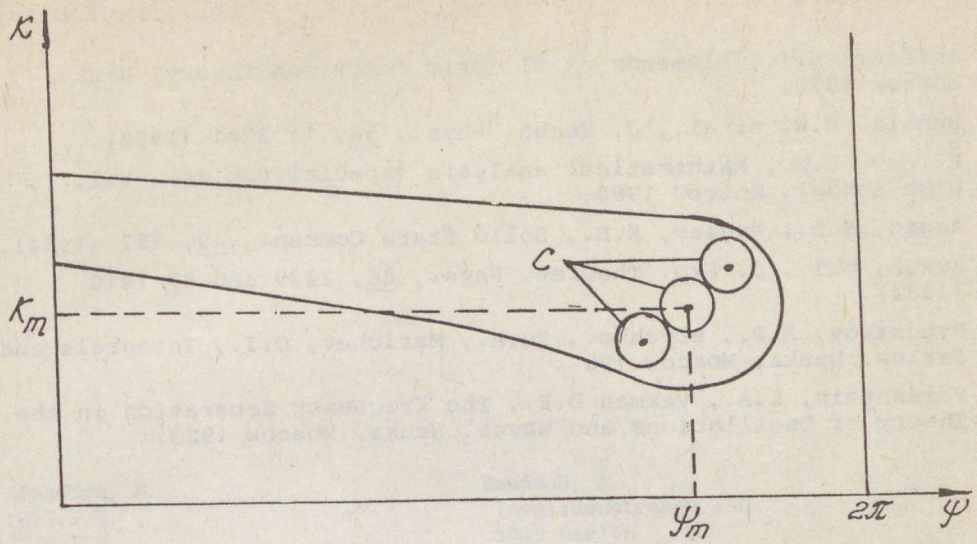

Fig. 2. Pattern of oscillation stability zone on the phase plane and distribution of the concentration regions. C - concentration regions.

Relaxation within each mode can also be represented as certain distributions, P_1 (K, ψ) and P_2 (K, ψ), on the amplitude-phase plane. As they are mixed up, the weight of each distribution is proportional to time, therefore one can expect to obtain the 1/f fluctuation spectrum. The question whether the 1/f component is present is the fluctuation spectrum cannot be answered with the help of summed distribution, P (K, ψ), obtained in the computer-based experiment. P (K, ψ) is a distribution with three concentration regions. In each of these regions the amplitude of the probability density and their relationships are strongly dependent on the whole time of the computer experiments, which implies the presence of 1/f-type properties in the fluctuation spectrum. To obtain stationary distribution, an enormous computer time is needed, hence we present here only a qualitative pattern of distribution obtained by extrapolation to the infinitely large averaging time.

REFERENCES

Ahiezer, N.I., Elements of Elliptic Functions Theory. Nauka, Moscow 1970.

Bunkin, F.W. et al., J. Techn. Phys., 58, 11, 2241 (1988).

Efimov, A.W., Mathematical analysis (special topics). Vol. 1, High School, Moscow 1980.

Kogan, S.M., Nagaev, K.E., Solid State Commun., 49, 387 (1984).

Kozub, V.I., J. Exp. Theoret. Phys., 86, 2239 and 87 1410 (1984).

Prudnikov, A.P., Brychkov, Yu.A., Marichev, O.I., Integrals and Series. Nauka, Moscow 1981.

Vainshtein, L.A., Vakman D.E., The Frequency Separation in the Theory of Oscillations and Waves. Nauka, Moscow 1983.

Alabedra, R.
U.S.T.L.
C.E.E.S.
Place Eugene Bataillon
34060 Montpellier
France

Ambrózy, A.
Dept.of Electronics Technology
Technical University of Budapest
1521 Budapest
Hungary

Anton, K.
Institut für Angewandte Physik
Universität Frankfurt
Robert Mayer Str. 2-4.
6000 Frankfurt 1
FRG

Baciocchi, M.
C.N.R. - I.E.S.S.
Via Cineto Romano 42
00156 Roma
Italy

Bakshee, I.,S.
Inst. Semicond.
Acad. Sci.USSR
252650 Kiev - 28
USSR

Bareikis, V.
Inst. of Semiconductor Physics
Academy of Sciences Lithuanian SSR
K. Poshelos 52, Vilnius 232600
USSR

Baudach, A.
Invalidenstrasse 110
1040 Berlin
GDR

Beben, J.
Institute of Experimental Physics
Wrocław University
Cybulskiego 36., 50-205 Wrocław
Poland

Belan, J.
Department of Microelectronics
Slovak Technical University
Mlynska dolina
81219 Bratislava
Czechoslovakia

Ben-Yaakov, S.
Dept. of Electrical Computer Eng.
Ben-Gurion University
Beer Sheva
Israel

Briggmann, J.
Max Planck Institut für Metallforsch.
Heisenberg str. 1
7000 Stuttgart 80
FRG

Brophy, J.J.
University of Utah
210 Park Building
Salt Lake City, Ut 84112
USA

Bulsara, A. R.
NOSC Code 633
8780 Taurus Pl.
San Diego, Ca 92152
USA

Castagnetti, R.
Institute of Quantum Electronics
HPT H8
8093 Zürich
Switzerland

Chang, J.
308 Westwood Plaza #578
Los Angeles
USA

Chen, Ch. T.M.
Dept. of Electrical Engineering
College of Engineering
University of South Florida
Tampa, Fl 33620
USA

Cherevko, A.G.
Inst. of Communication Systems
Novosibirsk
Tereshkova St 6-86
Novosibirsk 630090
USSR

Chovet, A.
Lab. Physique des Composants
ENSERG
23 Rue des Martyrs
38016-Grenoble Cedex
France

Codastefano, P.
Dipartimento di Fisica
Universita di Roma
Ple Amoro 2, Roma 00185
Italy

Cottle, J.G.
Electrical Engineering Dept.
Univ. of South Florida
Tampa, Fl. 33620
USA

Damgov, V.N.
Space Research Institute
Bulgarian Acad. of Science
6 Moskowska Str.
1000 Sofia
Bulgaria

Decoutere, S.
IMEC
Kapeldreef 75
3030 Leuven
Belgium

De Felice, L. J.
Dept. Anatomy & Cell Biology
Emory University
Atlanta, Ga 30322
USA

Dierickx, B.
IMEC
Kapeldreef 75
3030 Leuven
Belgium

Dmowski, K.
Inst. Microelectr. Optoelectr.
Technical Univ. of Warsaw
Koszykowa 75
00-662 Warsaw
Poland

Doutreloigne, J.
Rug-Labo voor Elect. en Meetechniek
Sint-Pietersnieuwstraat 41
9000 Gent
Belgium

Fronen, R.J.
Grp. Elect. Materials, Dept. Elect. Eng.
Eindhoven University of Technology
Postbus 513
5600 MB Eindhoven
The Netherlands

Ghibaudo, G.
Lab. des Comp. à Semiconducteurs
ENSERG/PCS
23 rue des Martyrs
38016 Grenoble
France

Gombos, G.
MTA MÜFI
P.O. Box 76
1325 Budapest
Hungary

Gouyet, J.F.
Lab. Physique
Ecole Polytechnique
91128 Palaiseau
France

Gottwald, P.
Dept. of Electron Devices
Technical Univ., Budapest
1521 Budapest
Hungary

Green, M.
Dept. of Chemistry
City College, University of NY
Convent Ave. at 138th Street
New York NY 10031
USA

Grmela, L.
Boreticka 13
Brno 62800
Czechoslovakia

Güttler, H.,H.
Festkörperforschung
Max Planck Inst.
Heisenbergstr. 1.
7000 Stuttgart 80
FRG

Gunnarsson, K.
Technikum
University of Uppsala
Box 534
75121 Uppsala
Sweden

Handel, P.H.
Physics Dept.
Univ.of Missouri
St Louis
Mo 63121
USA

Hashiguchi, S.
Dept. of Electronics
Yamanashi University
Kofu 400
Japan

Hasse, L. Z.
Politechnika Gdanska
Wydriat Elektronik
Majakowskiego 11/12
80-952 Gdansk
Poland

Heiden, C.
Inst. für Angew. Physik
Universität Giessen
Heinrich Buff-ring 16
6300 Giessen
FRG

Hofman, F.
Fysisch Laboratorium
Princetonplein 5, Postbus 80000
3508 TA Utrecht
The Netherlands

Hooge, F.N.
Dept. of Electrical Engineering
Techn. Univ. Eindhoven
P.O. Box 513
Eindhoven
The Netherlands

Jindal, R.P.
Bell Laboratories
Room 2 A - 142
600 Mountain Avenue
Murray Hill NJ 07974
USA

Jones, B.K.
Dept. of Physics
University of Lancaster
Lancaster LA1 4YB
UK

Karapatnitski, I.A.
High Energy Physics Inst.
Academy of Sciences
480082 Alma-Ata
USSR

Katilius, R.
Semiconductor Physics Institute
Lithuanian SSR Academy of Sci
K.Pozhelos 52.
Vilnius 232600
USSR

Kimmerle, J.
SEL AG, Dept. ZT/FZW
Lorenzstr. 10
7000 Stuttgart 40
FRG

Kiss L. B.
Kisérleti Fizika Tanszék
JATE
Dóm tér 9
6720 Szeged
Hungary

Klason, C.
Dept. of Polymer Materials
Chalmers University
41296 Gothenburg
Sweden

Kleinpenning, T. G. M.
Dept. of Electrical Engineering
University of Technology
P.O. Box 513
Eindhoven
The Netherlands

Kogan, Sh.M.
Inst. of Radioengineering
and Electronics
Acad. Sci. of the USSR
Marx prospect 18
103907 Moscow
USSR

Kolodziejski, J.F.
Institute of Electron Technology
Al. Lotnikow 32/46
02-668 Warszawa
Poland

Konczakowska, A.
Inst.Technologii Electronicznej
Politechnica Gdanska
ul. Majakowskiego 11/12
80-952 Gdansk
Poland

Kozub, V.
A.F.Ioffe Physico-Technical Inst.
Leningrad 194021
USSR

Kravtsov, Y.
Engineering Centre "Lidar"
P.O.Box 512
Moscow-57 125057
USSR

Kubat, J.
Sweden

Kugler, S.
Univ. of Duisburg
FB9/HLT
4100 Duisburg 1
FRG

Kurths, J.
Zentr.Inst. Astrophysik
1501 Tremsdorf bei Potsdam
GDR

Kusy, A.
Politechnika Rzeszowska
W. Pola 2
35-959 Rzeszów
Poland

Lecoy, G.
Cent. d'Etude d'Elect. des Solides
Université du Languedoc
34060 Montpellier Cedex
France

Liedermann, K.
Katedra Fyziky FE VUT
Konevova 131
63900 Brno
Czechoslovakia

Macicci, M.
Via Diotisalvi 2
I-56126 Pisa
Italy

Madhu, S.
Dept. of Electr. Engineering
Rochester Inst. of Technology
1, Lomb Memorial Drive
Rochester, New York 14623
USA

Magarshak, A.S.
P.O. Box 512. "Lidar"
125057 Moscow
USSR

Makovijtchuk, M.
Univ.of Microelect.Acad.of Siences
Universitetskaya 21.
Yaroslavl 150007
USSR

Matulionis, A.
Semiconductor Physics Institute
Lithuanian Academy of Sciences
Vilnius
USSR

May, E.J.P.
Dept of Engineering Science
University of Exeter
Exeter EX4 4QF Devon, UK

Mazzetti, P.
I.E.N.G.F.
Cs. M. D'Azeglio 42
10126 Torino
Italy

Meade, M.L.
Faculty of Technology
Open University
Walton Hall
MK7 6AA Milton Keynes, UK

Montorsi, A.
C.so Duca degli Abruzzi 24
10129 Torino
Italy

Moss, F.E.
Dept. of Physics
University of Missouri
St. Louis
Missouri 63121
USA

Munakata, T.
Faculty of Engineering
Tamagawa University
6-1-1 Tamagawa-gakuen Machida-shi,
Tokyo
Japan

Musha, T.
Dept. of Applied Electronics
Tokyo Inst. of Technology
Nagatsuta, Midoriku
Yokohama 227
Japan

Mykolaitis, H.
Dept. of Radiophysics
Vilnius University
Vilnius
USSR

Nathan, A.
Physical Electronics Laboratory
Institute of Quantum Electronics
ETH-Hönggerberg
8093 Zürich
Switzerland

Naumburger, V.
Zentr. Wiss. Gerätebau, Betr. Rahnsdorf
Akad. der Wissenschaften der DDR
Seestraße 82.
1166 Berlin Rahnsdorf
GDR

Neidenoff, A.
Fachhochschule des Saarlandes
Saaruferstr. 66
6600 Saarbrücken
FRG

Neri, B.
Istituto Elettronica e
Telecomunicazioni.
Università di Pisa
Via Diotisalvi 2
56126 Pisa, Italy

Neustroev, L.N.
Yogorskii pr. 18/14. kv.34
Moscow 129347
USSR

Nougier, J.P.
Univ. des Sciences et Tech.
du Languedoc
34060 Montpellier Cedex
France

Orsal, B.
Centre Electronique de Montpellier
USTL
34060 Montpellier
France

Osipov, V.V.
kv. 195, d. 5, Voronsovskie prudu
Moscow
USSR

Ostrava, S.O.
Department of Applied Physics
Kazan Aviation Institute
K. Marx ul. 10. 8-69.
420111 Kasan
USSR

Palenskis, V.
Dept. of Radiophysics
Vilnius University
Sauletekio Al.9
232054 Vilnius
USSR

Pellegrini, B.
Istituto di Elettronica e
Telecomunicazioni
Università di Pisa
Via Diotisalvi 2
56126 Pisa
Italy

Peransin, J.M.
C.E.E.S.
U.S.T.L.
Place Eugene Bataillon
34060 Montpellier Cedex
France

Potemkin, V.
Noise Laboratory
Physical Department
Moscow State University
Moscow 119899
USSR

Reggiani, L.
Dip. di Fisica
Università di Modena
Via Campi 213/a
41100 Modena
Italy

Ren, L.
P.O. Box 513
Eindhoven
The Netherlands

de la Rubia, F.J.
Fisica Fundamental,UNED
Apdo. Correos 60141
28080 Madrid
Spain

Saletti, R.
Centro Studi Radiotrasmissioni
Via Diotisalvi 2
56126 Pisa
Italy

Savelli, M.
Univ.des Scie.et Tech. du Languedoc
34060 Montpellier Cedex
France

Shi, Z.M.
EPFL Departement de Physique
Inst. de Micro- et Optoelectronique
1015 Lausanne
Switzerland

Šikula, J.
Dept. of Physics
Technical University of Brno
Barvicova 85
66237 Brno
Czechoslovakia

Sinkevich, A.Yu.
P.O. Box 512 "Lidar"
125057 Moscow
USSR

Šostarec, I.
A.Einstein 2.
24000 Subotica
Yugoslavia

Stepanescu, A.
Ist. Elettrotecnico Nazionale
G.Ferraris
Cso M. D'Azeglio 42
10129 Torino
Italy

Stolarski, E.
Institute of Electron Technology
Al. Lotnikow 32/46
02-668 Warszawa
Poland

Storm, L.
Institut für Angewandte Physik
Westfälische Wilhelms Universität
Corrensstrasse 2/4
4400 Münster
FRG

Strásky, L.
Tesla
Purkynova 99., 61245 Brno
Czechoslovakia

Szentpáli, B.
MTA MÜFI
P.O. Box 76
Budapest
Hungary

Tartaglia, P.
Ple Amoro 5
00185 Roma
Italy

Tetzlaff, R.
Institut für Angewandte Physik
Universität Frankfurt
Robert Mayer Strasse 2-4
6000 Frankfurt a.M. 1
FRG

Thomae,R.
Zentr. f.Wissenschaftliche Gerätebau
Rudower Chausser Nr.6
1199 Berlin
GDR

Trefán, Gy.
JATE Kísérleti Fizika Tanszék
Dóm tér 9., 6720 Szeged
Hungary

Van der Ziel, A.
4405 Grimes Ave South
Minneapolis, Mn 55424
USA

Van Sterkenburg, S.
Dept. of Electronic Eng.
Eindhoven Univ. of Technology
P.O. Box 513
5600 MD Eindhoven
The Netherlands

Van Vliet, C. M.
Cent. de Recherches Mathématiques
Université de Montréal
Case Postale 6128 - A
Montréal, Québec H3C 3J7
Canada

Vandamme, L.K.J.
Dept. of Electrical Engineering
Eindhoven Univ. of Technology
P.O. Box 513
5600 MB Eindhoven
The Netherlands

Vasina, P.
Dept. of Physics
Technical University
Voronezska 8.
61600 Brno-16
Czechoslovakia

Vavriv, D.
Kharkov University
Dzerzhinsky Sq. 4
310077 Kharkov
USSR

Viswanathan, C.R.
7731 Boelter Hall, Ucla
Los Angeles, Ca. 90024
USA

Voshchinskii, Yu.A.
P.O. Box 512 "Lidar"
125057 Moscow
USSR

Weber, B.
Institut für Angewandte Physik
Universität Frankfurt
Robert Mayer Str. 2-4
6000 Frankfurt 1
FRG

Wolf, D.
Institut für Angewandte Physik
Universität Frankfurt
Robert Mayer Str. 2-4
6000 Frankfurt 1
FRG

Zaklikiewicz, A.M.
Ite Cemi
Al. Lotnikow 32/46
02-668 Warszawa
Poland

Zhukov, A.
University of Solid State Physics
Chernogolovka
Moscow 142432
USSR

Zijlstra, R.J.J.
Fysisch Laboratorium
Rijksuniversiteit Utrecht
Princetonplein 5
Utrecht
The Netherlands

Bibliotheca Academiae Scientiarum Hungaricae
MAGYAR TUDOMÁNYOS AKADÉMIA KÖNYVTÁRA

AL-CHARCHAFCHI, S.H. 411
ALABEDRA, R. 159, 251, 585
ALOE, P. 237
AMBRÓZY, A. 109, 455, 569, 573
ANDRE, J.D. 171
ANISHCHENKO, V.S. 625
ANTON, K. 331
ARUGA, H. 437

BAKSHEE, I.S. 389, 397
BALESTRA, F. 495
BALTES, H.P. 543
BÁNLAKI, P. 537, 573
BAREIKIS, V. 53, 189
BARKAUSKAS, R. 45
BÉAL-MONOD, M.T. 71
BEBEN, J. 57
BEHN, U. 663
BELAN, J. 263
BELOGORTSEV, A.B. 657
BENZ, A.O. 605
BERTOTTI, G. 113
BIRKEMEYER, U. 605
BORBÉLY, G. 385
BORDONE, P. 99
BOUGHALEB, Y. 401
BROPHY, J.J. 77, 87
BULASHENKO, O.M. 61
BULSARA, A.R. 621

CARBONE, A. 285
CASTAGNETTI, R. 543
ČERMÁKOVÁ, A. 479
CHANG, J. 499, 503
CHEN, T.M. 515, 519
CHEREVKO, A.G. 125
CHERNESHOV, I.Yu. 651
CHOVET, A. 471
CLAEYS, C. 275, 483
COMALLONGA, J. 565
COS, S. 275
COTTLE, J.G. 515, 519

DAMGOV, V.N. 593, 615
DARGYS, A., 91
De BAETS, J. 511
DEBNATH, G. 29
DECLERCK, G. 483
DECOUTERE, S. 483
DEDULEVIČ, S. 49
DeFELICE, L.J. 303
DEFERM, L. 483
DEKHTYARUK, N.T. 259
DEMICHELIS, F. 285
De RYCKE, I. 511
De SMET, H. 511
DIERICKX, B. 275
DILIGENTI, A. 237
DIMOPOULOS, G. 471
DMOWSKI, K. 589
DOUTRELOIGNE, J. 511
DUMAS, J.M. 281
DUTOIT, M. 427

FANG, P. 515
FENG, S. 67
FLACHET, J.C. 251
FORGÁCS, G. 71
FRONEN, R.J. 475

GAFIJCHUK, V.V. 609
GAL'PERIN, Yu.M. 407
GANTSEVICH, S.V. 45
GARBAR, N.P. 461
GHIBAUDO, G. 271, 495
GINGL, Z. 335, 569, 573
GLADYSZ, H. 241
GOMBOS, G. 39
GOTTWALD, P. 109, 455
GOUYET, J.F. 401

GREEN, M.E. 313
GRIN', V.F. 397
GRMELA, L. 209, 217
GUNNARSSON, K. 437
GUREVICH, V.L. 407
GÜTTLER, H.H. 487

HAFEZ, I.M. 495
HANDEL, P.H. 155, 167, 179, 351, 365, 433
HASHIGUCHI, S. 393, 507
HASSE, L. 247, 599
HEIDEN, C. 175
HEIME, K. 201
HENNING, J.C.M. 205
HERAULT, D. 221
HEVESI, I. 569, 573
HLÁVKA, J. 217
HOFMAN, F. 205
HOOGE, F.N. 375
HRISTOV, T.S. 615
HÜTTEL, I. 217, 293

ILEGEMS, M. 427
IRIE, H. 507
ISLIKER, H. 605
ITO, A. 437

JACOBS, E.W. 621
JAKUBOWSKI, A. 589
JAMES, M. 29
JINDAL, R.P. 289
JOINDOT, I. 159
JONES, B.K. 213, 531
JUNG, G. 135

KANAYAMA, T. 393
KANCLÉRIS, Ž. 49
KARACHEVTZEVA, L.A. 397
KARAPATNITSKI, I.A. 465
KARPOV, V.G. 407
KATILIUS, R. 45, 189
KERNER, B.S. 609
KHIZHNYAK, B.I. 389, 397
KIL, A.J. 171
KISS, L.B. 319, 335, 569, 573
KLEINPENNING, T.G.M. 443
KOCHELAP, V.A. 61
KODALASHVILI, M.Z. 397
KOGAN, Sh.M. 129
KOKTAVÝ, B. 297, 479
KOLEK, A. 343
KONCZAKOWSKA, A. 241, 247
KONOPKA, J. 135
KOUADIO, A. 221
KOZUB, V.I. 407
KRATĚNA, L. 209
KRAVTSOV, Yu.A. 625

KUGLER, S. 201
KUROPYATNIK, I.N. 125
KURTHS, J. 605
KUSY, A. 343

LATTA, V. 263
LAUČIUS, J. 117
LECOY, G. 221
LEVEQUE, G. 251
LIBERIS, J. 53
LINDENBERG, K. 639
LUKYANCHIKOVA, N.B. 259, 461
LUNDGREN, L., 437

MAATOUGUI, A.H. 251
MAGARSHAK, A.S. 629, 667
MARINI, A. 267, 565
MASOERO, A. 561
MATISCAK, F. 263
MATUKAS, J. 231
MATULIONIS, A. 53
MATULIS, A. 49
MAY, E.J.P. 411, 417
MAZZETTI, P. 285
MEADE, M.L. 347
MIKOLAJ, V. 263
MILIUŠYTE, R. 53, 91
MIMAKI, T. 11
MITIN, V. 61, 99, 103
MONBLANC, P. 565
MONTORSI, A. 113
MORTEN, B. 561
MOSS, F. 29, 635
MOZZI, C. 237
MUNAKATA, T. 11
MUSHA, T. 385
MÜCK, M. 175
MÜLLER, R. 663
MYKOLAITIS, H. 117, 121

NAGAEV, K.E. 129
NATHAN, A. 543
NAUMBURGER, V. 581
NEIDENOFF, A. 19
NERI, B. 237, 267
NEUSTROEV, L.N. 421
NEVĚČNÝ, V. 227
NORDBLAD, P. 437
NOUGIER, J.P. 7

OLIVO, P. 267
ORSAL, B. 159, 251, 585
OSIPCHUK, L.K. 465
OSIPOV, V.V. 421, 609

PALENSKIS, V. 117, 231, 339
PANASHCHENKO, O.N. 421

PELLEGRINI, B. 3
PERANSIN, J.M. 281, 585
PETRICHUK, M.V. 461
PIKOVSKII, A.S. 625
PINCEVIČIUS, A. 231
POTEMKIN, V.V. 389
PRUDENZIATI, M. 561

RABARIOELINA, J. 565
RAMIREZ-PISCINA, L. 639
RANIRIHARINOSY, K. 159
REGGIANI, L. 95, 99
RIGAUD, D. 221, 281, 585
ROMANENKO, A.I. 125
ROSSO, M. 401
de la RUBIA, F.J. 639
RUSSELL, P.C. 531
RYABOV, V.B. 645

SAKALAS, P. 53
SALETTI, R. 267
SALKOV, E.A. 389, 397
SANCHO, J.M. 639
SAPOVAL, B. 401
SASČIUK, A.P. 461
SAVELLI, M. 251, 565
SCHAUER, P. 297
SCHIEVE, W.C. 621
SCHLAPP, W. 201
SEKINE, M. 365
SHI, Z.M. 427
SHOJI, M. 385
SHTEINGRADT, D.M. 629, 667
ŠIKULA, J. 209, 217, 227, 293, 297, 479
ŠIKULOVA, M. 227
SIMOEN, E. 275
SINHA, K. 29
SINKEVICH, A.Yu. 667
SMETONA, S. 231
ŠOBLICKAS, Z. 339
ŠOŠTAREC, I. 523
SPIRALSKI, L. 247, 599
STADALNIKAS, A. 339
STAFEEV, V.I. 465
STEPANESCU, A. 561
STOLL, H. 487
STORM, L. 551
STRAPKO, F. 263
STRÁSKÝ, L. 297
SUGIYAMA, Y. 393
SUN, M.I. 519
SVEDLINDH, P. 437
SYNEK, S. 293
SYRGABEKOV, I.N. 465
SZAKÁCS, T. 39
SZENTPÁLI, B. 189, 455

TÖRÖK, M. 569
TACANO, M. 393
TAYLOR, G.P. 213
TETZLAFF, R. 15
TREFÁN, GY. 569, 573

VAISSIÈRE, J.C. 7
VAJTAI, R. 335, 573
VALENZA, M. 221, 585
Van CALSTER, A. 511
van der ZIEL, A. 143
Van STERKENBURG, S. 577
Van VLIET, C.M. 103, 357
VANDAMME, L.K.J. 491
VANFLETEREN, J. 511
VARANI, L. 95, 99
VAŠINA, P. 209, 217, 227, 293, 297, 479
VASYUNYK, Z.I. 609
VAVRIV, D.M. 645, 651, 657
VERMEIREN, J. 275
VIGNAUD, P. 281
VISWANATHAN, C.R. 499, 503
VOSHCHINSKII, Yu.A. 629

WEBER, B. 351
WEIMANN, G. 201
WERNER, J.H. 487
WOLF, D 11, 15, 331, 351, 365

XU, Y.Z. 531

ZAKHLENIUK, N.A. 61
ZAKLIKIEWICZ, A.M. 369
ŽDÁNSKÝ, K. 209
ZHOU, T. 29, 635
ZIJLSTRA, R.J.J. 171, 205

Page numbers refer to the first page of the paper in which the index term appears.

activation energy 515
Al thin film 515
$Al_xGa_{1-x}As$ 205
ambipolar diffusion 45
amorphous semiconductors 77
amorphous silicon films 77
amplifier, operational 29
amplitude stability 663
analog circuit 29
analog simulator 29
analytic noise optimization 19
anodic oxidation 389
Arnold tongues 29
augmented 1/f noise 411

BCSCO (Bi-Ca-Sr-Cu-O) 135
bifurcation, topological 29
bipolar 483
bipolar transistor 443
bistable potential 635
bistable system 29
Boltzmann equation 7
Boltzmann-Langevin equations 189
breakdown 263,267
bulk noise 389
burst noise 227

cadmium selenide 511
carbon resistor 411
carbon/asbestos 417
carcinogens 417
carrier concentration 561
carrier density fluctuation 45
carrier mobility fluctuations 397
carrier number fluctuations 397
$Cd_xHg_{1-x}Te$ 397
chaos 29,663
chaotic return map 29
climate model 635
collision-controlled light scattering 45
colored noise 29
common source 507
conductance fluctuations 77,343
contact 561
convective noise 53,189
correlation function 29,95,189
correlators 589
counterdiffusion 561
critical exponents 343
critical point fluctuation 77
cross section noise 357
cross-spectrum 561
cryogenic temperature 499

deep centers 205
degradation 479,503
destabilization by noise 663
device modelling 491
device reliability 531,537
diagnostics 217
dichotomous noise 663
dielectric materials 293
diffusion 411,561
diffusion constant 103
diffusion noise 77,87,569,573
dissipative structure 663
distribution 667
DLTS 209
double limiting mode 667
double-well interatomic potentials 407
DX center 205,209

eccentricity, of Earth's orbit 635
electric field dependence of α_H 393
electrical fluctuations 171
electrohydrodynamic instabilities 663

electromagnetic fields 417
electromigration 515
electron gas 507
electron runaway 53
electron scattering 357
electron-photon interaction 357
electronic devices 443
electrostriction 577
elementary fluctuators 407
empirical relation 375
energetic stability 663
equivalent transfer of noise 19

Farey tree 29
feedback and noise 19
flicker noise 407,499,503
fluctuation conductivity 77
fluctuation phenomena 129
fluctuations 7,95,99
fluctuations of hysteresis loop 117,121
flux flow 135
flux of vacancies 515
focused ion beam implantation 393

G-R noise 171,205,227,393
GaAs 109,393,455,507
GaAs/AlGaAs heterostructures 171
gamma irradiation 523
gate-bias dependence of noise 507
general equivalent noise 19
generation-recombination 99

Hall device 393
Hall effect noise 397
HEMT 507
heterostructures 209,217
high electric fields 189
high electron-mobility transistor 507
high gate voltage 503
high speed devices 135,189
high T_c superconductors 77,135
Hooge's noise parameter 393
hot carriers 7
hot electron effects 103
hot electron fluctuations 53
hot electron noise 109,189
hot electron 91,95,99,189
hot-electron fluctuation length spectroscopy 189
hydrogenated amorphous silicon 77

ice ages, of Earth 635
impurity scatter 507
infrared divergence 357
InP 393
integral quantum Hall effect 171
integrator 29
interface noise 389
interface traps 483
intervalley fluctuations 45
intervalley noise 53,189
intervalley scattering 109
ion channel gating 313
ion channels 303
ionic conduction 87
ionic diffusion 87

JFET 443
Josephson contacts 129
Josephson effect 135
Josephson tunnel junction 443

kinetic theory of fluctuations 189
Kramer's rate 635

laser 29,635
laser diodes 475
laser simulator 29
lattice scatter 507
light output 475
light scattering 45
light scattering in electron-hole plasma 45
line-width of Josephson oscillations 129
linear filter 589
liquid helium temperature 499
liquid nitrogen temperature 499
localization 171
long-range fluctuations 53
low frequency noise 499
luminescent diodes 217

magnetic flux noise 77
magnetic noise 117,121
magnetic sensor 543
magnetron deposition 135
Markov systems 7
maximum of noise 19
membrane noise 303
MESFET 443
Michelson interferometer 577
microstructure 561
microwave noise emission 135
minimum of noise 19
mixed ionic conduction 77
mobility fluctuation 357,491
modulation 635
modulation noise 117,121
modulation noise vector model 117,121
Monte Carlo method 91,95,99
MOST 443,491
multicomponent semiconductor plasma 45

multiplication factor 263

nematic liquid crystals 663
neutron irradiation 523
noise factor 19
noise in amorphous magnetic alloy 121
noise in devices 227
noise in intermediate-length samples 189
noise in Josephson devices 129
noise in nonequilibrium system 189
noise in nonlinear system 117,121
noise in semiconductors 189
noise in superconductors 129
noise induced switching 635
noise matching 19
noise of capacitors 293
noise of p-n junctions 479
noise spectroscopy 77,209
noise spectrum 135
noise suppression 53
noise temperature 53,189
noiseless network 19
nonequilibrium electron-hole plasma 45
nonequilibrium fluctuations 189
nonequilibrium statistics 7
nonlinear dynamics 29
npn 483
nuclear irradiation 523
number fluctuation 491

$1/f$ noise 515
$1/f^2$ noise 515
operational amplifiers 523
optical characteristics 217
optical phonon emission 103
optoelectronic devices 209

parametric stochastic modulation 663
partial discharges 293
passivation 455
passive network components 293
percolation 343
percolation threshold 343
planar resistors 455
pn diode 443
pn junctions 479
pnp 483
power density 561
power spectrum 635
probability density 29
probability density function 343
probability density of residence times 635
probability density, hole in 29
probability density, skewing effect of 29
probability density, two-dimensional 29
pumping oscillator 667

quantum electrodynamics 357
quantum interferometer 135
quantum 1/f noise 357
quarter-micron filament 393
quasineutral fluctuations 45

random resistor network 343
random telegraph signal 635,667
random walk 569,573
real space renormalization group 343
relative noise 343
reliability 479,515
residence time 635
resistor 417,561
resolution 577
return map 29

sample stability 663
Schottky barrier diode 443
semiconductor 95,99
sheet resistance 561
signal to noise ratio, SNR 19,635
silicon 95,99
silicon MOSFET 499,503
simulation 569,573
single limiting mode 667
size effect 561
sodium β"-alumina 87
sodium β-alumina 87
soft potential model 407
spatially-inhomogeneous fluctuations 45
spectroscopy 205
spin fluctuation 77
stability 511,667
stabilization by noise 663
state occupancy fluctuations 189
state occupancy function 7
statistical thermodynamics 7
stochastic problems 29
stochastic resonance 635
stochastization 667
streaming 103
strong electric field 53
structural disorder 407
structure defects 479
subcritical transition 663
substrate, $LaAlO_3$, ZrO_2 135
supercritical transition 663
superionic conductors 77
surface noise 389
surface states 411,417
switching 635

technological conditions 19
terminations 561
theoretical SNR 589
thick film 561
thin film 109,135
thin film transistors 511
thin layers 455
thin silicon oxide 267
transient process 189
trapping-phenomena 95,99
tunneling 91
velocity fluctuation noise 103
velocity fluctuations 91
VLSI interconnections 515
voltage dependence of noise level 393

weighting factor of noise source 19
weighting function 589
white noise 29

YBCO (Y-Ba-Cu-O) 135

Zener reference 263

Bibliotheca Academiae Scientiarum Hungaricae
MAGYAR TUDOMÁNYOS AKADÉMIA KÖNYVTÁRA

1946

Any thermal equilibrium state or stationary state is only maintained by balancing opposite fluxes of thermodynamic variables. Whereas in statistical mechanics one is usually concerned with the averages of these variables, the study of the fluctuations, or in the spectral domain, noise, often reveals more of the nature of the stochastic processes responsible for the equilibrium or stationary state.

The Tenth International Conference on Noise in Physical Systems, including biological systems, dealt with a great variety of noise manifestations. Divided into eleven sessions, the Conference dealt with the fundamentals of noise as associated with statistical mechanics and stochastic mathematical theory, as well as with the manifestation of noise in many practical systems, be it physical, biological, or electronic in origin. Whether it be a specific noise problem or one of general aspects of fluctuations, this book with up to date references, will be most worthwhile for further research in this field.

674940

NOISE IN PHYSICAL SYSTEMS